Journal of Engineering and Technology for Industrial Applications

ISSN 2447-0228

December 2024

Volume 10 / No 50

Editor-in-Chief: J. C. Leite

www.itegam-jetia.org

ITEGAM - JETIA ISSN 2447-0228 Online
Journal of Engineering and Technology for Industrial Applications (JETIA)

O **ITEGAM-JETIA: Journal of Engineering and Technology for Industrial Applications** is a publication of the Galileo Institute of Technology and Education of the Amazon (ITEGAM), located in the city of Manaus since 2008. JETIA publishes original scientific articles covering all aspects of engineering. Our goal is the dissemination of research original, useful and relevant presenting new knowledge on theoretical or practical aspects of methodologies and methods used in engineering or leading to improvements in professional practice. All the conclusions presented in the articles It should be state-of-the-art and supported by current rigorous analysis and balanced assessment. Public magazine scientific and technological research articles, review articles and case studies.

JETIA will address topics from the following areas of knowledge: Mechanical Engineering, Civil Engineering, Materials and Mineralogy, Geosciences, Environment, Information and Decision Systems, Processes and Energy, Electrical and Automation, Mechatronics, Biotechnology and other Engineering related areas.

Publication Information:
ITEGAM-JETIA (ISSN 2447-0228), (online) is published by Galileo Institute of Technology and Education of the Amazon on a every two months (February, April, June, August, October and December).

Contact information:

Web page: www.itegam-jetia.org
Email: editor@itegam-jetia.org
Galileo Institute of Technology and Education of the Amazon (ITEGAM).

Joaquim Nabuco Avenue, No. 1950. Center. Manaus, Amazonas. Brazil.
Zip Code: 69020-031. Phone: (92) 3584-6145.

ITEGAM - JETIA ISSN 2447-0228 Online
Journal of Engineering and Technology for Industrial Applications (JETIA)

INSTITUTO DE TECNOLOGIA ITEGAM®

ITEGAM-JETIA. v.10, n.50. December of 2024. Manaus - Amazonas, Brazil. ISSN 2447-0228 (ONLINE)
https://www.itegam-jetia.org

SUMMARY

MECHANICAL PROPERTIES CHARACTERIZATION OF WELDED 3CR12 STAINLESS STEEL
Thabo Nelson Mathonsi **6**

A NEW PID TYPE CONTROLLER BASED ON MODIFIED CRISP LOGIC
Abdeslam Benmakhlouf , Ghania Zidani and Djalal Djarah **15**

DETECTION OF SUBSTATION POLLUTION IN DISTRICT HEATING AND COOLING SYSTEMS: A COMPREHENSIVE COMPARATIVE ANALYSIS OF MACHINE LEARNING AND ARTIFICIAL NEURAL NETWORK MODELS
Emrah Aslanand and Yıldırım Özüpak **22**

TECHNO-ECONOMIC EVALUATION OF RICE HUSK CO-FIRING AS A SUSTAINABLE BIOMASS FUEL ALTERNATIVE
Samsurizal, Revi Falka Azlinando and Arif NurAfandi **33**

EVALUATING PRODUCTIVITY AND COSTS OF CONCRETE CASTING FOR STRUCTURAL ELEMENTS
Fendi Hary Yanto **39**

DTC OF A 5LEVEL MMC FED3-Φ INDUCTION MOTORWITH PI AND FLC USING CBAPOD PWM TECHNIQUE
Sriramulu Naik Mudhavath, Kesana Gopikrishna and Venkat Anjani Kumar G **45**

ASSESSMENT OF THE ADEQUACY OF ELECTRICAL ENERGY DEMAND FORECAST MODEL FOR THE NIGERIA POWER DISTRIBUTION SYSTEM VIA STATIONARITY TEST
O.O Ade-Ikuesan, I.A Adejumobi, I.O Adebisi and G.A Dawodu **51**

THE IMPACT STUDY OF FLEXIBLE ALTERNATING CURRENTTRANSMISSION SYSTEM ON TRANSIENT STABILITY OF POWERSYSTEMS USING MATLAB CODE AND POWER WORLDSIMULATOR
Abdelhafid Hellal, Aissa Souli, Redha Djamel Mohammedi and Mohamed Elbar **59**

CAUSES, EFFECTS, AND PRACTICAL METHODS OF HARMONIC REDUCTION IN IRANIAN CEMENT FACTORIES WITH A FOCUS ON PLANT DEVELOPMENT
Mehdi Eslamian Koupaie **66**

USING BUSINESS ANALYSIS TO ENHANCE SUSTAINABILITY AND ENVIRONMENTAL COMPLIANCE IN OIL AND GAS: A STRATEGIC FRAMEWORK FOR REDUCING CARBON FOOTPRIN
Alliy Adewale Bello, Fredrick Fiyeboju Magi, Ogochukwu Gold Abaneme, Uzochi Achumba, Adebowale Martins Obalalu and Mobolaji Fakeyede **81**

MULTI CRITERIA MODEL OF SUPPLY CHAIN SUSTAINABILITY EVALUATION &DEVELOPMENT STRATEGY FOR AGRITECH START-UP
Thabed Tholib Baladraf, Nita Kuswardhani, Winda Amilia, Mohammad Rondhi and Yuli Wibowo **91**

PROCUREMENT AND LOGISTIC PROCESSES
Neyfe Sablón-Cossío, Giselle Rodríguez-Rudi, Roberto Wilman Rosales Bonilla, Jessica Elizabeth Medina Arias, Ana Julia Acevedo-Urquiaga and Rogelio Suárez Mella **101**

MACHINING PARAMETERS OPTIMIZATION IN WET TURNING OF EN31 MATERIAL USING BOX-BEHNKEN APPROACH OF RSM
Shivaji Bhivsane, Arvind Chel and Siraj Sayyed **108**

ITEGAM - JETIA ISSN 2447-0228 Online
Journal of Engineering and Technology for Industrial Applications (JETIA)
INSTITUTO DE TECNOLOGIA ITEGAM®

A RADIO FREQUENCY SYSTEM FOR SMART ATTENDANCE IN SCHOOLS 117
Akeem Abimbola Raji, Joseph Folorunso Orimolade and Oluwaseun Ibrahim Adebisi

MICROSTRUCTURAL INVESTIGATIONS ON THE FRACTURAL BEHAVIOR OF SS304 BUTT JOINTS DEVELOPED THROUGH VIBRATORY WELDING 125
K. Ch Sekhar, Dr Rashmi Dwivedi and Dr. V. V. Rama Reddy

EFR-NET: ENHANCED FRACTURE PREDICTION IN OSTEOPOROSIS WITH U-NET-BASED ANALYSIS 133
Vidhya K, T.M. Thiyagu, Edward Naveen V and Jenefa A

SMART INTERSECTION AND IOT: PRIORITY DRIVEN APPROACH TO UBRAN MOBILITY 143
Okubanjo, Ayodeji A, Odufuwa Bashir, Akinloye Benjamin and Okakwu Ignatius

A REVIEW OF POLOXAMER 407 INDUCES HYPERLIPIDEMIA IN VIVO STUDIES 149
Neti Eka Jayanti and Rozzana Mohd Said

IMPACT OF NITROGEN INCORPORATION ON BAND GAP BOWING IN ZINC-BLENDE GAAS$_{1-x}$N$_x$: A FIRST-PRINCIPLES STUDY 154
Mimouna Oukli, Ghlam Karima and Seyfeddine Bechekir

USING MACHINE LEARNING TO EVALUATE INDUSTRY 4.0 MATURITY: A COMPREHENSIVE ANALYSIS HIGHLIGHTING LEAN'S IMPACT ON DIGITAL TRANSFORMATION 161
Oussama Ben Ali, Sondes Hammami, Marwa Hasni, Fehmi H'Mida and Ahmed Nait Sidi Moh

ENHANCED ESTIMATION OF TORQUE BASED ON COGNITIVE TRAINING MODEL FOR ROBUST PMSM IN EV APPLICATIONS 173
G. Sudeep1, J. N. and Chandra Sekhar

HYBRID UM-LT-AHE TECHNIQUE FOR CONTRAST ENHANCEMENT OF MEDICAL IMAGES 180
Kamoli A. Amusa, Olumayowa A. Idowu and Abolaji O. Ilori

ESTIMATION OF THE TIME OF OCCURRENCE OF THE MAXIMUM ELECTRICAL DEMAND BY SELECTING THE OPTIMAL CLASSIFICATION MODEL AND MAKING USE OF UNBALANCED DATA 189
César A. Yajure Ramírez and Valesca M. Fuenzalida Sánchez

AN OVERVIEW OF IMPROVING LOGISTICS PROCESSES IN HEALTH FACILITIES: ISSUES, SOLUTIONS, AND CHALLENGES 196
Zdenek Smutny and Katerina Svandova

IMPLEMENTATION OF IOT IN IMPROVING THE EFFICIENCY OF HOSTAGE RELEASE OPERATIONS WITH THE QHBM METHOD 202
Dekki Widiatmoko, Kasiyanto, and Mokhammad Syafaatl

ENHANCING OPTICAL DISTRIBUTION POINT PLACEMENT: A DECISION SUPPORT SYSTEM INTEGRATING WEIGHTED PRODUCT METHOD, CONTENT-BASED FILTERING, AND LOCATION-BASED SERVICES 211
Viktor Handrianus Pranatawijaya, Widiatry Widiatry and Dea Jeany Lestari

OPTIMIZING PORTER ASSIGNMENTS IN HOSPITAL: A MATHEMATICAL MODELING APPROACH FOR WORKLOAD BALANCING 219
Chawis Boonmee and Phavika Mongkolkittaveepol

NEURAL NETWORK EDDY CURRENT NON-DESTRUCTIVE EVALUATION OF CONDUCTIVE COATINGS THICKNESS 228
Islam Nacer Eddine El Ghoul, A.E. Lakhdari, S. Bensaid, A. Aissaoui, A.T. Ouamane

ITEGAM - JETIA ISSN 2447-0228 Online
Journal of Engineering and Technology for Industrial Applications (JETIA)

VAULTGUARD: THE ADVANCED KEYLESS SECURITY SYSTEM **235**
Dr. Yogita Mane , Dr. Neeta Patil, Akshay Agrawal, Sanketi Raut, Vishal Shinde

EVALUATION OF WI-FI MESH NETWORKS FOR READING ELECTRICITY CONSUMPTION **243**
Carlos Bazán Prieto and Alberto Bazán Guillén

Journal of Engineering and Technology for Industrial Applications

ITEGAM-JETIA

ISSN ONLINE: 2447-0228

Manaus, v10. n.50, p. 06-14. November./ December., 2024.
DOI: https://doi.org/10.5935/jetia.v10i50.1144

RESEARCH ARTICLE OPEN ACCESS

MECHANICAL PROPERTIES CHARACTERIZATION OF WELDED 3CR12 STAINLESS STEEL

Thabo Nelson Mathonsi

University of Johannesburg, Faculty of Engineering, Johannesburg, South Africa

https://orcid.org/0000-0003-4801-6856

Email: tmathonsi@uj.ac.za

ARTICLE INFO

Article History
Received: June 5, 2023
Revised: July 1, 2023
Accepted: August 10, 2024
Published: November 30, 2024

Keywords:
3CR12 Stainless Steel,
Welding,
Mechanical Properties
Microstructure,
Heat-affect-zone (HAZ)

ABSTRACT

The use of metal inert gas (MIG) welding for joining metals frequently results in the change of the mechanical properties and the microstructure of the metal at the welded areas. This is due to the welding heat input and heat transfer. 3CR12 is a low-cost special stainless steel containing 12% chromium. It is considered to have good mechanical properties and corrosion resistance as a base metal, and understanding how these properties change as a result of MIG welding enables the drawing of proper conclusions regarding the properties of MIG welded 3CR12 stainless steel. However, little is known about its properties and behavior after welding with metal inert gas (MIG) welding, which is the most common welding process for welding stainless steel, and little is known about its weldability. Due to inadequate information about MIG welded 3CR12 stainless steel, it is hard to make a reliable statement about its properties and behavior. Thus, necessitating the need to gain knowledge regarding MIG welded 3CR12 stainless steel. This paper aims to characterize the mechanical properties of welded 3CR12 stainless steel. The focus is on investigating how the mechanical properties and the microstructure of 3CR12 stainless steel evolve due to MIG welding.

I. INTRODUCTION

It must define the problem and importance of the research carried out, it presents a (not very extensive) review of the literature on the subject of the article, including the authors' contributions to the state of the art. If you use abbreviations or acronyms, first write the words that identify them and then, in parentheses, the acronym. This set also establishes the research question, the objectives of the work and hypothesis, if necessary, the importance and limitations of the study. Establishes the method used at work. It is written in the present tense. Industrial equipment and pipes can be made from a variety of metallic materials. However, carbon steel still has the greatest applicability in the construction of the majority of equipment [1]. Although carbon steels can be utilized in a wide range of applications, they do have some technical limits, particularly in low-temperature and corrosive conditions. This is why they are regarded as general-purpose materials. While carbon steels lack some characteristics, alloy and stainless steels do, but in comparison to carbon steel, they have substantially greater production costs as well as expenditures associated with welding and assembly for industrial installations [2]. Despite their lower cost, carbon steels are not resistant to corrosion or erosion condition which generates undesirable contaminant residues. For this reason, carbon steel cannot be used directly in situations where it can contaminate the final product. In these situations, carbon steel is coated with more durable metallic or non-metallic compounds or other alloys to provide protection at a lower cost. Stainless steels are an example of this that are easily weldable [3]. Austenitic stainless steels are used specifically for building and protecting equipment and pipelines made of carbon steel from corrosion. With the exception of some ferritic steels with a chromium content of up to 17%, which have acceptable weldability and an expansion coefficient that is comparable to that of carbon steel, it is not advised to use many types of stainless steel, such as ferritic and martensitic, as structural steel or welded steel [4].

Middleburg Steel and Alloy (Pty) Ltd (later known as Columbus Stainless Steel) developed 3CR12 from AISI 409 stainless steel in 1970 [5]. 3CR12 is a low carbon utility ferritic stainless steel that complies with ASTM A240 and EN 1008-2 requirements. The single ferrite phase that exists in AISI 409 at high temperatures causes substantial grain growth in the material, which is bad for toughness, ductility, and the ductile to brittle transition temperature (DBTT) [6], [7]. This prompted the creation of 3CR12, a corrosion-resistant steel that would successfully replace coated carbon steel in typical corrosive situations and be reasonably inexpensive compared to other stainless steels like austenitic stainless steel [8].

To create dual phase structure (ferrite and austenite) at high temperatures, where one phase inhibits the formation of the other's grain, 3CR12 was produced by carefully balancing ferrite and austenite stabilizers [9]. Subsequently it has been found that 3CR12 has a grain structure that is considerably finer than that of AISI 409, which improves its weldability and mechanical qualities [7]. So far, it's important to note that 3CR12 also experiences grain growth. The manufacturer asserts that 3CR12 maintains its toughness to this extent when welded to thicknesses of up to 30 mm without post welding heat treatment (PWHT) [10].

There are two variants of 3CR12 i.e., un-stabilized (3CR12L) and titanium (Ti) stabilized grade (3CR12Ti) with their chemical compositions presented in Table 1.

Table: Composition of unsterilized (3CR12Ti) and titanium stabilized (3CR12L).

Grade	3CR12Ti	3Cr12L
C	0.03	0.03
Si	1	1
Mn	2	1.2
P	0.04	0.04
S	0.03	0.015
N	-	0.03
Cr	10.5-12.5	0.3-1
Ni	1.5	-
Other	Ti:4(C+N)0.6	-

Source: [10].

3CR12 is an intriguing and less expensive option to austenitic stainless steels (304, 316L) is 3CR12 [11]. Currently, some companies in South Africa i.e., Transnet Freight Rail, and Anglo Gold use 3CR12 in mine train wagons, due to its excellent corrosion resistance [12]. Nevertheless, little information specifically dedicated to the understanding mechanical properties behavior when welding 3CR12 stainless steel is available in the literature whereas austenitic grades are much more covered [13], [14], [15], [16] The most common research outputs in relation to stainless steel 3CR12 is based on determining the optimum welding material [17], [18].

This paper aims to characterize the mechanical properties of welded 3CR12 stainless steel. The focus is on investigating how the mechanical properties and the microstructure of 3CR12 stainless steel evolve due to MIG welding.

II. EXPERIMETAL PROGRAM

II.1 MATERIAL

The base material used was 3CR12 stainless steel supplied by Macsteel as 100 ×100 × 3 mm off-cut plate (see Figure 1) Table 2-1 shows mechanical properties of the base metal (obtained from the manufacturer's catalogue). Several researchers [18], [19] found that 308L welding material is the most suitable material for welding 3CR12 stainless steel. Chemical composition of the 308L weld wire was obtained from the manufacturer's catalogue [20].

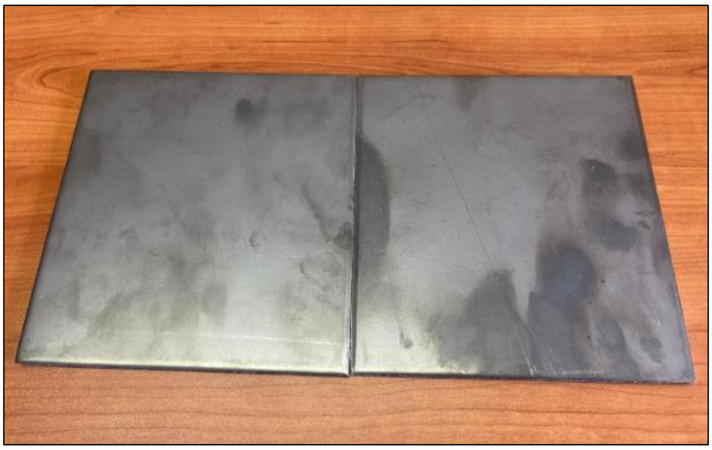

Figure 1: 3CR12 stainless steel.
Source: Author, (2024).

Table **Error! No text of specified style in document.**: Mechanical properties of 3CR12 stainless steel material.

Material	Tensile Strength (MPa)	Yield Strength (MPa)	%Elongation	Hardness (H)
3CR12	460	300-450	18	173

Source: [10].

III. WELDING PROCEDURE

Welding was conducted at Roan Engineering (Pty LTD) in Johannesburg, South Africa. The welding process was carried out using a six-axis MOTOMAN AR1440 arc welding robot (see Figure 2) with rated output current and voltage of 30-350A and 12-36V respectively.

Figure **Error! No text of specified style in document.**: Yaskawa robotic welder.
Source: [21].

The welder was configured to reverse polarity with welding grade argon shielding gas at 15 l/min flow rate. Welding was carried out (in accordance with the manufacturer's recommendation) as shown in Table 3.

Table 1: Welding procedure.

Welding Process	**MIG**
Filler Metal	308L (1.6 mm)
Tip to work distance	15 mm
Wire Feed Tare	6 m/min

Source: Author, (2024).

Source: Author, (2024).

III.1 WELDING PARAMETERS

According to [18], [19], [22] the optimum heat input (HI) input range for welding 3CR12 stainless steel is between 0.5 – 1.5 kJ/mm. To fully understand the mechanical behavior of 3CR12 stainless steel when welded, a variety of HI values (within and outside the optimum range) were selected. Since heat input is a function of the welding voltage, current, and speed. Based on the range of voltage, current, and welding speed used in welding 3CR12 stainless steel from the literature, the values resulting in the required HI values were selected. The mechanical properties were investigated at the parameters and the resulting heat input, as shown in Table 4.

Table 2: Welding parameters and resulting heat inputs.

Sample No.	Voltage (V)	Current (A)	Welding Speed (mm/s)	Heat Input (kJ/mm)
1	180	11.5	4.5	0.35
2	190	12.5	4.0	0.45
3	230	17.0	3.0	1
4	260	21.0	2.5	1.64
5	270	22.0	2.5	1.75

Source: Author, (2024).

IV. SAMPLE PREPARATION

IV.1 MATERIAL MICROSTRUCTURE AND MICROHARDNESS

Specimens for microstructure and microhardness examination were prepared through the following processes. Firstly, the samples were prepared by cutting 25 ×50 mm cross sections from the welded plates, then the specimens were mounted using a hot mounting press machine and polyfast mounting powder. Grinding and polishing was then carried out on the Struers Labopol 5. This was done in order to maintain an even and clean surface for usage on microscope and micro-hardness tester.

The specimens were then etched using Carpenters reagent [23]. During the etching process, grain boundaries were preferentially attacked, which resulted in a surface characterized by two-dimensional structure that is distinctive when viewed on the microscope. The samples were dipped into the reagent for 10-20 seconds. After the etching process, the samples were then taken to the microscope for observations.

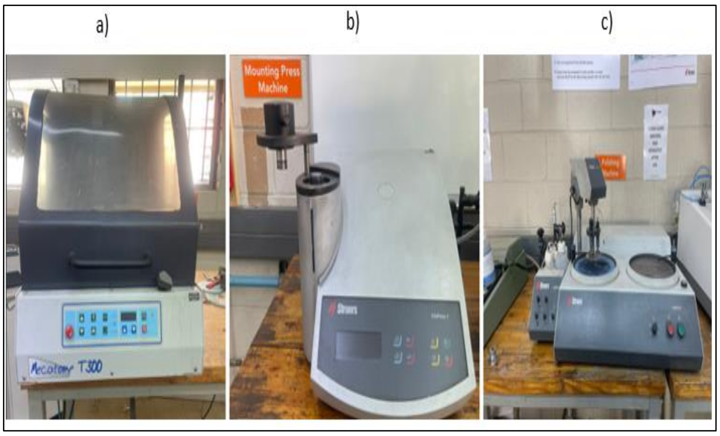

Figure 1: Sample preparation apparatus a) Mecatome T300 cutting machining, b) Hot mounting press machine, and c) Struers Labopol 5 polishing machining.

IV.2 TENSILE TEST

Specimens for tensile testing were machined to size using a Pinnacle PK-GRSM-V milling machine (see Figure 4). The machine specifications are outline in Table 5.

Figure 2: Pinnacle PK-GRSM-V milling machine.
Source: Author, (2024).

Table 3: Pinnacle PK-GRSM-V milling machine specifications.

Model	PK-GRSM-V
Table size	1270 x 254 mm
Max. Table Load (kgs)	300 kgs
T-Slot (width x number x distance)	16 x 3 x 63.5
Rapid feed rate	890 mm/min

Source: Author, (2024).

For each HI, three samples were prepared and tested. The tests were carried out in accordance with ASTM E8M-04's specifications as can be seen in Figure 5.

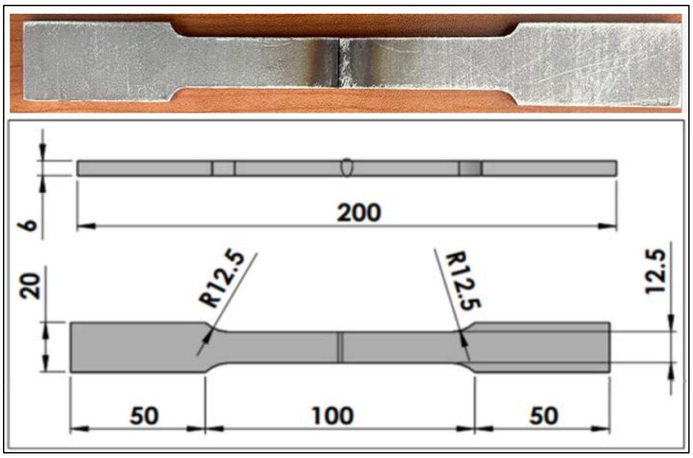

Figure 3: Tensile test specimen (a); dimensions of specimen according to ASTM E8M-04 (b) (units in mm).
Source: Author, (2024).

V. MEASUREMENT OF OUTPUT PARAMETERS

V.1 MICORSTRUCTURE MEASUREMENT

Metallographic analysis was conducted using Olympus-BX51M optical microscope, shown in Figure 6. The microscope has a magnification range of 5x to 100x.

Figure 4: BX51M Olympus optical microscope
Source: Author, (2024).

The system metallurgical microscope has X/Y high speed traveling stage that can position the sample very quickly. The microscope can achieve a resolution of about 100 µm, some of the BX51M Olympus optical microscope's specifications are shown in Table 6.

Table 4: BX51M Olympus optical microscope specifications.

Model	Application	Specifications	
BX51M	Microstructure Chip morphology, and Chip measurements	Resolution	0.37-3.36 µm
		Manual Zooming	5X – 10X
		Working stage	X/Y direction

Source: Author, (2024).

V.2 MICROHARDNESS MEASUREMENT

Figure 7 shows the Vickers microhardness tester that was used to evaluate the microhardness of the specimens. Depending on the indenter put on the indenter head, this machine can measure both Vickers and Knoop hardness. Eye observation is used to measure the indentation length.

Figure 5: TIME HM-6 digital microhardness tester.
Source: Author, (2024).

The specifications of the Vickers microhardness testing machine are presented in Table 7. This device features a built-in objective lens with two different magnification settings, 10X and 40X.

Table 5: Micro hardness tester specification.

Model	Application	Specifications	
MH-6	Microhardness	Range	10 - 1000 gf
		Objective	10X and 40X
		Loading rate	60 µm/sec

Source: [24].

The Vickers method is based on an optical measurement system. To create an indentation that can be measured and translated into hardness values, a diamond indenter is used in the microhardness test process described in ASTM C1327-15 [25]. A variety of materials can be processed using this technique. The Vickers scale uses a diamond with a square base and a pyramidal shape (see Figure 8). The load is typically applied for 15 to 30 seconds and ranges from 1 kgf to 120 kgf. Equation 2.1 [26] is used to compute the Vickers number (HV):

$$HV = 1.854 \times \frac{F}{D^2} \quad (2.1)$$

Where:

F = Applied load, kgf
D = Length of the impression diagonal, mm

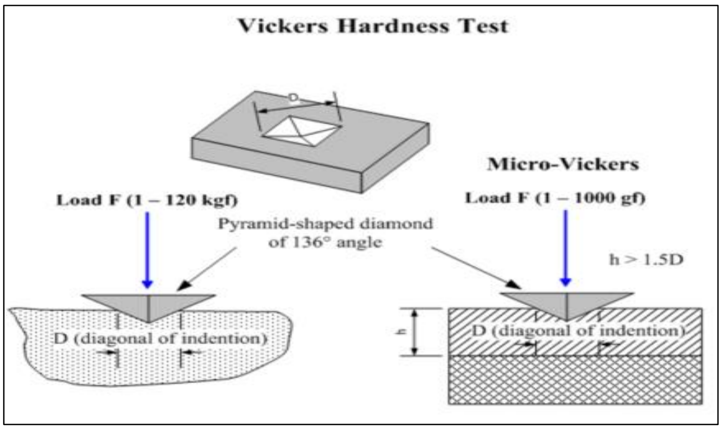

Figure 6: Vickers hardness tester indenter structure.
Source: [24].

A microscope, which is frequently a standard component of the Vickers Tester, is used to measure the length of the impression diagonal. ASTM E-384-99 was followed in conducting the test [27]. The hardness line and track indentation are displayed in Figure 9.

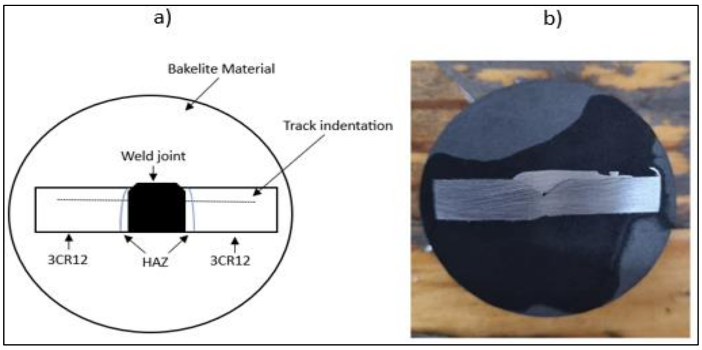

Figure 7: Microhardness test specimens' indentation locations (a) for MIG welded samples (b) after hot mounting.
Source: Author, (2024).

V.3. TENSILE TESTING

The Instron 9400 tensile testing machine (see Figure 10) was used to conducted tensile testing measurements. This machine is built around an electric motor with variable speed, a gear reduction system, and screws that raise or lower the crosshead. This movement applies tension or compression to the specimen. The motor's speed can be altered to alter crosshead speeds.

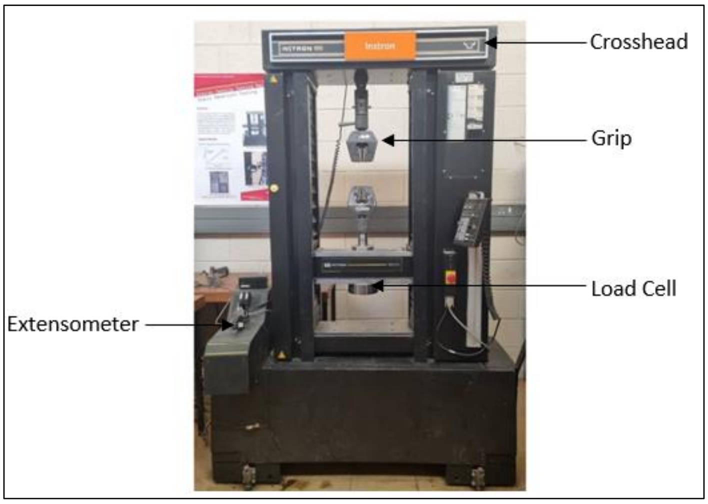

Figure 8: Instron 9400 tensile testing machine.
Source: Author, (2024).

To successfully test the specimen, the following steps were taken:

1. Put gage marks on the specimen.
2. Measure the initial gage length, width, and thickness.
3. Place the specimen between upper and lower jaw faces.
4. Perform the tensile test.
5. Get the $F - x$ and/or $\sigma - \varepsilon$ data.
6. Measure the final gage length and width.

VI. RESULTS AND DISCUSSIONS

Figure 11 shows a microstructure of a sample that was welded with a HI of 0.35 kJ/mm. The microstructure of the base metal contained ferrite grains with small islands of martensite. Since the 3CR12 stainless steel is Titanium stabilized, the titanium precipitate stabilizers could also be observed in the microstructure of the base metal. The heat-affected zone (HAZ) is characterized by larger coarse grains compared to the base metal, mainly due to the heat applied during the welding process. The grains observed in the microstructure of the HAZ are ferrite grains and small islands of martensite. The ferritic grains observed are dominant in the HAZ, and there is less martensite. Considerable grain growth is observed at the HAZ closer to the weld zone, and the grain size decreases when observed further away from the weld zone.

The microstructure observed in the weld zone mainly consists of fine grains of austenite and small portions of ferrite. The observed austenitic microstructure is due to the filler metal used in the welding process, which is 308L, an austenitic stainless steel grade, and the different phases present in the weld zone are due to welding a ferritic steel base metal using an austenitic grade filler metal.

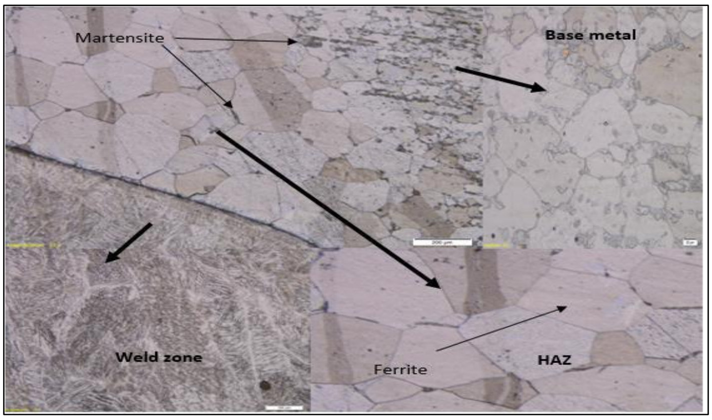

Figure 19: Sample welded at a heat input of 0.35 kJ/mm.
Source: Author, (2024).

Figure 12 shows a microstructure of a sample that was welded with a HI of 0.35 kJ/mm. The microstructure of the base metal contained ferrite grains with small islands of martensite, like the first sample. This is attributed to the fact that the increase in HI is insignificant (0.05kJ/mm) hence the similarities.

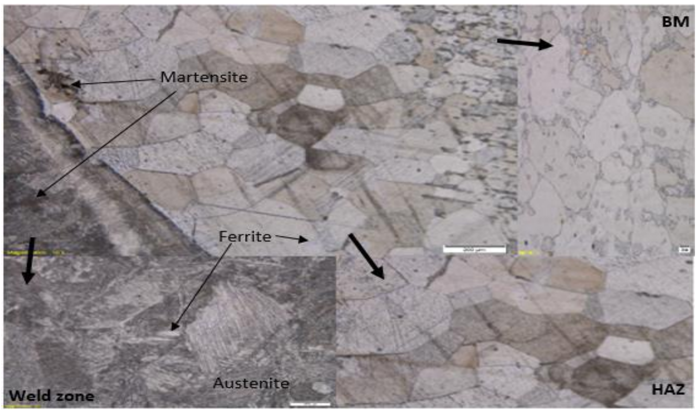

Figure 110: Sample welded at a heat input of 0.45 kJ/mm.
Source: Author, (2024).

Figure 13 shows a microstructure of the weldment using a HI of 1.0kJ/mm. the microstructure exhibited an acicular ferrite and lathe martensite. The lath martensite was widely dispersed. The presence of martensite was observed to be higher toward the center of the weld. This is mainly due to the high heat application and the higher rate of cooling at the center of the weld than in the zones toward the fusion zone.

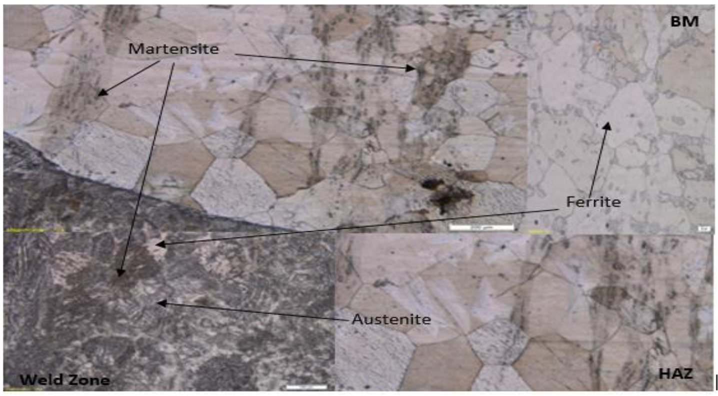

Figure 111: Sample welded at a heat input of 1.0 kJ/mm.
Source: Author, (2024).

Figure 14, and 15 shows the microstructures of the weldment using a HI of 1.65, and 1.75kJ/mm respectively. Both these HI are then the optimal recommended range of welding 3CR12. The microstructure also exhibited a lath martensite with a higher amount of martensite with a higher amount of martensite.

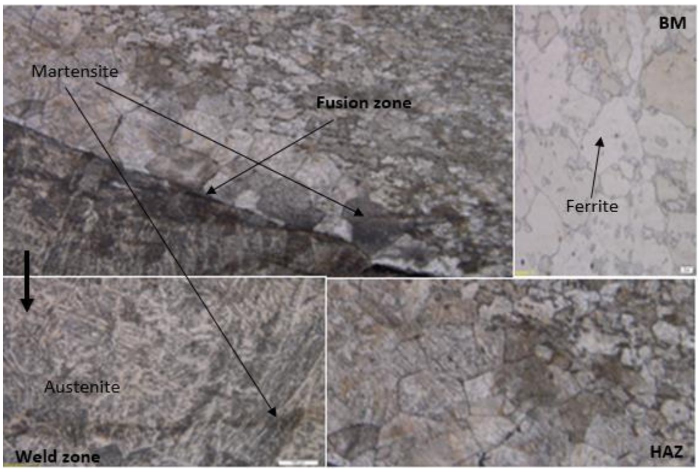

Figure 112: Sample welded at a heat input of 1.65 kJ/mm.
Source: Author, (2024).

Excessive grain deformation can be observed in the HAZ of sample 4. The HAZ is characterized by larger coarse grains similar to the other samples discussed. However, the grain boundaries of the observed grains are not as defined as those of sample 1 to sample 3. Martensite laths can be observed in the HAZ microstructure. The martensite presence observed is significantly more than in the first three samples due to the excessive heat input used to weld the sample. Considerable grain growth is observed at the HAZ closer to the weld zone, and the grain size decreases when observed further away from the weld zone.

The microstructure observed in the weld zone consists of fine grains of austenite and ferrite with martensite laths. The ferrite content in the weld zone is significantly less than in the first three samples. The martensite laths observed are at different orientations across the microstructure of the weld zone, and the presence of the martensite laths is more than in the first three samples as the heat input is also significantly higher than in the first three samples.

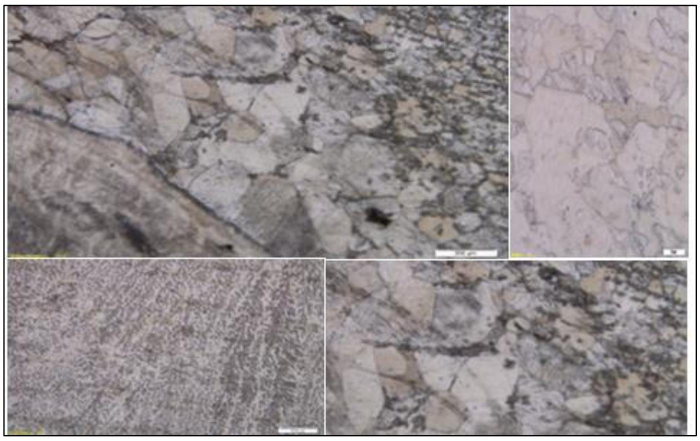

Figure 113: Sample welded at a heat input of 1.75 kJ/mm.
Source: Author, (2024).

Excessive grain deformation can be observed in the HAZ of sample 5, similar to the microstructure observed in sample 4. However, the grain deformation is more in sample 5 than in sample 4. The HAZ is characterized by larger coarse grains similar to all the samples discussed. However, the grain boundaries of the observed grains are not as defined as those of sample 1 to sample 3 and are defined similarly to those observed in sample 4. Martensite can be observed in the HAZ microstructure. The martensite presence observed is significantly more than all the other samples due to the excessive heat input welding the sample, which is 1.75kJ/mm. Considerable grain growth is observed at the HAZ closer to the weld zone, and the grain size decreases when observed further away from the weld zone. The microstructure observed in the weld zone consists of fine grains of austenite and ferrite with martensite laths. The ferrite content in the weld zone is significantly less than all the other samples. The martensite laths observed are at different orientations across the weld microstructure.

VI.1 MICROSTRUCTURE SUMMARY

The base metal's microstructure, 3CR12 stainless steel, was observed to have a dual phase of ferrite and martensite. This is consistent with the microstructure observed by Akinlabi and Akinlabi when characterizing the effect of heat treatment on 3CR12 stainless steel [28]. The ferrite grains were observed to be the white phase, whereas the martensite phase was the dark phase. This dual-phase presence in the base metal of 3CR12 stainless steel elucidates the fluctuations observed in the microhardness profile in the base metal. The higher values were due to the indentation occurring where martensite was present, and the lower values were due to the indentation occurring on the ferrite grains.

The microstructure in the weld zone of the welded sample was observed to have three phases: austenite, ferrite, and martensite. This mixture of phases is due to welding 3CR12 stainless steel, a ferritic steel base metal using an austenitic grade filler metal of 308L. The 308L was recommended to be the optimum filler material for welding 3CR12 stainless steel from the work of Molabe [29], and the observed microstructure is consistent with that observed from the same work. And hence the austenitic microstructure is due to the use of the 308L filler material grade. Martensite laths could be observed at different orientations in all the welded specimens, and higher heat inputs yielded more martensite presence. This elucidates the hardness values recorded in the weld zone, which were more than those observed in the HAZ and the base metal. An increase in the hardness values in the weld zone was influenced by the increase in the heat input and, thus, the presence of martensite.

VI.2 GRAIN SIZE CHARACTERIZATION

A solid metal's grain is made up of a variety of small crystals that are dispersed at random. Most mechanical qualities, such as hardness, yield strength, tensile strength, and impact strength, can be measured in relation to grain size. All these mechanical properties aforementioned increase with a decrease in grain size. Quantifying and characterizing the observed grain deformation that has happened in the changing microstructures of the welded material. The size of each grain in the microstructures was measured using the measuring instrument on the optical microscope.

During the microstructural analysis of the samples welded at various heat inputs, an alteration in the size of the grains in the heat-affected zone was observed. The areas of the 3CR12 stainless steel susceptible to heat application during the welding process showed a significant increase in grain size. The grain size affects the properties of a material, such as hardness. The grains that could be correctly observed in the different samples were measured using the optical microscope and presented in Figures 16 to 20.

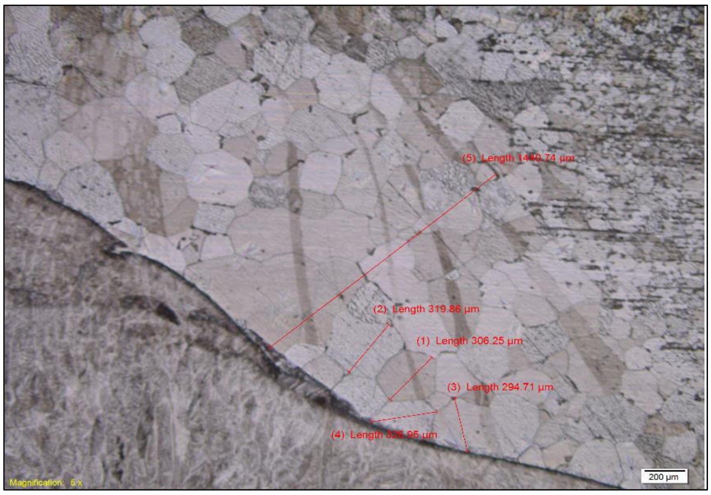

Figure 114: Sample welded at a heat input of 0.35 kJ/mm.
Source: Author, (2024).

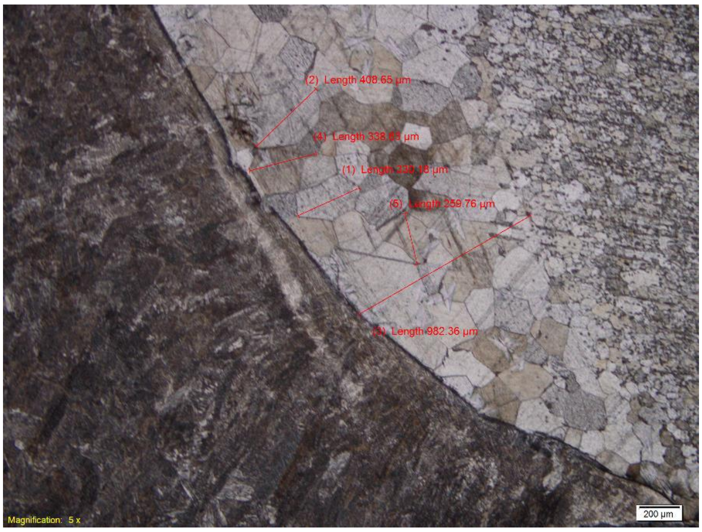

Figure 115: Sample welded at a heat input of 0.45 kJ/mm.
Source: Author, (2024).

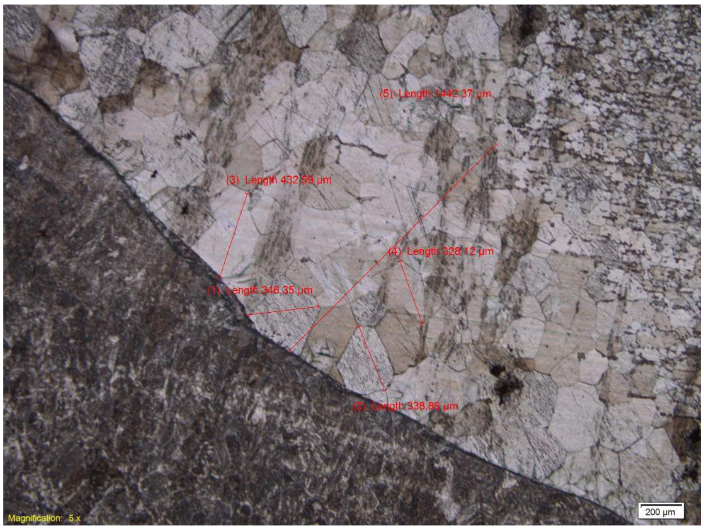

Figure 116: Sample welded at a heat input of 1.0 kJ/mm.
Source: Author, (2024).

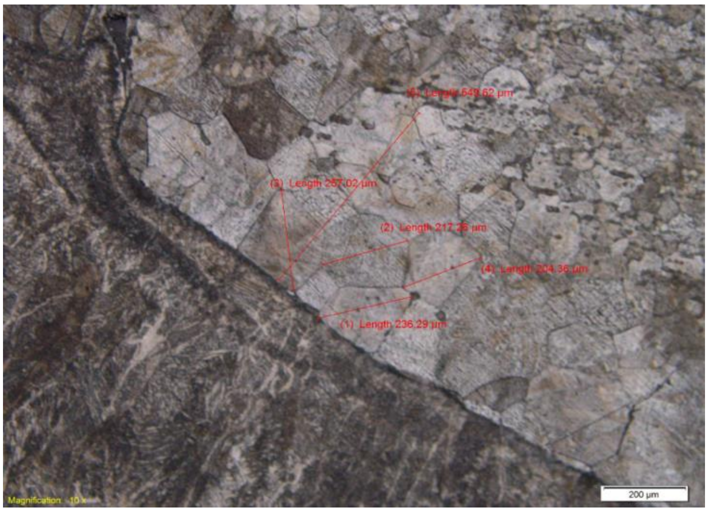

Figure 117: Sample welded at a heat input of 1.65 kJ/mm.
Source: Author, (2024).

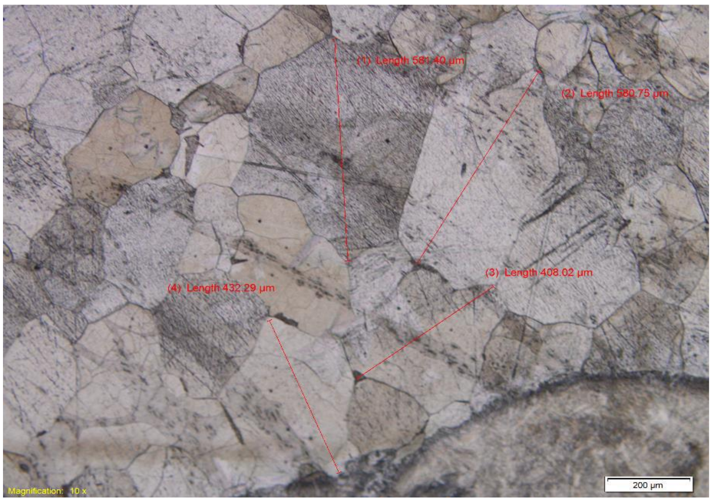

Figure 20: Sample welded at a heat input of 1.75 kJ/mm.
Source: Author, (2024).

VI.2.1 GRAIN SIZE CHARACTERIZATION SUMMARY

The grain sizes are summarized in Table 8, where the measurements of 4 grains per sample and an average value are determined.

Table 8: Summary of the grain sizes for each sample.

Measurement	**Grain size (µm)**				
	0.35kJ/mm	**0.45kJ/mm**	**1.0kJ/mm**	**1.65kJ/mm**	**1.75kJ/mm**
1	326.95	408.65	432.59	236.29	290.7
2	319.86	338.63	346.35	204.36	290.38
3	306.25	330.13	328.12	257.02	216.15
4	294.71	253.76	338.86	217.26	204.01
Average	311.9	332.79	361.48	228.73	250.31

Source: Author, (2024).

An interesting observation was seen that an increase in the HI resulted in an increase in the grain size, only up to a certain extent. (HI, 0.35-1.0kJ/mm). Future increase resulted in a reduction in grain size. The microstructure of the HAZ for all the welded samples is characterized by enlarged and coarse grains in all the welded samples due to the application of heat during welding. Similar results were observed [28], [30]. The increase in the grain size implies that fewer grain boundaries are present in the HAZ of the weld, and according to Vithi et al. [31] the presence of fewer grains in the microstructure makes the HAZ susceptible to dislocation movement. Dislocation movement results in a decrease in strength and thus makes the HAZ defenseless against fracture. An increase in the grain size resulted from the increase in the heat input. This also increased the volume of martensite precipitate present in the HAZ. The microstructure of the HAZ is characterized by the dual phases consisting of ferrite and martensite as with the base metal. This also elucidates the fluctuations observed in the microstructure of the HAZ is characterized by the dual phases consisting of ferrite and martensite as with the base metal. This also elucidates the fluctuations observed in the microhardness profile of the hardness in HAZ for all the welded samples. The higher values were due to the indentation occurring where martensite was present, and the lower values were due to the indentation occurring on the ferrite grains as with the base metal. An increase in grain size reduces the ductility and, thus, the material's toughness. However, according to Molabe [29], the grain growth was determined to have little to no effect on the tensile strength of 3CR12 stainless steel. This was due to the fracture during tensile testing occurring at the base metal instead of the HAZ. This is also consistent with the results obtained by Vithi et al. [31], where the fracture during tensile testing occurred in the base metal.

VI.3 MICROHARDNESS

The Vickers microhardness of the different samples was measured from the center of the weld to the base metal, and the profile obtained from the microhardness values for the different samples is shown in Figure 21. The different welded samples have the same base material, 3CR12 stainless steel. A fluctuation in the hardness profile can be observed in the base metal. This is mainly due to the alternating phases of ferrite and martensite found in the microstructure of the base metal. The martensite portions produce higher hardness values, whereas the ferrite grains produce lower hardness values, resulting in fluctuating values. However, the average hardness value found at the base metal is 178HV. The hardness values observed at the fusion zone (FZ), or weld cap are higher than the hardness values of both the base metal and the HAZ, with the lowest hardness observed at the HAZ. This phenomenon was observed for all the welded samples.

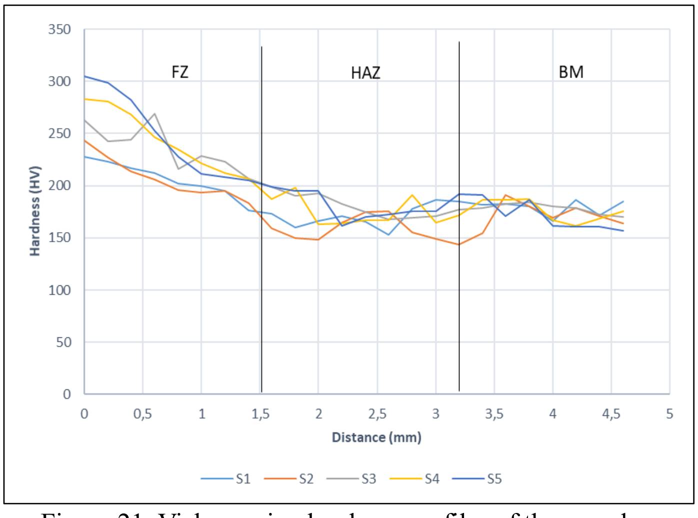

Figure 21: Vickers microhardness profiles of the samples.
Source: Author, (2024).

VI.4 TENSILE TESTING

According to the results of the tensile testing, all of the weldments have fractures in the weld zone (WZ) region (see Figure 22). This indicates that the WZ area, which has low tensile strength, is the weakest component of the joint. The site of the fracture was connected to the welding-induced decrease in the weld's hardness and strength. Precipitate coarsening in the over-aged zone was the main reason for the dramatic decrease in strength.

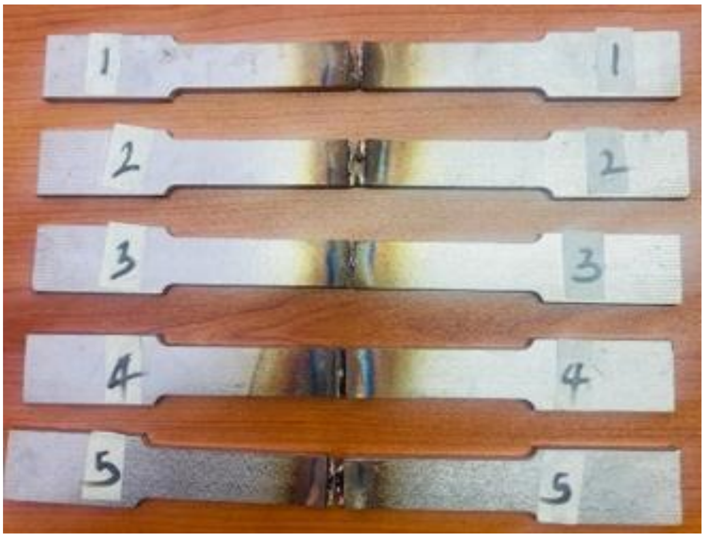

Figure 22: Fracture location of tensile testy samples
Source: Author, (2024).

Analyzing the results presented in Table 9, it can be argued that by changing the HI, it is possible to ensure the required strength of the welded joint. Controlled heat input welding procedures within the acceptable standard [18], [19], [22] ensures excellent strength of the welded joints.

The tensile tests of the welded specimens revealed a striking decrease in tensile strength when compared to values of the base material. About 45% of the base metal strength was the tensile strength of the weld joint.

Table 9: Summary of tensile test results.

HI (kJ/mm)	Load (N)	Average Load (N)
0.35	17349.85	16166.56
	15561.68	
	15588.16	
0.45	13355.09	17174.48
	21342.77	
	16825.57	
1.0	17989.06	20865.95
	21023.35	
	23585.45	
1.65	16838.97	22362.94
	23593.52	
	26656.34	
1.75	27431.8	24705.47
	20799.42	
	25885.2	

Source: Author, (2024).

V. CONCLUSIONS

Investigations were made into the ferritic stainless steel 3CR12's microstructure and mechanical characteristics. The study led to the following crucial conclusions:

- The coarse ferrite grains in the base metal are changed to fine grains of ferrite with some grain boundary lath martensite as a result of characteristic rapid solidification.
- The hardness at the mid cross-section of the fusion zone was found to be higher than the base material. This is mainly due to the fine solidification structure as a result of fast solidification.

VI. AUTHOR'S CONTRIBUTION

Conceptualization: Thabo Nelson Mathonsi.
Methodology: Thabo Nelson Mathonsi
Investigation: Thabo Nelson Mathonsi
Discussion of results: Thabo Nelson Mathonsi
Writing – Original Draft: Thabo Nelson Mathonsi.
Writing – Review and Editing: Thabo Nelson Mathonsi
Approval of the final text: Thabo Nelson Mathonsi

VIII. REFERENCES

[1] V. Balasubramanian, A. Lakshminarayanan, R. Varahamoorthy and S. Babu, "Application of Response Surface Methodology to Prediction of Dilution in Plasma Transferred Arc Hardfacing of Stainless Steel on Carbon Steel," International Journal of Iron Steel Res, vol. 16, pp. 44-53, 2009.

[2] AWS, "Welding Handbook: Welding Processes," in American Welding Society, vol. 2, 1992, p. 955.

[3] S. Brandi, S. Lui and T. Junior, "Welding, Brazing and Soldering, Electroslag and Electrogas Welding. ASM Handbook," ASM International, vol. 15, pp. 124-38, 2008.

[4] M. Butt, M. Ahmad and M. Azha, "Characterization for GTAWAISI 316 to AISI 316 & SA 516 Grade 70 Steels with Welded & Prewelded Annealing Conditions," Journal of Quality Technology Management , vol. 8, no. 2, pp. 119-33, 2012.

[5] N. G. Jungbacke, "The Influence of Substitutional Elements on the Transformability of 3CR12 Steel," University of Cape Town, Cape Town, 1996.

[6] A. K. Lakshminarayanan and V. Balasubramanian, "Evaluation of Microstructure and Mechanical Properties of Laser Beam Welded AISI 409M Grade Ferritic Stainless Steel," International Journal of Iron and Steel Research, vol. 19, no. 1, pp. 72-77, 2012.

[7] R. D. Knutsen, "A Microstructural Examination of Duplex Ferrite-martensite Corrosion Resisting Steels," University of Cape Town, Cape Town, 1989.

[8] J. Tarboton, " Johannes Paulus Hoffman The Technical Father of 3CR12," South African Institute of Mining and Metallurgy, vol. 116, no. 8, pp. 6-7, 2016.

[9] M. Greef, "The Influence of Welding Parameters of the Senitisation behaviour of 3CR12," University of Pretoria, Pretoria, 2006.

[10] "Stainless Steel," Columbus Stainless Pty Ltd, [Online]. Available: https://www.columbus.co.za/. [Accessed 10 July 2023].

[11] B. Rossi, "Mechanical Properties, Residual Rtresses and Structural behavior of Thin-walled Stainless Steel Profiles. PhD Thesis," University of Liège, Liège, 2008.

[12] A. Kaymakci, D. M. Madyira and N. Nkwanyana, "The Effect of Metal Transfer Modes on Mechanical Properties of 3CR12 Stainless Steel," Trascations of the Canadian Society for Mechanial Engineering, vol. 44, no. 2, 2019.

[13] S. S. R. Singh, R. V. Praneeth, V. S. Sankalp, S. S. Sashank and R. Karthikeyan, "Welding, Mechanical Properties and Microstructure of Different Grades of Austenitic Stainless Steels: A Review," Materials Today: Proceedings, vol. 62, pp. 3675-3680, 2022.

[14] F. S. d. Luz, W. A. Pinheiro, S. N. Monteiro, V. S. Candido and A. C. R. d. Silva, "Mechanical Properties and Microstructural Characterization of A Novel 316L Austenitic Stainless Steel Coating on A516 Grade 70 Carbon Steel Weld," Journal of Materilas Research and Technology, vol. 9, no. 1, pp. 636-640, 2020.

[15] S. Wu, T. Xu, M. Song and K. Guan, "Mechanical Properties Characterization of Welded Joint of Austenitic Stainless Steel using Instrumented Indentation Technique," Materials at High Temperature, vol. 33, no. 3, 2016.

[16] R. Krawczyk, J. Słania, G. Golański and T. Pfeifer, "Mechanical Properties and Microstructure of Austenite - Ferrite Duplex Stainless Steel Hybrid (Laser + GMAW) and SAW Welded Joint," Materials Basel, vol. 16, no. 7, 2023.

[17] R. M. C. Molabe, "Determining the Optimum Welding Material of 3CR12 Stainless Steel - Master Dessertation," Department of Mechanical Engineering - University Of Johannesburg, Johannesburg, 2018.

[18] J. Luijan, P. Surin and K. Eidhed, "The Effect of Welding Parameters on Joining Dissimilar Low Carbon Steel and 3CR12 Ferritic Stainless Steel by GTAW with ER308L Filler Metal," Journal of Physics: Conference Series, vol. 1519, 2020.

[19] K. Touileb, A. C. Hedhibi, R. Djoudjou, A. Ouis, A. Bensalama, A. Ibrahim, H. S. Abdo and M. M. Z. Ahmed, "Mechanical, Microstructure, and Corrosion Characterization of Dissimilar Austenitic 316L and Duplex 2205 Stainless-Steel ATIG Welded Joints," Materials (Basel), vol. 15, no. 7, p. 2470, 2022.

[20] "Stainless Steel 3CR12 Technical Data," Macsteel, [Online]. Available: https://macsteel.co.za/wp-content/uploads/2022/12/3CR12-data-sheet-2021.pdf. [Accessed 10 July 2023].

[21] "AR Series AR 1440 - Technical Details," Yaskawa, 2023. [Online]. Available: https://www.yaskawa.za.com/products/robots/welding-cutting/productdetail/product/ar1440_734. [Accessed 10 July 2023].

[22] K. Mogano, "Effect of Multipass Welding on Mechanical Properties of 3CR12 Steel - Masters Dessertation," Department of Mechanical Engineering University of Johannesburg, Johannesburg, 2021.

[23] K. B. Small, D. A. Englehart and T. A. Christman, "Technical Guide - A Guide to Etching Specialty Alloys for Microstructural Evaluation," Carpenter Technology, 2023. [Online]. Available: https://www.carpentertechnology.com/blog/a-guide-to-etching-specialty-alloys. [Accessed 11 July 2023].

[24] "Hardness Test Methods," SubsTech, 03 May 2014. [Online]. Available: https://www.substech.com/dokuwiki/doku.php?id=hardness_test_methods. [Accessed 15 April 2022].

[25] "Standard Test Method for Vickers Indentation Hardness of Advanced Ceramics," ASTM International C1327-15 (2019), 09 July 2019. [Online]. Available: https://compass.astm.org/document/?contentCode=ASTM%7CC1327-15R19%7Cen-US. [Accessed 15 March 2022].

[26] R. Smallman and A. Ngan, Modern Physical Metallurgy, Elsevier Ltd, 2014.

[27] "ASTM International - ASTM E384-99: Standard Test Method for Microindentation Hardness of Materials," ASTM International, 2023. [Online]. Available: https://standards.globalspec.com/std/3805697/ASTM%20E384-99. [Accessed 10 July 2023].

[28] E. T. Akinlabi and S. A. Akinlabi, "Characterising the Effects of Heat Treatment on 3CR12 and AISI 316 Stainless Steels," International Journal of Mechanical, Aerospace, Industrial and Mechatronics Engineering, vol. 8, no. 2, 2014.

[29] M. R. C. Molabe, "Determining the Optimum Welding Material of 3CR12 Stainless Steel," Department of Mechanical Engineering - University of Johnnesburg, University of Johnnesburg, 2018.

[30] C. C. Silva, J. P. Farias, H. C. Miranda, R. F. Guimarães, J. W. A. Menezes and M. A. M. Neto, "Microstructural characterization of the HAZ in AISI 444 Ferritic Stainless Steel Welds," Material Characterization, vol. 59, no. 5, pp. 528-528, 2008.

[31] N. L. Vithi, M. G. Maruma, A. Maleka and D. Chetty, "Microstructural and Mechanical Properties of Joining 3CR12 Stainless Steel and S355 Carbon Steel by GMAW Using 308L Filler Wire," Composite Materials, vol. 6, no. 1, pp. 1-6, 2022.

Journal of Engineering and Technology for Industrial Applications

ITEGAM-JETIA

Manaus, v10. n.50, p. 15-21. November./ December., 2024.
DOI: https://doi.org/10.5935/jetia.v10i50.1265

ISSN ONLINE: 2447-0228

RESEARCH ARTICLE OPEN ACCESS

A NEW PID TYPE CONTROLLER BASED ON MODIFIED CRISP LOGIC

Abdeslam Benmakhlouf [1], Ghania Zidani [2] and Djalal Djarah [3]

[1,3] Department of Electrical Engineering, Faculty of Applied Sciences, University of Kasdi MERBAH, Ouargla, 30000, Algeria.
[2] Department of Pharmacy, Faculty of Medecine, University of Batna 2, Batna, 05000, Algeria.

[1] http://orcid.org/0000-0003-0849-7229, [2] http://orcid.org/0000-0002-1338-3296, [3] http://orcid.org/0000-0002-2480-9731

Email: benmakhlouf.abdeslam@univ-ouargla.dz, g.zidani@univ-batna2.dz, djarah.djalal@univ-ouargla.dz

ARTICLE INFO

Article History
Received: August 24, 2024
Revised: October 16, 2024
Accepted: November 1, 2024
Published: November 30, 2024

Keywords:
Fuzzy Logic control,
Modified crisp logic,
PID, Self-tuning
Relative Rate Observer.

ABSTRACT

A PID type fuzzy logic controller (FLC) is a control scheme that utilizes fuzzy inference systems to replicate the behavior of a classical PID controller. This approach provides an alternative for systems where traditional PID control encounters difficulties, particularly in scenarios involving human expertise or non-linear behavior. In this study, we propose a novel PID-like controller that employs a modified crisp logic method—a rule-based approach designed to implement the reasoning process. This method aims to reduce processing time in fuzzy inference systems by using crisp sets instead of fuzzy sets and simple calculations to generate the output. Simulation results demonstrate the effectiveness of the proposed method, achieving comparable performance with the added benefit of reduced processing time.

I. INTRODUCTION

Fuzzy logic, introduced by Lotfi Zadeh in 1965, is a computational approach that allows for approximate reasoning, mimicking human decision-making processes [1]. Unlike traditional Boolean logic, where variables are strictly true or false, fuzzy logic employs membership functions to represent degrees of truth, with values between 0 and 1. This flexibility makes it particularly useful for handling uncertainty and ambiguity prevalent in real-world systems. Fuzzy logic control (FLC) is a direct application of fuzzy logic to control systems [2]. It allows us to incorporate human-like reasoning into control strategies. While it may not provide precise reasoning, it offers acceptable reasoning. Additionally, FLC can emulate deductive thinking, similar to how people infer conclusions from what they know. By using a set of linguistic rules and membership functions, FLC models the behavior of systems in a way that mimics human decision-making, providing robust and adaptive control solutions.

A PID type fuzzy logic controller combines the benefits of both PID control and fuzzy logic, resulting in a robust and adaptive control strategy. By utilizing fuzzy rules and membership functions, it effectively manages complex systems characterized by nonlinearities or uncertainties.

In the work by M. Mizumoto [3], the application of fuzzy logic to implement PID control strategies was explored. The study demonstrated that PID controllers can indeed be realized through specific fuzzy control methods, such as the “product-sum-gravity” and “simplified fuzzy reasoning” methods. Consequently, PID control is considered a special case within the broader context of fuzzy control. Notably, the min-max-gravity method lacks the ability to achieve PID controller functionality.

The PID type fuzzy logic controller (FLC) was extensively studied in the literature. The study in [4] presents a comprehensive exploration of crisp-type fuzzy controllers, delving into their fundamental principles, their basic structures, and operational characteristics. By conducting an in-depth analysis of their behavior, the unique attributes differentiating them from traditional fuzzy controllers are highlighted. Moreover, the chapter investigates strategies to optimize controller performance, focusing on enhancing efficiency and effectiveness in complex control scenarios. Through comparative studies and simulation-based evaluations, the potential benefits and real-world applications of crisp-type fuzzy controllers are demonstrated. The paper by Xu, Hang, and Liu introduces a novel approach to fuzzy PID control by employing a parallel structure [5]. This design involves combining independent fuzzy proportional and derivative controllers, offering increased flexibility and potential for improved performance compared to traditional fuzzy PID controllers. A key contribution of this work is the development of a tuning method based on gain and phase margins, facilitating controller design and optimization. In contrast to the complex rule-based structures often associated with fuzzy controllers, this research explores a simplified architecture with a reduced number of fuzzy sets. This streamlined approach enhances computational efficiency and enables stability analysis. By focusing on the core components of PID control, the authors demonstrate the effectiveness of this simplified fuzzy PID controller in achieving desired control objectives.

Parameter self-tuning is crucial for PID controllers to maintain optimal performance in dynamic environments by automatically adjusting control parameters to adapt to changing system conditions. The authors of [6] use Parameter Adaptive Method for real-time adjustment of PID parameters. The approach adopted in [7] introduce a novel PID type fuzzy controller that incorporates self-tuning scaling factors. This approach dynamically adjusts the proportional, integral, and derivative gains through a fuzzy inference system. By adapting to changing system conditions, the controller enhances performance and robustness. The authors demonstrate the controller's effectiveness through simulations and practical applications. Reference [8] proposes a novel self-tuning method for PID-type fuzzy logic controllers. By employing a relative rate observer to estimate system dynamics, the controller adaptively adjusts its scaling factors. This approach enhances the controller's ability to handle varying operating conditions and improve overall performance. This approach was implemented on a PLC [9] and compared with other self-tuning mechanisms in [10]. This methos was also used in a number of applications [11-16]. The self-tuning of different PID type fuzzy controllers was studied in literature [17-21].

Modified crisp logic is a simplified approach to fuzzy logic that aims to reduce computational complexity while retaining some of the benefits of fuzzy reasoning [22]. Unlike traditional fuzzy logic, which uses membership functions to represent degrees of truth, modified crisp logic employs crisp sets with defined thresholds. Essentially, it's a hybrid method that combines elements of both crisp logic and fuzzy logic. By simplifying the fuzzy inference process, modified crisp logic can potentially improve computational efficiency without sacrificing too much control performance. The main objective of this study is to use the modified crisp logic method to implement the PID type controller and the self-tuning mechanism.

The remainder of this paper is structured as follows. Section 2 provides a brief overview of PID type FLC. In Section 3, the principles of modified crisp logic are elaborated. Section 4 delves into the proposed self-tuning methods. Simulation results and their analysis are presented in Section 5. Finally, Section 6 summarizes the key findings and outlines potential directions for future research.

II. PID TYPE FLC

Figure 1 illustrates a typical closed-loop control system incorporating a standard PID type FLC [8]. The control signal generated by the PID type FLC is determined by:

$$u = \alpha U + \beta \int U dt \quad (1)$$

where U is the output of the FLC bloc.

Previous research [6] has demonstrated that fuzzy controllers employing product-sum inference, center of gravity defuzzification, and triangular input membership functions with a crisp output exhibit an input-output relationship defined by:

$$U = A + PE + D\dot{E} \quad (2)$$

Where $E = K_e e$ and $\dot{E} = K_d \dot{e}$.

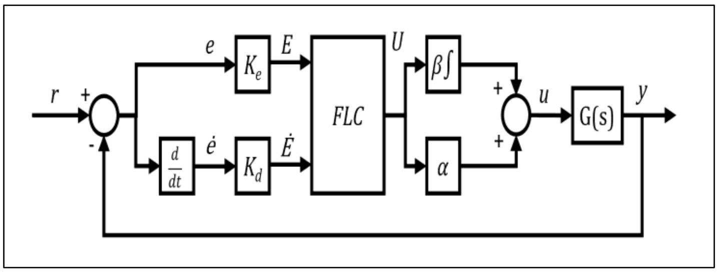

Figure 1: Closed-loop control structure for PID type FLC.
Source: Authors (2024).

Consistent findings in [23],[24] confirm that the minimum inference engine also produces the same input-output relationship. Combining equations (1) and (2) yields the controller output as follows:

$$u = \alpha A + \beta At + \alpha K_e Pe + \beta K_d De + \beta K_e P \int edt + \alpha K_d D\dot{e} \quad (3)$$

Consequently, the equivalent PID type FLC control components are derived as follows:

Proportional gain: $\alpha K_e P \beta K_d D$
Integral gain: $\beta K_e P$
Derivative gain: $\alpha K_d D$.

III. MODIFIED CRISP LOGIC

To streamline the fuzzy control process, modified crisp logic introduces two key modifications [22]. Firstly, crisp, non-overlapping membership functions are adopted for input variables. This simplification eliminates the need for complex membership degree calculations and rule inference, as each input belongs exclusively to one crisp set. Consequently, output sets are defined as singletons, thereby obviating the defuzzification stage. Secondly, to mitigate the potential abrupt transitions caused by crisp set-based outputs, a smoothing function is applied to generate the final control signal. This function effectively attenuates the discontinuous nature of the output, enhancing overall system performance. By incorporating these enhancements, the proposed controller offers a computationally efficient and robust alternative to fuzzy control.

The output value in the case of a system with 2 inputs and a single output is given by the following equation:

$$u = rule(i,j) - \frac{\Delta a + \Delta b}{2} \quad (4)$$

Here, rule (i,j) is a singleton output associated with the combination of input values belonging to crisp sets i and j, respectively.

$$\Delta a = c_a(i) - a \quad (5)$$

$$\Delta b = c_b(j) - b \quad (6)$$

Where a and b denote the input variables. The centers of the crisp sets corresponding to a and b are represented by ca(i) and cb(j), respectively. The difference between inputs (a, b) and their associated crisp sets are denoted by Δa and Δb.

The proposed controller architecture, illustrated in Figure 2, eliminates the need for fuzzification, complex fuzzy inference and defuzzification processes. By directly mapping input crisp sets to output singleton values, the controller significantly reduces computational burden. This streamlined approach enables real-time implementation without requiring specialized software or hardware.

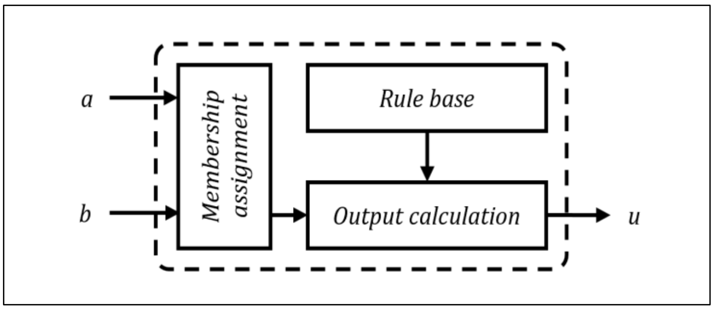

Figure 2: The architecture of the modified crisp logic controller.
Source: Authors (2024).

IV. MODIFIED CRISP LOGIC PID TYPE CONTROLLER

The proposed PID type controller shares the same architectural framework as its fuzzy counterpart (Figure 1), with the exception of the inference system, which is based on modified crisp logic. The conventional FLC block is replaced by a crisp logic equivalent as illustrated in Figure 2. For comparison, a standard PID type FLC utilizes the membership functions depicted in Figure 3(a), while the proposed PID employs those shown in Figure 3(b). The distinct characteristics of these membership functions are evident.

The rule base presented in Table 1 governs both the FLC inference process and the output calculation for the proposed controller.

Table 1: Rule base.

Ė/E	**N**	**P**
N	N	Z
P	Z	P

Source: Authors (2024).

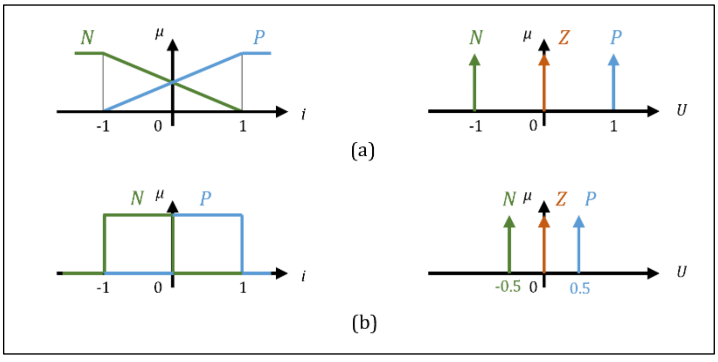

Figure 3: Membership functions (a) FLC, (b) Modified crisp logic.
Source: Authors (2024).

The control surfaces for both controllers are illustrated in Figure 4. Both methods yield identical decision surfaces. The FLC uses the product–sum inference mechanism and center of gravity defuzzification method.

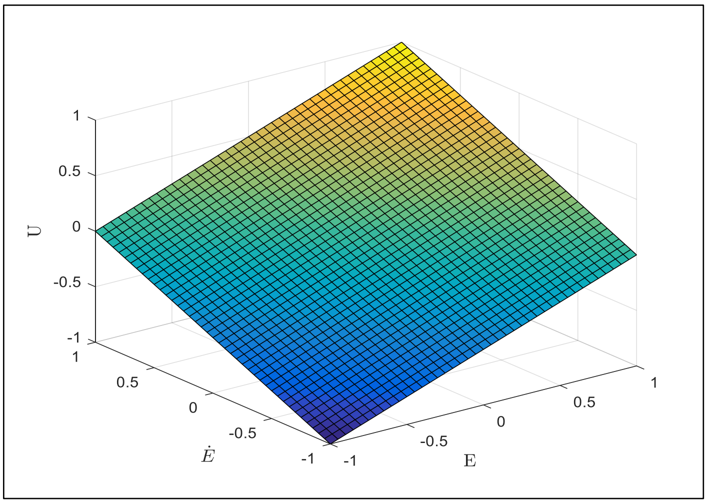

Figure 4: Control surface.
Source: Authors (2024).

V. SELF-TUNING OF A PID TYPE FLC

Numerous self-tuning strategies have been proposed to optimize PID type fuzzy logic controller parameters. One such approach is peak observer-based parameter adaptation, which leverages system peak responses to adjust controller settings in real-time [6]. By extracting information from these peaks, the method refines fuzzy controller scaling factors or membership functions. Alternatively, function tuners offer a more flexible approach, employing mathematical functions to correlate system behavior with desired parameter adjustments [23].

This paper focuses on the relative rate observer (RRO) method, which estimates system parameters based on output rate variations [8]. The architecture of PID type FLC with RRO self-tuning is illustrated in Figure 5. The proposed method leverages both system error and rate information to optimize PID type FLC performance. A fuzzy inference mechanism dynamically adjusts scaling factors associated with the derivative and integral coefficients. This mechanism employs two inputs: system error (e) and normalized acceleration (rv), as defined in [8]. The latter provides insights into system response dynamics, effectively functioning as a relative rate observer (RRO). The normalized acceleration rv(k) can be defined as:

$$r_v(k) = \frac{\ddot{e}(k)}{\dot{e}(\cdot)} \quad (7)$$

Where $\dot{e}(\cdot)$ is chosen as follows:

$$\dot{e}(\cdot) = \begin{cases} \dot{e}(k) & \text{if } |\dot{e}(k)| \geq |\dot{e}(k-1)| \\ \dot{e}(k-1) & \text{if } |\dot{e}(k)| < |\dot{e}(k-1)| \end{cases} \quad (8)$$

The fuzzy parameter regulator generates an output denoted as γ. The scaling factor for the derivative term, Kd, is modified by multiplying its initial value with γ. Conversely, the scaling factor for the integral term, β, is adjusted by dividing its initial value by γ.

$$K_d = K_{ds} K_{fd} K_f \gamma \tag{9}$$

$$\beta = \frac{\beta_s}{K_f \gamma} \tag{10}$$

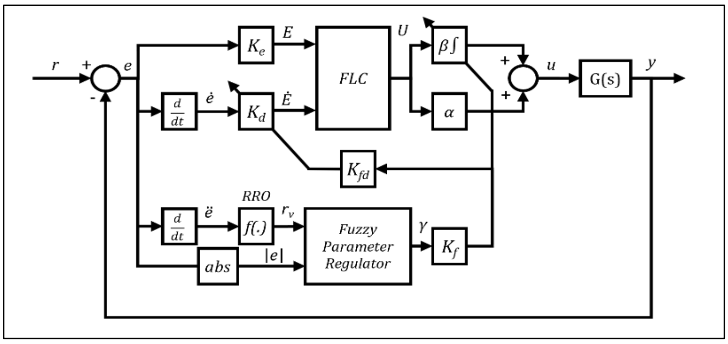

Figure 5: PID type FLC using RRO.
Source: Authors (2024).

Figure 6 and Figure 7 depict the input membership functions for the fuzzy and crisp modules respectively. It's important to note that output membership functions are singletons, specified within the corresponding rule tables.

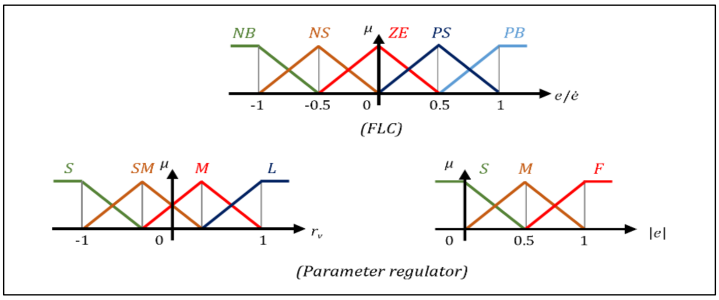

Figure 6: Membership functions for the fuzzy PID.
Source: Authors (2024).

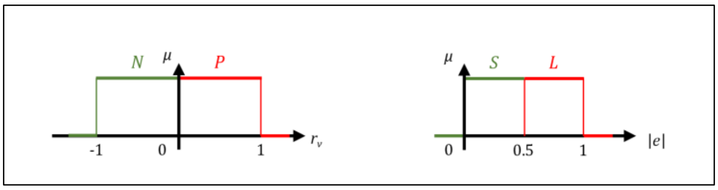

Figure 7: Membership functions for the crisp Parameter regulator.
Source: Authors (2024).

The symmetrical rule base outlined in [6] is presented in Table 3. This rule base serves as the foundation for the PID type FLC. The linguistic terms assigned to the input variables, error (E) and change in error (Ė), are: Negative Big (NB), Negative Small (NS), Zero (ZE), Positive Small (PS), and Positive Big (PB). The rule base for the crisp PID controller is the one presented in Table 1. Given that two crisp sets are employed for the input variables, the rule base is structured as a 2x2 matrix.

Table 2: Rule base of the fuzzy PID.

Ė/E	**NB**	**NS**	**ZE**	**PS**	**PB**
NB	-1	-0.7	-0.5	-0.3	0
NS	-0.7	-0.4	-0.2	0	0.3
ZE	-0.5	-0.2	0	0.2	0.5
PS	-0.3	0	0.2	0.4	0.7
PB	0	0.3	0.5	0.7	1

Source: Authors (2024).

Table 4 presents the rule base for the fuzzy parameter regulator [8]. The linguistic terms for the input variable $|e|$ and the output variable g are: Large (L), Small (S), Medium (M), and Small Medium (SM). For the other input variable, rv, the linguistic terms are: Fast (F), Moderate (M), and Slow (S). While Table 4 presents the rule base of the crisp parameter regulator.

Table 3: Rule base of the fuzzy parameter regulator.

$|e|/r_v$	**S**	**M**	**F**
S	M	M	L
SM	SM	M	L
M	S	SM	M
L	S	S	SM

Source: Authors (2024).

Table 4: Rule base of the crisp parameter regulator.

$|e|/r_v$	**N**	**P**
S	0.5	0.75
L	0.25	0.5

Source: Authors (2024).

VI. RESULTS AND DISCUSSION

In [8], the authors conducted a comparative analysis of the RRO method against conventional PID, peak observer, and function tuner approaches. The RRO method demonstrated superior efficiency due to its reduced parameter tuning requirements and enhanced robustness to system variations compared to its counterparts.

This section presents a comparative analysis of the proposed self-tuned PID controller based on modified crisp logic and a PID type FLC equipped with an RRO. Simulation studies were conducted on a second-order linear system characterized by varying parameters and transport delay defined by:

$$G_p(s) = \frac{K e^{-T_D s}}{s^2 + Ps + Q} \tag{11}$$

Discrete simulation with a sampling period of Ts = 0.1 s was employed for the experiments. Nominal system parameters were set as K = 16, P = 3, Q = 2, and TD = 0. To ensure consistency, parameters a = 0.2, b = 1, Ke = 0.8, and Kd = 0.25 remained constant for both controllers.

Two types of tests were performed: one-parameter and two-parameter adjustments. For the one-parameter case, the optimal value of Kf was found to be 4.35 while maintaining Kfd at 1. In the two-parameter adjustment scenario, Kf and Kfd were optimized to 1.9 and 2.45, respectively.

Figure 8 demonstrates that the proposed method with single-parameter adjustment yields a satisfactory response, comparable to the fuzzy PID with RRO. Figure 10 illustrates that simultaneous adjustment of both Kfd and Kf parameters results in an improved response. Figs. 9 and 11 present the control efforts exerted by both controllers. Notably, the crisp controller generates a smoother control signal with lower magnitude compared to the fuzzy controller.

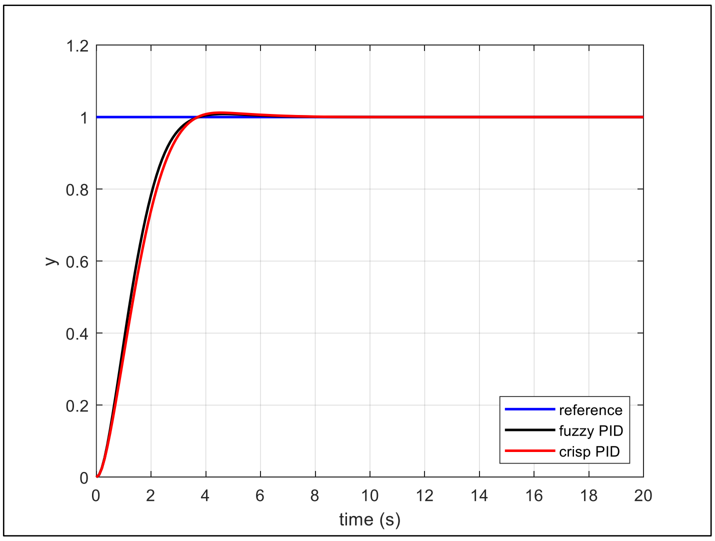

Figure 8: Unit step responses for the nominal system with one parameter adjustment.
Source: Authors (2024).

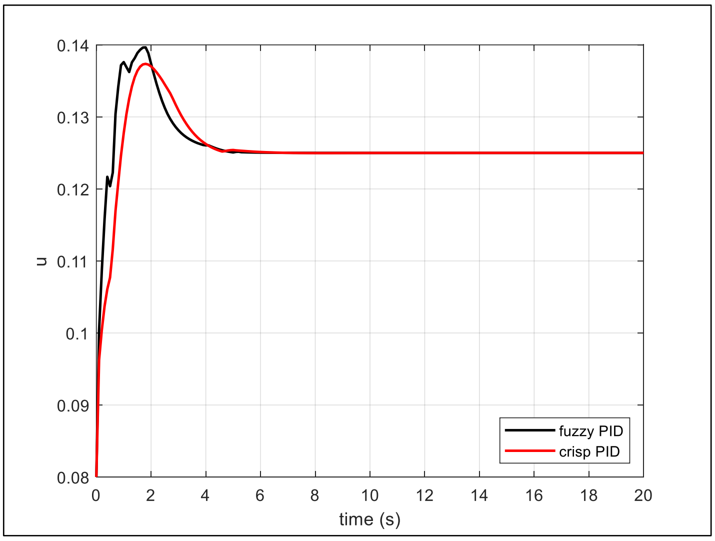

Figure 9: Control effort with one parameter adjustment.
Source: Authors (2024).

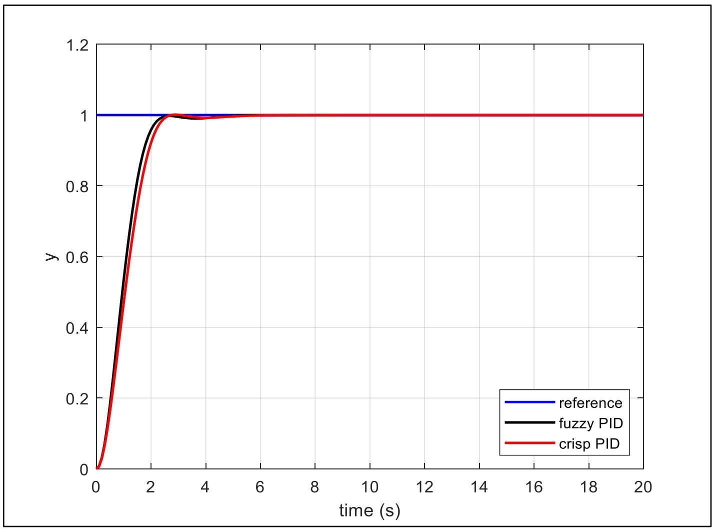

Figure 10: Unit step responses for the nominal system with two parameters adjustment.
Source: Authors (2024).

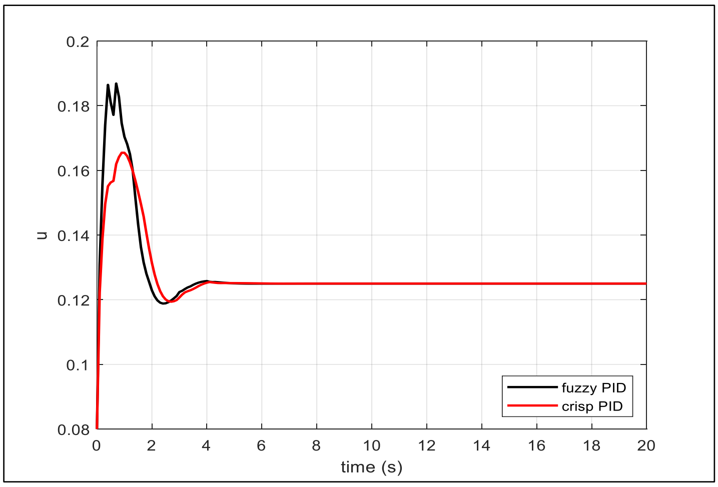

Figure 11: Control effort with two parameters adjustment.
Source: Authors (2024).

To evaluate and compare the proposed methods, a simulation study was conducted under varying system conditions. The plant transfer function denominator coefficients, P and Q, were systematically varied within the range of 0 to 4 without anytime delay, ensuring system stability by limiting pole locations to a left-half plane circle with a radius of 2. Four representative system configurations, labeled a to d, were examined. Specific parameter values and corresponding system types for each case are provided as follows:

Case a: $P = 2$ and $Q = 1$; overdamped stable system.
Case b: $P = 2$ and $Q = 0$; marginally stable system.
Case c: $P = 2$ and $Q = 2$; underdamped stable system.
Case d: $P = 0.5$ and $Q = 4$; almost oscillatory system.

For the remaining simulations, controller parameters were fixed at the optimal values determined for the nominal system. System responses for cases a to d are depicted in Figs. 12 to 15, respectively. Only the results for two parameter adjustments are presented. When at least one open-loop plant pole is located close to the imaginary axis, as in cases b and d. The PID type crisp controller demonstrates superior performance compared to the PID type fuzzy controller. To assess the impact of time delay, a 0.25s delay was introduced to the nominal system while maintaining fixed controller parameters. Figure 16 presents the resulting unit step responses for the compared methods. The crisp PID with two-parameter adjustment consistently outperforms the fuzzy PID controller under these conditions.

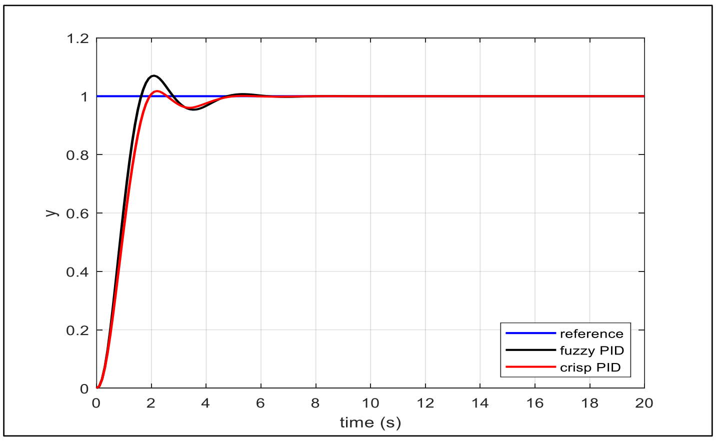

Figure 12: Unit step responses for case a.
Source: Authors (2024).

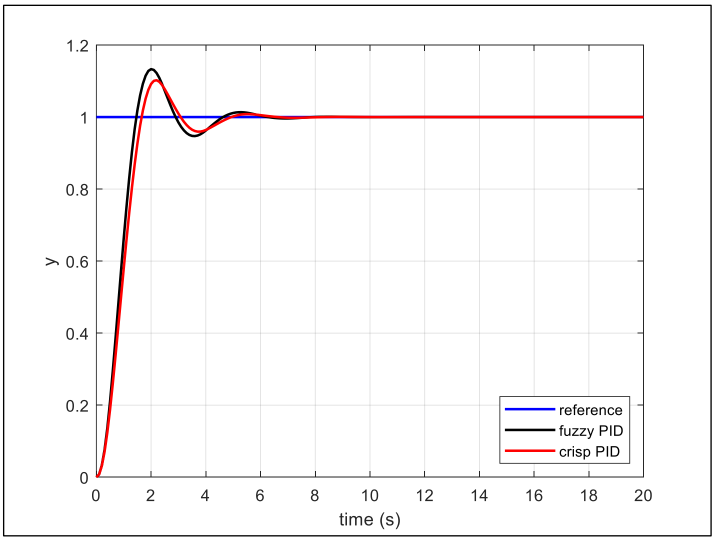

Figure 13: Unit step responses for case b.
Source: Authors (2024).

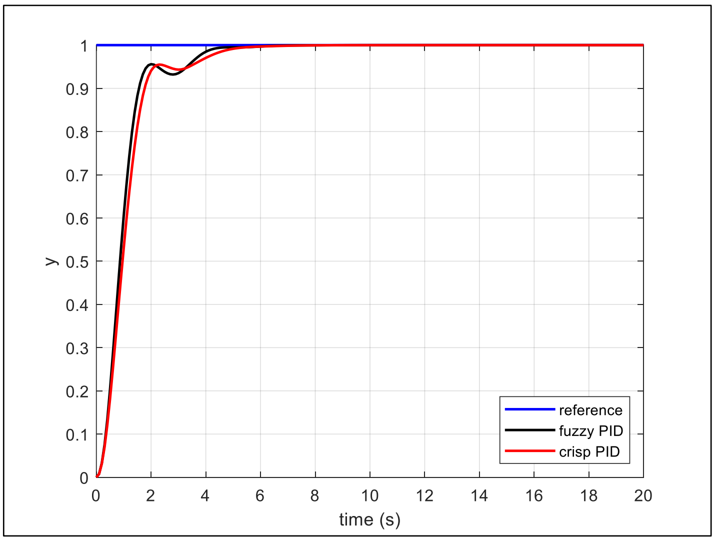

Figure 14: Unit step responses for case c.
Source: Authors (2024).

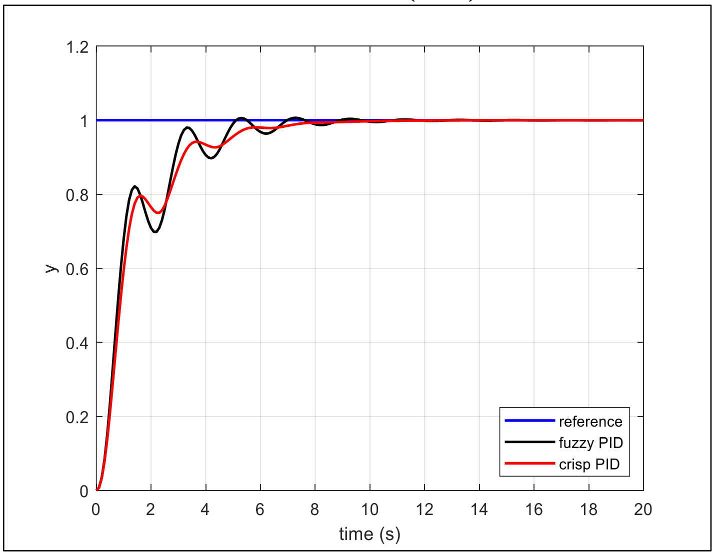

Figure 15: Unit step responses for case d.
Source: Authors (2024).

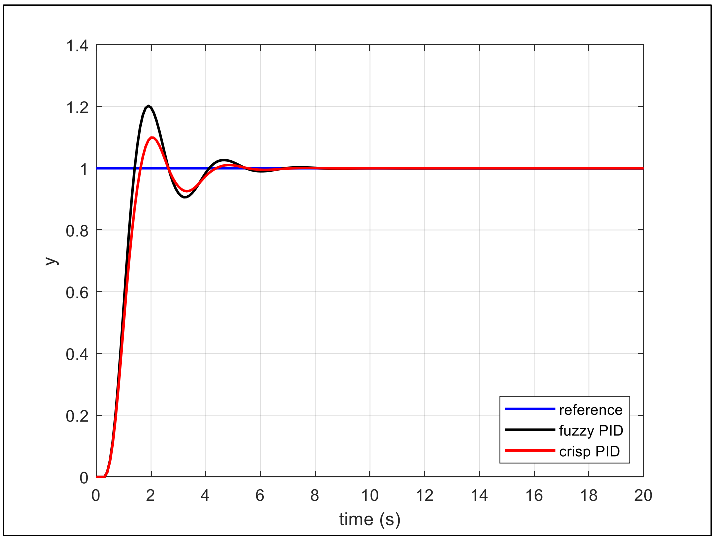

Figure 16: Unit step responses with TD = 0.25 s.
Source: Authors (2024).

VII. CONCLUSIONS

This research has successfully implemented a PID type controller utilizing modified crisp logic and a relative rate observer self-tuning mechanism. By simplifying the fuzzy inference process through crisp set theory, computational efficiency was significantly enhanced without compromising performance.

The proposed controller, while sharing a similar architecture with its fuzzy counterpart, demonstrated superior performance in terms of robustness and adaptability to system variations. Simulation results confirmed the effectiveness of the approach in handling complex system dynamics.

Future research will focus on applying this controller to more challenging and complex real-world applications.

VIII. AUTHOR'S CONTRIBUTION

Conceptualization: Abdeslam Benmakhlouf, Ghania Zidani and Djalal Djarah.
Methodology: Abdeslam Benmakhlouf and Ghania Zidani.
Investigation: Abdeslam Benmakhlouf and Ghania Zidani.
Discussion of results: Abdeslam Benmakhlouf, Ghania Zidani and Djalal Djarah.
Writing – Original Draft: Abdeslam Benmakhlouf.
Writing – Review and Editing: Ghania Zidani and Djalal Djarah.
Resources: Ghania Zidani.
Supervision: Djalal Djarah.
Approval of the final text: Abdeslam Benmakhlouf, Ghania Zidani and Djalal Djarah.

IX. DISCLAIMER

The authors declare that they received no financial support or grants from any public, commercial, or non-profit entities for this research. All the views expressed in this work are solely those of the authors.

X. REFERENCES

[1] Zadeh, L. A. (1965). "Fuzzy sets". Information and Control, 8(3), 338-353. https://doi.org/https://doi.org/10.1016/S0019-9958(65)90241-X

[2] Mamdani, E. H. (1974). "Application of fuzzy algorithms for control of simple dynamic plant". Proceedings of the Institution of Electrical Engineers, 121(12), 1585. https://doi.org/10.1049/piee.1974.0328

[3] Mizumoto, M. (1995). “Realization of PID controls by fuzzy control methods”. Fuzzy Sets and Systems, 70(2), 171-182. https://doi.org/https://doi.org/10.1016/0165-0114(94)00215-S

[4] Qiao, W. Z., & Mizumoto, M. (1996). “On the Crisp-type Fuzzy Controller: Behaviour Analysis and Improvement”. In M. J. Patyra & D. M. Mlynek (Eds.), Fuzzy Logic: Implementation and Applications (pp. 117-139). Vieweg+Teubner Verlag. https://doi.org/10.1007/978-3-322-88955-3_4

[5] Xu, J.-X., Hang, C.-C., & Liu, C. (2000). “Parallel structure and tuning of a fuzzy PID controller”. Automatica, 36(5), 673-684. https://doi.org/https://doi.org/10.1016/S0005-1098(99)00192-2

[6] Wu Zhi, Q., & Mizumoto, M. (1996). “PID type fuzzy controller and parameters adaptive method”. Fuzzy Sets and Systems, 78(1), 23-35. https://doi.org/https://doi.org/10.1016/0165-0114(95)00115-8

[7] Karasakal, O., Guzelkaya, M., Eksin, I., & Yesil, E. (2011). “An error-based on-line rule weight adjustment method for fuzzy PID controllers”. Expert Systems with Applications, 38(8), 10124-10132. https://doi.org/https://doi.org/10.1016/j.eswa.2011.02.070

[8] Güzelkaya, M., Eksin, İ., & Yeşil, E. (2003). “Self-tuning of PID-type fuzzy logic controller coefficients via relative rate observer”. Engineering Applications of Artificial Intelligence, 16(3), 227-236. https://doi.org/https://doi.org/10.1016/S0952-1976(03)00050-2

[9] Karasakal, Onur; Yeşil, Engin; Güzelkaya, Müjde; and Eksin, Ibrahim (2005) “Implementation of a New Self-Tuning Fuzzy PID Controller on PLC”, Turkish Journal of Electrical Engineering and Computer Sciences, 13(2), 277-286.

[10] Karasakal, O., Yesil, E., Guzelkaya, M., & Eksla, I. (2004, 28 June-1 July 2004). “The implementation and comparison of differenttype self-tuning algorithms of fuzzy pid controllers on PLC”. Proceedings World Automation Congress, 2004.

[11] Yeşil, E., Güzelkaya, M., & Eksin, İ. (2004). “Self tuning fuzzy PID type load and frequency controller”. Energy Conversion and Management, 45(3), 377-390. https://doi.org/https://doi.org/10.1016/S0196-8904(03)00149-3

[12] Mohamed, Ahmed H.; El Zoghby, Helmy M.; Bahgat, Mohiy; and Abdel Ghany, A. M. (2022) “Relative Rate Observer Self-Tuning of Fuzzy PID Virtual Inertia Control for An Islanded microgrid”, Future Engineering Journal, 3(2), 1-15.

[13] Abdel Ghany, M. A., Bahgat, M. E., Refaey, W. M., & Hassan, F. N. (2014). “Design of Fuzzy PID Load Frequency Controller Tuned by Relative Rate Observer for the Egyptian Power System”. The International Conference on Electrical Engineering, 9(9th International Conference on Electrical Engineering ICEENG 2014), 1-22. https://doi.org/10.21608/iceeng.2014.30368

[14] M. Abdel Ghany Mohamed, A. Ghany Mohamed Abdel Ghany, A. Bensenouci, M. -A. Bensenouci and M. Nazih Syed-Ahmad, “Fuzzy Fractional-Order PID Tuned via Relative Rate Observer for the Egyptian Load Frequency Regulation”, 2018 Twentieth International Middle East Power Systems Conference (MEPCON), Cairo, Egypt, 2018, pp. 103-109, doi: 10.1109/MEPCON.2018.8635142.

[15] P. Khan, Y. Khan and S. Kumar, “Activity-Based Tracking and Stabilization of Human Heart Rate Using Fuzzy FO-PID Controller”, in IEEE Journal of Emerging and Selected Topics in Industrial Electronics, vol. 3, no. 2, pp. 372-381, April 2022, doi: 10.1109/JESTIE.2021.3066902.

[16] P. Khan, Y. Khan and S. Kumar, “Tracking and Stabilization of Heart-Rate using Pacemaker with FOF-PID Controller in Secured Medical Cyber-Physical System”, 2020 International Conference on COMmunication Systems & NETworkS (COMSNETS), Bengaluru, India, 2020, pp. 658-661, doi: 10.1109/COMSNETS48256.2020.9027302.

[17] Jian-Xin, X., Yang-Ming, P., Chen, L., & Chang-Chieh, H. (1998). “Tuning and analysis of a fuzzy PI controller based on gain and phase margins”. IEEE Transactions on Systems, Man, and Cybernetics - Part A: Systems and Humans, 28(5), 685-691. https://doi.org/10.1109/3468.709617

[18] Faisal, M., & Kadri, M. B. (2013, 9-10 Dec. 2013). “Fuzzy PI-controller with self tuning scaling factors”. 2013 IEEE 9th International Conference on Emerging Technologies (ICET).

[19] Faisal, M., & Kadri, M. B. (2014, 8-10 Dec. 2014). “Fuzzy adaptive PI Smith control for Time Delay Systems”. 17th IEEE International Multi Topic Conference 2014.

[20] Chung, H.-Y., Chen, B.-C., & Lin, J.-J. (1998). “A PI-type fuzzy controller with self-tuning scaling factors”. Fuzzy Sets and Systems, 93(1), 23-28. https://doi.org/https://doi.org/10.1016/S0165-0114(96)00215-1

[21] Fereidouni, A., Masoum, M. A. S., & Moghbel, M. (2015). “A new adaptive configuration of PID type fuzzy logic controller”. ISA Transactions, 56, 222-240. https://doi.org/https://doi.org/10.1016/j.isatra.2014.11.010

[22] Benmakhlouf, A., Louchene, A., & Djarah, D. (2010). “Fuzzy Logic and Modified Crisp Logic Applied to a DC Motor Position Control”. Control. Intell. Syst., 38(3). https://doi.org/10.2316/JOURNAL.201.2010.3.201-2214.

[23] Woo, Z.-W., Chung, H.-Y., & Lin, J.-J. (2000). “A PID type fuzzy controller with self-tuning scaling factors. Fuzzy Sets and Systems”, 115(2), 321-326. https://doi.org/https://doi.org/10.1016/S0165-0114(98)00159-6.

[24] Tsung-Tai Huang, Hung-Yuan Chung and Jin-Jye Lin, “A fuzzy PID controller being like parameter varying PID”, FUZZ-IEEE'99. 1999 IEEE International Fuzzy Systems. Conference Proceedings (Cat. No.99CH36315), Seoul, Korea (South), 1999, pp. 269-276 vol.1, doi: 10.1109/FUZZY.1999.793247.

Journal of Engineering and Technology for Industrial Applications

ITEGAM-JETIA

ISSN ONLINE: 2447-0228

Manaus, v10. n.50, p. 22-32. November/ December., 2024.
DOI: https://doi.org/10.5935/jetia.v10i50.1289

RESEARCH ARTICLE OPEN ACCESS

DETECTION OF SUBSTATION POLLUTION IN DISTRICT HEATING AND COOLING SYSTEMS: A COMPREHENSIVE COMPARATIVE ANALYSIS OF MACHINE LEARNING AND ARTIFICIAL NEURAL NETWORK MODELS

[1] Emrah Aslan and [2] Yıldırım Özüpak

[1] Emrah ASLAN - Computer Programming Department, Silvan Vocational School, Dicle University, Diyarbakır, Turkey.
[2] Department of Electricity and Energy, Silvan Vocational School, Dicle University, Diyarbakır, Turkey.

[1]http://orcid.org/0000-0002-0181-3658, [2]http://orcid.org/0000-0001-8467-8702

Email: emrah.aslan@dicle.edu.tr, yildirim.ozupak@dicle.edu.tr

ARTICLE INFO

Article History
Received: September 9, 2024
Revised: October 16, 2024
Accepted: November 1, 2024
Published: November 30, 2024

Keywords:
Pollution Detection,
Grid Search Optimization,
Machine Learning,
CNN,
DHC.

ABSTRACT

This study analyzes the detection of substation fouling failures in District Heating and Cooling (DHC) systems using synthetic data. In the study, high, medium and low levels of contamination are considered and both machine learning and deep learning techniques are applied for the detection of these failure types. Within the scope of the analysis, machine learning algorithms such as K-Nearest Neighbors, XGBoost and AdaBoost are compared with the proposed Convolutional Neural Network (CNN) model. The machine learning algorithms and the Convolutional Neural Network model are trained to perform fault detection at different contamination levels. In order to improve the performance of the machine learning models, hyperparameter tuning was performed by Grid Search Optimization method. The results obtained show that the proposed Convolutional Neural Network model provides higher accuracy and overall success compared to machine learning methods. High performance measures such as Matthews correlation coefficient 0.944 and accuracy rate 0.972 were achieved with the CNN model. These findings reveal that contamination detection in substations can be done effectively with CNN-based approaches, especially for situations that require high accuracy. This study on fault detection in DHC systems provides a new and reliable solution for industrial applications.

I. INTRODUCTION

District Heating and Cooling (DHC) systems are a critical infrastructure component in modern urban energy management, providing efficient heating and cooling services to both residential and commercial buildings. These systems play an important role in improving energy efficiency and reducing operating costs. However, the reliability and performance of DHC systems can be affected by various failures, which can put the efficiency, safety and overall operational stability of the system at risk.

The development of effective fault detection and diagnosis (FDD) models for DHC systems is an important research area to ensure uninterrupted operation of the system and improve its reliability. Traditional fault detection methods are often based on manual checking and heuristic approaches, but these methods may not be sufficient to address the complexities of modern DHC systems. Recent advances in data-driven techniques, especially in the fields of machine learning (ML) and data analytics, offer promising solutions to these challenges. The lack of comprehensive datasets is a significant barrier to developing robust data-driven models. Existing studies emphasize that the lack of quality datasets limits the effectiveness of data-driven approaches [1]. To overcome this problem, researchers have focused on creating synthetic data sets through simulation or using open data sources. These data sets usually cover various system components such as generation units, distribution networks and storage facilities.

Numerous machine learning approaches for DHC system defect detection have been studied in recent research. For instance, because of its propensity to handle intricate patterns in data, XGBoost, Support Vector Machine (SVM), and Logistic Regression are often employed [2]. Studies have shown that these models can detect energy efficiency related faults with high accuracy, but there can be difficulties in detecting more subtle problems, e.g. thermal losses.

To improve the reliability of fault detection models, researchers are investigating integrating real-time data with simulation results and open data. This approach aims to increase the generalizability and robustness of the models, thus ensuring their applicability to a wide range of operational scenarios [3].

District Heating and Cooling (DHC) systems are increasingly being used to improve energy efficiency and reduce carbon emissions. DHC systems eliminate the need for individual heating or cooling systems by transmitting heat and cooling energy generated from a centralized source to buildings over a wide network. These systems play an important role in energy saving and environmental sustainability, especially in urban areas [4].

However, ensuring the long-term efficient operation of DHC systems poses a major challenge in terms of their maintenance and early detection of potential failures. Failures in substations, such as contamination, reduce the overall efficiency of the system and increase costs. In the past, the detection of such faults was mostly limited to physical checks or manual interventions in case certain critical limits were exceeded. Today, however, technological advances such as data analytics and machine learning offer the possibility to make these processes more automated and accurate [5].

In the past, fault detection processes in DHC systems were generally handled with a reactive approach. Physical inspections, periodic maintenance work and performance monitoring systems are among the classical methods that are activated after failures occur. These approaches are often time-consuming, lead to delays in fault detection and negatively affect the efficiency of the system. Furthermore, most of these methods are activated when there is a significant degradation in system performance, which often results in more costly repairs and system downtime. However, with the development of data collection and analysis techniques in recent years, methods such as machine learning and deep learning offer an important alternative for fault detection. By analyzing large amounts of data, these new methods provide the opportunity to detect signs and trends before failures occur [6]. Thus, early diagnosis of failures and implementation of preventive maintenance strategies become possible.

Machine learning and deep learning methods offer many advantages over traditional fault detection techniques [7]. Machine learning algorithms have achieved significant success in fault prediction by learning meaningful patterns from large datasets. Algorithms such as K-Nearest Neighbors (KNN), XGBoost and AdaBoost have the ability to automate fault prediction by training on data collected in the past. These algorithms have been successful in predicting system failures by analyzing correlations in the data and possible signs of failure. However, these methods are usually dependent on a more limited data structure and may be inadequate for complex or multidimensional data [8]. In contrast, deep learning methods, especially models such as Convolutional Neural Network (CNN), stand out with their capacity to process more complex data structures. CNN models provide higher success rates, especially in large and complex data sets, enabling the detection of previously undetected faults.

In this study, the failure conditions caused by contamination of substations in DHC systems are analyzed. Different machine learning algorithms (KNN, XGBoost, AdaBoost) and deep learning (CNN) models are compared using synthetic data for high, medium and low levels of contamination. Grid Search Optimization method was used to optimize the performance of the models and the best hyperparameters were selected. The results show that the CNN model outperforms the other models and achieves high accuracy rates.

The aim of this study is to develop a more accurate and efficient solution that goes beyond traditional methods for early detection of faults in DHC systems. In particular, it is aimed to detect complex failure types such as contamination of substations more effectively. The main advantage of the study is that higher accuracy rates are achieved with the CNN model and fault detection can be done at an earlier stage. This increases the overall efficiency of the system and reduces maintenance costs. However, the fact that deep learning models require large amounts of data and processing power is considered as a significant disadvantage of the study. Moreover, experiments with synthetic data need to be validated with real-world data, which is also one of the limitations of the study.

The study makes several important contributions to the literature. First, it demonstrates the applicability of deep learning methods for fault detection in DHC systems. Second, it proposes a solution for early detection of more complex fault types such as substation contamination. Finally, the high accuracy rates of the model proposed in the study provide a practical benefit for industrial applications. These findings not only contribute to the development of more efficient maintenance strategies in DHC systems, but also provide a new perspective on how deep learning algorithms can be applied in industrial processes.

Section 1 of this paper gives an overview of the problem. The following sections of the paper are as follows. Literature review related to the study is presented in Section 2. The implementation materials and methods are presented in Section 3, and the discussion and conclusions are presented in Section 4. Future work and conclusions are presented in Section 5.

II. THEORETICAL REFERENCE

In this study, problem diagnosis and detection techniques for District Heating and Cooling (DHC) systems are investigated. Using the IEA DHC Annex XIII as a framework, it offers a thorough study of typical DHC system faults. District heating systems have evolved from steam-based systems to ultra-low temperature networks, with future designs integrating distributed low-temperature sources and building-side heat pumps. A case study shows that while ultra-low temperature ring networks are 23% more expensive than 3rd generation systems, they are cost-effective when free waste heat is available [9].

France aims to decarbonize heating by expanding District Heating and Cooling Networks (DHCN) and identifying suitable areas for development. Using variables such as energy density, building age, and energy mix, the paper estimates the potential of DHN at 132 TWh/year and DCN at 7.8 TWh/year across France [10].

Decarbonizing energy sectors, especially heating, is crucial to combating climate change, as heating represents nearly half of global energy consumption. This paper reviews the role of heat pumps in reducing emissions and adding flexibility to renewable energy systems, but highlights economic, regulatory, and infrastructural challenges to their widespread adoption [11].

The article reviews 40 European thermal networks using distributed heat pumps and clarifies definitions of Fifth-Generation District Heating and Cooling (5GDHC). It finds that while 5GDHC systems in countries like Germany and Switzerland excel with renewable heat sources, they face higher pumping energy demands and variable control strategies compared to traditional district heating [12].

Even though the majority of research concur on a core set of typical failures, they frequently don't result in instant shutdowns and may thus go unreported. Although air-source chillers have received a lot of attention, DHC systems are also susceptible to identical issues that have been seen in water-source systems. This study looks on ways to diagnose and find faults in District Heating and Cooling (DHC) systems.

District heating and cooling systems have evolved over a century, serving over 70 million people in Europe with an estimated energy consumption of over 450 TWh. This paper reviews the current state of these systems, highlighting variations across countries in terms of technology, market structure, and regulations, and introduces a new socio-demographic approach to create indicators for modeling future systems [13].

Fifth-generation district heating and cooling (5GDHC) systems, tested in Melbourne, show 9-29% cost savings and 25-58% GHG emissions reduction compared to traditional systems. They offer economic and environmental benefits, especially in mild climates, and could expand to other regions with similar conditions [14].

Temperature control significantly impacts Fifth Generation District Heating and Cooling (5GDHC) systems. This study finds that constant temperature control can be more effective but is sensitive to setting changes, while simple multi-stage controls may underperform. Proper strategy selection and coordination are crucial for optimal system efficiency [15].

District heating and cooling networks offer benefits by integrating renewable energies and local thermal resources, but effective design and optimization are key. This review evaluates the use of Life Cycle Assessment (LCA) for assessing the environmental impact of these networks, revealing a wide range of emission factors. It emphasizes the need for improved management practices and proposes future research for developing a universal LCA tool for network analysis [16].

Due to the limited availability of real-world data, the development of optimized synthetic data sets is investigated to improve the accuracy of three different ML models such as K-Nearest Neighbors (KNN), Support Vector Machine (SVM) and Random Forest (RF). The integration of real and synthetic data improved the identification of initial faults using ML algorithms and the quality of the synthetic data obtained was found to be superior to existing methods [17].

A simulation-based dataset was developed to evaluate various types of failures in District Heating and Cooling (DHC) systems and tested with five machine learning models. The tests showed that the dataset provides high performance in fault detection and the applicability of the models to real systems [18].

Traditional and innovative methods used to achieve goals such as peak shaving, demand response and fast fault detection in advanced district heating and cooling systems are examined. The advantages and disadvantages of modern approaches such as model predictive control and machine learning are detailed [19].

A machine learning method is proposed to detect leakage faults with data from flow and pressure sensors. Using a delayed warning algorithm, a leak signal is sent and the model identifies the faulty pipe based on this signal. The method was successfully tested with 85.85% accuracy and a macro-F1 score of 0.99786 [20].

A machine learning model has been developed that performs well and can distinguish between data sets containing faults. The model is trained with data from a district heating substation in Sweden and tested with various parameters. The results show that the model successfully models the substation behavior and has high fault detection capability [21].

A study was conducted to develop an automatic fault detection and diagnosis (AFDD) framework for district heating substations. With data from Denmark, common faults are analyzed and the potential of AFDD to reduce energy use is highlighted. Additional indicators were proposed and improvements were made to detect future anomalies [22]. A study was conducted to show how smart meter data can be used for fault detection and maintenance processes. Faults were detected in advance with machine learning algorithms and maintenance improvements were provided with performance indicators. The findings were validated by experts and the importance of data utilization for smart heating networks was emphasized [23].

A two-level model was developed for fault detection in district heating systems. This model, which distinguishes high-level system faults and low-level sub-faults, provided high accuracy and reliability in tests. The results show that the model provides an effective solution for real-time monitoring [24]. In [25], a machine learning method is proposed to detect leakage faults with flow and pressure data. The delayed warning algorithm and the model ensure accurate identification of leaks. The method was successfully tested with 85.85% accuracy and a macro-F1 score of 0.99786.

III. MATERIALS AND METHODS

III.1 DATASET

This dataset contains synthetic fault data related to contamination in substations of District Heating and Cooling (DHC) systems. The dataset was developed as part of the International Energy Agency's (IEA) DHC Annex XIII project “Artificial Intelligence Fault Detection and Prediction of Heat Production and Demand in District Heating Networks”. This project develops artificial intelligence methods for the prediction of heat demand and production and evaluates algorithms for fault detection. The experiments in the dataset are simulations covering a period of 28 days, during which faults that can occur at various time points are observed [18]. Failures can occur with different intensities, either sudden or gradual. The failure intensity can be interpreted differently depending on the simulation model used. This dataset provides a valuable resource for the development of new approaches to fault detection in DHC systems. Table 1 lists the input names and basic statistics of the dataset [26].

Table 1: Basic statistical information about the data used in the dataset.

Variable	Explanation	Min	Max
BC	Id of the boundary conditions used for this experimen	0	12
F1_type	Type of fault used in the experiment	0	1
F1_start	Start time of the fault, in hours	0	671
F1_stop	Stop time of the fault, in hours	0	672
F1_init	İnitial intensity of the fault, in the range [0-1]	0	1
F1_final	Final intensity of the fault, in the range [0-1]	0	1

Source: [26].

III.2 K-NEAREST NEIGHBOR REGRESSION

K-Nearest Neighbor (KNN) regression is one of the supervised learning methods and is based on the idea of predicting a target data point by looking at the values of its neighboring data points.

KNN regression has a similar approach to the classification problem, but focuses on the prediction of a continuous target variable. The predicted value for a data point is determined by the average or weighted average of the target values of the selected “k” number of nearest neighbors. Since KNN regression is a parameter-free method, the structure of the model is shaped according to the data set and provides flexibility, especially for complex data distributions. However, the increase in computational costs for high-dimensional data sets and the impact of distance metrics on the performance of neighbor selection are important factors to be considered [27].

III.3 EXTREME GRADIENT BOOSTING REGRESSION

XGBoost (Extreme Gradient Boosting) is a powerful machine learning algorithm often used in supervised learning problems such as regression and classification. XGBoost is an ensemble learning method based on decision trees and minimizes errors by successively adding weak learners (usually decision trees). In regression problems, the main goal of XGBoost is to linearly improve the model's predictions as much as possible and minimize the loss function. The algorithm's innovations on gradient boosting include optimizations that make tree structures faster and more efficient, regularization (L1 and L2) and missing data management. This allows XGBoost to achieve high performance on large datasets while providing superior results in terms of speed and accuracy compared to other methods. The fact that it does not require as much computational power as deep learning techniques and its nonparametric structure have made it a frequently preferred method in regression analysis [28].

III.4 ADAPTIVE BOOSTING REGRESSION

Adaboost (Adaptive Boosting) is an ensemble learning method used to improve the performance of weak learners. Basically, by emphasizing the errors of each weak learner, weight is given to the next learner. In the regression problem, Adaboost successively combines weak regression models to minimize prediction errors. At each step, different weights are assigned to the samples, taking into account the model's previous prediction errors. This weighting allows the model to focus specifically on data points that have struggled with previous predictions. Adaboost regression is often applied with weak learners such as decision trees and is known for providing high accuracy in regression as well as in classification problems. However, it can be sensitive to overfitting and noisy data, so it requires careful model selection and parameter tuning. Adaboost's strength is that it can successfully combine weak learners to improve the overall performance of the model [29].

III.5 CONVOLUTIONAL NEURAL NETWORKS

Convolutional Neural Networks (CNNs) are deep learning architectures structurally inspired by the visual cortex of the human brain. They are particularly effective in computer vision tasks such as image recognition, object detection and classification.

The basic building blocks of CNNs are convolution layers that focus on capturing local features in the data, thereby reducing the number of parameters of the model through dimensionality reduction. These layers extract meaningful features from the input data through filters, and these features are abstracted in deeper layers, allowing more complex structures to be learned. CNNs offer high performance and accuracy, especially on large data sets, thanks to parameter sharing and local connections. Their advanced architecture and level of performance have made CNNs a popular solution in various fields such as medical imaging, autonomous vehicles, and face recognition [30].

III.6 GRID SEARCH OPTIMIZATION

Grid Search Optimization is a method of hyperparameter tuning used to improve the performance of machine learning models. Machine learning algorithms are structured with various hyperparameters that affect the behavior of the model, and choosing the optimal values of these parameters greatly affects the accuracy and overall performance of the model.

The Grid Search method aims to systematically scan all possible combinations of the specified hyperparameters and select the combination that gives the best result. This is accomplished by evaluating the model against a specified performance metric. Although Grid Search is usually used for smaller datasets and in environments with limited computational power, the processing time can increase considerably with large datasets or a large number of hyperparameters. In this case, the Grid Search method can become costly in terms of time and resources. Nevertheless, by finding the optimal parameters, the generalizability and accuracy of the model can be improved. Due to these features, Grid Search Optimization is widely used in the process of improving the success rates of machine learning and deep learning models.

III.7 GENERATION OF SYNTHETIC FAILURE

Synthetic failure data was generated using Modelica-based open source simulation models. First, potential failures in the system were identified by Failure Modes, Effects and Criticality Analysis (FMECA) and different failure scenarios were modeled. Simulations were performed by applying different failure profiles (step and ramp type) under boundary conditions such as outdoor temperature, solar radiation and heat demand. These profiles are defined by parameters such as fault onset time, severity and development time. Each simulation recorded the responses of the system for the faulted and unfaulted cases, forming a synthetic data set [19].

The data set was diversified with various failure types and boundary conditions. The onset time and severity of the faults were randomly selected, resulting in a data set that matches real-world conditions. As a result, for each simulation, variables such as boundary conditions, system inputs and outputs, and fault conditions were recorded to create a data set. This data set is structured in accordance with the machine learning models to be used in fault detection and diagnosis. Failure profiles are defined by the parameters given in Figure 1 below:

• Profile type: Failure can occur as a step or ramp.

• Start time (t_0): The moment when the fault occurs.

• End time (t_x): In the ramp profile only, the moment when the fault reaches maximum severity.

• Start intensity (v_0): Always starts at 0.

• Final severity (v_x): varies between 0 and 1, 1 being the maximum fault severity.

• These parameters were used to model different failure scenarios in the simulations.

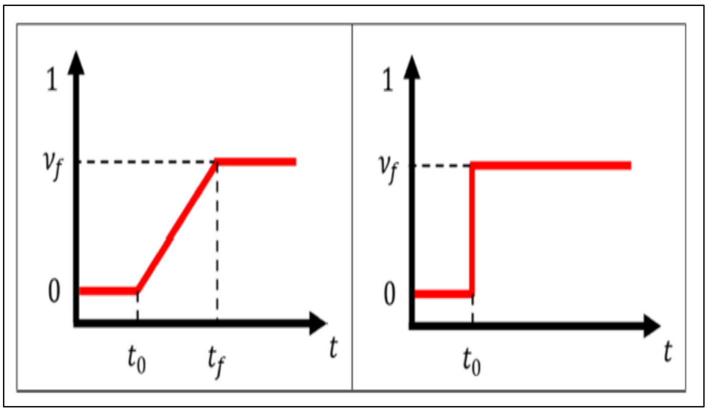

Figure 1: The simulation employed the following fault appearance profiles: ramp on the left for progressive faults and step on the right for sudden faults.
Source: [19].

The fault severity is represented by a number between 0 and 1, where 1 denotes the highest fault severity possible in the model. The model and type of fault will determine this.

IV. RESULTS AND DISCUSSIONS

In this section, the performance results and evaluation of the fault detection models developed for substation contamination are presented. The machine learning models KNN, XGBoost and AdaBoost along with the CNN model are tested and compared to detect faults at different contamination levels. Common performance metrics such as accuracy rate, Matthews correlation coefficient (MCC) and Accuracy are used to determine the performance of the models. The results show that the CNN model has a significant advantage over machine learning methods, especially in detecting more complex and low-level faults. In this section, the performance of each model is discussed in detail. The outstanding achievements of each model will be analyzed and the practical relevance of these findings for DHC systems will be evaluated.

The results of the KNN algorithm showed an accuracy rate of 86.4% and Matthews correlation coefficient performance of 72.3% for the detection of substation contamination faults. In order to improve the performance of the KNN model, hyperparameter optimization was performed with the Grid Search method. In this optimization process, important hyperparameters such as the number of neighbors (k) and distance metric for the KNN algorithm were selected from various values. In Table 2, the optimal hyperparameter values determined by the Grid Search method are presented in detail. These parameters aimed to improve the classification accuracy of the model, but it was observed that the performance of KNN was limited in complex data.

Table 2: KNN regression parameters.

Parameter	Value
n_neighbors	7
weight	distance
algorithm	auto
Leaf_size	30
p	2
n_jobs	10

Source: Authors, (2024).

The confusion matrix of the KNN algorithm is shown in Figure 2. In addition, Table 6 shows all performance metrics of the KNN algorithm.

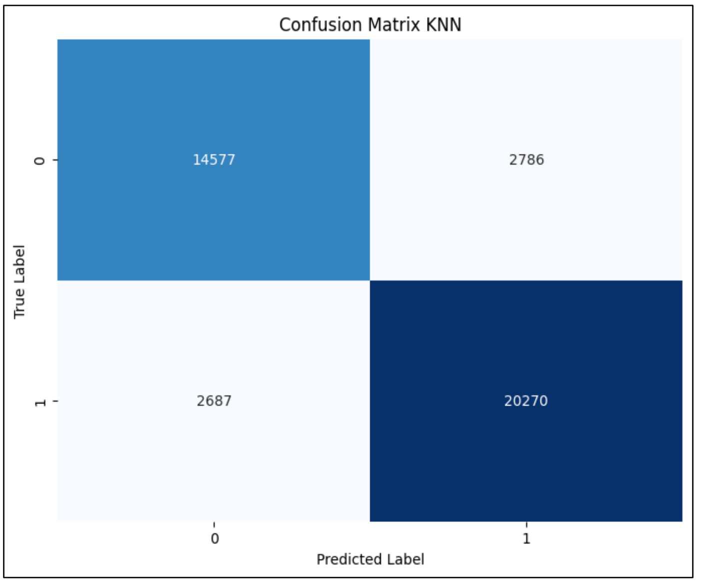

Figure 2: KNN regression confusion matrix.
Source: Authors, (2024).

Figure 3 presents the analysis for different levels of substation contamination in District Heating and Cooling (DHC) systems for the KNN algorithm. The graphs represent four different levels of contamination: very high fouling (75%), medium fouling (20% and 11%), and low fouling (5%). The expression UA [W/K] relates to the heat transfer coefficient in a heat exchange system or thermal system. There are two graphs for each level: The left-hand graphs show the probability of failure detection and the UA [W/K] values together. The graphs on the right-hand side show the correct and incorrect fault detections.

The case where the contamination in the system is very high is analyzed. In the left graph, the UA [W/K] values show a significant decrease with time, showing the effect of fouling and the loss of thermal performance of the system. The yellow dots represent the degree of fouling, while the blue line marks the point of failure. The right graph shows that the UA [W/K] value decreases continuously with time, indicating that the fouling is continuously increasing. In the case of moderate contamination, the spread of the yellow dots in the left graph is more regular and the UA [W/K] values are relatively more stable. However, after a certain point, there is a significant decrease in system performance with increasing fouling. In the right graph, the UA [W/K] value shows a later and slower decline compared to high contamination. It shows a similar pattern for a lower fouling level of 11%, which is lower than the medium level. In the left graph, the yellow dots are less diffuse and the UA [W/K] value decreases less over time. In the right graph, the decline in system performance is again observed, but it is later and less sharp.

Finally, for low levels of fouling, the graphs show a much more stable situation. In the left graph, the yellow dots are more concentrated at the upper levels and the UA [W/K] value remains stable for longer. In the right graph, it can be seen that the UA [W/K] remains largely stable and only slightly decreases.

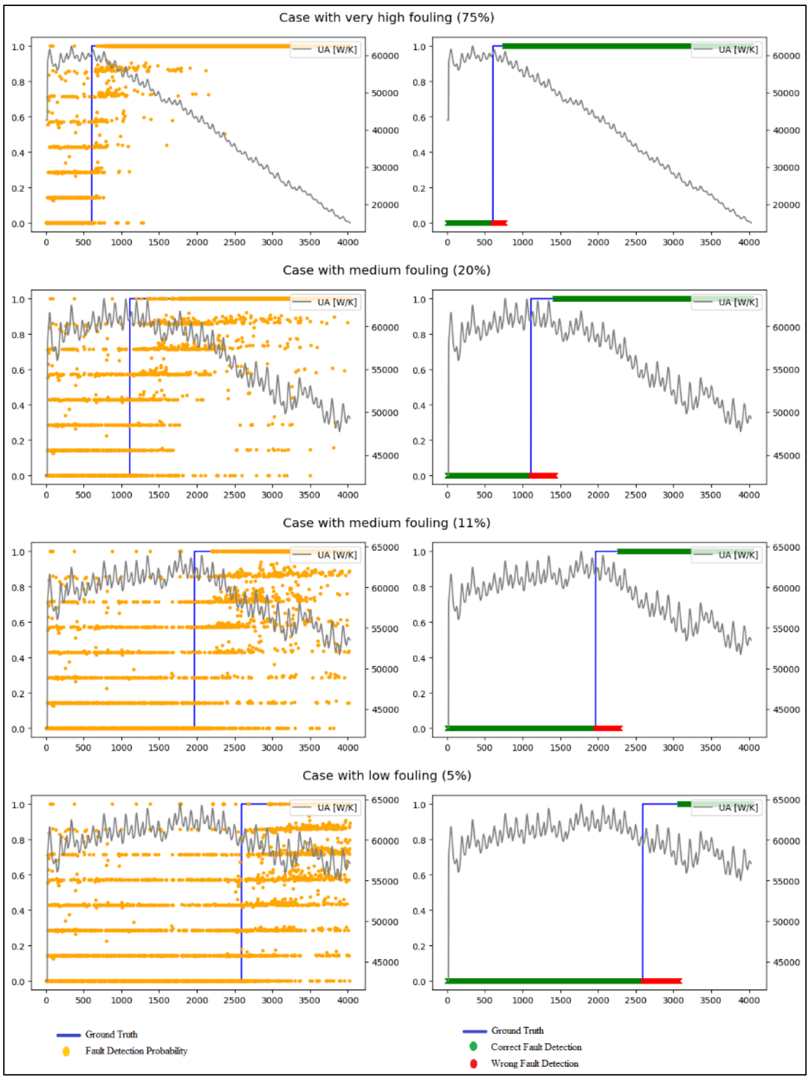

Figure 3: Analysis for different levels of substation contamination in DHC systems with KNN algorithm.
Source: Authors, (2024).

The results of the XGBoost algorithm were found to be highly successful for the detection of substation contamination faults. XGBoost achieved 96.1% accuracy rate and 92.0% Matthews correlation coefficient performance. In order to maximize the performance of the algorithm, hyperparameter tuning was performed using Grid Search Optimization. In this process, important hyperparameters such as learning rate and maximum depth (max_depth) were optimized.

Table 3: XGBoost regression parameters.

Parameter	Value
Base_score	0.7
booster	gbtree
Max_depth	5
Min_child_weight	5
Learning_rate	0.33
n_estimators	250
N_jobs	10
Random_state	5
Tree_method	approx

Source: Authors, (2024).

In Table 3, the optimal hyperparameters obtained as a result of this optimization process are presented in detail. The Grid Search optimization enabled the XGBoost model to detect fouling failures more accurately, resulting in an efficient model with high accuracy and short processing time. The confusion matrix of the XGBoost algorithm is shown in Figure 4. In addition, Table 6 shows all performance metrics of the XGBoost algorithm.

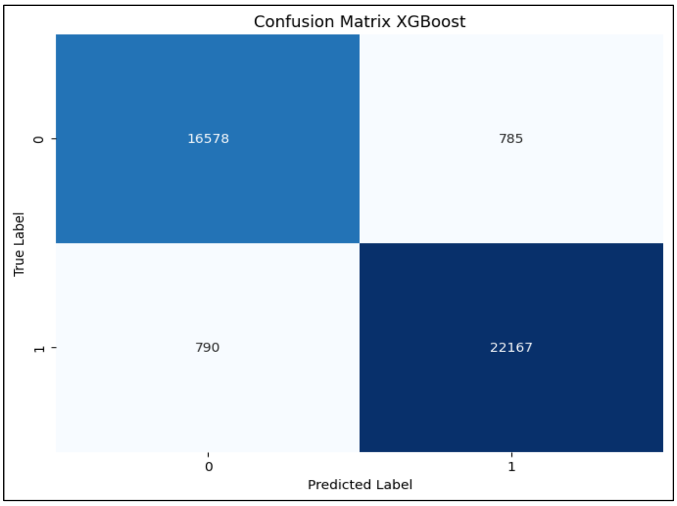

Figure 4: XGBoost regression confusion matrix.
Source: Authors, (2024).

Figure 5 presents the analysis for different levels of substation contamination in District Heating and Cooling (DHC) systems for the XGBoost algorithm. The left graph with high contamination shows the probability of fault detection and UA [W/K] values. In the case of very high contamination, the probability of fault detection increases rapidly from the point where the contamination starts and the system performance decreases significantly. In the right graph, the blue line represents the ground truth, the green area represents correct detections and the red area represents incorrect detections. In the case of very high contamination, the majority of correct failures are detected and the degradation of the system can be clearly observed. In the case of medium contamination, the left graph shows that at 20% contamination, the probability of fault detection fluctuates at first, but increases rapidly after a certain point. The UA [W/K] value shows a steady decrease over time. In the right graph, the correct detections are marked in green and it can be seen that the correct detection rate is high after the onset of contamination. However, false detections are observed for some points. At 11% contamination, the left graph shows that the probability of fault detection increases at a later stage compared to 20% contamination. The UA [W/K] value shows a less pronounced downward trend. In the right graph, correct detections are again indicated by green areas. At this level, correct detections are still predominant, but due to the low contamination, the system takes longer to detect a fault. At low contamination level, the left graph shows that the probability of fault detection remains low for a long time and only increases significantly in the later stages of contamination. The UA [W/K] values are more stable. In the right graph, the correct detections for this low level of contamination are highlighted in green, and the failure detection process is delayed compared to the other levels as the system performance is not degraded much.

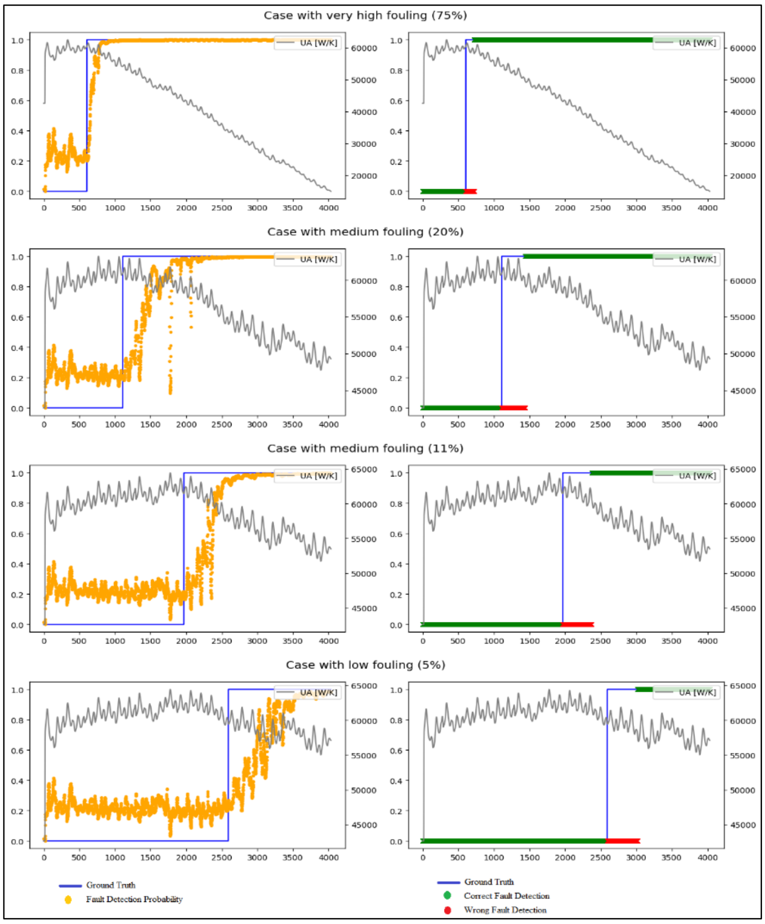

Figure 5: Analysis for different levels of substation contamination in DHC systems with XGBoost algorithm.
Source: Authors, (2024).

The AdaBoost model, a machine learning algorithm for the detection of substation contamination faults, achieved 91.3% accuracy and 82.6% Matthews correlation coefficient. Performance metrics such as model accuracy and Matthews correlation coefficient demonstrate the effectiveness of AdaBoost. In order to maximize the performance of the model, the hyperparameters were determined using the Grid Search Optimization method and the values are presented in Table 4. The confusion matrix of the Adaboost algorithm is shown in Figure 6. In addition, all performance metrics of the Adaboost algorithm are given in Table 6.

Table 4: Adaboost regression parameters.

Parameter	Value
Max_depth	5
Min_samples_leaf	5
Min_samples_split	10
n_estimators	250
Learning_rate	0.33
Random_state	5

Source: Authors, (2024).

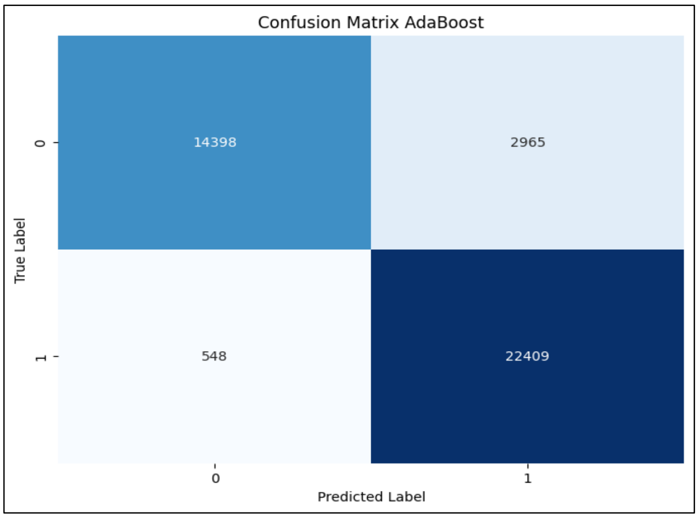

Figure 6: Adaoost regression confusion matrix.
Source: Authors, (2024).

Figure 7 shows the fault detection results for the Adaboost algorithm for different percentages of substation contamination levels. Very high contamination follows a curve with a very high probability of fault detection in the left-hand graph and a constant fault detection in a short time. There is a small difference between the onset of contamination and the point at which fault detection starts. The graph on the right shows that the system makes a correct detection in a very short time and there are almost no false detections. In the case of medium contamination, the probability of fault detection increases gradually and there is a steady detection trend after a value of about 1000. There is a slight delay in fault detection compared to the beginning of the contamination. The graph on the right shows that the system generally makes correct detections and there are few false detections. In the 11% contamination scenario, the probability of failure detection increases more slowly and stabilizes at a later time. This shows that the system is slower to detect lower contamination rates. The graph on the right shows that the correct detections are indicated by the green line and that these correct detections start later, as well as a few incorrect detections. At the lowest contamination level, the probability of fault detection increases significantly later and stabilizes over a longer period of time. This indicates that the system struggles to detect low contamination. The graph on the right shows that correct detections occur quite late and there are a relatively high number of false detections.

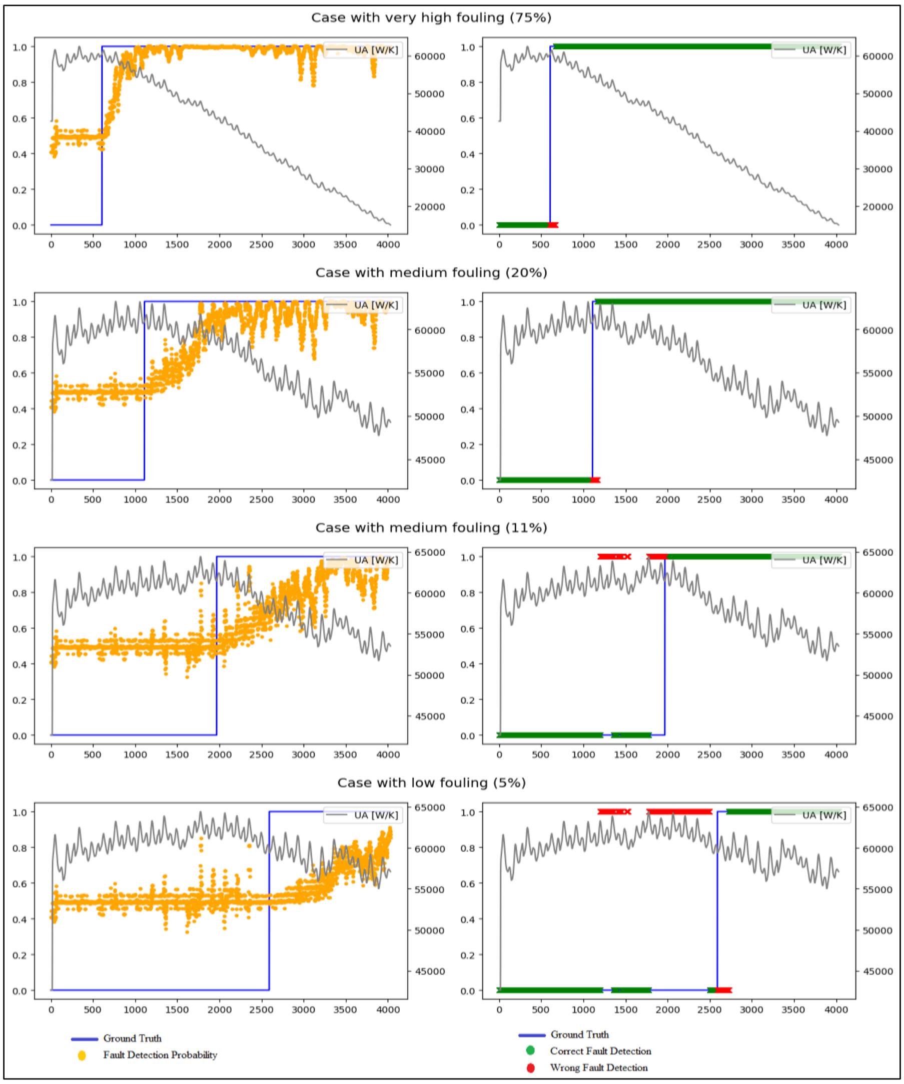

Figure.7: Analysis for different levels of substation contamination in DHC systems with Adaboost algorithm.
Source: Authors, (2024).

In the tests performed with the CNN algorithm, an accuracy rate of 97.2% and a Matthews correlation coefficient value of 94.4% were obtained.

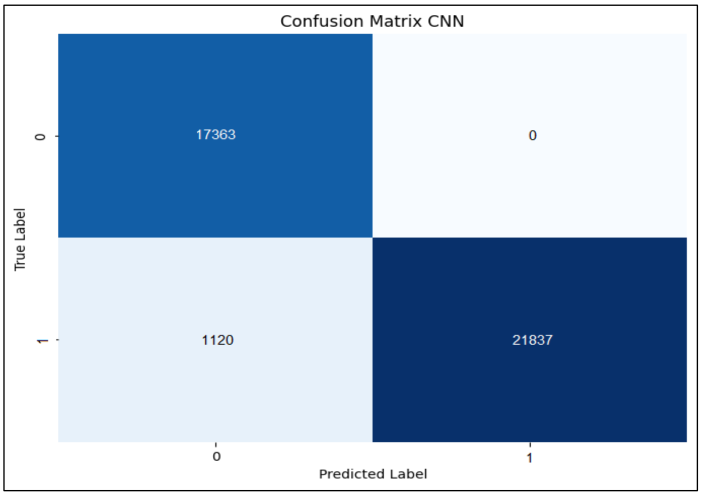

Figure 8: CNN algorithm confusion matrix.
Source: Authors, (2024).

A summary of the CNN model is given in Table 5. Figure 8 shows the confusion matrix of the CNN model. Table 6 shows the results obtained with the CNN algorithm.

Table 5: CNN model summary.

Layer	Output Shape	Param
dense	(None, 128)	1,280
batch_normalization)	(None, 128)	512
dropout	(None, 128)	0
dense	(None, 128)	16,512
batch_normalization	(None, 128)	512
dropout	(None, 128)	0
dense	(None, 64)	8,256
batch_normalization	(None, 64)	256
dropout	(None, 64)	0
dense	(None, 1)	65
Total params		**27,393**
Trainable params		**26,753**
Non-Trainable params		**640**

Source: Authors, (2024).

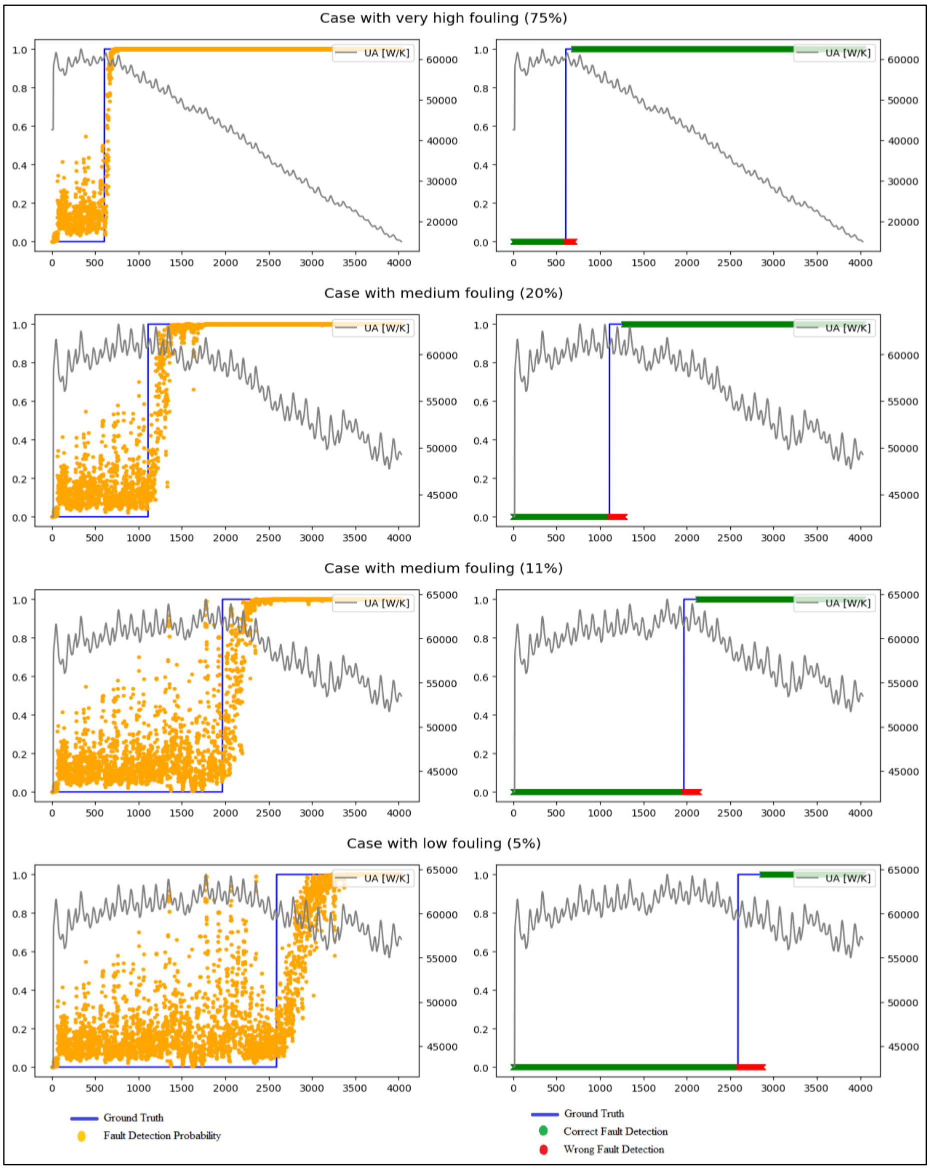

Figure 9: Analysis for different levels of substation contamination in DHC systems with CNN algorithm.
Source: Authors, (2024).

Figure 9 shows the fault detection results for the CNN algorithm for different percentages of substation contamination levels. In the case of very high levels of fouling, the graph on the left, the orange dots show the probabilities of fouling failure detection. The blue line shows the moment of actual fouling onset, while the gray line shows how the heat transfer coefficient (UA) value changes over time. Fouling was correctly detected with a high probability and at an early stage. In the graph on the right, the green and red horizontal lines represent correct and incorrect detections. The length of the green line indicates how long the model correctly detected contamination. In this case, the model has successfully detected very high contamination. The graph on the left shows that for medium contamination at 20%, the model made some incorrect detections but was generally correct. At the 11% contamination level, the detection success seems to be slightly lower, with a shorter green correct detection time and an increased number of incorrect detections. At the low contamination level, the model seems to have a lower probability of detection and a higher number of false detections. The blue line again shows the actual fouling time, while the gray line represents the heat transfer coefficient. In the graph on the right, the green correct detection line is quite short and the red false detection line is long. This indicates that the model struggles to detect the low fouling level.

In general, the graphs show that the accuracy and speed of fault detection varies depending on the contamination level. At very high contamination levels, the system makes fast and accurate detections, while at low contamination levels the detection time is longer and the number of false detections increases. This suggests that the system's ability to detect low levels of contamination is limited. These analyses highlight the importance of automatic fouling detection systems to improve the operational efficiency of DHC systems. Integrating systems with early warning mechanisms can play a critical role in saving energy and extending equipment lifetime.

Table 6: Comparison of algorithm results.

Algorithms	Accuracy	Matthews Corrcoef	Elapsed Time
KNN	86.4	72.3	67.55
XGBoost	96.1	92.0	26.96
AdaBoost	91.3	82.6	239.76
CNN Model	97.2	94.4	542.34

Source: Authors, (2024).

Table 6 shows the performance metrics of four different machine learning and deep learning algorithms for detecting substation contamination failures in District Heating and Cooling (DHC) systems. Accuracy, Matthews correlation coefficient (MCC) and Elapsed Time are evaluated for each algorithm. These metrics are important to understand the success and efficiency of the models in fault detection.

The KNN algorithm achieved 86.4% accuracy and 72.3% Matthews correlation coefficient. This shows that the model performs moderately well, but may misclassify some contamination cases. The KNN algorithm can perform well, especially when working with a small number of data points, but its performance may degrade with large datasets. The processing time was 67.55 seconds, which is a reasonable speed compared to other algorithms. The XGBoost algorithm performed very well with an accuracy of 96.1% and a Matthews correlation coefficient of 92.0%. These results show that XGBoost is capable of efficient classification and accurate detection at different contamination levels. Moreover, the processing time of the algorithm was very low at 26.96 seconds. The optimized nature of XGBoost makes it an effective option for users who want fast and accurate results.

The AdaBoost algorithm produced lower results than XGBoost, but better than KNN, with an accuracy of 91.3% and a Matthews correlation coefficient of 82.6%. AdaBoost uses the technique of strengthening weak classifiers to improve classification performance. Although it achieved a relatively high success rate, the processing time was considerably longer than the other algorithms at 239.76 seconds. This long processing time may limit AdaBoost's usefulness in scenarios with large datasets or fast results. The CNN model outperformed all other algorithms with the highest accuracy rate of 97.2% and the highest Matthews correlation coefficient of 94.4%. This high performance of the CNN model shows that deep learning models can work more effectively with large and complex datasets. However, the CNN model has the longest processing time of 542.34 seconds, indicating that the model requires high computational power and therefore runs for longer periods of time.

Comparing the performance of all algorithms, the CNN model gives the best results in terms of accuracy and Matthews correlation coefficient, but this superior performance is achieved at the cost of a longer processing time. XGBoost, on the other hand, produces almost as good results as CNN, but with a much shorter processing time, which makes it advantageous in practical applications. AdaBoost performs well in terms of accuracy, but is at a disadvantage in terms of processing time. The KNN algorithm, although one of the fastest algorithms, has lower accuracy and Matthews correlation coefficient compared to the other models. In conclusion, each algorithm offers different advantages and disadvantages in terms of accuracy, speed and computational cost.

V. CONCLUSIONS

In this study, various machine learning and deep learning algorithms are investigated for the detection of substation contamination faults in District Heating and Cooling (DHC) systems. The algorithms used include K-Nearest Neighbors (KNN), XGBoost, AdaBoost and Convolutional Neural Network (CNN) models. Contamination failures were analyzed at high, medium and low levels and hyperparameter optimization for the detection of these failures was performed by Grid Search method. The results show that the CNN model offers the best performance with 97.2% accuracy and 94.4% Matthews correlation coefficient. However, CNN has the longest processing time (542.34 seconds). XGBoost stood out as a fast and efficient alternative with 96.1% accuracy and short processing time (26.96 seconds). AdaBoost, despite having an accuracy of 91.3%, was quite slow with a processing time of 239.76 seconds. KNN, on the other hand, showed the lowest performance with an accuracy of 86.4%, and although it works fast, it is insufficient for complex data. In future studies, it is recommended to test these models on real-world datasets, optimize the processing time of CNN models, and investigate different types of failures more comprehensively.

VI. AUTHOR'S CONTRIBUTION

Conceptualization: Emrah Aslan and, Yıldırım Özüpak
Methodology: Emrah Aslan and, Yıldırım Özüpak
Investigation: Emrah Aslan and, Yıldırım Özüpak
Discussion of results: Emrah Aslan and, Yıldırım Özüpak
Writing – Original Draft: Emrah Aslan and, Yıldırım Özüpak
Supervision: Emrah Aslan and, Yıldırım Özüpak
Approval of the final text: Emrah Aslan and, Yıldırım Özüpak

VIII. REFERENCES

[1] Z. Ren, T. Lin, K. Feng, Y. Zhu, and Z. Liu, "A systematic review on imbalanced learning methods in intelligent fault diagnosis," IEEE Transactions on Instrumentation and Measurement, vol. 72, 2023. doi:10.1109/TIM.2023.3246470.

[2] L. Jin, D. K. Kim, K. Y. Chan, and A. Siada, "Deep Machine Learning-Based Asset Management Approach for Oil Immersed Power Transformers Using Dissolved Gas Analysis," IEEE Access, vol. 12, 2024. doi: 10.1109/ACCESS.2024.3366905.

[3] S. Zhou, Z. O'Neill, and C. O'Neill, "A review of leakage detection methods for district heating networks," Applied Thermal Engineering, vol. 137, pp. 567–574, 2018. doi: 10.1016/j.applthermaleng.2018.04.010.

[4] J. Zheng, Z. Zhou, J. Zhao, and J. Wang, "Effects of the operation regulation modes of district heating system on an integrated heat and power dispatch system for wind power integration," Applied Energy, vol. 230, pp. 1126–1139, 2018. doi: 10.1016/j.apenergy.2018.09.077.

[5] S. Månsson, I. L. Benzi, M. Thern, R. Salenbien, K. Sernhed, and P. J. Kallioniemi, "A taxonomy for labeling deviations in district heating customer data," Smart Energy, vol. 2, 2021. doi: https://doi.org/10.1016/j.segy.2021.100020

[6] Y. Wang, Q. Chen, T. Hong, and C. Kang, "Review of smart meter data analytics: Applications, methodologies, and challenges," IEEE Transactions on Smart Grid, vol. 10, no. 3, pp. 3125–3148, 2018. doi: 10.1109/TSG.2018.2818167

[7] D. Qu, W. Luo, Y. Liu, B. Fu, Y. Zhou, and F. Zhang, "Simulation and experimental study on the pump efficiency improvement of continuously variable transmission," Mechanism and Machine Theory, vol. 131, pp. 137–151, Jan. 2019. doi: https://doi.org/10.1016/j.mechmachtheory.2018.09.014.

[8] A. Rodler, S. Guernouti, M. Musy, and J. Bouyer, "Thermal behaviour of a building in its environment: Modelling, experimentation, and comparison," Energy and Buildings, vol. 168, pp. 19–34, Jun. 2018. doi: https://doi.org/10.1016/j.enbuild.2018.03.008.

[9] M. Jebamalai, K. Marlein, and J. Laverge, "Design and cost comparison of district heating and cooling (DHC) network configurations using ring topology – A case study," Energy, vol. 258, 2022, Art. no. 124777. [Online]. Available: https://doi.org/10.1016/j.energy.2022.124777.

[10] R. Patureau, C. T. Tran, V. Gavan, and P. Stabat, "The new generation of District heating & cooling networks and their potential development in France," Energy, vol. 236, 2021, Art. no. 121477. [Online]. Available: https://doi.org/10.1016/j.energy.2021.121477.

[11] A. S. Gaur, D. Z. Fitiwi, and J. Curtis, "Heat pumps and our low-carbon future: A comprehensive review," Energy Research & Social Science, vol. 71, 2021, Art. no. 101764. [Online]. Available: https://doi.org/10.1016/j.erss.2020.101764.

[12] S. Buffa, M. Cozzini, M. D'Antoni, M. Baratieri, and R. Fedrizzi, "5th generation district heating and cooling systems: A review of existing cases in Europe," Renewable and Sustainable Energy Reviews, vol. 104, pp. 504-522, 2019. [Online]. Available: https://doi.org/10.1016/j.rser.2018.12.059.

[13] V. Munćan, I. Mujan, D. Macura, and A. S. Anđelković, "The state of district heating and cooling in Europe - A literature-based assessment," Energy, vol. 304, 2024, Art. no. 132191. [Online]. Available: https://doi.org/10.1016/j.energy.2024.132191.

[14] K. Gjoka, B. Rismanchi, and R. H. Crawford, "Fifth-generation district heating and cooling: Opportunities and implementation challenges in a mild climate," Energy, vol. 286, 2024, Art. no. 129525. [Online]. Available: https://doi.org/10.1016/j.energy.2023.129525.

[15] Y. Zhang, M. Liu, Z. O'Neill, and J. Wen, "Temperature control strategies for fifth generation district heating and cooling systems: A review and case study," Applied Energy, vol. 376, Part A, 2024, Art. no. 124156. [Online]. Available: https://doi.org/10.1016/j.apenergy.2024.124156.

[16] K. Autelitano, J. Famiglietti, M. Aprile, and M. Motta, "Towards Life Cycle Assessment for the Environmental Evaluation of District Heating and Cooling: A Critical Review," Standards, vol. 4, no. 3, pp. 102-132, 2024. [Online]. Available: https://doi.org/10.3390/standards4030007.

[17] A. J. Patil, R. Naresh, R. K. Jarial, and H. Malik, "Optimized Synthetic Data Integration with Transformer's DGA Data for Improved ML-based Fault Identification," IEEE Transactions on Dielectrics and Electrical Insulation, 2024. doi: 10.1109/TDEI.2024.3421915.

[18] M. Vallee, T. Wissocq, Y. Gaoua, and N. Lamaison, "Generation and evaluation of a synthetic dataset to improve fault detection in district heating and cooling systems," Energy, vol. 283, p. 128387, 2023. doi: 10.1016/j.energy.2023.128387.

[19] S. Buffa, M. H. Fouladfar, G. Franchini, I. Lozano Gabarre, and M. Andrés Chicote, "Advanced Control and Fault Detection Strategies for District Heating and Cooling Systems—A Review," Applied Sciences, vol. 11, p. 455, 2021. doi: 10.3390/app11010455.

[20] P. Xue, Y. Jiang, Z. Zhou, X. Chen, X. Fang, and J. Liu, "Machine learning-based leakage fault detection for district heating networks," Energy and Buildings, vol. 223, p. 110161, 2020. doi: 10.1016/j.enbuild.2020.110161.

[21] S. Månsson, P.-O. J. Kallioniemi, K. Sernhed, and M. Thern, "A machine learning approach to fault detection in district heating substations," Energy Procedia, vol. 149, pp. 226-235, 2018. doi: 10.1016/j.egypro.2018.08.187.

[22] D. Leiria, K. H. Andersen, S. P. Melgaard, H. Johra, A. Marszal-Pomianowska, M. S. Piscitelli, A. Capozzoli, and M. Z. Pomianowski, "Towards automated fault detection and diagnosis in district heating customers: generation and analysis of a labeled dataset with ground truth," in Proceedings of Building Simulation 2023: 18th Conference of IBPSA. doi: https://doi.org/10.26868/25222708.2023.1576.

[23] F. Theusch, P. Klein, R. Bergmann, W. Wilke, W. Bock, and A. Weber, "Fault Detection and Condition Monitoring in District Heating Using Smart Meter Data," PHM Society European Conference, vol. 6, no. 1, p. 11, 2021. doi: 10.36001/phme.2021.v6i1.2786.

[24] M. Li, W. Deng, K. Xiahou, T. Ji, and Q. Wu, "A Data-Driven Method for Fault Detection and Isolation of the Integrated Energy-Based District Heating System," IEEE Access, vol. 8, pp. 23787-23801, 2020. doi: 10.1109/ACCESS.2020.2970273.

[25] P. Xue, Y. Jiang, Z. Zhou, X. Chen, X. Fang, and J. Liu, "Machine learning-based leakage fault detection for district heating networks," Energy and Buildings, vol. 223, p. 110161, 2020. doi: 10.1016/j.enbuild.2020.110161.

[26] M.Valle, "DHC substation fouling - synthetic faults," Kaggle, 2022. [Online]. Available: https://www.kaggle.com/datasets/mathieuvallee/ai-dhc-substation-fouling/data. Accessed: July. 29, 2024.

[27] B. Said, L. Mazouz, T. NAAS, Özüpak Yildirim, and R. Mohammedi, "Broken magnets fault detection in pmsm using a convolutional neural network and SVM", JETIA, vol. 10, no. 48, pp. 55-62, Jul. 2024. doi: https://doi.org/10.5935/jetia.v10i48.1185.

[28] P. Dimri, A. Nath, and P. Dimri, "Flood prediction and management", JETIA, vol. 10, no. 47, pp. 95-103, Jul. 2024. doi: https://doi.org/10.5935/jetia.v10i47.1103.

[29] E. Aslan, "Temperature prediction and performance comparison of permanent magnet synchronous motors using different machine learning techniques for early failure detection," Eksploatacja i Niezawodność – Maintenance and Reliability, 2024. doi: https://doi.org/10.17531/ein/192164.

[30] S. Gonjari, R. Pawar, R. Pawar, S. Kshirsagar, and R. Kokare, "Real time emotion recognition and classification for diverse suggestions using Deep Learning", JETIA, vol. 10, no. 48, pp. 14-20, Jul. 2024. doi :https://doi.org/10.5935/jetia.v10i48.1007.

Journal of Engineering and Technology for Industrial Applications

ITEGAM-JETIA

Manaus, v10. n.50, p. 33-38. November/ December., 2024.
DOI: https://doi.org/10.5935/jetia.v10i50.1292

ISSN ONLINE: 2447-0228

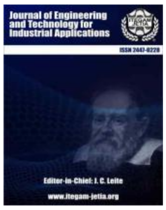

RESEARCH ARTICLE OPEN ACCESS

TECHNO-ECONOMIC EVALUATION OF RICE HUSK CO-FIRING AS A SUSTAINABLE BIOMASS FUEL ALTERNATIVE

[1]Samsurizal, [2]Revi Falka Azlinando and [3]Arif Nur Afandi

[1,2] Electrical Engineering, Institut Teknologi PLN. Jakarta, Indonesia
[3] Department of Electrical Engineering and Informatics, Faculty of Engineering. Malang, Indonesia

[1] https://orcid.org/0009-0001-2789-2876, [2]https://orcid.org/0000-0001-5852-3910 [3] https://orcid.org/0000-0001-9019-810X

Email: samsurizal@itpln.ac.id, revi1911195@itpln.ac.id an.afandi@um.ac.id

ARTICLE INFO

Article History
Received: October 02, 2024
Revised: November 6, 2024
Accepted: November 10, 2024
Published: November 30, 2024

Keywords:
Co-firing technology,
Rice husk biomass,
Power plant efficiency,
Renewable energy.

ABSTRACT

Co-firing is a technology that blends coal with biomass at a specific ratio in steam power plants. In the Lontar area, which is surrounded by vast rice fields, there is significant potential to utilize rice husk waste as a biomass feedstock. The aim of this design is to reduce Indonesia's dependence on coal, which is considered a non-renewable energy source, while promoting the transition to renewable energy. As coal consumption continues to rise each year, this research explores the potential to reduce coal usage by co-firing it with rice husk biomass. The co-firing design implements a biomass blending ratio of 2-5% with coal. The study's results indicate that, on average, only 0.608 kg of fuel is needed to generate 1 kWh of electricity. Additionally, the Net Plant Heat Rate achieved is 2,557.5 kcal/kWh, which, when compared to non-co-firing values, demonstrates an improvement in the power plant's efficiency. From an economic perspective, the power plant in the Lontar area could save fuel costs amounting to Rp 9.24 billion over a four-month period, with the average production cost of co-firing being only Rp 346.77/kWh. Based on these technical and economic results, the co-firing design is deemed feasible and promising for further implementation in the coming years.

I. INTRODUCTION

Steam Power Plants are one of the main energy sources in Indonesia that uses coal as the main fuel. With the growing awareness of the negative impact of coal on the environment, governments and researchers are looking for more environmentally friendly alternatives. One of the technologies that can be applied is co-firing technology. This technology allows the mixing of coal with biomass, such as agricultural waste, to reduce the use of coal as a non-renewable energy source [1].

Co-firing technology has great potential in areas such as Lontar, which are surrounded by large rice fields. This area produces abundant rice husk waste, which can be used as biomass for mixing with coal. By conducting co-firing, it is hoped that the use of coal can be significantly reduced, as well as provide economic and environmental benefits [2]. In the long term, this technology is one of the strategies to support the transition to new and renewable energy.

Currently, coal consumption in Indonesia continues to increase every year, so real efforts are needed to reduce dependence on coal [3]. One of them is by developing co-firing technology that utilizes rice husk biomass, which not only reduces carbon emissions, but also has the potential to improve the efficiency of power plants. The efficiency resulting from the application of co-firing can be seen from the savings in fuel consumption as well as lower electricity production costs.

With the growing urgency of the need for clean and efficient energy, co-firing technology shows that it is technically and economically feasible to be applied more widely. This opens up opportunities to increase the role of biomass in the national energy mix, while reducing the negative environmental impact of coal burning.

Applying coal-biomass co-firing power generation is the strategy to accelerate the renewable energy share in the energy mix to reach 23% by 2025. Although biomass co-firing trials have been carried out at several Coal-Fired Power Plants (CFPP), the potential for implementing biomass co-firing on a larger scale and for the long-term propose still needs to be identified [4].

In the National Electricity General Plan, PLN plans to implement Co-firing in 52 units (Steam Power Plants) [5]. Co-firing is the substitution of coal in a certain ratio with biomass materials such as wood pellets, palm shells and sawdust. In 2024, it is estimated that the total Co-firing capacity at electric steam power plant PLN will reach 18 GW. The Co-firing plan is aimed at supporting the development of NRE in Indonesia. By implementing Co-firing, the use of NRE can be carried out quickly without the need for the construction of new generators.

II. THEORETICAL REFERENCE

Biomass energy has great potential to help reduce dependence on fossil fuels, reduce greenhouse gas emissions, and promote energy sustainability. However, the utilization of biomass energy also requires careful management to ensure that its production and use do not result in negative consequences for the environment and sustainability.

There are types of solid biomass, including agricultural waste: Agricultural waste such as straw, rice husks, corn husks, and corn cobs are examples of solid biomass produced from agricultural processes. This waste can be used as fuel in the combustion process to generate heat or electricity. In addition, there are also types of wood chips, sawdust, wood fibers, and small pieces of wood are other examples of solid biomass that is often used in industry as fuel or raw materials. In addition, Plant Fibers: Plant fibers such as straw, bamboo, or coconut fiber can also be used as solid biomass for a variety of applications, including the manufacture of building materials and combustion as fuel.

Co-firing coal-fired power plants is a term that refers to the use of biomass fuels along with conventional fuels, such as coal, in the combustion operations of Steam Power Plants. This process aims to reduce dependence on fossil fuels, reduce greenhouse gas emissions, and improve sustainability and energy efficiency.

In coal-fired power plants, biomass fuels such as rice husks, sawdust, straw, agricultural waste, or other biomass are mixed and burned together with conventional fuels in the coal-fired power plant's incinerator. Co-firing technology has become quite popular technology in an effort to reduce the environmental impact of power plants and achieve energy sustainability goals.

Rice husk waste is a considerable waste generated in the agricultural industry, which is 20% of rice. The rice husk produced by Indonesia can reach around 15 million tons per year [6]. Rice husk is a waste product of rice milling that is separate from the grain of rice, where the rice husk has a hard layer, namely kariopsis which consists of two leaf shapes, namely crown husk and petal husk. Rice husks can be found in rural areas, as a by-product of rice milling which has a lot of potential. Rice husks are not flammable outdoors unless air is blown into them. Rice husks are highly resistant to moisture and decay by fungi, which makes it difficult for rice husks to decompose naturally. If the rice husk goes through the combustion process, it will produce rice husk ash. The density of rice husk tends to be low, namely 70-110 kg/m³, at the time of shaking, it is 145 kg/m³ or 180 kg/m³ in the form of briquettes or pellets. Therefore, rice husks require a large volume for storage and transportation, so long-distance transportation becomes uneconomical. The ash content obtained when rice husks are burned is 17-26%, much higher than other fuels (wood 0.2-2%, coal 12.2%). The caloric value of rice husks is high with an average of 3410 kcal/kg and can be used as one of the sources of renewable energy.

There are several studies that discuss the use of rice husks as co-firing. Ríos-Badrá et al., The research is focused on the properties and physical and chemical characteristics of husk pellets as well as efforts to improve the quality of husk pellets by using a mixture of husk with other materials such as the addition of husk charcoal, used cooking oil and others [7].

The energetic potential of the briquette with a standard mesh size of babassu coconut and rice. Mulch layer bagasse of the babassu mesocarp combined with rice straw powder was used. Both particle size and ash content were evaluated. The results show that there is a viability in the use of the briquette of 50% babassu and 50% rice straw. From this work can be raised questions about how other waste can be availed, generating new research on biomass [8].

Susanto, et.al., In his study, the results of the comparison of mixing sub-bituminous coal biopellets and rice husks in portable boilers with variations of 100%:0%, 95%:5%, 85%:15% showed that the highest data was found in sub-bituminous coal fuel. without a mixture of rice husk biopellets that produce a load of 17 watts with voltage parameters of 265 V, current of 1.17 A, temperature of 456HAIC and turbine rotation of 718 RPM. Sub-bituminous coal fuel with the mixing of rice husk biopellets with a ratio of 95%:5% with a load of 17 watts produces a voltage of 257 V, a current of 0.83 A, where the temperature produced in the ratio is 452HAIC and the turbine rotation is 664 RPM [9].

Meanwhile, Muniroh, et.al., discussed the Business Model Canvas and Business Strategy of BUMD Rice Husk PT Gerbang NTB Emas as a Co-Firing Material for Renewable Electrical Energy. The results of the study provide an overview of the nine elementts of BMC and the formulation of the rice husk business strategy of PT Gerbang NTB Emas. In addition, there is a need for a strategy to overcome the Business Model Canvas on customer segment, channel and customer relationship elements to support the success of PT Gerbang NTB Emas' rice husk business [10].

In this study, the physical properties and optimization of briquettes made from rice husk and sawdust were carried out. The bio-waste material of homogeneous particle sizes of 0.5mm and two binders of 90:10 percentage compositions which were sun-dried, prepared and compressed for the production of the briquettes. Energy valuation of the briquettes was carried out using a bomb Calorimeter. he results indicated that composite briquettes of mahogany sawdust and rice husk produced using starch gave the maximum energy value of 5.69kcal/g whereas those made with clay gave the least calorific value of 3.35kcal/g. This indicates that briquette from a composite of Mahogany sawdust/rice husk is, as a result, more appropriate for starting and retaining the fire for cooking and other domestic heating [11].

III. METHODOLOGY

In this article, the methods used in this study are qualitative and quantitative descriptive based on literature review. The literature review information on the analysis of the use of rice husk waste used comes from journals/scientific articles/books related to the same topic. The discussion of the study began by examining the origin of rice husk waste and its waste characteristics. Then continued with a study on the processing and utilization of rice husk waste based on the data that had been obtained in the previous study. Collection of data on boiler equipment operating parameters and other supporting data (data for NPHR and SFC calculations). Data collection was carried out before Co-firing and during the Co-firing process. Finally, the data that has been obtained from the joint literature review will be drawn into a conclusion of the analysis of the utilization of rice husk waste so that an informative data unit is obtained.

To determine the effect of biomass co-firing on production costs, a comparison of SFC and production costs was carried out when using coal and during co-firing. For the calculation of

Specific Fuel Consumption (kg/kWh) is obtained using the equation.

$$SFC = \frac{\text{Total Fuel}}{\text{Awakened kWh}} \quad (1)$$

NPHR (Net Plant Heat Rate) is an indicator of the reliability and efficiency of a thermal plant, especially coal-fired power plants. The smaller the NPHR value, the more efficient the coal-fired power plant is declared and vice versa. For the calculation of NPHR can use the equation:

$$NPHR = \frac{\text{Fuel Consumption} \times \text{Calorie Value}}{\text{Gen.output} - \text{Aux. power}} \quad (2)$$

To calculate the use of production costs so that they can be used as a comparative parameter for non-cofiring and co-firing, the equation.

$$\text{Production cost} = \text{Fuel Prices} \times SFC \quad (3)$$

Next, the NPHR and SFC calculations are carried out using the data that has been taken, after the calculation is completed, the data comparison process is carried out.

Data comparison is to compare data before Co-firing and after Co-firing which results in the form of deviation values in each co-firing process. The data that is compared are the operating parameters of boiler equipment during commissioning with the current (full coal and co-firing) The results of SFC and NPHR calculations are compared between full coal and Co-firing.

IV. RESULTS AND DISCUSSIONS

There is one steam power plant in the Lontar area, which uses rice husk biomass as a method of mixing coal fuel or so-called co-firing in order to carry out the government's program in 2021 as new and renewable energy (NRE) which is targeted in 2024 of 18 GW by using a biomass portion of 2%-5% biomass mixed with coal. This co-firing is carried out in the context of Renewable energy efforts which is a general plan for national electricity with co-firing is expected to help the target that is the purpose of this plan. The co-firing is carried out using a direct co-firing scheme where biomass is mixed directly with coal before the combustion process or put into a coal feeder. The implementation of Co-firing is carried out from the data obtained is that for a period of 4 months from January-April 2024, PLTU Lontar has 3 Power Generation Units where from the data obtained every month the implementation of co-firing is carried out alternately, this happens because of the availability of rice husk biomass fuel and the rules for the implementation of co-firing are carried out only up to 5% of the total biomass used.

Specific Fuel Consumption (SFC)

The SFC calculation is carried out to be able to find out the SFC value of how many Kg is needed to produce one kWh in a coal-fired power plant. Specific Fuel Consumption non-cofiring and cofiring for the period of January-April 2024, the dataused is one month of production where the total of 4 months of production is made per hour with the total data divided by 30 days and 24 hours, from the data obtained to be assumed the use of co-firing for 1 full month, for that the SFC calculation uses equation (1) which uses hourly parameters, Here's the equation (1).

Table 1: Data non-cofiring.

Moon	Total Fuel (Kg)	Awakened (kWh)
January	171,709.82	272,926.45
February	168,303.32	259,742.30
March	162,693.43	269,789.23
April	161,649.71	253,684.62

Source: Authors, (2024).

Using the data in the table, the Specific Fuel Consumption (SFC) value can be calculated using equation 1. Results of the calculation of Specific Fuel Consumption in January.

$$SFC = \frac{171{,}709.82}{272{,}926.45} = 0.629\ Kg/kWh$$

In the same way, the results of the calculation of the non-cofiring full consumption species for the period of January – April were obtained as shown in Table 1.

Table 2: Non-cofiring SFC calculation results.

Bulan	SFC (Kg/kWh)
January	0.629
February	0.647
March	0.603
April	0.637

Source: Authors, (2024).

The non-co-firing SFC value in Table 2 is influenced by the quality of coal fuel and the load conditions that must be accommodated by the coal-fired power plant, the lower the SFC value, the more efficient the fuel used. It can be seen that the SFC value from January to April has fluctuated although not significantly at only 0.6 kg/kWh, but this value has a great influence on the calculation of the production cost of a coal-fired power plant.

Furthermore, when using the husks in the data in Table 3 used Specific Fuel Consumption co-firing

Table 3: Data co-firing.

Moon	Total Fuel (Kg)	Awakened (kWh)
January	171,709.82	285,260.53
February	168,303.32	263,059.08
March	162,693.43	284,690.17
April	161,649.71	258,941.45

Source: Authors, (2024).

Using the data in Table 3, the value of Specific Fuel Consumption (SFC) co-firing can be calculated using equation 1. Co-firing coal with a percentage of 2%, 4%, and 5% biomass mixed with the direct co-firing method, the direct co-firing method is by mixing coal directly with rice husk biomass that has been sorted before the fuel enters the coal feeder. The results of the calculation of the Specific Fuel Consumption co-firing in January.

$$SFC = \frac{171{,}709.82}{285{,}260.53} = 0.601\ Kg/kWh$$

By using the same method, the results of the calculation of the Species full consumtion co-firing period for the period of January – April were obtained as shown in Table 4.

Table 4: SFC co-firing calculation results

Moon	SFC (Kg/kWh)
January	0.601
February	0.630
March	0.571
April	0.624

Source: Authors, (2024).

The data obtained by using 4% co-firing in January was 0.601 Kg/kWh, 5% co-firing in February was 0.639 Kg/kWh, 5% in March was 0.571 Kg/kWh, and 2% co-firing in April was 0.624 Kg/kWh can be compared with non-cofiring data, the less fuel used (Kg) is used to produce per kWh.

Net Plant Heat Rate (NPHR)

Net Plant Heat Rate is an indicator of the reliability and efficiency of a thermal plant, especially in coal-fired power plants. The result of the NPHR value is in the form of kcal/kWh assuming the use of co-firing for 1 month where how many calories are needed to produce one kWh, the smaller the NPHR value, the more efficient the coal-fired power plant is stated to be more efficient and vice versa (Table 5).

Tabel 5: Net Plant Heat Rate data with full coal.

Bulan	Bahan bakar (Kg)	Nilai Kalori (kcal)	Gen. output (MW)	Aux. Power (MW)
January	171,709.82	4594.00	267.47	13.33
February	168,303.32	4680.41	282.89	13.15
March	162,693.43	4665.53	288.62	13.50
April	161,649.71	4543.22	292.19	13.37

Source: Authors, (2024).

The calculation of NPHR looks at the burning hours with the parameters of coal consumption (Kg), the value of calories produced during combustion time (kcal/kg), generator output and aux power or self-use. The calculation uses equation 2. NPHR in January 2024.

$$NPHR = \frac{171709.82 \times 4590.00}{267.47 - 13.33} = 3{,}101.2 \text{ kcal/kWh}$$

With the same calculation, the NPHR value presented in table 6 is obtained.

Table 6: results of non-cofiring NPHR calculation.

Moon	NPHR kcal/kWh
January	3101.23
February	2945.33
March	2758.98
April	2633,99

Source: Authors, (2024).

The results of the NPHR calculation with fuel parameters (Kg), calorie value (kcal), generator output (MW) and self-use or aux power (MW) produce a kcal/kWh value in Table 6 shows that in January it is 3101.23 kcal/kWh which means that 3101.23 kcal is needed to produce 1 kWh, the MW calculation is changed to kW and subtracted by self-use, in February the NPHR value is obtained of 2945.33 kcal/kWh by using fuel lower than In January, in March 2024 the NPHR value was 2758.98 kcal/kWh with the use of fuel lower than in February, and in April it was produced from the calculation of the NPHR value of 2633.99 kcal/kWh which means that the NPHR value decreases every month, this value is also influenced by the fuel used and the amount of fuel recorded.

Meanwhile, the NPHR value with co-firing is obtained from the data presented in Table 7.

Table 7: net plant heat rate data with co-firing.

Moon	Bahan bakar (Kg)	Nilai Kalori (kcal)	Gen. output (MW)	Aux. Power (MW)
January	171,709.82	4213.98	267.47	13.33
February	168,303.32	4212.55	282.89	13.15
March	162,693.43	4132.23	288.62	13.50
April	161,649.71	4126.43	292.19	13.37

Source: Authors, (2024).

The data obtained is data that is recapped for 1 month for fuel consumption into /30 days and divided by 24 hours with the data obtained. The calculation of NPHR at the percentage of 1-5% mixing biomass with coal is calculated using the following equation 2:

NPHR in January 2024

$$NPHR = \frac{171{,}709.82 \times 4213.98}{267.47 - 13.33} = 2847.17 \text{ kcal/kWh}$$

The value obtained from the calculation will be compared with non-co-firing data, with the statement that the smaller the NPHR value, the more efficient a coal-fired power plant will be to produce 1 kWh. The following results of the NPHR calculation are shown in Table 8.

Table 8: Net Plant Heat Rate co-firing results.

Moon	NPHR (kcal/kWh)
January	2847.17
February	2628.28
March	2443.61
April	2392.34

Source: Authors, (2024).

Obtained from table 8 of 2847.17kcal/kWh for the month of January so per 1 kWh requires 2847.17 kcal needed to generate per kWh, in February the NPHR data of 2628.61 kcal/kWh this value is smaller than the value in January, in March the value obtained is also lower than the previous month with a value of 2443.61 kcal/kWh as well as in April where the NPHR value is lower than the month previously it was 2392.24, the NPHR value obtained from the calculation will be compared with non-cofiring data, with the statement that the smaller the NPHR value, the more efficient a coal-fired power plant will be to produce 1 kWh.

Cofiring and Non Co-firing

After obtaining the results of the SFC and NPHR calculations by comparing co-firing and non-co-firing assuming the use of 1 month of co-firing, this comparison was made in order to see the difference between SFC co-firing and non-co-firing as well as NPHR co-firing and non-co-firing, seeing how the comparison of the two parameters is shown in Table 9 and Table 10.

Table 9: *SFC* Co-firing and Non Co-firing.

Nilai SFC	January (Kg/kWh)	February (Kg/kWh)	March (Kg/kWh)	April (Kg/kWh)
Non Co-firing	0.629	0.647	0.603	0.637
Co-firing	0.601	0.639	0.571	0.0624

Source: Authors, (2024).

The results of the value in Table 9 can be said that SFC Co-firing is lower than the value of non-co-firing SFC, which means that the value of SFC Co-firing is better because it only requires a low value to produce 1 kWh.

Table 10: *NPHR* Co-firing and Non Co-firing.

Nilai NPHR	January (kcal/kWh)	February (kcal/kWh)	March (kcal/kWh)	April (kcal/kWh)
Non Co-firing	3101.23	2945.33	2758.98	2633.99
Co-firing	2847.17	2628.28	2443.61	2392.34

Source: Authors, (2024).

The results of the NPHR comparison in Table10, that with a lower co-firing value which means more efficient because it only requires a small amount of kcal needed to produce 1 kWh where the lower the NPHR value the better, the co-firing value and the non-co-firing value are compared with each other to see how much kcal it takes to produce 1 kWh.

Production Cost

The total cost incurred for coal and the calculation of production costs using equation 3. With the production cost of a sample of the January production as follows:

$$\text{Production cost} = \text{Rp}.1052{,}33 \times 0{,}629 = 661.91\ \text{Rp/kWh}$$

For the production cost with non-co-firing SFC requires Rp.661.91 per kWh, the results of the calculation are shown in Table 11 as follows.

Table 11: Coal Production Costs.

Moon	SFC (Kg/kWh)	Coal Fuel Prices (Rp)	Production Cost (Rp/kWh)
January	0.629	1052.33	661.91
February	0.6470	1052.33	680,85
March	0.603	1052.33	634,55
April	0.637	1052.33	670,33

Source: Authors, (2024).

Meanwhile, the cost of co-firing production which is the total cost incurred for coal and the calculation of production costs uses equation 3. The calculation for January is as follows:

$$\text{Production cost} = \text{Rp}.570.58 \times 0{,}601 = 342.91\ \text{Rp/kWh}$$

For the production cost with non-co-firing SFC requires Rp.342.91 per kWh, the results of the calculation are shown in table 12 as follows.

Table 12: Biomass Production Costs

Moon	SFC (Kg/kWh)	Coal Fuel Prices (Rp)	Production Cost (Rp/kWh)
January	0.601	570.58	342,91
February	0.639	570.58	364,60
March	0.571	570.58	325,80
April	0.624	570.58	356,04

Source: Authors, (2024).

Based on the results in Table 12, the calculation of SFC co-firing with a biomass price of Rp 570.58 per kg shows that the average cost required for producing 1 kWh is Rp 350.00. Without co-firing, the production cost in January amounted to Rp 135,948,091,753.98, while with co-firing, it was reduced to Rp 70,429,454,371.98. This indicates a cost reduction of nearly 50% when compared to using coal alone. In February, it is estimated that the monthly production cost was Rp 128,954,719,359.00, whereas the co-firing production cost was only Rp 69,056,166,084.00. Similarly, in March, the production cost without co-firing was Rp 130,068,104,586.00 compared to Rp 66,781,480,536.00 with co-firing. In April, the production cost without co-firing reached Rp 124,974,879,968.52, while the co-firing production cost was Rp 66,379,329,977.76. From these assumptions, it is concluded that using co-firing for one month can significantly reduce production costs.

V. CONCLUSIONS

Co-firing technology, which mixes coal with biomass such as rice husks, has the potential to reduce coal use in coal-fired power plants (PLTU) in Indonesia. In the Lontar area, which has a lot of rice husk waste, this co-firing design aims to support renewable energy and reduce dependence on coal.

The use of a mixture of 2-5% biomass showed an increase in PLTU efficiency, with significant fuel cost savings of IDR 9.24 billion in 4 months, and an average production cost of IDR 346.77/kWh. Therefore, from an economic and technical perspective, co-firing is worth continuing in the future.

VI. AUTHOR'S CONTRIBUTION

Conceptualization: Samsurizal, Revi Falka Azlinando and Arif Nur Afandi.
Investigation: Revi Falka Azlinando and Samsurizal.
Discussion of results: Samsurizal, Revi Falka Azlinando and Arif Nur Afandi.
Methodology: Samsurizal, Revi Falka Azlinando and Arif Nur Afandi.
Writing – Original Draft: Samsurizal, Revi Falka Azlinando and Arif Nur Afandi.
Writing – Review and Editing: Samsurizal, Revi Falka Azlinando and Arif Nur Afandi.
Supervision: Samsurizal and Arif Nur Afandi.
Approval of the final text: Samsurizal and Arif Nur Afandi.

VII. ACKNOWLEDGMENTS

The author would like to express his gratitude to all parties, starting from data collection and data processing so that this article can be compiled. Hopefully this article is useful and useful as learning material.

VIII. REFERENCES

[1] Sudarmadji, D. " Utilization of Rice Husk as Biomass in Co-Firing Technology," in Prosiding Seminar Nasional Energi. 10(1), 100-110., 2019.

[2] Darmawan, A., & Wibowo, S. "Implementation of Co-Firing Technology in PLTU: Case Study of PLTU Lontar," Journal of New and Renewable Energy, pp. 145-152, 2021.

[3] Ministry of Energy and Mineral Resources (ESDM), "Indonesia Renewable Energy Annual Report.," Ministry of ESDM, Jakarta, 2020.

[4] Triani, M., Tanbar, F., Cahyo, N., Sitanggang, R., Sumiarsa, D., & Utama, G. L. "The Potential Implementation of Biomass Co-firing with Coal in Power Plant on Emission and Economic Aspects: A Review," EXACT: Journal of Sciences and Data Analytics, vol. 3, no. 2, 2022.

[5] Ministry of Energy and Mineral Resources, "Co-firing Plan at PLTU," in the Ministry of Energy and Mineral Resources, Jakarta, 2021.

[6] E. Pramono, ""Straw and Rice Husk Waste Has the Potential to Become Alternative Fuel - Faculty of Agriculture and Animal Husbandry,"," 2022. [Online]. Available: https://fpp.umko.ac.id/2022/03/18/limbah-jerami-dan-sekam-padi-berpotensi-jadi-bahan-bakar-alternatif/.

[7] Ríos-Badrán, I. M., Luzardo-Ocampo, I., García-Trejo, J. F., Santos-Cruz, J., & Gutiérrez-Antonio, C. "Production and characterization of fuel pellets from rice husk and wheat straw," Renewable Energi, vol. 145, p. 500–507, 2020. https://doi.org/10.1016/J.RENENE.2019.06.048

[8] Silva, M., Lima, F., Soares, F., Caselli, F., & Costa, J., "Analysis of the Babassu as a source of biomass for the production of Briquettes in the Mid-North Region of Brazil," ITEGAM-JETIA, vol. 4, no. 14, pp. 51-56, 2018. https://doi.org/10.5935/2447-0228.201829

[9] Susanto, U., & Surjosatyo, A. "Analysis of Rice Husk Pellet Combustion Test for Co-Firing in Coal Crusher (PC) Boiler," International Journal of Business Engineering and Social Sciences, pp. 387-400, 2023.

[10] Muniroh, N. A., & Aminah, M. "Business Model Canvas and Rice Husk Business Strategy of BUMD PT Gerbang NTB Emas as Co-Firing Material for Renewable Electrical Energy," MANAJEMEN IKM: Jurnal Manajemen Pengembangan Industri Kecil Menengah, vol. 16, no. 1, pp. 38-52, 2021.

[11] Chukwuneke, J., Umeji, A., Obika, E., & Fakiyesi, O., "Optimization of composite briquette made from sawdust/rice husk using starch and clay binder. International Journal of Integrated Engineering," International Journal of Integrated Engineering, vol. 13, no. 4, pp. 208-16, 2021.

Journal of Engineering and Technology for Industrial Applications

ISSN ONLINE: 2447-0228

ITEGAM-JETIA

Manaus, v10. n.50, p. 39-44. November/ December., 2024.
DOI: https://doi.org/10.5935/jetia.v10i50.1293

RESEARCH ARTICLE OPEN ACCESS

EVALUATING PRODUCTIVITY AND COSTS OF CONCRETE CASTING FOR STRUCTURAL ELEMENTS

Fendi Hary Yanto[1,]

[1] Civil Engineering, Faculty of Vocational School Sebelas Maret University, Jalan Kolonel Sutarto Nomor 150K, Jebres, Surakarta City, Central Java 57126, Indonesia.

[1]http://orcid.org/0000- 0001-9316-4538.

Email: fendi@staff.uns.ac.id

ARTICLE INFO

Article History
Received: September 14, 2024
Revised: November 6, 2024
Accepted: November 10, 2024
Published: November 30, 2024

Keywords:
Cost,
Concrete Bucket,
Portable Concrete Pump,
Productivity,
Revit.

ABSTRACT

Indonesia has many construction companies due to its growing building construction sector. The productivity of heavy equipment plays a crucial role in project completion time and construction costs. A study comparing casting volume using Revit software is essential for the construction sector. Researchers are using Revit software to determine casting materials and assess casting equipment's productivity, such as portable pumps used for casting beams and floor slabs, concrete buckets used for casting columns, and casting costs. This quantitative research is a testament to our commitment to precision, as it utilizes actual project data, such as daily casting mapping and concrete supply. The data is then meticulously processed to produce output, such as differences in concrete volume between Revit software and on-site realization, the productivity of casting equipment, and casting costs. The analysis shows significant differences in material usage for casting on the 10th and 11th floors, directly impacting future construction projects' efficiency and cost-effectiveness.

I. INTRODUCTION

Project construction involves various activities to achieve specific objectives within a defined timeframe. It requires adequate resources such as skilled labor, materials, equipment, and practical implementation methods. Additionally, it involves managing costs and adhering to project timelines with a clear beginning and end [1]. A construction project is a series of well-planned, short-term activities that yield prompt and effective results. The 5M factors (man, materials, machine, money, and method) are pivotal in the decision-making process of a construction project [2],[3], [4]. These factors, which encompass human resources, building materials, construction equipment, project budget, and construction methods, guide the project's progression, ensuring the right tool weight, material selection, material volume, and workforce allocation.

Tool-heavy equipment is integral to civil engineering, as these specialized tools aid in various stages of the construction process, from laying the foundation to completing the roof [5]. They are particularly crucial in large-scale construction projects [6], where their use is essential for efficiency and timely task completion, resulting in the desired output within a shorter timeframe.

The tower crane is primarily composed of critical components such as the base section, mast section, climbing frame, support frame, slewing ring, slewing mast, cat head/tower top, jib, counter jib, counterweight, cabin sets, access ladder, trolley, hooks, and tie ropes[7],[8]. Each of these components plays a crucial role in the operation of the tower crane. The tower crane's functions include vertical movement (hoisting) for lifting and lowering loads, horizontal movement (trolley) for track traversal, and rotational movement (swing) for job rotation. The tower crane facilitates concrete movement from a truck mixer to the casting location using concrete buckets attached to the crane's hook[9],[10].

Nearly a century ago, Max Giese and Fritz Hull proposed pumping concrete [11]. This technique allows for quicker concrete delivery and `construction, setting new pumping height records. However, it can be complex and hazardous, leading to annual accidents [8],[12],[13]. Practical guidelines have been developed, and a versatile portable pump, the Frog Pump, can reach heights of over 200 meters, making it invaluable for high-rise construction [14-16]. On the other hand, a tower crane is a powerful and robust piece of equipment used for hoisting and transporting materials to elevated or high locations [17]. Typically employed in building construction projects, the tower crane is crucial in lifting heavy materials to facilitate construction work at great heights[18]. However, it is essential to note that in specific projects, using tower cranes may be challenging and necessary. Alternatives exist, and the decision to use this specific tool depends on the nature and requirements of the project, keeping in mind the substantial weight of the materials being handled.

These factors necessitate the contractor to carefully select suitable equipment, sources, power people, and project costs [19]. In project development, tools play a pivotal role in construction work. Emphasizes that a tool's operation's function and method, including its efficiency, safety features, and ease of use, must be thoroughly evaluated during the selection process to ensure optimal productivity [20]. This emphasis on efficiency empowers the audience, making them feel in control of the project's success [21].

Productivity is a critical factor that significantly influences the results of a construction project. Increased productivity can reduce the time spent on a project, reducing costs [22]. Conversely, tools that hinder productivity can inconvenience workers and inflate costs, underscoring the weight of each decision in project development. This highlights the audience's responsibility and accountability in ensuring optimal productivity, empowering them to make decisions integral to the project's success.

Chacón, highlight that work casting, as one component of many, significantly affects the speed of a project [23]. The large volume of construction beams and plates on the floor means that the productivity of all casting equipment directly impacts the project's time and costs [24-26]. It underscores the importance of your role in cost management. Your expertise and decisions are crucial in managing the costs and ensuring the project's success, making you an integral and valued part of the project's success.

Based on the description, the researcher will evaluate casting volumes in the field with volume calculation with Revit 3D software, productivity in tools casting concrete bucket and pump portable (Frog Pump), and cost foundry.

II. MATERIALS AND METHODS

II.1 MATERIALS

The research will analyze the casting columns, beams, and floor plates evaluation on Floor 10 and Floor 11 for the Surakarta Mother's Hospital Building construction project. The study will also analyze the productivity of crucial construction equipment such as the Portable Pump (Pump Frog) and the Tower Crane with a bucket, which plays a crucial role in the construction process. Count productivity on the 10th floor and 11th floor of the tool heavy pump portable for casting columns, beams, and plates, as well as productivity bucket on the Tower Crane For casting columns. The Unit Price Analysis Work (AHSP) for casting will also be evaluated. The project location can be seen in Figure 1, which depicts the conditions, environment, and boundaries of the construction site.

Figure 1: Mother's Hospital Building Construction Project Location.
Source: Author, (2024).

II.2 METHODS

Our data collection process is thorough and reliable. We will obtain primary data directly from sources for specific calculations and gather secondary data from oral or written sources for various preparations. Once all the necessary data for the final project is collected, it will be meticulously processed using Revit 3D software for 3D modeling software [27], [28], ensuring the results' reliability and your confidence in the project's outcomes.

Calculating time delay and adequate time will be required to calculate the productivity count for casting beams and floor plates using the Portable Pump (Pump Frog). The productivity count for casting columns using the Tower Crane with a bucket will involve necessary times for hoisting, slewing, trolley movement, landing, unloading, and loading. Furthermore, a calculation coefficient will be used to analyze price units, considering human resources, building materials, construction equipment, project budget, and construction methods. These factors guide the project's progress and ensure proper consideration for tool weight, material selection, material volume, and workforce allocation. Flow diagram research that can seen in Figure 2.

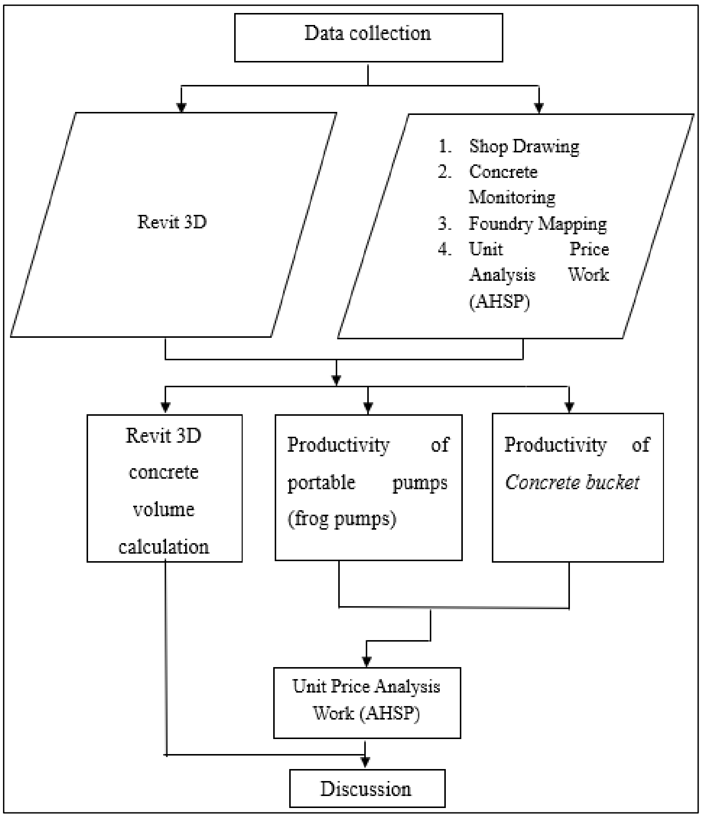

Figure 2: Research Method Flow Diagrams.
Source: Author, (2024).

III. RESULTS AND DISCUSSIONS

An evaluation casting was conducted to assess the suitability of the Revit 3D application in the field for constructing building. The analysis revealed that the casting zone on the 10th floor included casting head columns, beams, and plates. This information is presented in Figure 3. Figure 4 shows the 3D image of the casting zone on the 11th floor, including casting head columns, beams, and plates.

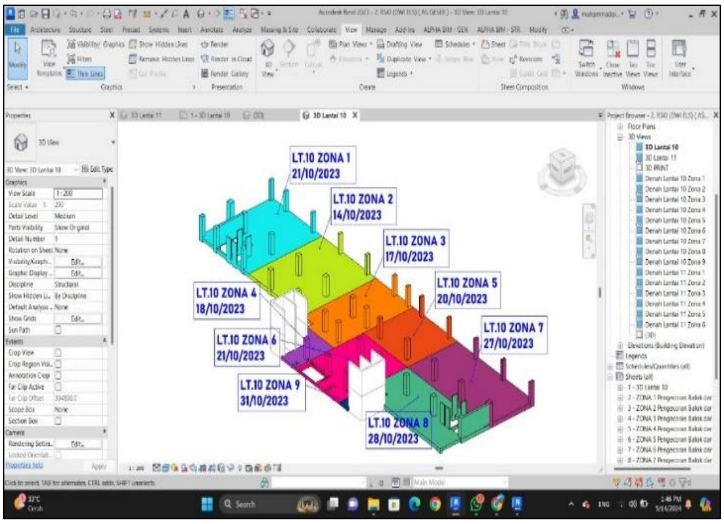

Figure 3: Displays the 3D view of the casting zone on the 10th floor of building.
Source: Author, (2024).

A comparison of the evaluation output results for casting concrete on the 10th floor using Revit 3D and the actual field conditions is presented in Table 1. The results indicate significant differences in the volume calculations for Zones 2, 3, 6, and 7. These differences, which are crucial for our project, may be attributed to waste and leftovers, as well as nonconformity in the plate floor or lack of precision by 125 mm. A graphical representation of the differences in the results is shown in Figure 5.

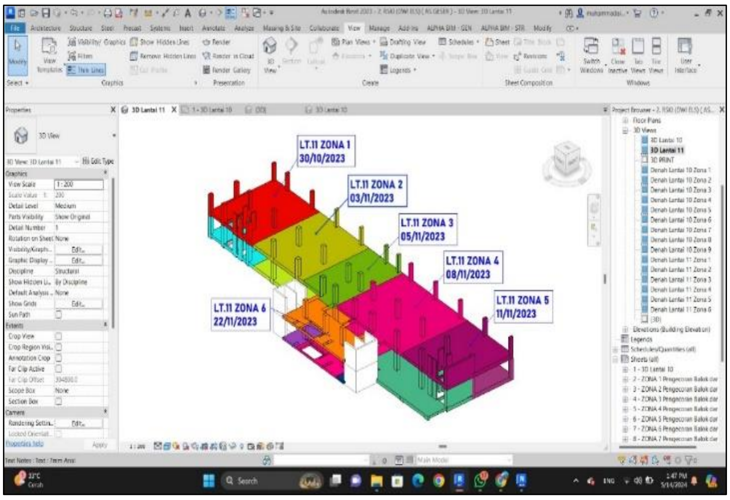

Figure 4: 3D View display 11th Floor Foundry.
Source: Author, (2024).

Table 1: Comparison Results of Concrete Volume with BIM Revit 3D and Realization 10th Floor Field.

Zone	Realization Field (m^3)	BIM Revit 3D (m^3)	Difference (m^3)
1	54	54.7	0.70
2	66	61.26	4.74
3	50.07	44.46	5.61
4	18.00	10.64	7.36
5	37.08	34.22	2.86
6	48	40.05	7.95
7	72	61.45	10.55
8	48	44.24	3.76
9	5,811	4.18	1.63

Source: Author, (2024).

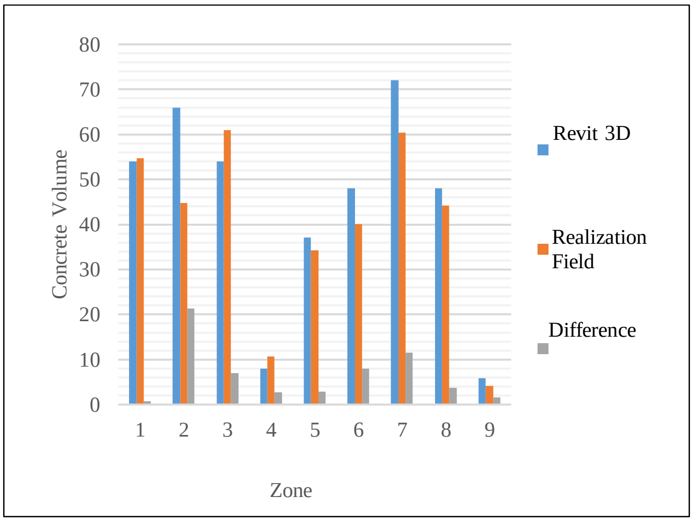

Figure 5: Concrete Volume Analysis Graph in the Field with Revit 3D.
Source: Author, (2024).

Similarly, the evaluation output results for casting concrete on the 11th floor are presented in Table 2, indicating differences in volume calculations for Zones 2, 5, and 6. These differences, which underscore the need for precision in our work, may be attributed to factors such as waste and leftovers, as well as nonconformity in the plate floor or lack of precision by 125 mm. A comparative analysis graph is presented in Figure 6.

Table 2: Comparison Results of Concrete Volume with BIM Revit 3D and Realization 11th Floor Field.

Zone	Realization Field(m^3)	BIMRevit 3D(m^3)	Difference(m^3)
1	54	53.72	0.28
2	72	60.62	11.38
3	60	52.52	7.48
4	84	80.26	3.74
5	66	52.47	13.53
6	42.8	31.27	11.53

Source: Author, (2024).

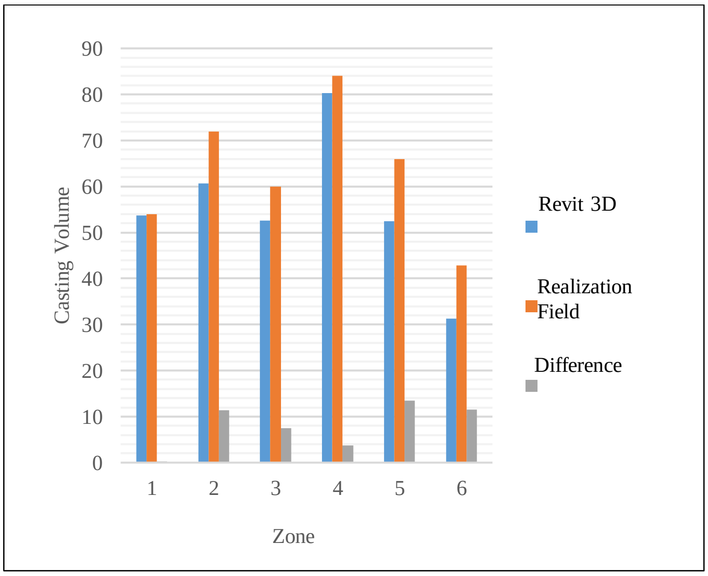

Figure 6: Comparative Analysis Graph of 11th Floor Concrete Volume.
Source: Author, (2024).

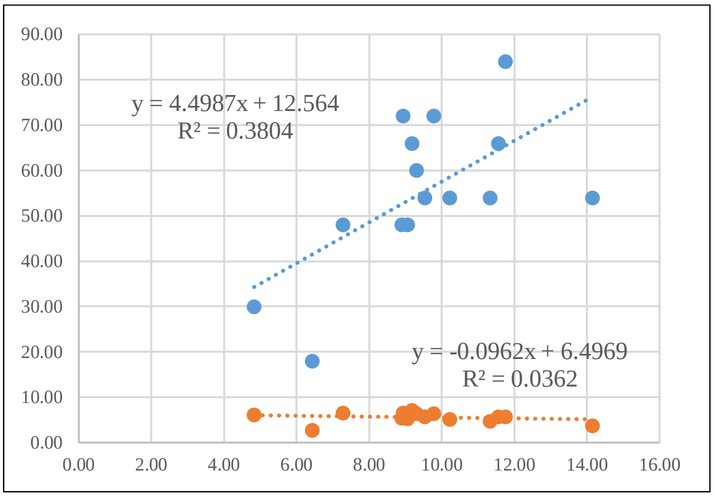

Figure 7: Effect of Volume and Time on Productivity of Portable Pumps.
Source: Author, (2024).

Calculating Portable Pump Productivity (Frog Pump) derived from concrete supply and sample intervals is a meticulous and precise process. This data is then analyzed, considering time delay, effectiveness, and total Time. The delay influences the total Time in the day. The average productivity of the portable pump at the foundry plate on the 10th floor and 11th floor, as seen in Table 3, is a result of these precise calculations, ensuring the accuracy of the results. This study comprehensively analyzes the effect of Volume and Time on productivity. Figure 7 illustrates the factors that significantly impact productivity, underlining the thoroughness and importance of this analysis, which is crucial for understanding the dynamics of portable pump productivity.

Table 3: Average Productivity of Portable Pumps in Foundries plate 10th Floor and 11th Floor.

Zone	10th floor (m^3/hour)	11th floor (m^3/hour)	10th floor (m^3/ day)	11th floor (m^3 / day)
1	14,15	11.32	113.19	90.63
2	11.55	8.92	92.36	71.4
3	9.53	9.18	76.24	73.50
4	6.43	11.74	51.43	93.99
5	8.89	9.30	71.11	74.42
6	7.27	10.22	58.18	81.77
7	9.77	-	78.19	-
8	9.06	-	72.45	-
9	4.83	-	38.61	-
Average	9.05	10,11	72.42	80.95

Source: Author, (2024).

The Figure 6 shows the R Square values (R2) for Volume (X1) and Time (X2) as predictors of productivity. Volume has a moderate R2 value of 0.3804, while Time has a weak R2 value of 0.0362. The correlation coefficients (r) for Volume and Time are 0.144 and 0.001, respectively, indicating weak correlations with productivity. This comprehensive analysis considers both variables simultaneously and independently. The results indicate a strong relationship between Volume and time (independent variables) and productivity (dependent variable), explaining 77.77% of the productivity.

Concrete buckets and heavy tower cranes are used at the foundry to construct columns. The tower crane GHD7032-12 is used for casting columns. It is fast, agile, and efficient. Table 4 shows the average productivity of tower cranes with concrete buckets on the 10th and 11th floors. This table also analyzes the influence of volume and time on productivity, as depicted in Figure 8.

Table 4: Average TC Productivity with Concrete Bucket Floor 10 and Floor 11.

Kolom	10th floor (m^3/hour)	11th floor (m^3/hour)	10th floor (m^3/ day)	11th floor (m^3 / day)
1	4.79	4.53	38.39	36.25
2	2.25	3.84	18.01	30.77
3	3.96	4.66	31.68	37.31
4	4.93	4.33	39.47	34.69
5	3.72	5.44	37.78	43.52
6	4.70	5.48	37.61	35.90
7	4.99	5.21	39.91	41.71
8	5.27	5.21	42.23	41.75
9	7.96	4.96	63.69	39.75
10	-	5.06	-	40.54
Average	4.84	4.78	38.76	38.22

Source: Author, (2024).

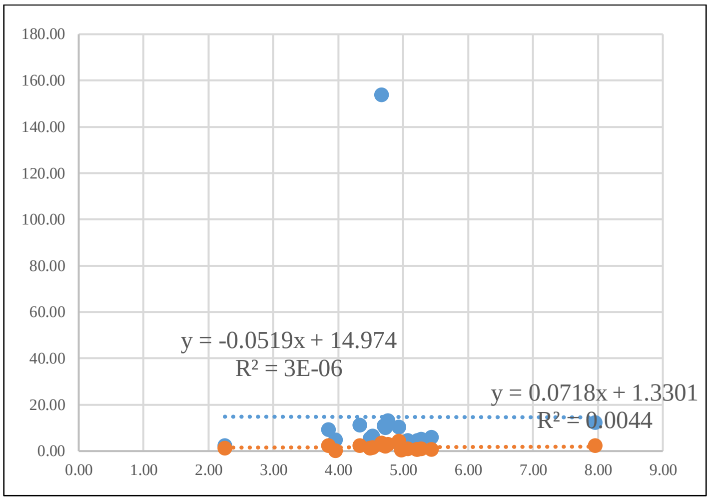

Figure 8: Chart Effect of Volume and Time on TC Productivity with Concrete.
Source: Author, (2024).

The R Square value determines how well the independent variables (volume and time) predict the dependent variable (productivity). The obtained R2 values for volume and time are considered weak, indicating a weak correlation between these variables and productivity. The analysis indicates that volume and time have a feeble influence on productivity, with an R2 value of 0.0056.

Based on the meticulously calculated productivity for casting columns, beams, and plate floors, the researcher can estimate the cost of the concrete volume using two different tools. The Portable Concrete Pump (Frog Pump) is used for casting beams and plate floors, while TC with Concrete Buckets is used for casting columns. By calculating the cost of casting one cubic meter for each zone, we can determine the total costs for casting columns on the 10th and 11th floors. The prices are based on Unit Price Analysis Work of Surakarta and can be found in Table 5.

Table 5: Recapitulation of Total Column Casting Prices.

Floor	Zone	Volume (m^3)	Cost 1 m^3 (IDR)	Total cost (IDR)
10	Zone 1	13.16	1,123,560	14,613,496
	Zone 2	2.52	1,135,618	2,806,825
	Zone 3	4.80	1,133,397	5,332,928
	Zone 4	10.36	1,124,434	11,506,935
	Zone 5	10.08	1,126,765	11,189,055
	Zone 6	10.92	1,124,129	12,126,075
	Zone 7	3.64	1,123,434	4,041,374
	Zone 8	5.04	1,126,957	5,594,942
	Zone 9	12.32	1,123,076	13,665,058
11	Zone 1	6.44	1,126,142	7,152,023
	Zone 2	9.24	1,124,933	10,266,891
	Zone 3	15.40	1,123,247	17,101,265
	Zone 4	11.20	1,124,434	12,439,929
	Zone 5	5.88	1,126,765	6,438,147
	Zone 6	5.32	1,125,060	5,908,361
	Zone 7	3.64	1,122,469	4,040,916
	Zone 8	4.48	1,130,292	5,908,361
	Zone 9	2.24	1,141,056	2,487,027
	Zone 10	4.48	1,130,584	4,973,799

Source: Author, (2024).

Evaluating the productivity and cost of concrete casting for structural elements, such as slabs and columns, involves a comprehensive analysis of various factors, including labor and equipment. As civil engineers, construction project managers, and professionals involved in concrete casting operations, your role is integral in this process. Casting productivity is greatly influenced by the efficiency of tools and labor, which directly affects the output in the casting process [29]. Research shows that the productivity of casting using a concrete pump is higher than using a tower crane. These differences highlight the importance of selecting the right tools to improve productivity metrics, which is essential for identifying areas for improvement in foundry operations [30]. In addition, labor efficiency is essential in reducing costs and increasing overall productivity in concrete casting [31]. Therefore, a thorough evaluation of labor and equipment and productivity metrics, with your active involvement, is essential to improve the efficiency and cost-effectiveness of concrete casting for structural elements [32].

IV. CONCLUSIONS

Our study analyzed casting productivity on the 10th and 11th floors. We found discrepancies in zones 1-9 on the 10th and 1-6 on the 11th floors. Productivity of foundry beams and plates, time with buckets, and TC productivity were compared. Our analysis revealed a significant influence of volume and time on productivity, with a correlation of 0.60. The cost for casting beams and plates on the 10th floor was IDR 530,670,938; on the 11th floor, it was IDR 469,403,363. The total cost for casting columns was IDR 80,876,688 on the 10th floor and IDR 75,781,783 on the 11th floor.

V. REFERENCES

[1] D. Arditi and H. M. Gunaydin, "Total quality management in the construction process," *Int. J. Proj. Manag.*, vol. 15, no. 4, pp. 235–243, 1997, doi: 10.1016/S0263-7863(96)00076-2.

[2] S. Khahro, S. Shaikh, N. Y. Zainun, B. Sultan, and Q. Khahro, "Delay in Decision-Making Affecting Construction Projects: A Sustainable Decision-Making Model for Mega Projects," *Sustainability*, vol. 15, p. 5872, Mar. 2023, doi: 10.3390/su15075872.

[3] E. Szafranko and J. Harasymiuk, "Modelling of Decision Processes in Construction Activity," *Appl. Sci.*, vol. 12, p. 3797, Apr. 2022, doi: 10.3390/app12083797.

[4] H. Movaffaghi and I. Yitmen, "Importance of decision-making in building materials selection," in *Materials Selection for Sustainability in the Built Environment*, 2024, pp. 71–85. doi: 10.1016/B978-0-323-95122-7.00004-6.

[5] R. Agha Majidi, *Building construction procedure*. 2021. doi: 10.13140/RG.2.2.28761.44644.

[6] J. E. Beavers, J. R. Moore, R. Rinehart, and W. R. Schriver, "Crane-related fatalities in the construction industry," *J. Constr. Eng. Manag.*, vol. 132, no. 9, pp. 901–910, 2006, doi: 10.1061/(ASCE)0733-9364(2006)132:9(901).

[7] A. H. Ali, T. Zayed, R. D. Wang, and M. Y. S. Kit, "Tower crane safety technologies: A synthesis of academic research and industry insights," *Autom. Constr.*, vol. 163, 2024, doi: 10.1016/j.autcon.2024.105429.

[8] A. H. Ali, T. Zayed, and M. Hussein, "Crane safety operations in modular integrated construction," *Autom. Constr.*, vol. 164, 2024, doi: 10.1016/j.autcon.2024.105456.

[9] A. W. A. Hammad, D. Rey, A. Akbar Nezhad, and A. Haddad, "Integrated mathematical optimisation approach for the tower crane hook routing problem to satisfy material demand requests on-site," *Adv. Eng. Informatics*, vol. 55, p. 101885, Jan. 2023, doi: 10.1016/j.aei.2023.101885.

[10] H. Ishak, Z. Mohamed, S. Fasih, M. Bello, R. Ezuan, and B. Adebayo, "Sway Control of a Tower Crane with Varying Cable Length Using Input Shaping," 2023, pp. 188–200. doi: 10.1007/978-981-99-7243-2_16.

[11] J. R. Illingworth, "Movement and distribution of concrete," 1972.

[12] D. Feys, G. De Schutter, S. Fataei, N. S. Martys, and V. Mechtcherine, "Pumping of concrete: Understanding a common placement method with lots of challenges," *Cem. Concr. Res.*, vol. 154, p. 106720, 2022, doi: https://doi.org/10.1016/j.cemconres.2022.106720.

[13] V. R. Kulkarni, "High performance concrete for high-rise buildings: Some crucial issues," *Int. J. Res. Eng. Technol.*, pp. 26–33, 2016.

[14] K. E. von Eckardstein, *Pumping concrete and concrete pumps: a concrete placing manual*. Schwing, 1983.

[15] R. A. Crepas, *Pumping Concrete: Techniques and Applications*. Crepas & Associates, 1997.

[16] N. R. Guptill *et al.*, "Placing concrete by pumping methods," *Am. Concr. Institute, Farmingt. Hills*, 1998.

[17] A. Kaveh and Y. Vazirinia, "An Upgraded Sine Cosine Algorithm for Tower Crane Selection and Layout Problem," *Period. Polytech. Civ. Eng.*, vol. 64, no. 2 SE-Research Article, pp. 325–343, Jan. 2020, doi: 10.3311/PPci.15363.

[18] A. Kaveh and Y. Vazirinia, "Optimization of Tower Crane Location and Material Quantity Between Supply and Demand Points: A Comparative Study," *Period. Polytech. Civ. Eng.*, vol. 62, no. 3 SE-Research Article, pp. 732–745, Jan. 2018, doi: 10.3311/PPci.11816.

[19] S. Ng, Z. Tang, and P. Ekambaram, "Factors contributing to the success of equipment-intensive subcontractors in construction," *Int. J. Proj. Manag.*, vol. 27, pp. 736–744, Oct. 2009, doi: 10.1016/j.ijproman.2008.09.006.

[20] A. Rathnayake and C. Middleton, "Systematic review of the literature on construction productivity," *J. Constr. Eng. Manag.*, vol. 149, no. 6, p. 3123005, 2023.

[21] S. Senaratne and M. G. Sexton, "Role of knowledge in managing construction project change," *Eng. Constr. Archit. Manag.*, vol. 16, no. 2, pp. 186–200, 2009, doi: 10.1108/09699980910938055.

[22] O. M. Elsahly, S. Ahmed, and A. Abdelfatah, "Systematic Review of the Time-Cost Optimization Models in Construction Management," *Sustain.*, vol. 15, no. 6, 2023, doi: 10.3390/su15065578.

[23] R. Chacón *et al.*, "Digital twinning of building construction processes. Case

study: A reinforced concrete cast-in structure," *J. Build. Eng.*, vol. 84, p. 108522, 2024.

[24] H. Tukundane and Y. Yang, "Effect of Project Control Practices on the Performance of Building Construction Companies in Uganda: A Case Study of the City of Kampala," *Buildings*, vol. 14, no. 6, 2024, doi: 10.3390/buildings14061818.

[25] M.-N. Li, X. Wang, R.-X. Cheng, and Y. Chen, "Aided design decision-making framework for engineering projects considering cost and social benefits," *Eng. Constr. Archit. Manag.*, 2024.

[26] P. S. Utomo, B. Sukindrawati, S. Sahadi, R. K. Fahma, and P. Astuti, "Productivity analysis of mixer trucks and a concrete pump in a multi-story building," in *AIP Conference Proceedings*, AIP Publishing, 2023.

[27] D. Lobos Calquin *et al.*, "Implementation of Building Information Modeling Technologies in Wood Construction: A Review of the State of the Art from a Multidisciplinary Approach," *Buildings*, vol. 14, no. 3, p. 584, 2024.

[28] S. Lagüela, L. J. Sánchez-Aparicio, E. González-González, A. Ospina-Bohórquez, M. Á. Maté-González, and D. González-Aguilera, "From 3D models to historic building information modeling (HBIM) and digital twins: A review," *Diagnosis Herit. Build. by Non-Destructive Tech.*, pp. 387–419, 2024.

[29] M. Wang Fu and J.-Y. Zheng, "Die Casting for Fabrication of Metallic Components and Structures," F. G. B. T.-E. of M. M. and A. Caballero, Ed., Oxford: Elsevier, 2022, pp. 54–72. doi: https://doi.org/10.1016/B978-0-12-819726-4.00037-5.

[30] R. Ds and A. Purwanto, "Increasing Factory Productivity Through Casting Machines with Cycle Time Analysis Using Theoretical Value Production & PDCA Methods," *Int. J. Innov. Sci. Res. Technol.*, pp. 965–975, Jul. 2024, doi: 10.38124/ijisrt/IJISRT24JUL828.

[31] P. Joshi and S. Shrestha, "Analysis of Labor Productivity During Concreting Operation in Building Construction of Kathmandu Valley," pp. 1–7, Jul. 2019.

[32] V. J. Mawson and B. R. Hughes, "The development of modelling tools to improve energy efficiency in manufacturing processes and systems," *J. Manuf. Syst.*, vol. 51, pp. 95–105, 2019, doi: https://doi.org/10.1016/j.jmsy.2019.04.008.

Journal of Engineering and Technology for Industrial Applications

ISSN ONLINE: 2447-0228

ITEGAM-JETIA

Manaus, v10. n.50, p. 45-50. November/December., 2024.

DOI: https://doi.org/10.5935/jetia.v10i50.1295

RESEARCH ARTICLE OPEN ACCESS

DTC OF A 5 LEVEL MMC FED 3-Φ INDUCTION MOTOR WITH PI AND FLC USING CBAPOD PWM TECHNIQUE

Sriramulu Naik Mudhavath [1], Kesana Gopikrishna [2], Venkat Anjani Kumar G[3].

[1 3] Assistant Professor, Department of E.E.E., Rajiv Gandhi University of Knowledge Technologies- Ongole, Andhra Pradesh.
[2] Assistant Professor, Department of E.E.E., Rajiv Gandhi University of Knowledge Technologies-Nuzvid, Andhra Pradesh.

[1]http://orcid.org/0000-0002-6602-9792, [2]http://orcid.org/0009-0007-9737-3338, [3]http://orcid.org/0009-0004-3111-0525

Email: msriramnaik@gmail.com, gopi52@gmail.com, anjishelectrical@gmail.com

ARTICLE INFO

Article History
Received: September 15, 2024
Revised: November 6, 2024
Accepted: November 10, 2024
Published: November 30, 2024

Keywords:
Direct Torque Control-DTC,
Modular Multilevel Converter – MMC,
Fuzzy Logic Controller- FLC.

ABSTRACT

Industrial motor drives, particularly three phase induction motor drives, have been adopting Modular Multilevel Converters (MMC). MMC is utilized in the design of power and control circuits to give the appropriate switching sequences that yield the corresponding output voltage levels. This paper describes the Alternate Phase opposition Disposition Pulse Width Modulation (APOD-PWM) method and fuzzy logic controller used to regulate the 5-level MMC topology of an induction motor. The MMC's switching mechanism is essential for enhancing the induction motor drive's power quality. The converter can be used as a source of controlled voltage because it has numerous distinct voltage levels accessible. Researchers have improved the application of fuzzy logic for Direct Torque Control (DTC) in variable speed drives that rely on multilevel inverters in the past few years. The MATLAB/SIMULINK simulator is the foundation of our suggested method, which measures the effectiveness of direct torque control with respect to ripple in current, speed, torque, and transient response. Both the fuzzy logic controllers (FLC) as well as the PID controller were compared in this study. THD content will significantly decrease as a result of this.

I. INTRODUCTION

Power electronic converters, such as multilevel inverters, are essential of the development of AC motors due to their excellent power abilities, reduced switching losses, and effective electrical performance, strong electromagnetic compatibility, and decreased output waveform harmonic content. Multilevel inverters provide a viable option for outdoor applications where it is not possible to cable AC power to the desired area and at which a driving unit with a fixed or varying speed is needed. Output waveforms inverter becomes significantly more similar to the sinusoidal waveform [1].

First described by [2], the Modular Multilevel Converter (MMC) is an architecture that offers benefits for high power utilizations. It is appropriate for HVDC of excellent performance [3]. Additionally, motor drives and STATCOM employ it [4],[5].
T. Nougouchi and Depenbrock [6],[7] developed the direct torque control approach for induction machine control, which was first published in the literature in the middle of the 1980s. The following severity is provided by this method: [8-10]. The disadvantages of a DTC system with hysteresis controllers are torque ripple, current, and variable switching frequency.

Because of their straightforward design and excellent performance under a variety of operating circumstances, PI-type controllers are the most often used controller in industrial applications [11]. The key issue with that controller is the proper selection of PI gains, as well as the fact that employing fixed gains may result in the controller failing to provide the appropriate control performance when plant characteristics and operating conditions change [12].

In [13-17], the performance of a 3-phase induction motor with DTC was reported when it was operated from MMC using the carrier-based Phase Opposition Disposition (POD PWM) approach. In [18],[19], 3-Level MMC employed a Fuzzy Logic Controller in conjunction with APOD-PWM technique. The current work used a simulator (MATLAB/SIMULINK) to determine the ripples in current, dynamic responsiveness, torque, and speed of a 3-Φ induction motor with DTC. The proposed architecture is a 5-level MMC with APOD-PWM strategy, which incorporates and combines both PI and fuzzy controllers.

II. PROPOSED MMC TOPOLOGY

As a unique hybrid arm multipolar cell topology, 100% of the arms' unipolar cells are connected to the grounding pole and 100% of the arms' bipolar cells are detached (Figure 1).

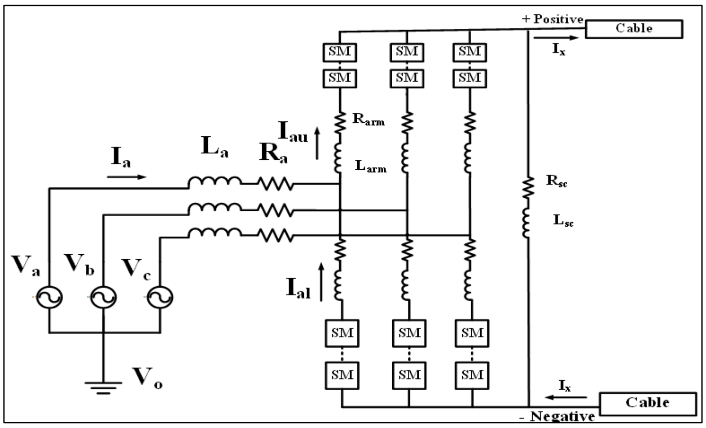

Figure 1: Depicts MMC's fundamental topology.
Source: Authors, (2024).

Basic formulas

All phase's SMs are arranged into two blocks according to the voltages Vla (lower arm) and Vua (upper arm). Per SM's capacitor is maintained full at a voltage of $Vc = V_{DC}/n$.

The equations connecting DC and AC voltage can be found using an upper or lower arm:

$$V_{oa} = \frac{V_{DC}}{2} - V_{ua} - L\frac{di_{ua}}{dt} \quad (1)$$

$$V_{oa} = -\frac{V_{DC}}{2} + V_{la} + L\frac{di_{la}}{dt} \quad (2)$$

For each of the arms, the currents are:

$$I_{ua} = \frac{I_a}{2} + \frac{I_{DC}}{3} + I_{za} \quad (3)$$

$$I_{la} = -\frac{I_a}{2} + \frac{I_{DC}}{3} + I_{za} \quad (4)$$

Where, I_{za}= circulating current

III. CONTROL AND MODULATION OF MMC

The regulation of terminal voltage as well as current is one of MMC's main challenges. Controlling both the ac and dc voltages is therefore essential.

The controlled variable may vary based on the subject of the investigation. MMC enable energy exchange between the input and output stages [20]. Further, significant considerations that must be made in the design and operation of MMC include arm current management, suppressing circulating currents, and balancing capacitor voltage [21]. Alternative research as listed in [22],[23] provide an extensive discussion of PWM approaches.

Several studies have been carried out [24-28] on the modulation of the MMC converter. PWM-based modulation techniques are most suited for MMC converters due to their modularity and simplicity of implementation. For MMC control, several pulse width modulation (PWM) approaches were examined [29].

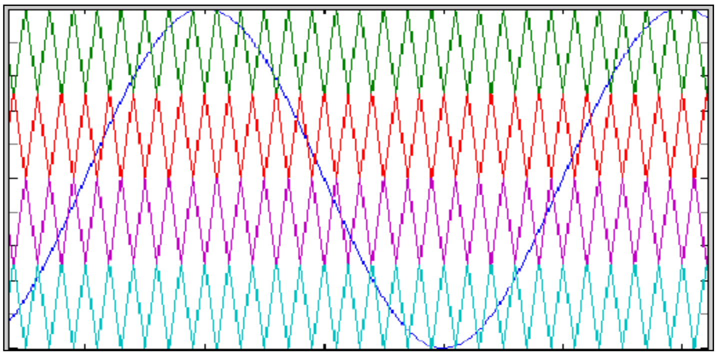

Figure 2: Illustrates the carrier-based APOD-PWM method.
Source: Authors, (2024).

The carry signal (message signal) and a reference signal (sinusoidal, triangle, ramp, etc.) are compared when carried-based PWM is used. This results in the generation of gating pulses, which in turn activate the switches on the arms. PWM technique refers to the signal generation process. An Alternative Phase Opposition Disposition PWM (APODPWM) technique (Figure 2) was taken into consideration in this work. This system alternates between using out-of-phase and in-phase carrier waveforms.

IV. FUZZY LOGIC CONTROLLER

The concept of fuzzy logic is comparable to human senses and cognition. For the fuzzy logic approach to be used in a real usage, the three steps that follow need to be completed:

1. The process of converting crispy or traditional information into fuzzy data, also known as Membership Functions (MFs), is called fuzziness.

2. Fuzzy Synthesis Procedure: Blend control constraints and functions for membership to produce the fuzzy outcome.

3. Defuzzification is: Various techniques are applied to determine each related result, which is then arranged in an array known as a lookup table.

According to the information being provided, choose the appropriate output from the lookup table for an application. The electromagnetic torque error is fizzed using five fuzzy subsets: Negative Big (NB), Negative Small (NS), Zero (Z), Positive Small (PS), and Positive Big (PB). Figure 3 (a) shows an assessment of their membership functions. Three fuzzy subsets of the error of flux are fuzzy: Negative (N), Zero (Z), and Positive (P). Figure 3(b) provides an assessment of their membership functions.

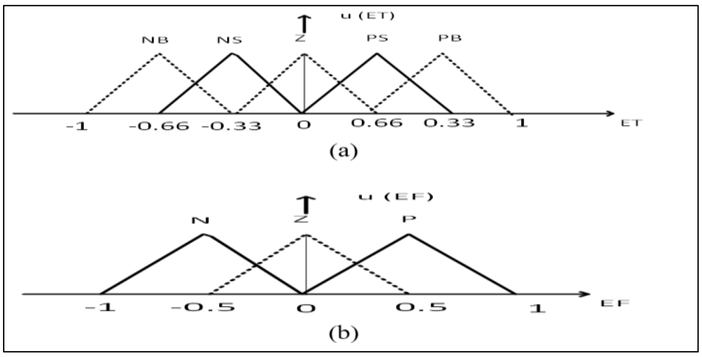

Figure 3. Fuzzy membership functions for input variables (error of torque and flow).
Source: Authors, (2024).

V. DIRECT TORQUE CONTROL

DTC for induction machines is becoming the superior substitute for field-oriented control techniques. In comparison to the vector control system, the configuration is significantly less complicated because PI regulators and positional conversions between synchronous and stationary frames are not included. Additionally, it does not require a position encoder or PWM, which add latency and call for mechanical transducers, respectively. DTC-based drives don't use the current regulation loop; instead, they are managed similarly to a closed loop system (Figure 4).

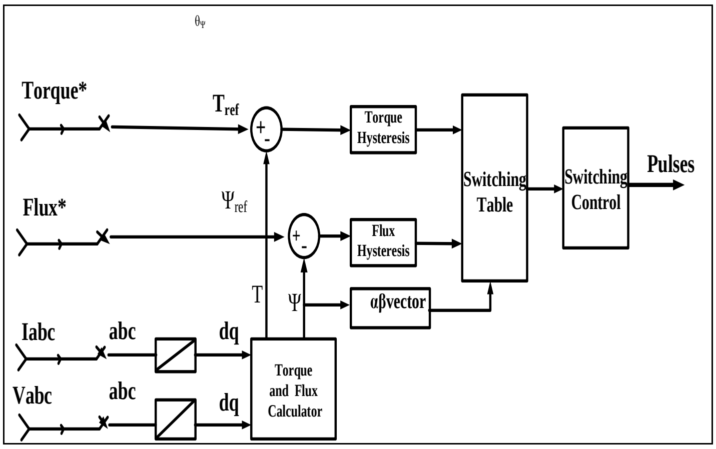

Figure 4: DTC based circuit.
Source: Authors, (2024).

Stator voltage is $u_s = R_s i_s + \frac{d}{dt}\lambda_s$ (5)

To calculate torque

$$T_e = \frac{3}{2} p_n \lambda_s * i_s \quad (6)$$

Stator linkage flux

$$\lambda_s = L_s i_s + L_m i_r = \frac{L_s}{L_m}(\lambda_r - \sigma L_r i_r) \quad (7)$$

It's possible to calculate torque and flux using the formulae above.

The fundamental idea of DTC is to concurrently select the best inverter switching modes and directly manage the machine's electromagnetic torque and stator flux linkage.

VI. SIMULATION VIEW OF CIRCUIT

The values of induction motor were shown in Table 1.

Table 1: Induction Motor Details.

Parameter	Rating
Nominal power	2237VA
Voltage $_{\text{Line-Line}}$	220V
Stator resistance	0.436Ω
Stator inductance	0.003H
Rotor resistance	0.818Ω
Rotor inductance	0.003H

Source: Authors, (2024).

Speed was considered as 1000, 700, 500, 100, -600 at 0, 1, 3, 5, 7 seconds respectively.

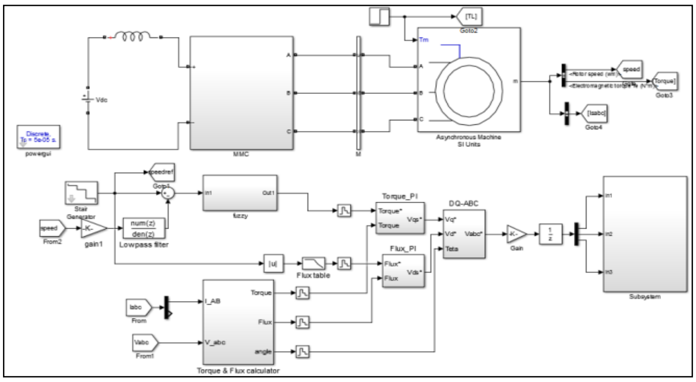

Figure 5: The simulation circuit.
Source: Authors, (2024).

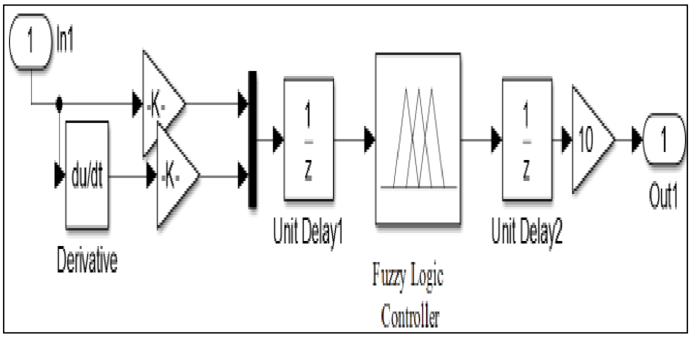

Figure 6: Inside the Fuzzy sub system.
Source: Authors, (2024).

Table 2: Controller details.

Controller	Gain Value
Torque	K_p =1.3, K_I = 100
Flux	K_p =200, K_I = 3000

Source: Authors, (2024).

VII. RESULTS AND DISCUSSION

PI CONTROLLER

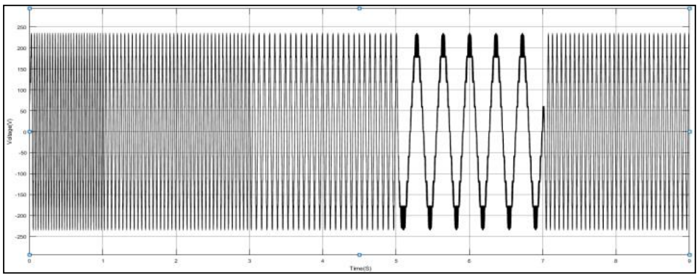

Figure 7: Voltage across inverter.
Source: Authors, (2024).

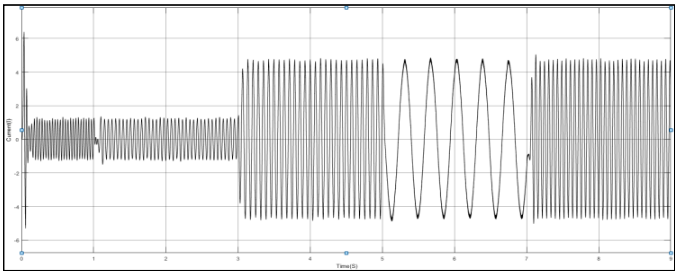

Figure 8: Current of inverter.
Source: Authors, (2024).

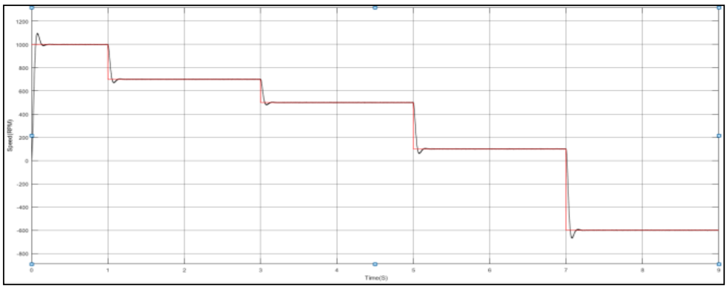

Figure 9: Speed of induction motor.
Source: Authors, (2024).

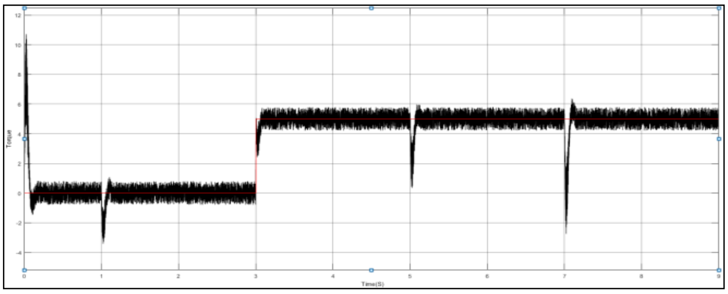

Figure 10: Torque of induction motor.
Source: Authors, (2024).

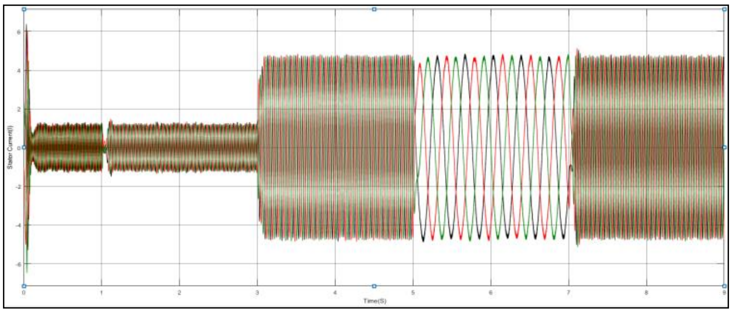

Figure 11: Stator current of motor.
Source: Authors, (2024).

FUZZY LOGIC CONTROLLER

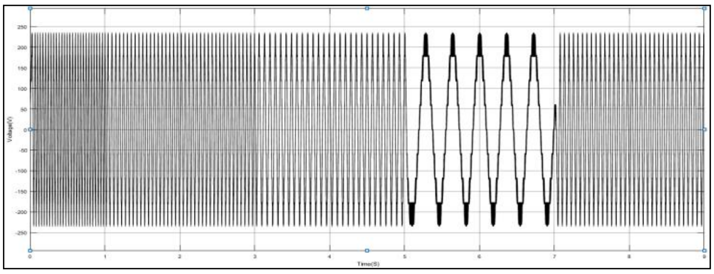

Figure 12: Voltage across inverter.
Source: Authors, (2024).

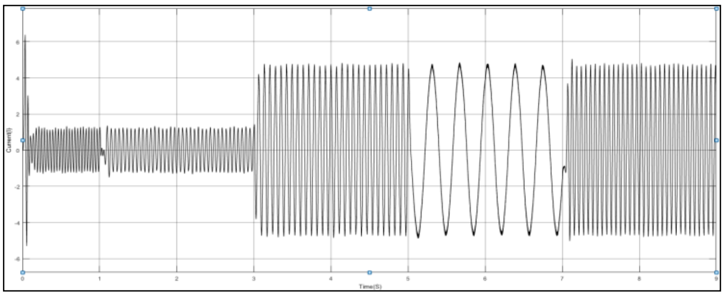

Figure 13: Current at inverter.
Source: Authors, (2024).

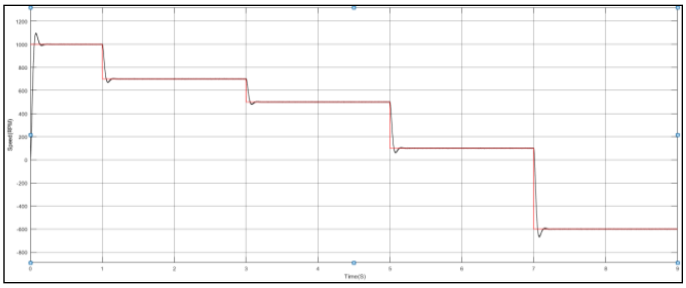

Figure 14: Speed of induction motor.
Source: Authors, (2024).

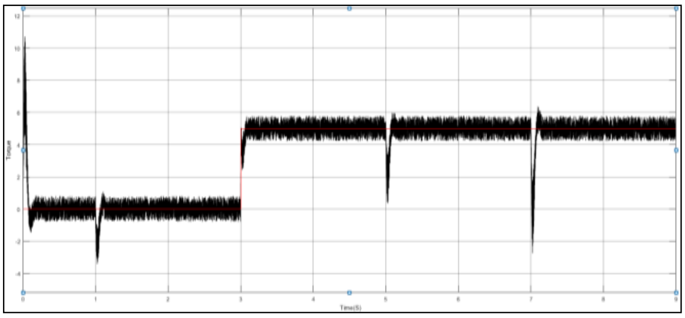

Figure 15: Torque of induction motor.
Source: Authors, (2024).

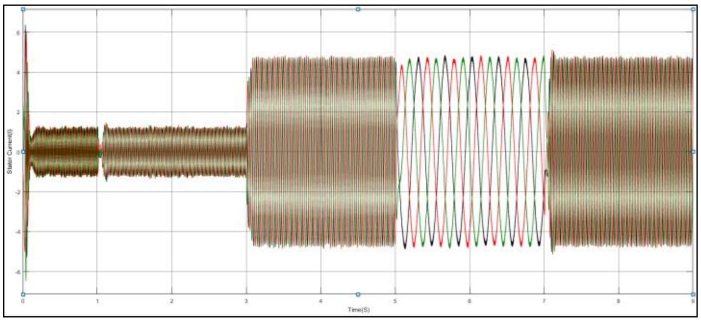

Figure 16: Stator current of induction motor.
Source: Authors, (2024).

The results seem to be the same for both scenarios, yet the Fuzzy MMC has a smaller percentage than the PI MMC when compared to THD values. The voltage THD value for PI MMC is 5.28%, while the fuzzy THD value is 4.52%. The maximum speed achieved with Fuzzy MMC is 997.28 rpm and with PI MMC is 996.46 rpm.

Table 3: Performance Comparison.

S. No	Parameter	5-L MMC	5-L F MMC
1	Voltage (V)	246.43	246.43
2	Current(A)	4.45	4.45
3	Speed (rpm)	996.46	997.28
4	Torque (N-m)	5.08	5.06
5	Stator Current(A)	4.39	4.32
6	THD	5.28%	4.52%
7	current ripple(p.u)	0.12	0.02
8	torque ripple(p.u)	0.001	0.0003
9	Peak Time(s)	0.073	0.03
10	Settling Time(s)	0.154	0.102

Source: Authors, (2024).

VIII. CONCLUSUION

Employing MATLAB/SIMULATION, the application of fuzzy MMC and PI MMC topology to the control of a three-phase induction motor was observed and compared. Fuzzy MMC topology performs better than PI MMC topology because it has a higher maximum speed attain value, a lower torque value, and less harmonic content.

IX. AUTHORS'S CONTRIBUTION

Conceptualization: Sriramulu Naik Mudhavath, Kesana Gopikrishna, Venkat Anjani Kumar. G
Methodology: Sriramulu Naik Mudhavath, Kesana Gopikrishna, Venkat Anjani Kumar. G
Investigation: Sriramulu Naik Mudhavath, Kesana Gopikrishna, Venkat Anjani Kumar. G
Discussion of results: Sriramulu Naik Mudhavath, Kesana Gopikrishna, Venkat Anjani Kumar. G
Writing – Original Draft: Sriramulu Naik Mudhavath, Kesana Gopikrishna, Venkat Anjani Kumar. G
Writing – Review and Editing: Sriramulu Naik Mudhavath, Kesana Gopikrishna, Venkat Anjani Kumar. G
Resources: Sriramulu Naik Mudhavath, Kesana Gopikrishna, Venkat Anjani Kumar. G
Supervision: Sriramulu Naik Mudhavath, Kesana Gopikrishna, Venkat Anjani Kumar. G
Approval of the final text: Sriramulu Naik Mudhavath, Kesana Gopikrishna, Venkat Anjani Kumar. G
Acknowledgments: If necessary, cite people or entities that supported the development of the research.

X. REFERENCES

[1] Bimal K. Bose, “Modern power electronics and AC drives”, The University of Tennessee, Knoxville, 2001, p.338.

[2] Ciftci, Baris, and Ahmet M. Hava. "Performance evaluation and selection of PWM switching and control methods for grid connected modular multilevel converters." 2015 IEEE Energy Conversion Congress and Exposition (ECCE). IEEE, 2015.

[3] Lawan, A. U., and Haider M. Abbas. "Level shifted PWMs comparison for a 5-level modular multilevel converter (MMC) topology inverter." 2015 IEEE Conference on Sustainable Utilization And Development In Engineering and Technology (CSUDET). IEEE, 2015.

[4] Merlin, M. M. C., et al. "A new hybrid multi-level voltage-source converter with DC fault blocking capability." (2010): 56-56. 9th IET International Conference on AC and DC Power Transmission (ACDC 2010).

[5] Lee, Sze Sing, and Yeh En Heng. "A tuning-less model predictive control for modular multilevel converter capable of unbalanced grid fault." International Journal of Electrical Power & Energy Systems 94 (2018): 213-224.

[6] M. Merlin, T. Green, P. Mitcheson, D. Trainer, D. Critchley, and R. Crookes, “A new hybrid multi-level voltage-source converter with dc fault blocking capability,” in Proc. 9th IET Int. Conf. AC DC Power Transmission., Oct. 2010, pp. 1–5.

[7] Indra, “Indirect current control techniques of Three Phase APF Using Fuzzy Logic and Proportional Integral Controller: Comparative analysis,” IEEE International Conference on Harmonics and Quality of Power ICHQP, pp. 362–367, 2004.

[8] Jiaqiang Yang. Jin Huang, “Direct torque control system for induction motors with fuzzy speed PI regulator,” Machine Learning and Cybernetics, 2005. Proceedings of 2005 International Conference IEEE, Vol. 2, pp. 778–783.

[9] Del Toro X. Jayne M G. Witting P A, “New DTC control scheme for the induction motor fed with a three-level inverter,” IEEE International Symposium on Industrial Electronics ISIE, Vol. 3, pp. 893 – 897, 2005.

[10] Abdalla T Y. Hairik H A. Dakhil A M, “Direct torque control system for a three phase induction motor with fuzzy logic based speed Controller,” 1st International Conference IEEE on Energy, Power and Control EPC-IQ, pp. 131 – 138, 2010.

[11] A. Hazzab, A. Laoufi, I.K. Bousserhane, M. Rahli “Real time implementation of fuzzy gain scheduling of PI controller for induction machine control”, International Journal of Applied Engineering Research, vol.1, nº.1, 2006, pp. 51-60.

[12] Shady M. Gadoue, D. Giaouris, J.W. Finch, “Tuning of PI speed controller in DTC of Induction Motor based on genetic algorithms and fuzzy logic schemes”, IEEE, 2006, pp.

[13] Sriramulu Naik Mudhavath, Dr. Gudapati Sambasiva Rao, “Speed and Flux Control of 3-Phase Induction Motor with MMC Topology by Using DTC Technique”, JARDCS, Vol. 11, 07-Special Issue, 2019, ISSN 1943-023X, Pages: 757-765.

[14] Sriramulu Naik Mudhavath, Gudapati Sambasiva Rao, “Control of Modular Multilevel Converter Fed 3-Phase Induction Motor using DTC with PI Controller”, DOI: 10.35940/ijitee.C8591.019320, ISSN: 2278-3075, Volume-9 Issue-3, January 2020, Page No. 3451-3456.

[15] Sriramulu Naik Mudhavath, Dr. Gudapati Sambasiva Rao, ” Performance comparison of 5 -level modular multilevel converter fed 3-phase induction motor with direct torque control using pi and fuzzy logic controller”, DOI: 10.5373/JARDCS/V12I2/S202012554, Vol. 12, Issue-02, 2020, Pages: 2084-2095.

[16] Mr. Sriramulu Naik Mudhavath, Dr. Gudapati Sambasiva Rao, “Direct Torque Control of MMC FED 3-Phase Induction Motor Using Fuzzy Logic Controller”, ISSN: 2005-4238 IJAST, Vol. 29, No. 6, (2020), pp. 2113 – 2121.

[17] Sriramulu Naik Mudhavath, Gudapati Sambasiva Rao, “DTC of 3-Level Npc Inverter and Mmc Fed 3-Phase Induction Motor”, IJITEE, DOI: 10.35940/ijitee. G4977.059720 , ISSN: 2278-3075, Volume-9 Issue-7, May 2020, Page No. 1156-1160.

[18] Mr. Sriramulu Naik Mudhavath, Dr. Gudapati Sambasiva Rao, “Performance Comparision Between MLI and MMC Topology of Direct Torque Control Induction Machine Drive With Apod-Pwm Technique”, ISSN: 1936-7317, Advanced Science Letters, Vol. 26, No. 6, (2020), pp. 1513.

[19] Mr. Sriramulu Naik Mudhavath, Dr. Gudapati Sambasiva Rao, “Fuzzy Based Three-Level MMC Topology for Direct Torque Control of Three Phase Induction Motor Drive with APOD-PWM Technique”, Issn: 1934-7197, Journal Of Engineering, Computing & Architecture, Vol. 10, Issue 7, (2020), pp. 89.

[20] J. J. Jung, H. J. Lee, and S. K. Sul, “Control strategy for improve dynamic performance of variable-speed drives with Modular Multilevel Converter,” IEEE J. Emerg. Sel. Top. Power Electron, vol. 3, no. 2, pp. 371–380, 2015.

[21] B. Li, S. Shi, D. Xu, and W. Wang, “Control and analysis of the modular multilevel dc de-icer with statcom functionality,” IEEE Trans. Ind. Electron., vol. 63, no. 9, pp. 5465–5476, 2016.

[22] Q. Tu and Z. Xu, “Impact of sampling frequency on harmonic distortion for modular multilevel converter,” IEEE Trans. Power Deliv., vol. 26, no. 1, pp. 298–306, 2011.

[23] Bina, M. Tavakoli. "A transformerless medium-voltage STATCOM topology based on extended modular multilevel converters." IEEE Transactions on Power Electronics 26.5 (2010): 1534-1545.

[24] B. Li, S. Shi, D. Xu, and W. Wang, “Control and analysis of the modular multilevel dc de-icer with statcom functionality,” IEEE Trans. Ind. Electron., vol. 63, no. 9, pp. 5465–5476, 2016.

[25] F. Xu, Z. Xu, H. Zheng, G. Tang, and Y. Xue, "A tripole HVDC system based on modular multilevel converters," IEEE Trans. Power Deliv., vol. 29, no. 4, pp. 1683–1691, 2014.

[26] Yin Li, Student Member, IEEE, Lingling Fan, Senior Member, IEEE, "Modular Multilevel Converter Based Induction Machine Drive" International Conference of North American Power Symposium (NAPS) on 4-6 Oct-2015, IEEE-2015.

[27] J. J. Jung, H. J. Lee, and S. K. Sul, "Control strategy for improve dynamic performance of variable-speed drives with Modular Multilevel Converter," IEEE J. Emerg. Sel. Top. Power Electron., vol. 3, no. 2, pp. 371–380, 2015.

[28] B. Li, R. Yang, D. Xu, G. Wang, W. Wang, and D. Xu, "Analysis of the Phase-Shifted Carrier Modulation for Modular Multilevel Converters," IEEE Trans. Power Electron., vol. 30, no. 1, pp. 297–310, Jan. 2015.

[29] A. António-Ferreira, C. Collados-Rodríguez, and O. Gomis-Bellmunt, "Modulation techniques applied to medium voltage modular multilevel converters for renewable energy integration: A review," Electr. Power Syst. Res., vol. 155, pp. 21–39, 2018.

Journal of Engineering and Technology for Industrial Applications

ITEGAM-JETIA

Manaus, v10. n.50, p. 51-58. November/ December., 2024.

DOI: https://doi.org/10.5935/jetia.v10i50.1299

ISSN ONLINE: 2447-0228

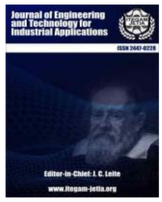

RESEARCH ARTICLE OPEN ACCESS

ASSESSMENT OF THE ADEQUACY OF ELECTRICAL ENERGY DEMAND FORECAST MODEL FOR THE NIGERIA POWER DISTRIBUTION SYSTEM VIA STATIONARITY TEST

O.O Ade-Ikuesan[1*], I.A Adejumobi[2], I.O Adebisi[3], G.A Dawodu[4]

[1]Department of Electrical/Electronic Engineering, Olabisi Onabanjo University, Ago-Iwoye, Nigeria.
[2,3]Department of Electrical and Electronics Engineering, Federal University of Agriculture Abeokuta, Nigeria.
[4]Department of Statistics, Federal University of Agriculture Abeokuta Ogun State Nigeria.

[1]http://orcid.org/0000-0002-0312-4637, [2]http://orcid.org/0000-0002-4587-6239, [3]http://orcid.org/0000-0001-8958-4951, [4]http://orcid.org/0000-0091-6683-7362

Email: olanike.adeikuesan@oouagoiwoye.edu.ng, engradejumobi@yahoo.com, adebisioluwaseun@funaab.edu.ng, dawoduga@funaab.edu.ng

ARTICLE INFO

Article History
Received: September 17, 2024
Revised: November 6, 2024
Accepted: November 10, 2024
Published: November 30, 2024

Keywords:
Stationarity,
Augmented Dickey-Fuller,
Peak- Load,
Feeders,
Differencing

ABSTRACT

Electric energy demand forecasting model is an essential tool in the course of planning in electricity industry. Though, there has been increasing concern to fix models for various domains. The adequacy and accuracy of these models for forecasting reasonable energy generation capacity, scheduling and system management planning are paramount. Inaccurate model will give forecasting that are either underrated that will incapacitate socio-economic growth by not supply enough electrical energy for development, or overestimated leading to excess electrical energy generation without commensurate returns on investment, another form of economic jeopardy. In this paper, Assessment of the adequacy of Electrical Energy Demand Forecasting Model for the Nigeria Power Distribution System via Stationarity test was performed as crucial stage in development of time series technique of energy demand forecast model. In the stationarity investigation of data set under the null hypothesis as a test tool for the confirmation of stationarity and non-stationarity of energy demand data for processing and further analyses of energy demand in power distribution system in Nigeria. Data were collected from five 33kV feeders each with sixty-point of monthly peak Load demand for five years (2015-2019) from Ibadan Electricity distribution Company (IBEDC). R- Software was used as optimization tool for the analyses. The end result was interpreted by Critical values for Augmented Dickey-Fuller method. Findings shows that data from three of the feeders were non-stationary they will go through data differencing to make the data suitable for further investigations as a mixture of an autoregressive integrated moving average ARIMA while two are stationary and can be authenticated for further analyses. The application of this test to further difference the datapoints that are non-stationary will lead to stationary dataset, hence, give viable model for accurate energy demand forecasting model development.

I. INTRODUCTION

Nigeria a nation producing electrical energy in anticipated large quantity for more than a decade, the rate at which electrical energy supply support structure and expansion in the country is poor, hence, power supply remains insufficient to meet the people demand [1]. Nigeria been the most populous country in Africa with over two hundred million population, meeting the electrical energy demand of the inhabitants in this era is a big task, a high volume of production activities and more demand for electrical energy is expected, for these reasons the government privatized Power sector in 2013, in anticipation to bridge demand-supply gap. However, the result was far from expectation, rather the heights of the tasks was changed, the gap is wider with population and socio-economy growth [1],[2].

Currently, over forty percent of the total inhabitants of Nigerians are off national grid [3]. The remaining 59.3% though connected, reliable power supply poses serious challenges nearly ninety-percent of the energy demanded is not met. In the Nigerian

Energy sector study, it was estimated that electricity demand will rise to the tune of 213,122 MW by 2040**.** Although the results of these studies be at variance extensively, the fact remains that there is wide gap in electrical energy demand and supply profile. In the coming years, industrial, commercial and domestic electricity demand is expected to rise considerably. Domestic demand with lion share will have rapid growth as a result of expansion at a reasonable rate yearly and growth in population that is estimated at 2.7% per annum. [4],[5]

Reliable power supply is an inevitable infrastructure for the economic growth of any nation. Yet, insufficient energy supply, in the presence of ever-increasing energy demand characterized by the unreliability, forced power outage, and unplanned load-shedding is rampant in Nigeria a supposed developing nation. Energy management and planning is one of the major ways of obtaining a reliable power supply and forecasting of energy demand is an optimization tool in power system planning and management. To obtain adequate and reliable forecasting algorithm is an immense challenge. The decision, therefore, to eliminate or minimize the risk of either inadequate or over-estimated power demand with the aid of careful planning and application of useful tools such as forecasting that is accurate is a necessity [6].

In the light of above-mentioned facts, there is a need for adequate planning using the appropriate forecasting model as a tool for accurate energy demand for the teeming population. However, time series model is one of the most effective models for energy demand because it gives room for trends and variations, this is of course the choice for this study, however, to achieve this the historical data for the time series analysis must be stationary [6]. Identification of stationary data phases in time series is an essential step in data mining and analysis. By statistical rule, data with constant mean, variance and covariance are stationary [7],[8]. Stationarity indicates that the mathematical features of a time series or the data mining that produced the series does not vary for some period of time [7]. Time series data may either stationary or not. Stationarity sequences are values that are unchanging and near to an average value of the data mining and other value of statistical central tendency [9]. A stationary time series will tend to return to its mean called mean reversion and fluctuate around this mean. Stationarity is diverse in nature, it could be wide, weak, strict or second order if it has a constant average and variance value [10].

Strictly stationary serial data has constant auto-covariance configuration in addition to mean and variance. When a series holds this covariance stationarity, the covariance configuration is steady over time [9]. Explicitly, the auto-covariance maintain constant measure of central tendency and dispersion irrespective of the point of sequential reference. Periodic systems are easy to predict, in the sense that their gesture has an iterating pattern. Interestingly, stationarity procedures circumvent the challenges of unauthentic regression [11]. Stationary is essential in data mining since its absence can muddled the appropriateness of developed model hence rubbish the forecasting result at intervals. The result of which will not give the desire model for accurate planning. Moreover, typical authentication tests to confirm adequacy of developed model such as Chi-squared, Q and Durbin-Watson statistic T, F, etc. are effective when variables are stationary otherwise, these tests cannot be bank upon.

Stationarity can be ascertained in several ways: graphical representation, autocorrelation and partial autocorrelation valuations, autocorrelation coefficients and quantified examinations. Several methods is applicable in stationarity specified tests such as: Unit root test, Dickey-Fuller and Augmented Dickey-Fuller, Kwiatkowski Phillips-Schmidt-Shin (KPSS), Zivot and Andrews, Variance Ratio Test (VRT). However, when the data point is average in real life time series, which is the case of this study, sixty datapoints per feeder, Augmented Dickey-Fuller (ADF) technique is preferable because of its robust result [12]. The application of Augmented Dickey-Fuller examination is comfortable through consecutive correlation. The ease of ADF test in complex series modeling is grandeur than others in its class. The method has more advantages of being more potent, specific and straight forward [12]. Results from ADF analysis are: p-value, value of the test statistic, number of lags, the critical value cutoffs. The interpretation of these and the significance will confirm stationarity and non-stationarity of the series [13]. Consequently, stationarity investigation should take the lead in sound data analysis for time series modeling. Principally, the exploration is highly crucial especially when dealing with systems for which the data acquisition procedure does not guarantee stationarity: if only short and unique time series is accessible and if the experimental circumstances is not amendable or the amenability is restricted. However, this scenario is a common occurrence in many fields of endeavor especially, electrical energy operation and management [13],[14].

R-software application for statistical analyses was used for the studies. There are now thousands of Packages for R specifically designed for specialized data manipulation or data analysis which enhance data visualization that produce publication-ready quality charts [15]. These graphs for pictorial valuation of the sequence revolved around the analyses of autocorrelation and partial autocorrelation plots. Relationship between a time series with trends in the autocorrelation explain the connection of the series and its features [14],[16]. To compute autocorrelation, the correlation are computed, and the lagged series is noted which is preliminary successions copy, this proceed a once or a multiple of times in the. A lagged sequence with single lag is the original series proceeding once; whereas, lag-2 is the initial series moved forward two time periods, on between the series and a lagged version of the series. Interpretation of the autocorrelation function (ACF) and partial autocorrelation function PACF plot will faction out stationarity and non-stationarity functions in collaboration with the p-value and lag order [17].

Peak load forecast is ideal for preparation of power system operation at the time of highest demand from the consumers, hence ideal for this analysis. [18],[19]. Peak load contribution, also referred to as peak power, peak demand, critical demand, or maximum demand is usually caused by spikes in usage which may result from a variety of factors. Peak demand, although the period is transient, all the same very crucial, when electricity is in high demand because the sharp the evidence of peak load curve is a necessity for adequacy in forecasting processes. However, the electricity companies must generate the maximum capacity and have the transmission and distribution infrastructure to handle the peak demand for economic reasons non-conventional methods of generation can serve as standby for such periods [20]. In Nigeria, stakeholders were focusing much attention on electric power generation plants and transmission systems with little responsiveness on distribution. With extraordinary increase in energy demand by all classes of consumers and population expansion, the complication of power distribution system became more elaborate. This led to daily challenges in Nigeria power distribution system that draw thoughtfulness and careful planning [21]. Therefore, the interest of this study was to assess the adequacy of the energy demand data via stationarity test for accurate model development in Nigeria power distribution system for effective planning to mitigate these myriad challenges in power sector.

II. METHODOLOGY

II.1 TIME SERIES MODELLING

A time series is a succession of data or action that follows a particular order or trend in an interval of time. Time series forecasting uses a procedure to calculate future ideals founded on previously observed and present occurrence. Its values are in progressive order hence makes the analysis diverse from cross-sectional studies, without natural ordering of the observations, action or information [22]. Time series analysis may be in frequency or time domain [23]. The time domain includes an algorithm that estimate the strength and wavelet while frequency domain takes account of autocorrelation and cross relationship analysis [24]. The flawless examination of time series data by inspection is graphical illustrations. However, other approaches are entails; autocorrelation analysis to examine serial dependence, spectral analysis to study recurrent performance which may not be seasonal, separation into components representing trend, seasonality, variation of diverse mode, and cyclical anomaly splitting a time-series into a sequence of sections. Models for time series data can be in various form and characterize diverse stochastic procedures. In model building there are variations in the level of a process, three classes, the autoregressive (AR) models, the integrated (I) models, and the moving average (MA) models. These classes depend linearly on previous data points. Combinations of these ideas produce autoregressive moving average (ARMA) and autoregressive integrated moving average (ARIMA) models [24].

II.2 AUGMENTED DICKEY-FULLER (ADF) MODELLING EQUATIONS

The mathematical models of Augmented Dickey-Fuller (ADF) test are expressed by equation (1) to (3). In a series with the sequence of $Y_1, Y_2, \dots\dots\dots\dots\dots .. Y_N$

The noble scholars Dickey and Fuller considered sets differential-form autoregressive equations [25].

$$\Delta Y_t = \gamma Y_{t-1} + \sum_{j=1}^{p} (\delta_j \, \Delta Y_{t-j}) + e_t \quad (1)$$

$$\Delta Y_t = \alpha + \gamma Y_{t-1} + \sum_{j=1}^{p} (\delta_j \, \Delta Y_{t-j}) + e_t \quad (2)$$

$$\Delta Y_t = \alpha + \beta t + \gamma Y_{t-1} + \sum_{j=1}^{p} (\delta_j \, \Delta Y_{t-j}) + e_t \quad (3)$$

Where:

t is the time of operation,

α is the intercept constant called a drift,

β is the coefficient on a time drift,

γ is the coefficient awarding process root, i.e., the focus of testing,

p is the lag order of the first-differences autoregressive procedure,

e_t is the left-over term for similar distribution.

The dissimilarity in the three equations in the presence of the deterministic elements α (a drift term) and βt (a linear time trend). The effort of testing is neither the coefficient γ equals to zero, what means that the original $Y_1, Y_2, \dots\dots\dots\dots\dots .. Y_N$, process has a unit root; hence, the null hypothesis of γ = 0 (random walk process) is tested in contrast to the alternative hypothesis γ < 0 of stationarity. More comprehensive, the null and alternative hypotheses corresponding to the models above are as follows in expression (4) to (9) [25],[26].

$$H_0 : Y_t \text{ is random walk OR } \gamma = 0 \quad (4)$$

$$H_1 : Y_t \text{ is random walk OR } \gamma < 0 \quad (5)$$

$$H_0 : Y_t \text{ is random walk around a drift OR } \{= 0, \alpha \neq 0\} \quad (6)$$

$$H_1 : Y_t \text{ is level stationary process OR } \{< 0, \alpha \neq 0\} \quad (7)$$

$$H_0 : Y_t \text{ is random walk around a trend OR } \{= 0, \beta \neq 0\} \quad (8)$$

$$H_1 : Y_t \text{ is level stationary process OR } \{< 0, \beta \neq 0\} \quad (9)$$

II.3 DESCRIPTION OF SITE LOCATION

In this study the feeders used are located in Ogun State, Nigeria. Ogun is one of the western states of Nigeria. The state is prominent in a high concentration of citadel of learning and localization of industries in Nigeria. The state has the most industrialised local Government area in Nigeria with Agbara and Ota Industrial estates. Ogun is blessed with higher schools of learning and the famous in Nigeria both private and public. It has a large arable landmass with good fertility for agricultural practice for plant and animal production. The settlement in the state comprises of urban, sub-urban and rural which account for the energy demand pattern of the state. The State energy demand pattern can serve as a good subset for Nigeria because of its growth rate and characteristics [27]. The electrical energy structure of the state is of six district sections with the headquarters at the state capital Abeokuta. The transmission stations include Sagamu with 132/33/11/0.415kV step down power transformers and five others. These six stations feed twenty-seven injection substations managed by Ibadan Electricity Distribution Company (IBEDC) that supplies forty-seven feeders out of which five are chosen for this study.

II.3.1 SYSTEM CONFIGURATION

In electric power distribution, Feeders are voltage power line conveying power from a supply substation to the distribution transformers. They convey power from a transformer or switch gear to the consumer via a distribution panel. The 11kV lines are used in residential and commercial areas feeding the distribution power transformers that distributes power to the structures in the area. Whereas, 33kV lines serves higher voltages rating that distribute power from one sub-station to another and unit point load in industries with high voltage consumption.

The data was acquired from the Ibadan Distribution Company (IBEDC), the monthly peak load for five years (2015 to 2019) in five different 33kV feeders in Ogun state for the study. These are presented in Table 1 to 5 the feeder are: Sagamu, Ikene, NNPC/OGIJO, Owode Egba, and Phoenix (Real).

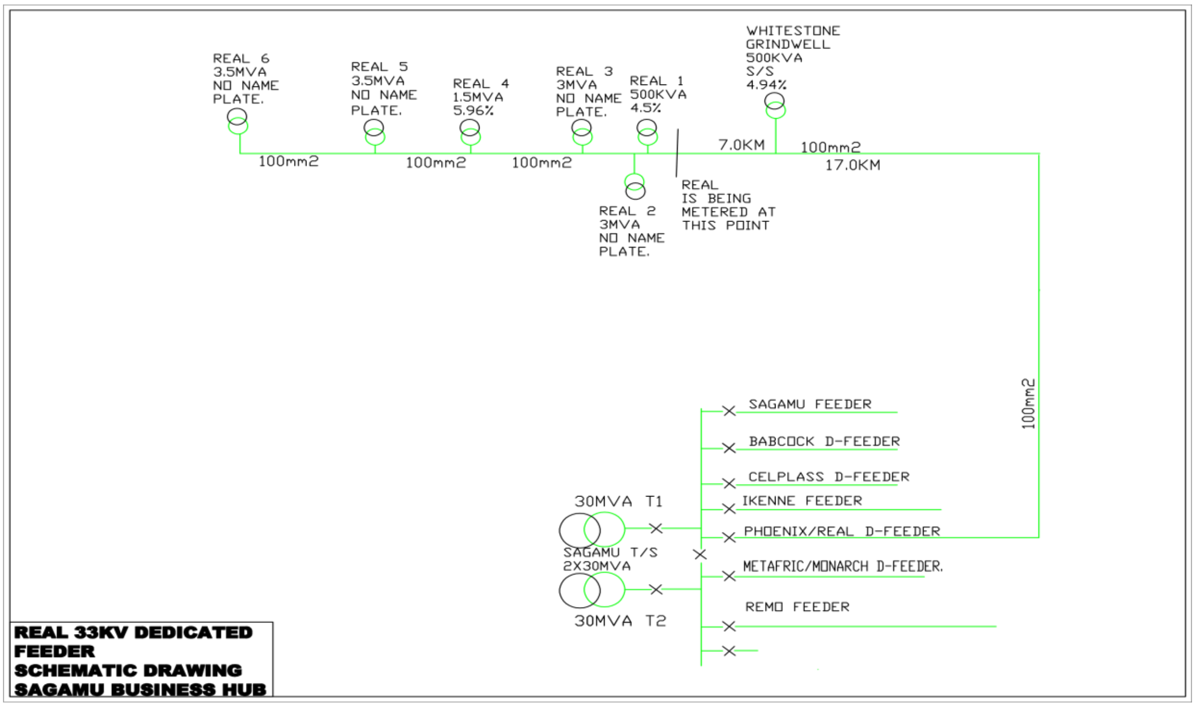

Figure 1: Line Diagram 33kV Feeders.
Source: Authors, (2024).

Table 1: Sagamu 33kv Feeder Monthly Peak Load 2015-2019 (MW/hr).

Year	Jan	Feb	Mar	Apr	May	Jun	Jul	Aug	Sep	Oct	Nov	Dec
2015	14.4	14.3	13.8	17.9	14.8	18.1	16.8	15.9	21.5	21.2	17.0	21.2
2016	18.2	18.0	17.5	22.1	18.6	22.4	20.9	19.9	26.0	25.7	21.1	25.7
2017	22.5	22.1	21.7	26.8	22.9	27.0	25.5	24.4	31.1	30.8	25.7	31.0
2018	27.2	25.6	26.4	32.0	27.2	32.3	30.6	29.3	36.7	36.3	30.8	36.5
2019	32.3	30.7	31.5	37.7	32.5	38.0	36.1	34.7	42.7	42.3	36.3	42.0

Source: Authors, (2024).

Table 2: Ikene 33kv Feeder Monthly Peak Load 2015 2019(MW/hr).

Year	Jan	Feb	Mar	Apr	May	Jun	Jul	Aug	Sep	Oct	Nov	Dec
2015	10.0	8.4	7.6	8.8	18.6	13.4	15.4	16.2	15.5	16.7	14.5	17.3
2016	13.1	11.3	10.3	11.8	23.0	17.1	19.3	20.2	19.4	20.7	18.3	21.5
2017	16.7	14.7	13.5	15.2	27.8	21.2	23.7	24.7	23.8	25.2	22.6	26.1
2018	20.8	18.5	17.2	19.1	33.1	25.8	28.6	29.7	28.7	30.2	27.4	31.2
2019	25.4	22.8	21.4	23.5	38.9	31.9	34.0	35.1	34.1	36.7	32.6	36.8

Source: Authors, (2024).

Table 3: NNPC/Ogijo 33kv Feeder Monthly Peak Load 2015-2019 (MW/hr).

Year	Jan	Feb	Mar	Apr	May	Jun	Jul	Aug	Sep	Oct	Nov	Dec
2015	14.4	17.6	22.2	19.9	19.2	16.6	20.1	18.8	19.6	17.1	17.7	20.2
2016	19.8	21.8	26.9	24.4	23.6	20.7	24.6	23.1	24.0	21.2	21.9	24.7
2017	24.2	26.5	32.0	29.3	28.5	25.2	29.6	27.9	28.9	25.8	26.6	29.7
2018	29.1	31.6	37.7	34.7	33.9	30.2	35.0	33.2	34.3	30.8	31.8	35.1
2019	34.5	37.2	43.8	40.6	39.7	35.7	40.9	38.9	40.1	36.5	37.4	41.0

Source: Authors, (2024).

Table 4: Owode/Egba 33kv Feeder Monthly Peak Load 2015-2019 (MW/hr).

Year	Jan	Feb	Mar	Apr	May	Jun	Jul	Aug	Sep	Oct	Nov	Dec
2015	17.5	14.7	19.0	21.5	17.0	12.5	10.4	16.0	13.8	17.1	10.8	11.5
2016	21.8	18.5	23.4	26.2	21.1	16.0	13.6	20.0	17.8	21.2	14.1	14.9
2017	26.5	22.8	28.2	31.3	25.7	20.0	17.3	24.5	22.0	25.6	17.9	18.8
2018	31.6	27.6	33.5	36.9	30.8	24.5	21.5	29.4	26.7	30.8	22.1	23.1
2019	37.2	32.9	39.3	43.0	36.3	29.4	26.1	34.8	31.9	36.4	26.8	27.9

Source: Authors, (2024).

Table 5: Phoenix Real 33kv Feeder Monthly Peak Load 2015-2019 (MW/hr.).

Year	Jan	Feb	Mar	Apr	May	Jun	Jul	Aug	Sep	Oct	Nov	Dec
2015	19.4	18.9	13.2	14.0	11.8	11.8	11.4	12.0	8.8	12.1	11.3	13.3
2016	23.8	23.2	16.8	17.8	15.2	15.3	14.8	15.5	11.8	15.6	14.7	16.9
2017	28.7	28.0	20.9	22.0	19.1	19.2	18.7	19.4	15.2	19.5	18.5	21.0
2018	34.1	33.3	25.5	26.7	23.5	23.6	23.0	23.8	19.1	23.4	22.8	25.6
2019	39.9	39.1	30.5	31.9	28.3	28.4	27.8	28.7	23.5	28.8	27.5	30.6

Source: Authors, (2024).

II.4 DATA ANALYSIS

The Augmented Dickey-Fuller (ADF) testing technique Modelling Equations (1) to (3) and expression (4) to (9) were used for the coding. The test were carried out with R-Software codes in Rstudio that give the Autoregressive Functions (ACF) and Partial Autoregressive Functions (PACF) plot for interpretation of stationarity and nonstationarity. The data was processed to confirm its stationarity status as indicated in Table 6. (Decision Rule: Reject Ho-hypothesis if the p-value is less than or equals to α(0.05), otherwise, do not reject.). Statistics tests value, lag order and p-value were computed by the R software for proper analyses, inferences and confirmations. Rstudio is an integrated development environment (IDE) for R. It comprises a console, syntax-highlighting editor that backings direct encryption implementation, as well as apparatuses for maneuvering, the past, mending and workspace management [28]. The package is for mathematical design that supports the development of applications in R environment. Rstudio requires R version 3.0. 1 or higher. Since R versions can be installed juxtaposed on a system. Code for the analysis is as follows:

```{r,echo=FALSE,comment= "",warning=FALSE,eval=T}

library ("tseries")

```

**Reading data in**

```{r,echo=FALSE,comment= "",warning=FALSE}

dat <- read.csv("mamaData.csv",header = T)

a = ts(dat$SAGAMU, frequency = 12,start = c(2015,1))

b = ts(dat$IKENE, frequency = 12,start = c(2015,1))

c = ts(dat$NNPC.OGIJO, frequency = 12,start = c(2015,1))

d = ts(dat$OWODE.EGBA, frequency = 12,start = c(2015,1))

e = ts(dat$PHOENIX.REAL, frequency = 12,start = c(2015,1))

```**Autocorrelation and partial autocorrelation plot of Data**

```{r,echo=FALSE,comment= "",warning=FALSE}

acf2(a, main = "SAGAMU ")

acf2(b, main = "IKENE ")

acf2(c, main = "NNPC OGIJO ")

acf2(d, main = "OWODE EGBA ")

acf2(e, main = "PHOENIX REAL ")

```

**Augmented Dickey F. Test**

**```{r,echo=FALSE,comment= "",warning=FALSE}**

adfSAGAMU <- adf.test(a)

adfIKENE <- adf.test(b)

adfNNPC <- adf.test(3c)

adfOWODE <- adf.test(d)

adfPHOENIX <- adf.test(e)

adfSAGAMU

adfIKENE

adfNNPC

adfOWODE

adfPHOENIX

```
```

III. RESULT AND DISCUSSION

III.1 CRITICAL VALUES FOR AUGMENTED DICKRY-FULLEY

The augmented Dickey–Fuller (ADF) value, is a negative number. The higher the negative value the more effective the refusal of the hypothesis that there is a unit root at some level of confidence. However, in the work of Fuller the standard in the Table 6 was established as the yardstick for interpretation of ADF test.

Table 6: Thresholds values for (ADF).

	DATA WITHOUT DRIFT	DATA WITH DRIFT		DATA WITHOUT DRIFT
No of data in the set	1%	5%	No of data in the set	1%
T = 25	-3.75	-3.00	T = 25	-3.75
T = 35	-3.64	-2.96	T = 35	-3.64
T = 50	-3.58	-2.93	T = 50	-3.58
T = 75	-3.54	-2.91	T = 75	-3.54
T = 100	-3.51	- 2.90	T = 100	-3.51
T = 150	-3.48	-2.89	T = 150	-3.48
T = 250	-3.46	-2.88	T = 250	-3.46
T = 500	-3.44	-2.87	T = 500	-3.44
T = ∞	-3.43	-2.86	T = ∞	-3.43

Source: [20].

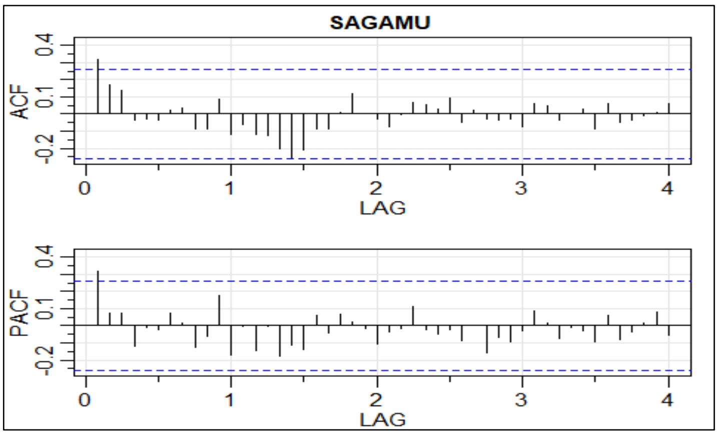

Figure 2: Sagamu feeder 33kV Autoregression and Partial Autoregression plot.
Source: Authors, (2024).

Hypothesis Result of Sagamu 33KVA feeder Augmented (ADF Dickey-Fuller)
Dickey-Fuller = -4.9325,
Lag order=3,
p-value=0.01
alternative hypothesis: stationary

The ACF and PACF graphs in Figure 2 show that the part of data that falls within the range of dotted lines are high in fact only one line is in the significant range which implies that this data are not significant and high possibility that a result or relationship is caused by something other than chance, in addition the ACF scatter along the horizontal axis with more negative parts which make the stationarity status a bit confusing. PACF plot show scatter functions that is neither decaying nor sine waves. As regards the test- statistics -4.9325 is quite low for a data point is sixty between fifty and hundred with threshold of -3.50 to -3.45, this show element of doubt in the validity of the test. However the lag order of 3 for real life data of this form may lead to complex analyses hence will require further analysis on transformation and authentication with adequacy test before field application, p-value of 0.01 (1%) this is sufficiently low, this validate the stationary of the series [29].

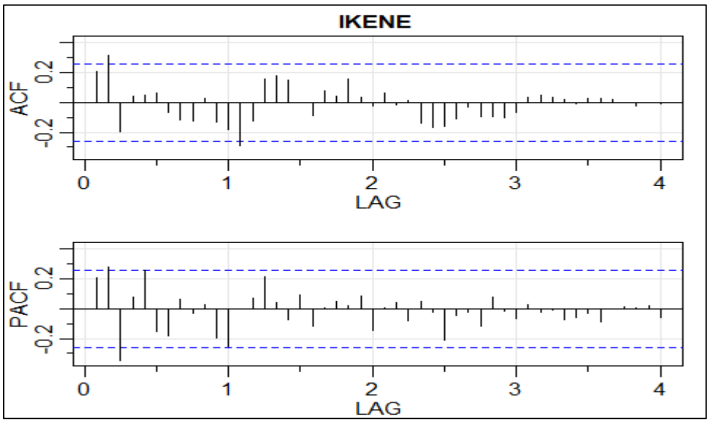

Figure 3: Ikene feeder 33kV Autoregression and Partial Autoregression plot.
Source: Authors, (2024).

Hypothesis Result of NNPC/OGIJO 33kVA feeder Augmented Dickey-Fuller (ADF)
Dickey-Fuller = -0.81603
Lag order = 3
p-value = 0.9551
alternative hypothesis: nonstationary

The ACF and PACF graphs in Figure 3 show that the proportion of data that are within the range of dotted lines are high which implies that this data are not significant and high possibility that a result or relationship is caused by something other than chance, in addition the ACF scatter along more in negative parts of the plot. As regards the test- statistics -0.81603 is tremendously high for the data point, with threshold of -3.50 to -3.45, this show component of ambiguity in the judiciousness of the test. However the lag order of 3 for real life data of this form may lead to multidimensional analyses hence will require further analysis (authentication with adequacy test) before field application, p-value of 0.9551 as against ≤ 0 .05 is too high, hence, the validation of nonstationary feature of the series [29].

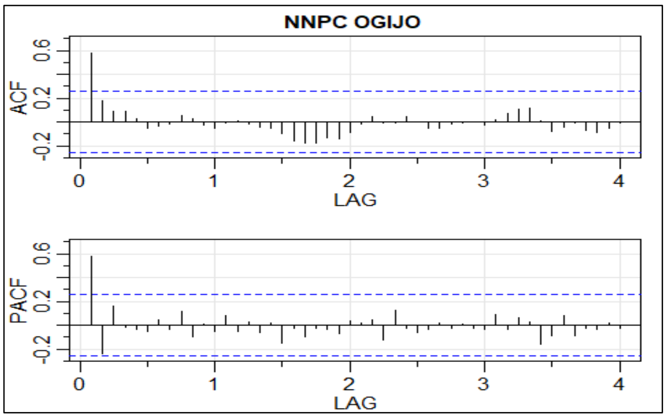

Figure 4: NNPC/OGIJO feeder 33kV Autoregression and Partial Autoregression plot.
Source: Authors, (2024).

Hypothesis Result of NNPC/OGIJO 33kVA feeder Augmented Dickey-Fuller (ADF)
Dickey-Fuller = -0.81603
Lag order = 3
p-value = 0.9551
alternative hypothesis: nonstationary

The ACF and PACF graphs in Figure 4. show that the proportion of data that are within the range of dotted lines are high which implies that this data are not significant and high possibility that a result or relationship is caused by something other than chance, in addition the ACF scatter along more in negative parts of the plot. As regards the test- statistics -0.81603 is tremendously high for the data point, with threshold of -3.50 to -3.45, this show component of ambiguity in the judiciousness of the test. However the lag order of 3 for real life data of this form may lead to multidimensional analyses hence will require further analysis (authentication with adequacy test) before field application, p-value of 0.9551 as against ≤ 0 .05 is too high, hence, the validation of nonstationary feature of the series[29].

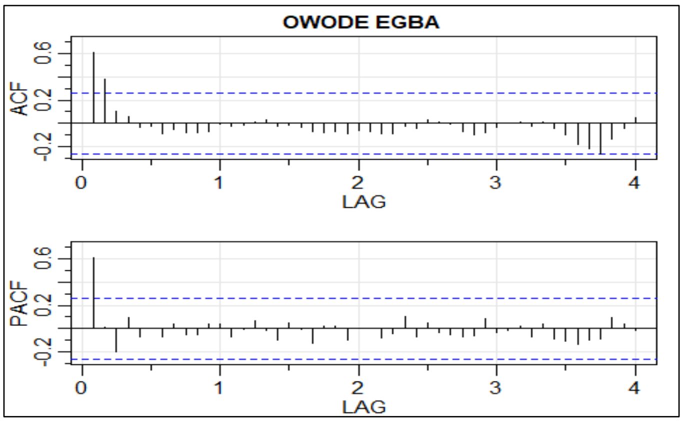

Figure 5: Owode Egba feeder 33kV Autoregression and Partial Autoregression plot.
Source: Authors, (2024).

The ACF and PACF graphs presented in Figure 5. above show that the ratio of data that falls within the range of Blue dotted lines are high which implies that this data are not significant and high possibility that a result or relationship is caused by something other than chance, in addition the ACF scatter along more in negative arts of the plot. As regards the test- statistics -1. 4093, is extremely high for the data point, with threshold of -3.50 to -3.45 this show component of uncertainty in the rationality of the test. However the lag order of 3 for real life data of this form may lead to multifaceted analyses hence will necessitate further investigation (authentication with adequacy test) before field application, p-value of 0.8135 in contradiction of ≤ 0 .05 is too high, hence, the validation of nonstationary feature of the series [29].

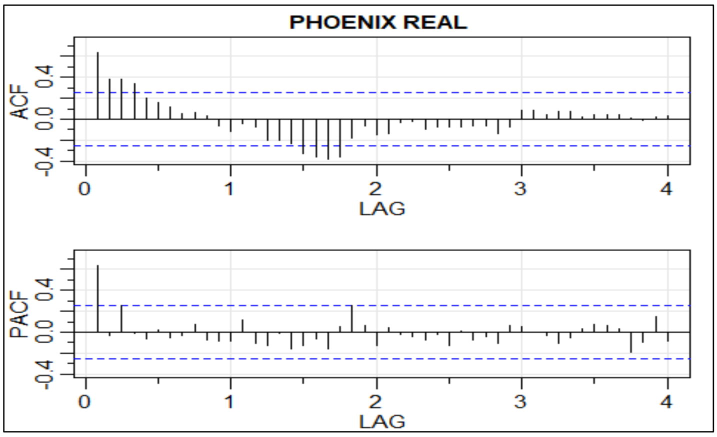

Figure 6: Phoenix 33kV feeder Autoregression and Partial Autoregression plot
Source: Authors, (2024).

Hypothesis Result of Phoenix 33kVA feeder Augmented Dickey-Fuller (ADF)
Dickey-Fuller = -2.0736
Lag order = 3,
p-value=0.545
alternative hypothesis: nonstationary

The ACF and PACF graphs in Figure 6 show that the proportion of data that falls within the range of Blue dotted lines are high which implies that this data are not significant and high likelihood that a result or relationship is caused by something other than chance, in addition the ACF scatter along more in negative parts of the plot. As regards the test- statistics -2.0736 is very high for the data point, (with threshold of -3.50 to -3.45), this show component of uncertainty in the rationality of the test. However the lag order of 3 for real life data of this form may lead to multifaceted analyses hence will necessitate further investigation for authentication with adequacy test before field application, p-value of 0.545 as against ≤ 0 .05 is too high, hence, the validation of nonstationary feature of the series.

III.2 SYSTEM CONFIGURATION

Ho = the series is non-stationary, Hi = the series is stationary: [26],[29].

Decision Rule: Reject Ho if the p-value is less than or equals to α (0.05); otherwise, do not reject. ADF Hypotheses rejecting the null hypothesis means that the given guess is not fit for application for lack of numerical significance; Acceptance of the null hypothesis is an indication that Ho is not rejected. The ADF test makes sure that the null hypothesis is accepted unless there is strong evidence against it to reject in favour of the alternate stationarity hypothesis [30-32].

IV. REFERENCES

[1] Precious C. Akanonu (2018) Challenges and Interventions Needs in the Nigerian Electricity Supply Industry (NESI).

[2] Doris Dokua Sasu (2023), Electricity in Nigeria - statistics & facts Nigeria. Energy and Environment.

[3] Nigeria Electricity Report Q3 2023 National Bureau of Statistics.

[4] Chukwuka Onyekwena, Joseph Ishaku, Precious C. Akanonu (2017) Electrification in Nigeria: Challenges and Way Forward. Centre for the Study of the Economies of Africa (CSEA) Abuja, Nigeria.

[5] Nigerian Electricity Supply and Installation Standards Regulations 2015 regulation no: nerc/reg/1/2015.

[6] Debnath, K. B. and Mourshed, M. (2018b). Forecasting methods in energy planning models. Renewable and Sustainable Energy Reviews, 88, 297-325

[7] Shay Palachy, (2019) Detecting stationarity in time series data Towards Data Science. A Medium publication sharing concepts, ideas, and codes.

[8] DeLurgio, S. A. (1998). Forecasting Principles and applications: Irwin Professional Publishing.

[9] Harvey A.C, (2017) Time Series Forecasting Based on the Logistic Curve Journal of the Operational Research Society, Volume 35, 1984 – Issue 7.

[10] Matthieu.Stigler, (2008).Stationarity Definition, meaning and consequences Matthieu Stigler Version 1.1, the document is released under the Creative Commons Attribution-Noncommercial 2.5 India license.

[11] Eduard Baumöhl & Štefan Lyócsa, 2009. Stationarity of time series and the problem of spurious regression. Online at https://mpra.ub.uni-muenchen.de/27926/MPRA Paper No. 27926, posted 07 Jan 2011 20:50 UTCAlfares, H. K., and Nazeeruddin, M. (2002). Electric load forecasting: literature survey and classification of methods. International journal of systems science, 33(1), 23-34.

[12] Stephanie: www.statisticshowto.datasciencecentral.com › adf-augmented-dickey-fuller, Jun 7, 2016.

[13] Academic library - free online college e textbooks - info {at}ebrary.net - © 2014 – 2020 Stationary and unit root test.

[14] Adejumobi, I. A. (2005) Forecasting Models and Diagnostic Checking with respect to Box-Jekins Time Series analysis. Nigeria Journal of Pure and Applied Science 20(1).1822-1834.

[15] Paul Torfs & Claudia Brauer (2017). A (very) short introduction to R Hydrology and Quantitative Water Management Group, Wageningen University, The Netherlands 4 August 2017.

[16] Galit, S and Kenneth C. L Jr.(2016), Time series forecasting with hands-on guide second edition Axelrod Schnall Publisher ISBN-13: 978-0-9978479-1-8 ISBN-10: 0-9978479-1-3.

[17] Robert H Shumway. David S. Stoffer (2011). Time Series Analysis and its Applications with Examples Spinger New York Dordrecht Heidelberg London. Third Edition.

[18] Gupta, J. (2009). A course in power systems: SK Kataria and Sons.

[19] Pabla, A.S (2004), Electric Power Distribution (5th Edition), Teta McGraw, Hill Publishing Company Ltd, New Delhi.

[20] Wikipedia, the free encyclopedia.

[21] Adejumobi, I. A (2021). Electricity, Man and Development: The complexity of the distribution system management in a power network 64th Inaugural lecture, Federal University of Agriculture Abeokuta Nigeria.

[22] Shirato, G., Andrienko, N., Andrienko, G., (2021). What are the topics in football? Extracting time-series topics from game episodes. In IEEE VIS 2021 Poster. URL http://geoanalytics.net/and/papers/vis21poster.pdf.

[23] Shirato, G., Andrienko, N., Andrienko, G., (2023). Identifying, exploring, and interpreting time series shapes in multivariate time intervals. Visual Informatics Published by Elsevier Volume 7, Issue 1, March 2023, Pages 77-91.

[24] Debnath, K. B. and Mourshed, M. (2018a). Challenges and gaps for energy pslanning models in the developing-world context. Nature Energy, 3(3), 172.

[25] Fuller, W. A. (1976). Introduction to Statistical Time Series. New York: John Wiley and Sons. ISBN 0-471-28715-6.

[26] Augmented Dickey–Fuller test – Wikipedia] en.wikipedia.org › wiki › Augmented_Dickey–Fuller_test.

[27] Wikipedia, the free encyclopedia Ogun.

[28] Ade-Ikuesan O.O, Osifeko M. O, Okakwu, I. K, Folaranmi K. S and Alao P.O (2018). Prediction of Electricity Consumption Demand Pattern for 2018 in Ogun state Nigeria. Journal of Applied Sciences &Environmental Management (JASEM) 22(6). 22(6):883-886.

[29] FinMath.Statistics.HypothesisTesting, Testing Of Stationarity Copyright © 2013, Deltix, Inc. RTMath, division of Deltix Inc.

[30] Hyndman, R.J., & Athanasopoulos, G. (2019) Forecasting: principles and practice, 3rd edition, OTexts: Melbourne, Australia. OTexts.com/fpp3. Accessed on <20200208>.

[31] Mehmed Kantardzic J. B, (2003). Data Mining—Concepts, Models, Methods, and Algorithm John Wiley & sons, Inc., Publication. The Institute of Electrical and Electronics Engineers, Inc.

[32] Akpanta, A, and Okorie, I. (2014). Application of Box-Jenkins Techniques in Modelling and Forecasting Nigeria Crude Oil Prices. International Journal of Statistics and Applications, 4(6), 283-291.

Journal of Engineering and Technology for Industrial Applications

ISSN ONLINE: 2447-0228

ITEGAM-JETIA

Manaus, v10. n.50, p. 59-65. November/ December., 2024.
DOI: https://doi.org/10.5935/jetia.v10i50.1300

RESEARCH ARTICLEOPEN ACCESS

THE IMPACT STUDY OF FLEXIBLE ALTERNATING CURRENT TRANSMISSION SYSTEM ON TRANSIENT STABILITY OF POWER SYSTEMS USING MATLAB CODE AND POWER WORLD SIMULATOR

Abdelhafid Hellal[1], Aissa Souli[2], Redha Djamel Mohammedi[3] and Mohamed Elbar[4]

[1] Polytechnic National School of El Harrach, Algiers, Algeria
[2] Electrical Engineering Department. Nuclear Research Center of Birine. Djelfa, Algeria
[3,4] Applied automation and industrial diagnostic Laboratory (LAADI), Faculty of Science and Technology, University of Djelfa, Algeria.

[1]http://orcid.org/0009-0000-2823-7868, [2]http://orcid.org/0009-0001-5463-8267, [3]http://orcid.org/0000-0003-4170-543X ,[4]https://orcid.org/0000-0002-2636-9469

Email: [1]hfdhellal@gmail.com, [2]a.souli@crnb.dz, [3]r.mohammedi@univ-djelfa.dz, [4]m.elbar@univ-djelfa.dz

ARTICLE INFO

Article History
Received: September 18, 2024
Revised: November 6, 2024
Accepted: November 10, 2024
Published: November 30, 2024

Keywords:
Transient Stability,
FACTS,
MATLAB,
Power World Simulator.

ABSTRACT

The purpose of this work is the study of the influence of FACTS on transient stability of power systems using a Power World Simulator software, and the computer code transient stability code 'TRANS_STAB_CODE' 'which was created in MATLAB. We tried in the introduction of this work to provide a description on the transient stability: definition, transient stability criteria, and equations. Then we gave an overview on the modelling of FACTS in power systems, the definition and types of Flexible Alternating Current Transmission System, their schemes, and their equations, then presented the model of UPFC (Unified Power Flow Controller) as an example. Secondly, we discussed the code, 'TRANS_STAB_CODE' that was created in MATLAB by giving a description of the code and their structure with graphics windows, and then I described privately the Power World Simulator simulation software. Then we presented the test electrical network, and the results of transient stability of this network systems with the code 'TRANS_STAB_CODE' 'and with Power World Simulator where no and where there Flexible Alternating Current Transmission System. At the end, we analyzed the results of both programs in both cases: with and without Flexible Alternating Current Transmission.

I. INTRODUCTION

Transient stability analysis is used to investigate the stability of power system under sudden and large disturbances, and plays an important role in maintaining security of power system operation [1],[2].

The transient stability analysis is performed by combining a solution of the algebraic equations describing the network with numerical solution of the differential equations.

However, due to the non-linearity of the differential equations, the solving process is tedious and complicated.

Flexible alternating current transmission systems (FACTS) technology opens up new opportunities for controlling power and enhancing the usable capacity of present, as well as new and upgraded lines.

The Unified Power Flow Controller (UPFC) is a second-generation FACTS device, which enables independent control of active and reactive power besides improving reliability and quality of the supply. This paper describes the transient stability in power systems by placing the UPFC at the sending end of an electrical power transmission system. The transient stability of power systems with the UPFC is compared with that without UPFC [3],[4].

Simulations are carried out in MATLAB Code 'which was created in MATLAB, and with Power Word Simulator to validate the results obtained and to see the performance of the UPFC.

Behavior of the power system transient is usually obtained on the basis of a model consisting of a differential equation system with a strong nonlinearity; the solution based on time can be obtained in the general case only by applying some suitable numerical integration methods [5],[6] Behavior of a synchronous machine for stable and unstable operation is illustrated in the Figure 1.

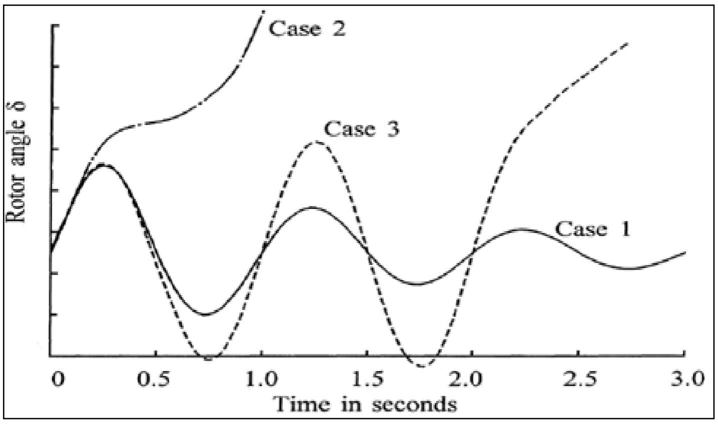

Figure 1: Rotor angle responses to transient disturbances.
Source: Authors, (2024).

In case 1, the rotor angle increases to a maximum and then decreases and oscillates with decreasing amplitude until it reaches a study state.

In case 2, the rotor continues to increase steadily until synchronism is lost. This type of instability is referred to as first swing instability and is caused by insufficient synchronizing torque.

In case 3 the system is stable in the first swing but becomes unstable as a result of growing oscillations as the end is approached. This form of instability generally occurs when post fault steady state condition itself is small signal unstable, and this is not necessarily as a result of the transient disturbance [7].

II. THE FACTS DEVICES

FACTS is a Flexible Alternating Current Transmission System, these devices have been developed by (EPRI) in the 80s.

It is a Power Electronic based system and other static equipment that provide control of one or more transmission system parameters to enhance control ability and to increase power transfer capability [8],[9].

FACTS devices are used to optimize already the existing transmission lines

FACTS devices are:

1. Serial Controllers: SSSC, IPFC, TCSC,
2. Parallel Controllers: STATCOM, SVC,
3. Serial - serial controllers,
4. Series - parallel controllers: UPFC, IPC,

II.1 USES OF FACTS DEVICES

1. To enhance the control ability of the transmission Network.
2. To increase the power transfer capability of transmission network.

II.2 OPPORTUNITIES OF FACTS

FACTS technologies opens up new opportunities for controlling power and enhancing the usable capacity of present as well as new and upgraded transmission lines .

FACTS controller controls the inter-related parameter that governs the operation of transmission lines including series impedance, Shunt impedance, current, voltage, Phase angle.

FACTS technologies also lead to extending usable transmission limits in step-by-step manner with incremental investment as and when required.

II.3 BENEFITS OF FACTS CONTROLLER

1. It increases the loading capability of the lines to their thermal capabilities.
2. It provides secured tie-line connections to the neighboring utilities.
3. It provides greater flexibility in setting new generations.
4. It helps in upgrading the transmission network.
5. It increases the utility of lowest cost generation.
6. It reduces Reactive Power flow thus allowing the lines to carry more active Power.

II.4 UNIFIED POWER FLOW CONTROLLER (UPFC)

The UPFC is made out of two voltage-source converters (VSCs) with semiconductor devices having turn-off capability, sharing a common dc capacitor and connected to a power system through coupling transformers. The basic structure of UPFC is shown in Figure 2.

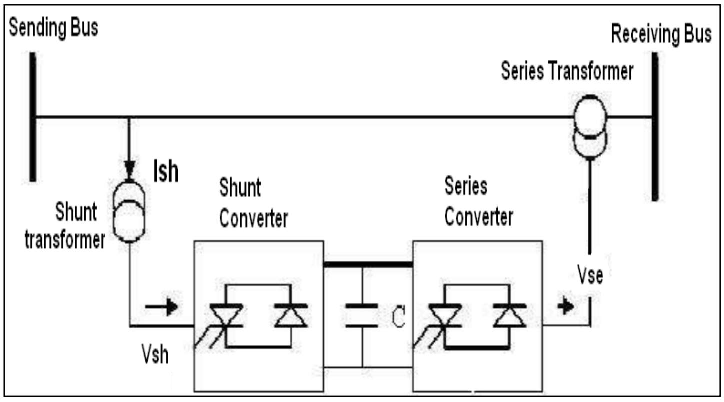

Figure 2: Basic Structure of an UPFC.
Source: Authors, (2024).

The shunt converter is primarily used to provide the real power demand of the series converter at the common dc link terminal from the ac power system. It can also generate or absorb reactive power at its ac terminal, which is independent of the active power transfer to (or from) the dc terminal.

Therefore, with proper control, it can also fulfill the function of an independent advanced static VAR compensator providing reactive power compensation for the transmission line and thus executing indirect voltage regulation at the input terminal of the UPFC [10].

II. DESCRIPTION OF THE COMPUTER TOOLS

II.1 MATLAB-CODE

Our program is called TRANS_STAB_CODE was developed to studies of transient stability of electrical networks [11],[12].

TRANS_STAB_CODE can analyze and studies of transient stability of electrical networks in two cases:

Trans_Stab_Linear_Loads where the loads are linear and Trans_Stab_Harmonic _Loads where there are non-linear loads (SVC, TCR, and UPFC) [13],[14].

TRANS_STAB_CODE is a computer code produced in MATLAB [15], and allows you to run multiple applications and functions (MATLAB files).

TRANS_STAB_CODE structure is based on graphical interfaces [16] performed by MATLAB (GUI).

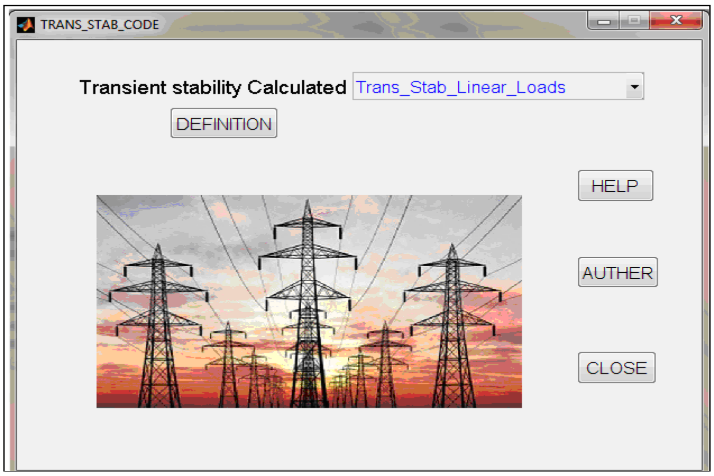

Figure 3: Principal Window of TRANS_STAB_CODE program.
Source: Authors, (2024).

The graphical interface TRANS_STAB_CODE program (Figure 3) contains a title, which signifies the objective of this program "Transient Stability Calculated", and two functions:

Trans_Stab_Linear_Loads, and Trans_Stab_Harmonic Loads with four push buttons:

The first button Definition: the definition of transient stability of power systems.

The second button Help: gives an overview of the program

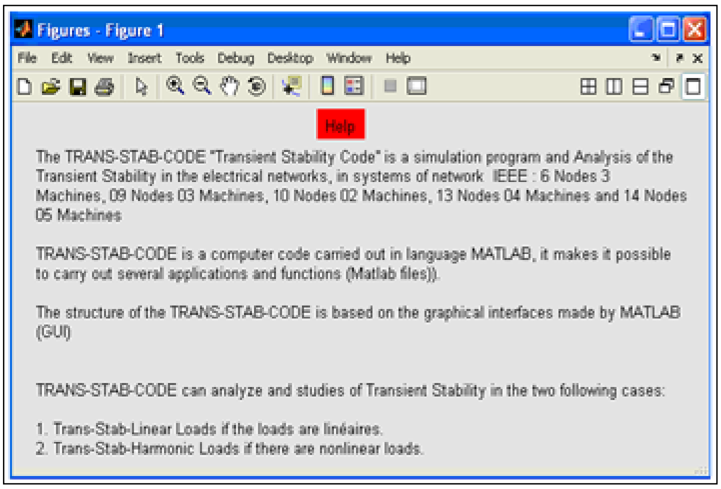

Figure 4: Help window of TRANS_STAB_CODE program.
Source: Authors, (2024).

The third button Réalised by: the author of this program.

The fourth button close: You can quit the programTRANS_STAB_CODE (Figure 4).

If we click on Trans_Stab_Linear_Loads, another window pops up and we can choose to study the electrical network systems (Figure 5).

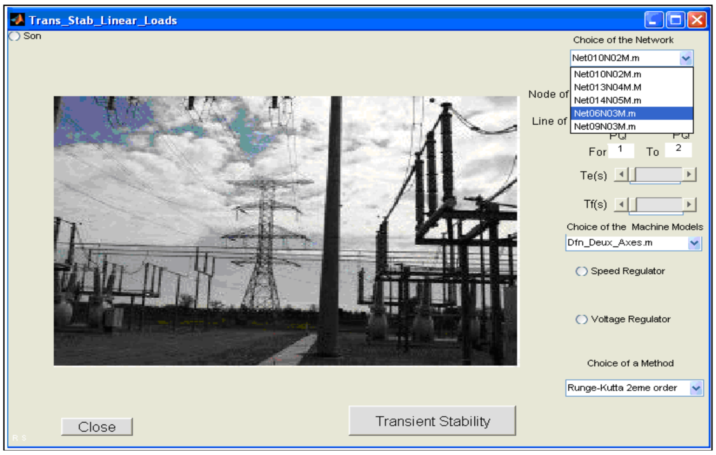

Figure 5: Electrical network system selection for studies of transient stability with linear loads.
Source: Authors, (2024).

If we press the button "Net06N03M, the block diagram of the network appears as follows (Figure 6):

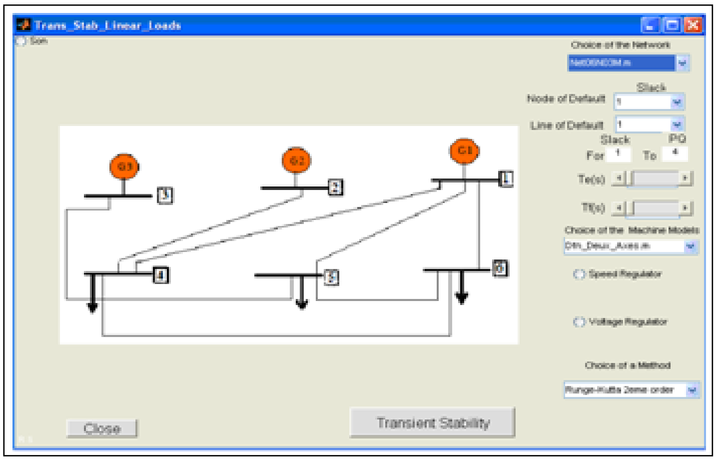

Figure 6: Synoptic diagram of network system 03 machines 6 bus.
Source: Authors, (2024).

If we press the button "Net09N03M (Figure 7), the block diagram of the network appears as follows:

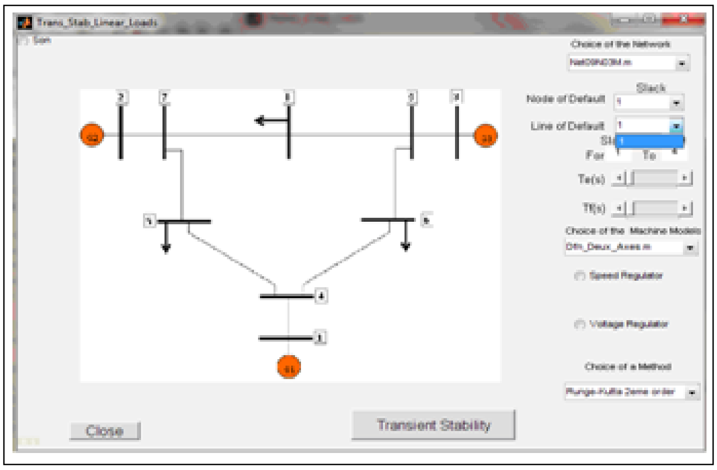

Figure 7: Synoptic diagram of network system 03 machines 09 bus.
Source: Authors, (2024).

If we click on Trans_Stab_Harmonic_Loads, another window pops up and we can choose to study the electrical network systems (Figure 8).

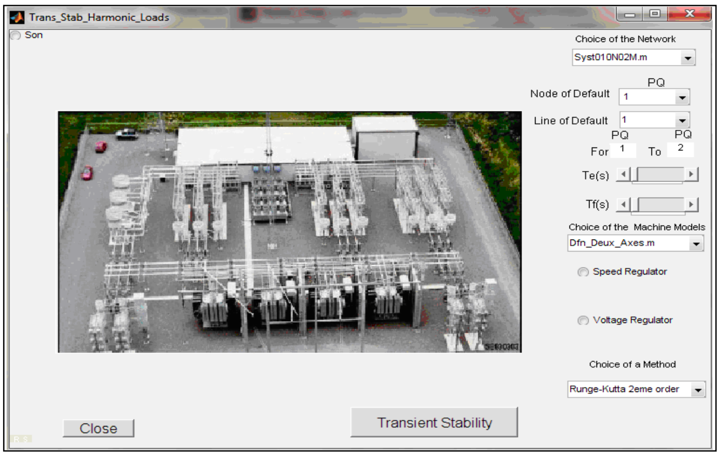

Figure 8: Electrical network system selection for studies of transient stability with non-linear loads.
Source: Authors, (2024).

If we press the button "Syst06N03M (Figure 9), the block diagram of the network appears as follows:

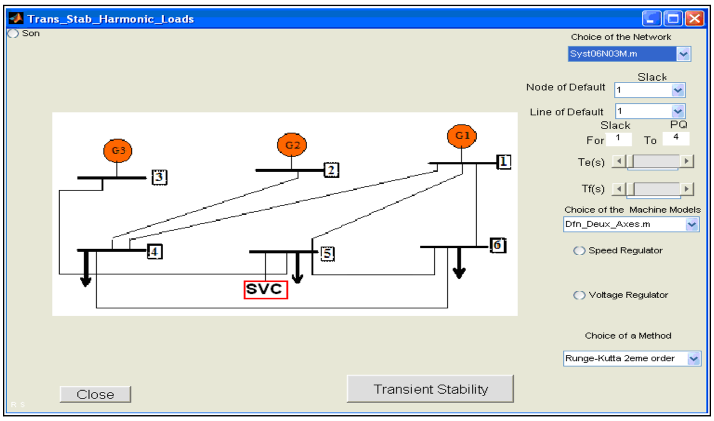

Figure 9: Synoptic diagram of network system 03 machines 6 bus with SVC.
Source: Authors, (2024).

If we press the button "Net09N03M (Figure 10), the block diagram of the network with UPFC appears as follows:

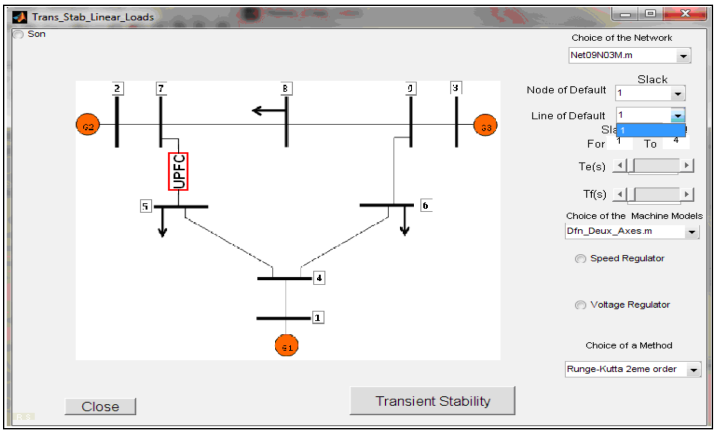

Figure 10: Synoptic diagram of network system 03 machines 09 bus, with UPFC.
Source: Authors, (2024).

II.2 POWER WORLD SIMULATOR

Power World Simulator [17] is an interactive power system simulation package designed to simulate high voltage power system operation on a time frame ranging from several minutes to several days. The software contains a highly effective power flow analysis package capable of efficiently solving systems of up to 100,000 buses.

Simulator runs under Microsoft Windows 95, 98, 2000, NT, or XP.

Key elements of power systems that are modelled include:

1. Load flow (power flow study),
2. Short circuit,
3. Transient stability,
4. Optimal dispatch of generating units (unit commitment),
5. Transmission (optimal power flow).

III. TEST NETWORK

A 9-bus 3-machine system [18], the system includes three generators and three large equivalent loads connected in a meshed transmission network through transmission lines as shown in Figure 11.

The total generation is 519.5MW and total load is 315MW.

The test system contains six lines connecting the bus bars in the system. Each generator is connected to network through step up transformer at 230kV transmission voltage.

We study the transient stability (a three-phase fault on bus 8 at 0.2 sec) in two cases:

1. Where linear loads,
2. Where non-linear loads (UPFC in line (5-7))

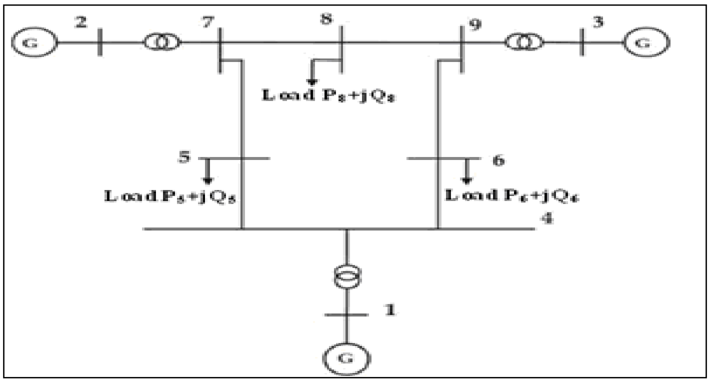

Figure 11: Synoptic scheme of System IEEE, 9 Bus.
Source: Authors, (2024).

Figure 12 shows the Network Test with Power Word Simulator.

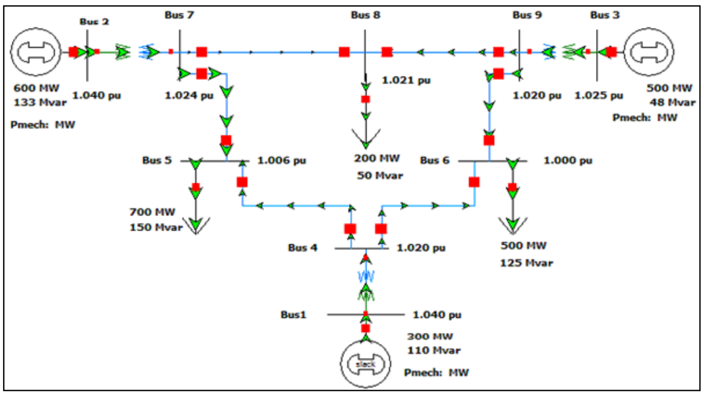

Figure 12: Test network with Power Word Simulator.
Source: Authors, (2024).

IV. RESULTS AND DISCUSSION

IV.1 With Power World Simulator

Without FACTS

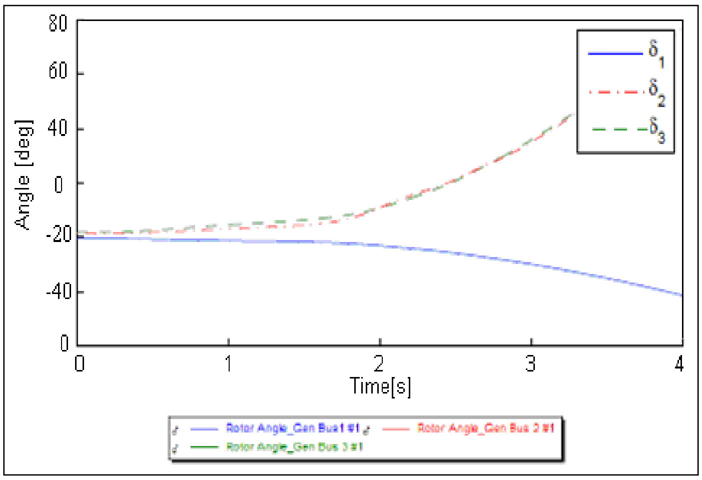

Figure 13: Rotor Angle of generators.
Source: Authors, (2024).

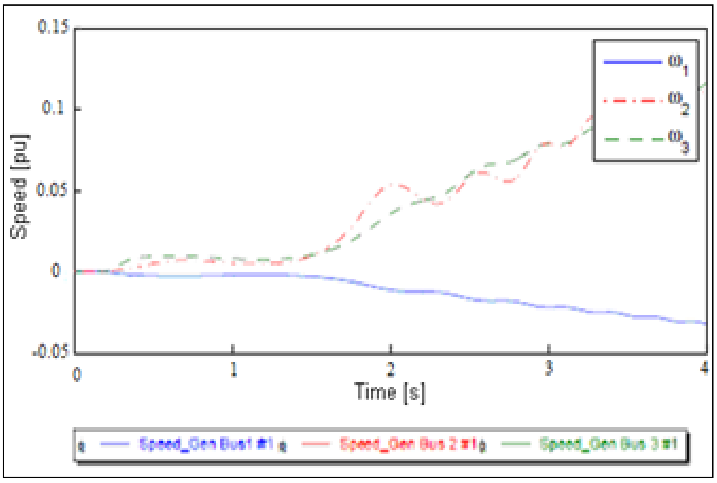

Figure 14: Angular speed of generators.
Source: Authors, (2024).

With FACTS

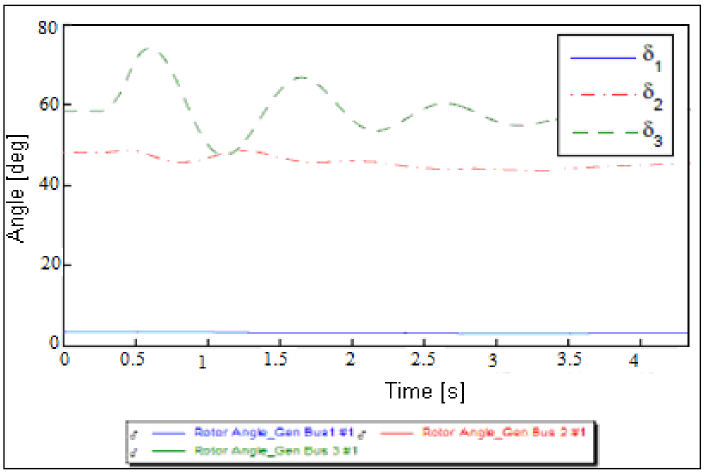

Figure 15: Rotor Angle of generators.
Source: Authors, (2024).

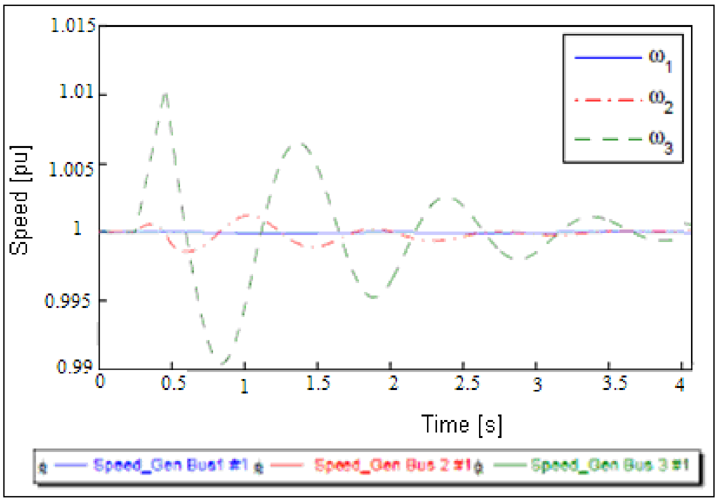

Figure 16: Angular speed of generators.
Source: Authors, (2024).

IV.2. With MATLAB CODE

Without FACTS (UPFC)

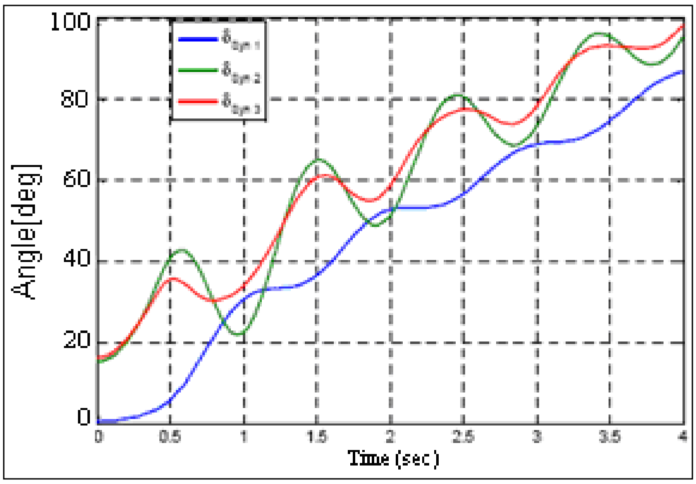

Figure 17: Rotor Angle of generators.
Source: Authors, (2024).

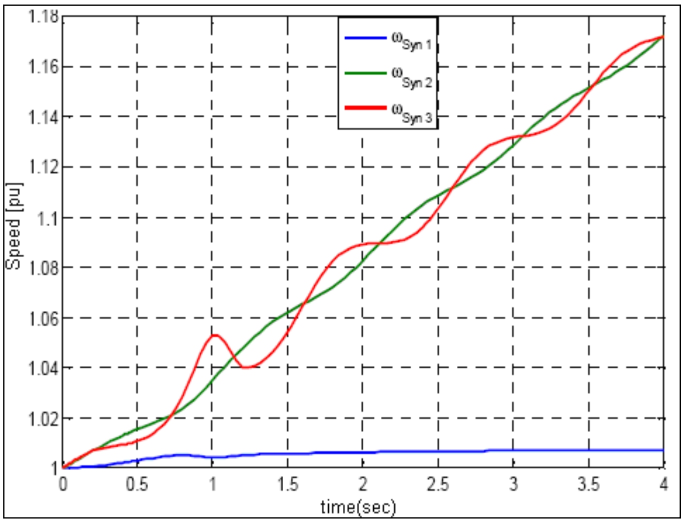

Figure 18: Angular speed of generators.
Source: Authors, (2024).

With FACTS (UPFC)

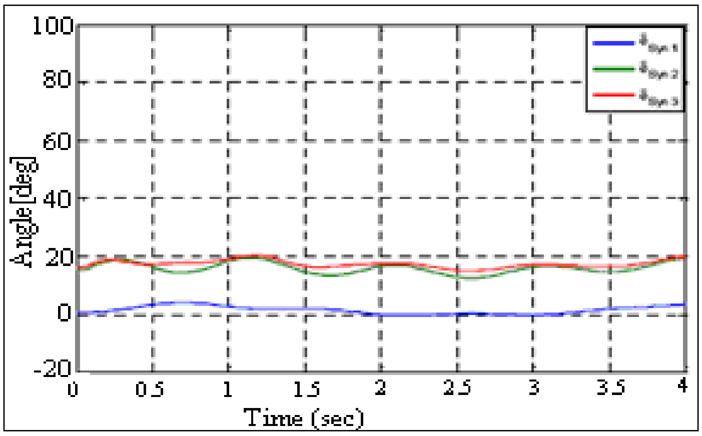

Figure 19: Rotor Angle of generators.
Source: Authors, (2024).

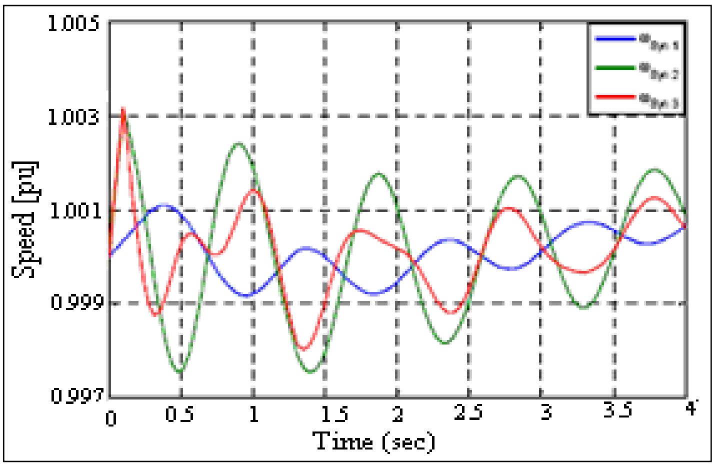

Figure 20: Angular speed of generators.
Source: Authors, (2024).

For our network system IEEE9 bus nodes, and a short circuit fault at the bus 8 (f t = 0.2 sec, c t=0.7sec) in the case where the normal load (not a UPFC), we note that the rotor angles curves of generators (2 3 d,d) of our network system are diverged by using the both software's: Power World Simulator (Figure 13), and MATLAB CODE (Figure 17), we observe also that after the fault the speed generators curves (2 3 w,w) are diverged by using the both software's: Power World Simulator (Figure 14), and MATLAB CODE (Figure 18), and consequently therefore the network system is not stable even after cleared the fault.

For the same system (IEEE 9bus) and for the same fault but if we set an UPFC in the line (5-7) as presented in the block diagram of (Figure 10), the curve of the rotor angles of machines2 and machine3 (2 3 d,d) of our network system are converged by using the both software's: Power World Simulator (Figure 15), and MATLAB CODE (Figure 19), we note also that after the fault the speed generators curves (2 3 w,w)are converged by using the both software's: Power World Simulator (Figure 16), and MATLAB CODE (Figure 20), and consequently therefore the network system is stable after cleared the fault.

IV. CONCLUSION

In this paper, the transient stability of the standard network system IEEE 9bus with and without using UPFC is studied.

FACTS device such as UPFC is employed for enhancing transient stability. The simulation results obtained from the use of different softwares shown in figure15, figure19 illustrates how the transient stability has been improved through the use of the UPFC.

The TRANS_STAB_CODE program is called « Transient Stability CODE ", developed in MATLAB environment has been tested on several nonlinear loads such as: SVC, TCR, UPFC, and gave entire satisfaction for the simulations performed confirming the relevance of this code.

Through these results one can say that the transient stability enhancement is achievable with UPFC, As well as the UPFC is extremely effective by handling disturbances of dynamic system.

The results have virtually the same appearance and overlap completely with those obtained with the Power World Simulator and MATLAB CODE, which shows the reliability of software Power World Simulator and MATLAB CODE in the study of the Transient Stability.

V. AUTHOR'S CONTRIBUTION

Conceptualization: Abdelhafid Hellal, Aissa Souli, Redha Djamel Mohammedi and Mohamed Elbar.
Methodology: Abdelhafid Hellal, Aissa Souli, Redha Djamel Mohammedi and Mohamed Elbar.
Investigation: Abdelhafid Hellal, Aissa Souli, Redha Djamel Mohammedi and Mohamed Elbar.
Discussion of results: Abdelhafid Hellal, Aissa Souli, Redha Djamel Mohammedi and Mohamed Elbar.
Writing – Original Draft: Abdelhafid Hellal, Aissa Souli, Redha Djamel Mohammedi and Mohamed Elbar.
Writing – Review and Editing: Abdelhafid Hellal, Aissa Souli, Redha Djamel Mohammedi and Mohamed Elbar.
Resources: Abdelhafid Hellal, Aissa Souli.
Supervision: Abdelhafid Hellal, Aissa Souli, Redha Djamel Mohammedi and Mohamed Elbar.
Approval of the final text: Abdelhafid Hellal, Aissa Souli, Redha Djamel Mohammedi and Mohamed Elbar.

VI. REFERENCES

[1] T. Ye, H. Wei, H. Yang et al., Coordinated control of multi-FACTS to enhance the small disturbance stability of the power system, s.l.: IEEE PES Innovative Smart Grid Technologies, (2012).

[2] MARLINK; Réseaux Electriques Aspects Actuels", électricité de France, Editura tehnica, Bucuresti 2000.

[3] CORAN; Modeling and Analysis of Electric power systems; EEH power systems Laboratory, ETH Zurich, 2004.

[4] Ganesh, and All, '' Improvement of Transient Stability Through SVC '' International Journal of Advances in Engineering & Technology, Nov. 2012.

[5] Prechanon Kumkratug, ''the Effect of the Static Var Compensator and R/X Ratio of Short Transmission Line on Transient Stability of Single Machine Infinite Bus System", American Journal of Applied Sciences 9(4): 468-471, 2012 ISSN 1546-9239 © 2012 Science Publications.

[6] Redha Djamel Mohammedi1, Aissa SOULI, Abdelhafid HELLAL, "Design of a computer code to evaluate the influence of the harmonics in the transient stability studies of electrical networks," PRZEGLĄD ELEKTROTECHNIC-ZNY, ISSN 0033-2097, R. 99 NR 12/2023, doi:10.15199/48.2023.12.04

[7] Whitaker, Jerry C. "Power Quality Standards"AC Power Systems Handbook, 2nd Edition. Jerry C. Whitaker Boca Raton: CRC Press LLC, 1999.
[8] Ravi Kumar and S. Siva Nagaraju, '' Transient Stability Improvement Using UPFC And SVC", ARPN Journal of Engineering and Applied Sciences, VOL. 2, NO. 3, June 2007.

[9] G. Naveen Kumar, M.S. Kalavathi, Reactive power compensation for large disturbance voltage stability using FACTS controllers, 2011 3rd International Conference on Electronics Computer Technology, Kanyakumari, India, (2011).

[10] Y. Wang, Y. Sun and S. Mei, Modeling of Short-term Large-disturbance Voltage Stability Considering Induction Motors, IEEE PES Innovative Smart Grid Technologies, Tianjin, China (2012).

[11] M. Elbar, A. Souli, A. Beladel, B. Ali, and A. Benhaimoura, "Impact study of flexible alternating current trans-mission system on power flow and power loss in power systems using MATLAB and PSAT", SEES, vol. 4, no. 1, pp. 348–369, Dec. 2023. https://doi.org/10.54021/seesv4n1-021.

[12] Mihai Gavrilaş1, Radu Toma,'' Flexible alternating current transmission system optimization in the context of large disturbance voltage stability'', Rev. Roum. Sci. Techn.–Électrotechn. et Énerg, Vol. 66, 1, pp. 21–26, Bucarest, 2021.

[13] Eslami M., Shareef H., Mohamed A., Application of PSS and FACTS devices for intensification of power stability. Inter. Rev. Electr. Eng., 5 (2010) No. 2, 552-570.

[14] A. Hashmani, Y. Wang, and T. T. Lie, "Enhancement of power system transient stability using a nonlinear coordinated excitation and TCPS controller," Int. J. Electr. Power Energy Syst., vol. 24, 201-214, 2002.

[15] MATLAB 7.1.0.246, Service Pack 3, August 2005, License Number 161051, Copyright 1984-2005.

[16] MATLAB®Creating Graphical User Interfaces© COPYRIGHT 2000– 2012 by The MathWorks, Inc.

[17] Simulator 16 User Guide - PowerWorld, User's Guide, 2011

[18] Swaroop Kumar. Nallagalva, Mukesh Kumar Kirar, Dr. Ganga Agnihotri, '' Transient Stability Analysis of the IEEE 9-Bus Electric Power System'', ISSN: 2277-1581, 01 July 2012.

Journal of Engineering and Technology for Industrial Applications

ITEGAM-JETIA

ISSN ONLINE: 2447-0228

Manaus, v10. n.50, p. 66-80. November/ December., 2024.
DOI: https://doi.org/10.5935/jetia.v10i50.1302

RESEARCH ARTICLE OPEN ACCESS

CAUSES, EFFECTS, AND PRACTICAL METHODS OF HARMONIC REDUCTION IN IRANIAN CEMENT FACTORIES WITH A FOCUS ON PLANT DEVELOPMENT

Mehdi Eslamian Koupaie

[1]. Department of Electrical Engineering- Isfahan (Khorasgan) Branch, Islamic Azad University Iram.

[1] https://orcid.org/0000-0002-4924-34x3

Email: 67mehdi@gmail.com

ARTICLE INFO

Article History
Received: September 24, 2024
Revised: November 6, 2024
Accepted: November 10, 2024
Published: November 30, 2024

Keywords:
Cement Industries,
Harmonics,
Variable Speed Drives,
Power Quality.

ABSTRACT

Cement factories in Iran are considered among the oldest industries. Due to favorable domestic and international markets, these plants have pursued development, whether willingly or unwillingly. Development involves improving the existing structure to enhance efficiency and adding production lines parallel to the old ones. In this situation, the presence of very large nonlinear loads in these industries, which are mostly formed by high-power variable-speed electric drives, has always caused serious problems due to harmonic distortions imposed on the factory and distribution lines. These effects should be considered in various sections when developing and designing new electrical systems. Despite various studies on this subject, none has presented a comprehensive approach specifically for this industry. This article delves into a thoroughly practical and empirical examination of the causes and consequences stemming from harmonics, alongside the constraints posed by standards. It also scrutinizes implementable techniques for solving harmonic-related problems and mitigating their effects with a focus on the development outlook of cement factories.

I. INTRODUCTION

Cement factories in Iran are considered among the oldest and largest industries. Due to the presence of large DC and AC motors and the necessity of controlling them, high-power AC and DC drives are used in various divisions such as mills, induced draft fans (known as ID fans), crushers, separators, and rotary kilns. The input voltage levels of the drives are typically in MV (6.3 KV) and LV (400 V, 690 V, and 800 V) levels. Most of Iran's cement factories operate within these voltage ranges and other voltage levels rarely observed. Motors and large drives in Iran's cement industries are often DC, but in development departments and modern factories, only AC motors and drives are utilized. Figure 1 illustrates a single-line diagram (SLD) of the development section of one of the major cement producers in Iran. The presence of large AC motors and drives in this factory signifies high energy consumption within this industry and as a result a large volume of harmonics with high amplitudes. Generally, the energy consumption of the cement industry accounts for nearly 5% of the total global industrial energy consumption [1], and the advantage of controlling harmonics caused by variable speed drives (a major source of nonlinear loads in the cement industry), besides its impact on the protection and lifespan enhancement of electrical equipment, can result in a reduction in losses, thereby decreasing global energy consumption, as well as return on investment in a cement plant [2].

So far, various studies, measurements and practical investigations have been carried out in the field of harmonics, methods of reducing them and improving power quality specifically for the cement industry [2-8]. However, these studies have been few and do not offer a comprehensive perspective to the reader for decision-making in electrical designs aimed at cement plant development. This paper attempts to not only present the causes, effects, measurement techniques, and practical comparison of control and reduction methods for harmonics in the cement industry but also provide a succinct review of relevant standards. Such insights can significantly assist electrical engineers in the design of electrical systems and the development of cement plants.

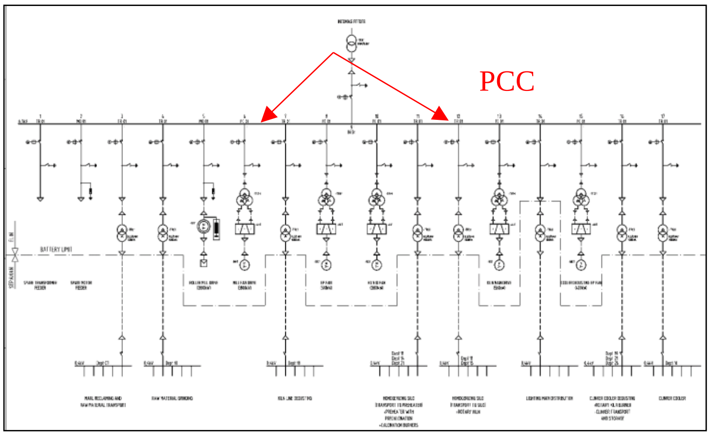

Figure 1: Single-line diagram of development section of modern cement plant in Iran.
Source: Authors, (2024).

From the point of view of the utility power system, only the amount of distortions in the input medium voltage (MV) levels holds significance, whereas in industrial plants, distortions at low voltage (LV) levels are crucial [5]; But in a cement factory, due to the existence of a dedicated substation and the use of both voltage levels, the values of harmonics in both sides of the grid and the plant are important. Therefore, the approach of this manuscript is to provide appropriate solutions while considering this aspect.

II. HARMONICS AND THEIR GENERATION CAUSES IN CEMENT INDUSTRIES

In accordance with IEEE 519-1992, harmonic is defined as a sinusoidal component of a periodic waveform or quantity (such as voltage or current), possessing a frequency that is a whole-number multiple of the fundamental frequency (50 or 60 Hz) [9]. Harmonics arise from all nonlinear sources within a cement plant. A source is considered nonlinear if its impedance varies with the applied voltage at any moment of time. Due to this impedance variation, the current drawn by the nonlinear load is also nonlinear [10]. Essentially, when a non-linear load is connected to a sinusoidal voltage source, the waveform becomes non-sinusoidal. Power electronic converters (AC/AC, AC/DC, DC/AC, DC/DC) and transformers are considered as sources of non-linear loads. Non-linear loads present in a cement plant include variable speed drives (variable frequency), uninterruptible power supplies (UPS), generators, power and distribution transformers, lighting systems (including LED or gas discharge lamps), computers, programmable logic controllers (PLCs), static var compensators (SVCs), and some laboratory equipment equipped with switching power supplies or rectifiers; nonetheless, the most influential nonlinear load in cement industries are large variable speed drives. They are the most important sources of harmonics and inter-harmonic distortions in cement industries [6]; although, one should not overlook the effects of arc furnaces that exist in a few cement factories in Iran. Table 1, inspired by the SLD of Figure 1, illustrates the power of large AC variable speed drives of the development segment of the sample factory, which can be relatively generalized for other cement plants in Iran.

Table 1: Large AC variable speed drives in a modern cement plant sample in Iran.

Equipment	Power
Mill fan drive	3800 kW
Kiln ID fan	2800 kW
Roller mill drive	2800 kW
Kiln main drive	560 kW
EP fan	500 kW
Cooler Dedusting EP fan	400 kW

Source: Authors, (2024).

The mentioned drives draw large non-linear or so-called non-sinusoidal currents from the grid and distort the power supply voltage waveform at the point of common coupling (PCC). Typically, the PCC is defined as the closest point to the user in the power system, so that the operator (system owner) can provide services to other subscribers from that point. For industrial users, the PCC is often considered at the high-voltage (HV) side of the transformer, while for commercial users, it is situated at the LV side of the transformer [9]. From the point of view of a cement plant with a dedicated substation, this point is considered to be on the MV side of the distribution transformers, i.e. the 6.3 kV side of the SLD in Figure 1 (where all the distribution transformers are connected). Figure 2 shows the equivalent circuit of a factory distribution system with non-linear load connection. The voltage in PCC is displayed as V_{PCC} and is calculated by subtracting the source voltage from the source impedance voltage drop (LS) caused by the passage of the nonlinear current i_{ac} as follows

$$V_{PCC} = (V_s - V_L) = \left\{ V_S - L_s \frac{d(i_{ac})}{dt} \right\} \quad (1)$$

By reason of the nonlinear nature of the current flow i_{ac} through the LS impedance, distortions in V_{PCC} will be observed. To mathematically express the non-linearity of current and voltage at the PCC, Fourier analysis is employed. Accordingly, the waveforms of complex alternating voltage and current can be expressed as the sum of an infinite number of sinusoidal oscillatory functions with different frequencies and amplitudes, which are integer multiples of the fundamental frequency.

Equations (2) and (3) represent symmetrical AC current and voltage without DC component at PCC point respectively, where i_{ac1} and V_{PCC1} are the fundamental frequency components (50 or 60 Hz), and i_{ach} and V_{PCCh} are components at the h_{th} harmonic frequency [10]. Figure 3 illustrates the practical measurement of root mean square (rms) values of voltages and currents containing harmonics at the PCC of a cement factory.

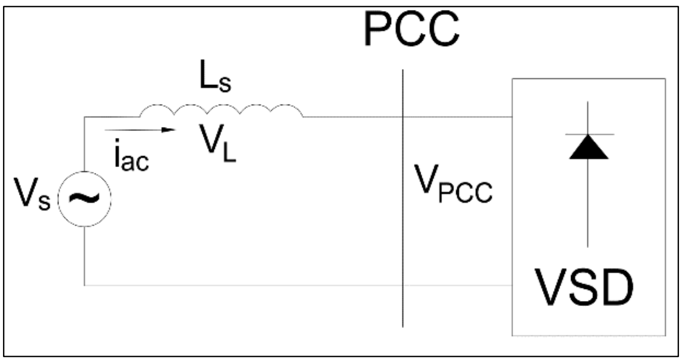

Figure 2: Equivalent circuit of the distribution system and PCC location.
Source: Authors, (2024).

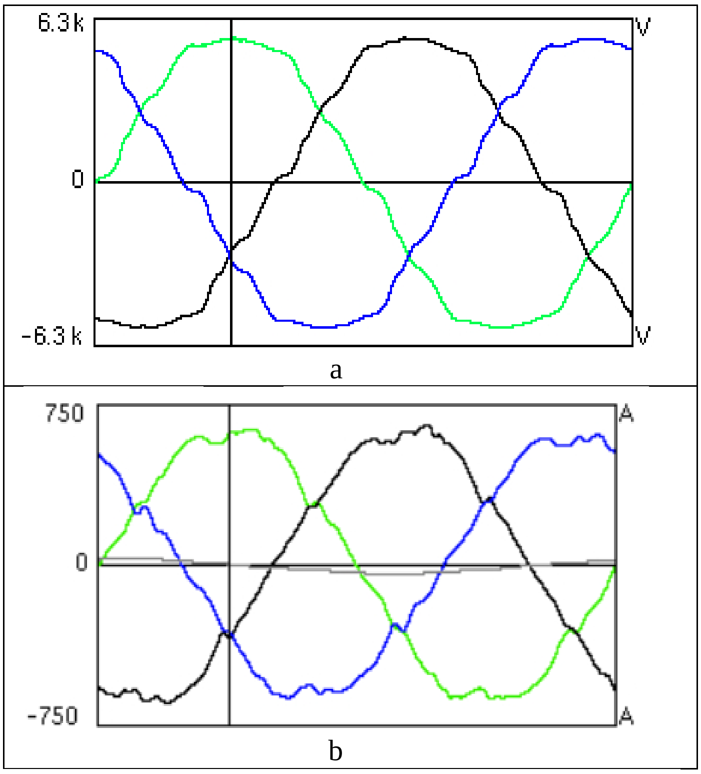

Figure 3: Measured rms voltage (a) and current (b) containing harmonics at the PCC of a cement factory.
Source: Authors, (2024).

$$i_{ac}(t) = i_{ac1}(t) + \sum_{h=2}^{\infty} i_{ach}(t) \quad (2)$$

$$V_{PCC}(t) = V_{PCC1}(t) + \sum_{h=2}^{\infty} V_{PCCh}(t) \quad (3)$$

The characteristic harmonics of electrical drives (or all power electronic converters) in steady-state are obtained from equation (4) [10],[11] and the amplitude of harmonic currents for an ideal square wave from equation (5) [11], where h represents the harmonic order, P is the number of pulses per cycle, n is any integer, I_h is the harmonic current of the h_{th} order, and I_1 is the fundamental current.

$$h = nP \pm 1 \quad (4)$$

$$I_h = \frac{I_1}{h} \quad (5)$$

Based on equations (4) and (5), for prevalent electrical drives in cement plants, whether with DC or AC motors, the characteristic or dominant harmonics and the percentage of harmonic currents, are as follows:

- Predominant harmonics in 6-pulse drives: 5, 7, 11, 13, 17, 19, 23, 25, ...
- Predominant harmonics in 12-pulse drives: 11, 13, 23, 25, 35, 37, ...
- Predominant harmonics in 18-pulse drives (currently not common in Iranian cement plants): 17, 19, 35, 37, ...
- The magnitude of harmonic currents for the 5^{th}, 7^{th}, 11^{th}, 13^{th}, 17^{th}, orders are, in turn, 20%, 14.3%, 11.1%, 7.7%, 5.8%, ...

The amount of distortion in voltage and current waveforms at the PCC are determined by the Total Harmonic Distortion (THD) index and calculated by equations (6) and (7) respectively.

$$\%THD_{V_{pcc}} = \frac{\sqrt{\sum_{h=2}^{\infty} V_{pcch}^{\ 2}}}{V_1} \times 100 \quad (6)$$

$$\%THD_I = \frac{\sqrt{\sum_{h=2}^{\infty} I_h^{\ 2}}}{I_1} \times 100 \quad (7)$$

IEEE 519-2014 introduces an additional metric, known as Total Demand Distortion (TDD), to assess the overall impact of distortion on the current waveform at the PCC. TDD is a percentage of the maximum demand current at the PCC and is computed using equation (8):

$$\%TDD = \frac{\sqrt{\sum_{h=2}^{\infty} I_h^{\ 2}}}{I_L} \times 100 \quad (8)$$

In the above equation, I_h represents the magnitude of individual harmonic components (rms amps), h denotes the harmonic order, and I_L stands for the maximum demand load current (rms value) at the PCC, typically defined as the sum of load currents associated with maximum demand during each of the twelve previous months divided by 12. TDD can also be represented as a measured $\%THD_I$ per unit of load current [10]; however, TDD is utilized at the PCC instead of THD_I.

Normally, harmonics up to the 50^{th} order (in typical industrial applications, which Iran's cement factories also follow, up to the 25^{th} order [10]) are used to measure THD_{Vpcc}, THD_I and TDD. Harmonic components beyond the 50^{th} order are measured only if necessary (for sensitive applications) [9]. Additionally, IEEE 519-2014 introduces the following relationships under the headings of very short time and short time harmonic measurements. These measurements were not present in previous IEEE standards. Very short time harmonic values are evaluated over a 3-second interval by aggregating 15 consecutive sections and 12 (or 10) cycles for 60 (or 50) Hz power systems, and are calculated using equation (9). In practice, the duration of this measurement is 24 hours. Short time harmonic values are also assessed for a specific frequency component over a 10-minute interval based on summing up 200 consecutive very short-time values by equation (10). Practically, the duration of this measurement is one week.

$$F_{n,vs} = \sqrt[2]{\frac{1}{15}\sum_{i=1}^{15} F_{n.i}^2} \quad (9)$$

$$F_{n,sh} = \sqrt[2]{\frac{1}{200}\sum_{i=1}^{200} F_{(n,vs),i}^2} \quad (10)$$

In equations (9) and (10), F represents the rms values of voltage or current, n denotes the harmonic order, i is a simple counter, and the subscripts vs and sh correspond to "very short" and "short", respectively.

The recommended values and limits for voltage and current distortion are outlined in Section IV. It's noteworthy that in cement plants without arc furnaces (similar to the majority of cement plants in Iran), odd harmonics are predominantly present, and in most cases, even harmonics can be disregarded. odd harmonics are often dominant and even harmonics can be ignored in most cases.

III. HARMONIC EFFECTS ON CEMENT PLANT DEVELOPMENT

The penetration of new equipment such as mills, fans, crushers, rotary kilns, etc., into the development divisions of a cement factory significantly alters harmonic conditions. An empirical recommendation suggests conducting harmonic studies in the current state of the factory prior to the design of development sections; Because changes in new harmonic conditions can lead to damage to old equipment, reduce power factor, increase maintenance costs, and energy consumption [3], [8], [10], [12]. The effects of harmonics in cement factories vary depending on the type of electrical equipment and the sensitivities of different departments. Usually, the problems caused by harmonics are not obvious at first glance and operators only observe secondary effects such as sudden production line interruptions, transformer overheating, and electronic equipment malfunctions. In many cases, attempts are made to solve the problem (such as increasing transformer capacity, increasing cable size, and so on) regardless of the root cause of these issues (i.e., harmonics). However, it should be noted that even if there are no apparent problems in the existing factory, it is uncertain how close it is to a critical situation [8]. Minor developments or optimizations in cement factory production lines (such as using power factor compensators, changing DC drives to modern AC drives, etc.) will reveal these effects. It should be noted that all protective relays, capacitor banks, reactors, cables, transformers, and switches are not designed and sized for the effects caused by harmonics. It should be acknowledged that none of the protective relays, capacitor banks, reactors, cables, transformers, and switches are designed and sized to mitigate the effects caused by harmonics.

The addition of new equipment means an increase in non-linear current drawn from the AC source. These harmonic currents pass through all impedances between the load and the source, causing voltage drops for each harmonic frequency. The total voltage distortion, resulting from the vector summation of all individual voltage drops, is substantially influenced by the impedance between the source and the load. The significant effects of harmonics in cement factories are briefly discussed below. The significant impacts of harmonics in cement factories are succinctly addressed herein. It is noteworthy that other effects have been neglected owing to fewer problems in this type of plants.

III.1 POWER QUALITY

The first tangible effect can be considered as the reduction in power quality. Harmonics cause distortion in the waveform and a decrease in the power factor. While initially, the power factor may appear to be determined solely by reactive power, theinfluence of harmonics on reducing the power factor cannot be disregarded. While power factor may initially be perceived solely as reactive power dependence, the effects resulting from harmonics cannot be overlooked in power factor reduction. Reference [13] expresses equation (11) as the relationship between THD_I and power factor. Consequently, an increase in harmonics results in a decrease in power factor. In this equation, $\cos\phi_1 = P_1 / S_1$, P_1 and S_1 respectively refer to active and reactive power at the fundamental frequency.

$$PF \approx \frac{\cos\phi_1}{\sqrt{1+THD_I^{\,2}}} \tag{11}$$

It is worth mentioning that power factor correction capacitors in the cement factory power grid are also affected by harmonics and may be subject to overloading and premature failure. This is because the capacitive reactance is inversely proportional to the frequency, thus acting as a harmonic current consumer.

III.2 TRANSFORMERS

Harmonics induce heightened flux dispersion and iron losses within transformers, attributed to amplified eddy and hysteresis currents. These effects culminate in elevated thermal dissipation and insulation stress on winding conductors, ultimately diminishing the transformer's operational longevity. Harmonics also intensifies the vibration of the core laminations and result in the production of additional acoustic noise. Moreover, due to the increase in the rms current values, copper losses in the transformer (RI^2) are also elevated [3],[10],[14].

III.3 ELECTRICAL MOTORS

Electrical motors employed within cement factories, whether DC or AC, will be affected by harmonics, necessitating meticulous attention during their design or procurement processes [15], as harmonics manifest in the outputs of converters and directly impact motors. Analogous to transformers, their adverse effects include losses from eddy and hysteresis currents. These effects lead to increased heat losses, winding insulation stress, lubrication degradation of bearings, and diminished motor longevity. For every 10 degrees temperature increase above the rated temperature of the motor, the insulation life of the motor may decrease by 50% [10]. Another effect is the generation of bearing currents, which, if left unaddressed, significantly reduce bearing lifespan. Practical solutions to prevent them include employing insulated bearings, insulated couplings, and installing shaft grounding brushes [16]. Figure 4 demonstrates an example of the use of shaft grounding brushes installed on the shaft of a large motor to ground bearing currents. Harmonics can lead to an increase in torque ripple (one of the factors causing vibration and audible noise) and torsional oscillations of the motor’s shaft (especially AC motors). Furthermore, under harmonic conditions,

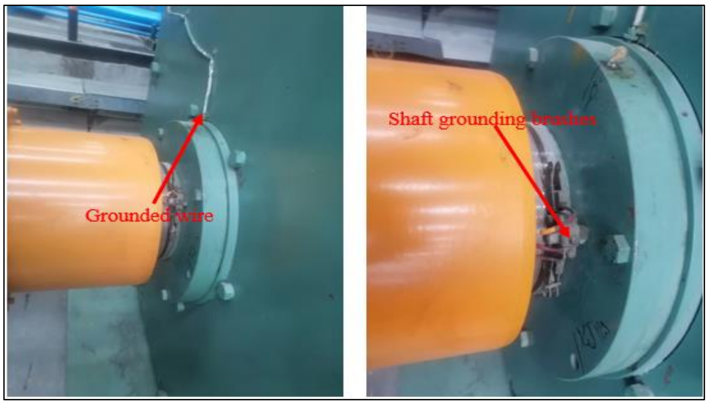

Figure 4: The installed grounding brushes on the shaft of a 1000 MW DC motor in a cement factory.
Source: Authors, (2024).

serious damage to the shaft and mechanical structure of the motor may occur due to the frequency matching of oscillations with the natural mechanical frequency of the shaft.

III.4 GENERATORS

The use of emergency power generators in cement factories is inevitable due to the critical nature of uninterrupted power supply. Generators typically exhibit an impedance three to four times higher than that of distribution transformers, rendering them more susceptible to the effects of harmonics. Similar to transformers and electrical motors, harmonics contribute to increased generator temperature by amplifying iron and copper losses, as well as inducing torque fluctuations and torsional vibrations [10].

Another significant concern is the potential for generators to trip unexpectedly under harmonic conditions due to protection system interventions. Generators are equipped with voltage and frequency controllers, and excessive voltage distortion caused by nonlinear loads can disrupt these settings. Specifically, the generator controller monitors the zero-crossing points of the phase to determine the frequency of the AC line. Voltage distortion introduces a "fuzzy" characteristic to the voltage waveform at these zero crossings, leading to imprecise and unreliable frequency calculations. The controller actively responds to fluctuations in the line frequency, striving to stabilize it towards the desired target frequency (typically 50 or 60 Hz). In extreme cases, the generator may experience surges or oscillations in its effort to reach the target frequency, ultimately necessitating disconnection from the grid [17].

Design engineers involved in cement plant development must consider the derated range of generators under harmonic conditions. Alternatively, they should request generators with specified tolerance levels to harmonic distortions from manufacturers.

III.5 CABLES

Cable resistance (especially AC resistance) is subject to skin effects and proximity. Both of these effects depend on the frequency, spacing between cables, the size, and cable structure. Consequently, notable increases in RI^2 losses may occur in harmonic conditions [10,18]. In the development of cement factory plants, neglecting to address harmonic control or not considering the derated range for cable size during the design phases may lead to excessive conductor heating and insulation damage under nominal loads.

It's important to note that in a four-wire power system (comprising three phases and a neutral), three-phase currents return to the grid via the neutral cable. Under linear balanced load conditions, neutral cable current is zero. Whereas, in harmonic conditions, even if the three-phase system is balanced, currents caused by odd harmonics combine, resulting in additional neutral cable current (up to 172% of phase current). For clarity, Figure 5 depicts practical measurements of three-phase currents and neutral wire for lighting of LED lamps in the development hall of a cement factory.

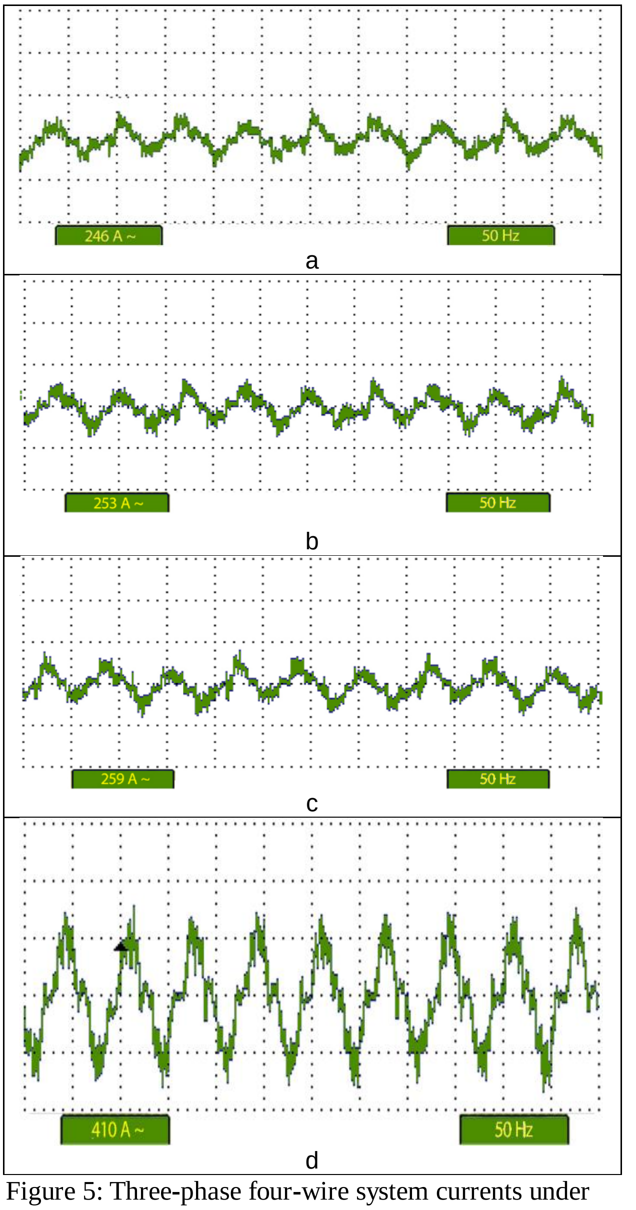

Figure 5: Three-phase four-wire system currents under harmonic conditions: (a) Phase A current (b) Phase B current (c) Phase C current (d) Neutral wire current.
Source: Authors, (2024).

III.6 CIRCUIT BREAKERS AND FUSES

As previously discussed, in the presence of nonlinear loads, the rms current value increases. Therefore, if the trip level of circuit breakers remains unchanged, premature and unwarranted trips may occur. On the other hand, the circuit breakers are designed to interrupt current at the zero crossing point of phase currents, and under harmonic conditions, false zero crossings may occur due to waveform distortion and high rates of di/dt at this point, leading to premature tripping of circuit breakers without any actual fault occurrence [10],[18]. To overcome this issue, some manufacturers suggest a derated range of circuit breaker or the utilization of electronic control circuits for precise detection of the zero crossing point.

In the case of fuses, the rise in rms current diminishes their current carrying capacity and introduces changes in both their time-current characteristic and melting time [18]. Additionally, under harmonic conditions, proximity effects cause non-uniform current distribution in fuse elements, ultimately leading to thermal stresses [10].

III.7 PROTECTION RELAYS AND MEASUREMENT EQUIPMENT

Harmonics may lead to errors and incorrect operation of some protection relays (especially traditional relays) [18],[19]. Despite efforts in today's relay structures to ensure proper performance even under the most challenging harmonic conditions, various reports indicate the vulnerability of relays to harmonic effects [20-22]. Henceforth, in the development of cement factories and the alteration of harmonic conditions, these effects should be taken into account in the selection or adjustment of protective relays to prevent future damages.

Common measurement equipment is typically designed to read sinusoidal quantities at the fundamental frequency. Non-linear currents and voltages induce errors in measurement circuits that cause wrong readings [10]. For instance, electromechanical kilowatt-hour meters may overestimate consumption under harmonic conditions [18],[23], while analog power factor meters may indicate lower power factor values [18].

III.8 RESONANCE

One of the undesirable effects of harmonics that can occur with the development of an industrial plant (increasing inductive and capacitive loads) is the phenomenon of resonance. This effect becomes more obvious especially with the installation of capacitor banks or SVCs for power factor correction. Resonance leads to higher levels of harmonic voltage and current distortions [9], resulting in damage to capacitor banks, cable overvoltage incidents, occurrences of corona discharge, increased inrush currents in transformers, and prolonged decay rates (especially during simultaneous switching of capacitors and transformers), as well as heightened duty of switching equipment [18]. Practically, to mitigate or eliminate resonance, series reactors are commonly employed with loads, functioning as low-pass filters to attenuate higher harmonic components. It is crucial to note that even the addition of a small capacitor to a large power system can create resonance. Equation (12) can be used to estimate the harmonic order of the parallel resonant frequency during the installation of capacitor banks [24].

$$h_R = \sqrt{\frac{MVA_{SC}}{MVAR_{CAP}}} \qquad (12)$$

In equation (12),

$$MVA_{SC} = \frac{S_T}{U_{CC}} \qquad (13)$$

Where MVA_{SC} denotes the short-circuit power of the transformer at the desired bus in terms of MVA, and $MVAR_{CAP}$ represents the reactive power of the capacitor bank in terms of MVAR. S_T indicates the power of the MV/LV transformer (or the sum of several parallel MV/LV transformers) in terms of MVA, while UCC expresses the short-circuit voltage of the MV/LV transformer as a percentage. Figure 6 illustrates the resonance effect in a power system with a six-pulse drive and power factor correction capacitor in a simple simulation conducted using MATLAB.

IV. CONTROL STANDARDS AND PRACTICAL METHODS FOR HARMONIC MEASUREMENT

Various international standards have been introduced for the measurement, control, and limitation of harmonics, which are categorized and listed in references [25-28]. Based on these references and the current common guidelines in Iran's cement industries, the relevant standards can be divided into two sections: measurement standards and limits on harmonic ranges at the PCC. In general, IEC 61000-4-7 can be considered the most suitable standard for THD and TDD measurements in an industrial plant because this document provides a detailed examination of harmonic measurement methods and has been endorsed by other common standards. In most standards, THD is used to express voltage distortion and TDD for current distortion. Industrial plants must consistently be responsible to controlling harmonic currents and take steps to reduce harmonics within the permissible range at the PCC. Figure 7 shows a practical connection example of a portable power analyzer model DW-6095 for harmonic measurement at the PCC.

Regarding the permissible ranges of THD and TDD, international standards IEEE 519 and EN50160, as well as the national standard [29], are recognized as the preferred references in Iranian industrial plants, irrespective of their different revisions. However, in plants with dedicated high-voltage lines or dedicated power plants, only two mentioned international standards are considered for setting limits on harmonic ranges. Nevertheless, there is no difference between the Iranian national standard and IEEE 519 in terms of the permissible range of THD_{Vpcc}. In a comparative analysis between EN 50160 and IEEE 519, it can be said that EN 50160 focuses on a wider spectrum of parameters related to power quality besides harmonics, while IEEE 519 specifically and precisely addresses only harmonics and their limitations for acceptable levels in power systems. Investigations indicate that IEEE 519 is currently accepted as the best reference for permissible levels of harmonics in cement plants in Iran and is also endorsed by power distribution companies. This standard was initially introduced in 1981 and has been continually updated due to the increasing nonlinear loads, experiences gained, and the various conditions arising in power systems. Tables 2 and 3 from IEEE 519-2022 respectively show the limits of THD and TDD at the PCC. It is important to clarify that Table 2 exclusively presents voltage distortion limits at the PCC for Iranian cement plants, (that is, LV and MV voltage levels), and the information pertaining to voltage levels other than LV and MV is omitted from the table.

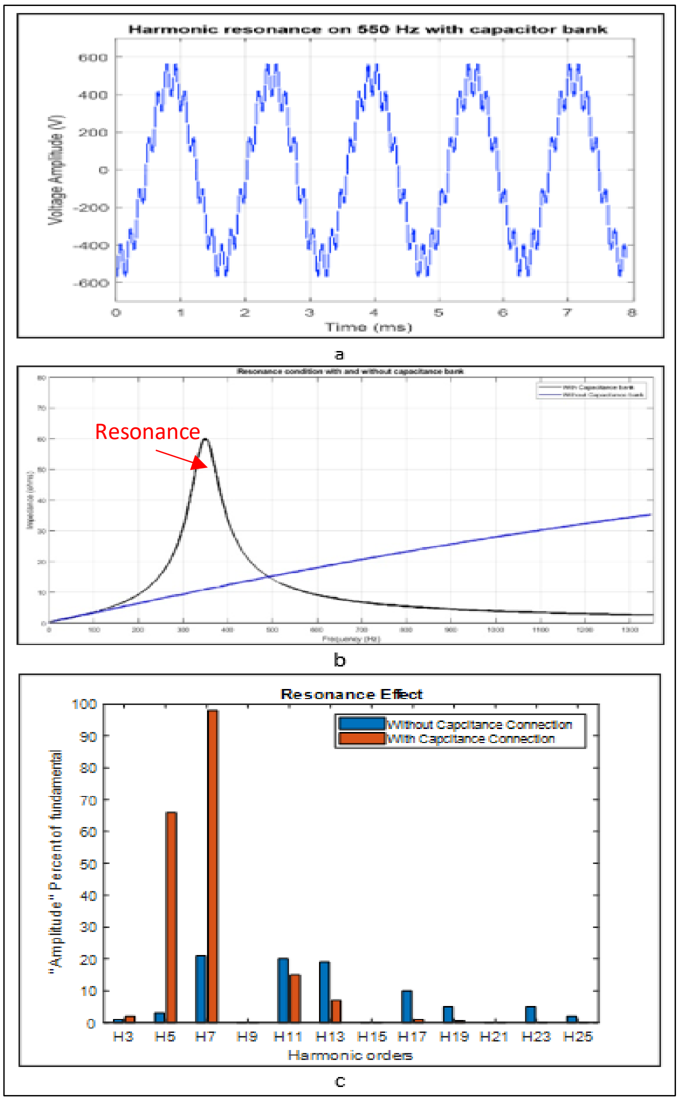

Figure 6: Resonance conditions and harmonic voltage amplification: (a) Resonance example at 550 Hz and harmonic voltage enhancement (b) Impedance profile of the network before and after the addition of the capacitor bank (c) Comparison of voltage harmonic distortion levels before and after the addition of the capacitor bank.
Source: Authors, (2024).

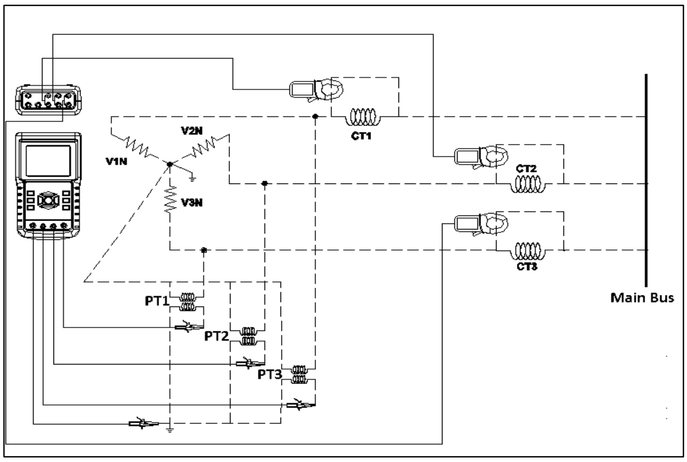

Figure 7: An example of the practical connection method of a portable power analyzer for measuring harmonics.
Source: 3 Phase power analyzer-Model DW-6095-Operation manual, (2010).

By comparing Tables 2 and 3, it can be said that voltage distortion limitations are absolutely and clearly stated in the standard, while current distortion limitations are contingent upon the electrical source impedance and harmonic suppression capability. According to Table 3, as I_{SC} increases relative to I_L, the likelihood of the circuit being impacted by harmonic presence decreases; in other words, According to Table 3, as ISC increases relative to IL, the probability of the circuit being impacted by harmonic presence decreases; in other words, while a strong grid can effectively reduce current harmonics with minimal impact on voltage, a weak grid may encounter greater voltage fluctuations in its efforts to suppress harmonics. In extremely weak grids, both voltage and current distortions may have similar magnitudes. Thus, it could be contended that current emission requirements must be stricter in weaker grids.

A notable aspect of existing standards is their focus solely on low frequencies (up to the 50th harmonic) and very high frequencies (above 150 kHz). Modern active harmonic mitigation devices, such as Active Power Filters (APFs) and Active Front End (AFE) drives (introduced in Section V), generate harmonic frequencies through switching operations. These frequencies typically range between 2 kHz to 150 kHz, a spectrum not currently addressed by existing standards. This gap enables manufacturers to employ less effective and cost-efficient LCL passive filters [30].

Table 2: Voltage distortion limits.

Bus voltage V at PCC	Individual harmonic (%)	Total harmonic distortion THD (%)
$V \leq 1.0$ kV	5.0	8.0
1 kV $< V \leq 69$ kV	3.0	5.0

Source:[31].

V. PRACTICAL STRATEGIES FOR HARMONIC MITIGATION OR ELIMINATION

Various methods for mitigating or eliminating harmonics have been scrutinized and analyzed in the literature [10], [26], [31], [32], [33], [34], [35]. Based on these references, methods for reducing harmonics can be broadly categorized into three main groups. The first category includes effective and optimal design methods for harmonic-generating equipment (such as electrical drives, motors, and transformers). When developing cement plants, proactive measures should be taken to mitigate this issue prior to equipment procurement. Considering the return on investment, it is advisable to acquire production lines that inherently produce much lower levels of harmonics. The second category comprises power management techniques and power system resilience (such as active power management, current distribution improvement, proper management and distribution of nonlinear and linear loads, appropriate sizing of motors and transformers, and techniques for enhancing power network stability). This aspect should be incorporated into the power system design phase of cement plant projects. The third category relates to additional methods (such as adding active and passive filters, isolated transformers, and reactors). These types of methods are implemented after a detailed study of harmonic sources and analysis of injected harmonics into the network.

In general, it is preferable for harmonics to be limited at their sources unless conditions make it technically and economically infeasible. The selection of optimal methods or their combination for harmonic reduction depends on the characteristics and structure of each plant's power system, and requires a precise evaluation of the electrical system, financial budget, and operational environment. Herein, the most common practical techniques currently employed in Iran's cement industries are examined in more detail and ultimately compared from both technical and economic standpoints with a view to plant development.

Table 3: Current distortion limits for systems with rated voltages from 120 V through 69 kV.

I_{SC}/I_L	**Harmonic limits [a,b] $2 \le h < 11$**	**Harmonic limits [a,b] $11 \le h < 17$**	**Harmonic limits [a,b] $17 \le h < 23$**	**Harmonic limits [a,b] $23 \le h < 35$**	**Harmonic limits [a,b] $35 \le h \le 50$**	**TDD Required**
< 20 [c]	4.0	2.0	1.5	0.6	0.3	5.0
20 < 50	7.0	3.5	2.5	1.0	0.5	8.0
50 < 100	10.0	4.5	4.0	1.5	0.7	12.0
100 < 1000	12.0	5.5	5.0	2.0	1.0	15.0
> 1000	15.0	7.0	6.0	2.5	1.4	20.0

[a] For $h \le 6$, even harmonics are limited to 50% of the harmonic limits shown in the table.
[b] Current distortions that result in a dc offset, e.g., half-wave converters, are not allowed
[c] Power generation facilities are limited to these values of current distortion, regardless of actual I_{SC}/I_L unless covered by other standards with applicable scope.
Where:
I_{SC} = maximum short-circuit current at PCC
I_L= maximum demand load current (fundamental frequency component) at PCC under normal load operating conditions

Source:[31].

V.1 UTILIZATION OF LARGE AC OR DC CHOKES (REACTORS)

It is one of the most common methods of reducing harmonics in industrial factories and is known as an effective, simple and inexpensive way to reduce harmonics of electrical drives [10],[26],[36],[37]. In AC drives, chokes can be implemented in three configurations: on the AC line side (commonly known as AC chokes, which is a very popular method), in the DC link circuit (known as DC chokes, which are integrated within the drive itself), or both (especially in very large drives where the short-circuit capacity of a dedicated source is relatively low compared to the drive's apparent power). The choice of configuration depends on the drive's design and the power system [10],[36]. Figure 8 illustrates the configurations of AC and DC chokes in electrical drives [36]. There are varying approaches on the comparative effectiveness of AC versus DC chokes in reducing harmonic currents [38],[39]. However, it is generally accepted that using chokes not only limits harmonic currents but also reduces harmonic voltage distortion and protects the drive against voltage disturbances and imbalances (such as surges, spikes, and transients) [10],[11],[26],[36],[38],[39]. For better understanding, Figure 9 shows the effects of chokes on reducing current ripple [40],[41].

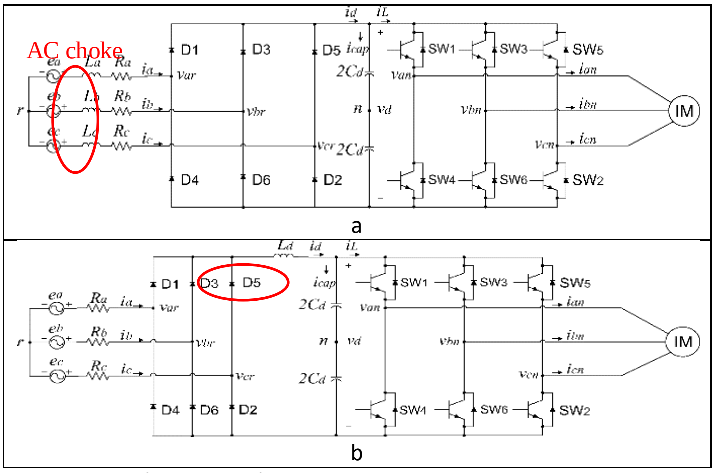

Figure 8: Configuration of utilizing DC and AC chokes: (a) Reactors La, Lb, and Lc on the AC line side of the induction motor drive (b) Reactor Ld in the DC link of the induction motor drive.
Source: [36].

From a practical standpoint, in most cases, chokes alone are insufficient for effective harmonic reduction. They need to be used in combination with other harmonic mitigation techniques to achieve optimal results [10],[38]. Typically, chokes are available in standard impedance ranges (such as 2%, 3%, 5%, and 7.5%) [10] and are only necessary for 6-pulse drives [38]. A drawback of using chokes is the voltage drop they cause [10],[38],[39], which can lead to under-voltage faults and negatively affect drive performance under unstable input voltage conditions.

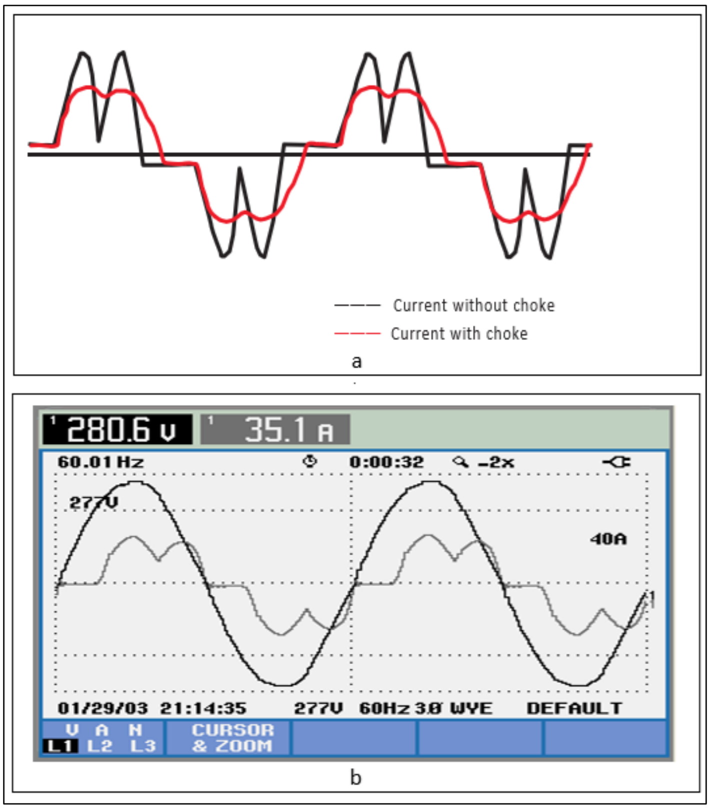

Figure 9: Effects of utilizing chokes: (a) Schematic waveforms showing the effect of a choke on the input current to a six-pulse drive (b) Practical results of using an AC choke with 3% impedance for a 480-volt, 30-horsepower motor at full load.
Source: (a) [40], (b) [41].

V.2 ISOLATION TRANSFORMERS

The use of isolation transformers is common in many cement factory structures in Iran and is considered an appropriate solution for reducing harmonics. Similar to chokes, they utilize their reactance to reduce harmonics. Additionally, due to their conventional delta-star configuration, they help mitigate triple harmonics [42]. However, the reason for using them is not solely limited to harmonic reduction. They do not perform significantly better than simple chokes and have higher costs [10],[26],[42]. Their advantages include the ability to step up or step down voltage levels, establishing a neutral ground reference for nuisance ground faults [10],[42], and eliminating certain common-mode frequency disturbances [26],[42]. This harmonic reduction method can be considered the best solution when using AC and DC drives that have SCRs in the rectifier bridge structure [10], as it not only reduces harmonics but also facilitates voltage level changes and protective measures.

The size (or capacity) and impedance of transformers play crucial roles in reducing voltage harmonics. In simpler terms, on the low-voltage side, larger transformer sizes or lower impedance result in a more pronounced reduction in voltage harmonics [40]. It's imperative, particularly in the development or procurement of cement production lines, to adhere to IEEE C57.110-2018 standards when manufacturing, ordering, or utilizing transformers.

V.3 QUASI 12-PULSE ELECTRICAL DRIVES

Quasi 12-pulse drives incorporate phase-shifting transformers in their structure. These transformers are employed in various configurations and vector groupings to mitigate harmonics in different industries [26]. However, it has been observed that most cement factories in Iran use two transformers with configurations of delta (primary)-delta (secondary) and delta (primary)-star (secondary), each supplying equal nonlinear loads (6-pulse variable speed drives with equal loads). Typically, instead of using two transformers, a single transformer with two separate secondary windings, as shown in Figure 10, is used. Each secondary winding supplies an electrical drive for a motor. with both motors having equal power and being mechanically coupled. These motors have equal power and are mechanically coupled to each other. This type of structure creates a quasi-12-pulse converter configuration, offering nearly the same advantages as a true 12-pulse electrical drive, significantly reducing the 5th and 7th harmonics and overall total harmonic distortion (THD) [10],[43],[44],[45]. In this configuration, the predominant harmonics are the 11th and 13th, while the amplitudes of other harmonics, such as the 17th, 19th, and higher orders, are effectively minimized [45].

The advantages of this arrangement include not only providing the required voltage for the drives via the transformer but also leveraging cost-effective 6-pulse drives, achieving a notable reduction in total harmonic distortion, and attaining lower inertia by using two series-connected motors instead of a single larger motor. Additionally, if one drive or motor fails, the production process can continue at reduced power. The disadvantages include the predominant 11th and 13th harmonics and the potential complete system shutdown in the event of any failure in the primary winding of the transformer.

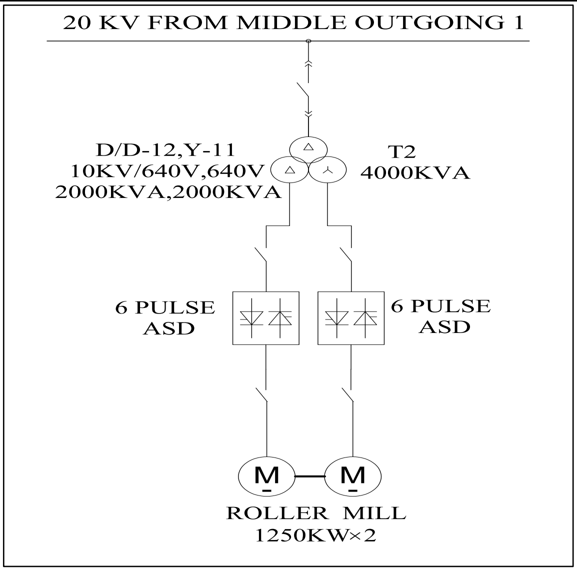

a)

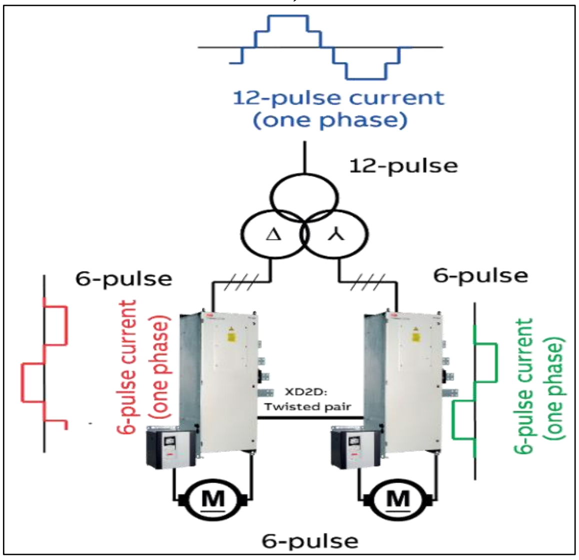

b)

Figure 10: Quasi-12-pulse drive configuration: (a) A section of the single-line diagram of a sample cement plant in Iran equipped with a quasi-12-pulse drive, (b) Implementation of the quasi-12-pulse structure using two ABB DCS880 drives. Source: (a) Authors, (2024), (b) [45].

V.4 PASSIVE HARMONIC FILTERS

Passive harmonic filters are a highly practical and widely used method for reducing harmonics in the power systems of cement plants [3],[8],[46],[47]. After series chokes, they are considered the simplest and most cost-effective technique for reducing THD [26]. Passive harmonic filters, also known as harmonic trap filters [10], can be categorized into series and shunt types. Among these, the shunt type is more commonly used to create a low-impedance path for specific harmonics [48]. In the single-line diagram shown in Figure 1, an example of a shunt connection of a passive harmonic filter to a roller mill drive can be seen. These filters are composed of passive elements such as inductors, capacitors, and often resistors (for damping) [8],[10],[48] and are available in various topologies. Figure 11 depicts different topologies of shunt passive filters, which can be used either in combination or individually, depending on the power system of the cement plant and the load characteristics [49]. Observations indicate that in Iranian cement plants, typically at low voltage levels (800V, 690V, and 400V), one or more single-tuned filters are used, and at medium voltage levels (mostly 6.3kV and rarely 33kV, 20kV, and 11kV), sometimes other topologies are used in combination. Nevertheless, the application of single-tuned filter topologies in the cement industry is much more common due to their simple structure, lower cost, and effective performance. It is recommended to place passive filters near the harmonic source, as by reducing harmonics at the source, in addition to eliminating the need for oversizing electrical equipment, losses can be minimized, voltage distortions can be effectively reduced, and the filter can be sized for a specific load [48]. Figure 12 shows an example of connecting a double-branch filter to a nonlinear load in a cement plant to eliminate the 5th and 7th harmonics. As detailed in the accompanying SLD, each passive filter is designed and tuned for a specific harmonic frequency that needs to be reduced or eliminated.

From a practical standpoint, passive harmonic filters are predominantly used to eliminate or control lower-order predominant harmonics, especially the 5th, 7th, 11th, and 13th harmonics. They perform poorly for harmonics above the 13th order and are rarely used for higher-order harmonics [10]. Their operating principle is based on the resonance phenomenon (due to changes in filter components as a result of frequency variations) to create minimal impedance for a specific harmonic (or in some cases, with a combined structure for a specific frequency band [48]) [8],[10],[48],[50]. The resonance frequency or tuning frequency for a single-tuned filter is calculated using equation (14) [10],[33],[50],[51]. In this equation, L is the inductance of the filter in henries, and C is the capacitance of the filter in farads. At this frequency, the filter provides low impedance for the harmonic frequency f_r and high impedance for other harmonics [50,51].

$$f_r = \frac{1}{2\pi\sqrt{LC}} \tag{14}$$

In practice, due to the risk of filter resonance with the power system frequency, the tuning frequency of the filter is set slightly below the harmonic frequency [11],[48],[49],[50]. For example, a 5th harmonic filter is tuned to the 4.7th harmonic [11],[50].

Besides harmonic reduction, improving power quality through reactive power compensation is another advantage of these filters [8],[48],[50],[51]. However, it should also be noted that these filters can absorb harmonics from other sources [10], and to prevent filter resonance with the power system and ensure their effective performance, thorough studies of load, power quality, and network impedance during their design are essential [52].

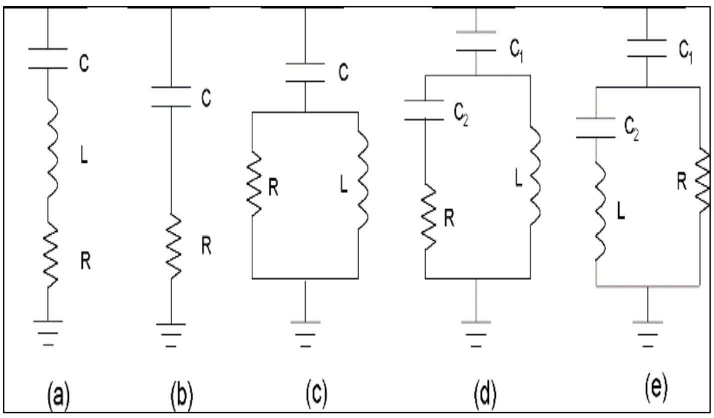

Figure 11: Types of passive shunt filter topologies: (a) single tuned, (b) first order, (c) second order, (d) third order, (e) C-type.
Source: [49].

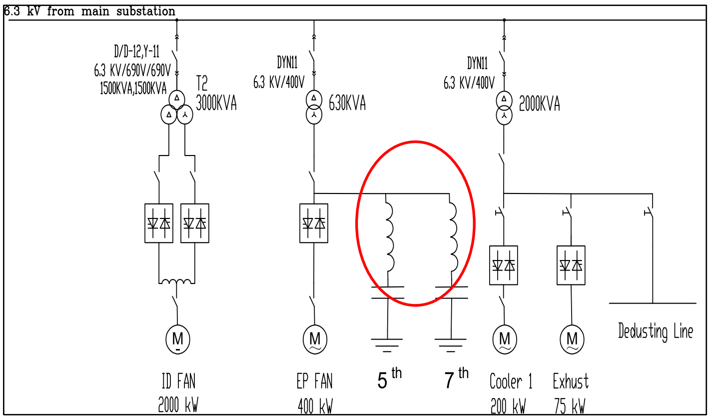

Figure 12: Part of the single-line diagram of a cement plant and the connection of a double-branch passive filter to the nonlinear load.
Source: Authors, (2024).

V.5 HIGH PULSE CONVERTERS

From an industrial perspective, electric drives with 12-pulse, 18-pulse, 24-pulse, 30-pulse, 36-pulse, 42-pulse, and 48-pulse converters [53] are recognized as high-pulse converters. Among these, 30-pulse and 42-pulse converters are rarely produced due to the special requirements for transformers. Normally, only 12-pulse, 18-pulse, 24-pulse, and 36-pulse converters can be found in various industries with different structures, the most common topologies of which are shown in Figure 13 [53],[54].

According to equations (4) and (5), as the number of pulses of power converters increases, the amplitude of harmonic currents and ultimately the THD decreases. Invariably, increasing the number of converter pulses not only mitigates harmonic distortion in the AC input current, but also delivers a smoother and higher average DC output level [10]. Since it is not feasible to find all common high-pulse drives in one factory with completely similar supply and loading conditions for practical investigation, simulation methods have been used here to analyze the harmonic injection of various converters. Figures 14 and 15 respectively compare the input current of phase a and the level of harmonic currents of various common high-pulse converters with configurations shown in Figure 13 under ohmic full load conditions (THD_I equals TDD). As observed, increasing the number of pulses significantly affects reducing THD_I. Despite this, based on field studies and as shown in the SLDs of Figures 1 and 12, only 12-pulse drives are prevalent in the cement industry in Iran, and other high-pulse converters are not used. This can be attributed to the considerably higher cost of high-pulse converters and their more intricate circuits (which consequently render them more susceptible to disturbances and failures) [8], as well as the necessity for large and specialized transformers to achieve phase shifting [10],[53]. Different configurations of industrial 12-pulse DC and AC drives (known as True 12-pulse) currently deployed in numerous cement factories can be found in [45], [55].

As evident from Figure 15, the advantage of 12-pulse converters lies in their ability to mitigate not only the 5th and 7th harmonics but also higher-order frequency components, where the 11th and 13th emerge as predominant [10],[38],[43],[45],[54]. While this technique diminishes the amplitude of harmonics, it does not entirely eradicate them [10]. Among the drawbacks of 12-pulse drives compared to prevalent industrial six-pulse drives are the more intricate converter architecture, higher price [10],[40], and decreased overall drive efficiency due to voltage drop caused by the phase-shifting transformer [10].

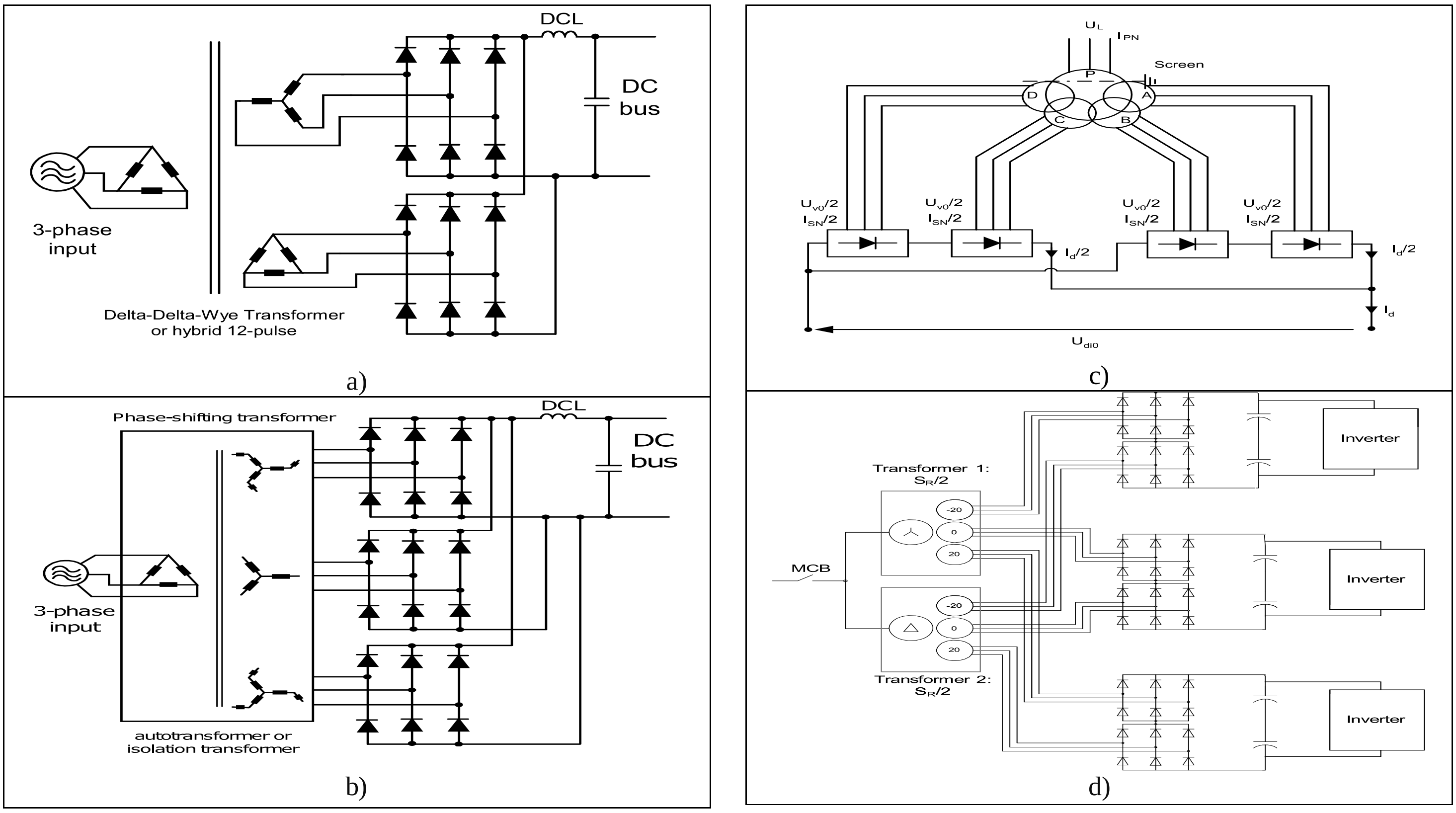

Figure 13: Some common configuration of high pulse industrial drives: a) 12-pulse converter b) 18-pulse converter c) 24-pulse converter d) 36-pulse converter.
Source: (a) , (b) [54],(c), (d) [53].

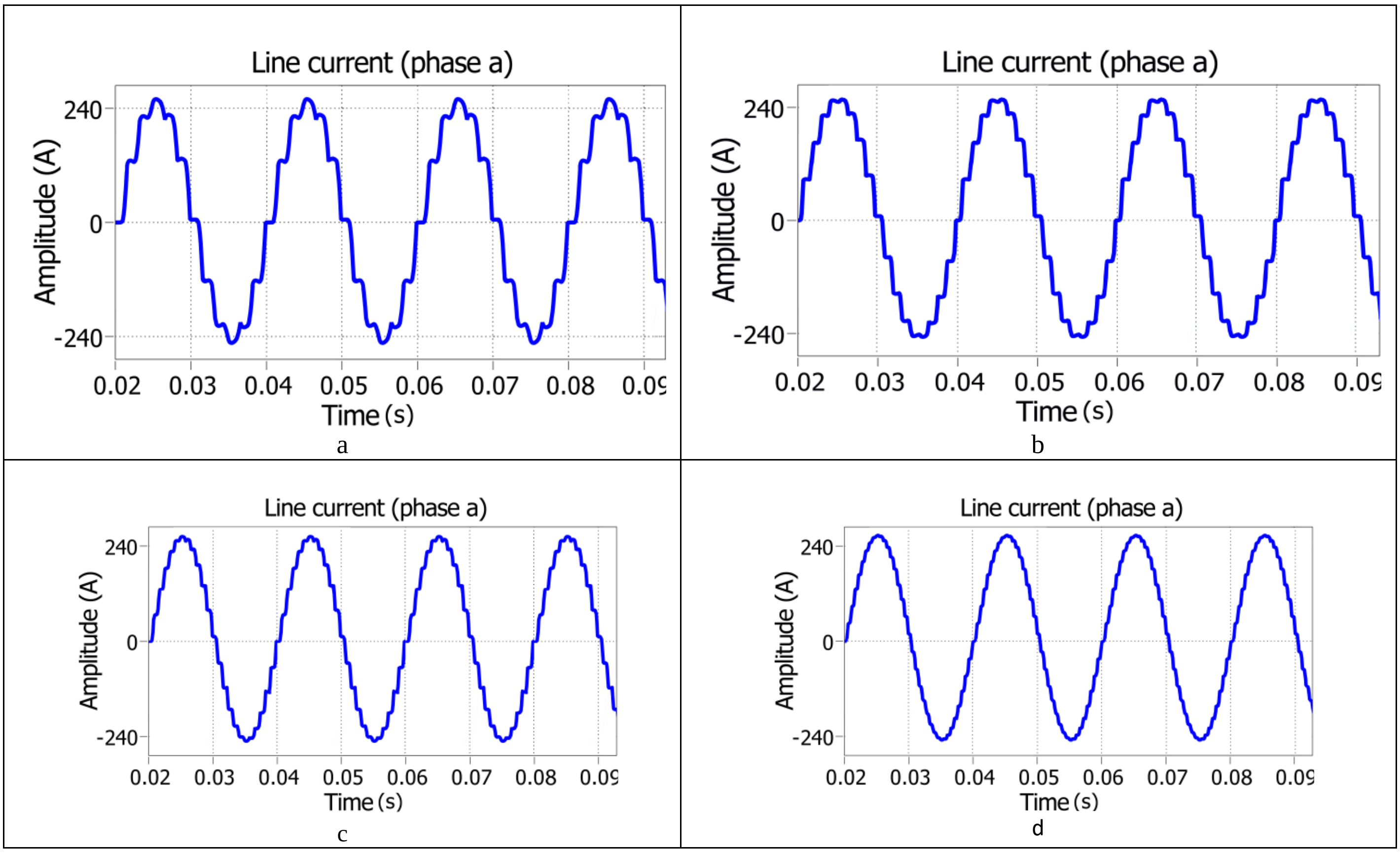

Figure 14: Comparison of the input current of phase a from various high pulse converters with diode rectifier and ohmic load: (a) 12-pulse converter (b) 18-pulse converter powered by a three-phase to nine-phase autotransformer (c) 24-pulse converter (d) 36-pulse converter.
Source: Authors, (2024).

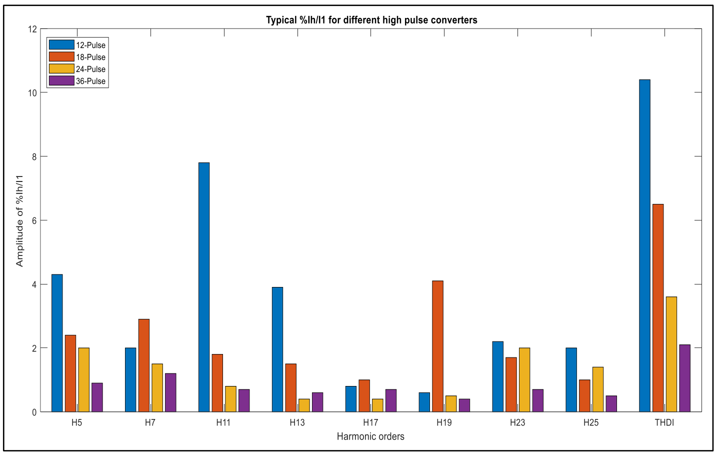

Figure 15: Comparison of the harmonic orders of the input current of high pulse converters with diode rectifier and ohmic load: (blue) 12-pulse converter (THDI=10.4%), (red) 18-pulse converter powered by a three-phase to nine-phase autotransformer (THDI=6.5%), (orange) 24-pulse converter (THDI=3.6%), (purple) 36-pulse converter (THDI=2.1%).
Source: Authors, (2024).

V.6 ACTIVE HARMONIC FILTERS

Although active harmonic filters (AHFs) have gained traction in diverse industries for their effective reduction of harmonics and compensation of reactive power [7],[10], they are not commonly used in the cement industry due to their significantly high cost [8]. However, their deployment in the cement industry is recommended due to the return on investment and their proper effectiveness [2],[7],[47]. AHFs can be classified into four categories: series, shunt, a combination of both, and hybrid (a combination of active and passive filters) [31],[33], among which the shunt configuration is much more prevalent [10],[30],[33]. The operating principle of a shunt AHF involves monitoring and measuring the distortions of nonlinear load currents by filtering the main current and subsequently injecting equal but opposite harmonic currents in real-time to eliminate harmonics [10],[28],[32],[43]. In fact, the voltage distortion caused by harmonic currents passing through the system impedance can be corrected by injecting a nonlinear current with the opposite polarity. This process can restore the voltage to its sinusoidal state [31]. Figure 16 depicts its operating principles [52].

AHFs are capable of removing harmonics up to the 50th order [26],[43], achieving a total harmonic distortion of current (THDI) lower than 5% [7],[26],[28],[43],[47], and improving the power factor close to unity [25],[28]. Compared to passive harmonic filters, AHFs offer several advantages: they do not resonate with the power network [10],[28],[33], are insensitive to changes in source and load impedance [10],[28], are not limited to specific frequencies, and operate over a wide frequency range [8],[34]. Additionally, AHFs do not require detailed harmonic studies of the power system [52], especially in self-tuning models. Nevertheless, investigations suggest that these types of filters currently do not have a place in Iranian cement factories. This could be attributed to the complex control systems of AHFs, which lead to very high costs and increased maintenance expenses [8],[10],[25],[33], relatively high levels of electromagnetic interference (EMI) [30], and possibly the leniency of regional power companies in Iran, especially at dedicated 63 kV substations.

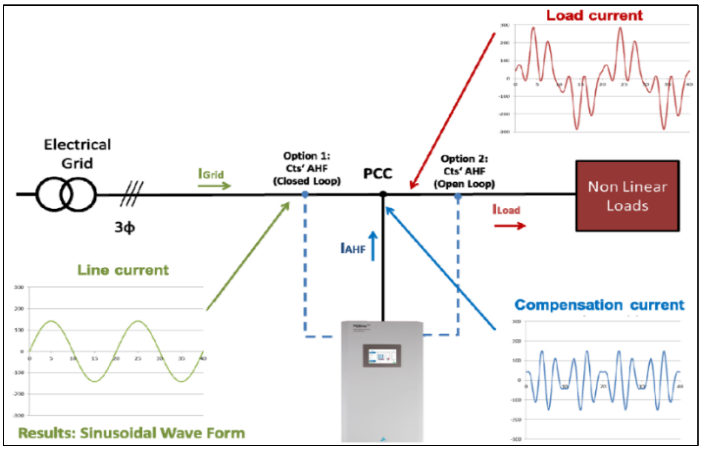

Figure 16: Principles of active shunt filter operation.
Source: [52].

V.7 LOW HARMONIC DRIVES

Some manufacturers of industrial electric drives have introduced and marketed a variety of low harmonic electric drives to meet IEEE 519 requirements. These types of drives are generally active front end (AFE) [5],[10],[30],[56],[57], and in some cases, drives with an integrated active filter [58]. Figures 17 and 18 show examples of the configuration of this type of industrial drives. As observed in Figure 17, unlike the common six-pulse industrial drives, the AFE drive utilizes a fully controlled IGBT bridge instead of a diode bridge rectifier at the input of the drive. This IGBT bridge allows the drive to draw a more sinusoidal current from the grid, significantly reducing low-order harmonics (below 50th) [10], [30], [56], [57]. Therefore, these drives are also referred to as drives with a sinusoidal input rectifier [10]. It should be acknowledged that the switching losses of the IGBTs in the input unit of the AFE drive reduce its efficiency compared to the traditional six-pulse drive. However, when considering the overall system losses, including those caused by harmonic reduction filters, the total losses of AFEs are the same or less [56]. In addition to significant reduction in harmonic distortions (even below the limits specified in IEEE 519), the advantages of AFE drives include inherent four-quadrant operation, regenerative capability (returning energy to the grid in braking mode), high dynamic response, reactive current control capability, unity power factor operation, elimination of the need for external filters and special transformers, and voltage drop elimination at motor terminals (usually caused by commutation or voltage disturbances in the source) [5],[10],[40],[56],[57]. While the features of AFE drives compared to commonly used six-pulse VSDs can result in some capital return due to a reduction in cable size by approximately 10%, distribution transformer capacity by 20%, generator capacity by 50%, and energy storage [59], their economic justification is currently lacking due to nearly 2.5 times production costs [40], especially in conditions where significant regenerative or braking modes are absent. Therefore, their utilization in cement factories is not widespread [8], and their application is mostly found in downhill conveyor belts in very large cement production complexes [60]. Other disadvantages of industrial AFE drives include the inherent generation of harmonics higher than 50th and relatively high levels of EMI in the range of 2 to 150 kHz [10,30], which must be carefully considered when using them in various industries.

In industrial drives with an integrated active filter, an AHF as shown in Figure 18 is employed to mitigate harmonics. As previously discussed regarding AHFs, despite their presence, the drive can draw a much more sinusoidal current with a unity power factor from the grid [58]. The disadvantages of this type of drive are similar to those of AHFs, but in terms of cost, depending on the technology used, it may be somewhat cheaper than modern AFE drives.

Field studies and investigations indicate the lack of utilization of low harmonic industrial drives in Iranian cement factories due to their very high cost. It is obvious that currently replacing existing six-pulse drives in a cement factory, whether in operation or nearing the end of their life cycle, with an AFE drive is not ideal and cost-effective. However, with the growth of production and technology, it is expected that in the not-too-distant future, advanced AFE drives will replace six-pulse drives and even 12-pulse or quasi-12-pulse drives in modern cement factories.

Table 4, derived from the analysis of data recorded in four Iranian cement factories with almost similar characteristics, compares the types of practical methods available for harmonic reduction in terms of THD_I level and total cost (including all necessary components such as transformers, additional cables, etc.) for a 500 kW EP fan at the PCC (primary side of transformers). Considering the absence of completely identical conditions in the studied factories, all values in the mentioned table are relative. This information can assist engineers in selecting harmonic reduction techniques for development or control in current conditions in cement factories and even other industrial complexes. An interesting conclusion that can be drawn from Table (4) is the comparison between 12-pulse and quasi-12-pulse converters. It is observed that a quasi-12-pulse converter may have economic advantages and superior THD_I reduction compared to the conventional structure of 12-pulse converters in the cement industry.

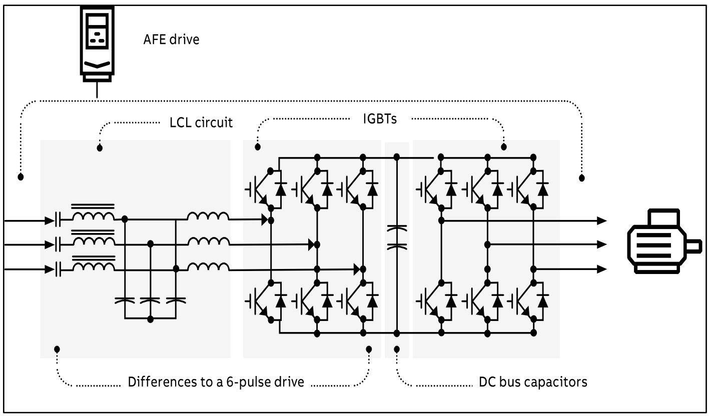

Figure 17: A simplified hardware configuration of an AFE drive.
Source: [56].

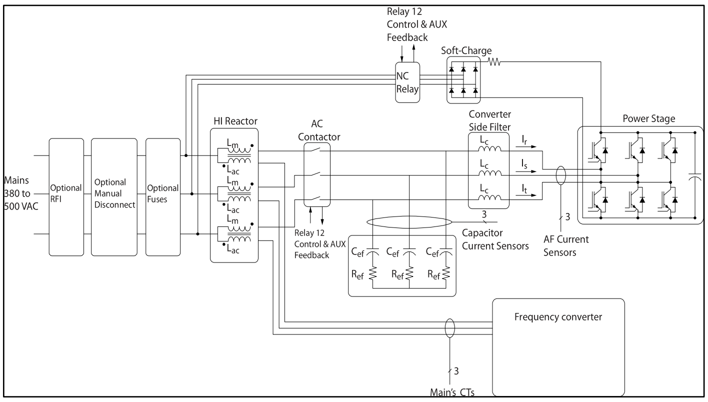

Figure 18: Basic topology of a low harmonic drive with integrated active filter.
Source: [58].

Table 4: Technical and economic comparison of harmonic reduction strategies at full load.

	Current harmonic orders ($\%I_h/I_1$)								THD_I	Cost
	5th	**7th**	**11th**	**13th**	**17th**	**19th**	**23th**	**25th**		
6-pulse without choke	84%	63%	20%	11%	8.9%	7.2%	5.6%	2.8%	**108.24%**	100%
6-pulse with 3% AC choke	41.6%	16%	7.8%	6.1%	5%	3.9%	2.5%	2.5%	**46.23%**	104%
6-pulse with 5% AC choke	33.4%	10.2%	5%	3.2%	2.9%	2%	1.6%	1.2%	**35.65%**	106%
6-pulse with passive harmonic filter	2.7%	3%	2.5%	2.3%	1.4%	1%	0.5%	0.4%	**5.58%**	183%
Quasi 12-pulse	3.5%	1.5%	6.7%	3.4%	0.3%	0.3%	1.5%	1.3%	**8.66%**	188%
12-Pulse with Dd-Dy transformer	4.8%	2.7%	9.3%	5.3%	1%	0.8%	3.5%	2.6%	**12.86%**	194%

Source: Authors, (2024).

VI. CONCLUSIONS

Cement factories in Iran are recognized as significant sources of harmonics due to the presence of very large nonlinear loads. Therefore, it is necessary to conduct fundamental studies on the causes, effects, and methods of harmonic reduction in this industry. Controlling and reducing harmonics are considered important and mandatory both from the perspective of distribution network standards and the lifespan of electrical equipment. However, major problems caused by harmonics typically become apparent during the development of such factories. This is because the addition of new equipment in the development divisions or even optimization of the existing production line can significantly alter the harmonic conditions.

Based on comprehensive studies and investigations regarding the causes and effects of harmonics, it is strongly recommended that power quality studies be conducted for the current conditions before designing the development divisions, and that the harmonic effects be considered when procuring new equipment. Various standards recommend measuring harmonics up to the 50th order at the PCC but in cement factories, this is typically done up to the 25th order. The PCC in a cement factory can be at the LV (Low Voltage) level or, given the presence of dedicated high-voltage substations, at the MV (Medium Voltage) level. Most standards use THD to express voltage distortion and TDD to express current distortion.

In general, it is better to limit harmonics at their sources unless it is technically and economically unfeasible. The cost issue is an important factor in selecting harmonic reduction techniques; currently, Iranian cement factories only use AC chokes, passive harmonic filters, and quasi-12-pulse and 12-pulse drives. Field research results indicate that a quasi-12-pulse converter can somewhat outperform the conventional 12-pulse converter in the cement industry both economically and in terms of harmonic reduction. Although many new techniques, such as active filters or low-harmonic drives, are considered suitable methods, they currently have no place in the Iranian cement industry due to their very high costs. Nonetheless, it is expected that advanced AFE drives will replace six-pulse and even 12-pulse or quasi-12-pulse drives in modern cement factories in the future.

VII. AUTHOR'S CONTRIBUTION

Conceptualization: Author One, Author Two and Author Three.
Methodology: Author One and Author Two.
Investigation: Author One and Author Two.
Discussion of results: Author One, Author Two and Author Three.
Writing – Original Draft: Author One.
Writing – Review and Editing: Author One and Author Two.
Resources: Author Two.
Supervision: Author Two and Author Three.
Approval of the final text: Author One, Author Two and Author Three.

VIII. ACKNOWLEDGMENTS

We extend our sincere gratitude to Mr. Mohammad Ali Haji Abadi, Electrical Manager at Sepahan Cement Company in Isfahan, for providing drawings and practical analyses. We also wish to thank the electrical engineering departments at the Fars, Khuzestan, Tehran, and Abyek Cement factories for their invaluable information, practical results, measurements, and experiences.

IX. REFERENCES

[1] M. Soomro, V. W.Y. Tam, A.C. J. Evangelista, "2 - Production of cement and its environmental impact", Recycled Concrete Technologies and Performance, Woodhead Publishing Series in Civil and Structural Engineering, 11-46, 2023, https://doi.org/10.1016/B978-0-323-85210-4.00010-2.

[2] Asia Power Quality Initiative (APQI) Company, "Mitigation of Harmonic and Reduction in Operating Cost for a Cement Plant-Case Study 37", 2013.

[3] E. Schmitz, M. Pendo and A. Hasan, "A study of harmonics at Dacotah Cement," 1998 IEEE/PCA Cement Industry Technical Conference. XL Conference Record (98CH36070), Rapid City, SD, USA, pp. 27-40, 1998, doi: 10.1109/CITCON.1998.679235.

[4] R. L. Smith and R. P. Stratford, "Application Considerations in Handling Effects of SCR Generated Harmonics in Cement Plants," in IEEE Transactions on Industry Applications, vol. IA-17, no. 1, pp. 63-70, Jan. 1981, doi: 10.1109/TIA.1981.4503901.

[5] M. Holland, "Fundamentals on harmonics," 1999 IEEE/-IAS/PCA Cement Industry Technical Conference. Conference Record (Cat. No.99CH36335), Roanoke, VA, USA, pp. 55-67, 1999, doi: 10.1109/CITCON.1999.767026.

[6] V. Suresh Kumar, P. S. Kannan and V. Saravanan, "Harmonic distortion in a modern cement industry-a case study," 2006 IEEE Power India Conference, New Delhi, India, pp. 6 pp.-, 2006, doi: 10.1109/POWERI.2006.1632630.

[7] Y Kusumalatha, Y P Obulesh, Ch Saibabu, "Harmonics Mitigation of Industrial Motor Drives with Active Power Filters in Cement Plant-A Case Study", International Journal of Power Electronics and Drive System (IJPEDS), Vol.2, No.1, pp. 1~8, 2012, doi: 10.11591/ijpeds.v2i1.120.

[8] M. Ahrens and Z. Konstantinovic, "Harmonic filters and power factor compensation for cement plants," Conference Record Cement Industry Technical Conference, 2005., Kansas City, MO, USA, pp. 77-103, 2005, doi: 10.1109/CITCON.2005.1516354.

[9] "IEEE Recommended Practice and Requirements for Harmonic Control in Electric Power Systems," in IEEE Std 519-2014 (Revision of IEEE Std 519-1992), vol., no., pp.1-29, 11 June 2014, doi: 10.1109/IEEESTD.2014.6826459.

[10] N. Shah, "Harmonics in Power Systems, Causes, Effects and Control", White Paper, Siemens Industry, Inc., 2013.

[11] J. W. Gray and F. J. Haydock, "Industrial power quality considerations when installing adjustable speed drive systems," in IEEE Transactions on Industry Applications, vol. 32, no. 3, pp. 646-652, May-June 1996, doi: 10.1109/28.502177.

[12] L. P. Raj Nadimuthu et al., "Energy Conservation Approach for Continuous Power Quality Improvement: A Case Study," in IEEE Access, vol. 9, pp. 146959-146969, 2021, doi: 10.1109/ACCESS.2021.3123153.

[13] M. Abdul-Wahhab, "Harmonic Analysis of a Power Distribution Network in Baghdad City", Engineering and Technology Journal. Vol.34, Part (A), No.6, 2016, doi: 10.30684/etj.2016.113130.

[14] D. Pejovski, K. Najdenkoski, M. Digalovski, "Impact of different harmonic loads on distribution transformers", Procedia Engineering, Volume 202, Pages 76-87, ISSN 1877-7058, 2017, https://doi.org/10.1016/j.proeng.2017.09.696.

[15] "IEEE Recommended Practices for Cement Plant Electric Drives and Related Electric Equipment," in IEEE Std 499-1983, vol., no., pp.1-21, 4 March 1983, doi: 10.1109/IEEESTD.1983.114396.

[16] K.B. Tawfiq, M. Güleç, P. Sergeant, "Bearing Current and Shaft Voltage in Electrical Machines: A Comprehensive Research Review" Machines Journal, Published by MDPI, 11(5):550. 2023, https://doi.org/10.3390/machines11050550.

[17] "Back-up generators and harmonic levels-Acceptable level of harmonics" Technical Note 127, Published by ABB company, LVD-EOTKN127U-EN, REV B, 2023.

[18] J. C. Das, "Effects of Harmonics", in Power System Harmonics and Passive Filter Designs Book, IEEE, pp.331-378, 2015, doi: 10.1002/9781118887059.ch8.

[19] W. A. Elmore, C. A. Kramer and S. E. Zocholl, "Effect of waveform distortion on protective relays," in IEEE Transactions on Industry Applications, vol. 29, no. 2, pp. 404-411, March-April 1993, doi: 10.1109/28.216551.

[20] P. M. Donohue and S. Islam, "The Effect of Nonsinusoidal Current Waveforms on Electromechanical and Solid-State Overcurrent Relay Operation," in IEEE Transactions on Industry Applications, vol. 46, no. 6, pp. 2127-2133, Nov.-Dec. 2010, doi: 10.1109/TIA.2010.2070054.

[21] A. Benjamin and S. K. Jain, "A Review of Literature on Effects of Harmonics on Protective Relays," 2018 IEEE Innovative Smart Grid Technologies - Asia (ISGT Asia), Singapore, pp. 407-412, 2018, doi: 10.1109/ISGT-Asia.2018.8467876.

[22] H. Farzin, M. Monadi, M. Fotuhi-Firuzabad, M. Savaghebi,"A reliability model for overcurrent relays considering harmonic related malfunctions", International Journal of Electrical Power & Energy Systems, Volume 131, 2021, https://doi.org/10.1016/j.ijepes.2021.107093.

[23] A. A. Hossam-Eldin and R. M. Hasan, "Study of the effect of harmonics on measurments of the energy meters," 2006 Eleventh International Middle East Power Systems Conference, El-Minia, Egypt, pp. 547-550, 2006.

[24] D.J. Carnovale, "Power Factor Correction and Harmonic Resonance: A Volatile Mix", EC&M Mag., Vol. 102, No.6, p. 16, June 2003.

[25] S. Jain, "Chapter one - power quality: An introduction", in: S.K. Dwivedi, S. Jain, K.K. Gupta, P. Chaturvedi (Eds.), Modeling and Control of Power Electronics Converter System for Power Quality Improvements, Academic Press; p. 1–29. 2018, https://doi.org/10.1016/B978-0-12-814568-5.00001-6.

[26] A. Kalair, N. Abas, A.R. Kalair, Z. Saleem, N. Khan, "Review of harmonic analysis, modeling and mitigation techniques" Renewable and Sustainable Energy Reviews, Vol 78, pp 1152-1187, 2017, https://doi.org/10.1016/j.rser.2017.04.121.

[27] J. C. Das, "Harmonic Distortion Limits According to Standards," in Power System Harmonics and Passive Filter Designs , IEEE, pp.427-451, 2015. doi: 10.1002/9781118887059.ch10.

[28] R .Pinyol, "Harmonics: causes, effects and minimization" SALICRU white papers. ref. JN 004a01 ed. august 2015.

[29] "Iran Power Industry Standards - Power Quality Part Two : Permissible Ranges of Harmonics" in Persian, Iran Power Generation & Transmission Management Organization - Head Office (Tavanir), April 2002.

[30] A. Hoevenaars, M. Farbis and M. McGraw, "Active Harmonic Mitigation: What the Manufacturers Don't Tell You," in IEEE Industry Applications Magazine, vol. 26, no. 5, pp. 41-51, Sept.-Oct. 2020, doi: 10.1109/MIAS.2020.2982484.

[31] IEEE Standard for Harmonic Control in Electric Power Systems. IEEE, 519-2022.

[32] M.L Duc, L. Hlavaty, P. Bilik, R. Martinek, "Harmonic Mitigation Using Meta-Heuristic Optimization for Shunt Adaptive Power Filters: A Review". Energies Journal, Published by MDPI, 16(10):3998. 2023, https://doi.org/10.3390/en16103998.

[33] A. Habash, and G. Todeschini, "Harmonic Mitigation Project, Work Package 1a: Literature Review", Report produced as part of the project 'Harmonic mitigation' carried out with Western Power Distribution, Swansea University, 2020, https://cronfa.swan.ac.uk/Record/cronfa55773.

[34] A. Taghvaie, T. Warnakulasuriya, D. Kumar, F. Zare, R. Sharma and D. M. Vilathgamuwa, "A Comprehensive Review of Harmonic Issues and Estimation Techniques in Power System Networks Based on Traditional and Artificial Intelligence/Machine Learning," in IEEE Access, vol. 11, pp. 31417-31442, 2023, doi: 10.1109/ACCESS.2023.3260768.

[35] D. Fallows, S. Nuzzo, A. Costabeber, and M. Galea, "Harmonic reduction methods for electrical generation: a review", IET Generation, Transmission and Distribution, 12(13), 3107-3113, 2018, https://doi.org/10.1049/iet-gtd.2018.0008.

[36] K. Lee, T. M. Jahns, T. A. Lipo, G. Venkataramanan and W. E. Berkopec, "Impact of Input Voltage Sag and Unbalance on DC-Link Inductor and Capacitor Stress in Adjustable-Speed Drives," in IEEE Transactions on Industry Applications, vol. 44, no. 6, pp. 1825-1833, Nov.-dec. 2008, doi: 10.1109/TIA.2008.2006308.

[37] Electromagnetic Compatibility (EMC)—Part 3–6: Limits—Assessment of Emission Limits for the Connection of Distorting Installations to MV, HV and EHV Power Systems, IEC/TR 61000-3-6:2008, Apr. 2008.

[38] X. Liang, O. Ilochonwu and J. Lim, "Influence of Reactors on Input Harmonics of Variable Frequency Drives," in IEEE Transactions on Industry Applications, vol. 47, no. 5, pp. 2195-2203, Sept.-Oct. 2011, doi: 10.1109/TIA.2011.2161858.

[39] "Advantages of the integrated DC link reactor: SINAMICS Power Module PM240-2/PM240P-2, SINAMICS G120C and SINAMICS G120X", Siemens Industry, Inc. FAQ-0H7B4HG0, Entry ID: 109749021, Version 1.4, 09/2019.

[40] "ABB DRIVES: Technical guide No. 6 - Guide to harmonics with AC drives", ABB Automation Group Ltd, Ident.No. 3AFE64292714 REV F, 27 November 2017.

[41] "Low Voltage Drives Harmonic Mitigation Comparison: AC Line Reactors vs. DC Link Chokes", Application Note: AP040109EN, EATON Company, Effective March 2015.

[42] K. H. Sueker, "Comments on "Harmonics: the effects on power quality and transformers"," in IEEE Transactions on Industry Applications, vol. 31, no. 2, pp. 405-406, March-April 1995, doi: 10.1109/28.370291.

[43] T. C. Sekar and B. J. Rabi, "A review and study of harmonic mitigation techniques," 2012 International Conference on Emerging Trends in Electrical Engineering and Energy Management (ICETEEEM), Chennai, India, pp. 93-97, 2012, doi: 10.1109/ICETEEEM.2012.6494450.

[44] J. K. Phipps and J. P. Nelson, "A harmonic distortion control technique applied to six-pulse bridge converters," in IEEE Transactions on Industry Applications, vol. 29, no. 3, pp. 616-624, May-June 1993, doi: 10.1109/28.222434.

[45] "ABB INDUSTRIAL DRIVES: DCS880 drives-12-pulse manual", ABB Automation Products, Ident.No. :3ADW000533R0101 Rev A, 06/2019.

[46] J. M. Barcus and S. Ihara, "Harmonic assessment of cement plants", 30th IEEE Cement Industry Technical Conference, Quebec, QC, Canada, pp. 55-88, 1988, doi: 10.1109/CITCON.1988.13238.

[47] B. Segal, "Energy efficiency improvement in the cement industry," IEEE-IAS/PCS 2002 Cement Industry Technical Conference. Conference Record (Cat. No.02CH37282), Jacksonville, FL, USA, pp. 54-62, 2002, doi: 10.1109/CITCON.2002.1006493.

[48] J. C. Das, "Passive Filters," in Power System Harmonics and Passive Filter Designs , IEEE, pp.685-743, 2015, doi: 10.1002/9781118887059.ch15.

[49] A. B. Nassif, W. Xu and W. Freitas, "An Investigation on the Selection of Filter Topologies for Passive Filter Applications", in IEEE Transactions on Power Delivery, vol. 24, no. 3, pp. 1710-1718, July 2009, doi: 10.1109/TPWRD.2009.2016824.

[50] B. Turkay, "Harmonic filter design and power factor correction in a cement factory", 2001 IEEE Porto Power Tech Proceedings (Cat. No.01EX502), Porto, Portugal, pp. 4 pp, vol.1-, 2001, doi: 10.1109/PTC.2001.964642.

[51] T. Thasananutariya and S. Chatratana, "Planning Study of Harmonic Filter for ASDs in Industrial Facilities," in IEEE Transactions on Industry Applications, vol. 45, no. 1, pp. 295-302, Jan.-feb. 2009, , doi: 10.1109/TIA.2008.2009503.

[52] L. Motta and N. Faúndes, "Active / passive harmonic filters: Applications, challenges & trends," 2016 17th International Conference on Harmonics and Quality of Power (ICHQP), Belo Horizonte, Brazil, pp. 657-662, 2016, doi: 10.1109/ICHQP.2016.7783319.

[53] H. Escarria, " ABB Special Transformers-Variable Speed Drive Applications", ABB Group, July 2011.

[54] Jun-koo Kang, "Multi-Pulse Rectifier Solutions for Input Harmonics Mitigation", Applicable Product: F7, G7, P7 and E7, Doc#: WP.AFD.02, White Paper, Yaskawa Electric America, Inc., December 1, 2005.

[55] "Application Guidelines for 12-Pulse Operation of PowerFlex 750-Series AC Drives", Rockwell Automation, Inc., Publication 750-AT003B-EN-P, October 2023.

[56] "Ultra-low harmonic and regenerative drives for increased efficiency and reliability of processes and systems", White paper, ABB Motion, Ident.No.: 3AXD50000795550, 2021.

[57] "Active Front End Drives: Lower Harmonics, Higher Energy Savings", Rockwell Automation, Inc., Publication PFLEX-WP001A-EN-P – October 2018.

[58] "VLT- Low Harmonic Drive Instruction Manual- VLT Automation Drive FC 300", Danfoss company, doc No. MG34O222, Rev. 23 January 2012.

[59] M.Fedorovicheva, "Improving data center efficiency with VSDs for cooling" ABB HVAC WEBINARS, 30 July 2020.

[60] P. Luchinger, U. Maier and R. A. Errath, "Active front end technology in the application of a down hill conveyor," IEEE Cement Industry Technical Conference, 2006. Conference Record., Phoenix, AZ, USA, pp. 20 pp., 2006, doi: 10.1109/CITCON.2006.1635717.

Journal of Engineering and Technology for Industrial Applications

ITEGAM-JETIA

ISSN ONLINE: 2447-0228

Manaus, v10. n.50, p. 81-90. November/ December., 2024.
DOI: https://doi.org/10.5935/jetia.v10i50.1303

RESEARCH ARTICLE OPEN ACCESS

USING BUSINESS ANALYSIS TO ENHANCE SUSTAINABILITY AND ENVIRONMENTAL COMPLIANCE IN OIL AND GAS: A STRATEGIC FRAMEWORK FOR REDUCING CARBON FOOTPRIN

Alliy Adewale Bello[1], Fredrick Fiyeboju Magi[2], Ogochukwu Gold Abaneme[3], Uzochi Achumba[4], Adebowale Martins Obalalu[5] and Mobolaji Fakeyede[6]

[1]Northeastern Universitty, Boston, USA.
[2]Western Michigan University, Mallinson Institute of Science Education, Kalamazoo MI, USA.
[3,4] Northeastern University, Roux Institute College of Professional Studies, Boston USA.
[5]Kwara State University, Malete, Kwara -Nigeria.
[6]Chevron Corporation, Bollinger Canyon Road - San Ramon, USA.

[1] http://orcid.org/0009-0005-6617-8578, [2] https://orcid.org/0000-0002-6102-2428, [3] http://orcid.org/0009-0007-5427-9640, [4] https://orcid.org/0009-0007-7178-8957, [5] https://orcid.org/0000-0001-5059-9830, [6] https://orcid.org/0009-0007-1059-9562

Email: alliybello2@gmail.com, fredrickfiyeboju.magi@wmich.edu, abaneme.o@northeastern.edu, uzochi.achumba@gmail.com, adebowale.obalalu17@kwasu.edu.ng, Mobolaji.Fakeyede@gmail.com

ARTICLE INFO

Article History
Received: September 23, 2024
Revised: November 6, 2024
Accepted: November 10, 2024
Published: November 30, 2024

Keywords:
Business Analysis,
Sustainability,
Oil and Gas,
Carbon Footprint.

ABSTRACT

The oil and gas industry has been identified also as a major source of greenhouse gases and contributes approximately 42% of the total global CO_2 emissions. As the world continues to strive towards sustainable development goals including those of the Paris accord, this industry is under pressure to decrease its emission of carbon. This review discusses the application of business analysis tools on a strategy that supports sustainability and aligns oil and gas companies with environmental standards. The framework is centred on the deployment of next-generation technologies as carbon capture and storage, on establishing global standards of corporate climate policies, on engaging stakeholders, on optimizing business processes, on facing climate risks and on experimenting with new forms of biofuels. Some of the problems include high costs, complications due to state regulations, and negative attitudes from the public and stakeholders.These issues can be overcome through effective public-private partnerships, sharing of information, and diversification of research spending. In addition to mitigating emissions the envisaged framework is designed for companies to derive strategies that will keep them competitive and socially responsive. The present review also underlines the necessity to use a complex approach to increasing the sustainability of the oil and gas industry.

I. INTRODUCTION

The oil and gas industry is the major emitter of greenhouse gases contributing to nearly 42% of the global emission of CO_2. and is therefore a major contributor to climate change [1]. These emissions result from various processes, including the extraction, refining, and combustion of fossil fuels, as well as routine practices like flaring and methane leaks during production [2]. As the primary contributor to global emissions, the industry's activities have a profound impact on climate change, driving global warming, rising sea levels, and extreme weather events [1]. Given its central role in the climate crisis, the oil and gas sector faces increasing pressure to adopt more sustainable practices to reduce its carbon footprint [3]. Similarly, due to globalisation and the signing of the Paris Accord among other international acts, this sector has no option but to cut its footprint when it comes to the environment to meet international emission targets [4],[5]. Industry's pressures on those issues have been varied, some firms are advanced in sustainable practices integration, while others have not been able to adopt sustainable practices without compromising the firm's performances, [6],[7].

The concept of sustainability in the oil and gas industry involves two key dimensions: environmental sustainability and the economic or social sustainability of companies in the sector [8,9]. Achieving a balance between these aspects is critical, as companies must minimize their environmental impact while ensuring their long-term economic viability and maintaining social responsibility toward the communities in which they operate [8]. The sector's capital intensity, extensive value chain, and reliance on non-renewable resources pose challenges to meeting sustainability goals [10],[11]. The industry's dependence on fossil fuels conflicts with the principles of sustainable development, which prioritize long-term resource conservation and minimizing environmental harm [3]. As oil and gas operations require significant investments in infrastructure, the capital intensity of the sector makes transitioning to sustainable practices more complex [10]. Additionally, the global economy's reliance on oil and gas for energy security further complicates the industry's efforts to reduce its environmental footprint [1]. Growing energy demands, driven by population growth and industrialization, increase the pressure on companies to balance environmental sustainability with energy supply [12].

To achieve sustainability, oil and gas companies must adopt strategies that integrate environmental, economic, and social dimensions [12]. This includes reducing carbon emissions, improving energy efficiency, and transitioning to renewable energy sources [9]. However, these environmental measures must be aligned with the companies' profitability and investments in cleaner technologies [8]. Social sustainability involves ensuring equitable benefits for local communities while mitigating social harms like displacement and health risks [13]. The implementation of sustainability strategies is also complicated by varying regulatory requirements and geopolitical factors [11].

This manuscript aims at formulating a strategic framework that adopts business analysis techniques to tackle these issues thereby promoting sustainability and compliance with environmental standards in the oil and gas sector [6-8]. In this way, the industry will be able to reposition its business models in harmony with the SDGs and contribute to lowering carbon intensity without compromising economic rationality and social standards [14],[15].

II. THEORETICAL REFERENCE

II.1 OVERVIEW OF THE GLOBAL NEED FOR SUSTAINABILITY IN THE OIL AND GAS SECTOR

Sustainability in the oil and gas sector requires balancing environmental impacts, economic growth, and people's welfare in the sector. The industry has come to the stage of a cross-road of providing solutions to global economic growth, while at the same time upholding the Social Responsibility Safety Management about environmental conservation [10],[16],[17]. Due to awareness of environmental protection, the oil and gas industry is continuously evolving towards sustainable development goals, and is linking its further discussion with climate change, emission and sustainable energy for the world [13]. Currently, there is a noticeable trend towards increasing sustainability in the global oil industry on the part of both the global oil and gas sector and governments, with goals set for emission reductions, energy efficiency, and the shift to clean energy [18],[19]. This is based on International Climate Policies, including the Paris Agreement, which calls for emission reduction measures to raise the global temperature by only one degree. In this regard the global temperature should not exceed 5°C above the level of pre-industrialization [3],[20].

The oil and gas sector operates at the intersection of complex geopolitical and societal dynamics, where energy security, economic stability, and environmental sustainability are deeply intertwined [21]. As global concerns about climate change intensify, the industry faces mounting pressure to align with sustainability goals and reduce its carbon footprint [22]. This pressure stems from both international agreements, such as the Paris Agreement, and shifting societal expectations. Business analysis, particularly through strategic frameworks, can play a crucial role in enhancing sustainability and ensuring environmental compliance within this sector [23]. Geopolitically, the reliance on fossil fuels has far-reaching implications for national and global stability [21]. Oil-rich countries often experience economic volatility due to fluctuations in global oil prices and geopolitical conflicts. For example, nations like Venezuela and Nigeria have faced economic instability linked to their heavy dependence on oil revenues. This economic vulnerability highlights the need for these countries to diversify their economies away from fossil fuels. The shift towards cleaner energy sources and the adoption of sustainable practices are becoming essential strategies for maintaining economic stability and reducing vulnerability [24].

Societal implications are equally significant. As governments implement policies aimed at reducing carbon emissions, oil-dependent economies must adapt to avoid socio-economic disruptions. For instance, Saudi Arabia's Vision 2030 represents an ambitious effort to reduce its reliance on oil by investing in diverse sectors such as tourism and technology. Similarly, Kazakhstan is focusing on renewable energy projects to create new economic opportunities and lessen its dependence on fossil fuels. These examples underscore the necessity for oil-dependent nations to foster economic resilience through diversification and innovation [25].

From a business analysis perspective, developing a strategic framework for reducing the carbon footprint involves several key components. First, integrating renewable energy technologies into oil and gas operations can substantially lower emissions and enhance sustainability [23]. For instance, companies can adopt solar, wind, and geothermal energy to power their facilities and reduce reliance on conventional fossil fuels. The use of photovoltaic solar panels on infrastructure, wind turbines near facilities, and geothermal heat pumps can significantly contribute to energy diversification and emissions reduction [26],[27]. Moreover, effective waste management and recycling practices are essential for minimizing the environmental impact of oil and gas operations. Implementing source reduction, material substitution, and process optimization can help reduce waste generation at facilities [28]. Recycling materials such as metal scrap and drilling muds can divert waste from landfills and promote a circular economy. Additionally, converting organic waste into renewable energy sources through technologies like anaerobic digestion and biogasification can offset fossil fuel consumption and reduce greenhouse gas emissions [21].

The strategic framework also emphasizes the importance of compliance with environmental regulations and standards. Companies must regularly monitor environmental parameters, emissions, and adherence to permit conditions to ensure regulatory compliance [26]. Environmental management systems [EMS], such as ISO 14001, can help establish proactive measures for identifying and mitigating environmental risks. Engaging with local communities and stakeholders is crucial for building trust and ensuring the successful implementation of sustainability initiatives [23].

II.2. INTERNATIONAL AGREEMENTS AND REGULATORY FRAMEWORKS: IMPACTS ON THE OIL AND GAS SECTOR

International agreements like the Paris Agreement have played a crucial role in shaping global climate policies by setting ambitious goals to curb greenhouse gas emissions and control global temperature increases. Since its adoption in 2015, the Paris Agreement has sought to limit the rise in global temperatures to well below 2°C above pre-industrial levels, aiming for an even more stringent 1.5°C limit [28],[29]. This framework has driven governments to adopt stricter environmental regulations and to encourage the transition to renewable energy sources. Governments worldwide are responding with increasingly stringent environmental standards. For example, the European Union Emissions Trading System [EU ETS] imposes a cap on total emissions and allows for trading of emission allowances, creating economic incentives for companies to reduce their emissions [30]. Similarly, national carbon taxes are designed to reduce carbon emissions by making high-emission activities more costly [28]. In response to these regulations, there has been a notable shift towards renewable energy. Policies like Germany's Energiewende are promoting significant investments in renewable energy sources, such as wind and solar power [31] Major oil and gas companies, including BP and TotalEnergies, are adapting by investing in these cleaner technologies to comply with regulatory expectations and lessen their environmental impact [32].

Maintaining a social license to operate is increasingly important. Companies must navigate these evolving regulations to retain public trust and avoid financial penalties. Enhanced reporting and ESG disclosures are becoming essential, as illustrated by ExxonMobil's improved climate disclosures following shareholder demands [33]. This regulatory environment compels oil and gas firms to integrate sustainability into their core strategies and operations. This pressure emanates from governments, investors, and civil society who are demanding companies to be more responsible in the manner they deal with their impact on the environment. Different governments in the world are coming up with even tighter restrictions on emissions and environmental conservation thus forcing industries to become environmentally tolerant to meet their set standards [7],[34].

Integrating sustainability into key business operations is now widely recognized as a significant competitive edge [35]. Companies that take the initiative to implement eco-friendly practices, such as cutting down emissions, enhancing energy efficiency, and investing in renewable energy sources, are better prepared to comply with future regulations, attract investors, and enhance their corporate image [36]. Sustainability has shifted from being a peripheral issue to becoming a central element of strategic decision-making, particularly in the oil and gas sector. Business analysis provides the tools needed to measure the financial returns of sustainable investments, ensuring these efforts support both environmental objectives and financial success [37]. Oil and gas companies are experiencing global investors' attention due to Environmental, Social, and Governance [ESG] considerations, which influence the business' sustainability and market capitalization [17],[38].

II.3. IMPORTANCE OF REDUCING CARBON FOOTPRINT IN THE INDUSTRY

Minimizing carbon emissions helps with sustaining oil and gas by lessening greenhouse emissions, advancing along the globe's climate objectives, and promoting sustainable actions in the long term [39]. Currently, the oil and gas sector is one of the highest emitters accounting for about 42% of total global CO_2 emissions [1],[3]. If these emissions are not significantly lowered, the world cannot achieve the existing climate goals, like the Paris Agreement that intends to limit global warming to 1. 5°C above pre-industrial levels [2],[4],[7]. In addition, when the limit of the usage of carbon is set and the cost of carbon increases, firms unable to decrease their emissions will be at a higher risk of suffering financially and could even lose market advantage. While carbon pricing mechanisms like carbon taxes and cap-and-trade systems are in place, they operate to increase the operating costs of oil and gas firms and thereby make capital-intensive projects less economically feasible for investors [17,38]. Digital emission estimation minimizes the carbon footprint of the oil and gas sector providing accurate real-time estimation, and efficient design changes at lower costs: as a result, enhancing the sustainability goals [32]. Organizations that develop a strategic approach to decreasing carbon emissions, including allocating resources to low-carbon technologies as well as increasing the efficiency of energy usage, not only address climatic risks but also strengthen their economic performance and competitive advantage [5].

Integrating renewable energy sources into oil and gas operations offers a promising route to reducing carbon emissions and enhancing sustainability. Technologies like solar, wind, and geothermal power can offset the energy-intensive processes of extraction, transportation, and refining [40]. Solar panels installed on infrastructure such as drilling rigs and refineries can generate electricity, reducing reliance on fossil-fuel-based grid power [41]. Wind turbines, both onshore and offshore, can supplement energy needs and lower greenhouse gas emissions. Geothermal systems, utilizing heat from the Earth, can provide essential power and thermal energy, especially in remote areas with limited grid access. To mitigate climate change, reducing greenhouse gas emissions is crucial. Advanced technologies and practices can minimize methane leaks, flaring, and venting, and enhance energy efficiency throughout the oil and gas value chain [40]. Advanced detection methods, including optical gas imaging and drones, can improve leak identification and repair [41]. Alternatives to flaring, such as gas-to-power conversion and gas reinjection, can help recover resources and reduce emissions. Carbon capture and storage [CCS] technologies can capture and store CO_2 emissions from industrial processes, including oil and gas operations, preventing atmospheric release [40]. Minimizing waste generation and encouraging recycling are key components of sustainable resource management in oil and gas operations [42]. Companies can lessen their environmental impact, conserve natural resources, and improve operational efficiency by reducing waste streams, recycling [43] materials, and implementing waste-to-energy technologies. Strategies such as source reduction, material substitution, and optimizing processes help reduce waste generation at oil and gas facilities [37]. Designing products and packaging for durability, recyclability, and reusability also minimizes waste throughout a product's life cycle [44]. Recycling programs for materials like metal scrap, plastic containers, and drilling muds can divert waste from landfills, decreasing the need for raw materials. Recycling facilities can extract valuable resources from waste, reintegrating them into production and fostering a circular economy [41].

Additionally, organic waste, such as biomass and wastewater sludge, can be converted into renewable energy, reducing fossil fuel consumption and greenhouse gas emissions. Technologies like anaerobic digestion and biogasification convert waste into biogas, biofuels, and heat for onsite energy generation

[45]. Ensuring compliance with environmental regulations is vital for maintaining social license to operate. Environmental management systems [EMS] such as ISO 14001 provide a structured approach to identify and manage environmental risks. Moreover, engaging local communities and stakeholders enhances transparency, builds trust, and enables collaboration on minimizing environmental impacts [45].

The objective of this review is to identify the application of business analysis in increasing sustainability and Conformity to the environmental standards in the Oil and gas industry. Through business analysis, a company gains a structured model of performing decision-making processes, which eventually helps to determine the most appropriate strategies for minimizing carbon emissions and maintaining the company's profitability [6],[7]. Furthermore, it endeavours to present a conceptual framework for managing the carbon reduction strategy within the industry with an emphasis on informed decision-making processes and best practices.

Business analysis is crucial in advancing sustainability and ensuring environmental compliance in the oil and gas industry. By relying on data-driven approaches, companies can enhance operational efficiency, cut down emissions, and boost profitability. Through the use of real-time data and predictive analytics, firms are able to make smarter decisions about energy consumption and emissions control, helping them meet their environmental targets [46]. Additionally, business analysis aids companies in evaluating regulatory risks, allowing them to anticipate changes in environmental policies and adapt strategies to ensure compliance [38]. This foresight minimizes risks while enhancing the company's overall sustainability efforts. Business analysis further informs investment in low-carbon technologies by assessing the cost-effectiveness of such investments, ensuring that the most sustainable solutions are also economically viable [6]. Moreover, optimizing supply chains through business analysis helps companies identify inefficiencies in logistics and production processes, leading to reduced emissions [3]. Business analysis also aligns Corporate Social Responsibility [CSR] efforts with stakeholder expectations, promoting transparency and strengthening trust through clear sustainability reports [20]. Business analysis equips oil and gas companies with the necessary tools to confront environmental challenges, cut their carbon footprint, and remain sustainable while maintaining profitability. Despite these advancements, there remains a gap in integrating business analysis with strategic frameworks specifically tailored for reducing carbon footprints. This journal aims to bridge this gap by proposing a comprehensive framework that leverages business analysis to address sustainability challenges, offering actionable insights for enhancing both environmental performance and economic viability in the oil and gas industry.

III. MATERIALS AND METHODS

The steps used in this review reflected rigorous and efficient identification and synthesis of data. The sources of data collection were academic and peer-reviewed journals, business reports, and case studies that revolved around sustainability, environmental standards, and business reporting on the oil and gas industry. The literature review was conducted by searching multiple databases like Scopus, Web of Science, and Google Scholar using such keywords as "business analysis in oil and gas", "sustainability", "environmental compliance", and "carbon footprint reduction". The inclusion criteria were articles published in the last decade, devoted to global and gas sectors and written in English, which analyzed the role of business analysis for sustainability in the given industry. Studies that did not contain features of any of these articles were dropped out of the review process.

Besides journal articles, several industry reports developed by key oil and gas companies as well as by the International Energy Agency [IEA] and the World Bank were reviewed to identify the current best practices and trends in the industry. Information from these sources was subjected to thematic analysis to find out various themes, strategies and challenges on sustainability and environmental compliance within the industry. The analysis was also identified how various business analysis tools and techniques have been employed in the process of solving these challenges.

To ensure a thorough review, data was categorized based on relevance and impact. Key areas of focus included the effectiveness of various business analysis tools, the influence of technological advances on sustainability, and the strategies that leading firms use to improve environmental compliance. The synthesis process involved cross-comparing findings from different sources to highlight similarities and differences, offering a detailed view of current practices and industry gaps.

The review also assessed the research methods used in the studies, evaluating the strength of research designs, data collection techniques, and analysis methods to ensure the conclusions were credible and sound. Additionally, the review took into account the geographic and sectoral diversity of the studies to provide a well-rounded perspective on sustainability practices in various contexts. The resulting framework, derived from academic research, industry reports, and thematic analysis, offers a comprehensive strategy for reducing the carbon footprint in the oil and gas sector. It provides actionable recommendations and best practices that can be tailored to different operational scenarios within the industry.

III.1 FRAMEWORK DEVELOPMENT

The literature and case study analysis used to inform the development of the strategic framework for lowering the carbon footprint of the oil and gas industry also guided the development of the strategic framework. The above framework was built in several phases. First, the general tools that are applied to business analysis in sustainability practices, including SWOT analysis, PESTEL analysis, and value chain analysis, were described and compared in the context of the oil and gas sector. These tools were then incorporated into a coherent framework specific for improving the decision-making and operational processes about sustainability and environmental management.

The development of the framework was also an iterative process where feedback from other experts and professionals would be incorporated. This feedback played an important role of making certain that the framework is not only theoretical, but it is also realistic and implemental. The framework was intended to be rather general so that it could be easily customized to the peculiarities of individual companies operating in the industry.

III.2 CRITERIA FOR SELECTING CASE STUDIES

When choosing cases, several factors were taken into nconsideration to make sure that only relevant and appropriate cases were included in the review. First, the study had to include eight cases of companies within the global oil and gas sector that have applied business analysis strategies to enhance sustainability and decrease carbon footprint, and are located in the United States of America. Second, these cases had to show some market impact:

emission changes, upgraded compliance, or improved efficiency. The cases were selected from different geographical locations to capture variations in the regulation and the market covering that stream of the profession to get a feel of how business analysis comprehensively can be deployed in several settings.

Additionally, where the description of the problem encountered, the tools used for business analysis, and its outcome were well captured, such cases were considered first. This selection criterion ensured that the case studies presented recommendations which could be applied or could be borrowed by other firms in the industry. The last choice of cases was carried out by comparing the theoretical literature and numerous reports of successful and failed strategies.

Table 1: Key Components of the Framework.

Strategic Framework Component	Description	Business Analysis Tool	Application of the Tool
Policy Alignment	Ensuring company policies are aligned with international environmental regulations and sustainability goals.	PESTEL Analysis	Analyzes the Political, Economic, Social, Technological, Environmental, and Legal factors affecting policy alignment.
Technology Integration	Adoption and integration of advanced technologies to minimize emissions and improve energy efficiency.	SWOT Analysis	Assesses the Strengths, Weaknesses, Opportunities, and Threats related to adopting and integrating new technologies.
Stakeholder Engagement	Engaging with stakeholders, including governments, communities, and investors, to support sustainability initiatives.	Stakeholder Analysis	Identifies and prioritizes key stakeholders and their interests to develop engagement strategies that align with sustainability goals.
Operational Optimization	Streamlining operations to reduce energy consumption and emissions throughout the value chain.	Value Chain Analysis	Examines each stage of the value chain to identify opportunities for reducing carbon footprint and enhancing operational efficiency.
Risk Management	Identifying and mitigating risks associated with environmental compliance and sustainability.	Failure Models and Effects Analysis [FMEA]	Evaluates potential failure points in processes and systems to prioritize risks and implement preventive measures to enhance environmental compliance.
Sustainability Reporting and Monitoring	Implementing systems for tracking and reporting sustainability metrics and progress towards carbon reduction goals.	Balanced Scorecard	Provides a framework for tracking performance across financial, customer, internal process, and sustainability perspectives.
Innovation and Research Development	Investing in R&D to develop new methods and technologies for reducing emissions and enhancing sustainability.	Innovation Mapping	Identifies areas for innovation and tracks the development and implementation of new technologies and practices.
Continuous Improvement	Implementing processes that ensure ongoing improvement in sustainability and operational efficiency.	Lean Six Sigma	Applies Lean Six Sigma methodology to reduce waste, improve efficiency, and enhance sustainability in operations.
Problem Solving and Process Improvement	Identifying and addressing underlying issues that impede environmental compliance and sustainability.	Root Cause Analysis	Investigates the root causes of problems related to environmental performance, enabling targeted solutions that enhance sustainability and compliance.

Source: Authors, (2024).

Table 2. Characteristics of Included Case Studies.

Author & Year	Objective	Case Study	Methodology	Description	Potential Challenges	Suggested Solutions
Tonge [2019]	To examine sustainability trends and technology integration in the oil and gas sector.	BP's Technology Integration for Emission Reduction	Case Study Analysis	BP implemented advanced carbon capture and storage [CCS] technology to reduce emissions in its oil and gas operations.	**High Initial Costs:** Implementing CCS technology involves significant upfront investment.	**Public-Private Partnerships:** Collaborate with governments to secure funding and subsidies for CCS projects.
Alnuaim [2019]	To explore the alignment of corporate policies with international climate goals.	ExxonMobil's Policy Alignment with Paris Agreement	Policy Review and Case Study	ExxonMobil adjusted its internal policies to align with the Paris Agreement's goals, focusing on reducing scope 1 and 2 emissions.	**Regulatory Compliance:** Variations in local regulations across different countries may complicate implementation.	**Global Standardization:** Advocate for more consistent international regulatory standards to simplify compliance.
Intykbayeva [2021]	To assess the impact of stakeholder engagement on sustainability initiatives,	Shell's Stakeholder Engagement in the Netherlands	Stakeholder Analysis and Case Study	Shell engaged local communities and stakeholders in the Netherlands to support its transition to renewable energy.	**Community Resistance:** Some stakeholders may resist changes due to perceived economic or social impacts.	**Transparent Communication:** Develop clear communication strategies to inform stakeholders of long-term benefits.

Mojarad et al. [2018]	To optimize operations for reducing energy consumption and emissions in the oil and gas industry.	Chevron's Operational Optimization in Downstream Operations	Value Chain Analysis and Case Study	Chevron streamlined its downstream operations to reduce energy consumption and emissions using value chain analysis.	**Operational Disruption:** Optimizing operations may temporarily disrupt existing processes.	**Phased Implementation:** Gradually implement changes to minimize disruptions and maintain operational continuity.
Menéndez et al. [2022]	To explore innovation in biofuels as a sustainable alternative in the energy sector.	TotalEnergies' Innovation in Biofuels Development	Innovation Mapping and Case Study	TotalEnergies invested in R&D to develop biofuels as part of its sustainability strategy, reducing reliance on fossil fuels.	**Technological Uncertainty:** The success of new technologies like biofuels is not always guaranteed.	**Diversified R&D Portfolio:** Invest in multiple technologies to mitigate the risk of any single project's failure.
Garbie [2016]	To evaluate risk management practices in ensuring environmental compliance in the oil and gas industry.	Saudi Aramco's Risk Management for Environmental Compliance	Risk Assessment and Case Study Analysis	Saudi Aramco developed a comprehensive risk management framework to ensure compliance with environmental regulations.	**Complex Risk Assessment:** Identifying and mitigating environmental risks can be complex and resource-intensive.	**Advanced Analytics:** Utilize data analytics and AI to enhance risk identification and mitigation processes.
Alnuaim [2019]	To investigate the effectiveness of sustainability reporting in tracking environmental goals.	Eni's Sustainability Reporting and Monitoring System	Sustainability Reporting and Case Study	Eni implemented a robust sustainability reporting system, tracking progress towards carbon reduction goals.	**Data Accuracy:** Ensuring the accuracy of sustainability data across multiple operations can be challenging.	**Integrated Reporting Tools:** Implement integrated software solutions that consolidate and verify data from different sources.

Source: Authors, (2024).

III.3 STRATEGIC FRAMEWORK FOR REDUCING CARBON FOOTPRINT

The following are the elements of the proposed Strategic Framework for Reducing Carbon Footprint namely; policy and regulation matching, incorporation of superior technology, stakeholder involvement, operation optimization, risk management, sustainable assessment, and investment in innovation (Table 1). All the components incorporate tools for business analysis such as PESTEL, SWOT, Value Chain Analysis, Failure Models and Effects Analysis [FMEA], Balanced Scorecard, Stakeholder Analysis, Innovation Mapping, Lean Six Sigma and Root Cause Analysis to enhance effectiveness in attaining sustainable outcomes. As can be evidenced by the case studies presented in this paper, the sustainability effort in the oil and gas industry varies (Table 2). BP engaged in the use of carbon capture and storage which was however characterized by high initial costs through public-private partnerships. ExxonMobil adjusted the policies to the Paris Agreement and promoted the standards for internationalization. Shell was focused on identifying Paths Towards Renewables to involve stakeholders. Through phased implementation, Chevron improved downstream operation efficiency. Biofuels were another important investment for TotalEnergies; it addressed the technological risks by having balanced research and development programs. The participants' actions include Saudi Aramco, which initiated the creation of the framework for risk management, integrated with big data, and also Eni, which focused on improving sustainability reporting, using integrated tools.

IV. RESULTS AND DISCUSSIONS

In the case of the oil and gas industry, there are several effects of the framework in the achievement of the sustainability goals as the following cases have shown. For instance, BP has adopted more refined carbon capture and storage [CCS] technology as an illustration of how technology holds the potential to lower emissions, albeit at a greater start-up cost, which may be moved by PPPs [47]. This approach highlights the role of innovative technology in achieving long-term sustainability goals, demonstrating that while initial costs may be high, the benefits of CCS in significantly reducing emissions can be substantial when supported by strategic partnerships. Such collaborations can help distribute the financial burden and facilitate the scaling of CCS technology across the industry.

Similarly, while addressing the policies of the organization, namely, ExxonMobil, on the requirements of the Paris Agreement, which indicate the importance of the regulation alignment to achieve the objective of sustainability, the variations of the local regulations noticed in this case show that there is a need for international standardization. The variations in local regulations observed in this case underscore the necessity for international standardization. A unified global framework could streamline compliance and foster more consistent implementation of sustainability practices, thereby enhancing the overall effectiveness of regulatory measures. Standardization would reduce the complexity faced by multinational corporations operating in diverse regulatory environments, enabling more coherent and widespread adoption of sustainable practices [10]. Furthermore, Shell's interaction with the stakeholders in the Netherlands shows the need to involve the locals in the support of a shift to renewable energy as the main resistance hinders communication [48]. The other significant factors for sustainability improvement in the oil and gas industry are operational improvement and innovation. Chevron, therefore, sues downstream optimization to minimize energy usage as a demonstration of how value chain analysis reduces emissions, though operational changes impact continuity and are manageable through a phased approach [15].

The resistance encountered in engaging local stakeholders illustrates the importance of effective communication and collaboration. Involving local communities early in the decision-making process and addressing their concerns can mitigate resistance and enhance support for renewable energy projects. This engagement is crucial for successful implementation and acceptance of sustainability initiatives, as demonstrated by Shell's experience [48]. Another significant factor for sustainability improvement in the oil and gas industry is operational enhancement and innovation [44]. Chevron's use of downstream optimization to minimize energy consumption is a prime example of how value chain analysis can contribute to emission reductions. The phased approach to implementing operational changes demonstrates the feasibility of incremental improvements in reducing emissions while maintaining operational continuity. Such strategic optimization not only lowers energy usage but also enhances overall operational efficiency, thereby aligning with sustainability goals [15].

TotalEnergies' commitment to biofuels as a sustainable option shows how variation in the portfolios can help manage risks arising from the issues of technological volatility to improve the robustness of sustainability approaches [20]. By investing in biofuels, TotalEnergies addresses the challenge of technological uncertainty and demonstrates how a diversified approach to sustainability can enhance resilience. This strategy not only supports sustainability objectives but also provides a buffer against market fluctuations and technological changes, reinforcing the robustness of sustainability efforts [49].

In addition to defensive capabilities, there are more effective risk management practices, including the one in Saudi Aramco, to ensure compliance with the environmental standards whereby risk management enables the application of advanced analytics to tackle complexities of risk assessments [8]. Advanced analytics and risk management strategies enable companies to navigate the complexities of environmental compliance more effectively. By leveraging sophisticated analytical tools, companies can better assess and manage environmental risks, thereby enhancing their ability to meet regulatory requirements and achieve sustainability objectives [50].

The outlined approaches, which could present some problems, contribute to the improvement of the oil and gas sector's performance of sustainable development objectives altogether. The strategic initiatives reflected in these examples highlight the importance of integrating technological innovations, policy alignment, stakeholder engagement, and risk management into a comprehensive framework for enhancing sustainability and minimizing carbon footprints. These elements, when combined, provide a robust foundation for advancing sustainability efforts across the industry [51].

The following are some of the strategic initiatives, which are included in the development of the proposed framework for enhancing sustainability and minimising carbon footprint in the oil and gas industry: For example, BP has employed the best CCS technology that shows that technology is a key factor in addressing emissions even though it might entail high initial costs, which may be eased with public-private partnerships aimed at sourcing capital [47].

Despite the high initial costs, CCS technology represents a critical tool for reducing carbon emissions. The involvement of public-private partnerships can help mitigate these costs and facilitate the broader adoption of CCS, thus contributing to long-term sustainability goals [52]. Similarly, the fact that ExxonMobil changed its internal policies to abide by the Paris Agreement speaks to the power of policy as the crucial factor affecting sustainability; if the policies were more standardized around the world, the company would be more likely to adhere to them and engage in more sustainable practices across different regions [10]. The need for international standardization is evident, as consistent global policies would simplify compliance and encourage more widespread adoption of sustainable practices across different regions [36].

When comparing the proposed framework with several similar strategies in the oil and gas industry that are not included in the analysis, it is possible to identify differences that could provide a better understanding of how to improve sustainability and minimize carbon footprints. For example, [1] focuses on renewable hydrogen as one of the promising options to address the carbonization problem of the oil and gas industry. Unlike the BP's reliance on CCS technology to cut down emissions, renewable hydrogen is a low-carbon fuel which does not have much distance to travel in terms of integration due to its compatibility with existing infrastructures, without the high initial investments that are required for CCS [1],[47]. Also, some companies have ventured into different types of renewable technologies, meaning that they are not concentrated in one particular kind of technology like ExxonMobil's single-focused strategy of policy commitment to the Paris Agreement outlined in this work by [20]. Moreover, this is further demonstrated by [3] on how digital twins and predictive analytics can design and manage the oil and gas industry in a way that maximises operations while also minimising emissions rather than just performing a 'value chain' analysis. This technology provides a dynamic and comprehensive view of operations, allowing for optimized performance and reduced emissions. Unlike traditional value chain analysis, digital twins and predictive analytics offer real-time insights and enhanced efficiency, thereby contributing [53] to more effective sustainability management [38]. This approach differs from the operational improvement strategies that have been embarked on at Chevron particularly because they feature more on the efficiency of current processes and the optimal use of digital tools, whereas the use of big data is still in an enhanced stage [15]. Furthermore, one form of partnership has seen manufacturers like Equinor seek to own certain assets to integrate renewable energy in their operation plans while lowering carbon footprints in a more consistent manner than through the use of posted emissions reduction technologies like CCS or biofuels [54]. These comparative examples emphasize the fact that a more synergistic approach is required to integrate av sophisticated technology, renewable energy investments, and policy changes to achieve overall carbon reduction and sustainability goals in the oil and gas industry. A more integrated and multifaceted strategy, incorporating various elements of technology, policy, and stakeholder engagement, is essential for addressing the complex challenges of sustainability in the oil and gas industry [49]. The strategies for increasing sustainability and decreasing carbon intensity within the oil and gas industry are long-term and have scalability potential across the sector. For example, BP as a company integrates efficient carbon capture and storage or CCS as a form of addressing emissions although the technology is large scale at the start it is costly thus the need for involvement of partner funding [10],[47]. Likewise, ExxonMobil's policy collaboration with the Paris Agreement is evidence of integrated business and climate objectives that can generate a uniform business model that makes compliance more manageable and perhaps more extensive

[8],[10]. Moreover, the practice of engaging stakeholders and coming up with innovative solutions for sustainable options also increases the possibility of expanding these sustainability efforts. Shell's lessons in engaging stakeholders for renewable energy transition show that traditional communications management practice also helps to negate community opposition to sustainable projects and thus increase the acceptance and implementation of such projects in a wide area [20],[48]. Furthermore, the investment in biofuels at TotalEnergies also demonstrated how the diversified research and development offset the risks associated with new technologies for fossil fuel use reduction in the energy sector as a scalable model as mentioned in [15],[20]. These strategies stress about the applicability on a large scale and long-term returns for the industry that fuels the change towards a more sustainable and compliant manner in the oil and gas sector**.** By adopting a synergistic approach that combines technological advancements, policy alignment, stakeholder engagement, and diversified investments, the industry can more effectively achieve its sustainability goals and reduce carbon footprints over the long term.

V. CONCLUSIONS

This review responds to the research questions showing the importance of the business analysis approach in improving sustainability and compliance to environmental conditions in the oil and gas industry. Some major research findings suggest that the use of modern technologies and the integration of corporate policies with international climate goals can significantly decrease emissions; meanwhile, high costs and bureaucratic obstacles can hinder these efforts [10],[47]. Engagement of stakeholders and efforts towards the development and utilization of other renewable energy sources such as bio-fuels are also found to be potential solutions for sustainability and low carbon footprint within this industry, especially when implemented with communication transparency and diverse investment in research and development [20],[48]. Strategic management, focusing on operational excellence, risk management and sound sustainability reporting are integral parts of a strategic management model that provides guidelines for improving organisational performance and targeting global sustainability goals without compromising on economic viability [8].

To reach sustainable and scalable development in the oil and gas industry, it is better to use several strategies: First and foremost, initial strategies include prioritizing the use of more advanced technologies, like CCS; however, it is crucial to find solutions to financial difficulties through public and private financing to reduce the overall costs, which is carried out through the development of funding mechanisms [8,47]. Also, integrating corporate policies with international climate deals including the Paris Agreement is important in lateral harmonization of sustainability regimes, thus minimizing compliance risks across jurisdictions [10]. Stakeholder communication and the involvement of stakeholders within sustainability processes can improve sustainability and easier transition towards renewable energy [48] However, risk management strategies are required to minimize the technological risks involved with newer technologies and rising environmental standards to achieve a diversified portfolio of renewable energy technologies [20]. Further studies should therefore consider examining the applicability of innovation tools like digital twin and predictive analytics for achieving better practical and environmental outcomes than conventional tools [3],[15]. It is also essential to analyse how other novel renewable energy resources such as renewable hydrogen and offshore wind affect the central idea of sustainability and carbon-cutting initiatives in the oil and gas industry [1],[54]. Further, it is necessary to study the community effects of sustainability transition, which involves how local communities can participate actively in this change and how knowledge regarding best practices in public involvement and communication can be shared in different countries [48]. Finally, researchers must assess the impacts of the policy initiatives that seek to synchronise regional and global regulation of sustainability practices seeking to achieve further improvements in the implementation of sustainable practices across the industry [10].

VI. AUTHOR'S CONTRIBUTION

Conceptualization: Alliy Adewale Bello, Fredrick Fiyeboju Magi, Ogochukwu Gold Abaneme, Uzochi Achumba, Adebowale Martins Obalalu and Mobolaji Fakeyede.
Methodology: Alliy Adewale Bello, Fredrick Fiyeboju Magi, Ogochukwu Gold Abaneme, Uzochi Achumba, Adebowale Martins Obalalu and Mobolaji Fakeyede.
Investigation: Alliy Adewale Bello, Fredrick Fiyeboju Magi, Ogochukwu Gold Abaneme, Uzochi Achumba, Adebowale Martins Obalalu and Mobolaji Fakeyede.
Discussion of results: Alliy Adewale Bello, Fredrick Fiyeboju Magi, Ogochukwu Gold Abaneme, Uzochi Achumba, Adebowale Martins Obalalu and Mobolaji Fakeyede.
Writing – Original Draft: Alliy Adewale Bello, Fredrick Fiyeboju Magi, Ogochukwu Gold Abaneme, Uzochi Achumba, Adebowale Martins Obalalu and Mobolaji Fakeyede.
Writing – Review and Editing: Alliy Adewale Bello, Fredrick Fiyeboju Magi, Ogochukwu Gold Abaneme, Uzochi Achumba, Adebowale Martins Obalalu and Mobolaji Fakeyede.
Supervision: Alliy Adewale Bello, Fredrick Fiyeboju Magi, Ogochukwu Gold Abaneme, Uzochi Achumba, Adebowale Martins Obalalu and Mobolaji Fakeyede.
Approval of the final text: Alliy Adewale Bello, Fredrick Fiyeboju Magi, Ogochukwu Gold Abaneme, Uzochi Achumba, Adebowale Martins Obalalu and Mobolaji Fakeyede.

VII. REFERENCES

[1] Int. Energy Agency [IEA], 2021. Global Energy Review 2021. Available: https://www.iea.org/reports/global-energy-review-2021.

[2] O. Schneising et al., "Advances in retrieving methane and carbon monoxide from TROPOMI onboard Sentinel-5 Precursor," Atmos. Meas. Techn. Discuss., vol. 2022, pp. 1-28, 2022.

[3] S. Paltsev, A. Ghandi, J. Morris, and H. Chen, "Global electrification of light-duty vehicles: impacts of economics and climate policy," Econ. Energy Environ. Policy, vol. 11, no. 10.5547, 2022.

[4] J. van den Broek, "Quantifying visions on the Dutch energy transition," 2020.

[5] S. Ghosh, A. K. Tiwari, B. Doğan, and E. J. A. Abakah, "The dynamic relationship between gas and crude oil markets and the causal impact of US shale gas," Comput. Econ., vol. 63, no. 6, pp. 2501-2524, 2024.

[6] Q. Abbas, M. Nurunnabi, Y. Alfakhri, W. Khan, A. Hussain, and W. Iqbal, "The role of fixed capital formation, renewable and non-renewable energy in economic growth and carbon emission: a case study of Belt and Road Initiative project," Environ. Sci. Pollut. Res., vol. 27, pp. 45476-45486, 2020, doi: 10.1007/s11356-020-10413-y.

[7] S. Thacker, E. Eaton, N. Healy, A. Scerri, J. C. Stephens, and G. Supran, "Fossil fuel industry influence in higher education: A review and a research agenda," *Wiley Interdisciplinary Reviews: Climate Change*, doi: 10.1002/wcc.904, May 2024.

[8] I. Garbie, "Sustainability in the service sector: oil and gas industry," in Sustainability in Manufacturing Enterprises: Concepts, Analyses and Assessments for Industry 4.0, 2016, pp. 217-236.

[9] T. Walker, S. Barabanov, M. Michaeli, and V. Kelly, "Sustainability in the oil and gas industry: An introduction," in *Sustainability in the Oil and Gas Industry*, 1st ed., Cham, Switzerland: Springer, 2023, doi: 10.1007/978-3-031-51586-6_1.

[10] S. Alnuaim, "Energy, Environment, and Social Development: What Does Sustainability Mean for Oil and Gas?" J. Petroleum Technol., 2018, doi: 10.2118/1218-0010-JPT.

[11] R. J. Lempert, B. Preston, S. M. Charan, L. Fraade-Blanar, and M. S. Blumenthal, "The societal benefits of vehicle connectivity," Transp. Res. D: Transp. Environ., vol. 93, no. 102750, 2021.

[12] A. Bello, "CSA implementation strategies unravelling success and challenges," ITEGAM-JETIA, vol. 10, no. 47, pp. 42-49, 2024, doi: 10.5935/jetia.v10i47.1070.

[13] T. Walker, S. Barabanov, M. Michaeli, and V. Kelly, "Sustainability in the oil and gas industry: An introduction," in *Sustainability in the Oil and Gas Industry*, 1st ed., Springer, 2023, doi: 10.1007/978-3-031-51586-6_1.

[14] Y. Yusuf, A. Gunasekaran, A. Musa, N. El-Berishy, T. Abubakar, and H. Ambursa, "The UK oil and gas supply chains: An empirical analysis of adoption of sustainable measures and performance outcomes," Int. J. Prod. Econ., vol. 146, pp. 501-514, 2013, doi: 10.1016/J.IJPE.2012.09.021.

[15] A. A. S. Mojarad, V. Atashbari, and A. Tantau, "Challenges for sustainable development strategies in oil and gas industries," in Proc. Int. Conf. Bus. Excellence, vol. 12, no. 1, pp. 626-638, 2018.

[16] E. Dadd, V. Kirou, J. Velasquez, S. Kalhori, and D. Galatro, "Sustainability and future of the oil and gas industry: a mini-review," DYNA, 2023, doi: 10.15446/dyna.v90n226.105963.

[17] I. Kostenok, Y. Khomenko, and A. Efimenko, "Today's interpretation of oil and gas companies' sustainability in global fuel and energy market," Vestn. Plekhanov Russ. Univ. Econ., 2020, doi: 10.21686/2413-2829-2020-1-93-107.

[18] N. Ekpecham, "Global Oil Industry: Environmental Sustainability Efforts by Corporations and Governments," J. Artif. Intell. Gen. Sci. [JAIGS], vol. 1, no. 1, pp. 166–167, 2024, doi: 10.60087/jaigs.v1i1.94.

[19] H. Dong, "Oil and gas industry: environmental and sustainability in the energy transition to net-zero," 2022, doi: 10.3997/2214-4609.2023101044.

[20] J. Menéndez-Sánchez, J. Fernández-Gómez, and A. Araujo-de-la-Mata, "Sustainability Strategies by Oil and Gas Companies, Contribution to the SDGs and Local Innovation Ecosystems," Energies, vol. 16, no. 6, pp. 2552, 2023.

[21] M. Hafner, P. P. Raimondi, and B. Bonometti, "Geopolitics of Oil and Gas in the MENA Region," in The Energy Sector and Energy Geopolitics in the MENA Region at a Crossroad, Springer, Cham, 2023, pp. 81-98. doi: 10.1007/978-3-031-30705-8_5.

[22] S. Bakhsh, W. Zhang, K. Ali, and J. Oláh, "Strategy towards sustainable energy transition: The effect of environmental governance, economic complexity, and geopolitics," Energy Strat. Rev., vol. 52, p. 101330, Mar. 2024.

[23] Q. Hassan, P. Viktor, T. J. Al-Musawi, B. M. Ali, S. Algburi, H. M. Alzoubi, A. K. Al-Jiboory, A. Z. Sameen, H. M. Salman, and M. Jaszczur, "The renewable energy role in the global energy transformations," Renewable Energy Focus, vol. 48, p. 100545, Mar. 2024.

[24] R. Vakulchuk, I. Overland, and D. Scholten, "Renewable energy and geopolitics: A review," Renew. Sustain. Energy Rev., vol. 122, p. 109547, Apr. 2020.

[25] A. Ibenrissoul, Z. Benjouid, and S. Kammoun, "Evaluating the compliance of environmental management systems: Evidence from Moroccan banks," Arab Gulf J. Sci. Res., Jun. 2023. [Online]. Available: https://ajieel.com/index.php/a/article/download/47/48.

[26] C. Okafor, C. Madu, C. Ajaero, J. Ibekwe, H. Bebenimibo, and C. Nzekwe, "Moving beyond fossil fuel in an oil-exporting and emerging economy: Paradigm shift," AIMS Energy, vol. 9, no. 2, pp. 379–413, 2021. doi: 10.3934/energy.2021020.

[27] J. Awewomom, F. Dzeble, Y. D. Takyi, et al., "Addressing global environmental pollution using environmental control techniques: a focus on environmental policy and preventive environmental management," Discover Environmental, vol. 2, p. 8, 2024. doi: 10.1007/s44274-024-00033-5.

[28] M. Dhali, S. Hassan, and U. Subramaniam, "Comparative analysis of oil and gas legal frameworks in Bangladesh and Nigeria: A pathway towards achieving sustainable energy through policy," Sustainability, vol. 15, no. 21, p. 15228, 2023. doi: 10.3390/su152115228.

[29] S. C. Dike and S. E. Osinachi-Nwandem, "Regulatory framework governing gas operations and utilization in the Nigerian petroleum industry," Afr. J. Ind. Eng. Environ. Res., 2023. [Online]. Available: https://ajieel.com/index.php/a/article/download/47/48.

[30] C. Yin, "International law regulation of offshore oil and gas exploitation," Environ. Impact Assess. Rev., vol. 88, p. 106551, May 2021.

[31] A. Rahuma and S. Fethi, "A new approach to evaluate environmental strategy: Empirical evidence from international petroleum companies using the balanced scorecard model," Bus. Strat. Environ., vol. 24, p. 3068, 2022. doi: 10.1002/bse.3068.

[32] C. Majumdar, K. C., A. Naik, H. Garg, A. Suryadi, A. Sabir, H. Hussain, and N. Singh, "Digital Emission Footprint Estimation as a Design Criteria to Fulfil Sustainable Development Goals," 2024, doi: 10.2523/iptc-23408-ms.

[33] J. Lee, A. M. Serafin, and C. Courteau, "Corporate disclosure, ESG, and green fintech in the energy industry," J. World Energy Law Bus., vol. 16, no. 6, pp. 473–491, 2023. doi: 10.1093/jwelb/jwad018.

[34] W. Ahmad, J. Rezaei, M. Brito, and L. Tavasszy, "The influence of external factors on supply chain sustainability goals of the oil and gas industry," Resources Policy, vol. 49, pp. 302-314, 2016, doi: 10.1016/J.RESOURPOL.2016.06.006.

[35] Y. Zhu, H. Zhang, A. B. Siddik, Y. Zheng, and F. A. Sobhani, "Understanding corporate green competitive advantage through green technology adoption and green dynamic capabilities: Does green product innovation matter?" Systems, vol. 11, no. 9, p. 461, 2023. doi: 10.3390/systems11090461.

[36] R. Fernández-González, F. Puime-Guillén, and J. E. Vila-Biglieri, "Environmental strategy and the petroleum industry: A sustainability balanced scorecard approach," J. Petrol. Explor. Prod. Technol., vol. 13, pp. 763–774, 2023. doi: 10.1007/s13202-022-01543-9.

[37] M. A. Roffé and F. A. I. González, "The impact of sustainable practices on the financial performance of companies: A review of the literature," Revista Científica "Visión de Futuro", vol. 28, no. 1, pp. 221–240, 2024.

[38] Y. Mahmood, T. Afrin, Y. Huang, and N. Yodo, "Sustainable development for oil and gas infrastructure from risk, reliability, and resilience perspectives," Sustainability, vol. 15, no. 6, p. 4953, 2023. doi: 10.3390/su15064953.

[39] R. Bhattacharya, D. Bose, G. Mitra, and A. Sarkar, "Prospects of Sustainability for Carbon Footprint Reduction," in Sustainable Development and Climate Change, 2024, doi: 10.1002/9781394174805.ch14.

[40] J. O. T. and V. U. Oguanobi, "Navigating business transformation and strategic decision-making in multinational energy corporations with geodata," Int. J. Appl. Res. Soc. Sci., vol. 6, no. 5, pp. 801–818, May 2024. doi: 10.51594/ijarss.v6i5.1103. [Online]. Available: www.fepbl.com/index.php/ijarss.

[41] A. E. Esiri, O. A. Babayeju, and I. O. Ekemezie, "Implementing sustainable practices in oil and gas operations to minimize environmental footprint," GSC Adv. Res. Rev., vol. 19, no. 03, pp. 112–121, 2024. doi: 10.30574/gscarr.2024.19.3.0207.

[42] N. O. Solomon, P. Simpa, O. A. Adenekan, and S. C. Obasi, "Sustainable nanomaterials' role in green supply chains and environmental sustainability," Eng. Sci. Technol. J., vol. 5, no. 5, pp. 1678–1694, 2024.

[43] S. C. Obasi, N. O. Solomon, O. A. Adenekan, and P. Simpa, "Cybersecurity's role in environmental protection and sustainable development: Bridging technology and sustainability goals," Comput. Sci. IT Res. J., vol. 5, no. 5, pp. 1145–1177, 2024.

[44] S. Yasemi, Y. Khalili, A. Sanati, and M. Bagheri, "Carbon capture and storage: Application in the oil and gas industry," Sustainability, vol. 15, no. 19, p. 14486, 2023.

[45] I. O. Ekemezie and W. N. Digitemie, "Carbon capture and utilization [CCU]: A review of emerging applications and challenges," Eng. Sci. Technol. J., vol. 5, no. 3, pp. 949–961, 2024.

[46] J. G. Vargas-Hernández, J. A. López-Lemus, and M. F. H. Cota, "Green human resources and its implications on green organizational social responsibility and organizational green image," Posgraduate and Research Department, Tecnológico Mario Molina Unidad Zapopan, Mexico, University of Guanajuato, Mexico. [Online]. Available: https://www.irma-international.org/viewtitle/304794/?isxn=9781668451137.

[47] P. Tonge, "Sustainability trends in oil and gas," APPEA J., 2019, doi: 10.1071/AJ18206.

[48] M. Intykbayeva, "Sustainable Path for the Oil and Gas Industry," 2021, doi: 10.5957/TOS-2021-23.

[49] R. Blay-Roger, M. Saif, L. F. Bobadilla, T. Ramirez-Reina, M. A. Nawaz, and J. A. Odriozola, "Embracing the sustainable horizons through bioenergy innovations: A path to a sustainable energy future," Frontiers in Chemistry, vol. 12, Catalytic Reactions and Chemistry, 2024. doi: 10.3389/fchem.2024.1416102.

[50] O. Amoo, F. Usman, E. Okafor, O. Akinrinola, and N. Ochuba, "Strategies for leveraging big data and analytics for business development: A comprehensive review across sectors," Comput. Sci. IT Res. J., vol. 5, pp. 562–575, 2024. doi: 10.51594/csitrj.v5i3.861.

[51] O. P. Agboola, F. M. Bashir, Y. A. Dodo, M. A. S. Mohamed, and I. S. R. Alsadun, "The influence of information and communication technology [ICT] on stakeholders' involvement and smart urban sustainability," Environ. Adv., vol. 13, p. 100431, 2023.

[52] D. Hariyani, P. Hariyani, S. Mishra, and M. K. Sharma, "Leveraging digital technologies for advancing circular economy practices and enhancing life cycle analysis: A systematic literature review," Waste Manag. Bull., vol. 2, no. 3, pp. 69–83, 2024.

[53] A. R. Patel, D. R. Vyas, A. Markana, and R. Jayaraman, "A conceptual model for integrating sustainable supply chain, electric vehicles, and renewable energy sources," Sustainability, vol. 14, no. 21, pp. 14484, 2022.

[54] S. Whitfield, "Offshore Wind: The New Frontier in Powering Platforms?" J. Petroleum Technol., vol. 72, no. 01, pp. 38-40, 2020.

Journal of Engineering and Technology for Industrial Applications

ISSN ONLINE: 2447-0228

ITEGAM-JETIA

Manaus, v10. n.50, p. 91-100. November/ December., 2024.

DOI: https://doi.org/10.5935/jetia.v10i50.1314

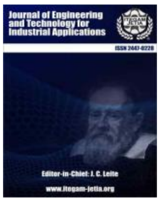

RESEARCH ARTICLE **OPEN ACCESS**

MULTI CRITERIA MODEL OF SUPPLY CHAIN SUSTAINABILITY EVALUATION & DEVELOPMENT STRATEGY FOR AGRITECH START-UP

Thabed Tholib Baladraf[1], Nita Kuswardhani [2], Winda Amilia[3], Mohammad Rondhi [4], and Yuli Wibowo [5]

[1] IPB University, Bogor, Indonesia
[2,3,4,5] University of Jember – Jember, Indonesia

[1] https://orcid.org/0000-0002-4953-1318, [2] https://orcid.org/0000-0001-7019-4590, [3] https://orcid.org/0000-0002-5098-5456, [4] https://orcid.org/0000-0002-6860-4957, [5] https://orcid.org/0000-0002-8825-7550

Email: thabedtholib@apps.ipb.ac.id, nita.ftp@unej.ac.id, winda.ftp@unej.ac.id, rondhi.faperta@unej.ac.id, yuliwibowo.faperta@unej.ac.id

ARTICLE INFO

Article History
Received: September 29, 2024
Revised: November 6, 2024
Accepted: November 10, 2024
Published: November 30, 2024

Keywords:
Agritech start up,
Multidimensional scaling,
Soft system methodology,
Supply chain management,
Sustainable supply chain.

ABSTRACT

The presence of agritech startups has successfully become a visionary solution at the agriculture supply chain to make it more efficient. Unfortunately, the supply chain in agritech start-ups is not sustainable and has various disadvantages. Therefore, this study aims to 1) analyze the current situation of supply chain at agritech start-ups, 2) analyze the sustainability index at agritech start-ups, and 3) analyze the strategy formulation needed by agritech start-ups through a soft system methodology approach. The research methods used were mixed methods. The stages of the research consisted of identifying current supply chain conditions, determining supply chain performance indicators by involving experts, assessing the supply chain sustainability index, and designing a conceptual model. The results showed the quality of the commodities produced did not meet standards and became a waste. The results of sustainability analysis in multidimensional results show a value of 48.84, economic 58.51, social 46.93, ecological 32.61, technology 42.36 and institutional 63.80. The results of the soft system methodology show that the strategies include contract farming, periodic coordination between stakeholders, GAP and OHS assistance, preparation of SOP for cultivation, application of borrowed tools under supervision, application of socialization of environmental literacy, and implementation of reserve supply chain.

I. INTRODUCTION

The supply chain has an important role, especially in the agricultural sector and fresh ingredients which are potential in Indonesia. The supply chain is fully responsible for the commodities distributed from upstream to downstream. According to Somapa et al. the supply chain consists of several components, namely purchasing, manufacturing, distribution, and storage [1]. A good supply chain has the characteristics of being visible, has the lowest possible costs, and is sustainable [2]. To meet these needs, innovations from agritech start-ups emerged that shortened the supply chain and helped farmers get more reasonable prices [3]. Agritech start-ups provide a marketplace for farmers, so that it is easier for farmers to sell agricultural products because they have direct market access.

Farmers as commodity suppliers in this case benefit because they get good market access. However, this solution is not balanced with the sustainability aspects of the process. This is because agritech start-ups want commodity quality with high standards without intensive and good cultivation assistance. This causes the majority of the commodities produced are not standardized and become waste. Based on the results of information from farmers, every time they make a commodity deposit to a company, ±20% of the commodity is returned to the farmer because it is not up to standard and ends up as food waste that cannot be sold. In addition, other problems were encountered, such as the absence of a guaranteed formal agreement and technological adoption, which was quite difficult. This shows that the existing supply chain is still not sustainable and threatens the sustainability of agritech start-ups and even causes agritech start-ups to go out of business [4]. To overcome these problems, further studies are needed to determine the root causes and the right strategies using sustainability analysis and soft system methodology to realize sustainable supply chain management.

According to Fahimnia et al. sustainable supply chain management (SSCM) is a supply chain that integrates social, environmental, economic, institutional, and technological pillars [5]. SSCM aims to protect the environment, advance the social condition of the community, and provide benefits to various parties [6]. The application of SSCM is proven to be able to overcome various problems and bring various benefits such as creating a circular economy that is prosperous and minimizing waste generation [7], increasing marketing, improving product image, and certainty [8]. On the other hand, soft system methodology (SSM) involves the development of system models related to problem situations. These models are used as a medium of discussion to bring changes to the actual situation.

Research related to SSCM in recent years has increased significantly in business and academia due to its positive impact [9-11]. However, SSCM research in developing countries, especially in agriculture, is still very limited and only recently considered important [12]. Research on the application of SSCM with SSM in agritech start-ups considering economic, social, environmental, technological, and institutional aspects has never been reported, so researchers in this case want to fill this gap. In this research, a study and analysis were conducted regarding the current condition of the supply chain, measurement of supply chain sustainability, and application of the soft system methodology. The calculation results will be used to formulate best strategy. Therefore, this study aims to 1) analyze the current situation and condition of supply chain at agritech start-ups, 2) analyze the sustainability index for each dimension at agritech start-ups, and 3) analyze the conceptual model and strategy formulation needed by agritech start-ups to create a sustainable supply chain through a soft system methodology approach.

II. THEORETICAL REFERENCE

II.1 AGRITECH START-UP

Agritech start-ups are start-up companies specifically engaged in the field of agricultural technology to solve various agricultural problems [13]. The presence of agritech start-ups during the current pandemic era plays an important role in meeting food needs and absorption of agricultural production [14]. According to Klerkx and Vilalobos, based on the business model and solved problems, agritech start-ups can be divided into four major groups, namely (1) financial group, (2) education and coaching group, (3) e-commerce group, and (4) technology development group [15].

II.2 SUPPLY CHAIN

The supply chain is a network of companies that are interconnected to produce and deliver products to consumers. Existing networks are generally grouped as suppliers, processing industries, distributors, shops, or retail, as well as supporting companies such as logistics service companies, packaging providers, and others. The supply chain has three kinds of flows that must be controlled, including the flow of goods that flows from upstream to downstream, the flow of finance that flows from downstream to upstream, and the flow of information from upstream to downstream and vice versa. According to Munizu, the goal of the supply chain is to maximize the value generated as a whole [16]. An integrated supply chain will increase the value generated. Supply chain management applications have the main objectives of increasing efficiency, reducing costs, reducing capital, improving service, and improving customer satisfaction. However, the supply chain applied to agriculture is currently not sustainable and causes various losses, so a strategy is needed to achieve this goal by implementing SSCM.

II.3 SUSTAINABLE SUPPLY CHAIN MANAGEMENT

Sustainable supply chain management (SSCM) is a network of companies that pays attention to the environment, advances the social condition of society and can still provide profit to various parties. SSCM consists of five pillars consisting of economic aspects, social aspects, environmental aspects, technological aspects, and institutional aspects. SSCM was created due to the many problems arising from unsustainable supply chains such as lack of access to reserve markets [17], improper handling of agricultural products [18], high food waste [19], unmet commodity needs [20], and material losses [21]. This is exacerbated by the fragmented pattern of relationships between actors [22]. The illustrative description of SSCM is presented in Figure 1.

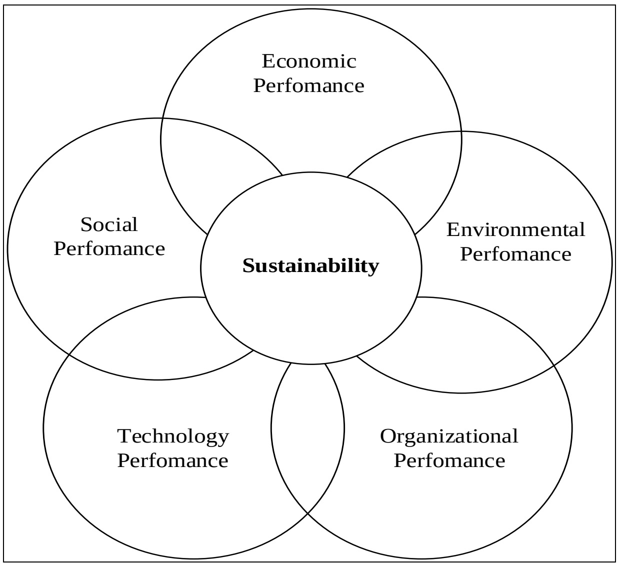

Figure 1: illustration sustainable supply chain management.
Source: [22].

II.3 MULTIDIMENSIONAL SCALING

Multidimensional Scaling Analysis (MDS) is an analytical model that can model nonlinear variables that can be used on nominal or ordinal data [23]. MDS is divided into two based on the scale of measurement of similarity data, MDS on a metric scale, which assumes that the data is quantitative, and MDS on a nonmetric scale, which assumes that the data is qualitative (nominal and ordinal). MDS has characteristics where comparisons will be made using diagrams or maps or graphs, so it can also be called a perceptual map. The application of MDS is done by calculating the shortest distance from the Euclidian Distance. In practice, MDS is an application derivative that is often used to measure the level of sustainability, namely Rapfish. According to previous research, MDS-Rapfish is often used in various sectors such as fisheries [24], agriculture [25], and supply chain [26]. The MDS-Rapfish analysis carried out will produce a sustainability index that is visualized in a two-dimensional image with a rating scale range of 0-100%.

II.3 SOFT SYSTEM METHODOLOGY

Soft system methodology is an approach used to deal with management problems that arise from human activity systems [27]. SSM can also be defined as a problem-solving framework where the nature of the problem is difficult to define [28]. The essence is to build a system model through understanding in depth the problem situation according to the phenomena encountered. SSM provides a coherent approach to group and individual thinking about context, complexity, and policy ambiguity [27]. This method is very reliable to be used to solve problems in various fields ranging from health [29], and engineering [30].

III. MATERIALS AND METHODS

The research was carried out in collaboration with several agritech start-ups and was carried out in three areas with relatively high agricultural and fishery productivity, namely Malang Regency, Jember Regency, and Banyuwangi Regency. The research begins with the identification of current supply chain conditions by describing the chain structure, chain management, chain resources, and chain business. The next step is to identify sustainability indicators through field observations, literature studies, and discussions with the six experts involved to obtain valid indicators. After identifying sustainability indicators, the supply chain sustainability index was then measured by involving ninety partner farmers using a Likert scale of 0-2 so that a sustainability value would be obtained. The sustainability value scale is presented in Table 1.

Table 1: Sustainability index scale.

Index	Sustainability Indicator
0-25,00	Bad
25,01-50,00	Less
50,01-75,00	Quite
75,01-100	Good

Source: Authors (2024).

In this study, several additional analyses were also carried out, including leverage and suitability analysis. Leverage analysis enabled us to determine the most sensitive/influential indicators. The indicator with the highest value is considered the most sensitive indicator. The suitability analysis consists of monte carlo analysis, s-stress, and R2. The results of a good monte carlo analysis have insignificant differences [31]. The results of a good stress value analysis have a value of less than 0.25 [32]. While the results of a good R2 have a value close to 1 [33]. The last stage is the preparation of a soft system methodology conceptual model to solve complex unstructured problem situations based on holistic analysis through a forum group discussion with experts.

IV. RESULTS AND DISCUSSIONS

IV.1 CURRENT CONDITION OF SUPPLY CHAIN

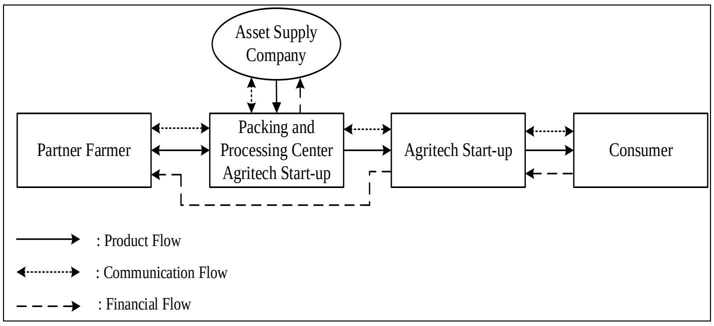

Figure 2: Current supply chain flow at agritech start-up.
Source: Authors (2024).

The supply chain structure in an agritech start-up consists of several members including primary and secondary members. Primary members in the supply chain are main actor that consist of partner farmers, agritech start-ups, and consumers. Secondary members consist of asset supply companies but are not directly involved in the process (Figure 2).

Supply chain management describes contractual agreements, transaction systems, and supply chain collaboration. In the contractual agreements, it was found that the majority of agritech start-ups still have not entered written and formal contractual agreements with partner farmers. This of course causes losses because according to Rustiani et al. relationships that are not formal have the potential to cause fraud and losses [34]. In the transaction system, it was found that the system applied between agritech start-ups and farmers is a credit transaction system. Partner farmers will receive payment after the partner farmers send the commodity. In supply chain collaboration, it was found that agritech start-ups were already transparent to partner farmers regarding price information. However, agritech start-ups do not provide regular assistance related to cultivation activities, causing many products that do not meet the criteria and become food waste.

The business process chain describes the business relationships between members of the supply chain through two perspectives, namely the cycle view and the push pull view. The cycle view in the supply chain business process consists of four stages, namely procurement, which is the stage of ordering raw materials. Manufacturing is the management of raw materials into ready-to-sell materials. Replenishment is the stage of replenishing the product or commonly known as the anticipation stage. Customer order is the stage of ordering by consumers. On the other hand, supply chain business processes, when viewed from a push or pull view, will be divided into two. The push stage has unknown consumer demand characteristics, while the pull stage has certain consumer demand characteristics. The agritech start-up supply chain business process is presented in Figure 3.

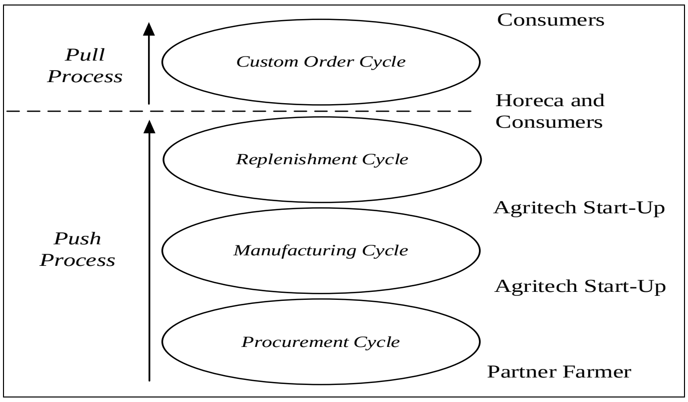

Figure 3: Agritech start-up supply chain business process.
Source: Authors (2024).

IV.2 MULTIDIMENSIONAL SUSTAINABILITY

In the sustainability analysis, 40 sustainability indicators are used based on the reality/observation on the ground and discussed with experts. The sustainability analysis was conducted multidimensionally in terms of the economic dimension, social dimension, ecological dimension, technological dimension, and institutional dimension. Multidimensional analysis was conducted in order to find out which dimensions must be improved and which dimensions must be maintained in performance. The results of multidimensional sustainability analysis are presented in Figure 4 and suitability testing using monte carlo, s-stress, and R^2 are presented in Table 2.

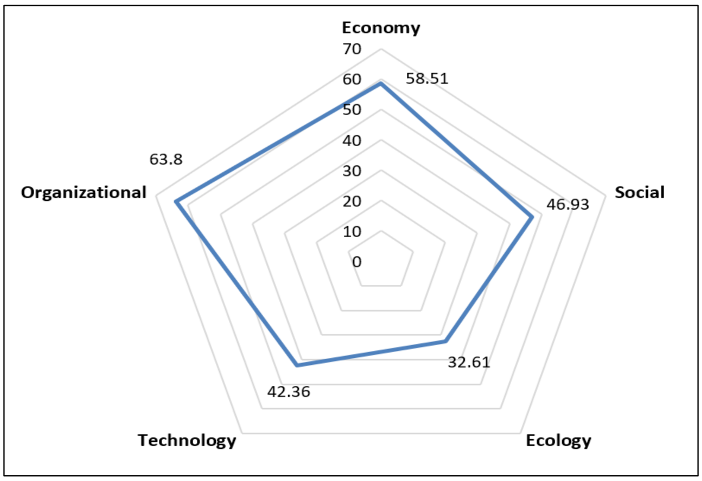

Figure 4: Multidimensional sustainability index kit chart.
Source: Authors (2024).

Table 2: Multidimensional and suitability analysis.

Dimension	MDS	Monte Carlo	S-Stress	R^2
Economy	58.51	57.47	0.143	0.946
Social	46.93	47.28	0.152	0.942
Ecology	32.61	33.16	0.138	0.943
Technology	42.36	42.26	0.148	0.944
Institutional	63.80	63.38	0.152	0.942
Multidimensional	**48.84**	**48.71**	**0.147**	**0.943**

Source: Authors (2024).

Based on Figure 4 and Table 2, it can be seen that the multidimensional scaling value on the economic is 58.51, the social is 46.93, the ecological is 32.61, the technological is 42.36, the institutional is 63.80, and multidimensional is 48.84. The ecological has the lowest value, followed by technological, social, economic and institutional. This shows that the principle of sustainability has not been balanced in the supply chain at agritech start-up. The results of the monte carlo analysis obtained values in the range 33.16-63.38 which showed no significant difference. The s-stress value gets in the range of 0.138-0.152 which means that the indicator has a reliable level of confidence because it is <0.25. The value of R^2 is in the range of 0.942-0.946 which means it is good. In order to find a more detailed explanation, sustainability analysis is then explained on the economic, social, ecological, technological, and institutional.

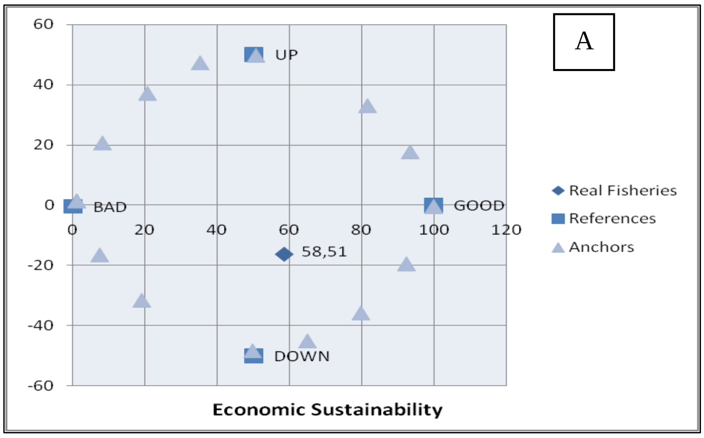

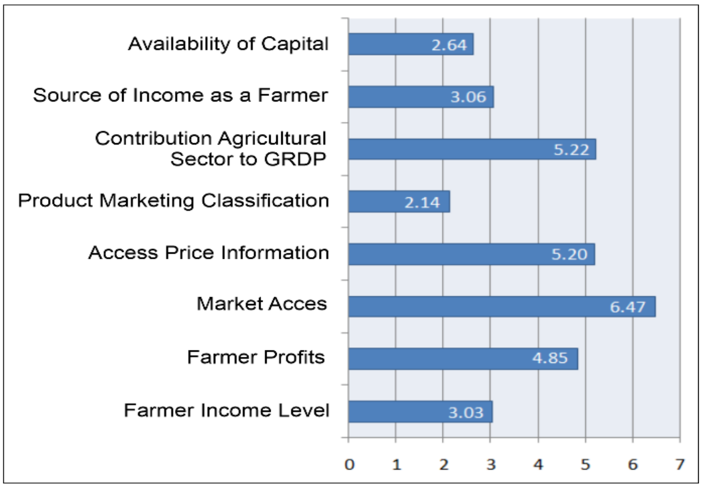

Figure 5: Sustainability index (a) and leverage analysis (b) on economic dimension.
Source: Authors (2024).

Figure 5 explains the sustainability index and leverage analysis of the economic dimension in the agritech start-up supply chain. The results of the economic dimension sustainability index get a value of 58.51, which is classified as quite sustainable. This is in line with the facts on the ground where agritech start-ups have succeeded in streamlining supply chains that were originally long and complex to become shorter and more efficient. According to Dolfsma et al. which states that the presence of agritech start-ups has succeeded in cutting supply chains to become more efficient [35]. Based on the results of the leverage analysis performed, the three most influential indicators were selected. The three indicators include market access (6.47), contribution agricultural sector to GRDP (5.22), and access price information (4.85). The first indicator is market access. The existence of flexible market access will certainly make it easier for farmers to sell their commodities. The presence of an agritech start-up has succeeded in making it easier for farmers to market their commodities because partner farmers can sell their commodities only through the application. According to Kanellos et al. sales through applications can reach a broad market and increase profits [36]. The second indicator is contribution agricultural sector to GRDP. The higher the contribution of a sector to GRDP, the more natural resources and potential livelihoods that exist in that area can be identified. Based on the facts on the ground, the majority of partner farmers are in the East Java region. The third indicator is price access. The more transparent access to price information, the easier it will be for farmers to run their business. This is in line with research conducted by Lam, which states that the easier it is to access price information, the easier to farming activities [37].

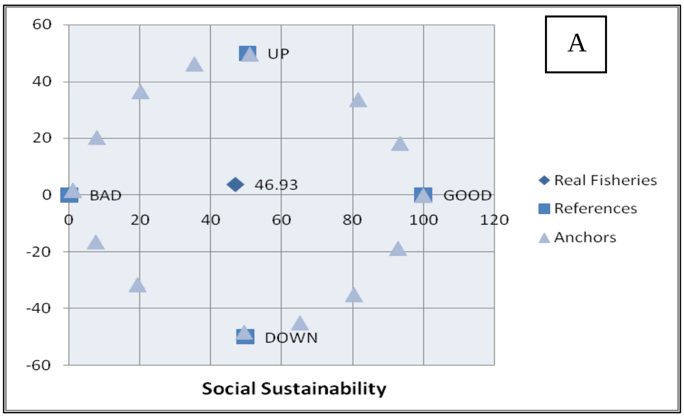

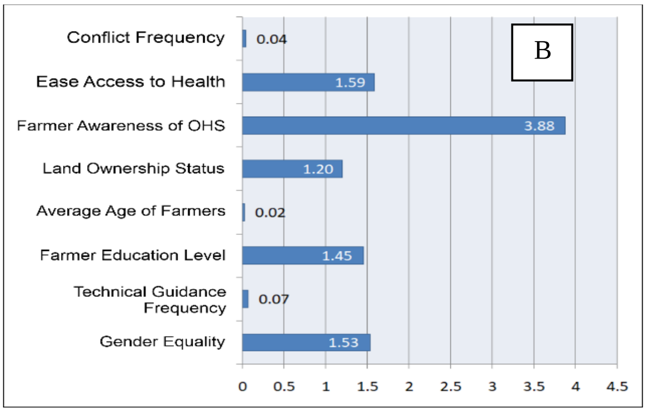

Figure 6: Sustainability index (a) and leverage analysis (b) on social dimensions.
Source: Authors (2024).

Figure 6 explains the sustainability index and leverage analysis of the social dimension in the agritech start-up supply chain. The results of the social dimension sustainability index get a value of 46.93, which is classified as less sustainable. This is caused by agritech start-ups that are still too focused on profits and are not yet intensive in providing assistance to farmers. This is further strengthened by the education level of farmers who are classified as lacking. According to Cook et al. the assistance provided to farmers plays an important role so that farmers can be relevant to developments [38]. In addition, debriefing can be a means of non-formal education for farmers. Based on the results of the leverage analysis performed, the three most influential indicators were selected. The three indicators include farmers' awareness of OHS (3.88), ease of access to health (1.59), and gender equality (1.53). The first indicator is farmers' awareness of occupational health and safety (OHS). Based on the facts in the field, it was found that the partner farmers did not have knowledge about OHS so they always ignored it. This is in line with research, which states that farmers do not apply OHS due to knowledge factors and no training has been carried out [39]. Of course, in the short and long term it will be detrimental to the health of farmers while at the same time hindering the process of production being carried out. The second indicator is easy access to health. Access to health needed by farmers can be in the form of health centers or personal protective equipment. Facts on the ground show that the majority of farmers are in rural areas and ease of access to health depends on the area or location of the farmer, however, partner farmers still feel that they do not have access to good health because they are far away. This is linear with research by Abaku and Odimarha, which states that ease of access to health is the most sensitive indicator for farmers, because farmers are often found to be sick but have difficulty access to health [40].

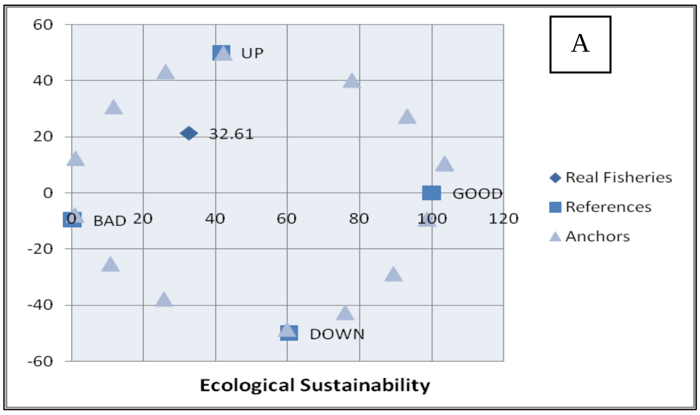

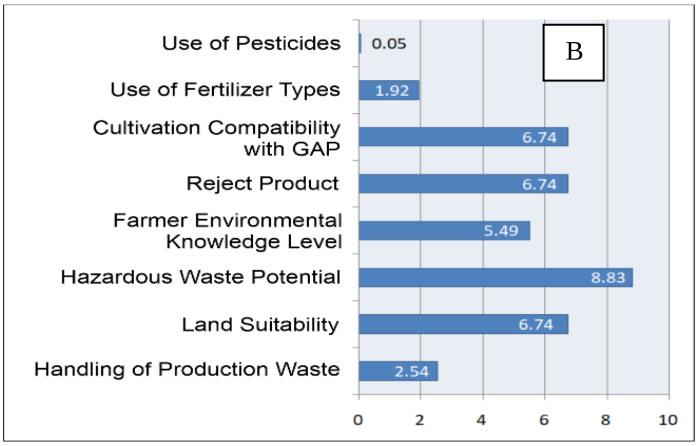

Figure 7: Sustainability index (a) and leverage analysis (b) on ecological dimensions.
Source: Authors (2024).

Figure 7 explains the sustainability index and leverage analysis of the ecological dimension in the agritech start-up supply chain. The results of the ecological dimension sustainability index get a value of 32.61, which is classified as less sustainable. This is because agritech start-ups have very high standards for the quality of commodities but are not matched by the implementation of training on cultivation, the environment and market provision by the company. According to Arifin, farmers need market certainty in order to have income, because commodities are perishable [41]. The lack of certainty and the provision of a reserve market from the company causes high product rejection and becomes food waste. This certainly causes losses for farmers and based on the results of direct observations in the field, partner farmers often complain about this. Based on the results of the leverage analysis performed, the three most influential indicators were selected. Some of these indicators include the potential for hazardous waste (8.83), and technical suitability of cultivation with GAP (6.74), and rejected products (6.74).

The first indicator is the potential for hazardous waste. The potential for hazardous waste will arise if farmers use inorganic fertilizers and pesticides because they will have an impact on soil health. Inorganic fertilizers and pesticides cause degradation of macronutrients such as potassium, nitrogen and phosphorus. In addition, according to El-Dewiny and Zaghloul. the use of inorganic fertilizers and pesticides affects soil fertility and health [42]. Based on the facts in the field, it was found that there is no potential for hazardous waste, because farmers use organic fertilizers and pesticides combined with inorganic within reasonable limits. The second indicator is the suitability of cultivation with GAP. GAP is a general guideline in carrying out correct cultivation to ensure product quality, safety for farmers and consumers. The application of GAP is very important because it acts as a quality assurance system as well as a series of sustainable supply chain management. However, the facts on the ground show that partner farmers still do not know and apply the GAP, causing the quality of the commodities produced to be not up to standard. The third indicator is reject product. Reject products are commodities that are returned to partner farmers because they are not up to standard. Facts in the field show that the reject product that occurs is still high. This is thought to be caused by the lack of supplies to partner farmers, as well as the absence of a reserve market. According to Beullens and Ghiami the high number of food waste is caused by products that do not meet demand criteria and there is no provision of a reserve market as an alternative option [43].

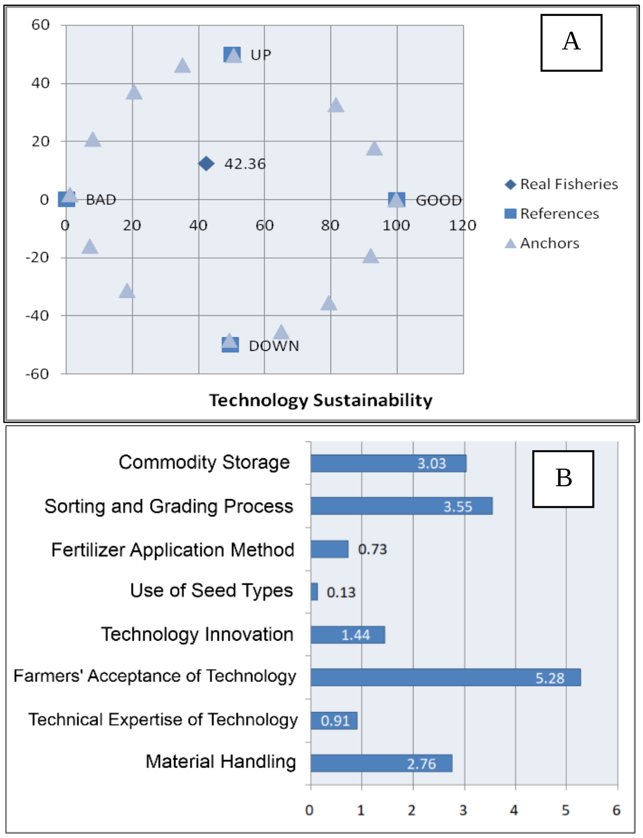

Figure 8: Sustainability index (a) and leverage analysis (b) on technological dimensions.
Source: Authors (2024).

Figure 8 explains the sustainability index and leverage analysis of the technology dimension in the agritech start-up supply chain. The results of the technology dimension sustainability index get a value of 42.36, which is classified as less sustainable. In its implementation, Agritech start-up has a mission to create a digital agricultural ecosystem. Digitalization in agriculture can increase productivity and cost savings [44]. However, the implementation of agricultural digitization encountered obstacles including the lack of knowledge by farmers, and infrastructure. In order to find out which indicators have the most influence, leverage analysis is then carried out. Based on the results of the leverage analysis conducted on the technology dimension, the three most influential indicators were selected. The three indicators include farmers' acceptance of technology (5.28), sorting and grading processes (3.55), and commodity storage (3.03).

The first indicator is farmers' acceptance of technology. Farmers' acceptance of technology is a basic thing that is needed. Facts on the ground show that partner farmers can accept technology well, this is reflected in the use of the applications provided. This is supported by Oktavia and Fathin who state that the applications used by agricultural start-ups in Indonesia are well received by farmers and make the farming process easier [45]. The second indicator is the process of sorting and grading. This process is a basic process that always exists in every agricultural commodity to ensure the quality of the criteria. If the commodity meets the standard criteria and market demand, then the commodity will be followed up and sent to PH and PPC and then distributed to consumers. Meanwhile, if the commodity does not meet the standard criteria, the commodity will be returned to the farmer. The facts in the field show that the majority of sorting and grading processes are still done manually, causing a less accurate level and longer time. This is in line with the research of Mhaski et al. which states that sorting and grading using machines is faster and more efficient than manual ones. The third indicator is commodity storage [46]. Commodity storage should ideally be placed in a refrigerator to extend shelf life and maintain quality. According to Muncan et al. storage at low temperatures can anticipate the occurrence of rot and prevent shrinkage in weight [47]. The fact is that partner farmers do not have a refrigerator after harvesting and only put it at room temperature.

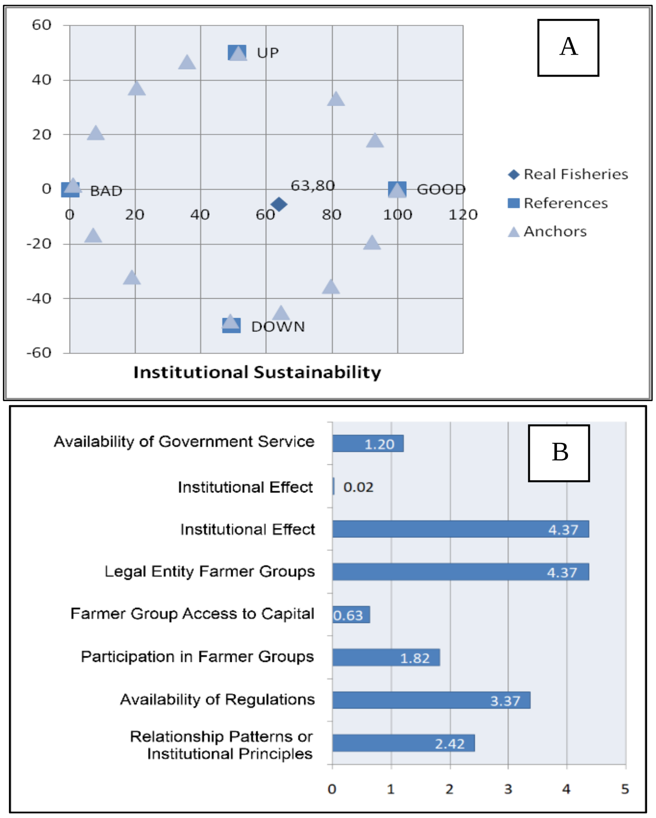

Figure 9: Sustainability index (a) and leverage analysis (b) on institutional dimensions.
Source: Authors (2024).

Figure 9 explains the sustainability index and leverage analysis of the institutional dimension in the agritech start-up supply chain. The results of the technology dimension sustainability index get a value of 63.80, which is classified as quite sustainable. According to Kusnandar et al. it is hoped that the presence of farmer institutions can help farmers in various aspects [48]. In its implementation, agritech start-ups are targeting farmer institutions because they are considered to be able to absorb more commodities. Based on the results of the leverage analysis, it was found that the three most influential indicators included the existence of farmer groups (4.37), legal entity farmer groups (4.37), and availability of regulations (3.37).

The first indicator is the existence of farmer groups. The existence of farmer groups has a fairly good effect on the development of farmers, because it can be a forum for farmers to work together with intra-institutions, fulfill aspects of capital, fulfill production facilities, assist marketing and provide information [48]. Facts on the ground show that partner farmers in the research area are all members of farmer groups and are actively partnering with agritech start-ups. The second indicator is legal entity farmer groups. According to Kusnandar et al. an ideal farmer group has several things, including (1) having a complete organizational structure, (2) being open to partnerships, and (3) having training and capacity building [49]. Facts on the ground show that all farmers are members of farmer groups that are legal entities, but there are no regulations governing farming activities. The third indicator is the availability of regulations. Rules or regulations in farmer groups have several weaknesses, including unclear rules and procedures for membership, the unclear profitability status of Gapoktan. Based on the facts in the field, it was found that the farmer groups studied had unclear rules so they were not implemented/implemented. The combined farmer groups only carry out partnership duties with external parties, in this case agritech start-ups.

IV.2 SOFT SYSTEM METHODOLOGY CONCEPTUAL

Based on the sustainability analysis carried out and combined with observations, several main issues were found that became problematic and presented in Figure 10.

1. There is no reserve supply chain provided for rejected commodities causing food waste. According to Crawford (2006), food waste can be mitigated by flexible market, one of which is the provision of market options.

2. The GAP cultivation system has not yet been implemented, causing the commodities produced to be non-standard. According to Vittersø et al. cultivation that applies GAP will produce quality commodities, good standards, and minimize food waste [50].

3. The cooperation that is implemented is still based on trust so that the cooperation that is established can cause fraud between the two parties which is mutually detrimental. This is reinforced by Putri and Rondhi's research which states that the application of contract farming has succeeded in reducing the risk of fraud by up to 39% [51].

4. The level of environmental knowledge and literacy possessed by partner farmers is still low, causing partner farmers to ignore ecological factors. This is supported by research by Yu et al. and Li et al. which states that environmental literacy in farmers has a significant relationship with sustainable production carried out in farming [52], [53].

5. There is no application of modern technology such as automatic sorting machines and refrigerators. The absence of technology such as automatic sorting machines and refrigerators causes low efficiency. Mhaski et al. states that the existence of technology using machines will increase efficiency while extending the shelf life of commodities [46].

6. Cultivation that pays attention to OHS and lack of access to health has not yet been implemented so that it risks harming the health of partner farmers. Riswal et al. states that the awareness of OHS farmers in rural areas is very low, so they are at high risk of health problems [54].

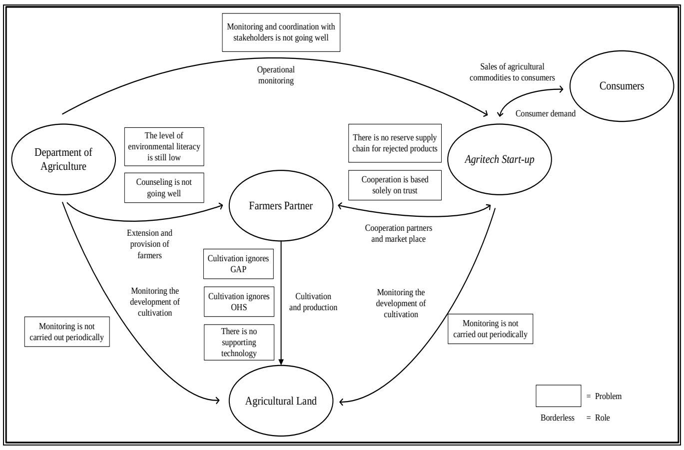

Figure 10: Rich picture agritech start up supply chain.
Source: Authors (2024).

Root definition and conceptual model development are the steps taken to identify the problem and determine the right solution in industry. After defining the problem in detail, then a catwoe analysis is carried out to find out in more detail the role of each supply chain actor involved in this case. This stage begins with Catwoe analysis (customers, actors, transformation, worldview, owner, environment constraints). The resulting Catwoe analysis at agritech start-up supply chain will be presented in Table 3.

Table 3: Catwoe analysis agritech start up supply chain.

Category	Explanation
Customers	Farmers partner
Actors	Farmers partner and agritech start-up
Transformation	Application of a contract farming system, farming assistance based on GAP and OHS, and application of a reverse supply chain
Worldview	Increasing the profitable cooperation system, knowledge of partner farmers, sustainability and reliability agritech start-up supply chain
Owner	Agritech start-up and government
Environment constraint	Low technology adoption and partner farmer acceptance of new knowledge

Source: Authors (2024)

The results of the Catwoe analysis are then arranged into several activities packaged in the form of a conceptual model that is called a purposeful human activity system (PHAS). The core of system thinking is the creation of conceptual model as intellectual tool used to discuss situation in the real world that is deemed problematic. Through the conceptual model, it is hoped that real conditions and ideal conditions can be compared. Based on Catwoe's analysis presented above, a conceptual model aimed at increasing the sustainability of agritech start-up supplies is presented in Figure 11.

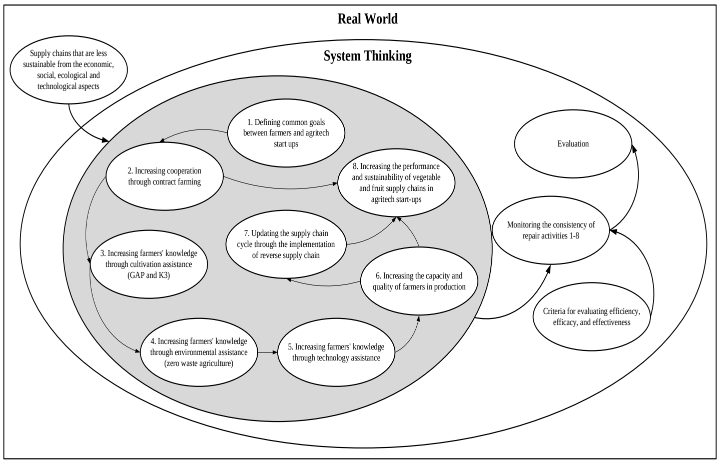

Figure 11: Conceptual model agritech start up supply chain
Source: Authors (2024)

In the comparison stage of the real conditions with the conceptual model (ideal conditions) an elaboration of current activities, gaps that occur, and action plans that can be carried out are carried out. It is hoped that this comparison of conceptual models can become a recommendation for agritech start-ups to implement the action plans that have been prepared and hope can improving performance and sustainabolity. In detail, current activities, gaps, and action plans are presented in Table 4.

Table 4: Current realities, gaps and plans of action.

Current Realities	Gaps	Plans of Action
The cooperation established between the parties is still based on trust. This creates the potential for fraud.	• There is no binding cooperation • Bad coordination between parties • Not yet optimal role of government institutions as supervisors	• Application of contract farming to partner farmers and agritech start ups • Implementation of periodic coordination between government as supervisor and agritech start up as operator
The knowledge of cultivation, technology and environment owned by partner farmers is still low so that it has a big impact on the farming process and the commodities produced	• Partner farmers have not implemented GAP and OHS-based cultivation • It is still quite difficult for partner farmers to adopt technology • Partner farmers still do not understand environmental literacy in agriculture	• Implementation of GAP and OHS assistance for partner farmers • Preparation of standard operating procedures for the cultivation process so that it complies with GAP and OHS • Application of borrowing tools • Application of socialization on the importance of environmental literacy for agricultural sustainability
The supply chain that is run is still not sustainable due to high waste	• The current supply chain does not provide a reserve market for reject products	• Provision of reverse logistics by agritech start ups in order to create a sustainable supply chain

Source: Authors (2024

V. CONCLUSIONS

Based on the research conducted, the following conclusions were obtained:

1. Analysis of the current condition of the supply chain descriptively shows that the supply chain is not working well. In the chain structure, it was found that the quality of the commodities produced by the majority did not meet standards and became a waste. In addition, it was found in chain management that contract agreements qwere not made with partner farmers.
2. The results of the sustainability analysis show that the multidimensional results show a value of 48.84 (less sustainable), economic 58.51 (quite sustainable), social 46.93 (less sustainable), ecological 32.61 (less sustainable), technology 42.36 (less sustainable) and institutional 63.80 (quite sustainable).
3. The results of the soft system methodology analysis show that there are three main problems, namely cooperation is still based on trust, farmers' knowledge (cultivation, technology, and the environment) is still low, and the supply chain that is being carried out is still not sustainable. The strategy formulated includes implementing contract farming, implementing regular coordination between stakeholders, assisting GAP and OHS, preparing standard operating procedure for cultivation, applying borrowed tools with supervision, implementing environmental literacy socialization, and implementing a reverse supply chain.

VI. AUTHOR'S CONTRIBUTION

Conceptualization: Thabed Tholib Baladraf, Nita Kuswardhani
Methodology: Thabed Tholib Baladraf, Nita Kuswardhani
Investigation: Thabed Tholib Baladraf, Winda Amilia
Discussion of results: Thabed Tholib Baladraf, Nita Kuswardhani
Writing – Original Draft: Thabed Tholib Baladraf
Writing – Review and Editing: Thabed Tholib Baladraf
Resources: Nita Kuswardhani, Winda Amilia.
Supervision: Nita Kuswardhani, Winda Amilia, Mohammad Rondhi, Yuli Wibowo
Approval of the final text: Nita Kuswardhani, Winda Amilia, Mohammad Rondhi, Yuli Wibowo

VII. ACKNOWLEDGMENTS

The authors acknowledge the support from the agritech start up for its willingness to be the object and location of the research, as well as the data and information support and discussion. The author also acknowledges to Dr. Nita Kuswardhani, S.TP., M.Eng., IPM, Winda Amilia, S.TP., M.Sc., M. Rondhi, S.P., M.P., Phd., and Dr. Yuli Wibowo, S.TP., M.Sc., IPM for his guidance and direction in carrying out the research.

VIII. REFERENCES

[1] S. Somapa, M. Cools, and W. Dullaert, "Characterizing supply chain visibility – A literature review," *Int. J. Logist. Manag.*, vol. 29, no. 1, pp. 308–339, 2018, doi: 10.1108/IJLM-06-2016-0150.

[2] U. D. Apeji and F. T. Sunmola, "Principles and Factors Influencing Visibility in Sustainable Supply Chains," *Procedia Comput. Sci.*, vol. 200, pp. 1516–1527, 2022, doi: 10.1016/j.procs.2022.01.353.

[3] D. Rafi and M. Mubeena, "Role of Agritech Start-Ups in Supply Chain—An Organizational Approach of Ninjacart," in *The Digital Agricultural Revolution*, 2022, pp. 289–299.

[4] E. Koberg and A. Longoni, "A systematic review of sustainable supply chain management in global supply chains," *J. Clean. Prod.*, vol. 207, pp. 1084–1098, 2019, doi: 10.1016/j.jclepro.2018.10.033.

[5] B. Fahimnia, J. Sarkis, A. Gunasekaran, and R. Farahani, "Decision models for sustainable supply chain design and management," *Annual Operation Research*, vol. 250, no. 2, pp. 277–278, 2017, doi: 10.1007/s10479-017-2428-0.

[6] R. Dubey, A. Gunasekaran, S. J. Childe, T. Papadopoulos, and S. Fosso Wamba, "World class sustainable supply chain management : critical review and further research directions" *Int. J. Logist. Manag.*, vol. 28, no. 2, pp. 1–42, 2017. doi: 10.1108/IJLM-07-2015-0112

[7] C. L. Martins and M. V. Pato, "Supply chain sustainability: A tertiary literature review," *J. Clean. Prod.*, vol. 225, pp. 995–1016, 2019, doi: 10.1016/j.jclepro.2019.03.250.

[8] C. R. Carter, M. R. Hatton, C. Wu, and X. Chen, "Sustainable supply chain management: continuing evolution and future directions," *Int. J. Phys. Distrib. Logist. Manag.*, vol. 50, no. 1, pp. 122–146, 2020, doi: 10.1108/IJPDLM-02-2019-0056.

[9] M. H. Islam, M. R. Sarker, M. I. Hossain, K. Ali, and K. M. A. Noor, "Towards Sustainable Supply Chain Management (SSCM): A Case of Leather Industry," *J. Oper. Strateg. Plan.*, vol. 3, no. 1, pp. 81–98, 2020, doi: 10.1177/2516600x20924313.

[10] A. Rajeev, R. K. Pati, S. S. Padhi, and K. Govindan, "Evolution of sustainability in supply chain management: A literature review," *J. Clean. Prod.*, vol. 162, pp. 299–314, 2017, doi: 10.1016/j.jclepro.2017.05.026.

[11] V. Kiousis, E. Nathanail, and I. Karakikes, "Assessing traffic and environmental impacts of smart lockers logistics measure in a medium-sized

municipality of Athens," *Adv. Intell. Syst. Comput.*, vol. 879, no. January, pp. 614–621, 2019, doi: 10.1007/978-3-030-02305-8_74.

[12] R. . Sánchez-Flores, S. . Cruz-Sotelo, S. Ojeda-Benitez, and M. Ramírez-Barreto, "Sustainable Supply Chain Management—A Literature Review on Emerging Economies," *Micro Macro Mark.*, vol. 12, no. 6972, pp. 1–27, 2020, doi: 10.3390/su12176972.

[13] K. E. R. Heerman, "Technology, ecology and agricultural trade," *J. Int. Econ.*, vol. 123, p. 103280, 2020, doi: 10.1016/j.jinteco.2019.103280.

[14] Central Bureau of Statistics, *Indonesia Statistic 2023*, vol. 1101001. 2023.

[15] L. Klerkx and P. Villalobos, "Are AgriFoodTech start-ups the new drivers of food systems transformation? An overview of the state of the art and a research agenda," *Glob. Food Sec.*, vol. 40, no. December, p. 100726, 2024, doi: 10.1016/j.gfs.2023.100726.

[16] M. Munizu, "The Effect of Trust, Commitment, and Information Technology on Supply Chain Performance (Case Study of Passion Fruit Processors in Makassar City)," *J. Manaj. dan Agribisnis*, vol. 14, no. 1, pp. 32–42, 2017, doi: 10.17358/jma.14.1.32.

[17] M. M. Magesa, K. Michael, and J. Ko, "Access and use of agricultural market information by smallholder farmers: Measuring informational capabilities," *Electron. J. Inf. Syst. Dev. Ctries.*, vol. 86, no. 6, pp. 1–21, 2020, doi: 10.1002/isd2.12134.

[18] A. Mrówczyńska-Kamińska, B. Bajan, K. P. Pawłowski, N. Genstwa, and J. Zmyślona, "Greenhouse gas emissions intensity of food production systems and its determinants," *PLoS One*, vol. 16, no. 4 April, pp. 1–20, 2021, doi: 10.1371/journal.pone.0250995.
[19] K. Schanes, K. Dobernig, and B. Gözet, "Food waste matters - A systematic review of household food waste practices and their policy implications," *J. Clean. Prod.*, vol. 182, pp. 978–991, 2018, doi: 10.1016/j.jclepro.2018.02.030.

[20] M. Bhatia and G. M. J. Bhat, "Agriculture Supply Chain Management-An Operational Perspective," *Brazilian J. Oper. Prod. Manag.*, vol. 17, no. 4, pp. 1–18, 2020, doi: 10.14488/bjopm.2020.043.

[21] N. Wani, L. Li, X. Wu, and J. Fan, "Coordination of a fresh agricultural product supply chain with option contract under cost and loss disruptions," *PLoS One*, vol. 16, no. 6 June, pp. 1–15, 2021, doi: 10.1371/journal.pone.0252960.

[22] E. M. Meemken and M. F. Bellemare, "Smallholder farmers and contract farming in developing countries," *Proc. Natl. Acad. Sci. U. S. A.*, vol. 117, no. 1, pp. 259–264, 2020, doi: 10.1073/pnas.1909501116.

[23] B. Manjunatha *et al.*, "Multidimensional Scaling Method and Some Practical Applications," *Arch. Curr. Res. Int.*, vol. 24, no. 6, pp. 586–599, 2024, doi: 10.9734/acri/2024/v24i6814.

[24] A. Laapo, D. Howara, S. Kassa, H. Sultan, and A. Rahim, "A Multidimensional Approach to Assessing the Leverage Factors of the Sustainability of Seaweed Farming in Coastal Area of Parigi Moutong District, Indonesia," *J. Aquac. Fish Heal.*, vol. 10, no. 3, p. 271, 2021, doi: 10.20473/jafh.v10i3.24281.

[25] I. Mucharam, E. Rustiadi, A. Fauzi, and Harianto, "Assessment of rice farming sustainability: Evidence from Indonesia provincial data," *Int. J. Sustain. Dev. Plan.*, vol. 15, no. 8, pp. 1323–13332, 2020, doi: 10.18280/ijsdp.150819.

[26] Whidya Utami *et al.*, "Supply Chain Model of Fresh Fisheries in the Waters of Fakfak, West Papua: An Overview from the Perspective of Evaluation of Performance and Sustainability of Supply Chain," *Int. J. Entrep. Res.*, vol. 3, no. 4, pp. 95–101, 2020, doi: 10.31580/ijer.v3i4.1537.

[27] R. Françozo, A. Paucar-Caceres, and M. C. N. Belderrain, "Combining Value-Focused thinking and soft systems methodology: A systemic framework to structure the planning process at a special educational needs school in Brazil," *J. Oper. Res. Soc.*, vol. 73, no. 5, pp. 994–1013, May 2022, doi: 10.1080/01605682.2021.1880298.

[28] E. Martin, B. Winarno, H. Purnomo, and N. Wijayanto, "Managing Conflict-Risk Forest Areas Through a Soft Systems Methodology Approach: The Case of Benakat Research Forest, South Sumatra," *J. Penelit. Sos. dan Ekon. Kehutan.*, vol. 5, no. 3, pp. 179–202, 2008, doi: 10.20886/jpsek.2008.5.3.179-202.

[29] H. Augustsson, K. Churruca, and J. Braithwaite, "Change and improvement 50 years in the making: a scoping review of the use of soft systems methodology in healthcare," *BMC Health Serv. Res.*, vol. 20, no. 1, pp. 1–13, 2020, doi: 10.1186/s12913-020-05929-5.

[30] F. Chukwunonso, "Soft Systems Methodology (SSM) as a Viable Methodology for Knowledge Engineering: A Literature Review," *Int. J. Informatics Commun. Technol.*, vol. 5, no. 1, p. 1, 2016, doi: 10.11591/ijict.v5i1.pp1-10.

[31] Suharno, N. Anwar, and E. Saraswati, "A technique of assessing the status of sustainability of resources," *IOP Conf. Ser. Earth Environ. Sci.*, vol. 250, no. 1, 2019, doi: 10.1088/1755-1315/250/1/012080.

[32] A. Eunike, D. Hardiningtyas, S. I. Kartika, and D. Andronicus, "Sustainability Analysis of Beach and Mangrove 1 Tourism in Clungup," *ECSOFiM Econ. Soc. Fish. Mar. J.*, vol. 06, no. 01, pp. 1–13, 2018, doi: 10.21776/ub.ecsofim.2018.006.01.01.

[33] M. Suresha Adiga, P. S. Ananthan, V. Ramasubramanian, and H. V. Divya Kumari, "Validating RAPFISH sustainability indicators: Focus on multi-disciplinary aspects of Indian marine fisheries," *Mar. Policy*, vol. 60, pp. 202–207, 2015, doi: 10.1016/j.marpol.2015.06.032.

[34] A. Arouna, J. D. Michler, and J. C. Lokossou, "Contract farming and rural transformation: Evidence from a field experiment in Benin," *J. Dev. Econ.*, vol. 151, no. January, p. 102626, 2021, doi: 10.1016/j.jdeveco.2021.102626.

[35] W. Dolfsma, G. Isakhanyan, and S. Wolfert, "Information Exchange in Supply Chains: The Case of Agritech," *J. Econ. Issues*, vol. 55, no. 2, pp. 389–396, 2021, doi: 10.1080/00213624.2021.1908800.

[36] N. Kanellos, P. Karountzos, N. T. Giannakopoulos, M. C. Terzi, and D. P. Sakas, "Digital Marketing Strategies and Profitability in the Agri-Food Industry: Resource Efficiency and Value Chains," *Sustain.*, vol. 16, no. 14, pp. 1–25, 2024, doi: 10.3390/su16145889.
[37] M. E. Lam, "The Ethics and Sustainability of Capture Fisheries and Aquaculture," *J. Agric. Environ. Ethics*, vol. 29, no. 1, pp. 35–65, 2016, doi: 10.1007/s10806-015-9587-2.

[38] B. R. Cook, P. Satizábal, and J. Curnow, "Humanising agricultural extension: A review," *World Dev.*, vol. 140, p. 105337, 2021, doi: 10.1016/j.worlddev.2020.105337.

[39] A. Farid, A. Pratiwi, and A. D. A. Fitri, "The Relationship of Farmers Characteristics and Perception of the Occupational Health and Safety (OHS) Application in Farming Activities in Wonosalam District, Jombang Regency, East Java," *Sodality J. Sosiol. Pedesaan*, vol. 7, no. 2, pp. 153–158, 2019, doi: 10.22500/sodality.v7i2.26974.

[40] Emmanuel Adeyemi Abaku and Agnes Clare Odimarha, "Sustainable Supply Chain Management in the Medical Industry: a Theoretical and Practical Examination," *Int. Med. Sci. Res. J.*, vol. 4, no. 3, pp. 319–340, 2024, doi: 10.51594/imsrj.v4i3.931.

[41] A. Rente, "Introduction to Agroindustry," *Bandung CV Mujahid Press*, vol. Cetakan 1, no. 23, pp. 301–316, 2016.

[42] C. El-Dewiny and A. Zaghloul, "Behavior of inorganic contaminants associated with agricultural fertilizers and their impact on soil and plant ecosystems," *Int. J. Environ. …*, vol. 6, no. 1, pp. 13–27, 2023.

[43] P. Beullens and Y. Ghiami, "Waste reduction in the supply chain of a deteriorating food item – Impact of supply structure on retailer performance," *Eur. J. Oper. Res.*, vol. 300, no. 3, pp. 1017–1034, 2022, doi: 10.1016/j.ejor.2021.09.015.

[44] F. da Silveira, F. H. Lermen, and F. G. Amaral, "An overview of agriculture 4.0 development: Systematic review of descriptions, technologies, barriers, advantages, and disadvantages," *Comput. Electron. Agric.*, vol. 189, no. August, p. 106405, 2021, doi: 10.1016/j.compag.2021.106405.

[45] H. F. Oktavia and S. Fathin, "Agriculture Start Up in Indonesia," *AGRISIA-Jurnal Ilmu-Ilmu Pertan.*, vol. 14, no. 2, pp. 51–60, 2022.

[46] R. R. Mhaski, P. B. Chopade, and M. P. Dale, "Determination of ripeness and grading of tomato using image analysis on Raspberry Pi," *Int. Conf. Commun. Control Intell. Syst. CCIS 2015*, pp. 214–220, 2016, doi: 10.1109/CCIntelS.2015.7437911.

[47] J. Muncan, S. Anantawittayanon, T. Furuta, T. Kaneko, and R. Tsenkova, "Aquaphotomics monitoring of strawberry fruit during cold storage – A comparison of two cooling systems," *Front. Nutr.*, vol. 9, no. December, pp. 1–21, 2022, doi:

10.3389/fnut.2022.1058173.

[48] K. Kusnandar, O. van Kooten, and F. M. Brazier, "Supporting self-organisation in farmer organisations in developing countries: A case with a group of farmer groups in Indonesia," *J. Co-op. Organ. Manag.*, vol. 11, no. 2, p. 100214, 2023, doi: 10.1016/j.jcom.2023.100214.

[49] K. Kusnandar, O. van Kooten, and F. M. Brazier, "Empowering through reflection: participatory design of change in agricultural chains in Indonesia by local stakeholders," *Cogent Food Agric.*, vol. 5, no. 1, 2019, doi: 10.1080/23311932.2019.1608685.

[50] G. Vittersø *et al.*, "Short food supply chains and their contributions to sustainability: Participants' views and perceptions from 12 European cases," *Sustain.*, vol. 11, no. 17, 2019, doi: 10.3390/su11174800.

[51] A. T. R. Putri and M. Rondhi, "Contract Farming And The Effect On Price Risk In Broiler Farming," *E3S Web Conf.*, vol. 142, pp. 1–5, 2020, doi: 10.1051/e3sconf/202014205002.

[52] L. Yu, W. Liu, S. Yang, R. Kong, and X. He, "Impact of environmental literacy on farmers' agricultural green production behavior: Evidence from rural China," *Front. Environ. Sci.*, vol. 10, no. November, pp. 1–19, 2022, doi: 10.3389/fenvs.2022.990981.

[53] S. Li, X. Huo, R. Si, X. Zhang, Y. Yao, and L. Dong, "Exploring the role of environmental literacy and social norms in farmers' LMTT adoption: evidence from China," *Int. J. Clim. Chang. Strateg. Manag.*, 2022, doi: 10.1108/IJCCSM-12-2021-0138.

[54] M. Riswal, F. Mallapiang, and A. Multazam, "Occupational Safety and Health Behaviors among Agricultural Workers in Rural Area Indonesia," *J. Aafiyah Heal. Res.*, vol. 2, no. 2, pp. 1–13, 2021, [Online]. Available: https://doi.org/10.52103/jahr.v2i2.558

Journal of Engineering and Technology for Industrial Applications

ISSN ONLINE: 2447-0228

ITEGAM-JETIA

Manaus, v10. n.96, p. 101-107. November/ December., 2024.
DOI: https://doi.org/10.5935/jetia.v10i50.1319

RESEARCH ARTICLE | OPEN ACCESS

PROCUREMENT AND LOGISTIC PROCESSES

Neyfe Sablón-Cossío[1], Giselle Rodríguez-Rudi[2], Roberto Wilman Rosales Bonilla[3], Jessica Elizabeth Medina Arias[4], Ana Julia Acevedo-Urquiaga[5] and Rogelio Suárez Mella[6]

[1,6] Universidad Técnica de Manabí, Ecuador.
[2]Universidad Anáhuac, Veracruz, México.
[3] CBSNETWORK ECUADOR S.A.S, Ecuador
[4] Universidad Regional Amazónica Ikiam, Ecuador
[5] Fundación Universitaria San Mateo, Colombia

[1]https://orcid.org/0000-0002-6691-0037, [2] https://orcid.org/0000-0002-0555-1376, [3] https://orcid.org/0000-0001-7857-6016, [4] https://orcid.org/0009-0009-4120-7810, [5] https://orcid.org/0000-0001-7867-1590, [6] https://orcid.org/0000-0002-5492-9339

Email: nsabloncossio@gmail.com, gisellerod1019@yahoo.es, roberto.rosales@cbsnetwork.com.ec, mgjessicamedina@gmail.com, anajuliaa@gmail.com, rogelio.suarez@utm.edu.ec

ARTICLE INFO

Article History
Received: October 3, 2024
Revised: November 6, 2024
Accepted: November 10, 2024
Published: November 30, 2024

Keywords:
Logistic,
compras,
supply chain,
process

ABSTRACT

Nowadays, managing procurement processes in companies and supply chains facilitates competitiveness among actors. In this study, the objective was to evaluate the performance of procurement processes in Ecuadorian companies. To achieve this, a modified verification instrument was used, composed of the dimensions: the importance of procurement and its relation to supply chains, procurement, suppliers, cycle, cost and human talent training. The instrument evaluated the performance of procurement areas in 162 Ecuadorian companies. The instrument was validated and the data was processed using descriptive and inferential statistics. The results of this study show a low performance level in the procurement areas in the observed companies. The weakest variables were: procurement, demand and providers. The study contributres with relevant data that can be used to create strategies to improve the procurement performance in Ecuadorian companies.

I. INTRODUCTION

Procurement is a very relevant process for supply chains and logistics. It allows linking demand forecasts with the material needs expressed to suppliers. Thus, procurement is a strategic leverage for organizations. This process becomes costly because it is dependent on multifunctional equipment, relations with suppliers, and contract management [1].

In this context, procurement performance is a factor that influences the sustainability of an organization. Some studies [2] focus their research on green procurement. They have emphasized the environmental impact that results from purchasing non-polluting resources, and how this is related to positive social en economic performance.

Other studies mention the need for applying technologies to procurement, to decrease time and costs. At the same, digitalization influences data training and treatment, which facilitates decision-making [3]. In this sense, it allows to have a data set that helps to identify the organization's client in relation to the demand forecasts, as well as decreasing logistic costs and projecting its niche into the market. Moreover, the use of AI to optimize [4] inventories, provider management, demand forecasts, demand provision, cycles, and costs.

In the Ecuadorian context, the country's logistic performance was analyzed [5]. The goal was to identify the sector's main issues in 2023, and provide useful information to the National Logistic Planning for the following years [5]. As a result, the following logistic estimations were defined: 40% belongs to transport, 23% to storage, 9% to procurement and supplies, and 12% to costumer service and order processing, and 9% to planning and inventory management. On the other hand, the logistic services related to procurement and provider management from companies is distributed as such: 79,1% is executed directly, 18,6% is executed by hiring external companies, and 2,3 % do not execute or apply them. Nonetheless, there are not many analysis of this kind, that promote data registration at a national level in terms of logistic, and that contribute to decision-making.

On the other hand, the index of logistic performance of competitiveness and service quality defined by the World Bank (1= lowest and 5= highest) for Ecuador was 2.75 in 2018; this is the last available data. This implies that the logistic performance is average, despite a low growth of 0.11 since 2007. When comparing this value to those of neighboring countries such as Colombia and Peru in 2022, Ecuador's growth is lower. Both countries have had regulations based on supply chains for more than a decade. This shows the need for regulations that support logistic development and supply chains in Ecuador.

Thus, the objective of this study was to evaluate the performance of the procurement process in Ecuadorian companies.

This work is structured as such: section 1 is composed of the introduction, section 2 of materials and methods for evaluating procurement; section 3 includes the results and discussion; and lastly, section 4 presents the conclusions of the study.

The motives of this study are:

✓ The identification of the relevant characteristics of procurement in Ecuadorian companies.

✓ The stimation of procurement cycles in Ecuadorian companies.

II. MATERIALS AND METHODS

Data Collection

Quantitative methodologies with a positivist approach were applied to the study [6]. The period for the study carried out between 2022-2024 on Ecuadorian companies. The study was descriptive, explicative and correlational because it characterized the procurement variables. The procurements were diagnosed following the criteria from the checklist [7]. A questionnaire on Google Forms was used and distributed all around the country.10 questionnaires were used for tests that were subsequently removed from the final sample. The sample contained 162 respondents. The questionnaire was in Spanish and the respondents were informed of their anonymity.

Questionnaire content

The objective of the questionnaire was to evaluate the performance of procurement in Ecuadorian companies. The questionnaire was organized into 7 dimensions and 57 items to fulfill the objective: general characteristics of the companies, the importance of procurement and its relation to the Supply Chain (SC), demand, suppliers, procurement, cycle, cost and human talent training.

✓ General characteristics of the company: this dimensión is focused on describing the companies on broad terms, specifically location, activity[8], and some demographic data [9].

✓ The importance of procurement and its relation to the supply chain: this dimensión included ítems such as evaluation of the procurement section's role, the strategic importance of procurement in the supply chain, and the reasons why it is crucial. The criteria were obtained from [10-13].

✓ Procurement: This dimension comprises 24 out 57 items. The ítems aim to describe the type of procurement, the process, the services they offer, and indicators. The criteria were obtained from [14-17].

✓ Demand: It is composed of 13 items, which are focused on forecasts, information, coverage, and product sales. The criteria were obtained from [16],[18],[19].

✓ Suppliers: This dimension included 9 items such as selection, classification, policies, evaluation, and logistic services. The criteria were obtained from [10],[19],[20]. Cycle: This dimension has three items that help to determine the timeframe from the identification of demand, to the moment arrives at the warehouse and unit. The criteria were obtained from [19].

✓ Cost: This dimension was comprised of questions 47 and 52, based on the application of the Activity Based Costing, and aims to estimate how much the procurement section can help to reduce costs in the supply chain. The criteria were obtained from [19], [21],[22].

✓ Human Talent Training: This dimension had 3 items, which aim to describe the traning and education of the workers from sales, demand management, and suppliers. The criteria were obtained from [19].

Instrument validation and reliability

With the goal of estimating the internal consistency of the instrument, the following were used: Cronbach's Alpha and McDonald's Omega [23]. Cronbach's alpha was interpreted from the intervals: $\alpha > 0.9$ excellent, $\alpha > 0.8$ good, $\alpha > 0.7$ questionable, $\alpha > 0.5$ poor and $\alpha < 0.5$ unacceptable [24].

Statistical Analysis

This instrument has several scales, so the statistical analysis was performed based on them.

✓ Descriptive statistics were applied to the dichotomous scale items, specifically the mode and frequency estimation.

✓ The frequency was estimated for the open-ended result items.

✓ Descriptive and inferential statistics were applied to the items with a Likert scale (1-5). In the first, the mean per variable and the cycles and their corresponding deviation were estimated.

✓ In the second, the Spearman's Rho correlation was applied to define the relationship between variables. And significant correlations were taken with a value greater than 0.5 [25], [26]. The chi-square test was applied to demonstrate the hypothesis that there is a relationship between staff training (university or not), the assessment of the function of the purchasing area in your organization (p8) and the number of people dedicated to logistics. These analyses allow for the evaluation of purchasing processes in Ecuadorian companies. Based on this analysis, strategies are identified to improve these processes in the companies under study.

IV. RESULTS AND DISCUSSIONS

The companies under study are classified by type and sector. Of these, 72.8% are classified as services and the rest as industries. This demonstrates the global trend, where services predominate over production. The most analyzed sector is the food sector (53.7% of the sample), followed by commerce (27.8% of the sample), Table 1.

Table 1: Classification of companies in the study.

Classification	Element	Frequency	Percentage	Valid Percentage	Cummulative percentage
Tipo	Industry	44	27.2	27.2	27.2
	Service	118	72.8	72.8	100
Sector	Food	87	53.7	53.7	53.7
	Artisan	9	5.6	5.6	59.3
	Commerce	45	27.8	27.8	87
	Logistics	3	1.9	1.9	88.9
	Chemicals	4	2.5	2.5	91.4
	Services	6	3.7	3.7	95.1
	Public Services	1	0.6	0.6	95.7
	Services	6	3.7	3.7	99.4
	Transport	1	0.6	0.6	100
	Total	162	100	100	

Source: Authors, (2024).

In the case of the location of the companies in the study, 65.4% are in Manabí, followed by 21.6% in Pastaza, Table 2. This infers that 67.8% belong to the Coast region of Ecuador, 27.8% are in the Amazon region and 4.3% in the Highlands region. This provides an opportunity for further in this area. At the same time, the research was developed in the country, demonstrating its importance.

Table 2: Socio-demographic characteristics.

Provinces	Frequency	Percentage	Valid Percentage	Cumulative Percentage	Regions
Chimborazo	3	1.9	1.9	1.9	Highlands
Cotopaxi	1	0.6	0.6	2.5	Highlands
Esmeraldas	2	1.2	1.2	3.7	Coast
Guayas	2	1.2	1.2	4.9	Coast
Manabí	106	65.4	65.4	70.4	Coast
Napo	10	6.2	6.2	76.5	Amazon
Pastaza	35	21.6	21.6	98.1	Amazon
Pichincha	2	1.2	1.2	99.4	Highlands
Tunguragua	1	0.6	0.6	100	Highlands
Total	162	100	100		

Source: Authors, (2024).

The results from the instrument's consistency were a Cronbach's Alpha of 0.945 and an Omega value of McDonald's of 0.943. These values demonstrate that the checklist is reliable because the internal consistency values are greater than 0.9, which are considered excellent.

On the other hand, the variables are estimated with an average between 2.18 and 3.54 (low and medium on the Likert scale). The variable with the greatest challenge is purchases and the one with the greatest strength is purchases and their relationship with the chain, Table 3.

Table 3: Results from the variables and their items.

Variables	Items	Median	Variable median
Procurement and it relation to the SC	p8	3.83	3.54
	p38	3.3	
Demand	p15	3.03	2.71
	p16	2.18	
	p17	2.96	
	p18	2.88	
	p19	2.52	
	p20	2.37	
	p21	3.15	
	p22	2.75	

	p23	2.92	
Suppliers	p31	2.05	2.18
	p36	2.08	
	p35	2.22	
	p34	2.4	
	p49	3.26	
Cost	p52	3.5	3.09
	p47	2.77	
Procurement	p48a	2.04	2.449
	p48b	2.17	
	p48c	1.72	
	p48d	2.16	
	p48e	2.73	
	p48f	2.48	
	p48g	2.71	
	p48h	2.9	
	p48i	2.59	
	p48j	2.74	
	p48k	3.14	
	p48l	3.01	
	p48m	2.89	
	p48n	2.05	
	p48p	2.84	
	p48q	1.78	
	p48r	2.53	
	p54	3.34	
	p55	3.33	
	p56	1.84	

Source: Authors, (2024).

In this sense, the weakest items: the degree to which credit purchases are used, the degree to which purchases are taken into account for the management of customs procedures, and the presence of a logistics operator service to carry out procurement activities. Despite this, there are another 27 items with values lower than 3, which are also weaknesses for the companies under study. Based on the results, the variables show the following behaviors in relation to the average: the importance of purchases and their relationship with the SC (3.54 average value), cost (3.09 average value), purchases (2.449 low value), demand (2.71 low value) and suppliers (2.18 low value).

In the case of the importance of procurement and their relationship with the supply chain, both questions present average values, despite the fact that this variable presents few items. In the demand dimension, questions p16; p17; p18; p19; p20; pp22 and 23 have low values. In suppliers, questions p31; p36; p35, and p34 have low values. In costs, question 47 has low values. In the procurement dimensipon, there are three questions with very low values (p48c; p48q and p56). At the same time, most of the questions have low values, with medium values for questions 48k; 48L; 54 and 55). These elements show that in companies, performance in terms of purchases is between low and very low. Although some items are located in the middle, none of their values are located high or very high.

In this context, the relationship between staff training (university or not), the assessment of the function of the purchasing area in the organization (p8) and the number of people dedicated to logistics; it is concluded that there is a relationship between staff trained in logistics skills and the assessment with the purchasing function (Table 4). This is due to the rejection of the null hypothesis in the chi-square tests.

Table 4: Results from the chi-squared test.

	Value	df	Asymptotic significance (bilateral)
Pearson’s squared-chi	13.833a	8	.086
Likelihood ration	14.542	8	.069
Linear association	8.492	1	.004
N of valid cases	328		
a. 6 checkboxes (40.0%) had a count lowe 5. The minimum expected count is .20.			

Source: Authors, (2024).

As for the procurement area playing a strategic role in SC, a mode of 1 was estimated (which means Yes), with Yes being the most frequent response. It is stated that the information on the product demand is not generated automatically (mode of 2 which means No). This refers to the need for automation in the sales processes to obtain reliable data for decision-making and for there to be a relationship between the client's needs and the purchases made. At the same time, the procurement process is carried out by product type and not by ABC classification. This shows that in most cases products are purchased that do not guarantee the profits that come from A products and this can generate shortages of them; which causes losses.

In this sense, with a mode of 1 (which means No), they do not present any procedure for in-store purchases. At the same time, with a mean of 1 (which means No), a procedure is not defined to incorporate new products into the purchasing system. With a mode of 1 (meaning No), it mentions that there is no record of the suppliers or their selection, qualification, or compliance processes. In the case of orders to suppliers, it mentions that in 55% of the cases, buyer visits are used and 27.1% are by telephone. This influences the need for buyers to travel and the increase in costs in this activity. In the case of the evaluation of suppliers, there is no trend, 16.6% affirm that it is done by product availability.

Spearman's Rho coefficient was used to determine the bivariate correlations between the dimensions of the scale, determined for the evaluation of the procurement processes. Significantly different coefficients are obtained from zero to 1%. Within the results, the strong significant correlation between p48n and p19 stands out with a value of 0.758**. This shows that in the sample there is a direct relationship between the purchasing processes in import management and the coverage to generate demand [27]. On the other hand, there is a strong significant correlation between p48l and p48k with an estimate of 0.700**. This affirms that there is a direct relationship between the control of accounts payable and negotiation with suppliers, both elements of the purchasing process.[28].

At the same time, there are other significant correlations with values between 0.609** and 0.683**. Regarding demand, there are p16 and p20 with a correlation of 0.623** and; p17 and p20 with a correlation of 0.637**. In the former, there is a direct relationship between the goods in transit and the packaging as a parameter to generate demand. In the latter, there is a relationship between the average daily sales of the product and the packaging as a parameter to generate demand. In both cases, the packaging is taken into account to generate demand [29].

On the other hand, purchases are correlated between the items of the same variable and the cost. For example: p48e and p48f (with a correlation of 0.609**) where contracting is interrelated with the evaluation and selection of suppliers; p48f and p48i (with a correlation of 0.630**) where contracting is related to customer information; p48g and p48e (with a correlation of 0.648**) monitoring and control with orders to suppliers together with evaluation and selection; p48g and p48i (with a correlation of 0.646**) monitoring and control with orders to suppliers and with customer information; p48g and p48m (with a correlation of 0.617**) monitoring and control with orders to suppliers with the management of merchandise transport influences purchases; p48g and p48p (with a correlation of 0.643**) monitoring and control with orders to suppliers and inventory management; p48l and p48e (with a correlation of 0.645**) negotiation with suppliers and evaluation and selection of suppliers; p48n and p48m (with a correlation of 0.603**) how import management influences the management of merchandise transportation; p48l and p48m (with a correlation of 0.620**) how negotiation of suppliers influences the management of merchandise transportation; p48p and p48h (with correlation of 0.683**) how inventory management affects the planning of needs, p48r and p54 (with correlation of 0.610**) management and control of credits affects the capabilities of the purchasing area for the identification of reliable and quality suppliers and; p48m and p47 (with a correlation of 0.622**) the management of the transportation of goods affects the application of the ABC costing technique.

In addition, there are 65 correlations with significance and values greater than 0.500**. Within these there are some of the interest, for example: p16 and p31 (with a correlation of 0.548 **) the merchandise in transit is a parameter to generate the demand with the selection and evaluation of the suppliers in a systematic way, p20 and p31 (with a correlation of 0.527 **) the packaging of merchandise is a parameter to generate the demand with the selection and evaluation of suppliers systematically, p8 and p34 (with a correlation of 0.509 **) how much they value the procurement areas in the supply chain and the organization uses in its processes the same identification of the loads, p38 and p48r (with a correlation of 0.543 **) the level of involvement of the purchasing area in the strategic decision making in the SC and the management and control of credits in the purchases, p52, and p23 (with a correlation of 0.502 **) to what extent the procurement area contributes to reducing costs in the SC with the sales forecast for the generation of demand. These elements demonstrate the strong interaction between the variables of the questionnaire.

Regarding purchasing performance, the purchasing cycle was estimated in several processes., Table 5.

Table 5: Results from the procurement cycles.

Cycles		Demand. Warehouse	Demand Delivery	Imports	National
N	Valid	162	161	162	162
	Lost	0	1	0	0
Median		20.00	19.66	9.19	7.20
Standard error deviation		.891	.838	1.177	.667
Dev. Devation		11.339	10.638	14.978	8.491
Percentiles	25	15.00	15.00	.00	1.00
	50	15.00	15.00	3.00	5.00
	75	15.00	15.00	15.00	10.00

Source: Authors, (2024).

The results from these elements are as follows:

✓ The time elapsed from when demand is detected until the product arrives at the warehouse is an average of 20 days.

✓ The time elapsed from when the demand is detected until the product reaches the unit is an average of 19.66 days.

✓ Expresses approximately in days what the cycle of an import procurement is, which is an average of 9.19 days. (From the moment the order is prepared until the merchandise is received in the warehouse).

✓ Expresses approximately in days what the cycle of a national procurement is, which is an average of 7.20 days. (From the moment the order is prepared until the merchandise is received in the warehouse).).

These values show a similar performance from the study by [30] even though the objectives of the two studies are different.

As a result of the weaknesses that are identified and the poor state of the purchasing processes, improvement strategies are developed that contribute to reducing these gaps. Among the strategies that can be implemented, the following stand out:

- ✓ Automate the procurement process to reduce costs for the company and become more competitive.
- ✓ Develop blockchain to have more safety in logistic transactions.
- ✓ Implement other management philosophies that could improve these processes, such as CRM (Client Relations Management), ERP (Enterprise Requirement Planning), VMI (Vendor-Managed Inventory), and, CPFR (Collaborative Planning, Forecast and Replenishment).
- ✓ Provide training for the staff to optimize logistic operations.
- ✓ Implement forecast systems according to the ABC classification.
- ✓ Promote the hiring of logistic operators for some activities in these processes to reduce costs and improve client's satisfaction Fomentar la contratación de operadores logísticos para algunas actividades en estos procesos para la mejora tanto de los costos como de la satisfacción del cliente.
- ✓ Value the use of credit purchases as a surplus of income through financial planning in the company.

V. CONCLUSIONS

This research focused on the evaluation of procurement processes in Ecuadorian companies. The results obtained reveal specific patterns and challenges faced by these companies in the country, offering valuable implications for both theory and practice in the field of logistics and procurement management. The predominance of the companies under study is centered in the service sector (72.8%) over industry (27.2%) reflecting a global trend towards the outsourcing of economies.

The behavior of the procurement role was evaluated through several key dimensions: the relationship of procurement with the supply chain, demand, suppliers, the procurement cycle, cost and human talent capabilities. The results indicate that the procurement area in these companies presents several challenges. The means obtained on a Likert scale from 1 to 5 vary between 2.18 and 3.54, suggesting a performance ranging from low to medium. In particular, the relationship between procurement and the supply chain is the most highly valued dimension (average of 3.54), which highlights the strategic importance that these companies attach to their integration in the supply chain. However, specific aspects such as the management of credit purchases, attention to customs procedures, and the use of logistics operators show significant weaknesses (values below 3 on the Likert scale), which indicates critical areas for improvement.

The cycle times for import and domestic purchases were analyzed. The results show an average time of 20 days for a product to reach the warehouse from the detection of demand and 19.66 days for it to reach the requesting unit. These times, together with the import (9.19 days) and domestic (7.20 days) procurement cycles, reveal a moderate efficiency in the purchasing processes, highlighting opportunities to optimize these operations and reduce waiting times.

VI. AUTHOR'S CONTRIBUTION

Conceptualization: Neyfe Sablón-Cossío and Giselle Rodríguez-Rudi.
Methodology: Neyfe Sablón-Cossío and Ana Julia Acevedo-Urquiaga.
Investigation: Neyfe Sablón-Cossío, Giselle Rodríguez-Rudi, Roberto Wilman Rosales Bonilla, Jessica Elizabeth Medina Arias, Ana Julia Acevedo-Urquiaga and Rogelio Suárez Mella.
Discussion of results: Neyfe Sablón-Cossío and Giselle Rodríguez-Rudi.
Writing – Original Draft: Neyfe Sablón-Cossío and Giselle Rodríguez-Rudi.
Writing – Review and Editing: Neyfe Sablón-Cossío, Giselle Rodríguez-Rudi and Rogelio Suárez Mella
Resources: Neyfe Sablón-Cossío, Roberto Wilman Rosales Bonilla and Jessica Elizabeth Medina Arias.
Supervision: Neyfe Sablón-Cossío and Giselle Rodríguez-Rudi.
Approval of the final text: Neyfe Sablón-Cossío and Giselle Rodríguez-Rudi.

VIII. REFERENCES

[1] P. Zhang, K. W. Pang, and H. Yan, "Coordinating inventory sharing with retailer's return in the consignment contracts," International Journal of Production Research, Article vol. 60, no. 4, pp. 1196-1209, 2022, doi: 10.1080/00207543.2020.1854485.

[2] C. P. Jayarathna, D. Agdas, and L. Dawes, "Viability of sustainable logistics practices enabling circular economy: A system dynamics approach," Business Strategy and the Environment, Article vol. 33, no. 4, pp. 3422-3439, 2024, doi: 10.1002/bse.3655.

[3] M. A. Al-Shboul, "RFID technology usage and supply chain global positioning information sharing system: An enablers of manufacturing enterprises' supply chain performance-fresh insights from the Middle East region as developing countries," Electronic Journal of Information Systems in Developing Countries, Article vol. 90, no. 2, 2024, Art no. e12304, doi: 10.1002/isd2.12304.

[4] D. N. Pozzo, R. A. M. Aguilar, J. A. A. Libreros, D. M. G. Tamayo, J. R. Borre, and U. H. Biegelmeyer, "International Purchase Transactions: An Analysis of the Decision Cycles in Colombian Companies' Operations," in Lecture Notes in Computer Science (including subseries Lecture Notes in Artificial Intelligence and Lecture Notes in Bioinformatics), 2022, vol. 13293 LNCS, pp. 146-159, doi: 10.1007/978-3-031-10539-5_11. [Online]. Available: https://www.scopus.com/inward/record.uri?eid=2-s2.0-85135050693&doi=10.1007%2f978-3-031-10539-5_11&partnerID=40&md5=17d8658170826e0f8e813a790de23ec3

[5] ASOLOG, "Informe de Resultados de la Encuesta Nacional Logística del Ecuador," 2023. [Online]. Available: https://clusterlogistico.ec/wp-content/uploads/2023/12/2023-12-11-Resultados-ENL-EC-2023.pdf

[6] R. Hernández-Sampieri and C. Mendoza, "Metodología de la investigación. Las rutas cuantitativa, cualitativa y mixta," ed: Mcgraw-hill México, 2018.

[7] J. Acevedo Suárez et al., La Logística Moderna en la Empresa. La Habana. Cuba: Editorial Félix Varela, 2017.

[8] M. Carreras-Simó, S. Codinach-Segura, N. Filimon, and F. Fusté-Forné, "Exploring consumer preferences for local food: The case of traditional coastal fishmongers in Costa Brava (Catalonia, Spain)," Journal of Agriculture and Food Research, Article vol. 11, 2023, Art no. 100527, doi: 10.1016/j.jafr.2023.100527.

[9] C. Fotopoulos, A. Krystallis, and P. Anastasios, "Portrait value questionnaire's (PVQ) usefulness in explaining quality food-related consumer behavior," British Food Journal, Article vol. 113, no. 2, pp. 248-279, 2011, doi: 10.1108/00070701111105330.

[10] A. Ghazvinian, B. Feng, J. Feng, H. Talebzadeh, and M. Dzikuć, "Lean, Agile, Resilient, Green, and Sustainable (LARGS) Supplier Selection Using Multi-Criteria Structural Equation Modeling under Fuzzy Environments," Sustainability (Switzerland), Article vol. 16, no. 4, 2024, Art no. 1594, doi: 10.3390/su16041594.

[11] G. Gereffi and J. Lee, "Why the World Suddenly Cares About Global Supply Chains," Journal of Supply Chain Management, Article vol. 48, no. 3, pp. 24-32, 2012, doi: 10.1111/j.1745-493X.2012.03271.x.

[12] M. Abolbashari, "Achieving procurement excellence through a Bayesian Network modelling approach," in Proceedings of the International Conference on Industrial Engineering and Operations Management, 2018, vol. 2018, JUL ed., p. 1877. [Online]. Available: https://www.scopus.com/inward/record.uri?eid=2-s2.0-85066956062&partnerID=40&md5=df72eb38c4b81119fc918662498f0a12. [Online]. Available: https://www.scopus.com/inward/record.uri?eid=2-s2.0-85066956062&partnerID=40&md5=df72eb38c4b81119fc918662498f0a12

[13] C. G. Lee, "Purchasing and sourcing," in Logistics Engineering Handbook, 2007, pp. 7-1.

[14] M. Martini, M. Paolanti, and E. Frontoni, "Open-world person re-identification with RGBD camera in top-view configuration for retail applications," IEEE Access, Article vol. 8, pp. 67756-67765, 2020, Art no. 9057668, doi: 10.1109/ACCESS.2020.2985985.

[15] A. R. D. Liang, "Enthusiastically consuming organic food: An analysis of the online organic food purchasing behaviors of consumers with different food-related lifestyles," Internet Research, Article vol. 24, no. 5, pp. 587-607, 2014, doi: 10.1108/IntR-03-2013-0050.

[16] D. Lin, C. K. M. Lee, M. K. Siu, H. Lau, and K. L. Choy, "Analysis of customers' return behaviour after online shopping in China using SEM," Industrial Management and Data Systems, Article vol. 120, no. 5, pp. 883-902, 2020, doi: 10.1108/IMDS-05-2019-0296.

[17] N. Hao, H. H. Wang, and Q. Zhou, "The impact of online grocery shopping on stockpile behavior in Covid-19," China Agricultural Economic Review, Article vol. 12, no. 3, pp. 459-470, 2020, doi: 10.1108/CAER-04-2020-0064.

[18] R. Guidotti, L. Gabrielli, A. Monreale, D. Pedreschi, and F. Giannotti, "Discovering temporal regularities in retail customers' shopping behavior," EPJ Data Science, Article vol. 7, no. 1, 2018, Art no. 6, doi: 10.1140/epjds/s13688-018-0133-0.

[19] M. Murfield, C. A. Boone, P. Rutner, and R. Thomas, "Investigating logistics service quality in omni-channel retailing," International Journal of Physical Distribution and Logistics Management, Article vol. 47, no. 4, pp. 263-296, 2017, doi: 10.1108/IJPDLM-06-2016-0161.

[20] S. Thiruchelvam and J. E. Tookey, "Evolving trends of supplier selection criteria and methods," International Journal of Automotive and Mechanical Engineering, Article vol. 4, no. 1, pp. 437-454, 2011, doi: 10.15282/ijame.4.2011.6.0036.

[21] C. Zhang, M. Venkatesh, and M. Ohana, "The impact of normative institutions on socially sustainable supply chain management: the role of individual cultural values," International Journal of Operations and Production Management, Article vol. 44, no. 4, pp. 790-812, 2024, doi: 10.1108/IJOPM-10-2022-0691.

[22] C. Zhang, D. Moosmayer, M. Wang, and M. Ohana, "Managing Chinese suppliers' sustainability performance: The double-edged role of guanxi governance," Industrial Marketing Management, Article vol. 118, pp. 189-199, 2024, doi: 10.1016/j.indmarman.2024.03.001.

[23] A. F. Hayes and J. J. Coutts, "Use Omega Rather than Cronbach's Alpha for Estimating Reliability. But…," Communication Methods and Measures, vol. 14, no. 1, pp. 1-24, 2020/01/02 2020, doi: 10.1080/19312458.2020.1718629.

[24] D. George and P. Mallery., "SPSS for Windows step by step: A simple guide and reference". Fourth Edition. (11.0 update). 2003. URL: https://wps.ablongman.com/wps/media/ objects/385/394732/george4answers.pdf. 2003.

[25] H. Akoglu, "User's guide to correlation coefficients," Turkish journal of emergency medicine, vol. 18, no. 3, pp. 91-93, 2018.

[26] E. Saccenti, M. H. Hendriks, and A. K. Smilde, "Corruption of the Pearson correlation coefficient by measurement error and its estimation, bias, and correction under different error models," Scientific reports, vol. 10, no. 1, p. 438, 2020.

[27] E. Karttunen, K. Lintukangas, and J. Hallikas, "Digital transformation of the purchasing and supply management process," International Journal of Physical Distribution & Logistics Management, vol. 53, no. 5/6, pp. 685-706, 2023, doi: 10.1108/IJPDLM-06-2022-0199.

[28] K. Stouthuysen, A. Van Den Abbeele, J. van der Meer-Kooistra, and F. Roodhooft, "Management control design in long-term buyer-supplier relationships: Unpacking the learning process," Management Accounting Research, vol. 45, p. 100643, 2019/12/01/ 2019, doi: https://doi.org/10.1016/j.mar.2019.06.001.

[29] D. Lima, R. F. Ramos, and P. M. Oliveira, "Customer satisfaction in the pet food subscription-based online services," Electronic Commerce Research, Article vol. 24, no. 2, pp. 745-769, 2024, doi: 10.1007/s10660-024-09807-8.

[30] P. Huddleston, M. T. Coveyou, and B. K. Behe, "Visual cues during shoppers' journeys: An exploratory paper," Journal of Retailing and Consumer Services, vol. 73, p. 103330, 2023/07/01/ 2023, doi: https://doi.org/10.1016/j.jretconser.2023.103330.

Journal of Engineering and Technology for Industrial Applications

ITEGAM-JETIA

Manaus, v10. n.50, p. 108-116. November/ December., 2024.
DOI: https://doi.org/10.5935/jetia.v10i50.1354

ISSN ONLINE: 2447-0228

RESEARCH ARTICLE OPEN ACCESS

MACHINING PARAMETERS OPTIMIZATION IN WET TURNING OF EN31 MATERIAL USING BOX-BEHNKEN APPROACH OF RSM

Shivaji Bhivsane[1], Arvind Chel[2], Siraj Sayyed[3]

[1] Research Scholar, Dr. Babasaheb Ambedkar Marathwada University, Aurangabad-431004, (MH) India.
[2] Department of Mechanical Engineering, Jawaharlal Nehru Engineering College, Aurangabad-431001, (MH) India.
[3] Department of Mechanical Engineering, Maharashtra Institute of Technology, Aurangabad-431010, (MH) India.

[1] https://orcid.org/0000-0002-1169-957X, [2] https://orcid.org/0000-0001-7817-8958, [3] https://orcid.org/0000-0001-8531-7258

Email: bhivsanesv@gmail.com, achel@mgmu.ac.in, lucky.sartaj@gmail.com.

ARTICLE INFO

Article History
Received: October 26, 2024
Revised: November 6, 2024
Accepted: November 10, 2024
Published: November 30, 2024

Keywords:
EN31 Material,
Wet Turning,
RSM,
Tribological Parameters,
Surface Finish,
Optimization.

ABSTRACT

Manufacturing sectors are always challenged to enhance surface quality and tool life while reducing machining costs and setup times in hard-turning operations. In line with this, the current study focused on surface roughness optimization employing machining parameters such as cutting speed: v (160-260 m/min), feed: f (0.1-0.2 mm/rev), depth of cut: d (0.05-0.15 mm), and tool nose radius: re (0.4-1.2 mm) as functions. The experiment was designed by using Box-Behnken approach of RSM and carried out on a commercial CNC machine using EN31 material at 47 HRC. The research found that machining parameters have a considerable effect on surface roughness, as do stresses, vibrations, heat generation, and increased material per pass. The experimental surface roughness observed in between 1.34-2.81 μm whereas estimated surface roughness have R2=0.9976. The Anova design model showed face value of 356.21 which indicates the developed model is noteworthy. The significant and marginal effect of machining parameters are evaluated by considering p-value and overcall error observed within the range of 1.613-1.974%..

I. INTRODUCTION

In recent years, turning operations have garnered a lot of attention in the machining of hard materials with hardnesses more than 45 HRC [1]. Hard machining involves material hardness ranging from 45 to 68 HRC, and the steel is classed as alloy, tools, hardened, hard-chrome, and heat-treated steels [2]. To turn such workpiece materials, turning inserts such as carbide, ceramics, CBN, and PCBN must have extremely high mechanical and thermal load capacities [3]. Hard turning has many advantages over grinding, including lower costs, faster and easier execution, and nearly identical surface roughness [4],[5]. Several elements influence the behavior of the cutting process, including tool variables, workpiece variables, and cutting circumstances such as material, mechanical properties, chemicals, and physical characteristics [6]. The selection of ideal process parameters is typically a challenging task, but it is a critical aspect of machining process management in order to achieve enhanced product quality, high productivity, and low cost. The optimization of machining parameters using experimental approaches and mathematical and statistical models has expanded significantly over time to meet the shared aim of increasing machining process efficiency [7].

II. LITERATURE REVIEW

Authors Thiele and Melkote [7] investigated the influence of CBN insert edge geometry on the Ra of AISI 52100 hardened steel and determined that a larger re gives greater Ra than a smaller one. Similarly Chou and Song [8] were studied influence of re and concluded that lower re provided a bigger uncut thickness of chip, which increased temperature in the shear plane and formed deeper white layers, and vice versa. Siraj et al. [9] studied the effects of tribological parameters, re and found that the created empirical correlation could predict with an accuracy of 97.71% [0.4 mm re], 99.92% [0.8 mm re], and 99.67% [1.2 mm re].

Numerous authors studied the effect to dry and wet turning on hard materials. For [10] studied the coated carbide [B4C] under sliding and the results indicated that B4C coating considerably reduce the sliding distance by 2m. Similarly [11] evaluated turning operations with hard materials in both dry and wet conditions utilizing HTMF. The study concluded that a large amount of the cutting fluid evaporated during chip production when a high velocity thin pulsed jet with an injection rate of only 3 ml/min was used. According to [12] evaluated SAE 52100 hardened steel with a minimal oil flow [10 ml/h] at various cutting speeds utilizing CBN inserts. After comparing dry and wet turning results, the study determined that flank wear was slightly lower in wet and Ra was comparable in both. The lowest Ra was reached at a cutting speed of 175 m/min, while lower cutting speeds had no effect on Ra or flank wear in both situations. According to [13] studied the effectiveness of several cooling strategies, including cryogenic cooling, MQL, NDM, HPC, and solid, liquid, and vapour coolants, in improving surface finish in turning with various inserts. The study found that cooling strategies extend the life of coated inserts such as ceramic, carbide, and CBN. Investigated the rheological and tribological properties of water-based lubricants in AISI 52100 bearing steels. The study showed that WBLs have increasing potential in the EV transportation sectors. It examined the role of high-pressure rheology and tribochemistry in wear mechanisms for several lubricants [14].

Many authors studied the effect of various inserts on surface roughness [Ra], tool wear [VB], material removal rate, etc. in hard turning operations. According to [15] used regression and neural networks as a predictive modeling approach to quantify Ra and VB using CBN insert. The study concluded that lowering the feed rate increases VB, but increasing roughness comes at the expense of increased VB. Additionally, honed edge geometry in CBN inserts delivers better outcomes in terms of Ra and VB during severe turning operations. Similarly For [16] investigated the effects of turning on hardened steel for automotive applications. The study examined the effects of several types of inserts, such as ceramics, carbide, CBN, and PCBN, on Ra, T, and VB. Tamizharasan et al. [17] investigated the Ra and VB of three types of CBN inserts on hardened materials used in crank pin manufacture. The study found that A-grade inserts had better Ra and T than low-grade CBN inserts. Used the Taguchi technique to optimize Ra and machining parameters in hard turning of AISI 1030 steel with titanium-nitrate coated insert. The study found that 1.2 mm re, 0.15 mm/rev f, and 0.5 mm d resulted in a 335% reduction in Ra when compared to the open literature [18]. According to [19] investigated the effect of machining parameters on hard turning of AISI 4140 steel at 51 HRC using a coated-carbide tool. The study found that feed rate had a substantial effect on Ra and Rz, as did the dual factor interaction. Hamdan et al. [20] improved the surface roughness of AISI 304 steel with a KORLOY coated carbide insert [APXT 11T3PDSR-MM]. The study was conducted with four input parameters utilizing a L9 orthogonal array, and the results showed a 25.3% reduction in cutting forces and a 41.3% rise in Ra. For [21] used a regression model to evaluate the tribological parameters of AISI 52100 steel [55 HRC] with carbide inserts. The study found that sharpened saw tooth chips in burnt blue have a substantial effect on Ra. The quadratic equation identified the optimal machining settings of v, f and d as 70m/min, 0.04 mm/rev, and 0.1 mm respectively for achieving lower VB of 0.218 mm and 1.28 μm According to [22] investigated the dry turning operation on EN 31 steel with a CBN insert, optimizing the Ra and cutting tool settings. The study discovered that Ra increases with feed rate for all v and d's under consideration. The optimal machining settings were determined to be v, f, and d 100 m/min, 0.04 mm/rev, and 0.2 mm respectively.

Numerous authors were applied statistical and optimization techniques to optimize the machining parameters such as v, f, d, re, cutting forces, and temperatures, etc. in hard turning operations. The investigated and compared the mistakes encountered in hard turning and grinding operations on hard materials [23]. The study discovered that hard turning delivers economic benefits on the basis of poorer precision as compared to grinding and superfinishing procedures. Similarly, for [24] investigated the 2D and 3D surface textures produced by rigorous turning and grinding processes. The study found that periodic-random surfaces based on 2D roughness were extremely unsafe. According to [25] used ANN to optimize Ra and tool wear in D2 hardened steel at 60 HRC. The study found that the multilayer precipitation model of ANN predicts with an accuracy of 0.979 and outperformed the multiple regression model. Chandrasekaran et al. [26] demonstrated using several computing approaches, such as ANN, GA, SA, and PSO, on four machining operations, including turning. The study found that PSO produced the best outcomes, followed by GA and ANN. According to [27] used a CBN implant to investigate AISI H11 steel with hardness varying from 40 to 50 HRC. The study used a four-factorial RSM approach for assessing Ra and the forces of cutting. The investigation found that feed and cutting forces significantly impacted the depth of cut [56.77% and 31.50%, respectively], but individual cutting speeds had only minor variances. For [28] used a multivariate statistical technique called principal component analysis to investigate surface finish in hard turning of AISI 52100 steel. The study concluded that using the Ra and Rt components of PCA to make decisions about the optimal parameters of hard turning, while reducing VB reduces Ra. According to [29] investigated the effect of machining settings on dry hard turning with CBN inserts using the MCDM approach TOPSIS. ANOVA analysis revealed that the optimal parameters for achieving 0.507 μm Ra were v, f, and d at 200/min, 0.1 mm/rev, 0.8 mm, and 1.2 mm re. According to [30] studied the impact of machining settings on AISI 52100 steel using the Box-Behnken design. The study found that temperature and power consumption had a substantial impact on the machining parameters measured in the FEM analysis. At the minimal conditions, the v, f, and d were 162.42 m/min, 0.247 mm/rev, and 1.395 mm, respectively.

Few authors also studied the various techniques to enhance the Ra in hard turning operations. For [31] investigated the Ra in PHT of AISI 52100 steel [60-62 HRC] with a CBN insert in relation to rolling contact fatigue. The study found a very fine white coating [<1μm] on the top surface and increased residual stresses in PHT, with a negligible effect on microstructural phases. RCF life rises at the expense of Ra degradation. Similarly, [32] proposed a new technique for determining VB using sonic emission signals in AISI 4340 steel. The investigation was carried out on coated and uncoated nanostructured AlCrN carbide inserts, and the study found that increasing the amplitude of power resulted in an increase in VB and density at the end of VB. According to [33] investigated the Ra optimization technique for AISI 1053 steel utilizing the Johnson-Cook constant and wear factors. The study found that the 3D oblique cutting forces model had a stronger relationship with the flank wear model, but Ra predicted using the empirical model differed significantly from the experimental results. For [34] investigated the UVAT machining technique using a coated-carbide insert in hard turning of 62 HRC steel. The study found that using these techniques resulted in a lower Ra of 1.12μm than standard turning operations. Studied machining parameters to study VB in AISI 52100 steel utilizing a long-term approach of solid-lubricant assisted machining [SLAM] in dry turning. The study found that the SLAM technique dramatically reduced cutting forces, vibrations, VB, and Ra by 60%, 29%, 17%, and 66%, respectively [35].

The current study attempts to investigate the influence of coated carbide inserts on hardened material with a hardness of 47 HRC. The experiment was designed utilizing the Box-Behnken approach of the RSM method to optimize surface roughness under varied machining parameters, including re circumstances. A total of 27 runs were calculated using the considered method, and graphs for estimated and experimental surface roughness are presented.

III. MATERIALS AND METHODS

The experimental program begins with material selection for experimentation, followed by machining parameters selection, turning processes (dry and wet), surface roughness, and optimization approach. Machinability in hard turning processes is affected by a number of elements, including the machine, tool, cutting, and workpiece. The current study focuses primarily on tool material and geometry, ν, f, and d, re, and material hardness. The experimentation has been performed on EN31 material formally known as bearing steel. The chemical composition and ranges for EN31 steel are given in Table 1. While executing machining operations, three different levels are chosen ranging from -1 to +1 for the machining parameters being considered. The machining parameters and levels are listed in Table 2.

Table 1: Chemical composition and ranges for EN31

Chemical Composition	Range (%)
Carbon	0.98-1.10
Manganese	0.25-0.45
Chromium	1.30-1.60
Silicon	0.15-0.30
Sulphur	0.025 max.
Phosphorous	0.025 max.
Nickel	-
Molybdenum	-

Source: Authors, (2024).

Table 2: Machining parameters and their levels

Parameters	Units	Levels		
		-1	0	+1
Cutting Speed (ν)	m/min	160	210	260
Feed (f)	mm/rev	0.1	0.15	0.2
Depth of cut (d)	mm	0.05	0.1	0.15
Tool Nose Radius (r_e)	mm	0.4	0.8	1.2

Source: Authors, (2024).

The raw EN 31 material's hardness was assessed using a Rockwell hardness tester and was determined to be between 25 and 27 HRC. Further raw materials were split into 27 samples for the hardening operation. At the preparatory stage, all 27 EN31 samples were faced and plane turned, followed by a hardening process. Again, the hardness of all the samples was assessed and found to be between 46 and 47 HRC, and runs were calculated using the Box-Behnken approach of the response surface method, which included ν, f, d, and re. The experiment is carried out using a 25 mm diameter EN31 material measuring 60 mm in length. To improve the accuracy of the turning operation, a center hole is drilled in each sample. The Ra of each sample is tested three times using a Mitutoyo surface roughness tester, and the average value has been utilized for computations. The number of runs in the current study is computed using RSM's Box-Behnken technique. A total 27 runs are calculated using the machining parameters under consideration, and a quadratic equation is produced for surface roughness. Table 3 shows the run table for the Box-Behnken technique, which includes the estimated and actual values of machining parameters as well as standard and run orders. The table also shows the experimental and estimated Ra using quadratic equations, along with their percentage errors for each sample.
Quadratic Equation:

$$R_a = -0.674 + 0.015v + 6.193f + 5.436d - 1.061r_e - 0.016v \times f - 0.012v \times d + 0.0005v \times r_e + 1.00f \times d + 8.508 \times 10^{-15} f \times r_e + 0.125d \times r_e - 0.000012v^2 - 2.166f^2 - 1.666d^2 + 0.044r_e^2 \quad (1)$$

Table 3: Run table for hard turning using Box-Behnken approach of RSM.

Std Order	Run Order	ν	f	d	r_e	Ra (Exp)	Ra (Est)	% Error
22	1	210	0.2	0.1	0.4	2.57	2.55	0.78
12	2	260	0.15	0.1	1.2	2.15	2.12	1.40
3	3	160	0.2	0.1	0.8	1.80	1.82	1.11
15	4	210	0.1	0.15	0.8	2.11	2.11	0.00
18	5	260	0.15	0.05	0.8	2.35	2.34	0.43
1	6	160	0.1	0.1	0.8	1.54	1.51	1.95
19	7	160	0.15	0.15	0.8	1.82	1.84	1.10
14	8	210	0.2	0.05	0.8	2.06	2.05	0.49
10	9	260	0.15	0.1	0.4	2.81	2.80	0.36
23	10	210	0.1	0.1	1.2	1.61	1.63	1.24
21	11	210	0.1	0.1	0.4	2.32	2.33	0.43
17	12	160	0.15	0.05	0.8	1.52	1.49	1.97
24	13	210	0.2	0.1	1.2	1.86	1.86	0.00
26	14	210	0.15	0.1	0.8	2.09	2.09	0.00
9	15	160	0.15	0.1	0.4	2.02	2.04	0.99
13	16	210	0.1	0.05	0.8	1.81	1.83	1.10
6	17	210	0.15	0.15	0.4	2.59	2.58	0.39
27	18	210	0.15	0.1	0.8	2.09	2.09	0.00
7	19	210	0.15	0.05	1.2	1.58	1.60	1.27
20	20	260	0.15	0.15	0.8	2.53	2.56	1.19
2	21	260	0.1	0.1	0.8	2.38	2.37	0.42
4	22	260	0.2	0.1	0.8	2.48	2.52	1.61
25	23	210	0.15	0.1	0.8	2.09	2.09	0.00
5	24	210	0.15	0.05	0.4	2.29	2.30	0.44
11	25	160	0.15	0.1	1.2	1.32	1.32	0.00
16	26	210	0.2	0.15	0.8	2.37	2.34	1.27
8	27	210	0.15	0.15	1.2	1.89	1.89	0.00

Source: Authors, (2024).

IV. RESULTS AND DISCUSSIONS

The results focuses primarily on experimental data, such as machining parameters versus Ra. Additional findings based on Box-Behnken design are presented about the effect of combined machining parameters on Ra. Finally, it includes a comparison of experimental and estimated Ra using standard error. During wet turning, Ra is estimated using a variety of machining parameters, including ν, f, d, and re. Figure 1 shows a box plot for various machining parameters and Ra. Figure 1(a) depicts the relationship between ν and Ra, while 1(b), 1(c), and 1(d) show the relationship between f, dc, and re against Ra, respectively.

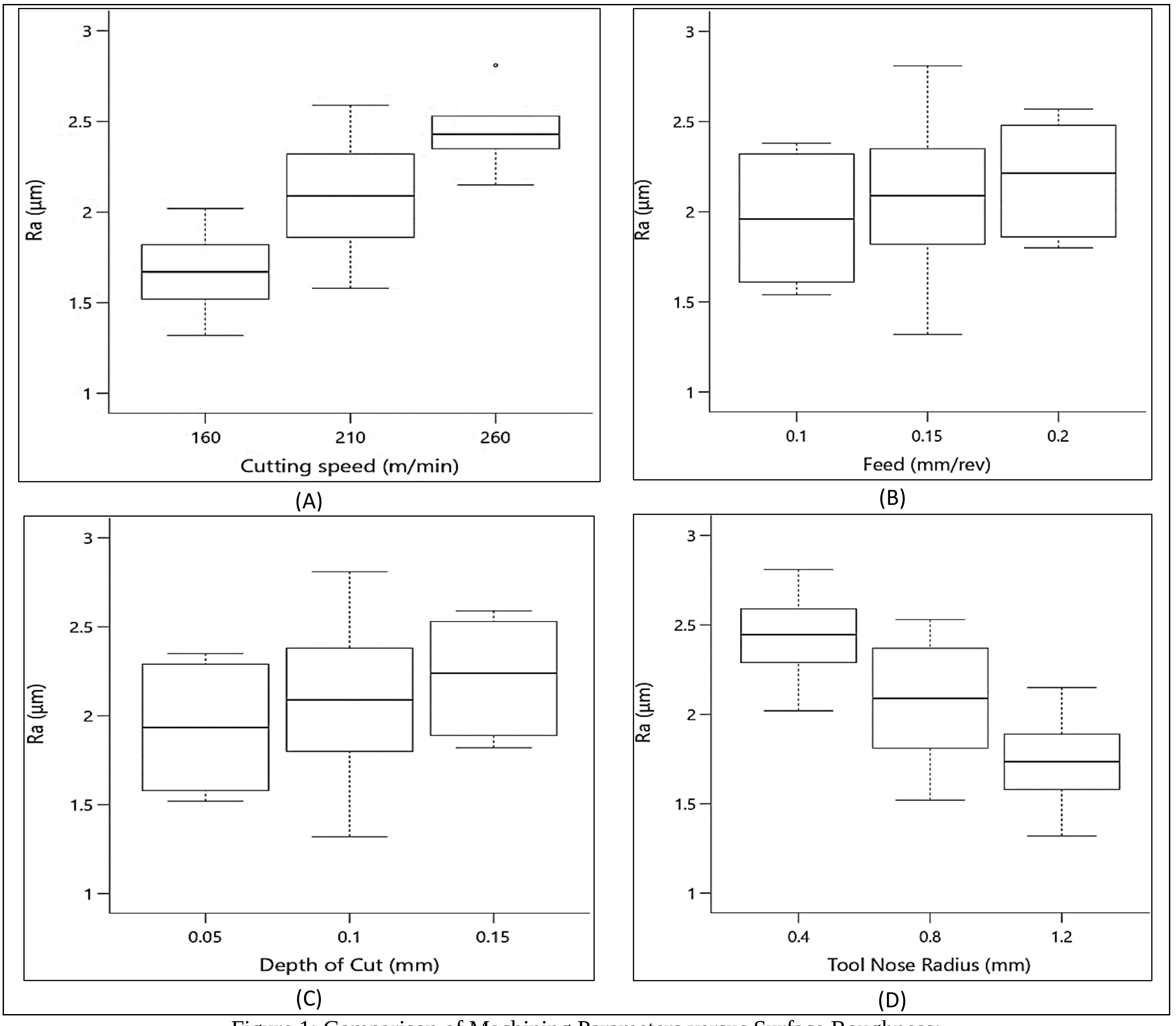

Figure 1: Comparison of Machining Parameters versus Surface Roughness:
a – Cutting speed vs Ra; b – Feed vs Ra;
c – Depth of cut vs Ra; d – Tool Nose Radius vs Ra.
Source: Authors, (2024).

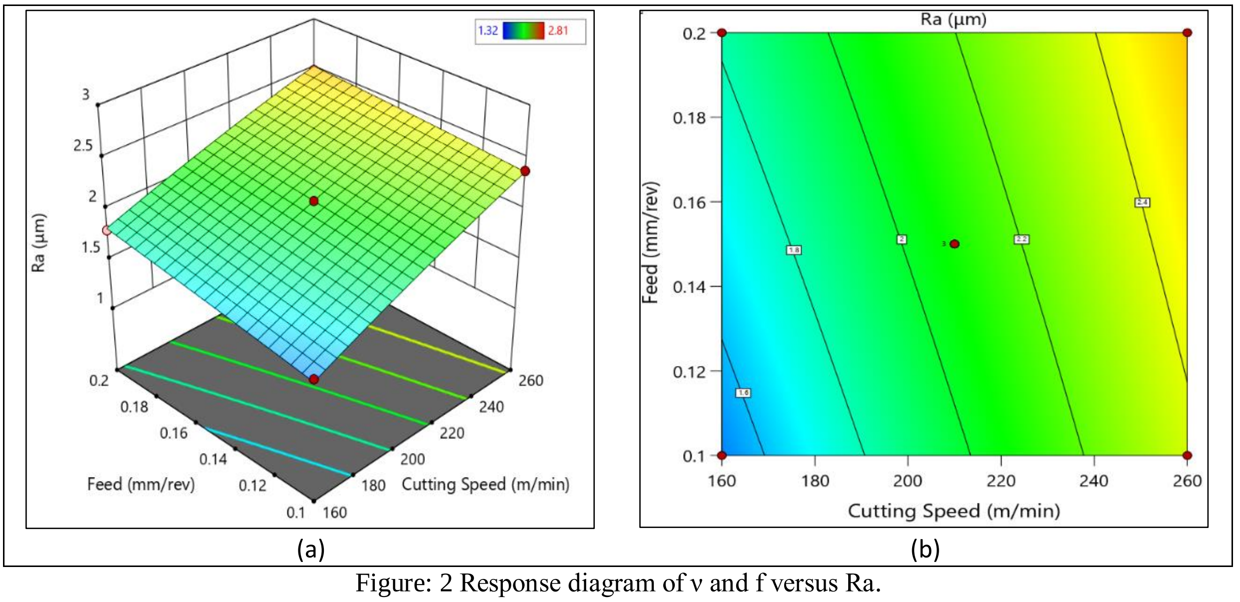

Figure: 2 Response diagram of ν and f versus Ra.
a – Feed and Cutting speed vs Ra; b – Contour plot.
Source: Authors, (2024).

Figure 1(a) shows that ν increases as Ra increases. At lower ν (160 m/min) Ra observed within the range of 1.5-1.8 µm whereas for 210 and 260 m/min observed within the range of 1.9-2.4 µm and 2.4-2.5 µm. At higher ν, the interquartile range is very closer and an outlier is observed for Ra near 3 µm. Similarly 1(b) and 1(c) shows that marginal variations in Ra for the range of f and d under consideration. Ra is observed within the range of 1.5-2.5 µm for both machining parameters and significant variations are observed for whiskers at 0.15 mm/rev f and 0.1 mm d in comparison with others. Figure 1(d) illustrates the relation between re and Ra. Ra decreases as re increases. The Ra is observed within the range of 1.4 to 2.9 µm and the interquartile range is observed larger at 0.8 mm re. The chip forming mechanism has a vital influence in Ra and re. A larger re lowers chip formation while improving Ra. Many researches have confirmed the relationship between Ra and re.

The number of runs in an experiment is computed using the Box-Behnken design of response surface approaches. The experimental application generates 3D response graphs and contour plots for machining parameters versus Ra. Figure 2 depicts the response diagram of f and ν versus Ra. A 3D surface plot is observed in Figure 2(a) while Figure 2(b) shows contour plot. A decreasing trend is observed in Ra when compared with f and ν. Figure 2(a) clearly shows that lower Ra is at 0.1 mm/rev f and 160 m/min ν, while Ra increases with increase in f and ν. The highest 2.8 µm Ra is observed when both machining parameters are set to higher levels. Contour plot 2(b) shows an increasing trend of Ra from 1.6 to 2.4 µm in relation to ν and f for all runs considered. A considerable contribution of f and ν is observed in turning operations. From the investigated range of both machining parameters, the least values give enhanced Ra leading to minimizing the intensity of forces and generation of heat at the surface.

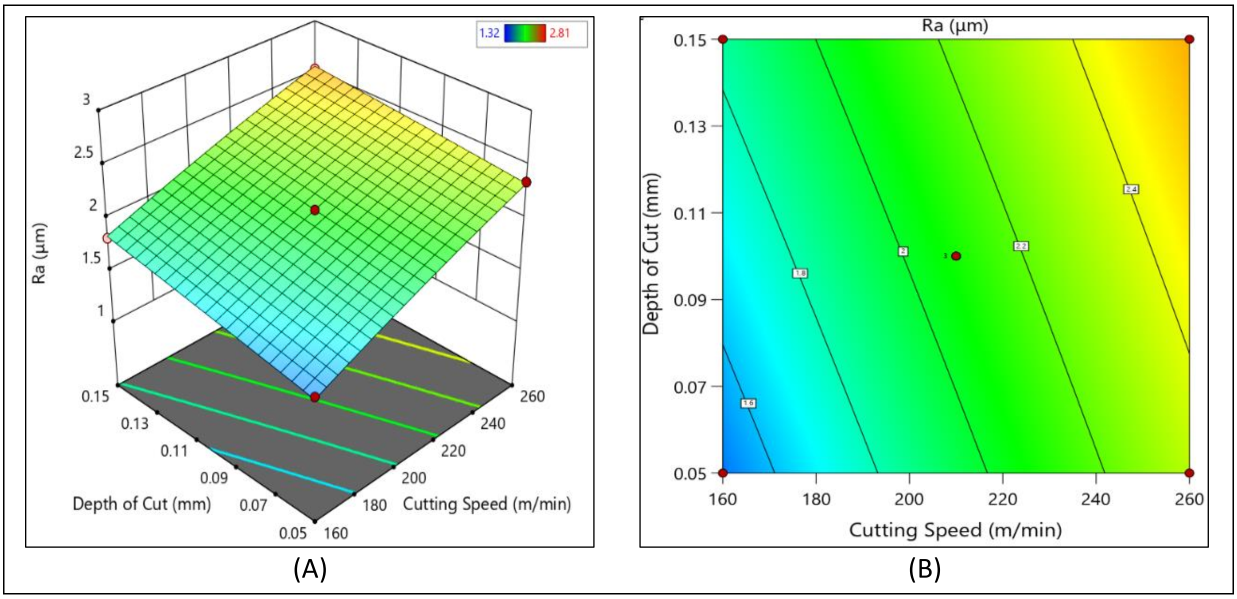

Figure 3: Response diagram of v and d versus Ra.
a – Depth of cut and Cutting speed vs Ra; b – Contour plot.
Source: Authors, (2024).

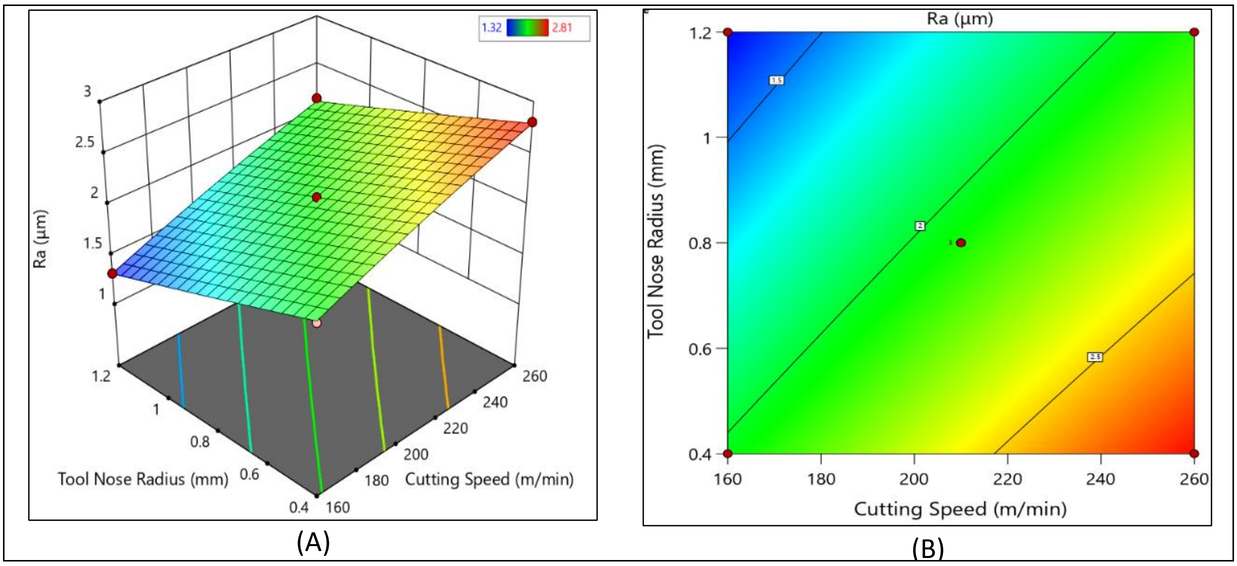

Figure 4: Response diagram of v and re versus Ra.
a – Tool nose radius and Cutting speed vs Ra; b – Contour plot.
Source: Authors, (2024).

Figure 3 depicts the response diagram of ν and d versus Ra. A similar trend like Figure 2 is observed in this section. Figure 3(a) shows the lowest Ra at 0.05 mm d and 160 m/min ν. If both the machining parameters are set to its higher levels provide greater Ra value 2.8 µm. Figure 3(b) also shows similar trend like Figure 2(b), an increasing trend of Ra from 1.6 to 2.4 µm in relation to ν and f for all runs considered. In turning operations, both d and ν play an important role. A smaller d improves Ra by removing less material per pass, resulting in less vibrations and resistance in tool materials.

Figure 4 depicts the response diagram of re and ν versus Ra. A 3D surface plot is observed in Figure 4(a) while Figure 4(b) shows contour plot. A decreasing trend in Ra with increase in re is observed and increasing in Ra with increase in ν is observed in Figure 4(a). Similar to a reduced d, a lower re with a lower ν significantly reduces Ra by removing fewer materials, but an increase in re with a lower ν increases Ra. At faster ν's and a smaller re, the tool material experiences more forces, vibrations, and resistance. From contour plot 4(b), the lowest Ra's are observed above 1 mm re whereas highest observed at above 220 m/min ν.

Figure 5 depicts the response diagram of d and f versus Ra. A 3D surface plot is observed in Figure 5(a) while Figure 5(b) shows contour plot. The deviations in f and d provides marginal variations Ra for all the runs under considerations. Some of the researches showed that the f significantly affects the Ra leading to increase in forces and vibrations in tool materials, but d do not have significant impact on forces and Ra. The Ra is observed within the range of 1.9 to 2.3 µm for both increase in f and d.

Figure 6 depicts the response diagram of re and f versus Ra. A 3D surface plot is observed in Figure 6(a) while Figure 6(b) shows contour plot. A decreasing trend in Ra with increase in re is observed and increasing in Ra with decrease in f is observed in Figure 6(a). The Ra is observed within the range of 1.8 to 2.4 µm for all the runs under considerations. From contour plot 6(b), the lowest Ra are observed above 1 mm re whereas highest observed at above 0.14 mm/rev f.

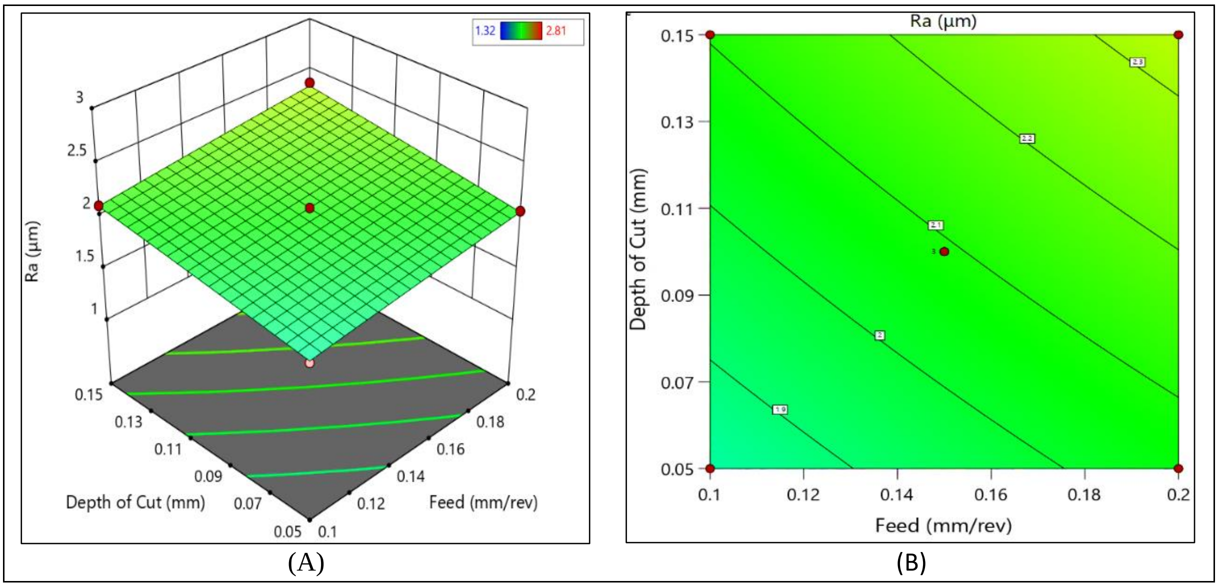

Figure 5: Response diagram of f and d versus Ra.
a – Depth of cut and Feed vs Ra; b – Contour plot.
Source: Authors, (2024).

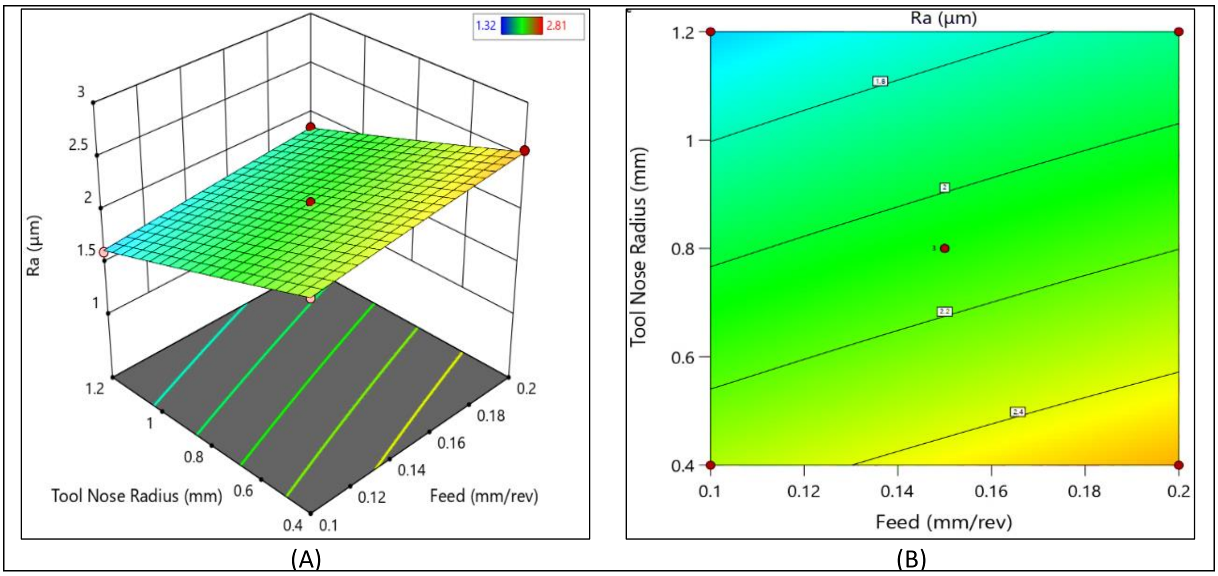

Figure 6: Response diagram of f and re versus Ra.
a – Tool nose radius and Feed vs Ra; b – Contour plot.
Source: Authors, (2024).

Figure 7 depicts the response diagram of re and d versus Ra. A 3D surface plot is observed in Figure 7(a) while Figure 7(b) shows contour plot. Similar to the Figure 6, a decreasing trend in Ra with increase in re is observed and increasing in Ra with decrease in d is observed in Figure 6(a). The Ra is observed within the range of 1.8 to 2.4 µm for all the runs under considerations. From contour plot 7(b), the lowest Ra's are observed above 1 mm re whereas highest observed at above 0.09 mm d.

Figure 8 shows a comparison of experimental and estimated Ra for all runs under investigation. The experimental value of Ra was measured three times and the average was used in computations. The expected Ra is anticipated using the quadratic equation obtained from the Box-Behnken method of the RSM approach. A substantial interconnectivity is observed between experimental and calculated Ra, and values predicted using a quadratic equation exhibit accuracy of prediction R^2=0.9976. Anova for the quadratic model yields a face value of 356.21, indicating that the developed model is noteworthy. Individual machining parameters such as ν, f, d, and re, as well as combinations of parameters such as ν and f, ν and d, and ν into ν, have a substantial effect on Ra. The remaining quadratic equation parameters had a minor effect on Ra and were observed using P-values.

Figure 9 displays f and ν versus design errors. Figure 9(a) shows a 3D surface plot, while 9(b) provides a contour plot of the same. Figure 9(a) and 9(b) clearly show that the outer margins of the surface plot have large inaccuracies, but the intensity reduces as one moves closer to the centroidal point. An asymptotic tendency is seen between 180 and 240 m/min ν and 0.12-0.18 mm/rev f. The similar results are also observed in different combinations of machining parameters. The percentage errors are in the range of 1.613-1.974%.

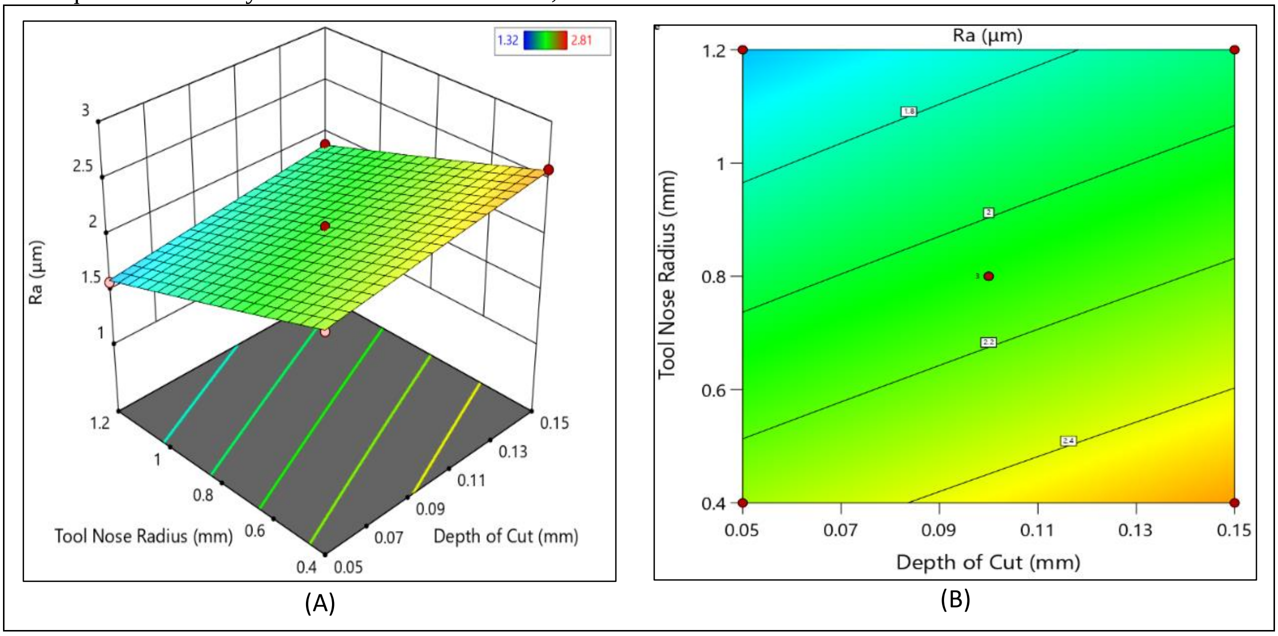

Figure 7: Response diagram of d and re versus Ra.
a – Tool nose radius and Depth of cut vs Ra; b – Contour plot.
Source: Authors, (2024).

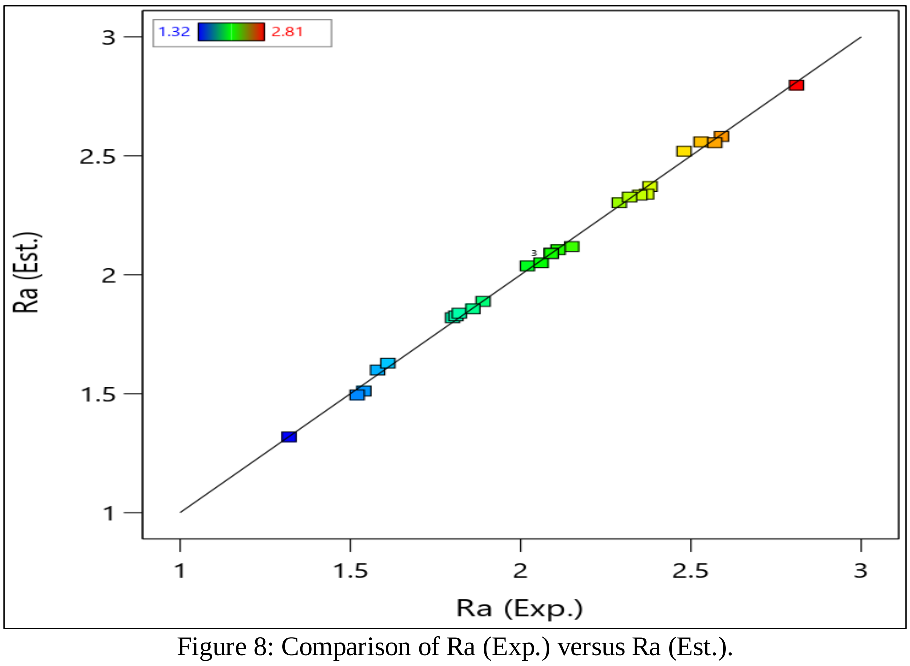

Figure 8: Comparison of Ra (Exp.) versus Ra (Est.).
Source: Authors, (2024).

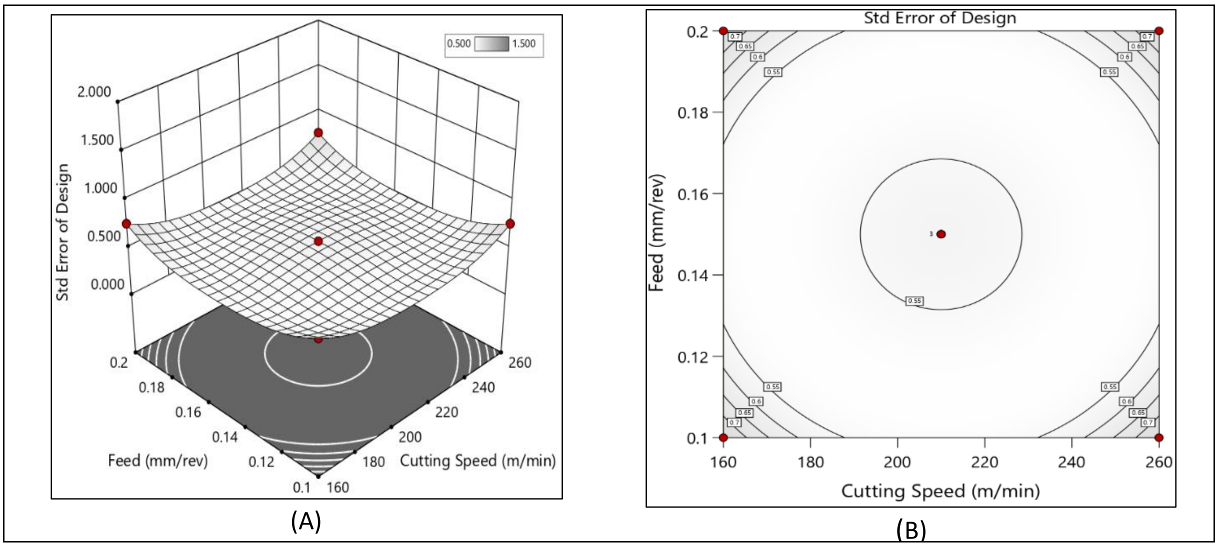

Figure 9: Response diagram of v and f versus Standard error of design:
a – Feed and Cutting speed vs Std. error of design; b – Contour plot.
Source: Authors, (2024).

The discussion based on current research work mainly focused on the problem statements and the conclusive findings from the current research. From the experimentation it has been observed that surface finish increases with increase in cutting speed, feed rate, and depth of cut, whereas it decreases with increase in tool nose radius. Several factors such as thermal expansion, built-up edge, chatter marks, contact timings and vibration may lead to increase the surface roughness due to increased cutting speed. The primary goal of the current research work was to use coated carbide inserts to optimize the surface finish of hardened EN31 alloy steel. The RSM Box-Behnken technique was used to formulate the procedure. The Box-Behnken approach yielded results in the form of contour plots, and it was noted how the machining parameters impacted the surface finish. Lower feed rate, depth of cut and cutting speed provides the excellent surface finish, this may be attributed due to fewer pass timings, heat generations and balanced forces. Larger contact area, which promotes smoother operation and balanced forces, may be the reason why higher tool nose radius combined with lower cutting rates improves surface smoothness. A sharper edge produced by a lower tool nose radius increases the intensity of cutting forces. The tight range of both feed rate and depth of cut may be the reason for the minor effects they have on surface roughness. Similar trends may be seen in the prediction of surface finish between tool nose radius and feed rate, as well as tool nose radius and depth of cut. Surface finish is not significantly affected by feed rate or depth of cut; instead, it is reduced by lower feed rate and depth of cut combined with a larger tool nose radius. The cutting forces' balancing may be the cause of this.

V. CONCLUSIONS

The experimentation on EN31 material was carried out with a coated carbide insert, and runs were estimated using the Box-Behnken approach of RSM. The machining parameters v, f, d, and re are all considered inputs, whereas Ra is predicted using the input parameters as a function. The conclusions are based on testing and optimization utilizing the Box-Behnken technique:

- The machining parameters v, f, d, and re significantly affects the Ra and it is observed within the range of 1.34-2.81 µm for all the runs under considerations.
- The Ra shows a decreasing tendency as compared to re, but an increasing trend with the remaining machining parameters.
- Reduced force intensity, heat generation, and fewer material per pass, forces and vibrations are noted at reduced v and f, and d with a larger re, resulting in smaller Ra.
- Marginal variations are observed in Ra when compared with d and f.
- The individual and combined effect of machining parameters on Ra are identified by considering p-value <0.05.
- The quadratic equation predicts Ra with an accuracy of R2=0.9976 and Anova model offers face value of 356.21 indicates the developed model is noteworthy.
- The errors are observed within the range of 1.613-1.974%. The Box-Behnken approach of RSM played a key role in optimizing machining parameters in hard turning.

VI. AUTHOR'S CONTRIBUTION

Conceptualization: Shivaji Bhivsane, Arvind Chel and Siraj Sayyed.
Methodology: Shivaji Bhivsane, Arvind Chel and Siraj Sayyed.
Investigation: Shivaji Bhivsane, Arvind Chel and Siraj Sayyed.
Discussion of results: Shivaji Bhivsane, Arvind Chel and Siraj Sayyed.
Writing – Original Draft: Shivaji Bhivsane, Arvind Chel and Siraj Sayyed.
Writing – Review and Editing: Shivaji Bhivsane, Arvind Chel and Siraj Sayyed.
Resources: Shivaji Bhivsane, Arvind Chel and Siraj Sayyed.
Supervision: Shivaji Bhivsane, Arvind Chel and Siraj Sayyed.
Approval of the final text: Shivaji Bhivsane, Arvind Chel and Siraj Sayyed.

VII. ACKNOWLEDGMENTS

Authors are thankful to the management of MIT College, Aurangabad for providing research facility.

VIII. REFERENCES

[1] D. Anoop, A. S. Sekhar, M. Kamaraj, and K. Gopinath, “Numerical evaluation of subsurface stress field under elastohydrodynamic line contact for AISI 52100 bearing steel with retained austenite,” Wear, vol. 330–331, pp. 636–642, 2015, doi: 10.1016/j.wear.2015.01.021.

[2] Attanasio, D. Umbrello, C. Cappellini, G. Rotella, and R. M'Saoubi, "Tool wear effects on white and dark layer formation in hard turning of AISI 52100 steel," Wear, vol. 286–287, pp. 98–107, 2012, doi: 10.1016/j.wear.2011.07.001.

[3] D. Bagawade, P. G. Ramdasi, R. S. Pawade, and P. K. Bramhankar, "Evaluation of Cutting Forces in Hard Turning of Aisi 52100 Steel By Using Taguchi Method," vol. 1, no. 6, pp. 1–5, 2012.

[4] G. Bartarya and S. K. Choudhury, "Effect of Cutting Parameters on Cutting Force and Surface Roughness During Finish Hard Turning AISI52100 Grade Steel," Procedia CIRP, vol. 1, no. mm, pp. 651–656, 2012, doi: 10.1016/j.procir.2012.05.016.

[5] I. S. Cho, A. Amanov, and J. D. Kim, "The effects of AlCrN coating, surface modification and their combination on the tribological properties of high speed steel under dry conditions," Tribol. Int., vol. 81, pp. 61–72, 2015, doi: 10.1016/j.triboint.2014.08.003.

[6]Y. B. Guo and C. R. Liu, "Mechanical properties of hardened AISI 52100 steel in hard machining processes," J. Manuf. Sci. Eng., vol. 124, no. 1, pp. 1–9, 2002, doi: 10.1115/1.1413775.

[7] J. D. Thiele and S. N. Melkote, "Effect of cutting edge geometry and workpiece hardness on surface generation in the finish hard turning of AISI 52100 steel," J. Mater. Process. Technol., vol. 94, no. 2, pp. 216–226, 1999, doi: 10.1016/S0924-0136(99)00111-9.

[8] Y. K. Chou and H. Song, "Tool nose radius effects on finish hard turning," J. Mater. Process. Technol., vol. 148, no. 2, pp. 259–268, 2004, doi: 10.1016/j.jmatprotec.2003.10.029.

[9] S. Siraj, H. M. Dharmadhikari, and N. Gore, "Modeling of Roughness Value from Tribological Parameters in Hard Turning of AISI 52100 Steel," Procedia Manuf., vol. 20, pp. 344–349, 2018, doi: 10.1016/j.promfg.2018.02.050.

[10] S. J. Harris, G. Krauss, M. T. Siniawski, Q. Wang, S. Liu, and Y. Ao, "Surface feature variations observed in 52100 steel sliding against a thin boron carbide coating," Wear, vol. 249, no. 10–11, pp. 1004–1013, 2001, doi: 10.1016/S0043-1648(01)00840-7.

[11] A. S. Varadarajan, P. K. Philip, and B. Ramamoorthy, "Investigations on hard turning with minimal cutting fluid application (HTMF) and its comparison with dry and wet turning," Int. J. Mach. Tools Manuf., vol. 42, no. 2, pp. 193–200, 2002, doi: 10.1016/S0890-6955(01)00119-5.

[12] E. Diniz, J. R. Ferreira, and F. T. Filho, "Influence of refrigeration/lubrication condition on SAE 52100 hardened steel turning at several cutting speeds," Int. J. Mach. Tools Manuf., vol. 43, no. 3, pp. 317–326, 2003, doi: 10.1016/S0890-6955(02)00186-4.

[13] V. S. Sharma, M. Dogra, and N. M. Suri, "Cooling techniques for improved productivity in turning," Int. J. Mach. Tools Manuf., vol. 49, no. 6, pp. 435–453, 2009, doi: 10.1016/j.ijmachtools.2008.12.010.

[14 J. Bosch and C. DellaCorte, "Rheological Characterization and Tribological Evaluation of Water-Based Lubricants in AISI 52100 Bearing Steel," Tribol. Lett., vol. 72, no. 1, 2024, doi: 10.1007/s11249-023-01811-7.

[15] T. Özel and Y. Karpat, "Predictive modeling of surface roughness and tool wear in hard turning using regression and neural networks," Int. J. Mach. Tools Manuf., vol. 45, no. 4–5, pp. 467–479, 2005, doi: 10.1016/j.ijmachtools.2004.09.007.

[16] S. K. Shihab, Z. A. Khan, A. Mohammad, and A. N. Siddiquee, "A review of turning of hard steels used in bearing and automotive applications," Prod. Manuf. Res., vol. 2, no. 1, pp. 24–49, 2014, doi: 10.1080/21693277.2014.881728.

[17] T. Tamizharasan, T. Selvaraj, and A. N. Haq, "Analysis of tool wear and surface finish in hard turning," Int. J. Adv. Manuf. Technol., vol. 28, no. 7–8, pp. 671–679, 2006, doi: 10.1007/s00170-004-2411-1.

[18] M. Nalbant, H. Gökkaya, and G. Sur, "Application of Taguchi method in the optimization of cutting parameters for surface roughness in turning," Mater. Des., vol. 28, no. 4, pp. 1379–1385, 2007, doi: 10.1016/j.matdes.2006.01.008.

[19] I. Asiltürk and H. Akkuş, "Determining the effect of cutting parameters on surface roughness in hard turning using the Taguchi method," Meas. J. Int. Meas. Confed., vol. 44, no. 9, pp. 1697–1704, 2011, doi: 10.1016/j.measurement.2011.07.003.

[20] A. Hamdan, A. A. D. Sarhan, and M. Hamdi, "An optimization method of the machining parameters in high-speed machining of stainless steel using coated carbide tool for best surface finish," Int. J. Adv. Manuf. Technol., vol. 58, no. 1–4, pp. 81–91, 2012, doi: 10.1007/s00170-011-3392-5.

[21] Panda, A. K. Sahoo, and A. K. Rout, "Statistical regression modeling and machinability study of hardened AISI 52100 steel using cemented carbide insert," Int. J. Ind. Eng. Comput., vol. 8, no. 1, pp. 33–44, 2017, doi: 10.5267/j.ijiec.2016.7.004.

[22] M. S. Karthik, V. R. Raju, K. Niranjan Reddy, N. Balashanmugam, and M. R. Sankar, "Cutting parameters optimization for surface roughness during dry hard turning of EN 31 bearing steel using CBN insert," Mater. Today Proc., vol. 26, no. xxxx, pp. 1119–1125, 2019, doi: 10.1016/j.matpr.2020.02.224.

[23] J. Kundrák, B. Karpuschewski, K. Gyani, and V. Bana, "Accuracy of hard turning," J. Mater. Process. Technol., vol. 202, no. 1–3, pp. 328–338, 2008, doi: 10.1016/j.jmatprotec.2007.09.056.

[24] W. Grzesik, K. Žak, and P. Kiszka, "Comparison of surface textures generated in hard turning and grinding operations," Procedia CIRP, vol. 13, pp. 84–89, 2014, doi: 10.1016/j.procir.2014.04.015.

[25] R. Quiza, L. Figueira, and J. P. Davim, "Comparing statistical models and artificial neural networks on predicting the tool wear in hard machining D2 AISI steel," Int. J. Adv. Manuf. Technol., vol. 37, no. 7–8, pp. 641–648, 2008, doi: 10.1007/s00170-007-0999-7.

[26] M. Chandrasekaran, M. Muralidhar, C. M. Krishna, and U. S. Dixit, "Application of soft computing techniques in machining performance prediction and optimization: A literature review," Int. J. Adv. Manuf. Technol., vol. 46, no. 5–8, pp. 445–464, 2010, doi: 10.1007/s00170-009-2104-x.

[27] H. Aouici, M. A. Yallese, K. Chaoui, T. Mabrouki, and J. F. Rigal, "Analysis of surface roughness and cutting force components in hard turning with CBN tool: Prediction model and cutting conditions optimization," Meas. J. Int. Meas. Confed., vol. 45, no. 3, pp. 344–353, 2012, doi: 10.1016/j.measurement.2011.11.011.

[28] G. Evangelista, R. S. Peruchi, T. G. Brito, P. R. Junior, and L. C. S. Rocha, "A Multivariate Statistical Quality Control of AISI 52100 Hardened Steel Turning," IEEE Access, vol. 8, no. June, pp. 109092–109104, 2020, doi: 10.1109/ACCESS.2020.3000585.

[29] P. Umamaheswarrao, D. Rangaraju, K. N. S. Suman, and B. Ravisankar, "Application of TOPSIS for multi response optimization of Process Parameters in dry hard turning of AISI 52100 steel," INCAS Bull., vol. 13, no. 1, pp. 211–224, 2021, doi: 10.13111/2066-8201.2021.13.1.22.

[30] A. Yıldız, L. Uğur, and İ. E. Parlak, "Optimization of the Cutting Parameters Affecting the Turning of AISI 52100 Bearing Steel Using the Box-Behnken Experimental Design Method," Appl. Sci., vol. 13, no. 1, 2023, doi: 10.3390/app13010003.

[31] N. Jouini, P. Revel, G. Thoquenne, and F. Lefebvre, "Characterization of surfaces obtained by Precision Hard Turning of AISI 52100 in relation to RCF life," Procedia Eng., vol. 66, pp. 793–802, 2013, doi: 10.1016/j.proeng.2013.12.133.

[32] L. H. A. Maia, A. M. Abrao, W. L. Vasconcelos, W. F. Sales, and A. R. Machado, "A new approach for detection of wear mechanisms and determination of tool life in turning using acoustic emission," Tribol. Int., vol. 92, pp. 519–532, 2015, doi: 10.1016/j.triboint.2015.07.024.

[33] J. Zhang, S. Y. Liang, J. Zhang, and S. Y. Liang, "Process Optimization of Finish Turning of Hardened Steels," vol. 6914, no. January, 2016, doi: 10.1080/10426910601016020.

[34] G. S. Ghule, S. Sanap, S. Adsul, S. Chinchanikar, and M. Gadge, "Experimental investigations on the ultrasonic vibration-assisted hard turning of AISI 52100 steel using coated
carbide tool," Mater. Today Proc., vol. 68, pp. 2093–2098, 2022, doi: https://doi.org/10.1016/j.matpr.2022.08.368.

[35] Borgaonkar and I. Syed, "Tool wear analysis in AISI 52100 steel machining with sustainable approach," Mater. Manuf. Process., vol. 39, no. 10, pp. 1369–1379, 2024, doi: 10.1080/10426914.2024.2323437.

Journal of Engineering and Technology for Industrial Applications

ISSN ONLINE: 2447-0228

ITEGAM-JETIA

Manaus, v10. n.50, p. 117-124. November/ December., 2024.
DOI: https://doi.org/10.5935/jetia.v10i50.1362

RESEARCH ARTICLE OPEN ACCESS

A RADIO FREQUENCY SYSTEM FOR SMART ATTENDANCE IN SCHOOLS

Akeem Abimbola Raji[*1], Joseph Folorunso Orimolade[2], Oluwaseun Ibrahim Adebisi[3]

[1] Department of Electrical and Electronics Engineering, Olabisi Onabanjo University, Ago-Iwoye, Ogun State Nigeria.
[2] Department of Electrical and Electronics Engineering, Afe Babalola University, Ado-Ekiti, Nigeria.
[3] Department of Electrical and Electronics Engineering, Federal University of Agriculture, Abeokuta, Nigeria.

[1] http://orcid.org/0000-0003-4303-4940, [2] http://orcid.org/0000-0002-7655-3651, [3] http://orcid.org/0000-0001-8958-4951

Email: rajiakeemabimbola@gmail.com, orimoladejf@abuad.edu.ng, adebisioluwaseun@funaab.edu.ng.

ARTICLE INFO

Article History
Received: October 28, 2024
Revised: November 6, 2024
Accepted: November 10, 2024
Published: November 30, 2024

Keywords:
Attendance,
RFID tag,
RFID reader,
Node MCU.
Smart system

ABSTRACT

Attendance is necessary in schools for curbing staff and students abseitism and lateness to classes. Traditional method of taking attendance where students write and sign on a sheet of paper is time consuming and labour intensive. This work presents smart attendance system that eases the way attendance is taken in lecture halls. The system integrates database with hardware components such as Radio Frequency Identification (RFID) card, RFID reader, I2C driver, display unit and Node Microcontroller Unit (NodeMCU) which has lower power consumption and better processing speed than Arduino microctontroller commonly used in the literature. Performance test conducted shows that the system performs its functions satisfactorily. The system reads and transfers students' data to the database in 3 seconds. In addition, students are asked to evaluate the performance of the sytem in terms of ease of use, functionality, efficiency, friendly user interface and speed of data transfer to the database. It is found that a good number of the students rate the ease of use, functionality, friendliness in the user interface and speed of data transfer excellent while more than average of the students rate the efficiency of the system good. The system is recomended for use in schools.

I. INTRODUCTION

Attendance is essential in schools and organizations for ensuring punctuality of students in classes and for preventing staff from lateness to work. Conventional methods of taking attendance include manual and swipe methods. Manual method involves students or staff writing and signing against his or her names on a sheet of paper. This approach can be easily manipulated as smart students or staff may impersonate and write on behalf of his or her colleagues making a mess of the method. The data generated from this approach cannot be relied upon and may be misleading. Though automated swipe card represents an upgrade on manual attendance where users swipe their cards on a system before gaining entry into the premises. The system can also be compromised to allow unauthorized access. In recent years, Radio Frequency Identification (RFID) technology is gaining wide usage in a number of applications including engineering construction [1-3], shopping malls and industries. The system utilizes RFID tag in line of sight with RFID reader for automatic detection and identification. The technology offers a number of advantages including security, reduced size, diversity and enhanced efficiency [3].

Previous works in the literature that have adopted this approach for different purposes include [4] which constructed RFID based robot for picking and placing an object. Researchers in [5] developed door control system that allowed users with preregistered RFID tags to gain entrance into a building. A digital sliding gate was developed in [6], where ATMEG8a microcontroller was utilized to control the servo meter. The gate opened when the system recognized the RFID card brought before it and denied access to unrecognized users. Authors in [7] constructed RFID library management system for controlling access to the library and for identification of books. Employee attendance management system was implemented in [8], where RFID tag was placed at a distance of 2cm from RFID reader before the data of the employee could be verified. RFID wireless car security system was presented in [9] for preventing car theft. Authors in [10] developed RFID system for disseminating information such as lecture and exam schedules to students. A database to track lecturer attendance in classes was developed in

[11] where each lecturer was provided with near field communication (NFC) card which was read by NFC reader. Authors in [12] introduced RFID based student attendance management system that eliminated time wastage in manual collection of attendance while works of [13-14] constructed digital attendance management system using RFID technology and Arduino uno microcontroller. According to [15] designed a tele-monitoring attendance system consisting of RFID device and photo cells. While RFID architecture was used for identification of students, photo cells were used to detect fraud. Research works in [16],[17] presented a graphical user interface application for students' attendance.

Authors in [18] developed attendance management system consisting of RFID hardware and Microsoft visual basic application as database. According to [19] developed student identification system for checking and admiting students into the examination hall. Authors made use of Arduino microcontroller series for configuring the sytem.

This work develops a smart attendance system where radio frequency technology is used for taking attendance of students in classes. In particular, ESP8266 microcontroller is used for improving the speed of information transfer from the hardware to the database and for improving the efficiency of the system. The microcontroller has better processing speed and requires less power than Arduino microcontroller hitherto used in the literature.

II. MATERIAL AND METHODS

II.1 OVERVIEW OF THE SYSTEM

Figure 1 illustrates the block diagram of the proposed smart attendance system which shows the interaction between the hardware and software parts. The hardware includes power supply unit, RFID card, RFID card reader, Node Microrolller Unit (NodeMCU) and display unit while the software part includes the database. Each unit is described as follows.

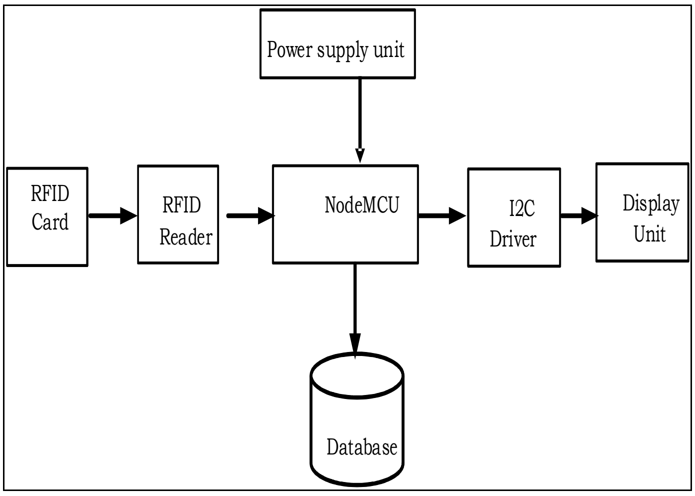

Figure 1: Block diagram of the proposed smart attendance system.
Source: Authors, (2024).

II.2 POWER SUPPLY UNIT

The power supply provides the required voltage for proper functioning of the system hardware components. It ensures that NodeMCU, RFID reader and display unit receive stable and regulated power required for reliable operation. NodeMCU and RFID reader typically operate at 3.3V or 5V, while the display unit requires a 5V supply. A 5V D.C battery from laptop or desktop is utilized to power the system.

II.3 RADIO FREQUENCY IDENTIFICATION (RFID) CARD

Radio Frequency Identication (RFID) cards contain a chip and an antenna. The chip stores a unique identification (UID) number and the antenna allows the card to communicate with the RFID reader. When an RFID card comes within the range of an RFID reader, the reader sends out a radio wave signal which is picked by the RFID card antenna. Figure 2 shows the RFID card.

Figure 2: RFID card.
Source: [20].

II.4 RFID READER

RFID reader is utilized to detect and read RFID cards, extracting their UID number on the card. It reads the UID number and determines if it corresponds to a known student or a new card. For recognized cards, it records attendance by linking the UID to student data, such as name and matriculation number. Students' details are transmitted to the database through Wi-Fi using HTTP request, typically formatted in JavaScript Object Notation (JSON). It is an essential component for efficient attendance tracking, ensuring seamless communication between RFID cards and digital records in the database. Figure 3 illustrates the RC522 RFID card reader.

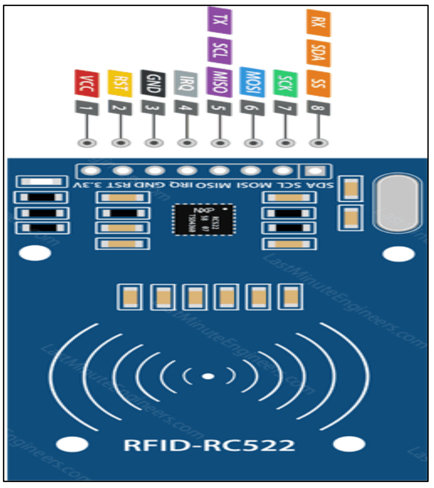

Figure 3: RC522 RFID Reader.
Source: [21].

II.4 NODE MICROCONTROLLER UNIT (NODEMCU)

Node Microcontroller Unit (NodeMCU) is an open source Internet of Things (IoT) platform that consists of ESP8266 Wi-Fi chip. Its primary function encompasses wireless connectivity, data processing, RFID communication, data storage and transmission. It is used to coordinate the activity of the system by interacting with various hardware components to enable efficient attendance tracking and database communication. It processes data from the RFID reader, manages display unit, and provides visual feedback. It connects to a local Wi-Fi network to facilitate communication with a database for data storage. Key pins associated with Wi-Fi connectivity in NodeMcU include transmitter (TX) and receiver (RX) pins. It communicates with the RFID reader using pins D8 (GPIO15) and D2 (GPIO4). Figure 4 illustrates the pin configuration of NodeMCU.

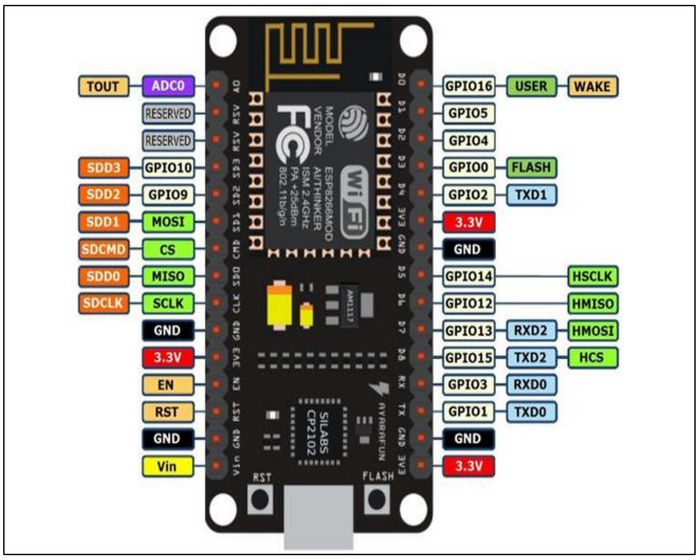

Figure 4: Pin configuration of NodeMCU.
Source: Authors, (2024).

II.6 DISPLAY UNIT

The Liquid Crystal Display (LCD) is used for providing a user-friendly interface for the smart attendance system. It is utilized for displaying important information to the users in real-time. It displays messages for successful scan and error messages when RFID cards are not scanned by RFID reader. In addition, it displays the activities of the the proposed smart attendance system at every point in time. It enhances the overall user experience by making the system more interactive and informative, facilitating efficient attendance tracking. Figure 5 shows the pin configuration of LCD.

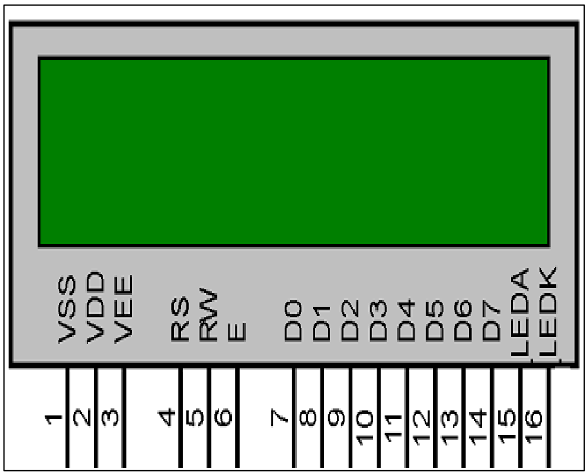

Figure 5: Pin configuration of 16X2 LCD.
Source: [22].

II.7 I2C DRIVER

The I2C driver handles communication between NodeMCU and LCD making it easier to display text. Figure 6 shows the I2C driver.

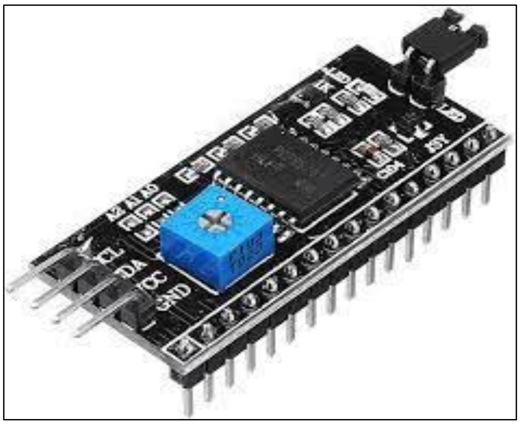

Figure 6: PCF 8574 I2C Driver
Source: Authors, (2024).

II.8 DATABASE

The database is used to store and keep the attendance of the students. Google spread sheet is utilized as database for keeping the students' attendance record.

The proposed smart attendance system is implemented using the the flow chart presented in Figure 7.

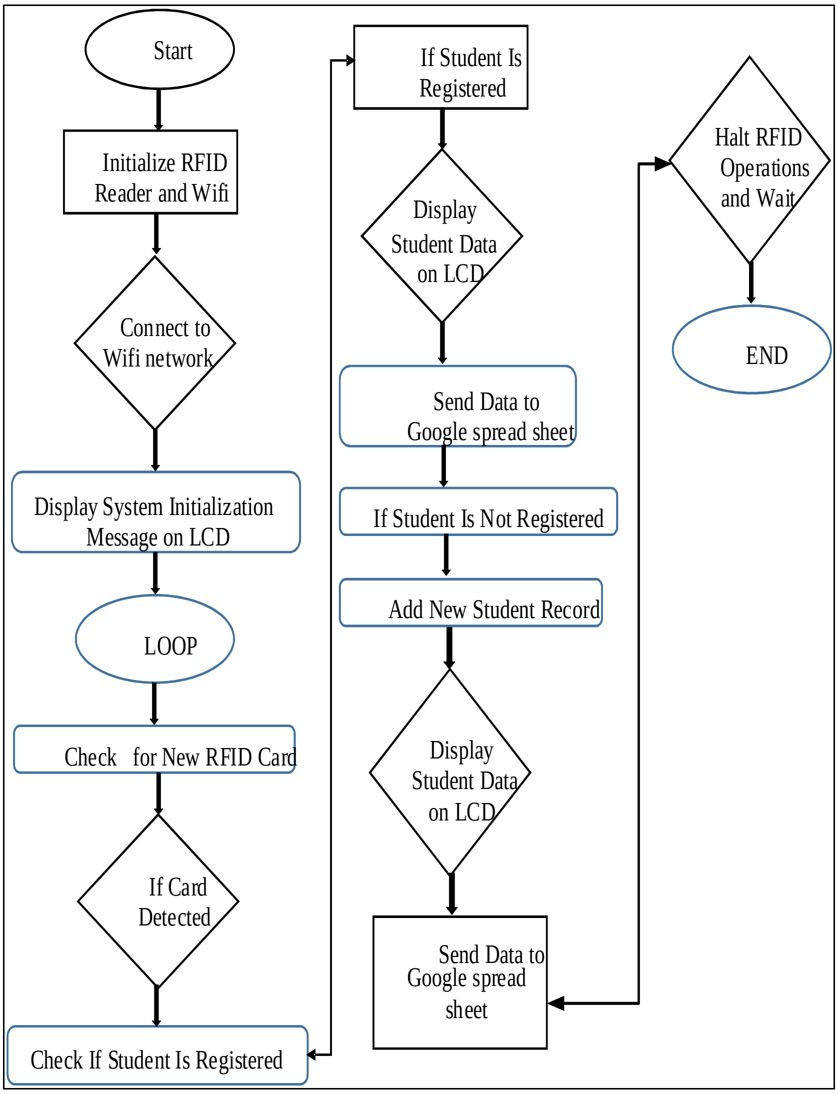

Figure 7: Flow chart of operation of the proposed RFID smarte attendance system.
Source: Authors, (2024).

II.8 DESIGN ALGORITHM OF THE PROPOSED SMART ATTENDANCE SYSTEM

The following algorithm highlights the steps taken in implementing the proposed smart attanance system which further explains the flow chart presented in Figure 7.

Algorithm: Operational sequence of wireless RFID system.

Step 1: Initialize the RFID reader and Wi-Fi module.
Step 2: Connect to the designated Wi-Fi network.
Step 3: Display a system initialization message on the LCD.
Step 4: Enter a continuous loop to monitor RFID card detection.
Step 5: If a new RFID card is detected:
Check if the student is registered in the system
If registered
Display the student's data on the LCD.
Send attendance data to the Google spreadsheet
If not registered
Add a new student record
Display the student's data on the LCD
Send attendance data to the Google spread sheet
Halt RFID operations temporarily to avoid multiple scans for the same card
Step 6: Repeat the loop
End

III. RESULTS AND DISCUSSION

III.1 SMART ATTENDNACE SYSTEM DEVELOPMENT RESULT

Figure 8 illustrated the internal circuit connection of the proposed smart attandance system where RST pin of the RFID card reader was connected to D3 (Digital GPIO Pin) of NodeMCU while MISO, MOSI, SCK, and SDA pins of RFID reader were connected to D6, D7, D5, and D4 (Digital GPIO Pins) of NodeMCU. These connections ensured communication between NodeMCU and RFID module which facilitated the reading of RFID tags. In addition, SDA and SCL pins of LCD were connected to D2 and D1 (Digital GPIO Pins) of NodeMCU. For power supply considerations, the VCC pins of both RFID card reader and LCD were connected to 3.3 V output of NodeMCU while GND pins of these components were connected to the ground (GND) of

NodeMCU. This hardware setup was complemented by a Google spreadsheet which was used as database for storage and retrieval of students' attendance data.

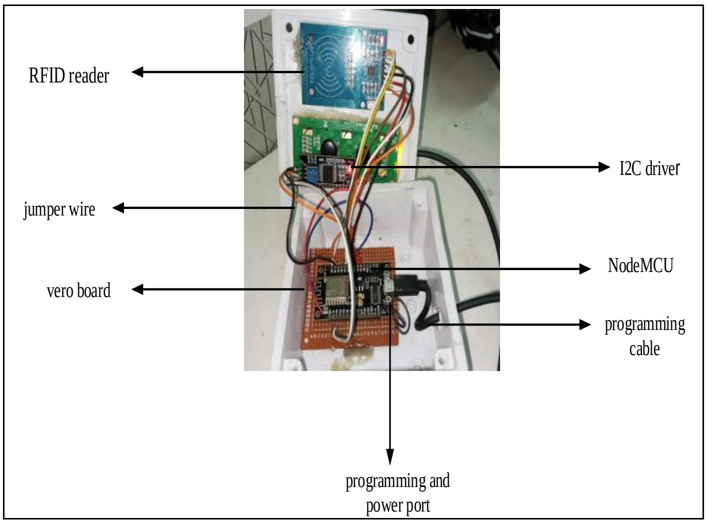

Figure 8: Internal components of the proposed smart attendance system.
Source: Authors, (2024).

III.2 PERFORMANCE EVALUATION RESULT

The proposed system was subjected to tests to verify and asses its performance. Figure 9a illustrated the proposed system connecting to Wi-Fi module on a laptop while Figure 9b depicted the snapshot of the prompt message which instructed the user to place the RFID card. Figure 10a illustrated the proposed system reading the information on RFID card while Figure 10b illustrated the transfer of the information on RFID card to Google spreadsheet. It was therefore seen that the system read RFID tag data successfully, constructed JSON payload, and utilized HTTP to communicate with Google sheet, displaying feedback on LCD screen.

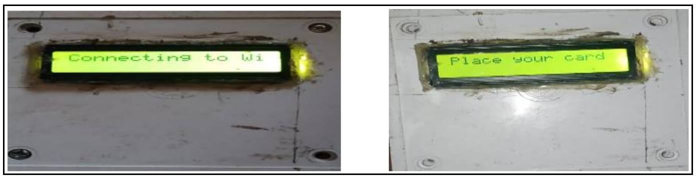

Figure 9: Proposed system under test, (a) system connecting to Wi-Fi module (b) system requesting for placement of card.
Source: Authors, (2024).

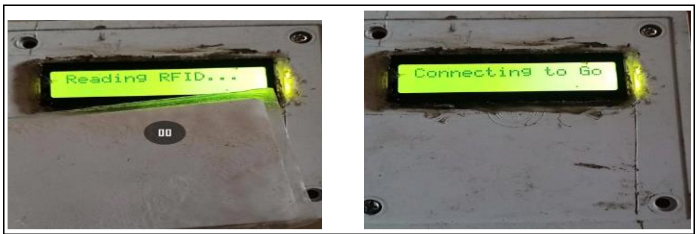

Figure 10: Proposed system under test (a) system reading the RFID card and (b) system directing the student details to the Google sheet.
Source: Authors, (2024).

Figure 11 presented the spreadsheet which revealed students's details such as the date of the class, time of the class, matric number and names of the students, UID number as well as the address of the students in the class.

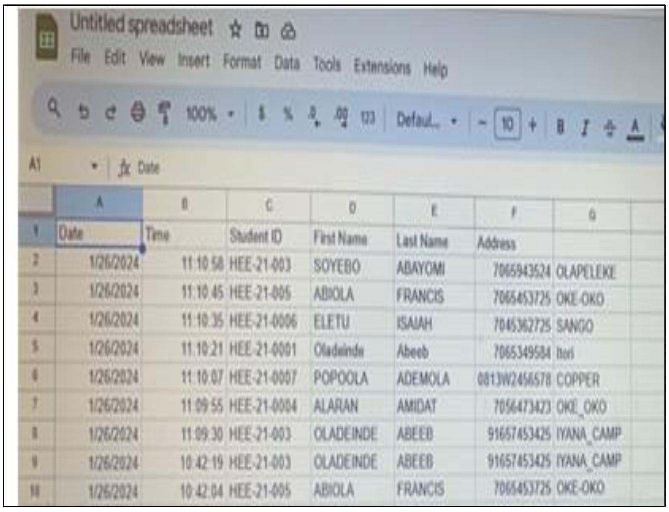

Date	Time	Student ID	First Name	Last Name	Address	
1/26/2024	11:10:58	HEE-21-003	SOYEBO	ABAYOMI	7065943524	OLAPELEKE
1/26/2024	11:10:45	HEE-21-005	ABIOLA	FRANCIS	7065453725	OKE-OKO
1/26/2024	11:10:35	HEE-21-0006	ELETU	ISAIAH	7045362725	SANGO
1/26/2024	11:10:21	HEE-21-0001	Oladeinde	Abeeb	7065349584	Ilori
1/26/2024	11:10:07	HEE-21-0007	POPOOLA	ADEMOLA	0813W2456578	COPPER
1/26/2024	11:09:55	HEE-21-0004	ALARAN	AMIDAT	7056473423	OKE_OKO
1/26/2024	11:09:30	HEE-21-003	OLADEINDE	ABEEB	91657453425	IYANA_CAMP
1/26/2024	10:42:19	HEE-21-003	OLADEINDE	ABEEB	91657453425	IYANA_CAMP
1/26/2024	10:42:04	HEE-21-005	ABIOLA	FRANCIS	7065453725	OKE-OKO

Figure 11: Snapshot of students' attendance.
Source: Authors, (2024).

A closer look of Figure 11 demonstrated the system's functionality which pointed to the fact that there existed synchronization and effective communication between hardware and software parts. This further implied that Google script in the spreadsheet communicated successfully with the NodeMCU, enabling real-time attendance taking and data transfer between the system and the spreadsheet. It was seen also that the Google App. script embedded in the spreadsheet, processed HTTP POST requests and updated the spreadsheet as more data were received. It was found that it only took 3s for the system to read and store information of students present in a class.

Furthermore, the students were tasked to assess the proposed system in terms of ease of use, efficiency, functionality, user interface friendliness and speed of data transfer to the database. The criteria and rating presented in Table 1 were used to assess the performance of the system. Table 2 therefore presented the summary of qualitative asssessment of the system.

Table 1. Rating criteria for assessing the system

Criteria	Excellent	Good	Average	Bad	Poor
Rating	5	4	3	2	1

Source: Authors, (2024).

Table 2: Summary of qualitative assessment of the system by the students

Criteria	Excellent	Good	Average	Bad	Poor
Ease of use	5	2	0	0	0
Functionality	4	3	0	0	0
Friendliness in user interface	5	1	1	0	0
Ffficiency	3	4	0	0	0
Speed of data transfer to the database	6	1	0	0	0

Source: Authors, (2024).

Using table 2, Figures 12-16 presented the percentage distribution of the scores of the assessment of the proposed system by the students.

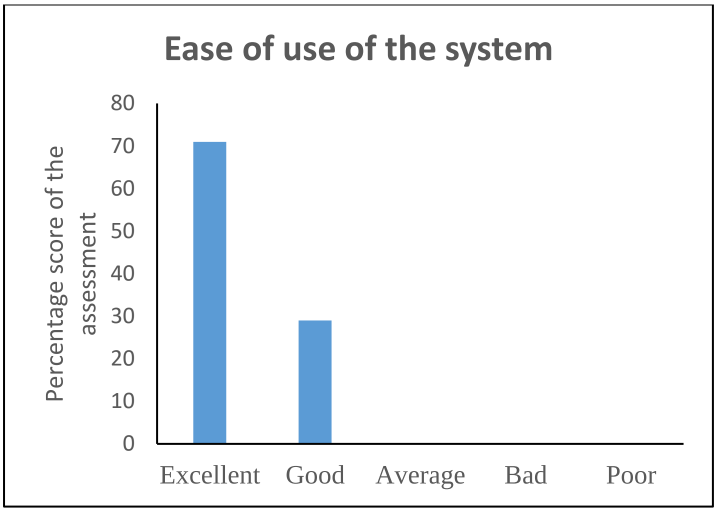

Figure 12: Result of the asseement of ease of use of the propsed system.
Source: Authors, (2024).

It was seen in Figure 12 that 71% of the students rated the ease of use of the sytem excellent while 29% rated it good. It was also oberved that average, bad and poor ratings of the proposed system had no scores.

Figure 13: Result of the asseement of functionality of the system.
Source: Authors, (2024).

It was observed from Figure 13 that 57% of the students rated the functionality of the system excellent while 43% rated it good. No score was howerver recorded for average, bad and poor ratings.

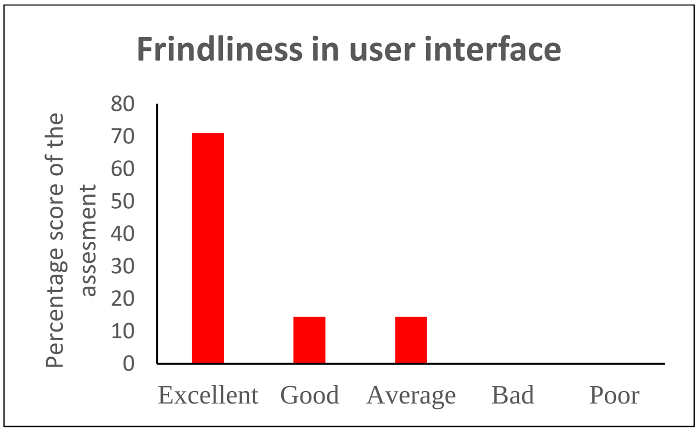

Figure 14: Result of the asseement of user interface friendliness
Source: Authors, (2024).

In terms of friendliness in the user interface of the proposed system, Figure 14 showed that 71% rated the system excellent while 14.5% and 14.5% rated the system good and average, respectively. It was seen also that bad and poor criteria had no score.

Figure 15: Result of the asseement of efficiency of the system.
Source: Authors, (2024).

Figure 15 showed that 43% of the students rated the efficiency of the system excellent, 57% rated it good while no student rated the system average, bad and poor.

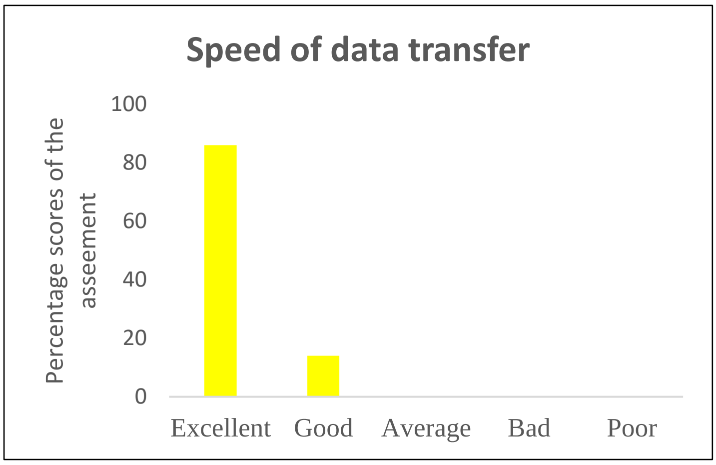

Figure 16: Result of the asseement of speed of data transfer of the system.
Source: Authors, (2024).

It was observed in Figure 16 that 86% of the students rated the speed of data transfer to the database excellent while 14% rated it good. Average, bad and poor ratings of the system had no scores.

Furthermore, the present work was compared with a few of existing works in the literature in terms of features such as connectivity, speed of information transfer, technology used, microcontroller used, power consumption and database. Table 3 presented the outcome of this comparison.

Table 3: Result of the comparison of the present work with previous works existing in the literature.

Characteristics features	Reference [12]	Reference [13]	Reference [14]	Reference [17]	Proposed work
Technology	RFID	RFID	RFID	RFID	RFID
Connectivity	Blue tooth	Blue tooth	Blue tooth	Blue tooth	Wi-Fi or IEE802.11
Speed of information transfer	Slow	Slow	Slow	Slow	Fast
Microcontroller used	Arduino	Arduino	Arduino	Arduino	NodeMCU (ESP8266)
database	Yes	No	No	Yes	Yes
Power consumption	Medium	Medium	Medium	Medium	low

Source: Authors, (2024).

It could be seen from Table 3 that the proposed work improved on the existing work in terms of the use of ESP8266 microcontroller which made the sytem to consume less power and enhanced the rate at which information was sent to the database.

IV. CONCLUSIONS

This work proposed a smart system based on radio frequency technology for taking attendance of students in a class. The system consisted of ESP8266 (Node Microcontroller Unit) for coordinating the activities of RFID reader, RFID card, I2C driver, display unit and database. The implementation of the overall system allowed students attendance to be taken and stored on Google spread sheet in a fast and efficient manner. The average time for the system to read RFID card and transfer students' details to the Google spreadsheet was 3s. In additon, the performance of the system was assesssed by the students based on the criteria such as ease of use of the system, functionality, friendliness in user interface, efficiency and speed of data transfer to the database. Results of the qualitative evaluation revealed that 71% of the students rated the ease of use of the system excellent while 29% rated it good. 57% and 43% of the students rated the functionality of the system excellent and good, respectively while 71%, 14.5%, and 14.5% rated the user interface excellent, good and average respectively. The efficiency of the system received 43% excellent and 57% good from the students. Moreover, 86% and 14% of the students rated the speed of transfer of data to the database excellent and good, resepectively. The system is recommended for use in schools and business outlets for taking the attendance of students and workers.

V. AUTHOR'S CONTRIBUTION

Conceptualization: Akeem Abimbola Raji
Methodology: Akeem Abimbola Raji, Joseph Folorunso Orimolade, Oluwaseun Ibrahim Adebisi
Investigation: Akeem Abimbola Raji, Joseph Folorunso Orimolade, Oluwaseun Ibrahim Adebisi
Discussion of results: Akeem Abimbola Raji, Joseph Folorunso Orimolade, Oluwaseun Ibrahim Adebisi
Writing – Original Draft: Akeem Abimbola Raji
Writing – Review and Editing: Joseph Folorunso Orimolade, Oluwaseun Ibrahim Adebisi
Resources: Akeem Abimbola Raji, Joseph Folorunso Orimolade, Oluwaseun Ibrahim Adebisi
Supervision: Akeem Abimbola Raji, Joseph Folorunso Orimolade, Oluwaseun Ibrahim Adebisi
Approval of the final text: Akeem Abimbola Raji, Joseph Folorunso Orimolade, Oluwaseun Ibrahim Adebisi

VI. ACKNOWLEDGMENTS

The authors are grateful to the several authors whose works formed the basis for the present work.

VII. REFERENCES

[1] C. Kim, Y. Ju and J-H Kim. "*Resource management in civil construction using RFID technology*", Proceedings of 26th International Symposium on Automation and Robotics in Construction, pp. 105-108, 2009.

[2] P. Patil and A. Shelake. "*An application of RFID technology to improve material management in construction sites*", International Research Journal of Engineering and Technology, vol. 8, no. 2, pp. 1000-1003, 2021.

[3] L-C Wang, Y-C Lim and P.H. Lim. " *Mobile construction RFID-based supply chain management portal system*," Joint International Conference on Computing and Decision making in Civil and Building Engineering, June 14-16, Montreal, pp. 2751-2761, 2006.

[4] P. Kumari, L. Mathew and N. Kumar, "*Combining Bio signals with RFID to develop a multimodal-shared control interface*", Journal of Engineering and Applied Science, vol. 70, no. 119, pp. 1-15, 2022.

[5] S.M.R. Rasid, F. Rashid, A-H Sabri and Rakibul Islam, "*Design and construction of automatic security system of a door using RFID technology*", International Journal of Scientific & Engineering Research, vol. 9, no. 9, pp. 1067-1073, 2018.

[6] A.M. Adebimpe, D. Chukunebikpe, D. Uguru-Okorie and D.V. Arise, "*Design and Implementation of a digital sliding gate using RFID technology*", Fuoye Journal of Engineering and Technology, vol. 7, no. 1, pp. 53-56, 2022.

[7] E.O. Edwards and P.E. Orukpe, "*Development of a RFID based Library management system and user access control*", Nigerian Journal of Technolgoy (NIJOTECH), vol. 3, no. 4, pp. 574-584, 2014.

[8] G.D.P Maramis and P.T.D Rompas, "*Radio frequency identification (RFID) based management system*", IoP Conf. Series: Materials Science and Engineering, 2018. Doi: 10.1088/1757-899x/306/11012045.

[9] A.S. Hassan and M.A Saleh, "*Design and construction of RFID wireless car security system*", International Journal of Scientific Engineering and Science, vol. 1, no. 6, pp. 61-65, 2017.

[10] Sambo et al, "*An RFID-based student information system*", Proceedings of 2017 IEEE 3rd International Conference on Electro-Technology for National Development, pp. 477-482, 2017.

[11] G.S.E. Putra, A. Lee I.M.T. Mahayara and I.G.A.W Dharmayasa, " *Design and development of lecturer attendance system using Radio Frequency Identification*", International Journal of Computer Science Engineering, vol. 10, no. 1, pp. 15-27, 2021.

[12] O.T. Arulogun, A. Olatunbosun, O.A. Fakolujo and O.M. Olaniyi, " *RFID-based students attendance*", International Journal of Scientific & Engineering Research, vol. 4, no. 2, pp. 1-9, 2013.

[13] A.C. Ohajianya, V.N. Ebomuche, C.E. Agbo, and G.A. Ikeh, " *Design and Development of a Radio Frequency Identification (RFID) based digital attendance system with master's E-identity card controlled access to the attendance taking mode*", ARPN Journal of Engineering and Applied Sciences, vol. 15, no. 20, pp. 2210-2219, 2020.

[14] O.C. Peter, O.L. Uwakwe, and C.C. Okoli, "*Implementation of an RFID technology based digital class attendance system for university students*", Journal of Emerging Trends in Engineering and Applied Sciences (JETEAS), vol. 13, no. 5, pp. 199-207, 2022.

[15] M.A.H. Ali, and N.A. Yusoff, "*Development of Tele-monitoring Attendance System using RFID and photo-cell*", Proceedings of 2018 IEEE International Conference on Automatic Control and Intelligent Systems, pp. 83-88, 2018.

[16] M. Kassim, H. Mazlan, N. Zaini and M.K. Salleh, "*Web-based student attendance system using RFID technology*", Proceedings of 2012 IEEE Control and System Research Colloquim (ICSGRC), pp. 213-218, 2012.

[17] A.A.Olanipekun and O.K. Boyinbode, "*A RFID based Automatic Attendance System in Educational Institutions in Nigeria*", International Journal of Smart Home, vol. 9, no. 12, pp.65-74, 2015

[18] T.C. Adeniran, Y. Sanni, N. Faruk, and A. Olawoyin, " *Design and Implementation of an Automated Attendance Monitoring System for a Nigerian University using RFID*", Africa J. Comp.& I.C.T. vol. 12, no. 2, pp. 72-89, 2019.

[19] A. Oyedeji, I. Okakwu, and O. Abolade, " *Development of an enhanced student identification system*", Firat University Journal of Experimental and Computational Engineering, vol. 2, no. 2, pp.80-86, 2024.

[20] S. Subashchandrabon and M. Pajany, " *Hybrid of Student Attendance Tracking System using RFID Device and Finger Print Sensor*", International Journal of Computer Science and Mobile Computing, vol. 4, no. 3, 271-278, 2015.

[21] S.H.V.K. Ashok, N.D. Divya, F. Samuel, U. Mande, "*RFID Based Attendance System" International Journal for Research in Applied Science & Engineering Technology*", pp. 2239-2248, 2022.

[22] A.I. Aniebiet and M. AbdulKadir, "*Design and Construction of an RFID based Automatic Attendance Management System*" International Journal of Scientific & Engineering Research, vol. 11, no. 12, pp. 1223-1264, 2020.

Journal of Engineering and Technology for Industrial Applications

ITEGAM-JETIA

Manaus, v10. n.50, p. 125-132. November/ December., 2024.
DOI: https://doi.org/10.5935/jetia.v10i50.1374

ISSN ONLINE: 2447-0228

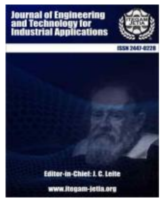

RESEARCH ARTICLE OPEN ACCESS

MICROSTRUCTURAL INVESTIGATIONS ON THE FRACTURAL BEHAVIOR OF SS304 BUTT JOINTS DEVELOPED THROUGH VIBRATORY WELDING

K. Ch Sekhar*[1], Dr Rashmi Dwivedi[2], Dr. V.V. Rama Reddy[3]

[1] Department of Mechanical Engineering, School of Engineering, Sri Satya Sai University of Technology & Medical Sciences, Sehore, M.P., India
[2,3] Department of Mechanical Engineering, Lendi Institute of Engineering and Technology, Vizianagaram, Andhra Pradesh, India

[1] https://orcid.org/0000-0002-6081-8571, [2] https://orcid.org/0000-0002-9755-5330, [3] http://orcid.org/0009-0000-5720-2525

Email: sekhar.lendi@gmail.com, rashmidwivedi29@gmail.com, siri_venkat@rediffmail.com

ARTICLE INFO

Article History
Received: June 11, 2024
Revised: November 6, 2024
Accepted: November 10, 2024
Published: November 30, 2024

Keywords:
vibratory welding,
fractural analysis,
mechanical properties,
crack sensitivity,
grain refinement.

ABSTRACT

Determination of weld strength through the fractural behaviour at different loads plays dominant role for selection of weld process in real-time applications. Assistance of vibratory treatment to the conventional welding process can bring major changes in the microstructure of weldment at greater extent. The intervention of increment and decrement in the mechanical properties at different vibratory welding parameters dependent on the grain refinement. The study focuses on analyzing microstructural transformations' influence in the weldments on different mechanical properties at various amplitudes and voltages of 2, 4, 6V. The tests such as tensile, Rockwell hardness and Charpy impact are conducted and fracture modes are identified. SEM analysis is performed to characterize the microstructure of different fractures between the developed butt joint on SS304 and susceptibility to crack is investigated. The fracture is exhibited as more ductile for samples developed with the assistance of vibratory treatment to the gas metal arc welding process. The decrease of columnar dendrites at weld zone and paradigmatic shift to equiaxed shapes under vibratory treatment prompted to achieve maximum enhancement in the mechanical properties and reduction of delta ferrite is responsible for decrement for further ranges.

I. INTRODUCTION

Substantial increment in the demands to produce superior standard products at low-cost driven advancements in the traditional manufacturing methods. Vibratory treatment is most notable advancement to the traditional welding process to minimize the defects of weldment and significant improvement in the weld strength [1],[2]. Studies are proven that the vibratory treatment can enhance the heat transfer at the weld pool which reduce the defects caused by porous regions, blow holes, spilling of weld material etc. [3]. But the analysis over influence of applied vibration parameters such as amplitude, frequency and time is essential to achieve maximum enhancement in the mechanical properties of the weldment [4].

According to [5] performed extensive analysis over influence of vibratory treatment parameters on the tensile strength of the joint in the pulsed ultrasonic tungsten arc welding process and heat evacuation is responsible for achieving maximum enhancement. Singh et al. investigated the influence of work piece frequency on the hardness of the butt joint made under vibratory treatment assistance to shielded metal arc welding process and achieved maximum enhancement at 250 Hz with fine grain structure [6]. Mostafapour and Gholizadeh studied the dependence of vibratory treatment parameters over the impact resistance of the weldments made on SS304 through TIG welding process and noted that the workpiece frequency, electrode voltage are the most dominant parameters among the amplitude, time, current, and welding speed [7]. Given high range frequencies of 15kHz for the welding of AZ31 sheet through TIG welding process and attained the greater reduction in grain size at interstitial sites is responsible for obtaining maximum enhancement in the microhardness [8]. Attempted to study the influence of various types of vibratory treatment in the gas metal arc welding (GMAW) process and observed that the reduction of temperature of molten droplet with the oscillation given to weld pool is essential to attain maximum heat transfer [9]. Weglowska and Pietras studied the grain refinement in the welding of thermoplastics through SEM analysis and stated that the orientation of finer grains is a responsible factor to attain the maximum enhancement in the tensile strength at highest electrode voltage of 20V [10].

Studied the influence of vibratory treatment over the microstructure and mechanical properties over the 316L stainless steel joints developed by using gas-tungsten arc welding and observed the columnar type dendrites exhibited lower length than the equiaxed dendrites which contributed to exhibit higher mechanical properties than the non-vibratory assistance [11]. Applied Taguchi analysis for optimizing process parameters in the vibratory welding to achieve maximum enhancement in the hardness of the butt joint and performed microstructural analysis to study the grain refinement in weldments. It is observed that the auxiliary vibrations supplied to weld zone prompted to significant refinement in the grain structure and leads to improvement in the studied mechanical property [12]. According to [13] applied flux cored arc welding supported with vibratory treatment and studied the influence over microstructure of the weldments. It is observed that proeutectoid ferrite occupied more than the ferrite side, acicular ferrite in the weld zone and observed the effective integrated balance achieved between the yield strength, toughness of the metal. Studied the mechanical properties of CO2 arc welding under the assistance of vibratory treatment and observed that the fatigue life, microhardness are significantly improved with the minimum deformation and residual stress formation [14]. For [15] investigated the microstructure of the weld zone formed through arc welding of AA-5083-H321 of similar metals and observed that the grain size is reduced from 200 to 50 µm under the influence of harmonic vibrations at the time interval of 30 mins.

The research is focused to investigate the microstructural behavior of the weldments developed through GMAW on SS304 under the assistance of vibratory treatment at different electrode voltages and analyze the response on tensile, impact strength [16]. Section-2 presents the materials used in this research along with the methods employed to produce the butt joint and conduct the experimentation. Section-3 presents the results obtained about the studying mechanical properties and SEM analysis to characterize the weldment in terms of enhancement or decrements in the studying properties at different electrode voltages and discusses the grain refinement with the introduction of vibratory treatment in the weld joint. Section-4 concludes the article by stating overall theme of conducted research and major identifications in the performed experimental investigations on vibratory treatment assisted GMAW process.

II. MATERIALS AND METHODS

Gas metal arc welding is preferred to develop the but joint with the assistance of vibratory treatment and SS304 of 5mm gauge is preferred as the base material for the similar welding. ER309 L is selected as the filler material and the chemical composition of the base and filler materials are listed in Table 1.

Table 1 Chemical composition of weld materials

Material	C	Mn	P	S	Ni	Si	Cr	Balance
SS304	0.09	<2.5	<0.048	<0.06	10.4	<1.02	18	Fe
ER309L	0.034	1.28	0.027	0.63	12	0.68	26	Fe

Source: Authors, (2024).

The single V-type butt joint is developed at the angle of 700 in the region of joint and opening of root is maintained as 3 and base is kept at 2mm by considering the thickness of the procured SS304 sheets. The line of welding is considered during the preparation of the samples and it is taken as the perpendicular to the direction of rolling [17]. A novel vibratory welding equipment is designed and fabricated in order to create butt joint through the dissimilar GMAW process from mild steel and stainless-steel plates. The butt joints are made at various frequencies from 600 to 1000 Hz while keeping the time period as constant at each frequency. For every cycle, the time period of each vibration is kept constant for 100 sec at each vibration frequency based on the crystallization temperature of the selected metals for welding. It is known that the SS304 and mild steel start crystallization at the temperature of 420 to 4600C [18]. Although the temperature for recrystallization is very low compared to actual weld pool temperature which is 26000C, still the experimentation is carried out up to maximum range and certain time is allowed for temperature drop to recrystallization state. The experimentation is carried out by manipulating at different ranges of frequences, amplitudes and the observations are made out to investigate the mechanical properties of butt joint at each parameter setting [19]. The highest frequency of workpiece is fixed at 1000 Hz based on the condition of making amplitude less than 0.5mm. Because after crossing the 1000 Hz, there is a possibility of crossing the spark gap greater than 3.0 mm which hinders the welding process [20].

The samples required to conduct the uniaxial tensile, Charpy impact and Brinell hardness tests are prepared according to ASTM D368, E10 and 23 standards. The weldability and susceptibility to crack of weldment is evaluated by conducting the Varestraint hot-ductility test. The microstructure at the welded zone for tensile, impact strength, hardness tested samples are characterized through SEM analysis [21]. The etching process is performed by using 5% Nital reagent {HNO3 (5ml) + ethyl alcohol (100ml)} over these samples in order to remove the blackspots and smoky layer created over the weld zone during the GMAW process.

III. RESULTS AND DISCUSSION

III.1 MICROSTRUCTURES AT DIFFERENT WELD ZONES

The microstructure of the developed butt joint through GMAW process under the assistance of vibratory treatment is characterized through scanning electron microscopy (SEM) technique. The weldments created between the two similar metals of SS304 are tested immediate to the welding process after their solidification. It is observed that the degree of dilution has major influence over the microstructure of the weldments and the increase in electrode voltage reduced the dilution process by rapid decrement in the temperature at the weld zone [22]. Similar effect is observed over the mechanical properties at which the increment in them is found with the decrease of dilution degree. The improvement in heat transfer through convection mode with the effective reduction of conduction to the non-involving (welding process) portions of base metal through the turbulence created by the vibratory treatment. As the convection mode heat transfer is higher, the lower melting of base metal is observed with the increase of electrode voltage.

Figure 1(a) represents the SEM analysis carried over the weld edges at where the interface between weld metal and base metal. It can be observed that the existence of fine side grains at the taken zone which are formed with the effect of higher cooling rates. The temperature gradient is significantly higher in this zone as there is no specific preheat treatment is employed before the GMAW process and it leads to generation of fine surface nuclei on SS304. In later stages, those nuclei are prompted for the effective conversion of fine side grains at the identified zone and those are incapable to exhibit greater resistance over the fracture due stretching of grains at the weld interface. The existence of equiaxed grains is very low in this zone due to the susceptibility of generating columnar dendrites towards the centre of the weldment instead the boundary zone [23].

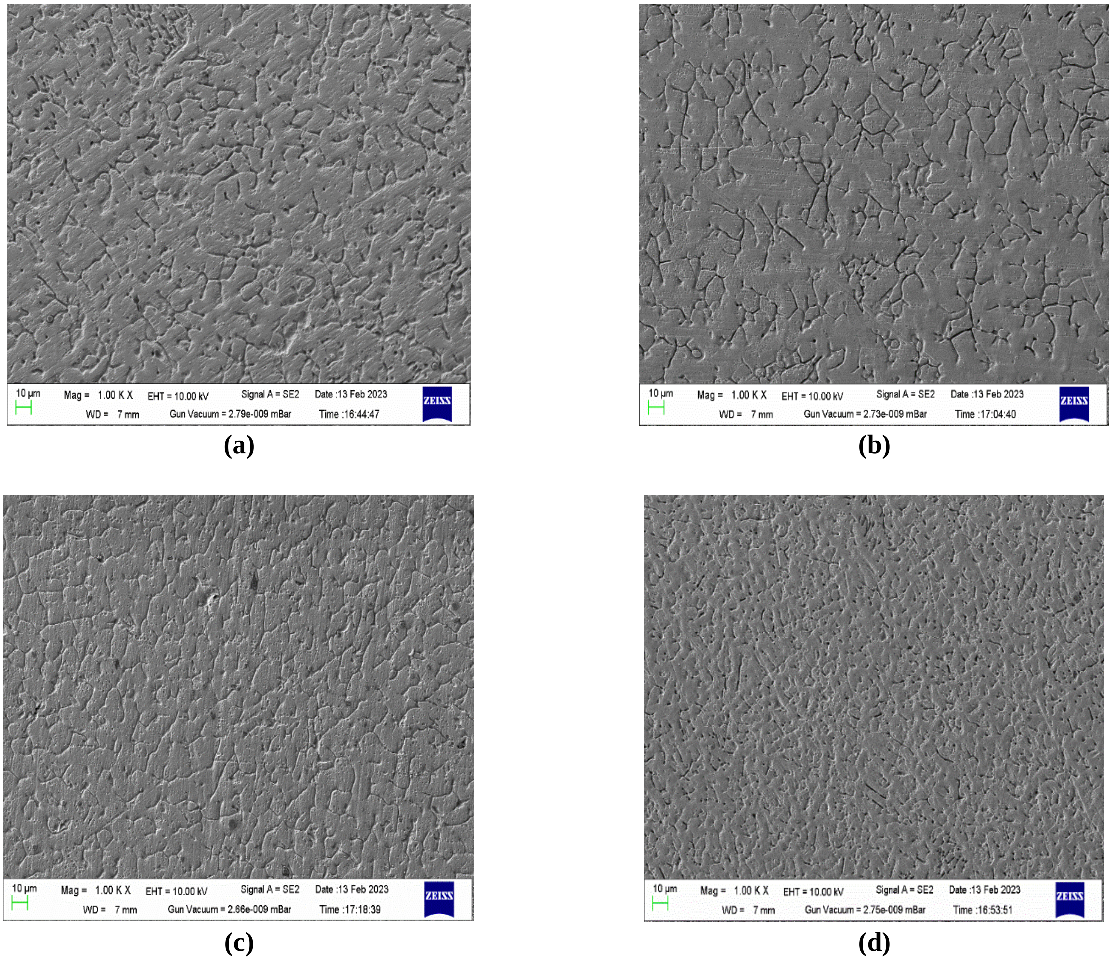

Figure 1: Microstructures at various vibratory weld conditions (a) at weld and base metal interface (b) at intermediate zone with electrode voltage of 2V (c) at intermediate zone with electrode voltage of V (d) at intermediate zone with electrode voltage of 6V.
Source: Authors, (2024).

Figure 1(b) represents the SEM analysis performed at the intermediate zone at where the complete dilution of base metal and filler material occurred at lower electrode voltage such as 2V. The appearance of smaller sized grains in the microstructure shown the existence of austenite with the combination of delta ferrite at the boundaries. The presence of ferrite stabilizing elements in the filler material have shown significant influence at this zone but the accumulation of such elements at the sub grain boundaries due to occurrence of eutectic reactions. The tendency to form of strength improvement barrier such as austenitic-ferritic at this zone is observed after the solidification [24]. The competitive growth into large number of bundles at grain boundaries are strong hinderance for the strength improvement.

Figure 1 (c) represents the SEM analysis performed at the intermediate zone at where the lower dilution of base metal and approximate dilution of filler material at 4V. It can be observed clearly that the growth of grain boundaries into different directions and great misorientations in the sub-grain boundaries. This phenomenon is mostly occurred in the ductile type materials such as SS304 which referred as "high-angle grain boundaries" and formation of such can lead to occurrence of cracks after solidification.

Figure 1 (d) represents the SEM analysis performed at the intermediate zone at where the lower dilution of base metal and complete dilution of filler material at 6V. It can be observed clearly that the growth of grain boundaries followed uniform orientation at the sub-grain boundary and clearly drawn a division between the dendrites, adjacent sub-grains. Although the misorientation is existed, still the degree of such is acceptable due to the growth of sub-grains along the crystallographic directions. It can be drawn a significant reduction in the size of dendrites in the weldment of SS304 from 648.02 to 93.67 µm. No cracks or discontinuities are appeared in the microstructure of butt joint and the areas are broadly stretched towards the centre of the weldment.

It is observed from the performed SEM analysis that the complete elimination of the unmixed weldments and greater heat gradients due to the applied vibratory treatment. The increase in the electrode voltage from 2 to 6V created a path for greater turbulence of weld pool and promote the heat evacuation. The movement of filler material towards to diluted base metal is improved and complete immersion become possible with the electromagnetic vibrations during GMAW process [25].

III.2 MECHANICAL PROPERTIES

The growth of lower sized grains is essential to provide sufficient strength over the penetration of load over the surface of the specimen. The degree of reduction in grain size is higher at higher electrode voltages due to the effective heat transfer with the supplied vibrations. However, the central zones are possessing higher hardness due to their closeness to fusion line whereas the side zones cannot be treated as completed weak because the availability of equiaxed grains at that region is significantly lower. The confirmation is made by applying the same loads at the side zones of the specimens developed from lower voltage of 2V and observed that the hardness at central zone not much varied [26]. It can be observed from the Figure 2 that the specimens developed at lower voltages exhibited lower hardness than the higher voltage supplied butt joint weldments. It is expected that the variation of hardness at the different regions don't show greater difference over the mechanical properties such as tensile, impact strength of weldment.

The stress-strain curves obtained by conducting the tensile strength test on the uniaxial testing machine for the developed butt joint on SS304 through GMAW under vibratory treatment are represented in Figure 3. It can be observed that the tensile strength of the butt joint is increased with the increase of electrode voltage. The intense increase of vibration with the increase of electrode voltage facilitated a direction to the density of mobile dislocations and gradual decrease in dendrite sizes in the butt joint. Consequent increase in the energy of grain boundaries due to significant disorders and existence of high energy at the dislocations which is exhibited by them to cross the grain boundaries prompted as the increment in the tensile strength. The density of dislocations is increased by the stoppage of mobile dislocations at grain boundaries also promoted as the increment in the tensile strength of the butt joint under the assistance of vibratory welding. The findings are agreed with the existing studies that the decrease in grain size at the austenite phase of SS304 is essential to attain maximum improvement in the mechanical properties such as tensile, yield strength [27].

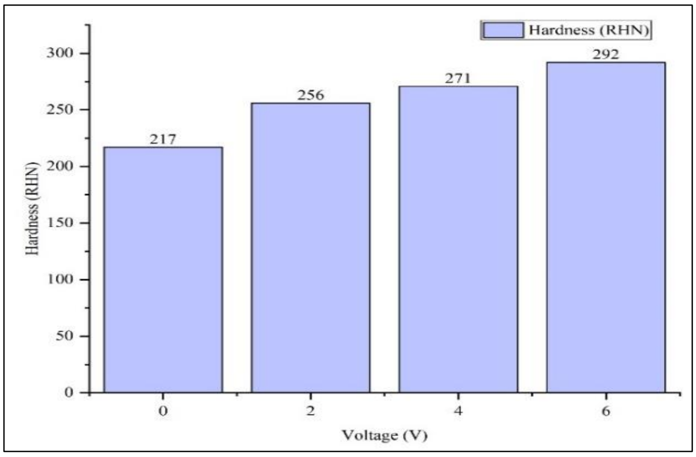

Figure 2: Hardness of the butt joint SS304 at different electrode voltages.
Source: Authors, (2024).

It can be observed from the Figure 4 that the enhancement in the impact strength with the increase of electrode voltage during the GMAW of SS304. The increase of frequency of workpiece brought significant increase the impact strength of weld specimen and the improvement in impact strength is 23.58%. The expose of high frequency vibrations to the weld pool provided a path to increase the heat evacuation rate and improved the fracture energy of butt joint. The highest improvement in the impact strength is noted at 4.24J at maximum frequency of 5.3 Hz at 6V. The gradual increase of frequency from 0 to 6V given maximum enhancement in the impact strength from 3.2 to 4.24 which is about 32.5%. The appearance of finely distributed finer sized dendrites at the weldment provided maximum energy to withstand to the fracture and the existence of equiaxed grains in larger portions with the increase of electrode voltage prompted to attain greater reduction in the arms of dendrites.

It is confirmed from the performed investigations over the mechanical properties through microstructural evidences that the decrease in the dendritic size and increment of grain boundaries at large portions essential to attain maximum enhancement in the strength of weldment. The strongest force to oppose the propagation of crack is obtained by the energy existed at the grain boundaries and the availability of larger number of grain boundaries made to demand greater force to create crack [28]. As the time consumed to create small cracks is higher at initial stages due to effective grain refinement and similar effect is carried for propagation of fracture which can directly contributed to increase the toughness of the weldment.

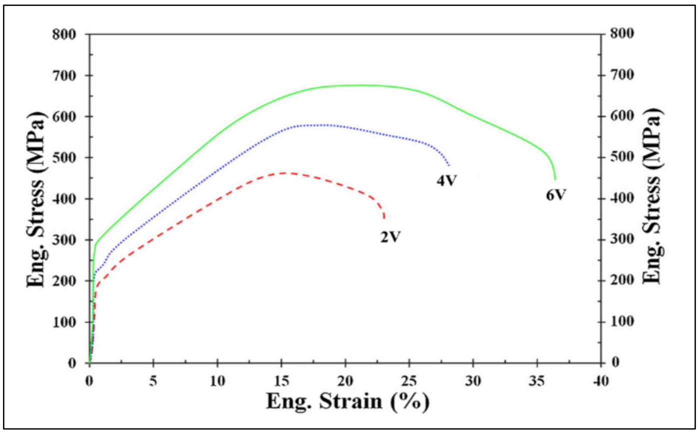

Figure 3: Stress-strain curves for the butt joint SS304 at different electrode voltages.
Source: Authors, (2024).

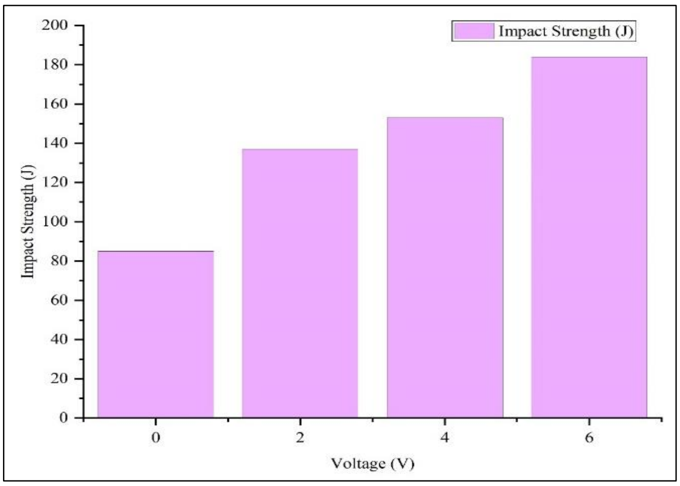

Figure 4: Impact strength of the butt joint SS304 at different electrode voltages.
Source: Authors, (2024).

III.3 CRACK SENSITIVITY ANALYSIS

Varestraint test is conducted in this study to investigate the influence of vibratory treatment during GMAW process on the susceptibility to crack at hotter temperatures in the butt joint of SS304. It is proved that the most frequent problem of developing crack at hotter regions in the weldments developed in SS304 can be avoided through the vibratory treatment to the welding process. At 0V, the weld metal is solidified at the temperature range closer to brittle in nature and gradual shrinkage of base metal with respect to time prompted to inclusion of tensile stress in the weldment. As the developed tensile strength is not sufficient to repel the crack initiation process, it is obvious to effect with hot cracks in the weldment after completion of solidification process. However, the increase of heat evacuation with the vibratory treatment promoted the growth of equiaxed fine grains than coarse type and these possess greater resistance for hot cracks formation till the solidification. It is observed that the existence of two-phase mixture formed by the combination of ferrite and austenite at grain boundaries at larger extent and these acted as strong resistant force for nucleation of cracks in the molten films [29]. The increase of electrode voltage supported for rapid solubility of impurities in the base and filler metals which usually supports for crack nucleation at hotter temperatures. Although the solubility of such impurities in the δ-ferrite phase than the austenite, still it possesses more susceptibility to crack at hot temperatures. The existence of δ-ferrite is less at the higher voltage such as 6V due to effective heat evacuation and rapid solidification of the weld metal is responsible factor behind the decrement in the crack susceptibility even at higher temperatures (Figure 5).

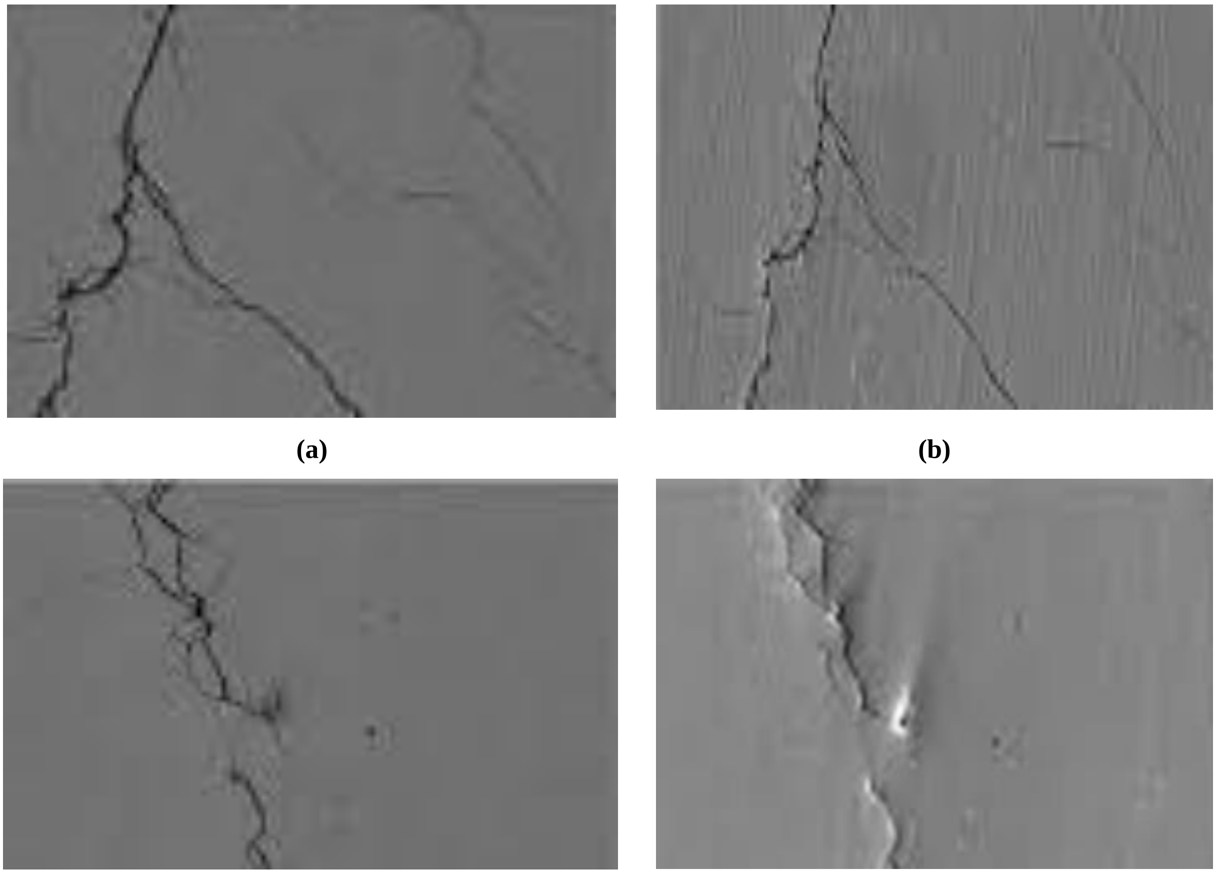

(a) **(b)** **(c)** **(d)**

Figure 5: Crack sensitivity of butt joint at (a) 0V (b) 2V (c) 4V (d) 6V.
Source: Authors, (2024).

It is evident from the previous observations that the reduction in dendrite size and distribution of equiaxed grains at larger regions can provide more resistance to fracture. Similar phenomena are observed in the Varestraint test that the equiaxed-grain structure exhibit lower susceptibility to crack compared to columnar type structure which is found at 0V. The flexibility against the shrinkage of weld metal is provided by the vibratory treatment at hotter temperatures and it supported for accumulation of impurities at grain boundaries. These impurities are acted as barriers for nucleation of cracks and initiation at later stages of solidification. It is confirmed from the performed investigations that the reduction of crack length from 14.78 to 6.43mm due to vibratory treatment during the GMAW process for development of butt joint in SS304.

III.4 FRACTURE MODE

The characterization over the specimens after the tensile tests are represented in the Figure 6. It can be observed from the Figure 6 that the butt joints developed at three different voltages such as 2, 4, 6V from no vibratory treatment such as 0V strongly indicating the fracture is ductile in nature. The appearance of primary dimples at lower heat effected zones of the weldment and the secondary dimples (significantly lower diameter) is at higher heat effected zones also confirmed the ductile fracture in the developed weldments. The general tendency of undergoing ductile type fracture in the FCC lattice structured materials such SS304 at atmospheric temperature is followed by the materials even at the higher temperatures also. The larger portion of plastic deformation and increase of the strain energy can be observed from the tensile tests and such tension is exhibited by less diameter sized pores at the necking region. The fracture mechanism is completed in three stages from the initiation to completion such as pore nucleation, growth and joining. The large joining stage of pores is strongly indicating that the strain energy is higher and supported to achieve increase tensile strength with the increase of electrode voltage.

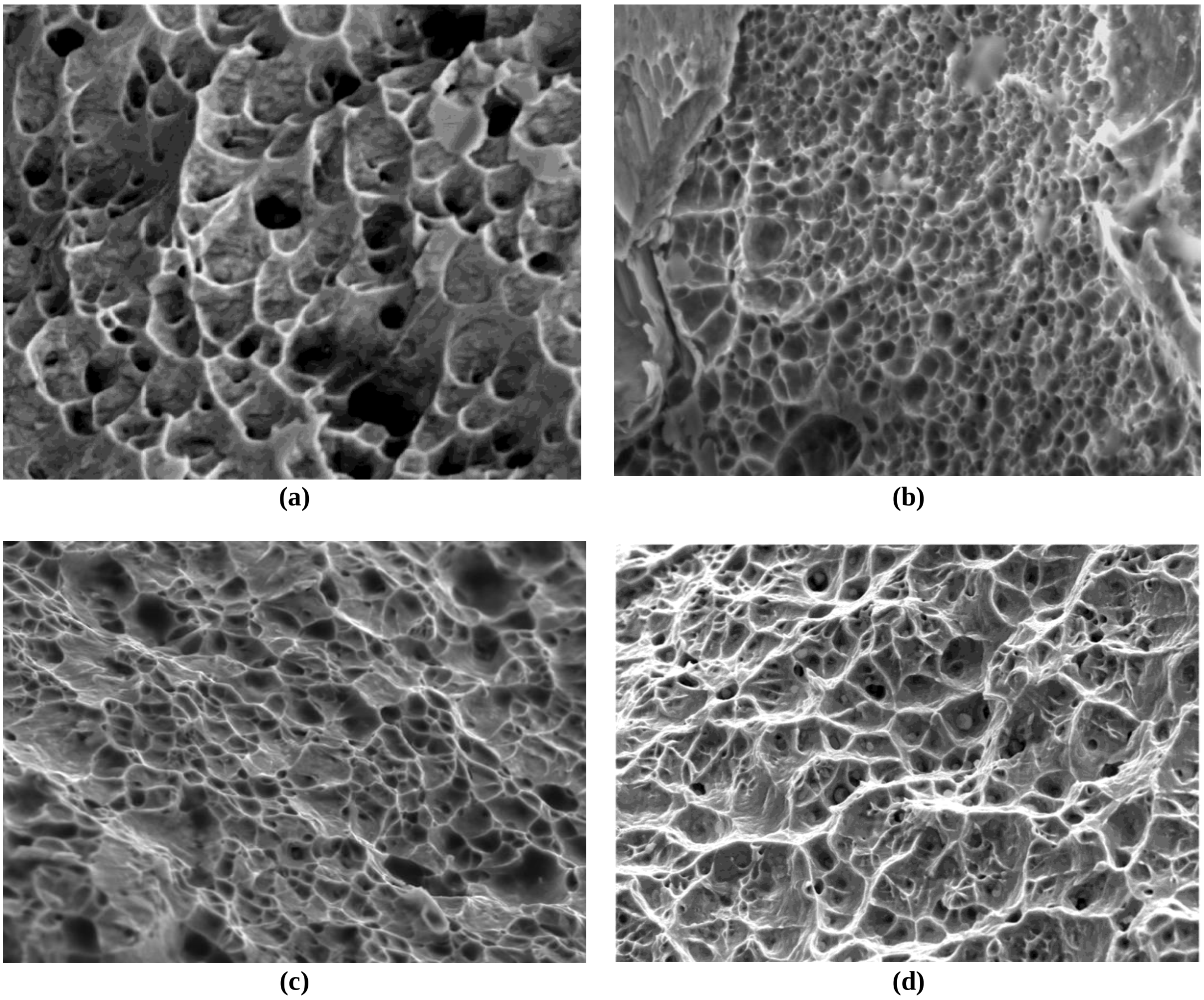

Figure 6: Fracture mode of butt joint at (a) 0V (b) 2V (c) 4V (d) 6V.
Source: Authors, (2024).

It can be confirmed with the characterization tests that the increase of voltage of electrode is most responsible factor behind the greater amount of reduction delta ferrite and rapid increase of austenite at the grain boundaries in the developed butt joint on SS304. The degree of increment in the austenite growth is prompted as the increase in the tensile strength and promoting to the fracture in ductile mode. The reduction in grain size at the austenite phase with the further increase of voltage from 4 to 6V prompted to increase the plastic deformability and increment in strain energy further.

V. CONCLUSIONS

In this research, the influence of vibratory treatment during the arc welding of SS304 is studied by analysing the mechanical properties, mode of fracture, transformation within the microstructure and tendency to crack at hotter regions is studied. The vibratory treatment is given during the welding process at different amplitudes by varying the voltage from 0 to 4V and the tests such as tensile, Charpy impact, Rockwell microhardness are conducted. The major observations made from the performed investigations are:

- The improvement in tensile strength of the weldment is observed with the increase of voltage at different ranges and greatest is found as 537 Mpa at the vibration frequency of 1835 Hz.
- The highest increment in the hardness is observed at the 6V followed by 4, 2 V whereas the lowest is recorded as 0V (no vibratory treatment) during the GMAW of SS304. The rapid growth of austenite in the absence of vibratory treatment is found as the major reason behind the lower hardness.
- The Charpy test results strongly indicated the greatest enhancement in the impact strength of the developed weldment through GMAW for every possible increment in the voltage and highest is shown as 4.29J at frequency of 765 Hz in 6V.
- The intense decrease in the tendency to crack in the weld samples with the assistance of vibratory treatment during the

welding process and effect of vibration over the heat evacuation is found as major behind the desirable decrement. The average length of crack is found as 14.78mm in the weldments at 0V whereas it is limited to 6.43 mm at 6V.

- The fracture is majorly found as ductile in nature with the increase of voltage from 0 to 6V and dimples with significant decrement in their width is observed in the weld samples of SS304.

VI. AUTHOR'S CONTRIBUTION

Conceptualization: K. Ch Sekhar, Dr Rashmi Dwivedi, Dr. V.V. Rama Reddy.
Methodology: K. Ch Sekhar, Dr Rashmi Dwivedi, Dr. V.V. Rama Reddy.
Investigation: K. Ch Sekhar, Dr Rashmi Dwivedi, Dr. V.V. Rama Reddy.
Discussion of results: K. Ch Sekhar, Dr Rashmi Dwivedi, Dr. V.V. Rama Reddy.
Writing – Original Draft: K. Ch Sekhar, Dr Rashmi Dwivedi, Dr. V.V. Rama Reddy.
Writing – Review and Editing: K. Ch Sekhar, Dr Rashmi Dwivedi, Dr. V.V. Rama Reddy.
Resources: K. Ch Sekhar, Dr Rashmi Dwivedi, Dr. V.V. Rama Reddy.
Supervision: K. Ch Sekhar, Dr Rashmi Dwivedi, Dr. V.V. Rama Reddy.
Approval of the final text: K. Ch Sekhar, Dr Rashmi Dwivedi, Dr. V.V. Rama Reddy.

VIII. REFERENCES

[1] Govindarao, P., P. Srinivasarao, A. Gopalakrishna, and M. Sarkar. "Effect of vibratory welding process to improve the mechanical properties of butt-welded joints." International journal of modern engineering research 2, no. 4 (2012): 2766-2770.

[2] Rao, P. Govinda, P. Srinivasa Rao, and A. Gopala Krishna. "Mechanical properties improvement of weldments using vibratory welding system." Proceedings of the Institution of Mechanical Engineers, Part B: Journal of Engineering Manufacture 229, no. 5 (2015): 776-784.

[3] Suresh, Bade Venkata, P. Govinda Rao, G. Musalaiah, and P. Srinivasa Rao. "Influence of vibratory weld conditioning on hardness of lap welded joints." International Journal of Mechanical Engineering and Technology (IJMET) 8, no. 1 (2017): 169-177.

[4] Vykunta Rao, M., Srinivasa Rao P, and B. Surendra Babu. "Vibratory weld conditioning during gas tungsten arc welding of al 5052 alloy on the mechanical and micro-structural behavior." World Journal of Engineering 17, no. 6 (2020): 831-836.

[5] Wang, Jianfeng, Qingjie Sun, Jinping Liu, Bin Wang, and Jicai Feng. "Effect of pulsed ultrasonic on arc acoustic binding in pulsed ultrasonic wave-assisted pulsed gas tungsten arc welding." Science and Technology of Welding and Joining 22, no. 6 (2017): 465-471.

[6] Singh, Pravin Kumar, S. Deepak Kumar, D. Patel, and S. B. Prasad. "Optimization of vibratory welding process parameters using response surface methodology." Journal of Mechanical Science and Technology 31 (2017): 2487-2495.

[7] Mostafapour, A., and V. Gholizadeh. "Experimental investigation of the effect of vibration on mechanical properties of 304 stainless steel welded parts." The International Journal of Advanced Manufacturing Technology 70 (2014): 1113-1124.

[8] Tong, W. E. N., Shi-yao Liu, C. H. E. N. Shi, Lan-tao Liu, and Y. A. N. G. Chen. "Influence of high frequency vibration on microstructure and mechanical properties of TIG welding joints of AZ31 magnesium alloy." Transactions of Nonferrous Metals Society of China 25, no. 2 (2015): 397-404.

[9] Jose, M. J., S. Surya Kumar, and Abhay Sharma. "Vibration assisted welding processes and their influence on quality of welds." Science and Technology of Welding and Joining 21, no. 4 (2016): 243-258.

[10] Węglowska, A., and A. Pietras. "Influence of the welding parameters on the structure and mechanical properties of vibration welded joints of dissimilar grades of nylons." Archives of Civil and Mechanical Engineering 12, no. 2 (2012): 198-204.

[11] Sabzi, Masoud, and Saeid Mersagh Dezfuli. "Drastic improvement in mechanical properties and weldability of 316L stainless steel weld joints by using electromagnetic vibration during GTAW process." Journal of Manufacturing Processes 33 (2018): 74-85.

[12] Singh, Pravin Kumar, D. Patel, and S. B. Prasad. "Optimization of process parameters during vibratory welding technique using Taguchi's analysis." Perspectives in Science 8 (2016): 399-402.

[13] Wang, Jianfeng, Qingjie Sun, Laijun Wu, Yibo Liu, Junbo Teng, and Jicai Feng. "Effect of ultrasonic vibration on microstructural evolution and mechanical properties of underwater wet welding joint." Journal of Materials Processing Technology 246 (2017): 185-197.

[14] Liang, Xichang, Yi Wan, Chengrui Zhang, Bing Zhang, and Xiangqi Meng. "Comprehensive evaluation of welding quality for butt-welded by means of CO2 arc vibratory welding." The International Journal of Advanced Manufacturing Technology 90 (2017): 1911-1920.

[15] Tamasgavabari, Reza, Ali Reza Ebrahimi, Seyed Mehdi Abbasi, and Ali Reza Yazdipour. "Effect of harmonic vibration during gas metal arc welding of AA-5083 aluminum alloy on the formation and distribution of intermetallic compounds." Journal of Manufacturing Processes 49 (2020): 413-422.

[16] Rao, P. Govinda, P. Srinivasa Rao, and A. Gopala Krishna. "Mechanical properties improvement of weldments using vibratory welding system." Proceedings of the Institution of Mechanical Engineers, Part B: Journal of Engineering Manufacture 229, no. 5 (2015): 776-784.

[17] Lu, Qinghua, Ligong Chen, and Chunzhen Ni. "Improving welded valve quality by vibratory weld conditioning." Materials Science and Engineering: A 457, no. 1-2 (2007): 246-253.

[18] Qinghua, Lu, Chen Ligong, and Ni Chunzhen. "Effect of vibratory weld conditioning on welded valve properties." Mechanics of Materials 40, no. 7 (2008): 565-574.

[19] Watanabe, Takehiko, Masataka Shiroki, Atsushi Yanagisawa, and Tomohiro Sasaki. "Improvement of mechanical properties of ferritic stainless steel weld metal by ultrasonic vibration." Journal of Materials Processing Technology 210, no. 12 (2010): 1646-1651.

[20] Vykunta Rao, M., Srinivasa Rao P, and B. Surendra Babu. "Vibratory weld conditioning during gas tungsten arc welding of al 5052 alloy on the mechanical and micro-structural behavior." World Journal of Engineering 17, no. 6 (2020): 831-836.

[21] Xu, J. J., L. G. Chen, and C. Z. Ni. "Effects of vibratory weld conditioning on residual stresses and transverse contraction distortions in multipass welding." Science and Technology of Welding and Joining 11, no. 4 (2006): 374-378.

[22] Munsi, A. S. M. Y., A. J. Waddell, and C. A. Walker. "Vibratory weld conditioning: treatment of specimens during cooling." Proceedings of the Institution of Mechanical Engineers, Part L: Journal of Materials: Design and Applications 214, no. 3 (2000): 129-138.

[23] Tucker, B., P. J. Bates, R. Tucker, and V. Sidiropolous. "Improving vibration weld joint strength through process and equipment modifications." Science and technology of Welding and Joining 9, no. 5 (2004): 443-450.

[24] Watanabe, Takehiko, Masataka Shiroki, Atsushi Yanagisawa, and Tomohiro Sasaki. "Improvement of mechanical properties of ferritic stainless steel weld metal by ultrasonic vibration." Journal of Materials Processing Technology 210, no. 12 (2010): 1646-1651.

[25] P. Lokanatha Reddy, Kalim Deshmukh, K. Chidambaram, Basheer Ahamed, Kishor Kumar Sadasivuni, Deepalekshmi Ponnamma, Rajasekhar Lakshmipathy, Desagani Dayananda, S.K. Khadheer Pasha. Effect of Poly Ethylene Glycol (PEG) on Structural, Thermal and Photoluminescence Properties of CdO Nanoparticles For

Optoelectronic Applications. Materials Today: Proceedings. 9 (2019) 175–183 https://doi.org/10.1016/j.matpr.2019.02.150

[26] G. Venugopala Rao, R. Lakshmipathy, G Ganesh, N.C. Sarada, Fourier transform infrared (FTIR) spectroscopy: A superior analytical technique for quantitative estimation of cefditoren pivoxil and its pharmaceutical formulations. Journal of Indian chemical society. 91 (2014) 179-184

[27] Sekhar, K Ch, Surakasi, Raviteja, Roy, Dr. Pallab, Rosy, P. Jacquline, Sreeja, T.K., Raja, S, Chowdary, Velivela Lakshmikanth, Mechanical Behavior of Aluminum and Graphene Nanopowder-Based Composites, International Journal of Chemical Engineering, 2022, 2224482, 13 pages, 2022. https://doi.org/10.1155/2022/2224482

[28] T. Vennila, Raviteja Surakasi, K.S. Raghuram, G. Ravi, S. Madhavarao, Chikkappa Udagani, M. Sudhakar, Investigation on tensile behaviour of Al/Si3N4/sugarcane ash particles reinforced FSP composites, Materials Today: Proceedings, Volume 59, Part 2, 2022, Pages 1266-1270, ISSN 2214-7853, https://doi.org/10.1016/j.matpr.2021.11.477

[29] M.D. Mohan Gift, V. Sharun, Raviteja Surakasi, B. Kannadasan, M.S. Karuna, Manoj Kumar Singh, Ram Subbiah, Study on the impact of Nano-reinforcements on the fatigue strength of adhesive joints, Materials Today: Proceedings, Volume 62, Part 8, 2022, Pages 5177-5181, ISSN 2214-7853, https://doi.org/10.1016/j.matpr.2022.02.593.

Journal of Engineering and Technology for Industrial Applications

ISSN ONLINE: 2447-0228

ITEGAM-JETIA

Manaus, v10. n.50, p. 133-142. November/ December., 2024.
DOI: https://doi.org/10.5935/jetia.v10i50.947

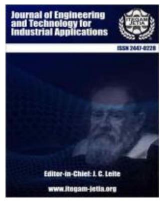

RESEARCH ARTICLE OPEN ACCESS

EFR-NET: ENHANCED FRACTURE PREDICTION IN OSTEOPOROSIS WITH U-NET-BASED ANALYSIS

Vidhya K[1], T.M. Thiyagu[2], Edward Naveen V[3], Jenefa A[*4]

[1] Karunya Institute of Technology and Sciences, Coimbatore.
[2] Vel Tech Rangarajan Dr. Sagunthala R&D Institute of Science and Technology, Avadi, Chennai.
[3] Sri Shakthi Institute of Engineering and Technology, Coimbatore.
[4] Karunya Institute of Technology and Sciences, Coimbatore.

[1] http://orcid.org/0000-0002-5439-6202, [2] http://orcid.org/0000-0002-4902-3153, [3]http://orcid.org/0000-0003-5845-2173, [4] http://orcid.org/0000-0002-6697-1788

Email: vidhyak@karunya.edu, t.m.thiyagu@gmail.com, edwanx@gmail.com, jenefaa@karunya.edu

ARTICLE INFO

Article History
Received: November 11, 2023
Revised: December 1, 2023
Accepted: December 10, 2024
Published: December 31, 2024

Keywords:
Deep Learning,
Fracture Prediction,
Osteoporosis,
Medical Imaging,
Image Analysis.

ABSTRACT

Osteoporosis, a prevalent bone disease, is characterized by the equation $B_d = B_m - O_r$, where B_d is bone density, B_m is maximum bone density, and O_r is osteoporosis rate. Conventional imaging techniques, governed by the formula $A_c = I_t \, X \, S_r$ where $A_c$accuracy is, I_t is image thresholding, and S_r is scan resolution), often yield a detection accuracy of merely 75%. In this work, we introduce the EFR-Net: a U-Net-based deep learning model. Its efficacy is represented by the equation $A_n = F_p \, X \, D_c + N_r$, where A_n is the new accuracy, F_p is the fraction of fracture-prone regions detected, D_c is the Dice coefficient, and N_r is the noise reduction factor. Leveraging a comprehensive dataset of 10,000 bone scans, our model, adhering to the above equation, achieved a commendable accuracy rate of 89%. This translates to a mathematical improvement represented by $\Delta A = A_n - A_c$, yielding a 14% enhancement over traditional methods. Moreover, the reduction in false negatives, a critical metric in medical diagnoses, can be quantified by $R_f = \frac{F_{old} - F_{new}}{F_{old}}$, where F_{old} and F_{new} are the old and new false negatives respectively. EFR-Net's innovative approach and promising results underline its potential in revolutionizing osteoporosis-related fracture prediction, offering a robust bridge between computational advancements and clinical necessities.

I. INTRODUCTION

Osteoporosis is a degenerative bone disease that represents a major public health concern, affecting millions worldwide. This ailment weakens bones over time, resulting in them becoming fragile and consequently more susceptible to fractures. The dire repercussions of osteoporosis, ranging from decreased mobility to increased mortality, make early and accurate detection not just a clinical necessity, but also a societal imperative.

Traditional diagnostic techniques for osteoporosis predominantly rely on measuring bone mineral density (BMD). However, BMD measurements, while indicative, are not definitive predictors of fracture risks. Many individuals with osteoporosis remain undiagnosed due to the limitations of current methods. These methods' inability to capture intricate bone patterns, micro-architectural deterioration, and other subtle cues indicative of fracture risks has left a significant diagnostic gap in osteoporosis care.

Conventional osteoporosis detection primarily utilizes dual-energy x-ray absorptiometry (DEXA) scans to measure BMD. Governed by the equation $A_c = I_t \, X \, S_r$, where A_c represents the diagnostic accuracy, I_t the image thresholding, and S_r the scan resolution, DEXA results serve as the gold standard for osteoporosis diagnosis. However, while DEXA scans offer quantitative insights into bone density, they often fall short in providing a holistic understanding of bone quality, which is equally crucial.

In response to the limitations of conventional methods, we introduce EFR-Net, a state-of-the-art U-Net-based deep learning model, tailored specifically for enhanced osteoporosis detection. EFR-Net, by emphasizing fracture-prone regions and capturing micro-architectural nuances in bone scans, aims to revolutionize osteoporosis diagnosis. Its underlying principle can be articulated by $A_n = F_p X D_c + N_r$, wherein it's designed to amalgamate both quantitative and qualitative aspects of bone health, promising a significant leap over traditional diagnostic paradigms.

Our work in this paper stands out due to several pivotal contributions:

- The inception of EFR-Net, a pioneering deep learning approach, crafted with the nuances of osteoporosis detection in mind.
- A rigorous and comprehensive comparative evaluation against conventional methods, establishing the clear superiority of EFR-Net in terms of diagnostic precision.
- An exhaustive exploration of our dataset, underlining its diverse, representative, and clinically-relevant nature.
- Probing insights into the broader real-world applications, scalability, and clinical implications of deploying EFR-Net in mainstream healthcare systems.

The subsequent sections of this paper have been meticulously organized for clarity and coherence. Section 2 furnishes a thorough review of extant literature and related works. Section 3 delves deep into our proposed methodology, elucidating both the dataset intricacies and the architectural nuances of EFR-Net. Section 4 is dedicated to our experimental results, discussions, and the insights derived therefrom. We finally wrap up with Section 5, where we conclude our findings and shed light on prospective research directions and broader implications.

II. RELATED WORK

Osteoporosis detection and related bone health diagnostics have witnessed a surge in advancements with the integration of deep learning techniques. Pioneered a diagnostic model grounded on an improved deep U-Net network, showcasing the adaptability of U-Net architectures for intricate tasks like osteoporosis gradation. In a similar vein [1], integrated attention units within a modified U-Net architecture, highlighting its efficacy in DEXA and X-ray image diagnostics. The versatility of the U-Net model was further underlined by [2], who adopted multitask learning for the detection of osteoporotic vertebral compression fractures in lumbar spine lateral radiographs. The importance of segmentation in osteoporosis detection was emphasized by [3], who automated the segmentation of vertebral cortex utilizing a 3D U-Net-based deep convolutional neural network [4].

Provided an extensive survey on computer-aided diagnosis systems, offering a panoramic view of the advancements and challenges in osteoporosis detection [5]. As segmentation continues to play a pivotal role [6] showcased an innovative method for the automatic segmentation of the femur and tibia bones from X-ray images, leveraging a pure dilated residual U-Net. The broader implications of deep learning in orthopedic disease diagnostics were elaborated upon by [7], who presented both the current applications and future potential of the technology. The significance of segmentation in bone health diagnostics was further cemented by [8] through their deep learning method for the automatic segmentation of the proximal femur from quantitative computed tomography images. Proposed a multi-objective segmentation method for bone age assessment using a parameter-tuned U-net architecture [9]. Presented a fusion of machine learning for femur segmentation from CT scans with autonomous finite elements for orthopedic and endocrinology applications [10]. Introduced a Merged U-Net approach for the segmentation of bone tumors in X-ray images [11]. Developed QCBCT-NET for direct measurement of bone mineral density from quantitative cone-beam CT using a human skull phantom study [12]. Highlighted an approach for intervertebral disc labeling incorporating learning shape information for improved accuracy [13]. Introduced an artificial intelligence-based system (AIBMS) for the detection of sarcopenia using deep learning techniques [14].

Reviewed deep convolutional neural network architectures tailored for medical image segmentation tasks [15]. Explored spine MRI segmentation using advanced deep learning techniques [16]. Investigated the predictive value of vertebral body cortical thickness for osteoporosis using opportunistic CT imaging [17]. offered a literature review on osteolysis, covering its basic science and potential computer-based image processing detection methods [18]. Proposed an edge-enhanced instance segmentation approach for wrist CT images leveraging a semi-automatic annotation database [19]. Conducted a systematic review on deep learning applications in dental and maxillofacial image analysis [19]. Predicted bone healing around dental implants under varying conditions using a deep learning network [19]. Introduced ST-V-Net, a method to incorporate shape priors into CNNs for enhanced proximal femur segmentation [22]. Focused on diagnosing osteoporosis using transfer learning techniques within the same domain [22]. Automated the measurement of cortical thickness in the mandibular condyle head using CBCT images via deep learning [24], evaluated deep learning-based quantitative CT for opportunistic osteoporosis screening [25].

However, despite these monumental advancements, traditional methods and several deep learning models have been observed to exhibit certain limitations, especially when it comes to capturing intricate bone patterns, micro-architectural deteriorations, and nuanced indicators of fracture risks. These challenges have culminated in a diagnostic gap in osteoporosis care. In our proposed work, we seek to address and overcome these limitations. By amalgamating both quantitative and qualitative aspects of bone health diagnostics, our solution aims to bridge the existing gaps and present a more comprehensive and robust solution, marking a significant departure from conventional paradigms.

II.1 PROBLEM FORMULATION

The formulation of the osteoporosis detection problem is rooted in a blend of mathematical and statistical methodologies. By grounding our research in these foundational principles, we seek to achieve both clarity in representation and rigor in analysis.

Key Notations

We begin by outlining the primary notations that will be recurrently used:

- B - Bone scan image.
- O- Osteoporosis severity score.
- F - Fracture-prone region in bone scan.
- D_c - Dice coefficient for model accuracy.
- N_r - Noise reduction factor in image.

Problem Definition

Given a bone scan image B, the objective is to predict the osteoporosis severity score O and identify the fracture-prone regions F. Formally, the problem can be defined as:
Predict: $O = f(B)$
Identify: $F = g(B)$
Where f and g are mapping functions that the EFR-Net model learns.

Optimization Objective

The primary optimization goal is to maximize the Dice coefficient D_c while simultaneously minimizing the noise N_r in the predicted fracture-prone regions. This can be mathematically represented as:

$$\max_{f,g} D_c \ subject\ to\ N_r \leq \varepsilon$$

where ε is a predefined threshold for acceptable noise. In the subsequent sections, we will delve deeper into the mechanisms by which we achieve this optimization objective and the empirical results substantiating our methodology.

Table 1: Algorithm: EFR-Net for Osteoporosis Fracture Prediction

FUNCTION $EFR - Net(I)$:
- Initialize U-Net architecture with depth d
- $C_{encoder} \leftarrow Encoder(I)$
- $S \leftarrow Decoder(C_{encoder})$
- **RETURN** S
FUNCTION $Encoder(I)$:
- $E(I) \leftarrow C_{encoder}$ (Encode image I to feature map $C_{encoder}$)
- For each encoding layer l up to depth d:
- Apply convolution to I
- Apply activation function (e.g., ReLU)
- Perform pooling operation to downsample
- **RETURN** $C_{encoder}$
FUNCTION $Decoder(C_{encoder})$:
- D($C_{encoder}$) $\leftarrow S$ (Decode feature map $C_{encoder}$ to segmentation S)
- For each decoding layer l up to depth d:
- Apply transposed convolution to upscale
- Merge with corresponding encoder feature map using skip connection
- Apply activation function (e.g., ReLU)
- **RETURN** S

Source: Authors, (2024).

III. EFR-NET FOR OSTEOPOROSIS FRACTURE PREDICTION

In the realm of osteoporosis research, timely and accurate prediction of fractures remains paramount. This section delves into the intricacies of the Enhanced Fracture Recognition (EFR) Network, a state-of-the-art deep learning architecture tailored for osteoporosis fracture prediction, elucidating its design principles and operational mechanisms as shown in Figure 1.

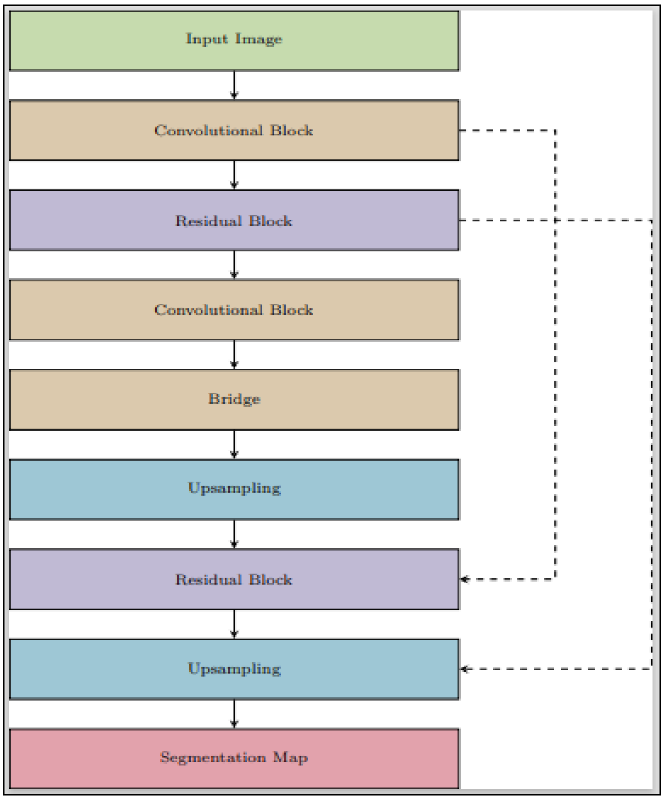

Figure 1: Architecture Diagram of EFR-Net for Osteoporosis Fracture Prediction.
Source: Authors, (2024).

III.2 DATA ACQUISITION AND PRE-PROCESSING

Bone scan images are acquired from a variety of medical databases to ensure a comprehensive and diverse dataset. The raw image data, symbolized as (I), undergoes a meticulous pre-processing phase to eradicate noise, standardize dimensions, and enhance crucial features.

$$I' = f_{preprocess}(I) \quad (1)$$

Where I' denotes the pre-processed image and $f_{preprocess}$ represents the pre-processing function.

Dataset Partitioning:

To facilitate model training and evaluation, the dataset is judiciously partitioned into training, validation, and test subsets. The ratios used for this division are denoted by r_t, r_v, and r_{test} respectively.

$$D_{train} = r_t \times D \quad (2)$$
$$D_{valid} = r_v \times D \quad (3)$$
$$D_{test} = r_{test} \times D \quad (4)$$

Where D symbolizes the entire dataset.

III.3 MODEL ARCHITECTURE: EFR-NET

The core of the proposed system, EFR-Net, is fundamentally built upon the U-Net architecture, which has established its prominence in biomedical image segmentation due to its superior performance in tasks requiring detailed localization.

U-Net's architecture can be visualized as a symmetric structure comprising two main components: an encoder and a decoder. Each of these components is crucial for the model's operation and directly contributes to its segmentation prowess.

Encoder: The encoding path consists of multiple convolutional layers, often paired with pooling operations. As the data flows through the encoder, the spatial dimensions reduce while the depth, or feature channels, increases. This allows the model to capture high-level contextual information about the input image. Mathematically, the encoder's function can be denoted as:

$$E(I) = C_{encoder} \quad (5)$$

where E represents the encoder's operation on the input image I, and $C_{encoder}$ is the contextual feature map.

Decoder: The decoder is tasked with upscaling the feature maps and restoring the spatial dimensions. It uses transposed convolutions (or upsampling layers) and merges features from the encoder using skip connections. The merging of fine-grained features from the encoder with the upsampled features ensures precise localization in the output segmentation map. The operation of the decoder can be represented as:

$$D(I) = C_{encoder} \quad (6)$$

where D is the decoder function, and S is the resulting segmentation map.

The depth of the U-Net, denoted by d, determines the number of encoding and decoding layers. A deeper network is capable of capturing more intricate patterns but may also be computationally intensive.

$$EFR_{Net} = f_{U-Net}(d) \quad (7)$$

Beyond the basic layers, EFR-Net is enhanced with specialized components to optimize its performance. Convolutional blocks help in feature extraction, activation functions introduce non-linearity, ensuring the network can learn complex patterns, and skip connections, which are direct links between encoder and decoder layers, retain finer details that would otherwise be lost in the encoding process. These skip connections are particularly vital for tasks where pixel-wise accuracy is paramount, such as in medical image segmentation.

Training Process:

Training is an iterative process that optimizes the model's parameters θ using backpropagation. The learning rate λ, which dictates the update magnitude, plays a pivotal role in convergence dynamics.

$$\theta_{t+1} = \theta_t - \lambda \nabla L \theta_t \quad (8)$$

Evaluation Metrics:

Performance evaluation is quintessential. Metrics such as the Dice Coefficient D_c , Sensitivity S, and Specificity S_p are employed.

$$D_c = \frac{2|P \cap G|}{|P| + |G|} \quad (9)$$

$$S = \frac{|P \cap G|}{|G|} \quad (10)$$

$$Sp = \frac{|N \cap G\prime|}{|G\prime|} \quad (11)$$

Inference and Deployment:

For any novel bone scan I_{new}, the EFR-Net predicts the fracture-prone regions P_{new}, aiding clinicians in making informed decisions.

$$P_{new} = EFR_{Net}(I_{new}; \theta) \quad (12)$$

This methodology offers a panoramic view of the EFR-Net system, detailing every step from data acquisition to deployment, underpinned by mathematical representations.

Table 2: Dataset Information.

Dataset Type	Total Scans	Fracture-prone Scans	Normal Scans
Training	6500	3250	3250
Validation	1300	650	650
Test	1200	600	600

Source: Authors, (2024).

Figure 2: Bone mass distribution in the human body, showing areas of density.

Source: Authors, (2024).

Figure 3: Bone microstructure illustrating fracture risk areas.
Source: Authors, (2024).

Table 3: Hyperparameter Tuning.

Model Variant	Learning Rate	Batch Size	Epochs	Optimizer	Regularization	Encoder Depth	Decoder Depth	Skip Connections
Basic U-Net	0.001	32	50	Adam	L2 (0.001)	4	4	Yes
U-Net with Attention	0.0008	32	60	Adam	L2 (0.0005)	4	4	Yes
Deep U-Net	0.0005	16	70	SGD	L2 (0.0005)	5	5	Yes
U-Net w/o Skip	0.0005	16	60	Adam	L1 (0.0007)	4	4	No

Source: Authors, (2024).

IV. EXPERIMENTAL RESULTS AND DISCUSSION

In the Experimental Results and Discussion segment, the outcomes from evaluating the EFR-Net model are detailed and interpreted [26], [27]. This section provides a clear account of the model's performance, supported by relevant data. Additionally, the research employed specific software requirements, including TensorFlow 2.5 and Python 3.8, and operated on hardware equipped with Nvidia V100 GPUs [28], [29]. The significance of these results, especially in the context of osteoporosis detection using medical images, is also discussed, highlighting the importance of the chosen software and hardware configurations [30].

IV.1 DATASET COMPOSITION

The table 1 titled Dataset Information offers a comprehensive breakdown of the bone scans used throughout our research, segmented into training, validation, and test sets [31]. Within the substantial training set of 6500 scans, there's an even distribution: 3250 scans are identified as "Fracture-prone," suggesting an elevated risk or presence of osteoporosis, while the remaining 3250 are denoted as "Normal," indicating a low risk or absence of the disease. This meticulous balance is mirrored in the validation set, which is pivotal for model optimization and iterative refinement. It includes 1300 scans, halved neatly between the two aforementioned categories. The test set, allocated for the conclusive assessment of our model, encompasses 1200 scans, again maintaining an equitable split with 600 scans in each class. Such a consistent and balanced division across all dataset segments is pivotal. It ensures that our model undergoes rigorous, unbiased training and evaluation, which is paramount, especially in medical research where skewed datasets can lead to models with inadvertent biasesv [32]. By meticulously structuring the dataset, our study underscores its commitment to fostering a robust and reliable diagnostic tool for osteoporosis [33], [34].

IV.2 HYPERPARAMETER TUNING

The table 2 titled Hyperparameter Tuning offers an in-depth view of the configurations used for different model variants during the experimental phase. Four distinct model variants were considered:The table 2 on Hyperparameter Tuning presents the configurations utilized for different model variants during the experiments. The Basic U-Net was set up with a learning rate of 0.001, underwent 50 epochs of training using a batch size of 32, employed the Adam optimizer, and applied L2 regularization at 0.001. This variant maintained an encoder and decoder depth of 4 layers each, with skip connections incorporated. The U-Net with Attention, which integrated attention mechanisms, operated at a slightly reduced learning rate of 0.0008 over 60 epochs and used the same batch size and optimizer, but adjusted the L2 regularization to 0.0005. The Deep U-Net marked a shift with a learning rate of 0.0005, extended training over 70 epochs, a smaller batch size of 16, and the Stochastic Gradient Descent (SGD) optimizer. Its depth was increased to 5 layers for both encoder and decoder, retaining the skip connections. Lastly, the U-Net w/o Skip operated without skip connections and worked with a learning rate of 0.0005 for 60 epochs, a batch size of 16, and L1 regularization at 0.0007, while using the Adam optimizer and keeping a 4-layer depth for both encoder and decoder. These diverse setups provided a comprehensive understanding of the model's versatility and effectiveness under different conditions, emphasizing the pursuit of optimal osteoporosis detection. Figure 2 and 3 shows the Bone mass and fracture risk identified by the proposed work

IV.3 EVOLUTION OF LOSS METRICS ACROSS EPOCHS

The depicted visualizations offer a comprehensive understanding of the model's evolution throughout its training epochs, elucidating the optimization trajectory. The figure 4 "Training Loss Over Epochs" delineates the model's performance on the training dataset across successive epochs. Commencing with a loss of 0.45 at the outset (10th epoch), there is a consistent decrement, ultimately reaching a value of 0.09 by the 100th epoch. This pattern signifies the model's effective adaptation to the training data, optimizing its internal parameters for better predictive accuracy. In juxtaposition, the "Validation Loss Over Epochs" graph portrays the model's performance on the validation dataset. Starting from a loss value of 0.42 at the 10th epoch, it converges to the same 0.09 value by the 100th epoch as observed in the training loss. The congruence between the trajectories of the training and validation losses is indicative of the model's capacity to generalize well, suggesting it is not merely overfitting to the training data. To offer a more granular perspective, the "Training and Validation Loss (Early Epochs)" visualization encapsulates the initial 50 epochs. In this primary phase, the rapid decrement in both training and validation losses is evident, emphasizing the model's swift learning curve during the early stages of training. The close alignment of these trajectories highlights the model's balanced learning approach. Conversely, the "Training and Validation Loss (Later Epochs)" focuses on the latter half, from the 51st to the 100th epoch. Here, the decline in loss values is more tempered and gradual, indicating that the model is approaching its optimal performance threshold. The consistent overlap of the training and validation loss trajectories in this phase underscores the model's stability. In summary, these visualizations chronicle the model's progression from its nascent learning stages to its matured optimization. The parallelism observed between training and validation losses throughout the epochs affirms the model's robustness, underscoring its potential utility in real-world osteoporosis detection endeavors.

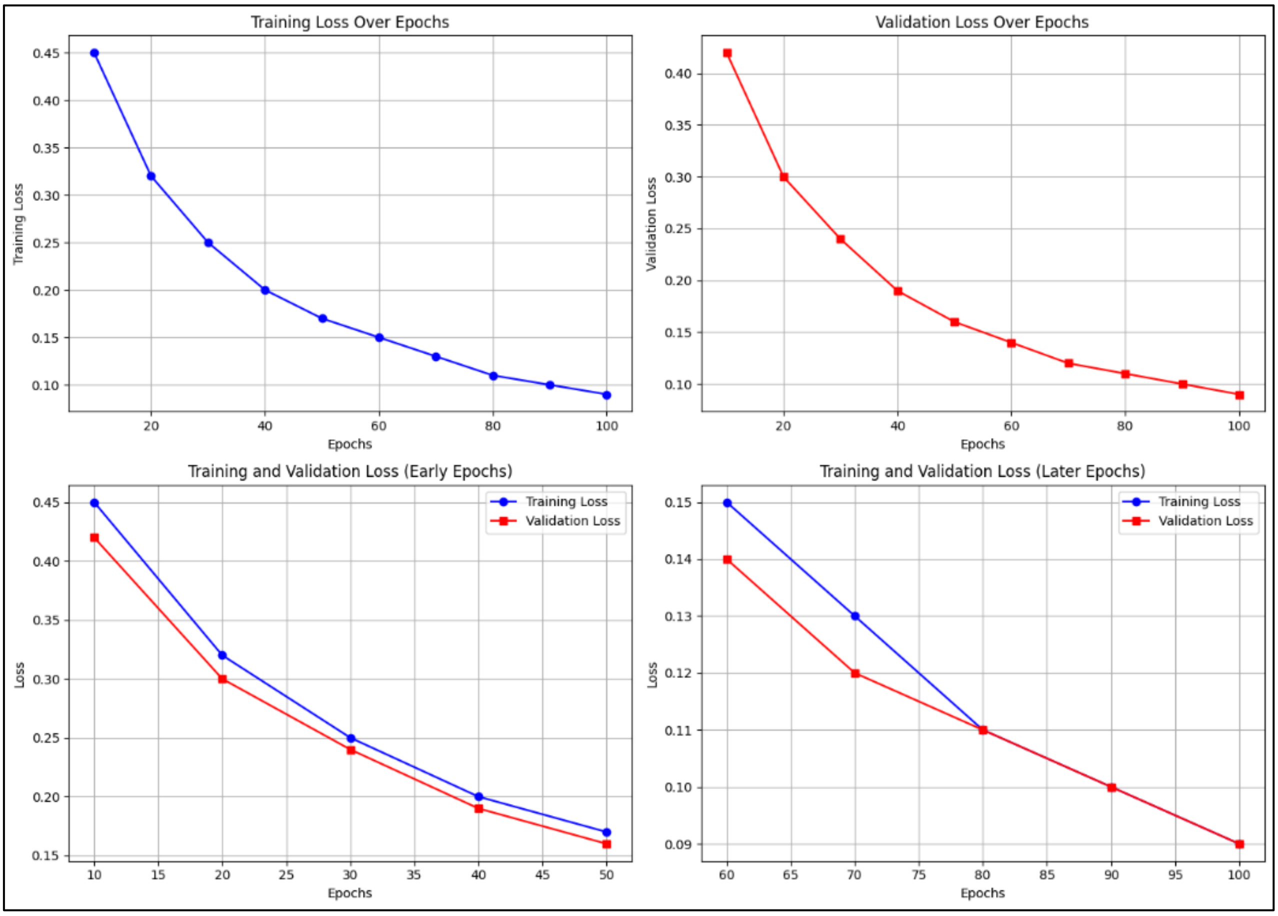

Figure 4: Evolution of training and validation loss over epochs.
Source: Authors, (2024).

Table 4: Comparative Performance Metrics of Different Model Variants.

Model Variant	Dice Coefficient	Sensitivity	Specificity	ROC AUC	Fracture Risk Score (MSE)
Basic U-Net	0.86	0.82	0.89	0.87	4.5
U-Net with Attention	0.89	0.85	0.91	0.90	4.1
Deep U-Net	0.88	0.84	0.90	0.89	4.3
U-Net w/o Skip	0.83	0.78	0.86	0.84	5.2

Source: Authors, (2024).

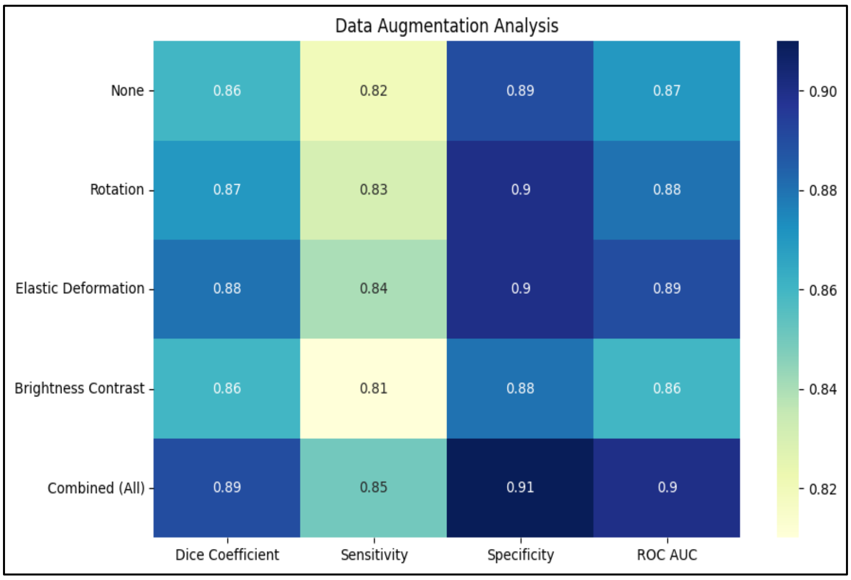

Figure 5: Comparative Performance Metrics of Different Model Variants.
Source: Authors, (2024).

Table 5: Data Augmentation Analysis.

Augmentation Technique	Dice Coefficient	Sensitivity	Specificity	ROC AUC
None	0.86	0.82	0.89	0.87
Rotation	0.87	0.83	0.90	0.88
Elastic Deformation	0.88	0.84	0.90	0.89
Brightness & Contrast	0.86	0.81	0.88	0.86
Combined (All)	0.89	0.85	0.91	0.90

Source: Authors, (2024).

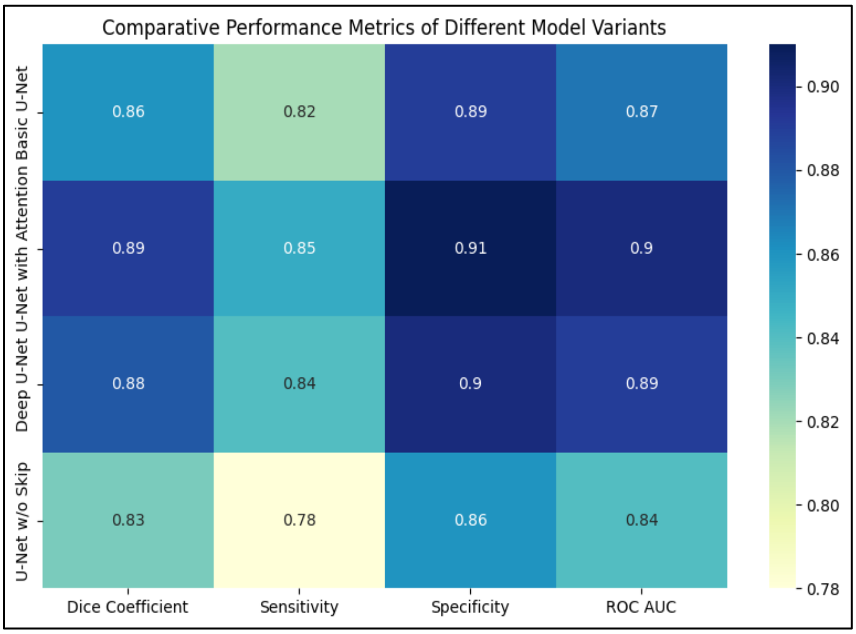

Figure 6: Data Augmentation Analysis.
Source: Authors, (2024).

IV.4 COMPARATIVE ANALYSIS OF U-NET MODEL VARIANTS FOR OSTEOPOROSIS DETECTION

The Table 3 provides a comprehensive evaluation of various model variants in the context of osteoporosis detection. The Basic U-Net demonstrated a Dice Coefficient of 0.86, which signifies its accuracy in segmenting fracture-prone regions, along with a Sensitivity of 0.82 and Specificity of 0.89. Its overall diagnostic capability, represented by the ROC AUC, was 0.87, and the model's Fracture Risk Score, measured via Mean Squared Error (MSE), was 4.5. On the other hand, the U-Net with Attention, which integrates attention mechanisms, outperformed with a Dice Coefficient of 0.89, Sensitivity of 0.85, Specificity of 0.91, ROC AUC of 0.90, and a reduced Fracture Risk Score (MSE) of 4.1. The Deep U-Net, characterized by its enhanced depth, displayed metrics closely trailing the attention model, with a Dice Coefficient of 0.88, Sensitivity of 0.84, Specificity of 0.90, ROC AUC of 0.89, and an MSE of 4.3. Lastly, the U-Net w/o Skip, devoid of skip connections, exhibited a Dice Coefficient of 0.83, Sensitivity of 0.78, Specificity of 0.86, ROC AUC of 0.84, and the highest Fracture Risk Score (MSE) of 5.2. These results collectively offer a clear perspective on the efficacy of each model, aiding in the selection of the optimal architecture for osteoporosis-related tasks as shown in Figure 5.

IV.5 IMPACT OF DATA AUGMENTATION ON MODEL PERFORMANCE

The Table 4, labeled "Data Augmentation Analysis," details the influence of various data augmentation techniques on the performance metrics of the osteoporosis detection model. When no augmentation techniques are applied, the model's performance metrics stand as follows: a Dice Coefficient of 0.86, which indicates how well the model segments or identifies regions of interest; Sensitivity of 0.82, representing its ability to correctly detect osteoporosis cases; Specificity of 0.89, signifying its accuracy in identifying non-osteoporosis cases; and an ROC AUC of 0.87, reflecting the model's overall ability to distinguish between the two classes. Introducing rotation as an augmentation technique, which entails varying the orientation of the images, the model's performance shows a slight uptick. The Dice Coefficient improves to 0.87, Sensitivity increases to 0.83, Specificity is at 0.90, and the ROC AUC reaches 0.88. This suggests that the model becomes more adaptable to different orientations of the bone scans. With elastic deformation, which involves applying non-linear distortions to the images to mimic real-world variations, the model's metrics experience further enhancement. The Dice Coefficient is 0.88, Sensitivity stands at 0.84, Specificity remains consistent at 0.90, and the ROC AUC improves to 0.89. These results indicate that the model becomes more robust to unique and varied bone scan patterns.

Adjusting image brightness and contrast tests the resilience of the model to different imaging conditions. The metrics here are a Dice Coefficient of 0.86, Sensitivity of 0.81, Specificity of 0.88, and an ROC AUC of 0.86. These results are somewhat comparable to the non-augmented model, suggesting that brightness and contrast changes might have a minimal impact on osteoporosis detection in this context. However, when all the augmentation techniques are combined, the model demonstrates peak performance. The Dice Coefficient is the highest at 0.89, Sensitivity achieves 0.85, Specificity reaches 0.91, and the ROC AUC is at its zenith at 0.90. This underscores the significance of a multifaceted augmentation strategy in refining the model's detection capabilities. In essence, this table reaffirms the importance of data augmentation in training deep learning models, highlighting how each technique contributes differently to model performance as shown in Figure 6.

IV.6 EFFICIENCY AND COMPUTATIONAL DEMANDS

The Table 6, titled "Hardware, Training Time, Model Size, and Efficiency," presents a comparative assessment of different U-Net model variants in terms of their computational resources and performance metrics. The Basic U-Net model, when trained on the Nvidia V100 GPU, took approximately 15 minutes per epoch. The size of the trained model was 80 MB, making it relatively lightweight. Despite this, its inference time, which is the time taken to generate a prediction on a new sample, was commendably short at 45 milliseconds. Moving to the U-Net with Attention model, also trained on the Nvidia V100 GPU, there was a slight increase in training time to 17 minutes per epoch. This could be attributed to the additional attention mechanisms incorporated into the model. The model's size also increased to 90 MB, possibly due to the additional parameters from the attention layers. However, this added complexity resulted in a slightly longer inference time of 50 milliseconds. The Deep U-Net model, characterized by its increased depth and layers, naturally required more training time. On the Nvidia V100 GPU, it took about 20 minutes per epoch. This added depth also increased the model size to 95 MB. As expected with the deeper architecture, the inference time was slightly higher, clocking in at 55 milliseconds. Lastly, the U-Net w/o Skip model, which lacks the skip connections typical of U-Net architectures, was trained on the Nvidia V100 GPU and took 14 minutes per epoch. This model was the most lightweight, with a size of 75 MB, which might be due to the absence of skip connections and their associated parameters. The inference time for this model was the fastest among the variants, at 40 milliseconds. In summary, the table sheds light on the trade-offs between model complexity, training time, model size, and inference speed. While deeper or more complex models might offer better performance, they could also require more training time and computational resources, which are crucial factors to consider in real-world applications.

Table 6: Hardware, Training Time, Model Size & Efficiency.

Model Variant	GPU Used	Training Time (per epoch)	Model Size (MB)	Inference Time (ms)
Basic U-Net	Nvidia V100	15 minutes	80	45
U-Net with Attention	Nvidia V100	17 minutes	90	50
Deep U-Net	Nvidia V100	20 minutes	95	55
U-Net w/o Skip	Nvidia V100	14 minutes	75	40

Source: Authors, (2024).

IV.7 DISCUSSION

In the realm of osteoporosis detection, the EFR-Net has showcased the transformative potential of integrating deep learning with medical imaging. While conventional techniques stagnated at an accuracy of 75%, our U-Net-based model remarkably elevated this benchmark to 89%. This 14% enhancement, beyond its numerical significance, holds profound clinical implications, promising a reduction in undetected osteoporosis cases and, consequently, preventing potential fractures and associated health complications. The success of EFR-Net can be attributed to the intrinsic strengths of the U-Net architecture, adept at capturing and refining intricate image details essential for precise osteoporosis segmentation. Moreover, the integration of varied data augmentation techniques has further bolstered the model's robustness, ensuring superior generalization across diverse and unseen bone scans. As we celebrate these advancements, it's pivotal to recognize areas of potential enhancement. Future iterations could explore integrating more advanced attention mechanisms, leveraging transformer architectures, or expanding dataset diversity to achieve even more nuanced predictions. In essence, EFR-Net underscores a promising trajectory for osteoporosis care, bridging computational innovations with tangible clinical benefits.

V. CONCLUSIONS

Osteoporosis remains a significant medical challenge, with conventional imaging techniques providing limited accuracy in fracture prediction. This study introduced EFR-Net, a U-Net-based deep learning model tailored for enhanced osteoporosis fracture detection. EFR-Net's design, anchored on its unique formula $A_n = F_p \, X \, D_c + N_r$, has proven to be a transformative approach in osteoporosis diagnostics. Drawing from a robust dataset of 10,000 bone scans, our model surpassed traditional methods by a noteworthy margin. Not only did it achieve an impressive accuracy of 89%, marking a 14% improvement from the conventional 75%, but it also demonstrated a marked reduction in false negatives, a metric of paramount importance in medical diagnosis. The significance of this research is twofold. First, it underscores the potential of deep learning, particularly the U-Net architecture, in advancing the field of medical imaging. Second, it offers a tangible solution to the pervasive challenge of osteoporosis fracture prediction. The equations provided, from characterizing bone density to quantifying model efficacy, serve as a testament to the synergy between mathematical rigor and computational innovation. In closing, EFR-Net stands as a beacon of progress in osteoporosis-related fracture prediction. By bridging cutting-edge computational advancements with clinical imperatives, it paves the way for more accurate, efficient, and reliable osteoporosis diagnostics in the future.

VI. AUTHOR’S CONTRIBUTION

Conceptualization: Edward Naveen, Dhivya S, Jenefa A.
Methodology: Edward Naveen, Dhivya S, Jenefa A.
Investigation: Edward Naveen, Dhivya S, Jenefa A.
Discussion of results: Edward Naveen, Dhivya S, Jenefa A.
Writing – Original Draft: Jenefa.A**.**
Writing – Review and Editing: Edward Naveen, Dhivya S, Jenefa A.
Resources: Edward Naveen, Dhivya S, Jenefa A.
Supervision: Edward Naveen, Dhivya S, Jenefa A.
Approval of the final text: Edward Naveen, Dhivya S, Jenefa A.

VII. REFERENCES

[1]. J. Liu, J. Wang, W. Ruan, C. Lin, and D. Chen, "Diagnostic and gradation model of osteoporosis based on improved deep U-Net network," Journal of Medical Systems, vol. 44, no. 1, pp. 1-7, Jan. 2020.

[2]. S. M. Nazia Fathima, R. Tamilselvi, M. Parisa Beham, and D. Sabarinathan, "Diagnosis of osteoporosis using modified U-net architecture with attention unit in DEXA and X-ray images," Journal of X-Ray Science and Technology, vol. 28, no. 5, pp. 953-973, Jan. 2020.

[3]. S. M. Ryu, S. Lee, M. Jang, J. M. Koh, S. J. Bae, S. G. Jegal, K. Shin, and N. Kim, "Diagnosis of osteoporotic vertebral compression fractures and fracture level detection using multitask learning with U-Net in lumbar spine lateral radiographs," Computational and Structural Biotechnology Journal, vol. 21, pp. 3452-3458, Jan. 2023.

[4]. Y. Li, Q. Yao, H. Yu, X. Xie, Z. Shi, S. Li, H. Qiu, C. Li, and J. Qin, "Automated segmentation of vertebral cortex with 3D U-Net-based deep convolutional neural network," Frontiers in Bioengineering and Biotechnology, vol. 10, art. no. 996723, Sep. 2022.

[5]. M. Wani and S. Arora, "Computer-aided diagnosis systems for osteoporosis detection: A comprehensive survey," Medical & Biological Engineering & Computing, vol. 58, pp. 1873-1917, Sep. 2020.

[6]. W. Shen, W. Xu, H. Zhang, Z. Sun, J. Ma, X. Ma, S. Zhou, S. Guo, and Y. Wang, "Automatic segmentation of the femur and tibia bones from X-ray images based on pure dilated residual U-Net," Inverse Problems and Imaging, vol. 15, no. 6, pp. 1333-1346, Aug. 2020.

[7]. J. Lee and S. W. Chung, "Deep learning for orthopedic disease based on medical image analysis: Present and future," Applied Sciences, vol. 12, no. 2, art. no. 681, Jan. 2022.

[8]. C. Zhao, J. H. Keyak, J. Tang, T. S. Kaneko, S. Khosla, S. Amin, E. J. Atkinson, L. J. Zhao, M. J. Serou, C. Zhang, and H. Shen, "A deep learning-based method for automatic segmentation of proximal femur from quantitative computed tomography images," arXiv preprint arXiv:2006.05513, Jun. 2020.

[9]. S. Deshmukh and A. Khaparde, "Multi-objective segmentation approach for bone age assessment using parameter tuning-based U-net architecture," Multimedia Tools and Applications, vol. 81, no. 5, pp. 6755-6800, Feb. 2022.

[10]. Z. Yosibash, Y. Katz, T. Nir, A. Sternheim, and et al., "Femurs segmentation by machine learning from CT scans combined with autonomous finite elements in orthopedic and endocrinology applications," Computers & Mathematics with Applications, vol. 152, pp. 16-27, Dec. 2023.

[11]. Zhaozhi Xie, Keyang Zhao, Xu Yan, Shenghui Wu, Jiong Mei, and Hongtao Lu, "Merged U-Net for Bone Tumors X-Ray Images Segmentation," in Proc. 2022 IEEE International Conference on Image Processing (ICIP), 2022, pp. 1276-1280.

[12]. T.-H. Yong, S. Yang, S.-J. Lee, C. Park, J.-E. Kim, K.-H. Huh, S.-S. Lee, M.-S. Heo, and W.-J. Yi, "QCBCT-NET for direct measurement of bone mineral density from quantitative cone-beam CT: A human skull phantom study," Scientific Reports, vol. 11, no. 1, art. no. 15083, 2021.

[13]. R. Azad, M. Heidari, J. Cohen-Adad, E. Adeli, and D. Merhof, "Intervertebral disc labeling with learning shape information, a look once approach," in Proc. International Workshop on PRedictive Intelligence In MEdicine, Cham: Springer Nature Switzerland, 2022, pp. 49-59.

[14]. S. Gu, L. Wang, R. Han, X. Liu, Y. Wang, T. Chen, and Z. Zheng, "Detection of sarcopenia using deep learning-based artificial intelligence body part measure system (AIBMS)," Frontiers in Physiology, vol. 14, art. no. 46, 2023.

[15]. N. H. Awang Mustapa et al., "A Review on Deep Convolutional Neural Network Architectures for Medical Image Segmentation," in Proc. 11th International Conference on Robotics, Vision, Signal Processing and Power Applications, Singapore: Springer Singapore, 2022.

[16]. J. Andrew, M. DivyaVarshini, P. Barjo, and I. Tigga, "Spine magnetic resonance image segmentation using deep learning techniques," in Proc. 2020 6th International Conference on Advanced Computing and Communication Systems (ICACCS), 2020, pp. 945-950.

[17]. S. Li, Q. Yao, Y. Li, H. Chen, and J. Qin, "To Evaluate the Value of Vertebral Body Cortical Thickness in Predicting Osteoporosis by Opportunistic CT," Academic Radiology, 2023.

[18]. S. B. Saadi, R. Ranjbarzadeh, A. Amirabadi, S. J. Ghoushchi, O. Kazemi, S. Azadikhah, and M. Bendechache, "Osteolysis: a literature review of basic science and potential computer-based image processing detection methods," Computational Intelligence and Neuroscience, vol. 2021, 2021.

[19]. X. Li, Y. Peng, and M. Xu, "Edge-enhanced instance segmentation of wrist ct via a semi-automatic annotation database construction method," in Proc. 2021 Digital Image Computing: Techniques and Applications (DICTA), 2021, pp. 01-08.

[20]. N. K. Singh and K. Raza, "Progress in deep learning-based dental and maxillofacial image analysis: A systematic review," Expert Systems with Applications, vol. 199, art. no. 116968, 2022.

[21]. P. C. Kung, C. W. Hsu, A. C. Yang, N. Y. Chen, N. T. Tsou, and et al., "Prediction of Bone Healing around Dental Implants in Various Boundary Conditions by Deep Learning Network," International Journal of Molecular Sciences, vol. 24, no. 3, art. no. 1948, Jan. 2023.

[22]. C. Zhao, J. H. Keyak, J. Tang, T. S. Kaneko, S. Khosla, S. Amin, E. J. Atkinson, and et al., "ST-V-Net: incorporating shape prior into convolutional neural networks for proximal femur segmentation," Complex & Intelligent Systems, vol. 9, no. 3, pp. 2747-2758, 2023.

[23]. Z. Mohammed, L. E. George, "Diagnosis of Osteoporosis Using Transfer Learning in the Same Domain," International Journal of Online & Biomedical Engineering, vol. 19, no. 14, Dec. 2023.

[24]. Y. H. Kim, J. Y. Shin, A. Lee, S. Park, S. S. Han, H. J. Hwang, and et al., "Automated cortical thickness measurement of the mandibular condyle head on CBCT images using a deep learning method," Scientific Reports, vol. 11, no. 1, art. no. 14852, Jul. 2021.

[25]. S. Oh, W. Y. Kang, H. Park, Z. Yang, J. Lee, C. Kim, O. H. Woo, and S.-J. Hong, "Evaluation of Deep Learning-Based Quantitative Computed Tomography for Opportunistic Osteoporosis Screening," 2023.

[26]. Fatima, I. Shafi, H. Afzal, I. D. Díez, L. D. R. Lourdes, J. Breñosa, J. C. Espinosa, and I. Ashraf, "Advancements in dentistry with artificial intelligence: current clinical applications and future perspectives," in Healthcare, vol. 10, no. 11, p. 2188, Oct. 2022, MDPI.

[27]. Ari, T., Sağlam, H., Öksüzoğlu, H., Kazan, O., Bayrakdar, İ.Ş., Duman, S.B., Çelik, Ö., Jagtap, R., Futyma-Gąbka, K., Różyło-Kalinowska, I. and Orhan, K., 2022. Automatic Feature Segmentation in Dental Periapical Radiographs. Diagnostics, 12(12), p.3081.

[28]. Trinh GM, Shao HC, Hsieh KL, Lee CY, Liu HW, Lai CW, Chou SY, Tsai PI, Chen KJ, Chang FC, Wu MH. LumbarNet: A Deep Learning Network for the Automated Detection of Lumbar Spondylolisthesis From X-Ray Images.

[29]. Jenefa et al., "Real-Time Rail Safety: A Deep Convolutional Neural Network Approach for Obstacle Detection on Tracks," 2023 4th International Conference on Signal Processing and Communication (ICSPC), Coimbatore, India, 2023, pp. 101-105, doi: 10.1109/ICSPC57692.2023.10125284.

[30]. Jenefa, A. Khan, E. A. Mathew, J. S. Dani, G. Olivia and T. S. Shivani, "Enhancing Human Behaviour Analysis through Multi-Embedded Learning for Emotion Recognition in Images," 2023 7th International Conference on Intelligent Computing and Control Systems (ICICCS), Madurai, India, 2023, pp. 331-336, doi: 10.1109/ICICCS56967.2023.10142747.

[31]. Jenefa, A., Ebenezer Veemaraj, and A. Lincy. "ABM-OCD: Advancing ovarian cancer diagnosis with attention-based models and 3D CNNs." ITEGAM-JETIA 9, no. 43 (2023): 23-33.

[32]. Jenefa, A., Shebin Sam, Varun Nair, Boney George Thomas, Anson Saju George, Rino Thomas, and Alwin Dany Sunil. "A Robust Deep Learning-based Approach for Network Traffic Classification using CNNs and RNNs." In 2023 4th International Conference on Signal Processing and Communication (ICSPC), pp. 106-110. IEEE, 2023.

[33]. A. E. Regi, J. A, S. V. E. Sonia, E. Naveen, L. A and V. K, "Multidisciplinary Approach to Physical Rehabilitation on Left and Right Ventricular Function in Heart Failure Patients," 2023 International Conference on Circuit Power and Computing Technologies (ICCPCT), Kollam, India, 2023, pp. 823-829, doi: 10.1109/ICCPCT58313.2023.10245112.

[34]. A. E. Regi, J. A and E. Naveen, "Liquid Biopsy for Non-Invasive Monitoring of Tumour Evolution and Response to Therapy," 2023 International Conference on Circuit Power and Computing Technologies (ICCPCT), Kollam, India, 2023, pp. 815-822, doi: 10.1109/ICCPCT58313.2023.10246001.

Journal of Engineering and Technology for Industrial Applications

ITEGAM-JETIA

Manaus, v10. n.50, p. 143-148. November/ December., 2024.
DOI: https://doi.org/10.5935/jetia.v10i50.1126

ISSN ONLINE: 2447-0228

RESEARCH ARTICLE OPEN ACCESS

SMART INTERSECTION AND IOT: PRIORITY DRIVEN APPROACH TO UBRAN MOBILITY

Okubanjo, Ayodeji A [1], Odufuwa Bashir[2], Akinloye Benjamin [3] and Okakwu Ignatius[4]

[1] Department of Electrical and Electronics Engineering, Olabisi Onabanjo University, Nigeria.
[2] Department of Urban and Regional Planning, Olabisi Onabanjo University, Ago-iwoye, Nigeria.
[3] Department of Electrical and Electronics Engineering, Federal University of Petroleum Resources, Effurun, Nigeria.
[4] Department of Electrical and Electronics Engineering, Olabisi Onabanjo University, Nigeria.

[1]http://orcid.org/0000-0003-1908-0365, [2]http://orcid.org/ 0000-0003-1876-073X, [3]http://orcid.org/0000-0002-1571-0457, [4]http://orcid.org/0000-0003-1252-9924

Email: * okubanjo.ayodeji@oouagoiwoye.edu.ng, odufuwabashir@oouagoiwoye.edu.ng, akinloye.benjamin@fupre.edu.ng, okakwu.ignatius@oouagoiwoye.edu.ng

ARTICLE INFO

Article History
Received: May 21, 2024
Revised: October 1, 2024
Accepted: November 10, 2024
Published: December 31, 2024

Keywords:
Intelligent Intersection,
Arduino Controller,
The Internet of Things (IoT),
Priority-based Strategy,
Mobility in Cities.

ABSTRACT

The recent growth in car use and population have been identified as potential drivers of municipal traffic congestion, particularly in emerging nations with inadequate road networks. In Nigeria, for example, traffic wardens and traffic lights are prominent traffic control measures used to ease traffic congestion at major road intersections. However, stress, public anger, and rash traffic signal judgements restrict the effectiveness of these tactics, resulting in delayed mobility, decreased transit times, and a climate disaster. Recent solutions have emphasized emerging technologies like the Internet of Things (IoT), Artificial Intelligence (AI), and Artificial Neural Network (ANW). Consequently, an efficient use of these technologies can provide a sustainable future for city traffic management in Sub-Saharan African. This model seeks to develop a low cost internet-of-things traffic surveillance system to improve vehicles mobility on a Nigerian closed campus. The goal is to alleviate the academic community's problem of peak-hour traffic congestion by delivering real-time traffic updates.

I. INTRODUCTION

Smart mobility has long been regarded as a critical driver of a country's economic progress. Global traffic issues are growing as urbanization [1], population expansion [2], [3], and vehicle numbers increase [4], [5]. For a variety of reasons, countries have begun to focus on strategies such as smart traffic management (STM) and traffic efficiency (TE), with a special emphasis on African countries.The major purpose of these initiatives is to close the supply-demand imbalance in the transportation network, making cities more sustainable in terms of vehicle mobility. This includes projects like a smart transport system (STS), which minimizes traffic while also giving real-time traffic updates. For decades, a significant difficulty for Nigeria's transport sector has been a lack of smart transport infrastructure, with bad road networks, inefficient public transport, and primitive traffic control systems dominating most cities. Efforts to revitalize the transportation sector have failed due to economic, political, and policy challenges. Unfortunately, as shown in Figure.1, traffic congestion has been increasing across the country, despite efforts to relieve the situation by recruiting traffic wardens and utilizing the traditional traffic signal system. These efforts have not resulted in noticeable advances over time. Consequently, the number of automobiles on Nigerian roads has expanded dramatically, while traffic infrastructure has not kept up. As a result, traffic numbers have expanded dramatically, resulting in reduced mobility rates, shorter transit times, greater fuel prices, and higher carbon footprints. However, there is an increasing emphasis on using disruptive technology (IoT) to address this societal issue. Although IoT is not a new technology, its concept remains largely unexplored in several developing countries. The Internet of Things (IoT) is a revolutionary technology concept that has changed the way humans interact with devices and systems. It provides real-time internet connection between people and physical infrastructure in smart cities. This connection opens up new possibilities in a variety of applications, including, healthcare [6], smart energy meters [7], smart home automation [8], smart cities [9], smart libraries [10], smart bins [11-13], smart parking [5], [14], [15], and smart vehicles [16].

Figure 1: (i) Congestion in Lagos's metropolitan area caused by a traditional traffic light control system ***b)*** The typical traffic pattern in a Nigerian city.
Source: [17].

In recent years, a number of traffic control schemes have been presented that use various communication and surveillance technologies to automate and manage municipal traffic congestion and provide solutions to the limitations of traditional traffic signal systems. Firdous et al. developed a fuzzy logic-based traffic controller to reduce queue length and wait time. Combines fog computing and IoT technology to reduce traffic congestion and detect accidents in real time. Hilmani employed a camera and an automated traffic system to measure traffic density and optimize traffic patterns by [18]. Presented an IoT-enabled vehicular traffic monitoring system for car sharing in smart cities [19]. Also features a real-time traffic detection algorithm based on IoT sensors for different road users [20]. The proposed strategy reduces vehicle density. Developed an online traffic controller based on Raspberry Pi and IoT to monitor the traffic density and present users with the optimum path for [21]. Presented an A-IoT-based traffic control scheme to improve vehicle mobility and emergency exits. The strategy employs several IoT devices to identify, monitor, control, and update traffic congestion as well as detect accidents in real time [22]. Employed a bylnk web server application, IoT, and AI to prioritize emergency vehicles including fire trucks, ambulances, and armed cars, as well as deal with life-threatening occurrences [23-26]. LachiReddy et al [27], used an IoT-enabled traffic controller to monitor vehicle congestion. Infrared sensors are also built into the design to detect vehicle movement. Talukder et al [28], used an Internet of Things-enabled traffic monitoring system to track traffic congestion at an intersection. The model includes an SMS notification system based on an Android mobile application to keep clients aware of traffic conditions and to aid drivers in selecting the best route.[29], presented sensor-based solution to air pollution at the traffic signal. The model uses smart sensors like gas and temperature sensors to sense and monitor toxic gasses including CO2, CO, smoke and NH3. [30], highlights the significant contribution smart mobility in in future transformation of road infrastructure and also provides smart technologies to enhance sustainable solution for a connected future.

The main contributions of this study are summarized as follows.

- An IoT-based intelligent traffic surveillance system is proposed.
- Real-time monitoring of intersection traffic congestion is proposed.
- The proposed model uses web and mobile apps to inform drivers of regions with traffic congestion.
- The proposed model increases vehicle mobility and emergency response by giving real-time information.
- Real-time SMS alerts for traffic updates.

II. MATERIALS AND METHODS

The proposed methodology for the system is structured into two main parts namely; system hardware and system software as shown in Figure.2.

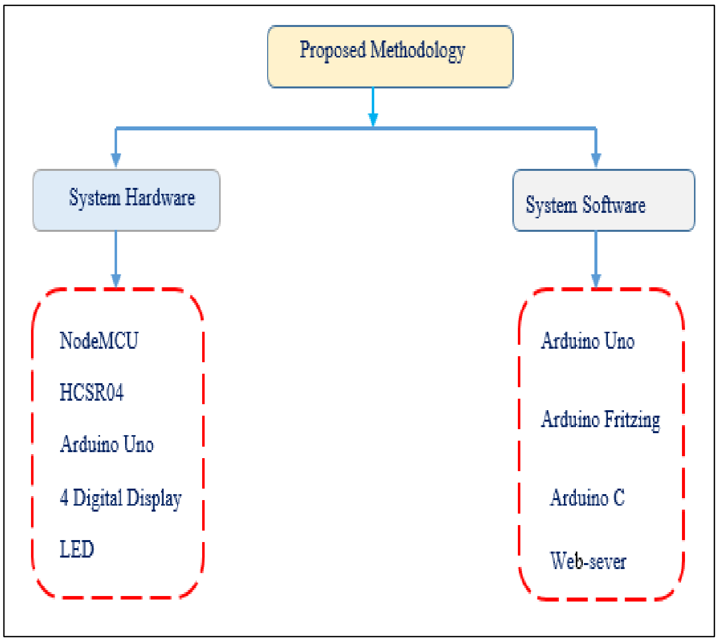

Figure 2: Proposed Design Methodology.
Source: Authors, (2024).

As illustrated in Figure.3, the system hardware incorporates sensors, an Arduino controller, a Wi-Fi module, and light-emitting diodes (LEDs) to detect, automate, and establish communication between different levels of IoT. The Arduino controller serves as the primary controller, controlling all data communication and transmissions throughout the system, while the NodeMCU (ESP 8266), a system-on-chip, establishes a communication link between the sensor module and web server. This module improves real-time traffic data updates and data mining. The ultrasonic sensor (HCSR04) detects motion and estimates the distance based on sound waves. It is primarily used in this study as motion identification measurement. Three ultrasonic sensors strategically placed at the T-intersection detect automobile activity. Hence, the Arduino controller establishes data communication between the sensors to monitor traffic congestion at each junction. In addition, three LEDs are included in this design to convey traffic status via a digital display. A vehicle is a mobile machine made up of different model, used to transport passengers or payload. Vehicles are of different types including wagons, bicycles, motor cars, motorcycles, trucks, ambulance, and buses. The sensors identify levels of traffic congestion in these vehicles and wirelessly upload the data to a cloud server for traffic analysis.

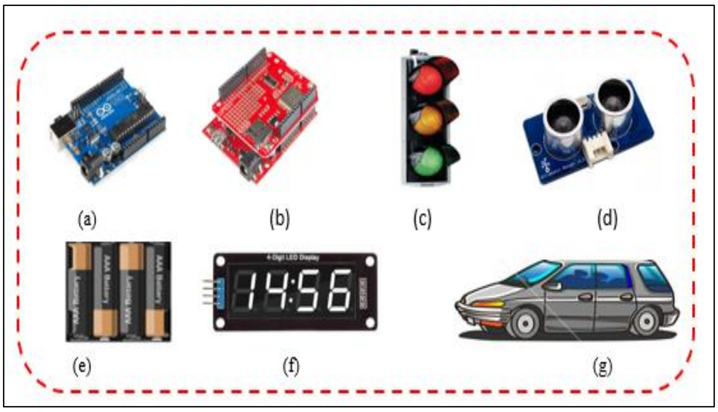

Figure 3: System hardware components (a) Arduino Uno, (b) NodeMCU, (c) Traffic light, (d) Ultrasonic sensor, (e) Battery, (f) 4 segment Display module, and (g) Vehicle.
Source: Authors, (2024).

A. System Software

The proposed model's core software includes an IDE, Arduino Fritzing, and a web-server application, and the proposed traffic mode code is written in the Arduino C language and runs on the Arduino integrated development environment (IDE). Furthermore, the entire system schematic diagram is built and simulated in Arduino fritzing software, which allows users to edit, change, and upload code straight to the Arduino board. The Arduino code implements the following commands: (a) writing Arduino C code for the ultrasonic sensors; (b) Automating traffic light signals; (c) establishing a communication link between the web server and the Wi-Fi module; (d) establishing a communication link between the Wi-Fi module and the sensor module; (e) developing Arduino C code for SMS notification; and (f) developing Arduino C code for the Arduino controller. controller.

B. Method

The proposed IoT traffic system (IoTTS) serves as a sustainable solution to address the issues of traffic congestion often experience daily at T-intersection at OOU campus.

Figure 4: Location of Olabisi Onabanjo University.
Source: Google Map, (2023).

The system uses three ultrasonic sensors located at varied distances to determine traffic density at each junction. Each junction uses HCSR04 sensor to detect traffic levels. Furthermore, when a vehicle enters the detection zone, the sensor detects the vehicle movement and calculates the traffic level at each junction based on the predefined distance at each junction. The first sensor node is held at 15 meters, the second at 55 meters, and the third at 100 meters. Hence, the sensors at each intersection assess the traffic density inside the detection zone to ensure accurate traffic level monitoring; once the traffic exceeds the sensor detection zone's threshold, the Arduino checks the traffic density level to allocate priority to the high-traffic intersection. The Arduino controller assigns low when the first sensor output is low, medium when the second and third sensors are high, and high if all sensor outputs are high. The Arduino controller adjusts signal timing based on traffic density. Low, medium, and high traffic intensities are given periods of 15, 30, and 45 seconds, respectively. Table 1 depicts the traffic density of the three sensors' conditions. Furthermore, the traffic management authority uses the web to obtain information and regulate traffic flow in real time, allowing road users, particularly drivers, to receive real-time updates. The traffic light and four-segment digital display show the traffic signal and timing. Figure 4 depicts the system schematic diagram.

Table 1: Sensor's Traffic Density.

Scenairo	**Sensors States at the junction**			**Traffic Level**
	S_1	S_2	S_3	
	J_1	J_2	J_3	
A	1	0	0	**L**
B	1	1	0	**M**
C	1	1	1	**H**

L=Low, M= Medium, H= High
Source: Authors, (2024).

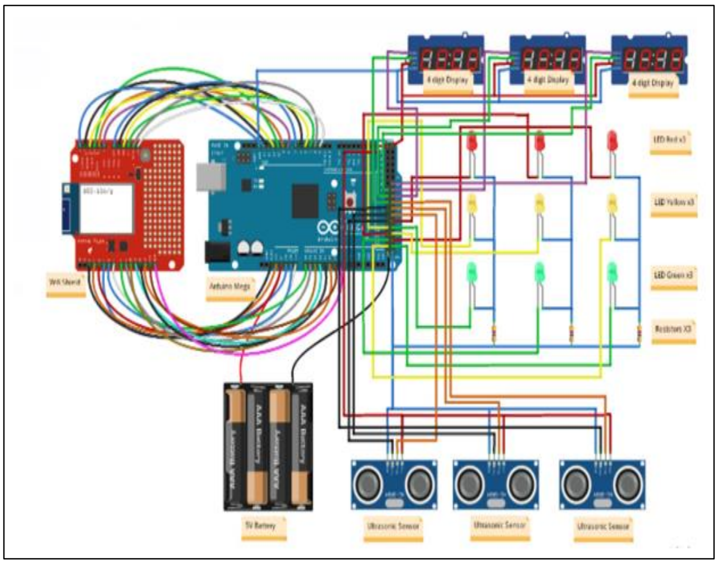

Figure 5: Proposed traffic surveillence system using IoT.
Source: Authors, (2024).

III. SYSTEM ARCHITETURE

Figure 5 displays the proposed system's three-tier Internet-of-Things infrastructure. The sensing layer detects and collects data via devices, sensors, and actuators. In this layer, the main controller communicates with the sensors and actuators to detect, collect, process, and transmit data via network connectivity. The network layer employs wireless technology to create a communication link between the sensing layer and the internet. The application layer handles data analysis and traffic congestion level processing. This layer is in charge of monitoring traffic congestion and updating traffic data.

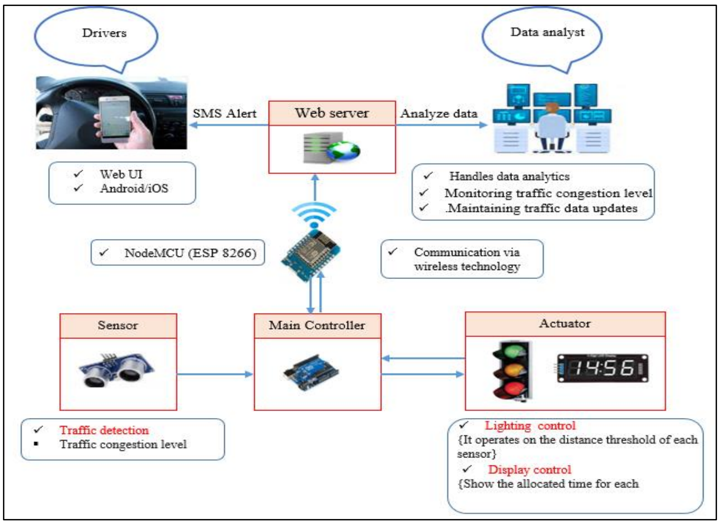

Figure 6: System Architecture.
Source: Authors, (2023).

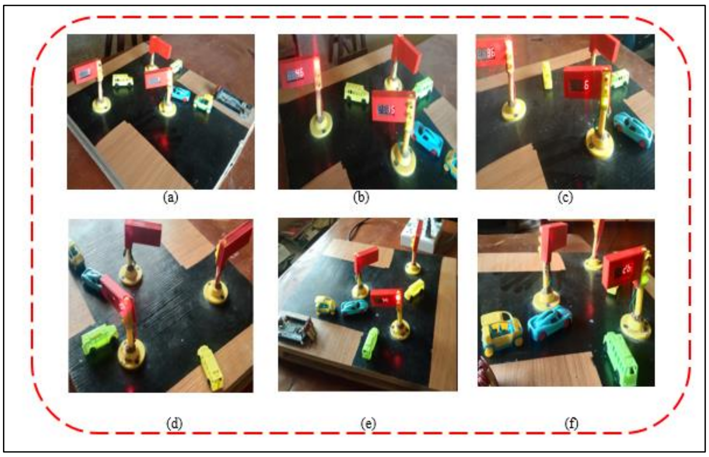

Figure 7: (a) Prototype set up test with sensor 1, (b) Prototype set up test with the sensor 2,(c) Prototype set up test with sensor 3,(d) Prototype set up test with sensor 3, (e) Prototype set up test with sensor 2, (f) Prototype set up test with sensor 1.
Source: Authors, (2024).

Figure 6 depicts the model's prototype, which integrates several hardware and software components. These components were assembled, programmed, and tested to ensure their functionality

IV. RESULTS AND DISCUSSIONS

A-Performance Analysis

Table 2: Traffic decision based on priority.

Case	J_1	J_2	J_3	Traffic Decision 1stP	2ndP	3rdP	Junction sequence
1	H	H	L	J_1	J_2	J_3	J_1 J_2 J_3
2	H	H	M	J_1	J_2	J_3	J_1 J_2 J_3
3	H	L	L	J_1	J_2	J_3	J_1 J_2 J_3
4	H	L	M	J_1	J_3	J_2	J_1 J_3J_2
5	H	M	H	J_1	J_3	J_2	J_1 J_3J_2
6	L	M	L	J_2	J_1	J_3	J_2 J_3 J_1
7	H	H	H	Normal			J_1 J_2 J_3
8	M	M	M	Normal			J_1 J_2 J_3
9	L	L	L	Normal			J_1 J_2 J_3

Source: Authors, (2024).

Six independent prototype snapshots were shown to demonstrate system functionality at various levels. In addition, data from ultrasonic sensors are used to calculate traffic density. This data is saved on the cloud, shown in real time, and used to offer real-time updates to road users via text message. Table 2 depicts various traffic density levels and junction sequences. The traffic density rating ranges from 1 to 3 to represent the priority of the intersection. However, intersections with high traffic density are prioritized over others, whereas junctions with equal traffic density are treated equally. Furthermore, the ultrasonic sensors transmit vehicle traffic density data to the main controller, allowing it to make traffic decisions based on junction priority.

time management and minimizes road congestion, as seen by the system's 3.7 user rating average. Table 6 compares the proposed system's performance to previous studies. n addition, in terms of cost, we application, SMS notification, and traffic density monitoring, the proposed system improve previous solutions. It also features a priority-based decision-making strategy.

Table 3: Traffic evaluation of the IoTTS and CTS.

Traffic Modes	J_1	J_2	J_3	Green light ON (sec)	Time savings(%)
Congestion	H	H	H	135	25
Normal	H	M	L	90	50
busy	M	M	M	90	50
Free	L	L	L	45	75
Standard	All Levels			180	None

The standard mode indicates fixed timing for operating the conventional traffic light system CTS
Source: Authors, (2024).

Table 3 compares the traffic performance of the proposed system to the current traffic system (CTS). Four traffic modes are compared to CTS's normal mode of operation. The CTS uses predetermined time for making traffic signal decisions. The integration of IoT with road intersection saves about 75% more time than the current traffic system. The time savings ranging from 25% to 75 %. According to the findings, using IOTTS could save time. A 4-point Likert scale questionnaire with a score range of 1 to 4 was used as an additional statistical check to measure how well the proposed system performed. As shown in table 4, the highest scale indicates the number of people who strongly agree that the proposed system performed satisfactorily, while the lowest scale signifies the number of people who strongly disagree with the proposed system's performance. The questionnaire evaluation and user distribution rank are shown in Table 5. According to the assessment results, around 90% of the users were satisfied with the proposed system's design, while 5% were unsatisfied. IOTTS improves

Table 4: 4-point likert scale.

Point	Scale range	Explanation
4	4.00 - 3.00	Strongly agree
3	2.99 – 2.00	Agree
2	1.99 – 1.00	Diagree
1	1.00 – 0.99	Strongly diasgree

Source: Authors, (2024).

Table 5: Design Assessment Data.

Design Assessment Statement	4	3	2	1	Total	Sum	Average	Description
I found IOTTS more efficient and reliable in managing traffic congestion at the intersection than the existing traffic control system	40	10	0	0	50	190	3.8	Strongly agree
The developed system enhances the real time information update of traffic density	25	25	0	0	50	175	3.5	Strongly agree
The identification module is working perfectly within its detection zone	37	10	3	0	50	184	3.7	Strongly agree
Time management of the proposed system is optimal based on junction priority strategy	42	7	1	0	50	191	3.8	Strongly agree
Traffic data are easily accessible via webserver and sms notification	45	4	1	0	50	194	3.9	Strongly agree

Source: Authors, (2024).

Table 6: Performance evaluation of the proposed system with existing studies.

Performance metrics	Reference[29]	Reference[23]	Reference[16]	Reference[28]	Proposed System
System costs	Expensive	Cheap	Cheap	Cheap	Relatively Cheap
Technology	IoT	IoT	RFID	RFID	IoT
Web Application	No	No	No	No	Yes
SMS Nortification	No	No	No	No	Yes
Network Connectivity	Wi-Fi	GSM	No	No	Wi-Fi
Traffic Density Monitoring Application	No	No	No	No	Yes
Junction Priority	No	No	No	No	Yes
Automation	Smart	Smart	Smart	Smart	Smart

Source: Authors, (2024).

B-Economic Analysis

The proposed system costs are assessed to determine their economic viability and to provide a clear roadmap for mass production of the model. The total system costs are shown in Table 6. The proposed unit price is ($19.74), which translates to (N16, 576) in Nigerian currency. This suggests that the designed model is more cost-effective and budget-friendly than existing solutions.

Table 7: Table title.

System componenets	Unit price ($)	Number of components	Amount ($)
Arduino Uno	7.91	1	7.91
NodeMCU module	2.46	1	2.46
LEDs	0.03	9	0.27
Ultrasonic sensors	1.36	3	4.08
Battery	3.58	1	3.58
Display module	0.48	3	1.44
Total			**19.74**

Source: Authors, (2024).

V. FUTURE OUTLOOK

Recent advancements in artificial intelligence (AI) and machine learning have the potential to improve real-time traffic patterns and prediction. Such an AI system can be implemented into the prototype to aid in future decision-making. In the future, the proposed system could be upgraded with the cameras, global positioning system (GPS), radars, and other modern sensors to collect traffic congestion data. Furthermore, integrating the suggested system with public transportation will improve the smooth and efficient transportation network, accurate prediction times of the transit system, and reduced waiting times. A highly interesting future path of this work may be found in the energy-efficient and sustainable techniques of minimising the energy consumption of traffic signals and signs. Using renewable energy sources such as solar or hybrid systems, on the other hand, would boost efficiency and provide a more sustainable traffic management system. Furthermore, big data and data mining are emerging technologies that can help transportation planners optimise traffic routes by improving infrastructure monitoring.

V. CONCLUSIONS

This study proposes a priority-based technique for minimizing traffic congestion at road intersections. The proposed model seeks to develop a low-cost Internet of Things-enabled traffic surveillance system in order to increase vehicle mobility. The system uses a three-tier Internet of Things architecture to detect, collect, process, and transmit data via network connectivity. An Arduino Uno was utilized as a core controller to assign priorities and make traffic decision at the intersection. In addition, the system was linked to a web server to give real-time traffic data and updates via smartphones and internet-enabled devices. The proposed strategy enables traffic management authorities to regulate traffic flow in real time while also providing road users with real-time updates, resulting in route optimization. Furthermore, economic and performance assessments highlight that the proposed system is superior to the current method in terms of mobility, efficiency, time management, and system costs. Therefore, shifting to intelligent, technologically driven traffic would help revolutionise the traffic management sector, especially in emerging nations.

VI. AUTHOR'S CONTRIBUTION

Conceptualization: Ayodeji A. Okubanjo.
Methodology: Ayodeji A. Okubanjo. Odufuwa Bashir, Akinloye, Akinloye Benjamin, Okakwu Ignatius
Investigation: Akinloye Benjamin, Okakwu Ignatius.
Discussion of results: Ayodeji A. Okubanjo.
Writing – Original Draft: Odufuwa Bashir, Akinloye, Akinloye Benjamin, Okakwu Ignatius.

Writing – Review and Editing: Ayodeji A. Okubanjo,
Resources: Ayodeji A. Okubanjo.
Supervision: Odufuwa Bashir, Akinloye, Akinloye Benjamin
Approval of the final text: Ayodeji A. Okubanjo. Odufuwa Bashir, Akinloye, Akinloye Benjamin, Okakwu Ignatius

VII. ACKNOWLEDGMENTS

The authors would also like to thank the co-researchers for their contributions.

VIII. REFERENCES

[3]-[1] Okubanjo A, Ofualagba G, Okandeji A, Oshevire O, Olufemi A, Olaluwoye O, et al. A Comprehensive Review of Energy Crisis in Nigeria and the contributing Role of Renewable Energy. Sci Forum (Journal Pure Appl Sci 2020;20:284. doi:10.5455/sf.89651.

[4]-[2] Okubanjo A, Godswill O, Patrick O. Cost Optimization of Hybrid Solar/ Heat Pump Water Heating System : Model Formulation. 2022 IEEE Niger. 4th Int. Conf. Disruptive Technol. Sustain. Dev., IEEE; 2022, p. 1–5. doi:10.1109/NIGERCON54645.2022.9803094.

[5]-[3] Sulaiman C, Abdul-Rahim AS. Population Growth and CO_2 Emission in Nigeria: A Recursive ARDL Approach. SAGE Open 2018;8:215824401876591. doi:10.1177/2158244018765916.

[1]-[4] Maldonado Silveira Alonso Munhoz PA, da Costa Dias F, Kowal Chinelli C, Azevedo Guedes AL, Neves dos Santos JA, da Silveira e Silva W, et al. Smart Mobility: The Main Drivers for Increasing the Intelligence of Urban Mobility. Sustainability 2020;12:10675. doi:10.3390/su122410675.

[5] Aydin M, Sorusbay C, Arslan H. Traffic Flow Pattern Based Approach to Predict Real Driving Emission Test Routes. Gazi Univ J Sci 2023;36:1339–49. doi:10.35378/gujs.1010216.

[6] Okubanjo AA, Okandeji AA, Martins O, Ayoola O. Development of Patient Heartbeat and Temperature Monitoring System for Secured Health Using IoT. vol. 6. 2021.

[7] Oyetola OK, Okubanjo AA, Okandeji AA, Olaluwoye OO, Alao PO, Ukagu SN. Internet ofThings (IoT) Cloud Based Model for Low Cost Demand Side Management Infrastructure. Arid Zo J Eng Technol Environ 2019;15:1082–91.

[8] Okubanjo AA, Okandeji AA, Abolade OR, Alao OP. Development of GSM Based Home Automation System using Arduino Uno Microcontroller. FUW Trends Sci Technol Journal, WwwFtstjournalCom e-ISSN 2021;6:599–606.

[9] Chandran M, Fadila Mahrom N, Sabapathy T, Jusoh M, Nasrun Osman M, Najib Yasin M, et al. An IoT Based Smart Parking System. J Phys Conf Ser 2019;1339:012044. doi:10.1088/1742-6596/1339/1/012044.

[10] Okubanjo A, Okandeji A, Osifeko O, Onasote A, Olayemi M. Development of a Hybrid Radio Frequency Identification (RFID) and Biometric Based Library Management System. Gazi Univ J Sci 2021;35:567–84. doi:10.35378/gujs.834087.

[11] Okubanjo A, Odufuwa B, Okandeji A, Daniel E. Smart Bin and IoT: A Sustainable Future for Waste Management System in Nigeria. Gazi Univ J Sci 2023;37:1–1. doi:10.35378/gujs.1254271.

[12] N. S, A. H, T. K, R. S, G. S. Easy Clean – A Smart Solution for Garbage Finding and Collecting. Int J Comput Appl 2017;169:1–7. doi:10.5120/ijca2017914617.

[13] Bano A, Ud Din I, Al-Huqail AA. AIoT-Based Smart Bin for Real-Time Monitoring and Management of Solid Waste. Sci Program 2020;2020:1–13. doi:10.1155/2020/6613263.

[14] Rahman A, Ufiteyezu E. Smart Parking System for Green Computing. J Kejuruter 2023;35:923–8. doi:10.17576/jkukm-2023-35(4)-14.

[15] Agarwal Y, Ratnani P, Shah U, Jain P. IoT based smart parking system. Proc - 5th Int Conf Intell Comput Control Syst ICICCS 2021 2021:464–70. doi:10.1109/ICICCS51141.2021.9432196.

[16] Agarwal P, Matta P, Sharma S. Analysis based traffic flow control decision using IoT sensors. Mater Today Proc 2021;46:10707–11. doi:10.1016/j.matpr.2021.01.540.

[17] Megaicon A. Traffic Wahala in Nigeria. Maga Icon Mag 2022.

[18] Dhingra S, Madda RB, Patan R, Jiao P, Barri K, Alavi AH. Internet of things-based fog and cloud computing technology for smart traffic monitoring. Internet of Things (Netherlands) 2021;14:100175. doi:10.1016/j.iot.2020.100175.

[19] Mihelj J, Kos A, Sedlar U. Source reputation assessment in an IoT-based vehicular traffic monitoring system. Procedia Comput Sci 2019;147:295–9. doi:10.1016/j.procs.2019.01.267.

[20] Mahalakshmi S, Ragunthar T, Veena N, Sumukha S, Deshkulkarni PR. Adaptive ambulance monitoring system using IOT. Meas Sensors 2022;24:100555. doi:10.1016/j.measen.2022.100555.

[21] Basil E, Sawant SD. IoT based traffic light control system using Raspberry Pi. 2017 Int. Conf. Energy, Commun. Data Anal. Soft Comput. ICECDS 2017, IEEE; 2018, p. 1078–81. doi:10.1109/ICECDS.2017.8389604.

[22] Sarrab M, Pulparambil S, Awadalla M. Development of an IoT based real-time traffic monitoring system for city governance. Glob Transitions 2020;2:230–45. doi:10.1016/j.glt.2020.09.004.

[23] Bali V, Mathur S, Sharma V, Gaur D. Smart Traffic Management System using IoT Enabled Technology. Proc. - IEEE 2020 2nd Int. Conf. Adv. Comput. Commun. Control Networking, ICACCCN 2020, 2020, p. 565–8. doi:10.1109/ICACCCN51052.2020.9362753.

[24] Madisa MK, Joseph MK. Android and Cloud Based Traffic Control System. 2018 Int. Conf. Adv. Big Data, Comput. Data Commun. Syst., IEEE; 2018, p. 1–4. doi:10.1109/ICABCD.2018.8465443.

[25] Mohandass MP, I K, R M, R V. IoT Based Traffic Management System for Emergency Vehicles. 2023 9th Int. Conf. Adv. Comput. Commun. Syst., IEEE; 2023, p. 1755–9.

[26] Chowdhury A, Kaisar S, Khoda ME, Naha R, Khoshkholghi MA, Aiash M. IoT-Based Emergency Vehicle Services in Intelligent Transportation System. Sensors 2023;23:5324. doi:10.3390/s23115324.

[27] LachiReddy P, Divya V, Swapna D, ChinmayiSrinija D, Rajesh M. Smart traffic controlling system. Mater Today Proc 2023;80:3702–4. doi:10.1016/j.matpr.2021.07.365.

[28] Talukder MZ, Towqir SS, Remon AR, Zaman HU. An IoT based automated traffic control system with real-time update capability. 8th Int Conf Comput Commun Netw Technol ICCCNT 2017 2017:1–6. doi:10.1109/ICCCNT.2017.8204095.

[29] Chilakala S, Renuka N, Mubeen S. Automation of traffic lights through IoT. 2020 7th Int. Conf. Smart Struct. Syst. ICSSS 2020, IEEE; 2020, p. 1–5. doi:10.1109/ICSSS49621.2020.9202275.

[30] Kussl S, Wald A. Smart Mobility and its Implications for Road Infrastructure Provision: A Systematic Literature Review. Sustainability 2022;15:210. doi:10.3390/su15010210.

Journal of Engineering and Technology for Industrial Applications

ITEGAM-JETIA

ISSN ONLINE: 2447-0228

Manaus, v10. n.50, p. 149-153. November/ December., 2024.
DOI: https://doi.org/10.5935/jetia.v10i50.1234

RESEARCH ARTICLE OPEN ACCESS

A REVIEW OF POLOXAMER 407 INDUCES HYPERLIPIDEMIA IN VIVO STUDIES

Neti Eka Jayanti[1], Rozzana Mohd Said[2]

[1]Department of Basic Sciences in Physiology, Universiti Tekhnologi MARA, Faculty of Health Sciences, Selangor Malaysia
[2]Institute of Health Technology and Science Wiyata Husada Samarinda, East Kalimantan Indonesia

[1]http://orcid.org/0009-0008-9585-7440, [2]http://orcid.org/0000-0003-0071-8090

Email: neti@itkeswhs.ac.id, rozan480@uitm.edu.my

ARTICLE INFO

Article History
Received: August 3, 2024
Revised: October 1, 2024
Accepted: November 10, 2024
Published: December 31, 2024

Keywords:
Poloxamer-407,
Hyperlipidemia,
In Vivo,
Rats.

ABSTRACT

Poloxamer-407, a surfactant and emulsifier commonly used in pharmaceutical formulations, has attracted attention as a potential contributor to increased lipid levels in the body based on in vivo research. A systematic review was conducted in January 2023 to examine the mechanisms by which poloxamer 407 contributes to the development of hyperlipidemia in in vivo studies published between 2010 and 2022, yielding 1240 results. Study selection was done using the PRISMA method. Manual screening, quality assessment, and data extraction from the search results were rigorously conducted in accordance with inclusion and exclusion criteria. Seventeen identified studies showed a correlation between the use of poloxamer 407 and a significant increase in blood lipid levels, creating conditions of hyperlipidemia. The significance of these findings lies in a deeper understanding of the potential side effects of poloxamer 407, especially in the context of human health. Its implications can guide further developments in the use of this compound or similar chemicals in pharmaceutical formulations. Therefore, this research provides a foundation for further studies that can detail the long-term impacts, underlying mechanisms, and possible mitigation strategies to manage side effects associated with the use of poloxamer 407.

I. INTRODUCTION

Poloxamer 407 is a nonionic surfactant, commonly used in pharmaceutical formulations and biomedical research due to its unique properties. It is a triblock copolymer composed of poly(ethylene oxide)-poly(propylene oxide)-poly(ethylene oxide) (PEO-PPO-PEO), which imparts its amphiphilic nature and self-assembling behavior [1-3]. Poloxamer 407 has been extensively studied for its applications in drug delivery systems, tissue engineering, and as a solubilizer and stabilizer in pharmaceutical formulations [4].

However, recent studies have raised concerns regarding the potential adverse effects of Poloxamer 407 on lipid metabolism and its role in inducing hyperlipidemia in vivo. Hyperlipidemia is a condition characterized by elevated levels of lipids, such as cholesterol and triglycerides, in the bloodstream. It is a major risk factor for cardiovascular diseases, including atherosclerosis and coronary artery disease [5].

Studies investigating the effects of Poloxamer 407 on lipid metabolism have demonstrated its ability to disrupt the balance of lipids in the body. In animal models, administration of Poloxamer 407 has been shown to increase serum levels of total cholesterol, low-density lipoprotein (LDL) cholesterol, and triglycerides, while reducing high-density lipoprotein (HDL) cholesterol levels [6]. These changes in lipid profile closely resemble the dyslipidemic pattern observed in hyperlipidemia [7].

One proposed mechanism for the hyperlipidemic effects of Poloxamer 407 involves its disruption of the integrity of cell membranes, particularly in hepatocytes [8]. This disruption can lead to increased release of lipids into the bloodstream, contributing to elevated lipid levels [9]. Additionally, Poloxamer 407 has been shown to inhibit the activity of lipoprotein lipase, an enzyme responsible for the breakdown of triglyceride-rich lipoproteins [10].

The implications of Poloxamer 407-induced hyperlipidemia are significant, especially considering its widespread use in pharmaceutical formulations and biomedical research. It highlights the need for caution when utilizing Poloxamer 407 in drug delivery systems and emphasizes the importance of assessing its potential effects on lipid metabolism [11].

This review aims to provide a comprehensive evaluation of the current literature on the relationship between Poloxamer 407 and hyperlipidemia in in vivo studies. By examining the available evidence, this review will contribute to a better understanding of the potential risks associated with the use of Poloxamer 407 and help guide future research and development efforts in the field.

II. METHODS

The systematic review methodology aims to identify and summarize research articles related to the use of Poloxamer-407 in treating metabolic syndrome. The systematic review is conducted using the Preferred Reporting Items for Systematic Reviews and Meta-Analyses (PRISMA) method [12] to ensure the process is transparent and reported accurately.

II.1 DATA SOURCES

Literature search was conducted using the keywords: Poloxamer-407, in vivo, rats, and hyperlipidemia. International databases were sourced from references or literature published on PubMed, NCBI, MDPI, Web of Science, and Springer, using connectors such as "and" or "or."

II.2 STUDY SELECTION

The study selection was conducted using the PRISMA flow diagram (Figure. 1). Search results were evaluated sequentially based on titles and abstracts. Inclusion criteria included: 1) publications in English, 2) literature published from 2010 to 2022, 3) literature related to hyperlipidemia, 4) involving only Poloxamer-407. Excluded literature comprised publications before 2010, non-English publications, literature unrelated to hyperlipidemia, and other Poloxamer variants. Selected literature was filtered for duplicates.

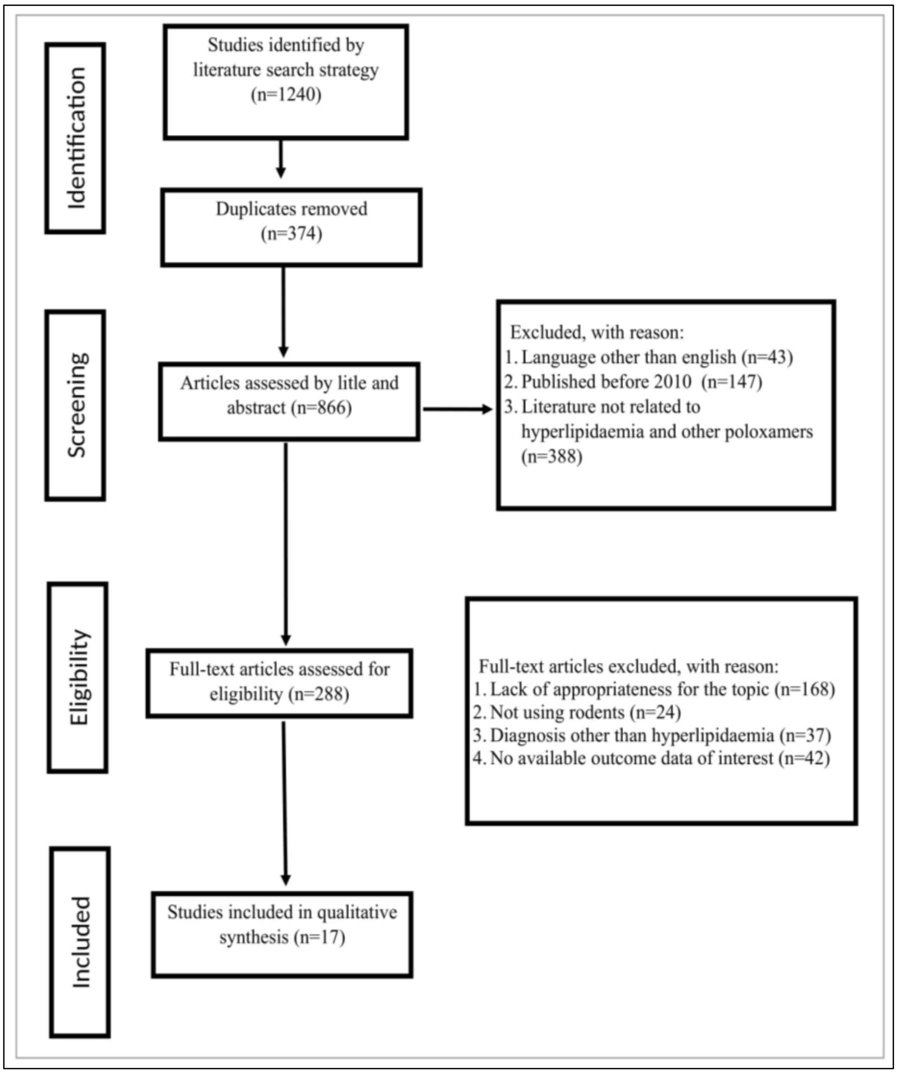

Figure 1: Flow chart for article selection.
Source: Authors, (2024)

II.3 DATA EXTRACTION

He matrix method was then employed to aid in summarizing and critiquing the selected studies. This matrix includes author (year), country, subject, dosage and method, key findings, as presented in Table 1. Data analysis was conducted by amalgamating relevant source references and adequate literature, facilitating data collection by providing sufficient understanding and explanation

III. RESULTS AND DISCUSSION

III.1 RESULT

Poloxamer copolymer, sometimes known as Poloxamer 407, is a hydrophilic non-ionic surfactant commonly used in various pharmaceutical and cosmetic formulations. Poloxamer 407 is a triblock copolymer consisting of two hydrophilic polyethylene glycol groups flanking a hydrophobic polypropylene glycol main group [13].

However, some studies have revealed that P407 can cause adverse side effects, including hyperlipidemia [14]. In this review, we will discuss and analyze findings from in vivo studies evaluating the relationship between P407 and the development of hyperlipidemia in experimental animals.

Animal-based studies on hyperlipidemia with the administration of Poloxamer-407 (P407) are presented in the table 1.

Table 1: Characteristics and key findings of selected articles (n=17).

AUTHOR, (YEAR)	COUNTRY	SUBJECT	DOSAGE AND METHOD	KEY FINDINGS
Hetal et al, 2013 [15]	Canada	Male Sprague Dawley rats	Single IP of 0.5 and 1g/kg	↑TC, ↑TG, ↑LDL, ↓HDL, and ↑leptin, ↓adiponektin
Thomas et al, 2012 [16]	Kansas City	Male Sprague Dawley rats	Single IP of 0.3 g/kg	↑TC and ↑HMG-CoA reductase activity
Yeom et al, 2018 [17]	Republic of Korea	Male Sprague Dawley rats	Single IP of 0.4 g/kg	↑TC, ↑TG, ↓HDL, and ↑LDL
Ruchel et al, 2016 [18]	Brazil	Male Wistar Rats	Single IP of 0.5 g/kg	↑TC, ↑TG, ↓HDL, and↑ LDL
Korolenko et al, 2013 [19]	Russia	Male CBA mice	IP of 0.5 g/kg twice per week for 1 month	↑TC, ↑TG, ↓HDL, and ↑LDL
Susana et al, 2017 [20]	Spain	Male Golden Syrian Hamsters	Periodically IP of 50 mg/kg every 72 h until 4 and 30 days	↑Lyso-PLs, ↓NEFAs, ↑TC, ↓HDL, ↑LDL, ↓LCAT, ↓sPLA2-IIA, ↑PON1
Leon et al, 2016 [21]	Canada	Male mice	IP of 0.5 g/kg	ACAT2 protein expression were not altered by P-407, ↑ LDL, ↑CL, ↑TG, ↑HMG-CoA reductase activity
Kumar et al, 2021 [22]	India	Male Wistar rats	Single IP of 0.5 g/kg	↑HOMA-IR index, ↑TG, ↑CL, ↓FRAP, ↓GSH, ↑PMRS, ↑AGE, ↑MDA, ↑PCO, ↑AOPP, ↓PON-1, ↑TNF-α and ↑IL-6, ↑SGPT and ↑SGOT
Jardan et al, 2021 [23]	Saudi Arabia	Male Wistar rats	Single IP of 1 g/kg	↑CYP3A, ↑TG, ↑CL, ↑LDL
Manzoni et al, 2020 [24]	Brazil	Male Wistar rats	Single IP of 0.5 g/kg	↑MDA, ↓SOD, ↓GST, ↓CAT, ↑ALT, ↑AST, ↑LDL, ↓HDL,
Zanwar et al, 2014 [25]	India	Male Wistar rats	Single IP of 0.5 g/kg	↑TC, ↑TG, ↓HDL, ↑VLDL
Yeom et al, 2018 [17]	Republic of Korea	Male Sprague Dawley rats	Single IP of 0.4 g/kg	↑TC, ↑TG, ↑ LDL, ↓HDL, ↑SREBP-2, ↑HMG-CoA reductase activity
Omari et al, 2016 [26]	Republic of China	Male Sprague Dawley rats	Single IP of 0.5 g/kg	↑TC, ↑TG, ↑ LDL, ↓HDL, ↓SOD, ↓GSH-PX, ↑MDA, ↑ALT, ↑AST
Ruchel et al, 2017 [18]	Brazil	Male Wistar rats	Single IP of 0.5 g/kg	↑TC, ↓HDL, ↑ LDL, ↑AST, ↑ALP, ↑ALT
Park et al, 2016 [27]	Republic of Korea	Male C57BL/6NTacSam mice	Single IP of 0.5 g/kg	↑TC, ↑TG, ↑ LDL, ↓HDL, ↑FAS, ↑ACC, ↑SREBP-2, ↑HMCR, ↑LDL, GAPDH, ↑SREBP-1c
Zuberu et al, 2017 [28]	Nigeria	Male Wistar rats	Single IP of 0.5 g/kg	↑TC, ↓HDL, ↑LDL, ↑AST, ↑ALP, ↑ALT
Manzoni et al, 2020 [29]	Brazil	Male Wistar rats	Single IP of 0.5 g/kg	↑TC, ↓HDL, ↑LDL, ↑AST, ↑ALP, ↑ALT, ↓SOD, ↓CAT, ↓GST

Source: Authors, (2024).

III.2 DISCUSSIONS

The Effect of Poloxamer-407 on Lipid Profile

Several in vivo studies have been conducted to evaluate the influence of P407 on lipid profiles in experimental animals. For instance, research conducted by Korolenko et al. (2013), using rats as an animal model, indicates that intravenous administration of P407 can elevate the levels of total cholesterol and triglycerides in the rats' blood [19]. Similar results were also reported by Naik et al. (2013), who found that oral administration of P407 to rabbits led to a significant increase in low-density lipoprotein (LDL) concentrations and plasma triglycerides [30].

The Mechanism of Inducing Hyperlipidemia by Poloxamer-407

The mechanism of hyperlipidemia has been investigated in numerous in vitro and in vivo experiments [31]. Currently, it is possible to induce hyperlipidemia in test animals in various ways. Hyperlipidemia can be triggered by certain chemicals, but only when consumed over an extended period and gradually over time [32]. One such substance is Poloxamer 407 (Pluronic®-M 127, P-407), which has been shown to significantly increase plasma triglyceride and cholesterol levels in several animal species, including rats [33], [34], mice [35-37], and rabbits [38]. Studies by Wasan et al. (2003) suggest that P407 can disrupt lipid metabolism by inhibiting the activity of lipoprotein lipase (LPL), which plays a role in breaking down lipoproteins and transporting triglycerides [39]. Another study by Leon et al. (2006) indicates that P407 can affect the expression of genes involved in lipid metabolism, including increased expression of genes regulating cholesterol synthesis in the liver [40]. One of the most intriguing hyperlipidemia models is P407, with a mechanism marked by increased TG levels due to: (1) inhibition of lipoprotein lipase; (2) increased TC levels due to indirect stimulation of 3-hydroxy-3-methylglutaryl coenzyme A reductase (HMG CoA reductase) activity, a rate-limiting enzyme in TC biosynthesis; and (3) reduced LDL receptor expression in all cholesterol-producing cells [41]. The P407 animal model can be influenced by the choice of: (1) various rodent species [20], [38], [41-43], (2) dose concentrations ranging from 300 mg/kg to 1500 mg/kg body weight [44], with the latter dose being preferred for mild hyperlipidemia; and (3) depending on the desired outcomes [45], either single treatment or chronic treatment [8], [20], [44], [46] via intraperitoneal (IP) injection.

Comparison with Other Studies

In addition to the studies mentioned above, several other studies have also reported the hyperlipidemic effects of P407 in experimental animals. For instance, Johnston et al. (2004) conducted a similar study using a rat model and found that P407 could also increase the levels of free fatty acids in the blood, which is a significant risk factor in the development of hyperlipidemia [47]. This finding aligns with the research by Johnson et al. (2010), indicating that P407 can influence the activity of adipose lipase enzymes, responsible for breaking down fats in adipose tissue [48].

IV. CONCLUSIONS

The findings from the discussed in vivo studies indicate that P407 has the potential to induce hyperlipidemia in experimental animals. The clinical implications of these findings need to be seriously considered, especially in the context of P407's use in pharmaceutical and cosmetic formulations. Furthermore, further research is required to understand the underlying mechanisms of the hyperlipidemic effects of P407 and to evaluate its potential risks in humans.

V. AUTHOR’S CONTRIBUTION

Conceptualization: Neti Eka Jayanti, Rozzana Mohd Said
Methodology: Neti Eka Jayanti
Investigation: Rozzana Mohd Said.
Discssion of results: Neti Eka Jayanti, Rozzana Mohd Said.
Writing – Original Draft: Neti Eka Jayanti
Writing – Review and Editing: Rozzana Mohd Said.
Resources: Neti Eka Jayanti, Rozzana Mohd Said.
Supervision: Neti Eka Jayanti, Rozzana Mohd Said
Approval of the final text: Neti Eka Jayanti, Rozzana Mohd Said.

VI. REFERENCES

[1] Varga, N., et al., The effect of synthesis conditions and tunable hydrophilicity on the drug encapsulation capability of PLA and PLGA nanoparticles. Colloids and Surfaces B: Biointerfaces, 2019. 176: p. 212-218.

[2] Varga, N., et al., Vitamin E-loaded PLA-and PLGA-based core-shell nanoparticles: synthesis, structure optimization and controlled drug release. Pharmaceutics, 2019. 11(7): p. 357.

[3] Varga, N., et al., Core-Shell Structured PLGA Particles Having Highly Controllable Ketoprofen Drug Release. Pharmaceutics, 2023. 15(5): p. 1355.

[4] Shi, J., et al., Self-assembled targeted nanoparticles: evolution of technologies and bench to bedside translation. Acc Chem Res, 2011. 44(10): p. 1123-34.

[5] Nelson, R.H., Hyperlipidemia as a risk factor for cardiovascular disease. Prim Care, 2013. 40(1): p. 195-211.

[6] Peng, X., et al., Poloxamer 407 Induces Hypertriglyceridemia but Decreases Atherosclerosis in Ldlr(-/-) Mice. Cells, 2022. 11(11).

[7] Al Quran, T.M., et al., Prevalence and Pattern of Dyslipidemia and Its Associated Factors Among Patients with Type 2 Diabetes Mellitus in Jordan: A Cross-Sectional Study. Int J Gen Med, 2022. 15: p. 7669-7683.

[8] Korolenko, T.A., et al., Effect of poloxamer 407 administration on the serum lipids profile, anxiety level and protease activity in the heart and liver of mice. Interdiscip Toxicol, 2013. 6(1): p. 18-25.

[9] Ma, H. and K.-J. Shieh, Cholesterol and human health. The Journal of American Science, 2006. 2(1): p. 46-50.

[10] Korolenko, T.A., et al., Influence of poloxamer 407 on fractional and subfractional composition of serum lipoproteins of mice. Health, 2010. 2(07): p. 722.

[11] Mahmoud, M.O., et al., Transdermal delivery of atorvastatin calcium from novel nanovesicular systems using polyethylene glycol fatty acid esters: ameliorated effect without liver toxicity in poloxamer 407-induced hyperlipidemic rats. Journal of controlled release, 2017. 254: p. 10-22.

[12] Liberati, A., et al., The PRISMA statement for reporting systematic reviews and meta-analyses of studies that evaluate health care interventions: explanation and elaboration. Annals of internal medicine, 2009. 151(4): p. W-65-W-94.

[13] Kumar, R., F. Akhtar, and S.I. Rizvi, Protective effect of hesperidin in Poloxamer-407 induced hyperlipidemic experimental rats. Biol Futur, 2021. 72(2): p. 201-210.

[14] Leon, C., et al., Acute P-407 administration to mice causes hypercholesterolemia by inducing cholesterolgenesis and down-regulating low-density lipoprotein receptor expression. Pharm Res, 2006. 23(7): p. 1597-607.

[15] Chaudhary, H.R. and D.R. Brocks, The single dose poloxamer 407 model of hyperlipidemia; systemic effects on lipids assessed using pharmacokinetic methods, and its effects on adipokines. Journal of Pharmacy & Pharmaceutical Sciences, 2013. 16(1): p. 65-73.

[16] Johnston, T.P. and W.K. Palmer, The Effect of Pravastatin on Hepatic 3-Hydroxy-3-methylglutaryl CoA Reductase Obtained from Poloxamer 407-Induced Hyperlipidemic Rats. Pharmacotherapy: The Journal of Human Pharmacology and Drug Therapy, 1997. 17(2): p. 342-347.

[17] Yeom, M., et al., Electroacupuncture ameliorates poloxamer 407-induced hyperlipidemia through suppressing hepatic SREBP-2 expression in rats. Life sciences, 2018. 203: p. 20-26.

[18] Ruchel, J.B., et al., Guarana (Paullinia cupana) ameliorates memory impairment and modulates acetylcholinesterase activity in Poloxamer-407-induced hyperlipidemia in rat brain. Physiology & Behavior, 2017. 168: p. 11-19.

[19] Korolenko, T., et al., Effect of poloxamer 407 administration on the serum lipids profile, anxiety level and protease activity in the heart and liver of mice. Interdisciplinary toxicology, 2013. 6(1): p. 18-25.

[20] Suárez-García, S., et al., Serum lysophospholipid levels are altered in dyslipidemic hamsters. Scientific Reports, 2017. 7(1): p. 10431.

[21] Leon, C., et al., Acute P-407 Administration to Mice Causes Hypercholesterolemia by Inducing Cholesterolgenesis and Down-Regulating Low-Density Lipoprotein Receptor Expression. Pharmaceutical Research, 2006. 23(7): p. 1597-1607.

[22] Kumar, R., F. Akhtar, and S.I. Rizvi, Protective effect of hesperidin in Poloxamer-407 induced hyperlipidemic experimental rats. Biologia Futura, 2021. 72: p. 201-210.

[23] Jardan, Y.A.B., et al., Assessment of glibenclamide pharmacokinetics in poloxamer 407-induced hyperlipidemic rats. Saudi Pharmaceutical Journal, 2021. 29(7): p. 719-723.

[24] Manzoni, A.G., et al., Hyperlipidemia-induced lipotoxicity and immune activation in rats are prevented by curcumin and rutin. International immunopharmacology, 2020. 81: p. 106217.

[25] Zanwar, A.A., et al., Antihyperlipidemic activity of concomitant administration of methanolic fraction of flax lignan concentrate and omega-3-fatty acid in poloxamer-407 induced experimental hyperlipidemia. Industrial Crops and Products, 2014. 52: p. 656-663.

[26] Omari-Siaw, E., et al., Tissue distribution and enhanced in vivo anti-hyperlipidemic-antioxidant effects of perillaldehyde-loaded liposomal nanoformulation against Poloxamer 407-induced hyperlipidemia. International Journal of Pharmaceutics, 2016. 513(1): p. 68-77.

[27] Park, J., M. Yeom, and D.H. Hahm, Fucoidan improves serum lipid levels and atherosclerosis through hepatic SREBP-2-mediated regulation. J Pharmacol Sci, 2016. 131(2): p. 84-92.

[28] Zuberu, J., et al., Hepatoprotective Effect of Camel Milk on Poloxamer 407 Induced Hyperlipidaemic Wistar Rats. Open Access Maced J Med Sci, 2017. 5(7): p. 852-858.

[29] Manzoni, A.G., et al., Hyperlipidemia-induced lipotoxicity and immune activation in rats are prevented by curcumin and rutin. Int Immunopharmacol, 2020. 81: p. 106217-106217.

[30] Naik, H.G., et al., Effect of poloxamer 407 on the serum cholesterol and triglyceride of rabbits. Int J Med Pharm Sci, 2013. 4(02).

[31] Hoffman, R., G.J. Brook, and M. Aviram, Hypolipidemic drugs reduce lipoprotein susceptibility to undergo lipid peroxidation: in vitro and ex vivo studies. Atherosclerosis, 1992. 93(1-2): p. 105-113.

[32] Connor, W.E. and S.L. Connor, The dietary treatment of hyperlipidemia: rationale, technique and efficacy. Medical Clinics of North America, 1982. 66(2): p. 485-518.

[33] Johnston, T.P. and W.K. Palmer, Effect of poloxamer 407 on the activity of microsomal 3-hydroxy-3-methylglutaryl CoA reductase in rats. J Cardiovasc Pharmacol, 1997. 29(5): p. 580-585.

[34] Johnston, T.P. and W.K. Palmer, Mechanism of poloxamer 407-induced hypertriglyceridemia in the rat. Biochem Pharmacol, 1993. 46(6): p. 1037-42.

[35] Johnston, T.P., et al., Potential downregulation of HMG-CoA reductase after prolonged administration of P-407 in C57BL/6 mice. J Cardiovasc Pharmacol, 1999. 34(6): p. 831-842.

[36] Johnston, T.P., et al., Regression of poloxamer 407-induced atherosclerotic lesions in C57BL/6 mice using atorvastatin. Atherosclerosis, 2000. 149(2): p. 303-313.

[37] Johnston, T.P., et al., Potency of select statin drugs in a new mouse model of hyperlipidemia and atherosclerosis. Int J Pharm, 2001. 229(1-2): p. 75-86.

[38] Blonder, J.M., et al., Dose-dependent hyperlipidemia in rabbits following administration of poloxamer 407 gel. Life Sci, 1999. 65(21): p. Pl261-6.

[39] Wasan, K.M., et al., Poloxamer 407-mediated alterations in the activities of enzymes regulating lipid metabolism in rats. J Pharm Pharm Sci, 2003. 6(2): p. 189-197.

[40] Leon, C., et al., Acute P-407 administration to mice causes hypercholesterolemia by inducing cholesterolgenesis and down-regulating low-density lipoprotein receptor expression. Pharmaceutical research, 2006. 23: p. 1597-1607.

[41] Johnston, T.P., The P-407-induced murine model of dose-controlled hyperlipidemia and atherosclerosis: a review of findings to date. J Cardiovasc Pharmacol, 2004. 43(4): p. 595-606.

[42] Korolenko, T.A., et al., Early-stage atherosclerosis in poloxamer 407-induced hyperlipidemic mice: pathological features and changes in the lipid composition of serum lipoprotein fractions and subfractions. Lipids in Health and Disease, 2016. 15(1): p. 16.

[43] Johnston, T.P. and W.K. Palmer, The effect of pravastatin on hepatic 3-hydroxy-3-methylglutaryl CoA reductase obtained from poloxamer 407-induced hyperlipidemic rats. Pharmacotherapy, 1997. 17(2): p. 342-7.

[44] Tanko, Y., et al., Effects of Fermented Ginger Rhizome (Zingiber officinale) and Fenu Greek (Trigonella foenum-graceum) Supplements on Oxidative stress and Lipid Peroxidation Biomarkers in Poloxamer-407 Induced -Hyperlipidemic Wistar Rats. Niger J Physiol Sci, 2017. 32(2): p. 137-143.

[45] Korolenko, T.A., et al., The influence of repeated administration of poloxamer 407 on serum lipoproteins and protease activity in mouse liver and heart. Canadian journal of physiology and pharmacology, 2012. 90(11): p. 1456-1468.

[46] Chaudhary, H.R. and D.R. Brocks, The single dose poloxamer 407 model of hyperlipidemia; systemic effects on lipids assessed using pharmacokinetic methods, and its effects on adipokines. J Pharm Pharm Sci, 2013. 16(1): p. 65-73.

[47] Johnston, T.P., The P-407–induced murine model of dose-controlled hyperlipidemia and atherosclerosis: a review of findings to date. Journal of cardiovascular pharmacology, 2004. 43(4): p. 595-606.

[48] Johnston, T.P., Poloxamer 407 as a general lipase inhibitor: its implications in lipid metabolism and atheroma formation in C57BL/6 mice. Journal of Pharmacy and Pharmacology, 2010. 62(12): p. 1807-1812.

Journal of Engineering and Technology for Industrial Applications

ISSN ONLINE: 2447-0228

ITEGAM-JETIA

Manaus, v10. n.50, p. 154-160. November/ December., 2024.
DOI: https://doi.org/10.5935/jetia.v10i50.1259

RESEARCH ARTICLEOPEN ACCESS

IMPACT OF NITROGEN INCORPORATION ON BAND GAP BOWING IN ZINC-BLENDE GAAS$_{1-x}$N$_x$: A FIRST-PRINCIPLES STUDY

Mimouna Oukli [1], Ghlam Karima[2], Seyfeddine Bechekir[3]

[1,3]Applied Materials Laboratory (A.M.L), Faculty of Electrical Engineering, Djillali Liabes University of Sidi Bel Abbes, Sidi Bel Abbes, Algeria.
[2]Laboratory of Intelligent control And Electrical Power System (ICEPS), Djillali Liabes University of Sidi Bel-Abbès, Sidi Bel-Abbès, Algeria

[1]http://orcid.org/0000-0002-4871-6919, [2]http://orcid.org/0000-0001-8276-0609, [3]https://orcid.org/0000-0002-6143-7164

Email: mounaoukli@yahoo.fr, ouklimouna22@gamil.com, Karighlam16@yahoo.fr,

ARTICLE INFO

Article History
Received: August 08, 2024
Revised: October 1, 2024
Accepted: November 10, 2024
Published: December 31, 2024

Keywords:
Ab–initio calculations,
Nitrides,
Structural properties,
Bowing parameter.

ABSTRACT

This study, utilizing full-potential linear muffin-tin orbital (FPLMTO) calculations within density functional theory (DFT), delved into the structural properties of zinc-blende GaAs$_{1-x}$N$_x$ alloys. By varying the nitrogen concentration (x= (0.125, 0.083, and 0.063), we observed deviations from Vegard's law for lattice parameters and nonlinear behavior of the bulk modulus. The band gap bowing was primarily attributed to volume deformation effects, as elucidated by the Ferhat approach. Our findings demonstrate that the electronic and structural properties of GaAs$_{1-x}$N$_x$ are strongly influenced by the nitrogen concentration. These variations present exciting opportunities for bandgap engineering and the design of wide-bandgap optoelectronic devices.

I. INTRODUCTION

Dilute nitride alloys, such as GaAs$_{1-x}$N$_x$ and GaSb$_{1-x}$N$_x$, have emerged as promising materials for infrared optoelectronic devices, particularly for telecommunications applications including solar cells [1], long-wavelength light-emitters (1.3 μm–1.55 μm), and tunable photodetectors [2-8]. These alloys offer unique properties, notably a significant reduction in their bandgap energy, rendering them highly attractive for various applications [9-10]. This band gap reduction is primarily attributed to the incorporation of a small amount of nitrogen [11] (typically less than 5%) into III-V compounds [12-14]. This phenomenon, known as "bowing," is linked to the strong curvature of the relationship between alloy composition and bandgap energy that has been experimentally observed for some dilute nitrides such as GaPN [15], [16], InPN [17] and GaAsN [18]. The "bowing factor," a key characteristic of these materials, is influenced by factors such as the electronegativity and atomic radius of nitrogen compared to those of arsenic [19].

While the band gap of a typical mixed compound exhibits a linear relationship with composition, as described by Vegard's law, certain materials, like GaNAs, GaInNAs, and GaNP, deviate significantly from this behavior, exhibiting a large band gap bowing with a bowing coefficient as large as 20 eV [20]. This anomalous decrease in band gap, often termed "large band gap bowing," has been extensively studied using theoretical and computational methods [21-32]. To gain a deeper understanding of the factors influencing this bowing effect, theoretical and computational methods have been extensively employed. However, the underlying mechanisms remain elusive.

To explore the underlying causes of this bowing phenomenon, measurements and calculations on semiconductor alloys indicate that the band gap energy deviates from the linear behavior given by Vegard's law [33], termed 'large band gap bowing'. The magnitude of the bowing factor varies significantly among different alloys and its physical origins are not fully understood. Our phenomenological model aims to elucidate these factors by investigating the structural properties of III-V ternary alloys containing nitrogen in zinc blend structure. To better understand the physical origins of the large dispersion and composition-dependent bowing in $A_{1\_x}B_xC$ alloys, we have used our recently developed phenomenological model Ferhat [34], which has been shown to account successfully for the optical band gap bowing of III–V semiconductor alloys.

This study investigates the impact of nitrogen incorporation on the gap bowing behavior of zinc-blende GaAs$_{1-x}$N$_x$ alloys. We will further explore the influence of nitrogen incorporation on this phenomenon. Full-potential linear muffin-tin orbital (FPLMTO) calculations within density functional theory (DFT) will be employed to systematically study these alloys over a range of compositions.

The paper is organized as follows. The method is briefly commented in Section 2. Results are discussed in Section 3. Finally, in section 4 we summarize the main conclusions of this work

II. COMPUTATIONAL DETAILS

This study employed the extended FPLMTO (PLW) method [35-37] for its calculations. This method, capable of handling all types of structures, including open ones, describes the electron exchange-correlation energy using the local density approximation (LDA) [38] and the Perdew et al. [39] parameterization. The computations were performed using the lmtART computer code [38], [40], which expands the potential within the non-overlapping muffin-tin sphere in spherical harmonics and the s, p, and d basis functions in plane waves in the interstitial regions. Convergence of the calculations was achieved when the total energy reached an accuracy of 10^{-4} Ry.

For the binary compounds under investigation, a cubic unit cell containing four atoms was considered. Each lattice site is occupied by two atoms: a gallium (Ga) atom located at the origin (0, 0, 0)a_0, and a nitrogen (N) or arsenic (As) atom positioned at (1/4, 1/4, 1/4)a_0 in the zinc blende structure (where a_0 is the lattice parameter for both binary compounds).

Tetragonal unit cells of 16, 24, and 32 atoms were used for ternary systems with x=0.125, x=0.083, and x=0.063, respectively. A primitive cell was used for binary systems.

The optical bandgap bowing (b) in a binary alloy system was analyzed by decomposing it into three contributions [34], [41]: volume deformation (VD), charge exchange (CE), and structural relaxation (SR). The VD term represents the response of binary compounds to pressure changes, the CE term relates to charge transfer at a = a(x), and the SR term describes the change in the ban dgap during relaxation.

For a given average concentration of x, the ternary alloy exhibits the following reaction:

$$(1-x)\mathrm{GaAs}_{(aGAS)} + x\mathrm{GaN}_{(aGaN)} \rightarrow \mathrm{GaAs}_{1-x}\mathrm{N}_x(a_{eq}) \quad (1)$$

Where aGaAs and aGaN are the equilibrium lattice parameters of the parent materials GaAs and GaN, respectively, the equilibrium lattice parameter of the ternary alloy $GaAs_{1-x}N_x$ varies with x.

Equation (1) can be decomposed into three steps:

$$\mathrm{GaAs}_{(aGAS)} + \mathrm{GaN}_{(aGaN)} \rightarrow \mathrm{GaAs}(a) + \mathrm{GaN}(a) \quad (2)$$

$$(1-x)\mathrm{GaAs}_{(aGAS)} + x\mathrm{GaN}_{(aGaN)} \rightarrow \mathrm{GaAs}_{1-x}\mathrm{N}_x(a) \quad (3)$$

$$\mathrm{GaAs}_{1-x}\mathrm{N}_x(a) \rightarrow \mathrm{GaAs}_{1-x}\mathrm{N}_x(a_{eq}) \quad (4)$$

The first step quantifies the impact of volume deformation on the bowing parameter by analyzing the relative response of GaN and GaAs to hydrostatic pressure. This is followed by considering the charge transfer between GaN and GaAs, and finally, the relaxation of the alloy's bonds. The overall bowing parameter is determined by summing up these three contributions.

These terms were calculated for various concentrations (x=0.125, x=0.083, and x=0.063) to determine the total bowing effect at the direct energy gap $E_{\Gamma\Gamma}$. The construction of total bowing is:

$$b = b_{VD} + b_{CE} + b_{SR} \quad (5)$$

Ferhat and Bechstedt proposed a model for the bandgap bowing parameter in the ternary $GaAs_{1-x}N_x$ alloy [42]. This model posits that the bowing parameter is composed of three distinct contributions, each dependent on the nitrogen concentration (x), which was investigated for x = 0.125, 0.083, and 0.063 in this study. These contributions are defined by specific mathematical relationships [2, 3]

$$b_{VD} = \frac{E_{GaAs}(a_{GaAs}) - E_{GaAs}(a)}{1-x} + \frac{E_{GaN}(a_{GaN}) - E_{GaN}(a)}{x} \quad (6)$$

$$b_{CE} = \frac{E_{GaAs}(a)}{1-x} + \frac{E_{GaN}(a)}{x} - \frac{E_{\mathrm{Ga1}-x\mathrm{N}x}(a_{eq})}{x.(1-x)} \quad (7)$$

$$b_{SR} = \frac{E_{\mathrm{GaAs1}-x\mathrm{N}x}(a) - E_{\mathrm{GaAs1}-x\mathrm{N}x}(a_{eq})}{x.(1-x)} \quad (8)$$

Where the equilibrium lattice constants of GaAs and GaN are represented by a_{GaAs} and a_{GaN} respectively, and the equilibrium lattice constant of the alloy with the average composition x is represented by *aeq*. The energy gaps of the binary compounds GaAs and GaN are represented by E_{GaAs} and E_{GaN} respectively, and the energy gap of the alloy $GaAs_{1-x}N_x$ for x=0.125, 0.083 and 0.063 is represented by E ($GaAs_{1-x}N_x$).

III. RESULTS AND DISCUSSIONS

In this section, we investigate the electronic properties of the parent binary compounds GaN and GaAs, as well as their ternary alloys, by computing their band structures using our calculated lattice parameters.

The total energy of each binary compound and the ternary GaAsN, as a function of volume, is depicted in Figures 1 through 5. These plots visualize how the total energy of the systems changes when their volume is altered.

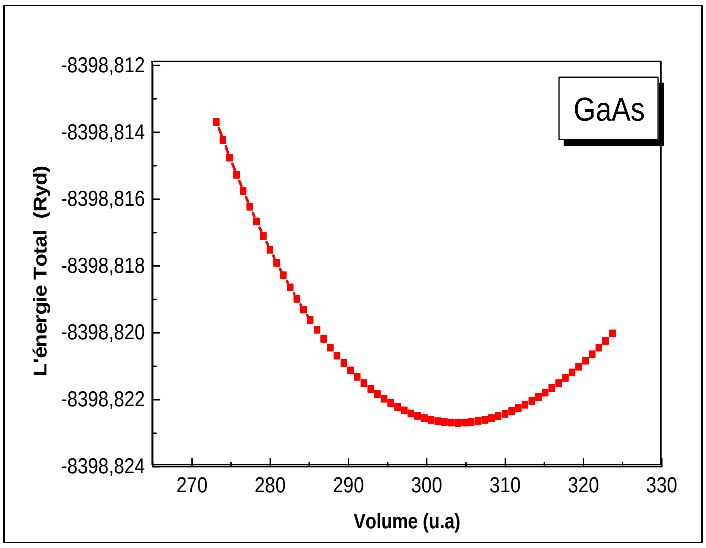

Figure 1: Total energy per molecule as a function of volume for GaAs using LDA calculation.
Source: Authors, (2024).

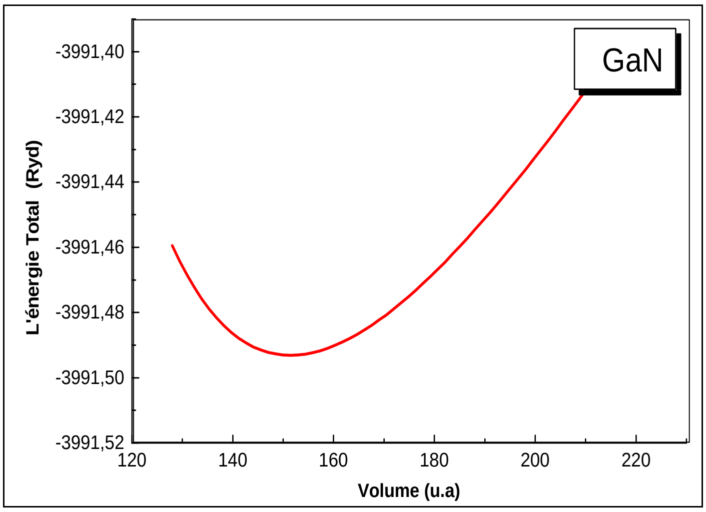

Figure 2: Total energy per molecule as a function of volume for GaN using LDA calculation.
Source: Authors, (2024).

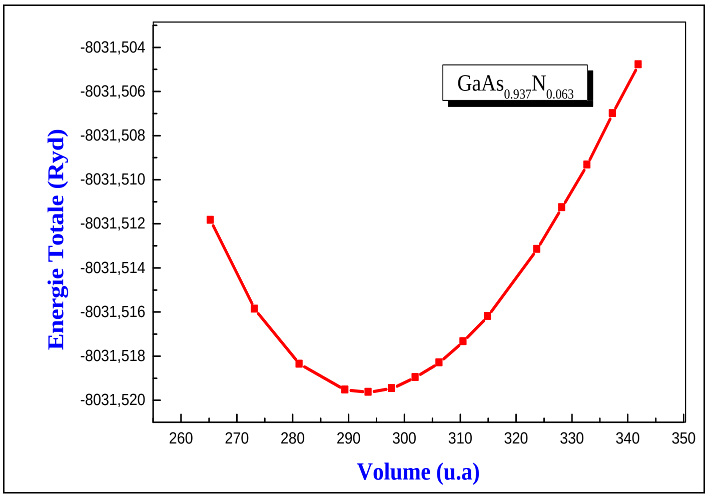

Figure 3: Total energy per molecule as a function of volume for $GaAs_{1-x}N_x$ (x= 0.063) using LDA calculation.
Source: Authors, (2024).

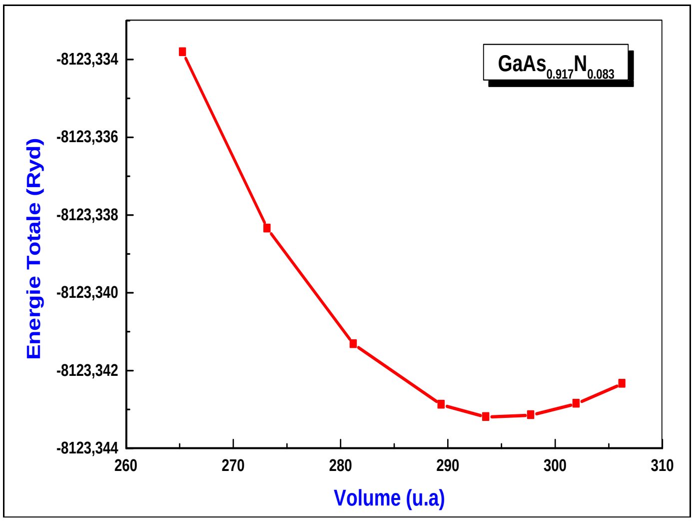

Figure 4: Total energy per molecule as a function of volume for $GaAs_{1-x}N_x$ (x=0.083) using LDA calculation.
Source: Authors, (2024).

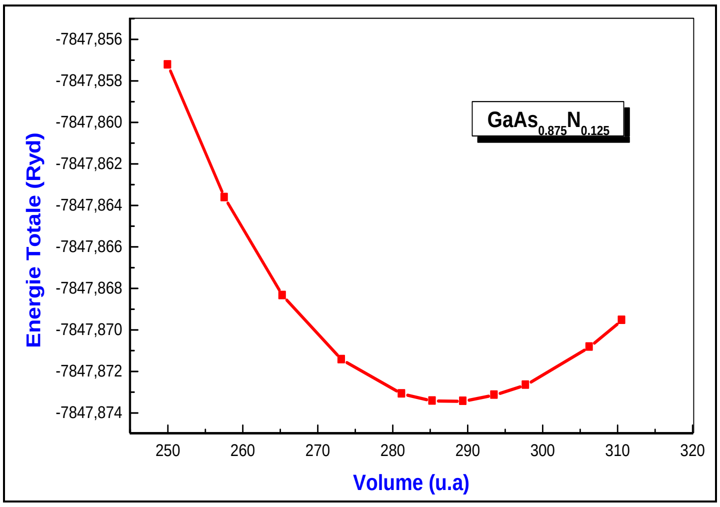

Figure 5: Total energy per molecule as a function of volume for $GaAs_{1-x}N_x$ (x=0.125) using LDA calculation.
Source: Authors, (2024).

To determine the equation of state, we fit our DFT total energy calculations, E(V), to the Murnaghan equation of state [43]:

$$E(V) = E_0 + \frac{B}{B(B-1)}\left[V\left(\frac{V_0}{V}\right)^{B_0} - V_0\right] + \frac{B_0}{B_0'}(V - V_0) \qquad (9)$$

where E_0 is the energy at equilibrium volume V_0, B0 is the bulk modulus, and B′ is its pressure derivative. By minimizing the total energy with respect to volume, we obtained the equilibrium lattice constant, bulk modulus, and its derivative for both binary and ternary compounds. These results are summarized in and Table I.

Table 1: The structural parameters of the investigated compounds. V_0 is the equilibrium volume per unit formula ($V_0 = a_0^3/4$ for binary, $V_0 = (c_0/a_0)$. $a_0^3/4$ for the tetragonal ternaries), a_0 represents the lattice constant for the binaries and ternaries, *B* is the bulk modulus and B' is its pressure derivative.

	V_0(Å^3)	**a_0 (Å^3)**	**c_0/a_0**	**B (GPa)**	**B`**
x = 0 **Exp** **Theoretical studies**	44.9 89	5.646 5.653[19]' 5.664[41] 5.666[42],	1	68.699 75.50[48] 69.71[41], 69.60[42], 76.47[14]	4.765 4.28 [14]
x = 1 **Exp** **Theoretical studies**	22.4 76	4.480 4.50 [43], [44] [46] 4.46[45] 4.48[48] 4.50[10], 4.56[49], 4.55[47]	1	192.564 190.932[45], 206.9[44] 189.488[10]	4.963 5.30[47] 4.46[10]
x = 0.125	42.6 00	5.544	2	73.701	4.556
x = 0.083	43.3 42	5.576	3	71.788	4.798
x = 0..063	43.7 16	5.592	4	71.935	4.789

Source: a Ref [19], b Ref [14], c Ref [10], d Ref [41], e Ref [42], f Ref [43], g Ref [44] , h Ref [45] , i Ref [48] , k Ref [49].

Our calculated equilibrium lattice parameters for GaN and GaAs are 4.480 Å and 5.646 Å, respectively, exhibiting deviations of only 0.69% and 0.75% from the experimental values of 4.511 Å and 5.6535 Å [14], [50]. The computed bulk modulus for zinc-blende GaAs and GaN is in good agreement with experimental data and previous theoretical studies [14]. Notably, GaN demonstrates a lower compressibility compared to GaAs.

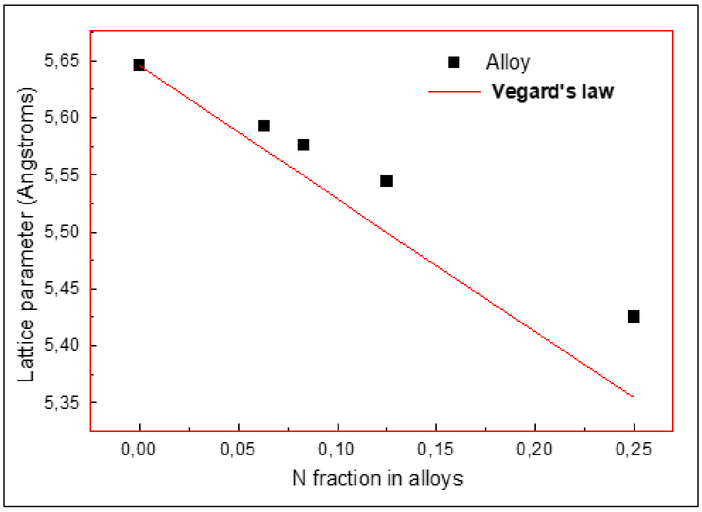

Figure 6: Lattice constant versus nitrogen concentration x in GaAs1-xNx.
Source: Authors, (2024).

For a given nitrogen concentration, the ternary alloys exhibit nearly identical equilibrium lattice parameters, displaying a linear variation (Figure 6).

However, a significant positive deviation from Vegard's law is observed for $GaAs_{1-x}N_x$, with an upward bowing parameter of -0.385 Å determined through polynomial fitting. This deviation is primarily attributed to the substantial size mismatch and lattice constant disparity between GaAs and GaN [33].

The bulk modulus of $GaAs_{1-x}N_x$ deviates notably from a linear concentration dependence, exhibiting a downward bowing of 45.82 GPa. This disparity results in a considerable deviation in rigidity for all systems studied. Notably, an increase in nitrogen concentration within $GaAs_{1-x}N_x$ correlates with a lattice parameter decrease and a bulk modulus increase, consistent with general trends observed in other III-V semiconductors and alloys [14], [51].

We began by calculating the band structures of the binary compounds GaAs and GaN. Both materials exhibited direct band gaps, with the valence band maximum (VBM) and conduction band minimum (CBM) located at the Γ point in the Brillouin zone. A comparison of our calculated bandgaps (0.206 eV for GaAs and 1.916 eV for GaN) with experimental values (1.52 eV for GaAs and 3.20 eV for GaN [14,51,52]) reveals an underestimation. However, given the focus of this study on qualitative trends rather than quantitative accuracy, this discrepancy does not significantly impact our conclusions.

Subsequently, we calculated the band structures for the ternary alloy $GaAs_{1-x}N_x$ and plotted the resulting gap variations (Fig. 7). A critical consideration when studying ternary alloys is the choice of unit cell. The unit cell employed in our calculations is a supercell, not a primitive cell. Consequently, the calculated band gaps may not always correspond to the true fundamental band gaps, which are typically obtained from calculations using primitive cells. This discrepancy arises from the zone folding effect inherent to supercell calculations.

Normally, if one of the binary constituents has an indirect band gap, the supercell of the ternary alloy might exhibit a spurious direct band gap due to zone folding. However, in the present case, both GaAs and GaN possess direct band gaps at the Γ point. Therefore, zone folding is not expected to alter the fundamental gap nature of the ternary alloy.

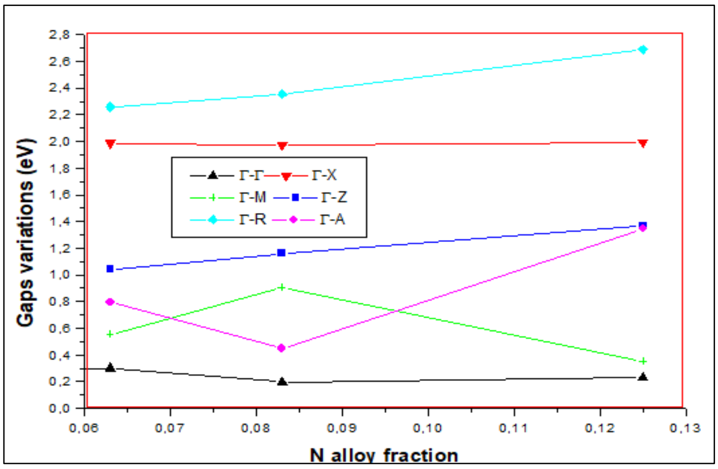

Figure 7: Gaps variation with the N fraction in the alloys.
Source: Authors, (2024).

For selected nitrogen concentrations (x = 0.0625, 0.083, and 0.125) within the dilute nitride regime, our calculations indicate direct band gaps located at the Γ point (Fig. 8, 9 and 10). However, as the nitrogen content increases from $GaAs_{0.937}N_{0.063}$ to $GaAs_{0.875}N_{0.125}$, a nonlinear variation in the Γ-Γ gap is observed. This behavior is similar to that reported for dilute nitride GaAsN alloys. Interestingly, the Γ-M and Γ-A gaps also exhibit nonlinear trends, with the Γ-M gap increasing while the Γ-A gap decreases. This complex behavior is likely attributed to zone folding effects, as the quantum states at these high-symmetry points are linear combinations of states from different high-symmetry points in the reciprocal lattice of the primitive cell.

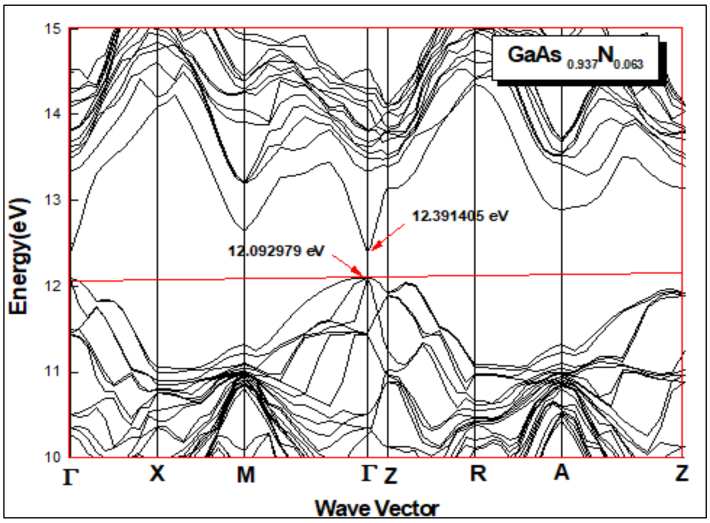

Figure 8: The band structure of the strained bulk $GaAs_{0.937}N_{0.063}$ alloy at a lattice parameter of a(x= 0.063).
Source: Authors, (2024).

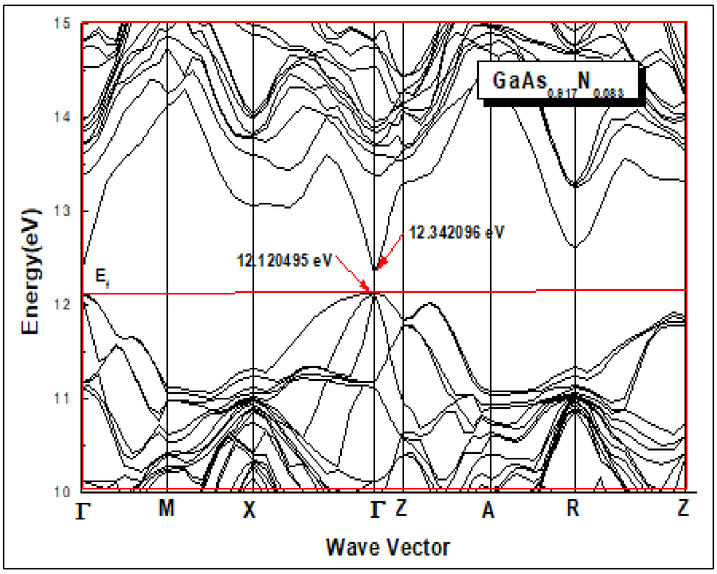

Figure 9: The band structure of the strained bulk $GaAs_{0.917}N_{0.083}$ .alloy at a lattice parameter of a(x= 0.0873).
Source: Authors, (2024).

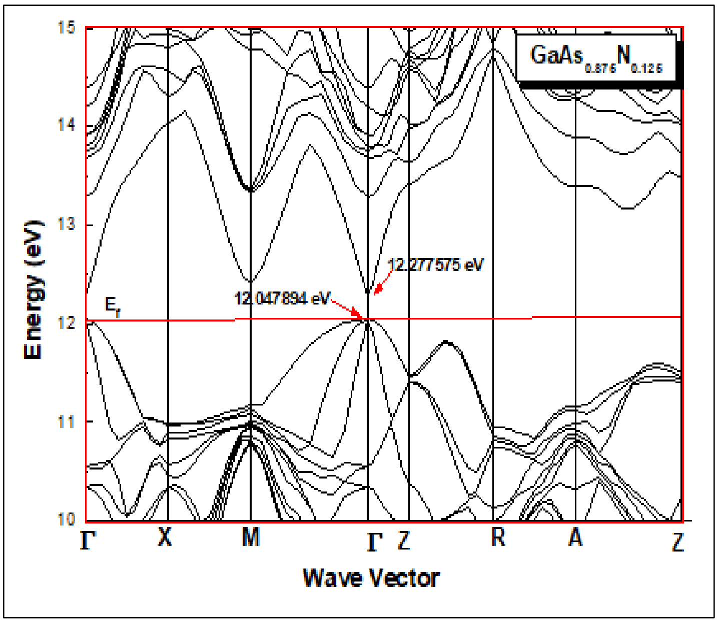

Figure 10: The band structure of the strained bulk $GaAs_{0.875}N_{0.125}$.alloy at a lattice parameter of a(x= 0.125).
Source: Authors, (2024).

The ternary $GaAs_{1-x}N_x$ alloys exhibit a direct bandgap character with both the valence band maximum (VBM) and conduction band minimum (CBM) located at the Γ point in the Brillouin zone. A notable trend is the increase in bandgap energy with increasing nitrogen content (x). However, this variation is nonlinear, indicating a more complex relationship between composition and bandgap than a simple linear interpolation.

Table 2 summarizes the calculated band gaps for the various samples. Our results indicate a strong dependence of the bandgap on nitrogen atom distribution within the supercell, highlighting the significant influence of nitrogen incorporation on the conduction band structure. Even small nitrogen concentrations (a few percent) can dramatically affect the electronic properties of GaAs.

Table 2: The gap energies (in eV) between the upper VB and the lower CB of the zinc blende (ZB) of all the present binary and ternaries.

	x=0	x =1	x= 0.063	x= 0.125	x=0.083
Γ- Γ	0,239	1,916	0.298	0,229	0,221
Γ –X	1,918	4.717	1,987	1,993	1,999
Γ –M	2,642	6.606	0.555	0.354	0.933
Γ –Z	--------	--------	1.043	1.365	1.186
Γ –R	0,828	4.874	2.259	2.688	2.380

Source: Authors, (2024).

Our calculations reveal a pronounced sensitivity of the calculated band gaps to the spatial distribution of nitrogen atoms within the supercell. This observation underscores the critical role of nitrogen incorporation in modifying the conduction band structure. Even a modest nitrogen content of a few percent in GaAs can significantly perturb the electronic properties of the material. This sensitivity arises from the formation of localized electronic states associated with nitrogen atoms, which act as perturbations to the host GaAs lattice. These localized states can introduce new energy levels within the band gap, leading to band gap narrowing and altering the overall electronic structure. Consequently, the precise arrangement of nitrogen atoms within the supercell has a substantial impact on the resulting band gap, highlighting the importance of considering configurational disorder effects in theoretical modeling of these materials.

According to the model proposed by Van Vechten and Bergstresser [29], the electronegativity difference between constituent atoms is a critical factor influencing the degree of disorder within an alloy system, which in turn affects the bandgap. In the case of $GaAs_{1-x}N_x$, the varying electronegativity between Ga, As, and N atoms results in different degrees of disorder for different alloy compositions. This disorder contributes to the nonlinear behavior of the bandgap.

To quantify the impact of disorder on the bandgap, we introduced the total curvature parameter (b) for the Γ-Γ transition. Our calculations summarized in the table 3 yielded values of 12.52 eV, 18.56 eV, and 24.66 eV for $GaAs_{0.875}N_{0.125}$, $GaAs_{0.917}N_{0.083}$, and $GaAs_{0.937}N_{0.063}$, respectively. These values suggest a significant increase in disorder with decreasing nitrogen content.

Another crucial factor affecting the bandgap is volume deformation (VD). Our calculations indicate that the contribution of VD to the total energy gap curvature parameter is substantial, especially for the $GaAs_{0.937}N_{0.063}$ alloy. This implies that the lattice expansion due to the incorporation of larger nitrogen atoms plays a dominant role in modifying the bandgap for this particular composition.

Table 3: Calculated bowing parameters b for $GaAs_{1-x}N_x$ alloys. The contributions due to volume deformation (b_{VD}), electronegativities (b_{CE}), and structural relaxations (b_{SR}) are also listed. All values are in eV.

Composition x	**x= 0.125**	**x=0.083**	***x=0.063***
$\mathbf{b_{VD}}$	14.585	22.609	30.044
$\mathbf{b_{CE}}$	-2.195	-4.210	-5.447
$\mathbf{b_{SR}}$	0.134	0.165	0.061
b	*12.525*	*18.564*	24.662

Source: Authors, (2024).

The significant role of volume deformation (VD) in contributing to the band gap bowing parameter is directly linked to the substantial lattice mismatch between the constituent binary compounds GaAs and GaN. In many alloy systems, the VD term is closely correlated with the overall volume of the unit cell, as represented by the lattice parameter (a). Consequently, the pronounced VD bowing parameter observed in $GaAs_{1-x}N_x$ can be attributed to the considerable difference in lattice constants between GaAs and GaN.

It is important to note that while charge exchange (ECB) can also influence bandgap bowing, its contribution is significantly smaller than that of VD in this system. This disparity is consistent with the relatively low ionicity of the constituent elements.

Structural relaxation (bSR), which accounts for atomic displacements from ideal lattice positions, is found to have a minimal impact on bandgap bowing in $GaAs_{1-x}N_x$ due to the limited lattice mismatch between the two binary compounds.
This study primarily focused on nitrogen concentrations above 7% (Figure 11). A comprehensive understanding of the bandgap bowing behavior at lower nitrogen levels would require further investigation.

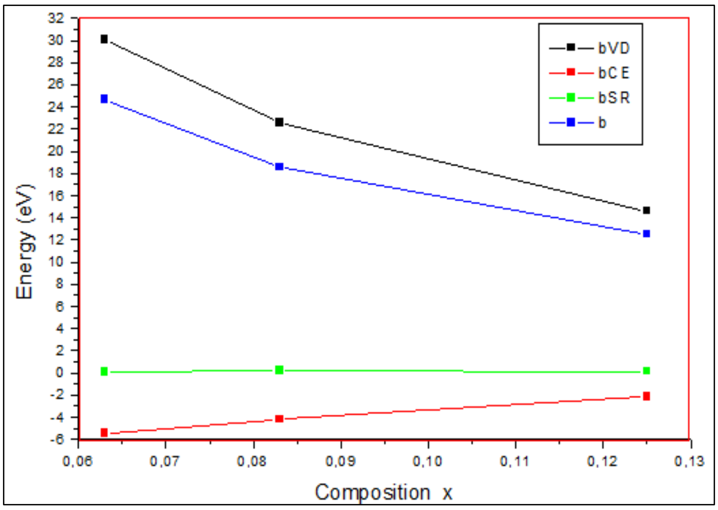

Figure 11: Curvature parameter variation b and the three contributions bVD, bCE, and bSR considering concentration x.
Source: Authors, (2024).

IV. CONCLUSIONS

This study employed ab-initio FPLMTO calculations to investigate the structural properties of cubic and tetragonal Ga(As,N) alloys, focusing on the critical role of interstitial regions, to clarify the mechanism of the large band gap bowing of the dilute nitride semiconductors, we calculated band edge energies of $GaAs_{1-x}N_x$.

Our findings indicate a complex interplay between volume deformation (VD), charge transfer (CE), and structural relaxation (SR) in determining the band gap bowing behavior of these alloys.

For the majority of compositions studied, VD emerges as the dominant factor influencing band gap bowing, with CE playing a comparatively minor role. Structural relaxation effects (SR) were found to be relatively weak in these systems. Collectively, VD and SR, constituting the structural component, primarily govern the overall band gap bowing.

It is important to note that the present investigation focused on nitrogen concentrations exceeding 7%. A comprehensive understanding of band gap bowing across the entire composition range would require further studies.

These results provide valuable insights into the fundamental mechanisms underlying band gap bowing in $GaAs_{1-x}N_x$ alloys, contributing to the development of more accurate theoretical models and facilitating the design of optoelectronic devices based on these materials.

V. AUTHOR'S CONTRIBUTION

Conceptualization: Mimouna Oukli , Ghlam Karima, Seyfeddine Bechekir.
Methodology: Mimouna Oukli , Ghlam Karima, Seyfeddine Bechekir.
Investigation:. Mimouna Oukli , Ghlam Karima, Seyfeddine Bechekir.
Discussion of results: Mimouna Oukli , Ghlam Karima, Seyfeddine Bechekir.
Writing – Original Draft: Mimouna Oukli , Ghlam Karima, Seyfeddine Bechekir.
Writing – Review and Editing: Mimouna Oukli , Ghlam Karima, Seyfeddine Bechekir.
Supervision: Mimouna Oukli , Ghlam Karima, Seyfeddine Bechekir.
Approval of the final text: Mimouna Oukli , Ghlam Karima, Seyfeddine Bechekir.

V. ACKNOWLEDGMENTS

One of the authors, O. M thanks the S.Y.Savrasov for Mindlab software freely available. This work has been supported by Applied Materials Laboratory (A.M.L).

VI. REFERENCES

[1] Paola Prete , Nico Lovergine, Progress in Crystal Growth and Characterization of Materials, Volume 66, Issue 4, November 2020, 100510,

[2] Z. Zaaboub , F. Hassen, H. Maaref, Solid State Communications. 314-315 (2020) 113913.

[3] Jian V. Lia, Man Hoi Wongb, Thin Solid Films 758 (2022) 139422. Volume 758, 30 September 2022, 139422.

[4]Takashi Tsukasakia, Naoki Mochidaa , Miki Fujitab , Toshiki Makimotoa, , Physica B: Condensed Matter, Volume 625, 15 January 2022, 413482.

[5] Arpad Kosaa,, Lubica Stuchlikovaa , Ladislav Harmathaa , Jaroslav Kovaca , Beata Scianab ,Wojciech Dawidowskib , Marek Tlaczalab, Materials Science in Semiconductor Processing, Volume 74, February 2018, Pages 313-318,

[6] Justin C. Goodrich, Damir Borovac, Chee-Keong tan & Nelson tansu, Scientific RepoRts | (2019) 9:5128.
[7] Wadi Bachir Bouiadjraa, Abdelkader Saidanea , Abdelkader Mostefaa Mohamed Heninib , M. Shafib ,Superlattices and Microstructures, Volume 71, July 2014, Pages 225-237.

[8] Takashi Tsukasaki , Naoki Mochida, Miki Fujita , Toshiki Makimoo, Physica B: Condensed Matter, Volume 625, 15 January 2022, 413482.

[9] Francesco Biccari, Alice Boschetti, Giorgio Pettinari, Federico La China, Massimo Gurioli, Francesca Intonti, Anna Vinattieri, MayankShekhar Sharma, Mario Capizzi, Advanced Material, Volume 30, Issue 21, May 24, 2018,1705450.

[10] S Gagui, H meradji, S Ghemid, Y Megdoud, B ZAIDI, B Ul haq, R Ahmed, B Hadjoudja , B Chouial, Bull. Mater. Sci. (2023) 46:63

[11] S gagui, S Ghemid, H Meradji, B Zaidi, Bakhtiar Ul haq, R Ahmed, B Hadjoudja, B Chouial and S A Tahir, Pramana , J. Phys. (2023) 97:145 **.**

[12] M. Lahoual, · A. Gueddim , · N. Bouarissa, Transactions on Electrical and Electronic Materials (2019) 20:344–349.

[13] Eßer et al. Appl. Phys. Lett. 107, 062103 (2015).

[14] Yibo Wang, Yan Liu, Genquan Han, Hongjuan Wang, Chunfu Zhang, Jincheng Zhang, Yue Hao, Superlattices and Microstructures, Volume 106, June 2017, Pages 139-146.

[15] I. Vurgaftman, J.R. Meyer, J. Appl. Phys. 94, 3675 (2003).

[16]. A. Gueddim, R. Zerdoum, N. Bouarissa,. J. Phys. Chem. Solids 67(8), 1618–1622 (2004).

[17] K.M. Yu, W. Walukiewicz, J. Wu, J.W. Beeman, J.W. Ager, E.E. Haller, W. Shan, H.P. Xin, C.W. Tu, Synthesis of III–Nx–V1-x thin _lms by N ion implantation. Appl. Phys. Lett. 78, 1077 (2001).

[18] S. Ben Bouzid, F. Bousbih, R. Chtourou, J.C. Harmand, P.Voisin, E_ect of nitrogen in the electronic structure of GaAsN and GaInAs(N) compounds grown by molecular beam epitaxy. Mater. Sci. Eng. B 112, 64 (2004).

[19] F. Hassena, Z. Zaabouba , M. Bouhlela , M. Naffoutia , H. Maarefa , N.M. Garni, Thin Solid Films, Volume 594, Part A, 2 November 2015, Pages 168-171.

[20] X.Z. Chen , D.H. Zhang , Y.J. Jin , J.H. Li , J.H. Teng , N. Yakovlev , Journal of Crystal Growth, 362 (2013) 197–201.

[21] Chuan-Zhen Zhao, Na-Na Li, Tong Wei, Chun-Xiao Tang, Ke-Qing Lu, Appl.Phys. Lett. 100 (2012) 142112.

[22] W. Shan, W. Walukiewicz, J.W. Ager III, E.E. Haller, J.F. Geisz, D.J. Friedman, J.M. Olson, S.R. Kurtz, Phys. Rev. Lett. 82 (1999) 1221.

[23] J. Wu, W. Walukiewicz, K.M. Yu, J.W. Ager III, E.E. Haller, Y.G. Hong, H.P. Xin, C.W. Tu, Phys. Rev. B 65 (2002) 241303.

[24] A. Lindsay, E.P. O'Reilly, Phys. Rev. Lett. 93 (2004) 196402.

[25] E.P. O'Reilly, A. Lindsay, S. Tomic, M. Kamal-Saadi, Semicond. Sci. Technol. 17 (2002) 870.

[26] W.J. Fan, M.F. Li, T.C. Chong, J.B. Xia, J. Appl. Phys. 79 (1996) 188.

[27] L. Bellaiche, S.-H. Wei, A. Zunger, Appl. Phys. Lett. 70 (1997).

[28] L. Bellaiche, S.-H. Wei, A. Zunger, Phys. Rev. B 54 (1996) 17568.

[29] Kurt A. Mader, A. Zunger, Phys. Rev. B 50 (1994) 17393.

[30] P.R.C. Kent, A. Zunger, Phys. Rev. B 64 (2001) 115208.

[31] V. Timoshevskii, M. Côté, G. Gilbert, R. Leonelli, S. Turcotte, J.-N. Beaudry, P. Desjardins, S. Larouche, L. Martinu, R.A. Masut, Phys. Rev. B 74 (2006) 165120.

[32] C.-K. Tan, J. Zhang, X.-H. Li, G. Liu, B.O. Tayo, N. Tansu, J. Display Technol. 9 (2013) 272L.

[33] S. T. Murphy, A. Chroneos, C. Jiang, U. Schwingenschlögl, R. W. Grimes, PHYSICAL REVIEW B 82, 073201 2010.

[34] M. Ferhat, Phys. Status Solidi b 241 (2004) R38.

[35] S.Y.Savrasov, Phys Rev B 54, 16470 (1996).

[36] S.Y.Savrasov, Phys Rev B 54, 16470 (1996).

[37] http://www.physics.ucdavis.edu/~mindlab/

[38]http://www.fkf.mpg.de/andersen/

[39] P. Hohenberg, W. Kohn, Phys. Rev. 136, B864 (1964).

[40] Perdew J P and Wang Y Phys. Rev. B 45, 13244 (1992).

[41] J.E. Bernard, A. Zunger, Phys. Rev. B 36 (1987) 3199.

[42] M. Ferhat, F. Bechstedt, Phys. Rev. B 65 (2002) 075213.

[43] F.D.Murnaghan, Proc. Natl. Acad. Sci. USA. 30, 5390 (1944).

[44] M.J. Espitia R et al. / Journal of Magnetism and Magnetic Materials 451 (2018) 295–299.

[45] L.I. Karaouzène et al. / Optik 168 (2018) 287–295

[46] M. Issam Ziane, et al., Mater. Sci. Semicond. Process. 16 (2013) 1138,

[47] M. Abu-Jafar, A.I. Al-Sharif, A. Qteish, Solid State Commun. 116 (2000) 389,

[48] S. Adachi, J. Appl. Phys. 61 (1987) 4869.

[49] H. Baaziz, Z. Charifi, A.H. Reshak, B. Hamad, Y. Al-Douri, Appl. Phys. A 106 (2012) 687.

[50] High-pressure band parameters for GaAs: first principles calculations S. Saib , N. Bouarissa b, Solid-State Electronics 50 (2006) 763–768

[51] K. Beladjal,A. Kadri,K. Zitouni,K. Mimouni - Superlattices and Microstructures, Vol. 155, (2021), pp 106901.

[52] M. Briki et al. / Superlattices and Microstructures 45 (2009) 80_90

Journal of Engineering and Technology for Industrial Applications

ISSN ONLINE: 2447-0228

ITEGAM-JETIA

Manaus, v10. n.50, p. 161-172. November/ December., 2024.
DOI: https://doi.org/10.5935/jetia.v10i50.1262

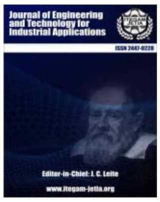

RESEARCH ARTICLE OPEN ACCESS

USING MACHINE LEARNING TO EVALUATE INDUSTRY 4.0 MATURITY: A COMPREHENSIVE ANALYSIS HIGHLIGHTING LEAN'S IMPACT ON DIGITAL TRANSFORMATION

Oussama Ben Ali[1], Sondes Hammami[2], Marwa Hasni[3], Fehmi H'Mida[4], Ahmed Nait Sidi Moh[5]

[1]National Engineering School of Tunis, University of Tunis El Manar, Tunisia
[2]National Engineering School of Tunis
[3]National Engineering School of Tunis, University of Tunis El Manar, Tunisia
[5] National Engineering School of Carthage, Université of Carthage, Tunisia
[4] Jean Monnet University, LASPI Laboratory, Roanne, France.

[1] http://orcid.org/0009-0000-6568-5387, [2] http://orcid.org/0000-0002-0044-1338, [3] http://orcid.org/0000-0002-4509-5563
[4] http://orcid.org/0009-0001-7009-823X, [5] http://orcid.org/0000-0002-2297-8603

Email: benalioussama1997@gmail.com, sondes.hammami@enicar.ucar.tn, marwa.gharbi@enib.ucar.tn, mohamedfehmi.hmida@enicar.ucar.tn, ahmed.nait@univ-st-etienne.fr

ARTICLE INFO

Article History
Received: August 21, 2024
Revised: October 1, 2024
Accepted: November 10, 2024
Published: December 31, 2024

Keywords:
Digital Transformation · Lean · Machine Learning · Industry 4.0 maturity. Data Analysis · Maturity level prediction

ABSTRACT

The rise of digital technologies in manufacturing and industries, known as the fourth industrial revolution, has created both opportunities and challenges for businesses. To succeed in this era of "Industry 4.0," companies need to assess their digital maturity. Through this study, we analyze the global state of Industry 4.0 maturity, identifying industry-specific trends, challenges, and potential growth. Leveraging advanced machine learning techniques, including data analysis, prediction, and recommendations. The study explores the complexities and evolution of Industry 4.0. Additionally, we show how machine learning plays a pivotal role in this analysis, contributing to enhanced insights and decision-making capabilities. Our research aims to not only assess the current state but also forecast future roadmaps while providing tailored recommendations for enhancing maturity levels. We aim to evaluate various machine learning based approaches for addressing these inquiries, focusing on Decision Tree, Support Vector Machine, and Random Forest models. We will choose the best performing model for our scenario. Initially, we use unsupervised learning through Hierarchical Clustering for grouping data, followed by data expansion. Subsequently, we employ supervised learning techniques, particularly Decision Tree, for descriptive, predictive, and perspective analysis. Among our recommendations for enhancing Industry 4.0 maturity levels, we advocate for extensive interventions, but exclusively for companies meeting predetermined criteria delineated within the decision tree node. Furthermore, we examine the influence of Lean on digital transformation. Through this interdisciplinary approach, our findings contribute to a deeper understanding of Industry 4.0 evolution and offer practical insights for strategic decision-making in the era of digitalization.

I. INTRODUCTION

The growth of Industry 4.0, often linked with the idea of the "smart factory" involves using high-tech tools like the Internet of Things (IoT), artificial intelligence (AI), advanced robots, 3D printing, and cloud computing in business operations. This shift completely changes how companies work and connect with their surroundings. It represents a new era in manufacturing marked by flexibility, creativity, and sustainability.

According to [1], there are five main reasons why Industry 4.0 is so important and groundbreaking: (1) Businesses can adapt quickly to market changes thanks to automation, (2) It boosts innovation and productivity, (3) It puts consumers at production, demanding new skills, and (5) it is posited to foster sustainable prosperity by leveraging modern technologies to address energy, resource, environmental, and socio-economic challenges.

Therefore, companies aim to align with the emerging trend of Industry 4.0 to maintain competitiveness in the market. To achieve this, it is essential to assess current levels of maturity and develop a clear roadmap for improvement.

Thus, companies stand to gain valuable insights by determining factors for their maturity level within the context of Industry 4.0. More particularly, we assess whether a company with a high maturity level in Lean is better positioned to enhance its Industry 4.0 maturity for becoming an advantageous endeavor. In other words, the process of improving the maturity level of Industry 4.0 could be smoother (quicker and less costly for the company) if it already has an established maturity basic level in this area.

To the best of our knowledge, there hasn't been a study that specifically outlines the key factors affecting the maturity level of Industry 4.0. While many studies have examined the correlation between Lean production and Industry 4.0 [2], [3], [4] they often neglect to specify how the maturity level of Lean impacts that of Industry 4.0.

The authors of [4] interviewed several companies to investigate the relationship between Lean practices and Industry 4.0. This investigation covered three main areas: Lean practices, Industry 4.0 technologies, and company performance indicators. The study revealed that combining Lean practices with Industry 4.0 adoption leads to significant improvements in operational performance. Additionally, it was observed that Lean practices were prevalent in companies with high operational performance improvement, while the adoption of Industry 4.0 was not significantly associated with such improvements. Despite this, there was a notable linkage between Industry 4.0 adoption and Lean practice implementation. While this study emphasizes the relationship between Lean Production, Industry 4.0 and operational performance, it does not show a tailored roadmap and improvement recommendations to companies. This gap is, indeed, undertaken in our current paper.

An additional study in [3] designed a questionnaire to categorize companies based on their commitment to Lean practices. The study discovered that companies that are deeply committed to Lean practices approached digital transformation differently from those with lower commitments. As such, two distinct digital transformation patterns have been identified: the Sustaining pattern, characterized by gradual digitalization involving the entire company horizontally. And the Disruptive pattern, marked by significant digital investments with a vertical focus. This research underscores the importance of understanding different digital transformation strategies for practitioners and scholars. Although this article indicates the difference between companies with low Lean level and high Lean level in adopting industry 4.0 technologies.

The contribution of other factors and their impact on industry 4.0 maturity level is not discussed.

Our proposed model allows to identify and analyze these factors. As a result, our approach is characterized by its customized and dynamic nature, that is meticulously aligned with the unique objectives and needs of the company.

Going into more details, Artificial Intelligence (AI) is used to identify the critical factors influencing the maturity level of Industry 4.0, particularly by assessing the impact of Lean on it. We have opted for AI due to its ability to explore complex patterns, detect nonlinear relationships, and adapt to evolving data [5]. Moreover, AI enables us to develop predictive and prescriptive models to anticipate future trends and recommend strategic actions. In summary, our AI-based approach offers a powerful and adaptable solution for understanding and enhancing the maturity level of Industry 4.0 in businesses.

The aim of our study is to conduct an analysis of the primary factors influencing the enterprise maturity level on Industry 4.0. Additionally, we are seeking to ascertain whether the maturity level of an enterprise in Lean practices affects its maturity level in Industry 4.0. We will also explore the existence of maturity models specifically tailored for Digital Lean initiatives.

Furthermore, we intend to identify suitable machine learning methodologies to address these inquiries. First, we use an unsupervised ML technique for data clustering and data augmentation which is Hierarchal clustering. Then, we use supervised ML techniques for the analysis issue. We mainly explore Decision Tree, Support Vector Machine and Random Forest for predictive analysis and Decision Tree for descriptive and perspective analysis.

The rest of this paper is organized as follows. In Section 2, we give a background and literature review regarding the addressed subject. Section 3 gives Dataset and methodology and in section 4, we represent results and discussion.

II. BACKGROUND

Before delving into our research questions, it is pertinent to establish a comprehensive definition of a maturity model. Subsequently, we will provide an overview of prominent maturity models relevant to Industry 4.0, Lean methodologies, and ascertain the existence of maturity models focused on digital Lean transformations. To this end, we will discuss potential examples of machine learning tools that could be explored to analyze and identify the key factors influencing the maturity level of enterprises in Industry 4.0 initiatives.

II.1 MATURITY MODEL

According to [6], maturity models are commonly used to assess the current situation, identify and prioritize improvement measures, and monitor progress in a given domain. These models are designed as a set of levels or stages describing the development of the examined object in a simplified manner, as described by [7].

Besides, the study in [8] highlights that maturity models allow us to define the current and desired levels of maturity along with corresponding improvement measures. In the same way, [9] describe maturity models as tools for continuous improvement and guides for organizations.

While maturity models may vary in their structural design and application domains, they typically comprise two fundamental components to serve their intended purpose as given in [6], [8]: (1) a series of levels or stages, and (2) dimensions or capabilities.

Dimensions serve as pivotal points in the evaluation process, with their selection tailored to the specific domain being assessed. Maturity models are inherently multidimensional. For example, in assessing the maturity of an enterprise in the context of Industry 4.0, considerations extend across various dimensions such as processes, personnel, and technology [10].

Similarly, when evaluating enterprises based on the maturity of their supply chain, dimensions such as reverse logistics, collaboration, processes, technology, and sustainability come into play [11]. Thus, the choice of dimensions to be evaluated is contingent upon the specific domain under scrutiny.

The authors of [6], [12], [8] classify maturity models into three categories based on their intended use:

- 1) descriptive, where the model is used to assess the maturity level of each dimension and the overall maturity level. Thus serving as a diagnostic tool to help companies focus on dimensions with mediocre maturity levels.

- 2) prescriptive, where the maturity model provides guidelines in the form of a roadmap to help the company improve its maturity level.

- 3) comparative, where the model allows for internal or external benchmarking with sufficient historical data from many assessment participants.

We note that maturity models are often associated within readiness models. They behave like maturity models but focus on assessing how prepared systems are for change. These models start by understanding the current state of the system, which helps in getting ready for improvements. They evaluate where a system stands before it undergoes any transformation towards maturity [13].

II.2 MATURITY MODEL IN INDUSTRY 4.0

In the context of Industry 4.0, maturity models play a crucial role. They help spread awareness of the concept and offer companies a better grasp of it. Additionally, they provide practical suggestions for implementing strategies to adapt to this transformative revolution. In this section, we focus on Industry 4.0 maturity and some readiness models developed in the literature.

Based on [13], maturity models are classified according two criteria:

1) the nature of the model's maturity (SIMMI 4.0 model [14]) or readiness (DREAMY model [15], FORRESTER model [12]).

2) the objective of the models: descriptive SIMMI 4.0 [14] and Impuls model [16], perspective models (the Connected Enterprise Maturity Model [17]), descriptive and perspective models (DREAMY model [15]), and finally comparative and perspective models.

For each model, the authors present dimensions. It's worth noting that dimensions vary significantly from one model to another. For instance, the SIMMI model considers Vertical integration, Horizontal integration, Digital product development, and Cross-sectional technology Criteria. On the other hand, The Connected Enterprise Maturity Model proposes dimensions such as Information infrastructure (hardware and software), controls and devices (sensors, actuators, etc., that feed and receive data), networks (that move all this information), and security policies (understanding, organization, enforcement).

Most models consist of five stages but with different labels. For example, SIMMI proposes these levels: Basic digitization level, Cross-departmental digitization, Horizontal and vertical digitization, Full digitization, and Optimized full digitization. While the Connected Enterprise Maturity Model proposes the levels: Basic digitization level, Cross-departmental digitization, Horizontal and vertical digitization, Full digitization, and Optimized full digitization.

Different methods are used to collect data for evaluating the maturity level, including an online self-assessment tool, a questionnaire combined with visits (Industrie 4.0 Maturity Index from ACATECH), and a general questionnaire, assisted by a third party (SIMMI 4.0).

According to [10], Industry 4.0 maturity models from the literature cannot adapt to small and medium-sized enterprises. They proposed an Industry 4.0 maturity model specifically tailored for small and medium-sized enterprises.

This model Comprises six dimensions and six levels. Based on the sub-dimensions, they developed a questionnaire and then they built a matrix to help them identify the gaps.

II.3. MATURITY MODEL IN LEAN

Lean methodology is based on the principle of continuous improvement. Maturity models play a crucial role in this context. By evaluating the current maturity level of Lean, companies can identify the gaps which could be the targeted areas for improvement. Accordingly, the maturity level of Lean can undergo continuous improvement.

Referring to [18], the discussion encompasses 24 key models. Within this collection, several models stand out as Lean Construction Maturity Models (LCMMs), explicitly illustrating the concept of Lean Construction (LC) maturity and offering a structured approach to assess LC maturity. Additionally, there is a subset of models that clearly consider Lean Construction as a foundational element. Lastly, three models were identified that lack a direct link to LC maturity but incorporate Lean principles and their adaptability into their frameworks [19].

Besides discuss combining Building Information Modelling (BIM), which is a process for creating and managing information on a construction project, and Lean Management (LM) to make construction projects more efficient. They agree that using BIM and Lean together can reduce waste and improve project results [20].

In addition, [21] presented LEAST which is a Lean Enterprise Self-Assessment Tool developed by an industry/government/academia team under the auspices of the Lean Aerospace Initiative (LAI). LEAST is organized into three sections:

- Section 1: lean transformation/leadership,

- Section 2: life cycle processes,

- Section 3: enabling infrastructure.

Each section is composed of multiple sub-sections and each sub-section contains multiple Lean practices. In total LEAST presents 54 Lean practices. For each practice, five maturity levels were assigned from level 1 (least capable) to level 5 (world class). Evaluating all the 2 will give the company a clear vision of its current state and the best way to prioritize the targeted areas for improvement measures.

In their research, [22] introduced a Lean maturity model tailored for operational-level planning. The study emphasizes the criticality of organizations implementing a comprehensive enterprise-wide Lean transformation plan, such as LESAT-LAI (Lean Enterprise Self-Assessment Tool) developed by the Lean Advancement Initiative (LAI), as a foundational requirement for the proposed model's effectiveness.

The model created has the dual capability of assessing both the degree of leanness and the effectiveness of Lean practices by evaluating Lean performance. The main purpose of this study is to develop a Lean maturity model adapted to the specifications of Manufacturing Cells.

Data is gathered through a case study approach involving two Manufacturing Cells, allowing for an investigation of Lean maturity in a real-life context. Both quantitative and qualitative data are analyzed inductively to enhance the theoretical framework, interpret Leanness and performance results, and formulate overall measurements.

II.4. MATURITY MODEL IN DIGITAL LEAN

Combining both paradigms will require a new maturity model that takes into account the relationship between Lean and Industry 4.0. In the relevant literature, only few articles have presented the Lean 4.0 maturity model. While there are articles proposing a Lean-Based Maturity Framework integrating Building Information Modeling (BIM) to offer valuable project insights including lessons learned, value generation, and continuous improvement [19], [20]. The convergence of Lean principles with Industry 4.0 within a maturity model context appears to be scarcely explored. To the best of our knowledge, [23] is the only article, published in 2023, to introduce a digital Lean maturity model in this intersection.

Exploring further both paradigms, [23] proposed a maturity model based on Lean and Industry 4.0 synergy. The model consists of four key elements: strategic pillars, perspectives dimensions and maturity levels. The model comprises two main strategic pillars: Lean and Industry 4.0. These pillars serve as the fundamental concepts guiding the framework. Additionally, there are three key perspectives termed as the "Smart" components, which include processes, people, and products.

These perspectives offer a holistic view of the organizational landscape. Moreover, the model defines maturity levels for both the strategic pillars, termed as strategic maturity levels, and the perspectives, termed as "Smart" maturity levels. This categorization aids in assessing the organization's progression within each aspect of the framework.

To our knowledge, all existing maturity models (Lean, industry 4.0 and Lean 4.0 models) use an assessment matrix to evaluate current maturity levels and rely solely on these levels to identify areas for improvement. Our machine learning model bridges this gap by leveraging similar use cases. Instead of offering generic recommendations, our model provides tailored roadmaps specific to each company's characteristics to enhance their maturity levels. Put simply, we learn from others' experiences to avoid errors and benefit from their successes. Instead of just using formulas and rules, we look at real-life examples to create a roadmap and help companies on their journey.

III. DATASET AND METHODOLOGY

The flowchart depicting our study's methodology is illustrated in Figure 1. Initially, the process involves obtaining a reliable database.

Due to the challenge of accessing databases containing real-world use cases of Lean 4.0 projects, primarily due to confidentiality concerns, we utilized a limited dataset as provided in reference [24]. The database consists of 19 companies and 53 attributes. Nevertheless, given the fact that we explore Machine Learning, a sufficient data amount should be provided to ensure obtaining an efficient model. Thereby, we use the segmentation-based data augmentation technique to increase the size of the data from 19 to 274 companies.

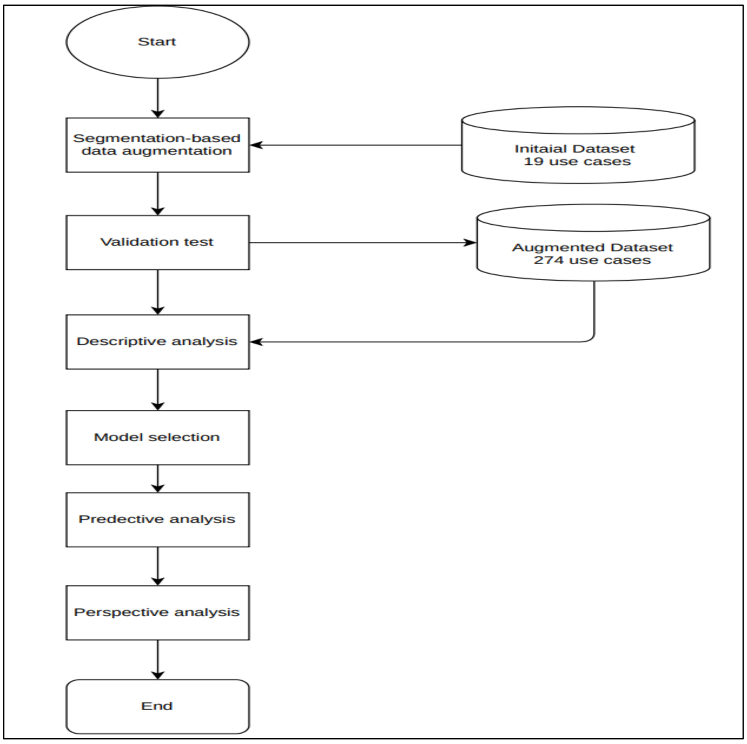

Figure 1: ML Workflow Chart.
Source: Authors, (2024).

Then, we verify the validity of our augmented data by calculating the percentage of maintained relationships between attributes in the generated data before incorporating it into our analysis. Before proceeding with predictive and perspective analysis, it is essential to select an appropriate model to ensure optimal results and insightful outcomes. This involved choosing the most suitable machine learning model that would effectively extract valuable insights from the data. This analysis process involves three key stages:

1.Descriptive Analysis: Here, we examine the correlations between different attributes and investigate the factors that have the most significant influence on the maturity of Industry 4.0.

2.Predictive Modeling: We utilize similar cases to predict the maturity level, leveraging predictive analytics techniques.

3.Perspective Enhancement: This stage involves offering customized and personalized recommendations aimed at enhancing the maturity level based on the insights gained from the analysis.

The authors of [24] focused on the difference between the companies with Low Lean maturity level and those with high Lean maturity level in the adoption of I4.0 technologies. Leveraging the same dataset, we aim to construct a maturity model, manifested as a machine learning (ML) model, designed to aid companies in forecasting their maturity levels and furnishing tailored recommendations based on analogous cases.

The contribution consists of: 1) Expanding the database using augmented data techniques to use in analyze phase; 2) Analyze the factors influencing maturity levels using machine learning tools; 3) optimize parameters of the model and 4) propose recommendations using decision tree.

III.1. DETAILS OF THE DATASET

The database (BD) presented in [24] consists of 19 use cases and 53 attributes. The companies involved in this study are confined to just two sectors: Machinery (M) and Metal Products (MP). These 19 companies fall into one of two categories: those with a Lean maturity level zero (0), indicating a low level of Lean maturity, and those with a Lean maturity level one (1), indicating a high level of Lean maturity.

These attributes are classified into four dimensions: 1) Industry 4.0 technologies and maturity level; 2) Targeted area of industry 4.0 investments; 3) purpose and expected performance of industry 4.0 investments and 4) magnitude of industry 4.0 investments. Each dimension has multiple sub-dimensions which are the variables of our model.

In this database, the authors consider 4 maturity levels (table 1) to evaluate six I4.0 technologies: 1) IoT; 2) Industrial analytics; 3) Advanced human–machine interface; 4) Cloud manufacturing; 5) Additive manufacturing and 6) Advanced automation. These technologies serve as the sub-dimensions falling under the primary dimension of "Industry 4.0 Technologies and Maturity Level."

Table 1: Maturity levels.

Level 0	Not Applicable
Level 1	Monitoring
Level 2	Control
Level 3	Control / Optimization Autonomy
Level 4	Optimization Autonomy

Source: [24]0.

In our study, we aim to assess the overall maturity level of the company by considering these different technologies. Therefore, we propose to replace the maturity level of each technology by an overall maturity level. This level is the weighted average of the maturity levels of the 6 technologies. The weights of each technology were defined in [25] using the Analytic Hierarchy Process (AHP) method. The weighting factors were assigned as follows:

- IoT Maturity level: 15.9%
- Industrial analytics Maturity level: 19.4%
- Advanced human–machine interface Maturity level: 40.2%
- Cloud manufacturing Maturity level: 11.7%
- Additive manufacturing Maturity level: 3.7%
- Advanced automation Maturity level: 3.2%
- Simulation Maturity level: 5.3 %

Here, we shall point out that these weights have been validated by calculating the consistency index of the related pay-off judgmental matrix. The obtained ratio is 0.02 which ensures that judgments established for computing these weights are coherent since the default risk is inferior to 0.1 (a conventional threshold that is typically considered).

Due to the absence of any mention of the "Simulation" technology in the responses gathered by [24] during their survey on technology investments, we propose excluding it from our analysis. In other words, since "Simulation" did not feature in the survey data, its value will be considered as 0. Thus, it will consequently be omitted from the equation used to determine the 'Overall Maturity Level'. The degree of Industry 4.0 development depends on the level of advancement in Industry 4.0 technologies, as shown by equation (1):

*data ['Overall Maturity Level'] = 0.159 * data ['IOT-Maturity Level'] + 0.194 * data ['Industrial analytics - Maturity level'] + 0.402 * data ['Advanced human–machine interface - Maturity level'] + 0.117 * data ['Cloud manufacturing - Maturity level'] + 0.037 * data ['Additive manufacturing - Maturity level'] + 0.032 * data ['Advanced automation - Maturity level']* *(1)*

To summarize, we have created a new column, **['Overall Maturity Level']**, in the **data** dataset. This new column replaces the six individual columns representing maturity levels in the six specified technologies. The value of **['Overall Maturity Level']** is calculated as the weighted sum of the maturity levels across these six technologies, as previously described.

III.2. DATA-SEGMENTATION BASED DATA AUGMENTATION

The dataset suggested in [24] is insufficiently large to construct a highly effective machine learning model. It only consists of nineteen use cases. To address this limitation, we can employ data augmentation techniques to generate additional case studies, thereby facilitating the development of a more accurate model.

The used approach customizes data augmentation to distinct data segments. It is fostering a more nuanced and effective learning process for machine learning models dealing with tabular data. It is valuable for tabular data due to its ability to preserve relationships and facilitate feature-specific augmentation. This technique is implemented through the following steps:

1. Hierarchical Clustering:

● Use hierarchical clustering to group data points into clusters based on their similarity.

● The optimal number of clusters is determined using the elbow method (in this case, it's set to 3).

2. Assigning Clusters:

● Assign each data point to a cluster based on the results of hierarchical clustering.

● This is done using the Agglomerative Clustering algorithm which is a bottom-up approach that starts by considering each data point as a single cluster and then progressively merges the closest pairs of clusters until only one cluster remains.

3. Data Augmentation Function:

● Define a function named augment_data that takes two arguments: data (the original dataset) and num_samples (the number of augmented samples to generate).
● Create a copy of the original data to store augmented data.
4. Loop Through Columns:
● Iterate over each column in the dataset except for the target column and the cluster column.
5. Augmentation Loop:
● For each column, loop through num_samples times to augment data.
● Randomly select a cluster from the clusters present in the dataset.
● Extract the data points belonging to the selected cluster.
● Randomly select one data point from the cluster.
● Perturb the value of the selected column in the chosen data point by randomly choosing a value from the unique values of that column in the original dataset.
● Append the augmented data point to the augmented dataset.
6. Return Augmented Data:
● Return the augmented dataset.

Prior to proceeding to data augmentation, we cluster it with a view to obtain homogeneous partitions. This would be of interest to apply the data augmentation safely by preventing high intra-variance. To do so, we referred to the Hierarchical clustering. According to [26], Hierarchical clustering is more suitable for categorical data. It also provides a hierarchical structure referred to as dendrogram that illustrates the relationships and the internal structure between clusters. This algorithm does not require the specification of the number of clusters in advance and can handle clusters of various shapes and sizes.

As depicted in Figure 2, the dendrogram displays various clusters of companies based on their similarities. The vertical lines linking companies are proportional to the level of similarity between the connected companies. The shorter the line, the more similar the companies are. For instance, from Figure 2, we observe that companies 17 and 5 are the most similar.

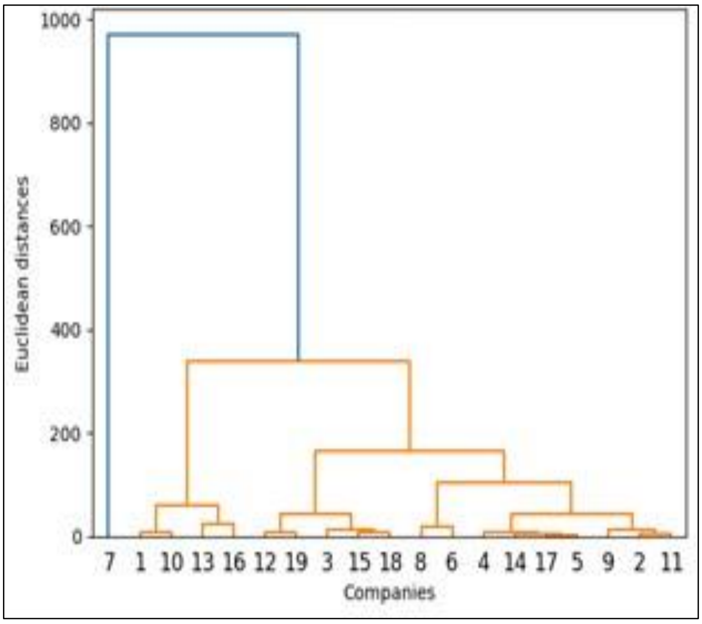

Figure 2: Dendrogramme des Entreprises : Analyse de Similarité et Clustering Hiérarchique.
Source: Authors, (2024).

We determined the number of clusters for our data using a method called the elbow method. This method involves plotting the within-cluster sum of squares (WCSS) against the number of clusters and looking for the point where the rate of decrease in WCSS slows down, forming an "elbow" shape in the plot. In our analysis, we observed that the elbow point occurred when we had three clusters. The next step consists of applying Data augmentation to each cluster.
The subsequent step involves applying Data augmentation to each cluster. The augmented data size amounts to 274.

Proposed a multivariate relationship analysis method to assess the fidelity of generated data compared to real data. This technique involves comparing Pairwise Pearson Correlation matrices between the real and generated data through heatmaps. A heatmap is a graphical representation of data where individual values are displayed using colors [27].

It is common practice to visualize the intensity or distribution of values across two dimensions, such as rows and columns in a matrix. By calculating the differences in correlations between the two datasets, the percentage of maintained relationships in the generated data is determined. If this percentage exceeds 0.6, the approach is classified as "Excellent"; between 0.4 and 0.6, as "Good"; and below 0.4, as "Poor".

In our case, the Percentage of numerical relationships maintained in generated data is 0.43 which means that our data augmentation approach is qualified as Good. This suggests that the generated data adequately preserves a substantial portion of the multivariate relationships observed in the real data.

III.3. UTILIZED MODELS AND TECHNIQUES

As shown in Figure 1, our analysis starts with descriptive analysis, then predictive analysis and finally perspective analysis. Each step from this process requires different techniques. For descriptive analysis, we selected Multiple Component Analysis (MCA) for multidimensional analysis and Heatmap.

By using these methods, we attempt to meet two objectives. First, identify pertinent features to the maturity level analysis by retaining only one example of each highly correlated pair of features. This would be of interest to refine the data to be fed to the machine learning model and prevent any overfitting issue. Second, identify the linkages between features and the maturity levels of companies. This allows to emphasize improvements scopes for the least performing. ML models enable us to achieve predictive analysis objectives.
In our scenario, we've opted for Decision Trees (DT), Random Forests (RF), and Support Vector Machines (SVM) to conduct our predictive analysis on forecasting the maturity level of a company. The selection of these specific ML models stems from their distinct strengths and suitability for the task at hand.
1. Decision Trees (DT): is chosen for its simplicity and interpretability. It's adept at handling categorical and numerical data, making it suitable for diverse datasets. The technical steps involved in building a decision tree include:
● Selecting the best attribute to split the data at each node, usually based on metrics like Gini impurity or entropy.
● Recursively partitioning the data based on these attributes until a stopping criterion is met, such as reaching a maximum depth or purity threshold.
2. Random Forests (RF): is an ensemble learning method that combines multiple decision trees to improve predictive performance and reduce overfitting. It's particularly useful when

dealing with high-dimensional data or datasets with a large number of features. The technical steps of RF involve:

● Building multiple decision trees on random subsets of the training data (bootstrapping).

● Aggregating the predictions of individual trees through voting or averaging to make the final prediction.

3. Support Vector Machines (SVM): is chosen for its effectiveness in handling both linear and non-linear classification tasks. It works by finding the hyperplane that best separates different classes while maximizing the margin between them. The technical steps of SVM include:

● Mapping the input data into a higher-dimensional space using a kernel function.

● Finding the optimal hyperplane that separates the classes with the maximum margin or minimizing classification errors.

By employing these models, we aim to leverage their unique capabilities to accurately predict the maturity level of companies. This predictive capability is crucial for strategic planning, as it empowers proactive decision-making to optimize processes and enhance overall maturity level.

IV. RESULTS AND DISCUSSIONS

IV.1. DESCRIPTIVE ANALYSIS

It is important to note that our dataset contains categorical variables. Therefore, we have selected Multiple Correspondence Analysis (MCA) technique which is a useful technique for multidimensional analysis of categorical data [28]. This technique enables the condensation of a group of categorical variables into a limited set of independent variables known as principal components. These components optimally summarize the data given in [28].

Now, let's explore the insights from the MCA graph (Figure 3):

a) Companies on the Upper Right Side of the Plot (Near Company 11):

The companies clustered closely together on the graph share remarkably similar characteristics, especially in their advanced industrial analytics, advanced automation, IoT, and human-machine interface maturity levels. What stands out is that they all show high levels of maturity in these areas, along with a significant use of extensive long-term interventions. This observation aligns with the conclusions drawn in reference [24]. In fact, it suggests that companies focusing on such interventions tend to have lower lean maturity levels but higher maturity in Industry 4.0. Therefore, this alignment strengthens the conclusion that these companies indeed demonstrate heightened maturity in Industry 4.0 technologies, backed by supporting evidence.

b) Companies on the Upper Left Side of the Plot (Close to Each Other):

This particular group of companies stands out as a cohesive cluster, evident from their close proximity on the individual-variable graph. Their distinguishing features include a preference for localized medium-term interventions, substantial investments in Industry 4.0 logistics, a modest maturity level in advanced automation (Level 0), and a leaning towards Lean principles. Our analysis suggests a correlation where companies with elevated Lean maturity prioritize logistics investments while demonstrating lower maturity levels in advanced automation.

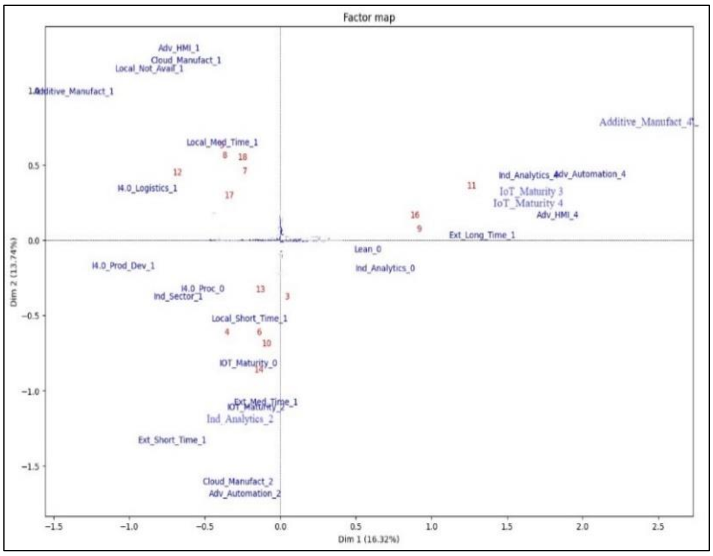

Figure 3: MCA Factor Map of Key Variables.
Source: Authors, (2024).

Now that we've explored the insights from the MCA graph, let's transition to discussing the heatmap. Transitioning from the Multiple Correspondence Analysis (MCA) graph to the heatmap serves a crucial purpose in our analysis. While the MCA provides an overview of relationships between categorical variables, the heatmap allows us to delve deeper into specific interactions and correlations. By visualizing the data in a heatmap, we can identify patterns, dependencies, and potential areas of interest. [29] describes the Heatmap (correlation matrix) as a necessary input for others who may wish to reproduce (and confirm) a study's results, as well as perform secondary analysis.

In this study, we employ heat maps as a powerful tool for conducting descriptive analysis of our dataset. Heat maps offer a visually intuitive means of summarizing and exploring the distribution of quantitative variables within our data, allowing us to identify prominent patterns and trends. By representing data values with varying colors, heat maps provide immediate insights into the relative magnitudes and spatial relationships of different variables or observations.

The heat map graph of Figure 4 provides a visual representation of the relationships between different variables in our dataset. These correlations offer several interpretations and insights into the factors influencing the overall maturity level of Industry 4.0 technologies. We summarize this into four factors:

a) 'Overall Maturity level' – Industry 4.0 inves - Assembly: 0.57:

The strong positive correlation suggests that organizations with higher levels of investment in assembly processes tend to have higher overall maturity levels in their Industry 4.0 technologies. This implies that a strategic focus on optimizing assembly operations through technology investments contributes significantly to the overall advancement of Industry 4.0 capabilities.

b) 'Overall Maturity level' - Quality -Governmental incentives: 0.46 / Overall Maturity level' - Productivity - Governmental incentives: 0.42:

The moderate positive correlations indicate that governmental support in the form of incentives for quality and productivity improvements is associated with higher overall maturity levels in Industry 4.0 technologies. Organizations that leverage such incentives may have access to resources or initiatives that facilitate the adoption of advanced technologies and practices, leading to enhanced quality and productivity outcomes.

c) 'Overall Maturity level' - Extensive interv - Long Time: 0.42:

The correlation of 0.42 between the overall maturity level and extensive interventions over a long time suggests that companies investing in long-term interventions tend to have higher maturity levels in Industry 4.0. This aligns with findings from [24], where such companies demonstrated higher Industry 4.0 maturity despite lower Lean maturity levels. In essence, sustained long-term efforts in adopting Industry 4.0 technologies positively impact overall maturity levels, indicating a strategic focus on digitalization and technological advancement over time.

d) 'Overall Maturity level' – Flexibility -Improving waste detection: 0.01 / 'Overall Maturity level' - Industry 4.0 invest - processing: 0.01:

The modest correlation between the "Overall Maturity Level" and the flexibility-improving waste detection suggests that companies prioritizing flexibility enhancements and waste detection in their industry 4.0

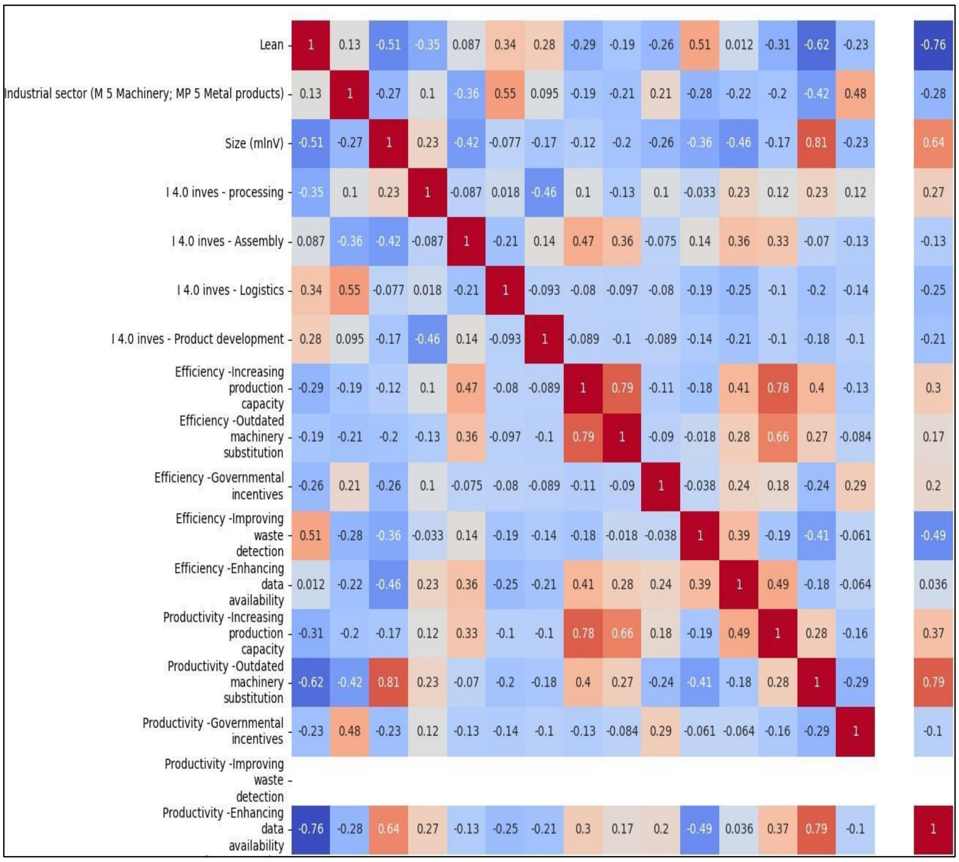

Figure 4: Partial Heat map Focus (correlation matrix).
Source: Authors (2024).

initiatives might not necessarily exhibit a high Industry 4.0 maturity level. These factors seem to have limited influence on the overall maturity level. Similarly, the weak correlation between investment in processing and overall maturity level implies that decisions regarding processing investment may not significantly impact Industry 4.0 maturity.

While analyzing the data, we observe that the "Lean" variable does not prominently appear among the influencing factors for the overall maturity level of Industry 4.0. Companies with Low Lean maturity level and High maturity level approach industry 4.0 differently. Despite these variations, the overall maturity level of Industry 4.0 remains consistent. In other words, although these companies implement Industry 4.0 differently, the overall maturity level shows only minor variations.

In summary, while the "Lean" factor does not significantly influence the overall maturity level of Industry 4.0, it plays a crucial role in shaping the implementation approach. Companies may adopt different strategies, yet the overall maturity level remains relatively consistent across both low and high Lean maturity companies.

IV.2. MODEL SELECTION

All of these models we used have the same phases. They first go through feature engineering which consists of feature selection and data cleaning. Following feature engineering, the models undergo training using labeled data to learn patterns and relationships between features and the target variable. During the training phase, model parameters are optimized to minimize a predefined loss function. Once trained, the models are evaluated using validation data to assess their performance and fine-tune hyperparameters if necessary. Finally, the models are deployed to make predictions on unseen data, providing insights into the maturity level of companies based on their features.

We chose Mean Squared Error (MSE), Mean Absolute Error (MAE), and R-squared (R2) score to evaluate the performance of our models because each metric offers unique insights into different aspects of model performance. MSE provides a comprehensive measure by penalizing larger errors more heavily, making it suitable for scenarios where large errors are critical. MAE, on the other hand, treats all errors equally, offering a simpler and more interpretable measure of performance that is less sensitive to outliers. Lastly, R2 score allows us to assess the goodness of fit of the model by indicating how well the independent variables explain the variability of the dependent variable. Together, these metrics provide a well-rounded evaluation of model accuracy, robustness to outliers, and overall fit to the data.

The MSE calculates the average of the squared errors (differences between predicted and actual values) [30]. The MAE represents the average absolute difference between the predicted values and the actual target values. Lower MSE and MAE (closer to zero) indicate better performing model.

R2 score assesses how well our model performs by measuring the proportion of explained variance. As far as the R2_score value gets near to one a better model performance is retrieved.

Table 2: Statistical performances of compared models.

AI model Metrics	**Decision Tree**	**Random Forest**	**SVM**
MSE	0.033	0.036	0.033
MAE	0.062	0.089	0.111
R2_score	0.863	0.851	0.863

Source: Authors, (2024).

As may be noticed from table 2, the Decision Tree model stands out as the most promising, demonstrating superior performance with an MSE of 0.033, MAE of 0.062, and an R2 score of 0.863. We note that, beyond its exemplary performance in this context, the Decision Tree model offers additional advantages that further justify its selection. Decision trees are inherently interpretable, allowing for straightforward visualization and understanding of decision-making processes. They are also computationally efficient and less sensitive to outliers compared to other models like SVM. Moreover, Decision Trees naturally handle feature interactions and nonlinear relationships, making them well-suited for datasets with complex structures. Hence, given its superior performance and inherent advantages, the Decision Tree model emerges as the optimal choice for this task, underscoring its versatility and efficacy in practical machine learning applications.

A Decision Tree is a machine learning technique that helps categorize (classification) or forecast values (regression). It divides data into sections based on their traits and assigns a label or predicts a value for each section. Key parameters for Decision Trees include:

1. Split Criteria: Defines how to assess the quality of a data split. Common choices include "Gini impurity" and "information gain."
2. Maximum Depth: Limits how deep the tree can grow, preventing excessive detail and reducing overfitting.
3. Minimum Split Samples: Sets the minimum number of data points needed to divide a node, helping to prevent splitting based on too little information.
4. Minimum Samples Leaf: Sets the minimum number of samples required for a node to be considered a leaf node (terminal node without any further splits).

With our Decision Tree model, we've carefully chosen parameters using grid search to optimize its performance. For the "min samples leaf" parameter, we initiated the numerical list in the grid search at 8. This decision reflects our commitment to creating a model that not only accurately captures patterns in the data but also ensures robustness, interpretability and generalization. By setting a minimum number of samples for each leaf node, we're encouraging the model to make decisions based on larger subsets of the data. This helps in extracting meaningful insights and interpretations from the decision tree, as we're analyzing patterns based on groups of data points rather than individual instances.

The grid search examines many combinations of params and provides us with the optimal combination which refers to the best performing model (Table 3).

Table 3: Best Hyperparameters of decision tree using Grid Search.

Split Criteria	Max_Depth	Min_Samples_Leaf	Min_Samples_Split
Gini impurity	None	8	2

Source: Authors, (2024).

In summary, Random Forest and SVM are only useful for descriptive and predictive analysis. However, the Decision Tree allows us to make the three (3) analysis (descriptive, predictive, and perspective). Besides, the Decision Tree is performing better than the other models. As a result, the Decision Tree is the most suitable choice for our analysis.

IV.3. PREDICTIVE ANALYSIS

After analyzing the key features, understanding the correlations and patterns in our data (Descriptive analysis), we can use these features for predicting the current maturity level of the company.

Figure 5 shows our Decision Tree model. Each node represents a question, and each branch corresponds to a response to that question [31]. Conceptually, we can view each node as a decision point. By traversing the tree and answering the questions at each node until reaching the last node, also called a leaf node, we can predict the maturity level based on the path followed.

To illustrate the application of the model, let's take the example of a case study (red circle in Figure 5). We start from the top of the decision tree (Figure 5). We observe that companies obeying the condition of the parent node (1st node) emphasize investments in Assembly. We move forward to the next node (2nd node), we go with companies that do not satisfy this condition. That means, companies who are not expecting Industry 4.0 performance improvements in Quality while also prioritizing enhancing data availability as an investment driver. For the next node (3rd node) we choose companies whose size exceeds 111. We reach the 4th node and observe that companies who are not adopting extensive interventions for long term tend to have an overall Industry 4.0 maturity level around 1.176 (5th node = Leaf node). By following this decision path (red circle), we can predict the maturity level for companies sharing these same attributes and decisions, which in this case corresponds to 1.176.

IV.4. PERSPECTIVE ANALYSIS

Our goal is to increase the maturity level. By examining the nodes following the leaf we can pinpoint actionable decisions contributing to maturity enhancement. It's crucial to distinguish between contextual variables like size or sector and actionable decisions, as changing contextual variables might not be feasible. By following this methodology, companies can pinpoint precise interventions necessary for advancing maturity levels, thereby leveraging the Decision Tree as a practical recommendation tool for organizational improvement.

Taking the example of the company associated with the leaf node displaying an overall maturity level of 1.176. By bringing together all companies that meet the same conditions present in the parent nodes of this sheet, it is likely that they share a similar maturity level because they conform to the same characteristics. Based on our model and considering similar cases, it is recommended that these companies emphasize extensive interventions for long term to improve their industry 4.0 maturity level. This recommendation is substantiated by findings from [7]—[24], who suggest that companies with low Lean maturity levels often require substantial interventions to foster significant improvements.

By adopting this strategy, there is a high probability, based on other similar cases, that this company can increase their maturity level from 1.176 to 1.381.

Furthermore, our analysis reveals a noteworthy observation: companies that neglect localized interventions exhibit a relatively lower maturity level of 0.755. However, by simply adopting localized interventions, this maturity level can be significantly enhanced to 0.876. This finding underscores the pivotal role of localized interventions in driving organizational maturity within the context of Industry 4.0. According to [7]—[24], companies that prioritize localized interventions typically demonstrate high levels of Lean maturity. This correlation suggests that by emphasizing localized interventions, companies not only enhance their Industry 4.0 maturity level but also align with established principles of Lean methodology. Therefore, integrating localized interventions into organizational strategies not only facilitates maturity enhancement but also fosters a culture of lean thinking and continuous improvement. Accordingly, it enables companies to position themselves for sustained success in the rapidly evolving landscape of Industry 4.0.

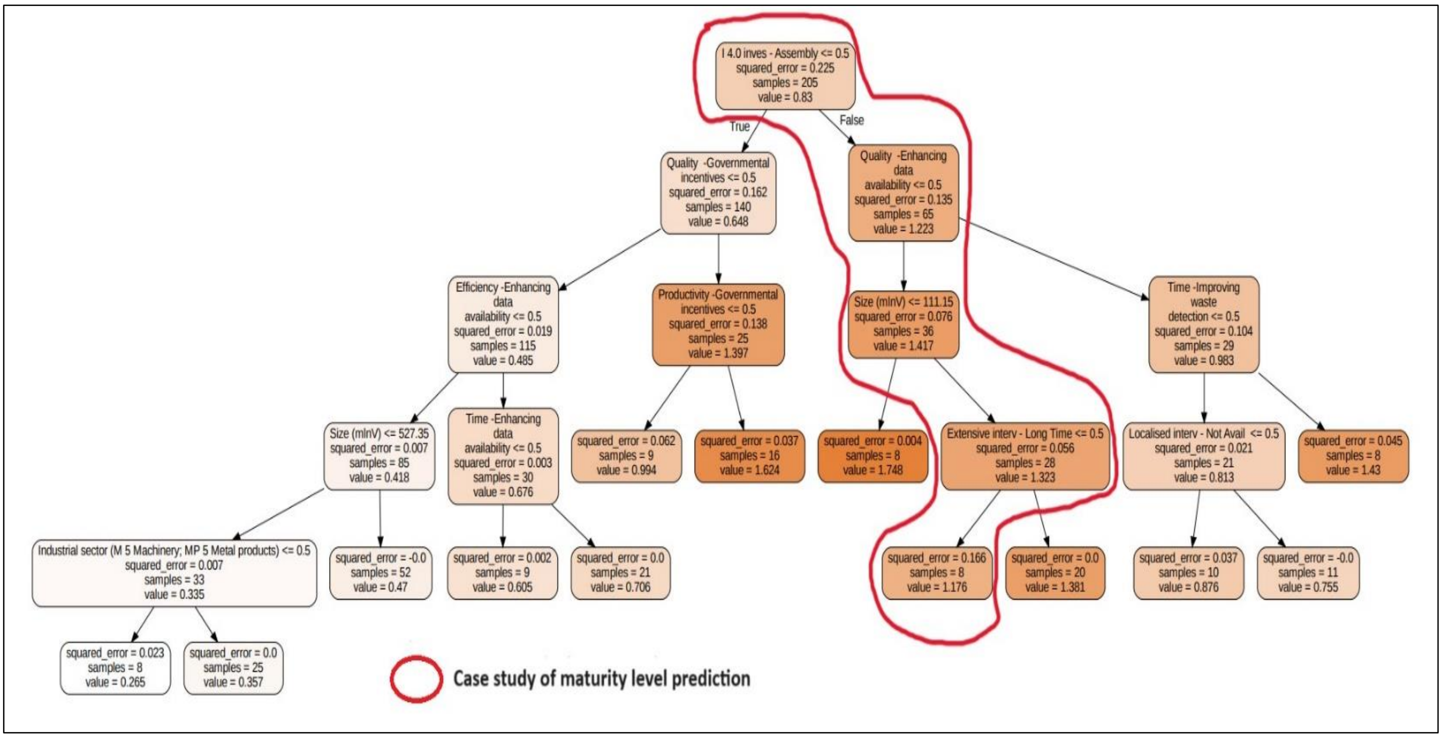

Figure 5: Decision Tree based ML model for maturity prediction and enhancement.
Source: Authors, (2024).

Besides, these companies can also follow a second path “Time – improve waste detection” which can significantly increase their overall maturity level from 0.755 to 1.43.

It indicates a crucial aspect influencing the maturity level of Industry 4.0 within the context of waste detection improvement. The presence of this column suggests that dedicating resources and efforts towards enhancing waste detection processes is pivotal for advancing Industry 4.0 maturity. This linkage between time-related performance improvement and waste detection aligns closely with Lean principles.

In Lean methodology, waste detection and reduction are fundamental pillars aimed at maximizing value and efficiency while minimizing resources and time. By focusing on improving waste detection as an Industry 4.0 investment driver, organizations align with Lean principles by identifying and eliminating non-value-adding activities or processes. The "Time – improve waste detection" column signifies an acknowledgment of the importance of time efficiency in waste detection efforts. Lean principles emphasize the elimination of waste to streamline processes and reduce lead times, thereby enhancing overall operational performance.

To create a straightforward plan of suggested actions, we looked at the decision tree (Figure 5) and collected possible recommendations along with the conditions that trigger them, putting everything together in a single table (Table 4).

Table 4 outlines the recommendations (Actions A1 to A6) corresponding to the conditions presented in the top section of the table (C1 to C12). It offers a customized roadmap of suggested actions for each company based on its features (conditions). In the table, 'Y' indicates that a condition is met by the company, 'N' indicates the opposite, and blank cells signify that the condition has no effect on the given actions. The recommended actions for each set of rules are denoted by 'X'.

Table 4: Recommendation table.

Conditions		Rules				
		1	**2**	**3**	**4**	**5**
C1	Are there Industry 4.0 investments in Assembly?	Y	Y	Y	N	N
C2	Is Quality targeted for Industry 4.0 performance improvement, with governmental incentives as the investment driver?				Y	N
C3	Is Quality targeted for Industry 4.0 performance improvement, with Enhancing data availability as the investment driver?	Y	Y	N		
C3	Is Time targeted for Industry 4.0 performance improvement, with Improving waste detection as the investment driver?	N	N			
C4	Is Time targeted for Industry 4.0 performance improvement, with Improving waste detection as the investment driver?			Y		
C5	Is company size <=111.15				N	
C6	Is Productivity targeted for Industry 4.0 performance improvement, with governmental incentives as the investment driver?					Y
C7	Is Efficiency targeted for Industry 4.0 performance improvement, with Enhancing data availability as the investment driver?	N	Y			
C8	Does the company refrain from adopting localized interventions?			N		
C9	Is the company implementing Extensive interventions for the long term?					
C10	Is Time targeted for Industry 4.0 performance improvement, with Enhancing data availability as the investment driver?					N
C11	Is company size <=527.35					
C12	Is the industrial sector Metal Products?					
Actions		**1**	**2**	**3**	**4**	**5**
A1	Target Industry 4.0 performance improvement using Time, with Improving waste detection as the investment focus.	X	X			
A2	Implement localized interventions.	X				
A3	Implement extensive interventions for long term.			X		
A4	Target Industry 4.0 performance improvement using Productivity, with gouvermental incentives as the investment focus.				X	
A5	Target Industry 4.0 performance improvement using Time, with Enhancing data availability as the investment focus.					X
A6	Target Industry 4.0 performance improvement using Quality, with gouvermental incentives as the investment focus.					X

Legend: Y: Yes, **Empty case:** Not Applicable, **N:** No, **X:** Recommended Action.
Source: Authors, (2024).

V. CONCLUSIONS

This paper deals with the factors influencing the industry 4.0 maturity level. To this end, we study the impact of lean maturity on Industry 4.0 maturity level. Besides, we explore maturity models and recommendations for digital Lean initiatives.

Thus, the integration of machine learning (ML) models, particularly the Decision Tree algorithm offers significant utility. Primarily, it is noticed in the context of predicting and enhancing maturity levels. Our study showcases the effectiveness of ML models in accurately predicting Industry 4.0 maturity levels based on company characteristics. This provides actionable recommendations for improvement. By leveraging the Decision Tree model, we were able to forecast maturity levels. In addition, we identify key factors influencing organizational maturity and suggest targeted interventions for enhancement. This approach serves as a valuable tool within the framework of maturity models, enabling organizations to systematically assess their current state, identify areas for development, and implement tailored strategies for advancement. Moreover, the interpretability and transparency of Decision Trees make them particularly suitable for decision-making processes in industry. They foster a deeper understanding of the underlying factors driving maturity levels. Overall, the utilization of Decision Trees, as decision support tools, offers a practical and efficient means of navigating the complexities of organizational maturity. Ultimately, Decision Trees facilitate informed decision-making and drive continuous improvement in industry practices.

The current study was initially confined to a relatively small data set comprising 19 real-world use cases and focused only on two sector activities, namely Machinery and Metal Products. Future research could involve expanding the dataset to encompass a more extensive range of sectors and varying sizes of companies. Additionally, there exists an opportunity to explore alternative targets within the same database to inform strategic decision-making processes. For instance, the columns representing targeted areas, such as processing and assembly, could be individually designated as targets to assess the feasibility. This enables the evaluation of potential benefits of investing in each area. Furthermore, by modifying the target variable in our model, insights into expected gains metrics like Return on Investment (ROI) could be achieved through survey-based approaches. This adaptation would facilitate a more comprehensive evaluation of the potential outcomes and benefits associated with different investment strategies.
Example:

VI. AUTHOR'S CONTRIBUTION

Conceptualization: Oussama Ben Ali, Sondes Hammami, Marwa Hasni, Fehmi H'Mida, Ahmed Nait Sidi Moh.
Methodology: Oussama Ben Ali, Sondes Hammami, Marwa Hasni, Fehmi H'Mida, Ahmed Nait Sidi Moh.
Investigation: Oussama Ben Ali, Sondes Hammami, Marwa Hasni, Fehmi H'Mida, Ahmed Nait Sidi Moh.
Discussion of results: Oussama Ben Ali, Sondes Hammami, Marwa Hasni, Fehmi H'Mida, Ahmed Nait Sidi Moh.

Writing – Original Draft: Oussama Ben Ali, Sondes Hammami, Marwa Hasni, Fehmi H'Mida, Ahmed Nait Sidi Moh.
Writing – Review and Editing: Oussama Ben Ali, Sondes Hammami, Marwa Hasni, Fehmi H'Mida, Ahmed Nait Sidi Moh.
Resources: Oussama Ben Ali, Sondes Hammami, Marwa Hasni, Fehmi H'Mida, Ahmed Nait Sidi Moh.
Supervision: Oussama Ben Ali, Sondes Hammami, Marwa Hasni, Fehmi H'Mida, Ahmed Nait Sidi Moh.
Approval of the final text: Oussama Ben Ali, Sondes Hammami, Marwa Hasni, Fehmi H'Mida, Ahmed Nait Sidi Moh.

VII. REFERENCES

[1] Weyer, S., Schmitt, M., Ohmer, M., & Gorecky, D. (2015). Towards Industry 4.0-Standardization as the crucial challenge for highly modular, multi-vendor production systems. Ifac-Papersonline, 48(3), 579-584. https://doi.org/10.1016/j.ifacol.2015.06.143

[2] Rosin, F., Forget, P., Lamouri, S., & Pellerin, R. (2019). Industrie 4.0 et Lean : Hiérarchie, amélioration ou complémentarité ? Conference: ClGl QUALITA 2019, "Le numérique et l'intelligence industrielle: défis et opportunités".

[3] Rossini, M., Cifone, F. D., Kassem, B., Costa, F., & Portioli-Staudacher, A. (2021). Being lean: how to shape digital transformation in the manufacturing sector. Journal of Manufacturing Technology. https://doi.org/10.1108/JMTM-12-2020-0467

[4] Rossini, M., Costa, F., Tortorella, G. L., & Portioli-Staudacher, A. (2019). The interrelation between Industry 4.0 and lean production: an empirical study on European manufacturers. The International Journal of Advanced Manufacturing Technology, 102, 3963-3976. https://doi.org/10.1007/s00170-019-03441-7

[5] Salehi, H., & Burgueño, R. (2018). Emerging artificial intelligence methods in structural engineering. Engineering structures, 171, 170-189. http://dx.doi.org/10.1016/j.engstruct.2018.05.084

[6] Iversen, J., Nielsen, P. A., & Norbjerg, J. (1999). Situated assessment of problems in software development. ACM SIGMIS Database: the Database for Advances in Information Systems, 30(2), 66-81. http://dx.doi.org/10.1145/383371.383376

[7] Wendler, R. (2012). The maturity of maturity model research: A systematic mapping study. Information and software technology, 54(12), 1317-1339. https://doi.org/10.1016/j.infsof.2012.07.007

[8] Pöppelbuß, Jens, and Maximilian Röglinger. (2011) "What makes a useful maturity model? A framework of general design principles for maturity models and its demonstration in business process management.". ***19***th European Conference on Information Systems, ECIS 2011

[9] Rummler, G. A., & Brache, A. P. (2012). Improving performance: How to manage the white space on the organization chart. John Wiley & Sons.

[10] Amaral, A., & Peças, P. (2021). A framework for assessing manufacturing SMEs Industry 4.0 maturity. Applied Sciences, 11(13), 6127. http://dx.doi.org/10.3390/app11136127

[11] Cheshmberah, Mohsen, and Safoura Beheshtikia (2020) "Supply chain management maturity: An all-encompassing literature review on models, dimensions and approaches." LogForum 16.1: 103-116. https://doi.org/10.17270/J.LOG.2020.377

[12] Maier, Anja & Moultrie, James & Clarkson, P. (2009). Developing maturity grids for assessing organizational capabilities: Practitioner guide. 1-29.

[13] Alcácer, V., Rodrigues, J., Carvalho, H., & Cruz-Machado, V. (2022). Industry 4.0 maturity follow-up inside an internal value chain: a case study. The International Journal of Advanced Manufacturing Technology, 1-12. http://dx.doi.org/10.21203/rs.3.rs-431651/v1

[14] Leyh C, Schäffer T, Bley K, Forstenhäusler S (2016) SIMMI 4.0 – a maturity model for classifying the enterprise-wide IT and software landscape focusing on Industry 4.0. Proceedings of the Federated Conference on Computer Science and Information Systems. 8:1297–1302. https:// doi. org/ 10. 15439/ 2016F 478.

[15] De Carolis A, Macchi M, Negri E, Terzi S (2017) A maturity model for assessing the digital readiness of manufacturing companies, in advances in production management systems. The Path to Intelligent, Collaborative and Sustainable Manufacturing, Cham 13–20. https:// doi. org/ 10. 1007/ 978-3- 319-66923- 6_2

[16] Rajnai Z, Kocsis I (2018) Assessing industry 4.0 readiness of enterprises. 2018 IEEE 16th World Symposium on Applied Machine Intelligence and Informatics (SAMI) 225–230. https:// doi. org/ 10.1109/ SAMI. 2018. 83248 44.

[17] Rockwell Automation (2014) The connected enterprise maturity model. https:// literature. Rockwell au tomation. com/ idc/ groups/ literature/ documents/ wp/ cie-wp002_- en-p. pdf

[18] Jayanetti, J. K. D. D. T., Perera, B. A. K. S., Waidyasekara, K. G. A. S., & Siriwardena, M. (2023). Critical Analysis of Lean Construction Maturity Models: A Systematic Literature Review. Buildings, 13(6), 1508. https://doi.org/10.3390/buildings13061508

[19] Demirdöğen, G., Diren, N. S., Aladağ, H., & Işık, Z. (2021). Lean based maturity framework integrating value, BIM and big data analytics: Evidence from AEC industry. Sustainability, 13(18), 10029. https://doi.org/10.3390/su131810029

[20] Mollasalehi, S., Aboumoemen, A. A., Rathnayake, A., Fleming, A. J., & Underwood, J. (2018). Development of an integrated BIM and lean maturity model. Conference: 26th Annual Conference of the International Group for Lean Construction http://dx.doi.org/10.24928/2018/0507

[21] Nightingale, D. J., & Mize, J. H. (2002). Development of a lean enterprise transformation maturity model. Information Knowledge Systems Management, 3(1), 15-30.

[22] Maasouman, M. A., & Demirli, K. (2016). Development of a lean maturity model for operational level planning. The International Journal of Advanced Manufacturing Technology, 83, 1171-1188. http://dx.doi.org/10.1007/s00170-015-7513-4

[23] Treviño-Elizondo, B. L., García-Reyes, H., & Peimbert-García, R. E. (2023). A maturity model to become a Smart Organization based on lean and Industry 4.0 synergy. Sustainability, 15(17), 13151. https://doi.org/10.3390/su151713151

[24] Rossini, M., Cifone, F. D., Kassem, B., Costa, F., & Portioli-Staudacher, A. (2021). Being lean: how to shape digital transformation in the manufacturing sector. Journal of Manufacturing Technology Management, 32(9), 239-259. https://doi.org/10.1108/JMTM-12-2020-0467

[25] Bhadu, J., Bhamu, J., & Saraswat, P. (2023). An Analytic Hierarchy Process (AHP) Approach for Prioritizing the Industries 4.0 Technologies (I4. 0T). https://doi.org/10.5109/6792813

[26] Kaushik, M., & Mathur, B. (2014). Comparative study of K-means and hierarchical clustering techniques. Int. J. Softw. Hardw. Res. Eng, 2(6), 93-98.

[27] Hernandez, M., Epelde, G., Alberdi, A., Cilla, R., & Rankin, D. (2023). Standardised metrics and methods for synthetic tabular data evaluation. Authorea Preprints. https://doi.org/10.36227/techrxiv.16610896.v1

[28] Riviére, C., & Marlair, G. (2010). The use of multiple correspondence analysis and hierarchical clustering to identify incident typologies pertaining to the biofuel industry. Biofuels, Bioproducts and Biorefining: Innovation for a sustainable economy, 4(1), 53-65. https://doi.org/10.1002/bbb.187

[29] Zientek, L. R., & Thompson, B. (2009). Matrix summaries improve research reports: Secondary analyses using published literature. Educational Researcher, 38(5), 343-352. http://dx.doi.org/10.3102/0013189X09339056

[30] Durap, A. (2023). A comparative analysis of machine learning algorithms for predicting wave runup. Anthropocene Coasts, 6(1), 17. http://dx.doi.org/10.1007/s44218-023-00033-7

[31] Hamoud, A., Hashim, A. S., & Awadh, W. A. (2018). Predicting student performance in higher education institutions using decision tree analysis. International Journal of Interactive Multimedia and Artificial Intelligence, 5, 26-31. http://dx.doi.org/10.9781/ijimai.2018.02.004

Journal of Engineering and Technology for Industrial Applications

ISSN ONLINE: 2447-0228

ITEGAM-JETIA

Manaus, v10. n.50, p. 173-179. November/ December., 2024.
DOI: https://doi.org/10.5935/jetia.v10i50.1271

RESEARCH ARTICLE OPEN ACCESS

ENHANCED ESTIMATION OF TORQUE BASED ON COGNITIVE TRAINING MODEL FOR ROBUST PMSM IN EV APPLICATIONS

G. Sudeep[1], J. N. and Chandra Sekhar[2]

[1,2] Department of EEE, Sri Venkateswara University, Tirupati, India

[1] http://orcid.org/0009-0005-0619-7996 , [2]http://orcid.org/0000-0003-2767-2467

Email: gaduputisudeep@gmail.com, chandu.jinka@gmail.com

ARTICLE INFO

Article History
Received: August 29, 2024
Revised: October 1, 2024
Accepted: November 10, 2024
Published: December 31, 2024

Feedforward Neural Network (FNN),
Permanent Magnet Synchronous Motors (PMSM),
Hyperband Algorithm.

ABSTRACT

Permanent Magnet Synchronous Motors (PMSM) which are used in commercial applications, requires precise torque calculation, which is necessary for the intended control. Conventional Model Predictive Control (MPC) performance is hampered by model parameter mismatches and high computational demands, precise torque control often necessitates the knowledge of rotor speed and position, which are traditionally obtained using mechanical sensors. The paper proposes Feedforward Neural Network model to estimate the parameter for desired switching of inverter for accurate position of rotor in optimized time. However, this model uses the d-q axis currents, voltages, rotor angle as inputs, and electromagnetic torque as the output. The model is developed with the help of Python programming based on Hyperband algorithm for hyperparameter tuning. Hyperband algorithm, efficiently optimizes hyperparameters by adaptive resource allocation, early stopping, reducing training time and improving accuracy. This integration allows the neural network(NN) to dynamically optimize its architecture, ensuring precise torque estimation. This approach addresses computational challenges and enhances the system's efficiency and responsiveness to real-time parameter variations and disturbances, leading to more robust and high-performing motor control applications.

I. INTRODUCTION

Electric vehicles (EVs) have emerged as a promising solution to address the growing concerns over environmental pollution and energy sustainability. PMSM have become a popular choice for EV propulsion systems [1] due to their high-power density, efficiency, and wide constant power speed range. The PMSM can provide high torque at low speeds, making them suitable for urban driving conditions. In addition, their compact size and lightweight design make them ideal for integration into the limited space available in EV.

One of the key aspects of utilizing PMSM in EV is the precise control of torque. The torque control in PMSM drives is crucial for achieving optimal performance and efficiency in EV propulsion systems. To achieve effective torque control, various control strategies can be employed, such as field-oriented control (FOC) or direct torque control (DTC) [2]. Advancements in motor control algorithms and sensor technologies have enhanced the accuracy and responsiveness of torque control in PMSM drives, leading to improved overall system efficiency and performance [3]. The integration of advanced sensor technologies has significantly enhanced the accuracy and responsiveness of torque control in PMSM drives. This level of control ensures smooth operation and optimal performance, further contributing to the overall efficiency of electric vehicle propulsion systems. In addition to advanced sensor technologies, there have been significant developments in sensor less control techniques for PMSM in EV. These techniques use algorithms and mathematical models to estimate the motor's operating conditions and rotor position without the need for physical sensors, thereby reducing cost and complexity in EV propulsion systems [4]. The offline torque estimation using sensors and torque transducers provides the necessary data for optimizing torque control strategies, ensuring that the PMSM meet the dynamic power requirements of electric vehicle propulsion systems. This approach further contributes to the smooth operation and overall efficiency of EV, addressing the specific needs of urban driving conditions and improving the driving experience for users [5]. Online torque estimations enable real-time monitoring and adjustment of torque in PMSM drives, ensuring optimal power delivery and responsiveness to dynamic power requirements. By incorporating advanced algorithms and sensor feedback, online torque estimations contribute to the seamless operation of EV in varied driving conditions, including urban settings with frequent starts and stops. One such approach is the use of Kriging-based techniques for online torque calculation in brushless DC motors, as highlighted in [6]. By leveraging improved estimation techniques, EV equipped with PMSMs can achieve enhanced performance and responsiveness, particularly in urban settings with frequent starts and stops.

Deep learning models, such as convolutional NN and recurrent NN, can be utilized to analyze and learn from large datasets of motor parameters and operating conditions. By training these models on a diverse set of torque measurements and corresponding motor states, the deep learning approach can provide accurate and real-time torque estimations for PMSMs in EV [7]. The block diagram Figure 1 depicts a system for controlling a PMSM. It includes components for current and voltage measurement, voltage source inverter, electrical angle measurement, sector identification, and lookup tables for estimators, ensuring accurate motor control and performance optimization.

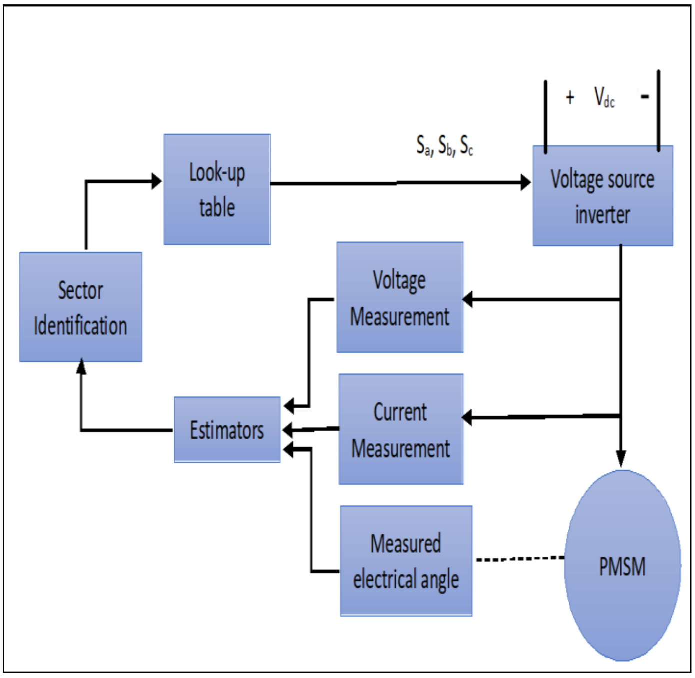

Figure 1: Torque control of PMSM Drive.
Source: Authors, (2024).

Accurately estimating motor torque is essential for the efficient control of PMSM. Torque estimation methods are generally categorized into online and offline techniques. Online methods use real-time electrical parameters—such as voltages, currents, and rotor position—to calculate instantaneous torque, offering the benefit of reduced system complexity and cost by eliminating the need for additional sensors. Offline methods, however, rely on detailed motor characterization through complex models and extensive testing. Although more complex, offline techniques can yield higher accuracy, particularly for motors with intricate magnetic structures. The choice between these methods depends on the application's specific needs, balancing complexity, cost, and accuracy.

Table 1: Related Literature Review.

Reference	Strength of Review
[8]	Suggests a technique for improving the identification of PMSM motor parameters through the use of a Chaotic Artificial Fish Swarm Algorithm (CAFSA) to optimize initial weights in a Back Propagation Neural Network (BPNN).
[9]	Introduces a sensor less speed tracking control method using polynomial equations and sliding mode-based control, validated on an embedded board.
[10]	Develops a feedforward NN for PMSM temperature estimation, achieving closed-loop errors under 4.5°C.
[11]	Assesses deep recurrent and convolutional NN with residual connections for PMSM temperature prediction, offering high performance without domain expertise.
[12]	Introduces sensor less robust optimum control strategy for PMSM with NN-based observers, validated by comparison tests and simulations.

Source: Authors, (2024).

The structure of this document is as follows. The suggested methodology framework is explained in Section 2, the results and discussion are covered in Section 3, and the conclusion is provided in Section 4.

II. PROPOSED METHODOLOGY

II.1 FRAME WORK FOR PROPOSED METHODOLOGY

This study presents a machine learning (ML) method for precise PMSM torque prediction. Data on currents, voltage and torque are collected cleaned and standardized. The model undergoes hyperparameter tunning and iterative training, with performance evaluated using R^2. Figure 2 visualization support model analysis, aiming to enhance motor control and optimization.

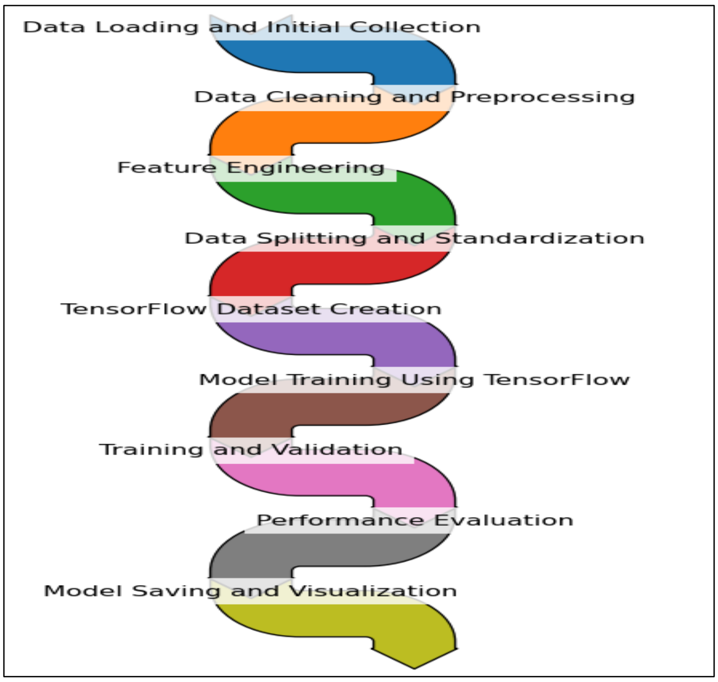

Figure 2: Flow chart of Proposed Methodology.
Source: Authors, (2024).

II.2. TORQUE ESTIMATION IN PMSM

Performance and efficiency can be significantly increased by integrating torque estimation techniques with PMSM control. For example, the application of DTC strategies—which can offer better dynamic responsiveness and fault tolerance than conventional vector control methods—can be made possible by the availability of correct torque information. Furthermore, the use of torque estimation in engine speed control can contribute to enhanced engine performance and efficiency, as demonstrated in the application of nonlinear observer-based torque estimation for engine speed control.

One widely adopted approach is to utilize the Clark and Park transformations to simplify the PMSM model and enable the implementation of field-oriented control techniques. The Clark transformation converts the three-phase stator voltages and currents into their equivalent two-phase stationary reference frame components, while the Park transformation further transforms these components into a synchronously rotating reference frame, relationships is explained in figure 3.

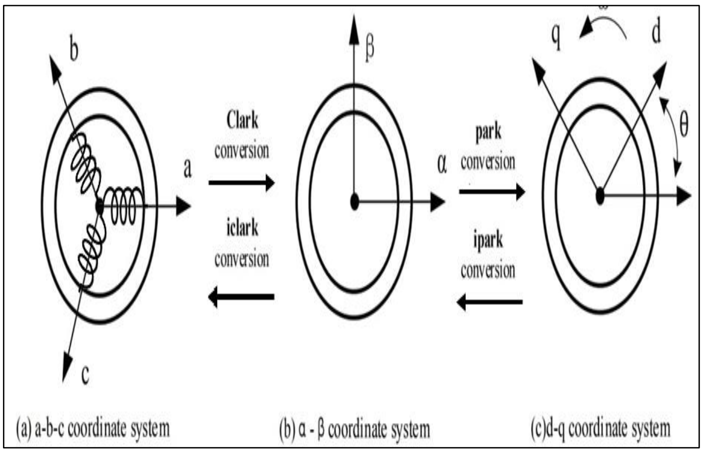

Figure 3: Transformation relationship in PMSM.
Source: Authors, (2024).

$$\begin{bmatrix} u_a \\ u_b \\ u_c \end{bmatrix} = \begin{bmatrix} R & 0 & 0 \\ 0 & R & 0 \\ 0 & 0 & R \end{bmatrix} \begin{bmatrix} i_a \\ i_b \\ i_c \end{bmatrix} + \begin{bmatrix} L & 0 & 0 \\ 0 & L & 0 \\ 0 & 0 & L \end{bmatrix} \frac{d}{dt} \begin{bmatrix} i_a \\ i_b \\ i_c \end{bmatrix} + \Phi\omega \begin{bmatrix} \sin \omega t \\ \sin(\omega t - 2\pi/3) \\ \sin(\omega t + 2\pi/3) \end{bmatrix} \quad (1)$$

$$\begin{bmatrix} i_\alpha \\ i_\beta \end{bmatrix} = \sqrt{\frac{2}{3}} \begin{bmatrix} 1 & -\frac{1}{2} & -\frac{1}{2} \\ 0 & \frac{\sqrt{3}}{2} & -\frac{\sqrt{3}}{2} \end{bmatrix} \begin{bmatrix} i_a \\ i_b \\ i_c \end{bmatrix} \quad (2)$$

$$\begin{bmatrix} i_a \\ i_b \\ i_c \end{bmatrix} = \sqrt{\frac{2}{3}} \begin{bmatrix} 1 & 0 \\ -\frac{1}{2} & \frac{\sqrt{3}}{2} \\ -\frac{1}{2} & -\frac{\sqrt{3}}{2} \end{bmatrix} \begin{bmatrix} i_\alpha \\ i_\beta \end{bmatrix} \quad (3)$$

$$\begin{bmatrix} i_d \\ i_q \end{bmatrix} = \begin{bmatrix} \cos\theta & \sin\theta \\ -\sin\theta & \cos\theta \end{bmatrix} \begin{bmatrix} i_\alpha \\ i_\beta \end{bmatrix} \quad (4)$$

$$\begin{bmatrix} i_\alpha \\ i_\beta \end{bmatrix} = \begin{bmatrix} \cos\theta & -\sin\theta \\ \sin\theta & \cos\theta \end{bmatrix} \begin{bmatrix} i_d \\ i_q \end{bmatrix} \quad (5)$$

In a PMSM, L represents the magnetic flux generated by the stator's permanent magnet and u_a, u_b and u_c are the voltages in each phase of the stator winding within a three-phase coordinate system. Similarly, i_a, i_b and i_c indicate the phase currents in this system, while R refers to the resistance of each stator winding phase. The three-phase voltage equations of a PMSM are inherently differential equations, which makes direct solutions complex and challenging. The angular velocity of rotation within the a-b-c coordinate system is denoted by ω. To effectively simplify the problem and enhance the motor's control capabilities, a suitable transformation is required to decouple these variables. This transformation process for the PMSM, which involves converting between various coordinate systems, is guided by the principles of preserving equivalent current, voltage, flux, and magnetomotive force. For instance, the Park transform converts the voltage model from the rotating d-q coordinate system to a form easier to manage, while the Clark transform shifts from the space vector to the a-b-c coordinate system for the static two-phase voltage model (α, β). These transformations yield a voltage model similar to that of a two-phase DC motor, making it easier to control. The transformations help determine the phase angle θ between the d-axis and q-axis, which is crucial for accurate motor control. Equations (2) through (5), in that order, display the park transformation relations between current and the Clark transformation in each coordinate system. Similar results can be obtained for the voltage transformation relationship in each coordinate system.

II.3. IMPLEMENTATION OF POLYNOMIAL LINEAR REGRESSION MODEL

The desired response for the variable PLRM is obtained using the estimated torque control, while the regressors are the observed torque and speed. The mathematical expectation of items with a higher order, k =0 in Equation (6), which presents the torque curve with respect to observed torque and speed, may then be fitted. It is assumed that the population size for things with a higher order "k" is minimal. But, bivariate k[th]-order PLRM [13], is the equation (6) is known as.

$$T_{cij} = \sum_{\gamma=0}^{k} \sum_{\lambda=0}^{k} \beta_{\gamma\lambda} T_{mij} \lambda + \varepsilon_{ij} \quad (6)$$

Where must be $k \geq 1$, and $i = 1,2,\ldots\ldots n$ & $j = 1,2,\ldots..q$

When $\beta_{\gamma\lambda}$ is the regression coefficient that needs to be determined, ε_{ij} is the torque error, and each εij is independent and has the same distribution. to acquire the linear regression of second order polynomials. In equation (6), the value of k is 2. Equation 2 shows how to use the regressors of the observed torque and speed to create the bivariate second order PLRM.

$$T_{cij} = \beta_{00} + \beta_{01}\omega_i + \beta_{02}\omega_i^2 + \beta_{10}T_{mij} + \beta_{11}T_{mij}\omega_i + \beta_{20}T_{mij}^2 + \varepsilon_{ij} \quad (7)$$

$$\text{where} T_{mij} = \begin{bmatrix} x_{i100} & x_{i101} & x_{i102} & x_{i110} & x_{i11} & x_{i120} \\ x_{i200} & x_{i201} & x_{i202} & x_{i210} & x_{i211} & x_{i220} \\ \vdots & \vdots & \vdots & \vdots & \vdots & \vdots \\ x_{iq00} & x_{iq01} & x_{iq02} & x_{iq10} & x_{iq11} & x_{iq20} \end{bmatrix} \quad (8)$$

$$\beta = [\beta_{00} \quad \beta_{01} \quad \beta_{02} \quad \beta_{10} \quad \beta_{11} \quad \beta_{20}]^T \quad (9)$$

The value of ω_i in equation (8) is 0. After that, as equation (10) shows how to generate the univariate second order PLRM using the observed torque's regressor. One way to rewrite equation (9) is as equation (11) shows.

$$T_{cij} = \beta_{00} + \beta_{10}T_{mij} + \beta_{20}T_{mij}^2 + \varepsilon_{ij} \quad (10)$$

$$\beta = [\beta_{00} \quad \beta_{10} \quad \beta_{20}]^T \quad (11)$$

II.4. IMPLEMENTATION OF DEEP LEARNING TECHNIQUE

The integration of deep learning with motor control systems holds the potential to revolutionize the field of PMSM torque estimation. It not only contributes to enhanced performance and energy efficiency but also facilitates the development of intelligent and autonomous electromechanical systems [14]. In this study, we explore the implementation of ML algorithms for torque estimation in PMSMs. Deep Learning models, especially NN, have emerged as an effective tool for accurate torque estimation in PMSMs.

Since the selection of hyperparameters can have a substantial impact on the model's performance, hyperparameter tuning in NN is an essential step in the creation of ML models. In particular for complicated models with several hyperparameters, traditional hyperparameter optimization techniques like grid search and random search can be computationally costly and time-consuming. [15]. To address this challenge, the Hyperband algorithm has been proposed as a novel and efficient approach to hyperparameter optimization shown in Figure 4 NN structure.

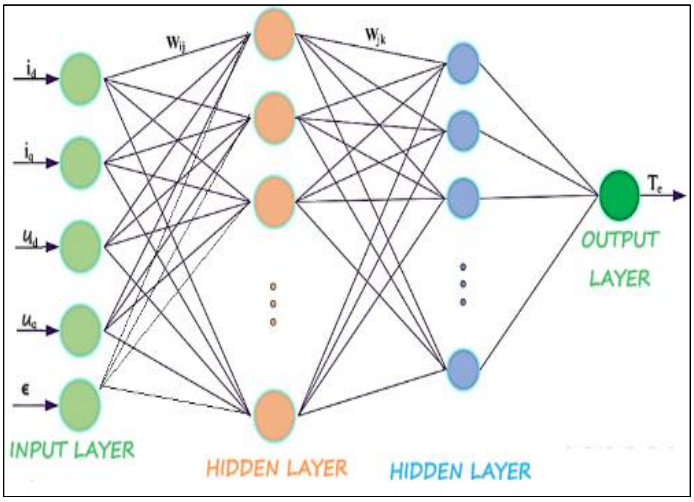

Figure 4: Neural Network Structure.
Source: Authors, (2024).

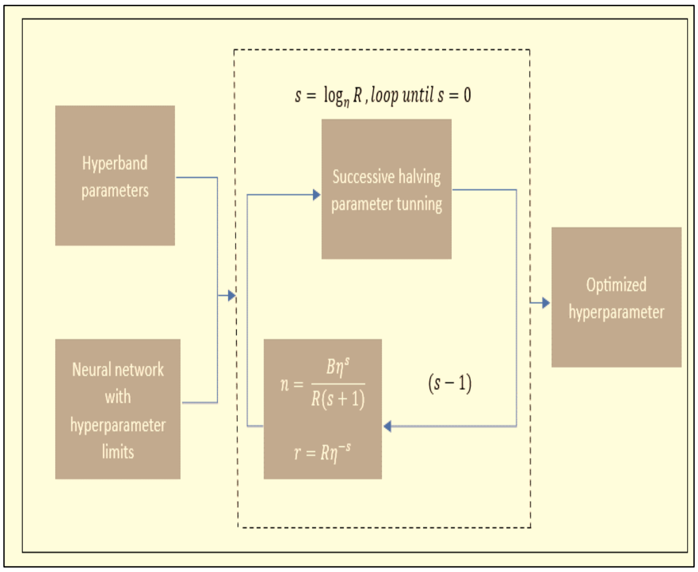

Figure 5: Hyperparameter optimization.
Source: Authors, (2024).

Scholars have investigated diverse methodologies for optimizing hyperparameters, encompassing extensive trials to comprehend the impacts of distinct hyperparameters and their mutual relations. Figure 5 illustrates one such strategy called Hyperband, a cutting-edge bandit-based technology that can offer appreciable speedups over conventional optimization techniques.

III.1 RESULTS AND DISCUSSION
III.1. DATA SET

This article proposes a comprehensive analysis on two datasets, namely Dataset 1 and Dataset 2, which contain measurements such as, the target variable torque T in Nm [16][17]. The dataset statistics as shown in figure 6 supports the torque T in Nm are as follows:

- Dataset 1: The dataset consists of 37 million samples with a mean value of -0.86 Nm and a standard deviation of 71.39 Nm. The minimum and maximum values are -133.90 Nm and 134.07 Nm, respectively. The interquartile range (IQR), spanning from the 25th percentile (-56.13 Nm) to the 75th percentile (55.40 Nm), indicates a wide spread of data points around the median (-1.08 Nm).
- Dataset 2: Similar to Dataset 1, this dataset also contains 37 million samples. The mean value is slightly lower at -0.90 Nm, with a higher standard deviation of 72.51 Nm. The minimum and maximum values are -136.84 Nm and 136.04 Nm, respectively. The IQR for Dataset 2 is slightly broader, with the 25th percentile at -59.40 Nm and the 75th percentile at 57.54 Nm, and a median of -1.37 Nm.

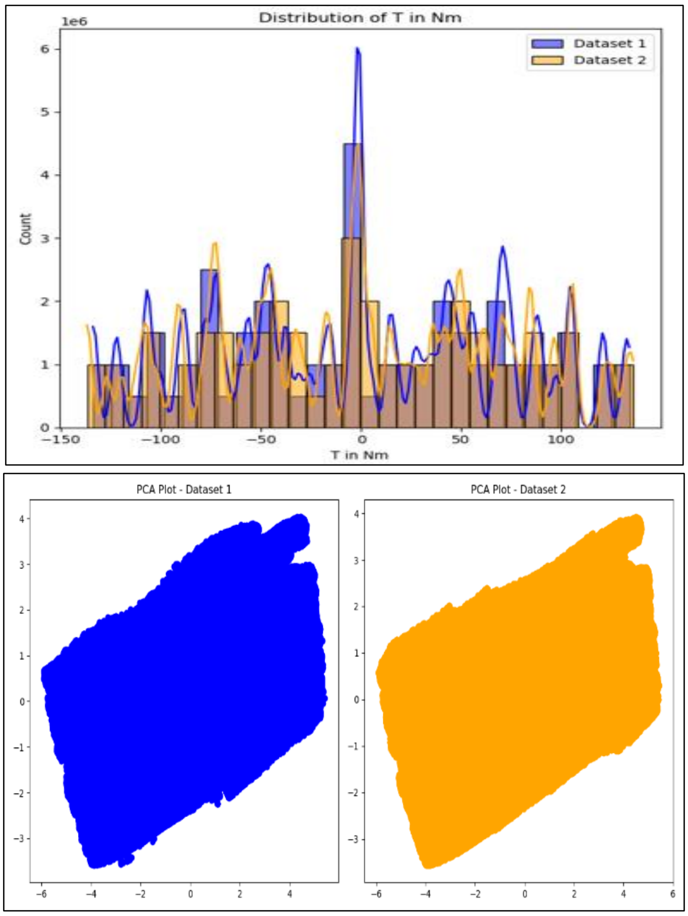

Figure 6: Dataset visualization.
Source: Authors, (2024).

III.2. RESULTS

The training process of the NN model loss values for both the training and validation datasets over 15 epochs. The tuning process yielded the following optimal hyperparameters:

Number of Neurons: 42, Layers: 8 and Learning Rate: 0.001, The model's training and validation loss over a period of 15 epochs conducted on dataset (2000RPM) is displayed in Figure 7 was developed in python version 3.12 with the help of keras tuner tool. Within the first few epochs, the model shows a quick decrease in both training and validation loss, followed by a stable plateau, suggesting that the model converged successfully and that there was not a large amount of overfitting during training Each hidden layer's dense component has 1,806 parameters (42 inputs * 42 outputs + 42 biases), while the output layer has 43 parameters (42 inputs * 1 output + 1 bias), leading to a total of 14,785 trainable parameters in the network. The developed model was pre-trained on NN was employed and subsequently trained on to adapt to a similar distinct dataset (120RPM). This process was carried out using TensorFlow with a distributed training strategy to optimize the model's performance. The training and validation loss over a period of 15 epochs is depicted in the graph as shown in figure 8. Early on, both losses exhibit a notable decline, pointing to a quick convergence of the model. The model may be well-tuned and not overfit if the validation loss is continuously less than the training loss. This steady performance demonstrates the resilience and generalizability of the approach.

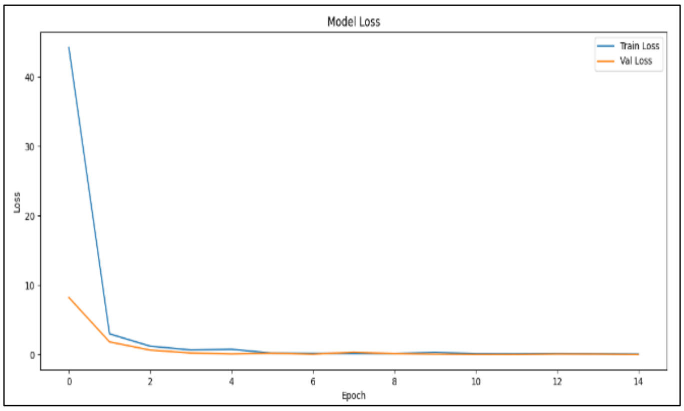

Figure 7: Loss curves for 2000RPM.
Source: Authors, (2024).

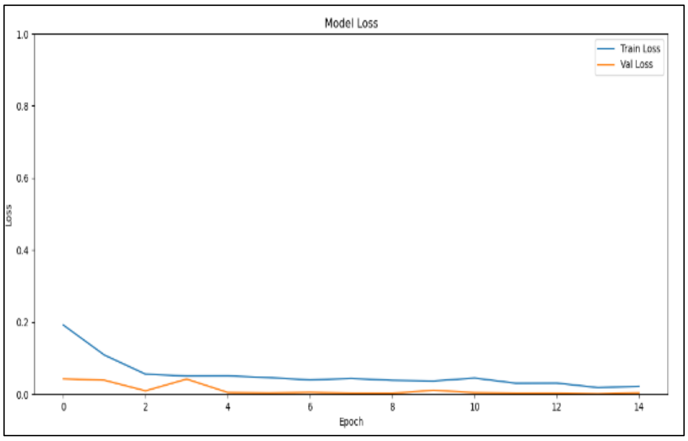

Figure 8: Loss curve for 120RPM.
Source: Authors, (2024).

Tables 2 and 3 compare the performance of polynomial linear regression and a fully connected feedforward neural network (NN) for torque estimation at two different speeds: 120 RPM and 2000 RPM. Table 2 shows that polynomial linear regression yields relatively high Mean Squared Error (MSE), Root Mean Squared Error (RMSE), and Mean Absolute Error (MAE) values, with MSEs of 212.850 and 206.064 at 120 RPM and 2000 RPM, respectively. These values indicate a moderate level of prediction accuracy, further corroborated by the R-squared values of 0.958 and 0.9608, suggesting that the model explains a substantial portion of the variance in the data but leaves some room for improvement. In contrast, Table 3 presents the results for the fully connected feedforward NN, which demonstrates significantly lower error metrics at both speeds. The MSE is reduced to 0.0009 at 120 RPM and 0.0093 at 2000 RPM, with corresponding RMSEs of 0.0301 and 0.0963. The MAE values are also much lower, at 0.0192 and 0.0542, respectively. The near-perfect R-squared values of 0.999 at both speeds indicate that the NN model almost entirely captures the variance in the dataset, showcasing its superior predictive capabilities over polynomial linear regression for this application. Overall, the NN model provides more accurate and reliable torque estimation across different speeds, making it a more suitable choice for this specific task compared to polynomial linear regression.

Table 2:Polynomial Linear Regression (Tourque Estimation).

Speed	MSE	RMSE	MAE	R-square
RPM 120	212.850	14.589	10.949	0.958
RPM 2000	206.064	14.354	10.714	0.9608

Source: Authors, (2024).

Table 3: Fully connected feedforward NN (Tourque estimation).

Speed	MSE	RMSE	MAE	R-square
RPM 120	0.0009	0.0301	0.0192	0.999
RPM 2000	0.0093	0.0963	0.0542	0.999

Source: Authors, (2024).

The scatter plot presented in Figure 9 and 10 illustrates the relationship between the direct axis current (i_d) and the quadrature axis current (i_q) for the PMSM. The data points, shown as dense clusters, reveal the operational characteristics and current interactions within the motor current dynamics. The plot showcases a distinctive pattern, indicative of the motor's response under varying load conditions and rotational speeds. The clustering and spread of data points highlight the motor's operational envelope and provide insights into the performance and efficiency of the PMSM.

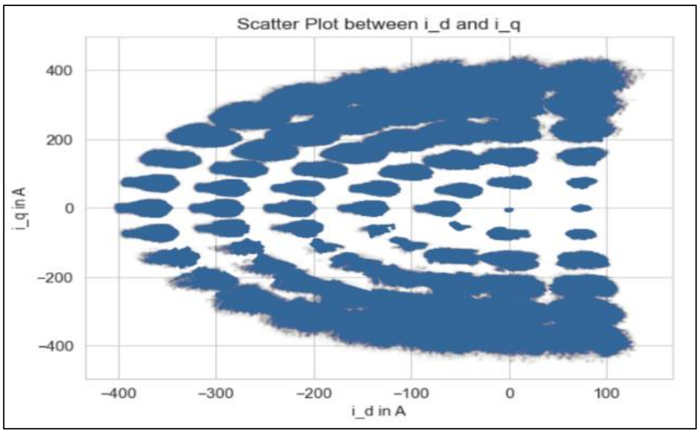

Figure 9: Scatter Plot of i_d vs. i_q for 120RPM.
Source: Authors, (2024).

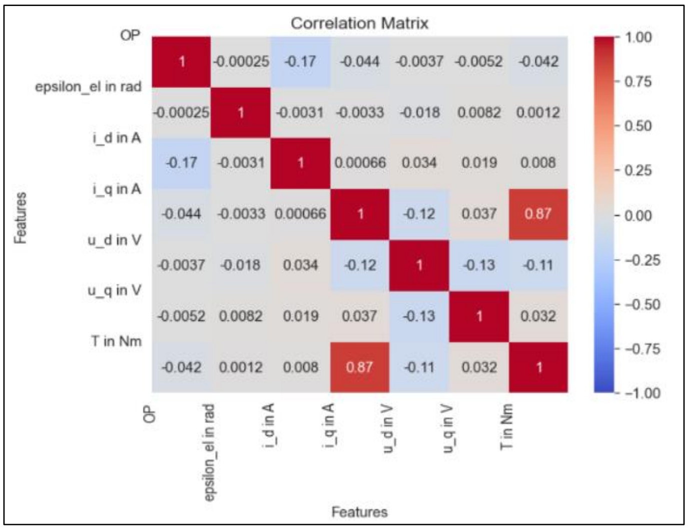

Figure 10: Scatter Plot of i_d vs. i_q for 2000RPM.
Source: Authors, (2024).

Heat Map

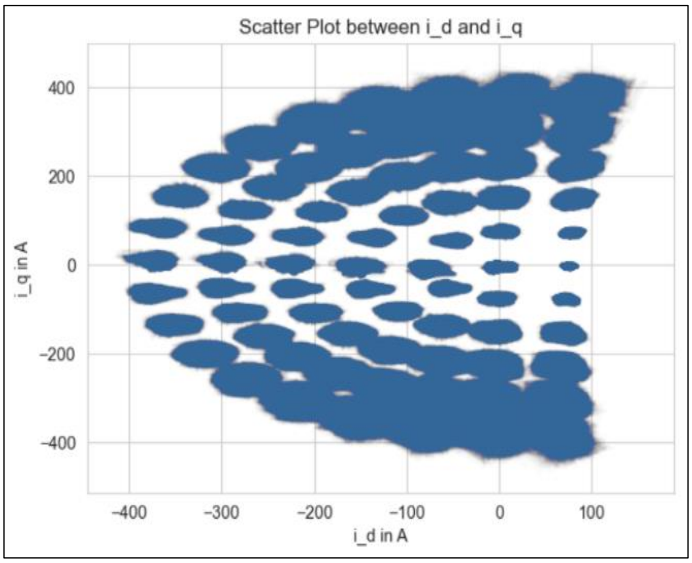

Figure 11: Heat Map at 120RPM.
Source: Authors, (2024).

Case 1: Correlation Matrix Heatmap at 120 RPM

Figure 11 presents the correlation matrix heatmap for various features of the PMSM dataset, including the electrical angle (ϵ_{el}), i_d, i_q, u_d, u_q, and torque (T). This heatmap visually represents the correlation coefficients between these features, providing insights into their linear relationships. The heatmap uses a colour gradient to depict the correlation values, where red shades indicate positive correlations, and blue shades signify negative correlations. The intensity of the colour corresponds to the magnitude of the correlation coefficient, with values ranging from -1 to 1.

Key observations from the heatmap include:

- A strong positive correlation (r=0.87) between the i_q and torque (T), suggesting that as i_q increases, the torque also increases.
- The correlations among other variables, such as i_d, u_d, u_q, and electrical angle(ϵ_{el}), are relatively weak, with coefficients close to zero, signifying little to no linear relationship.

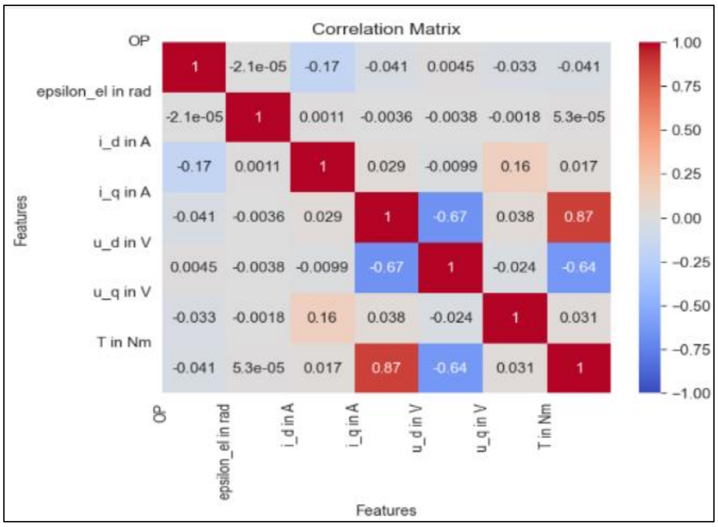

Figure 12: Heat Map at 2000RPM.
Source: Authors, (2024).

Case 2: Correlation Matrix Heatmap at 2000 RPM

Figure 12 shows the correlation matrix heatmap for various features of the PMSM dataset at 2000 RPM, including the electrical angle (ϵ_{el}), i_d, i_q, direct axis voltage (u_d), quadrature axis voltage (u_q), and torque (T).

Key observations from this heatmap include:

- A strong positive correlation (r=0.87) between the i_q and torque (T), indicating that an increase in i_q is associated with an increase in torque.
- A significant negative correlation (r=−0.67) between the u_d and the i_q, suggesting an inverse relationship between these variables.

IV. CONCLUSION

The article demonstrated the effective solution of deep learning for the torque estimation of PMSM. This utilizes the extensive datasets of currents, voltage and rotor angle was implemented in NN model with eight hidden layers, each layer contains 42 neurons. The model demonstrated the superior predictive performance, significantly reducing loss values and attaining high accuracy in torque estimation, outperforming polynomial linear regression models in terms of Mean Squared Error (MSE), Root Mean Squared Error (RMSE), Mean Absolute Error (MAE), and R-square metrics at both 120 RPM and 2000 RPM. Scatter plots of direct axis current (i_d) vs. quadrature axis current (i_q) revealed critical insights into motor behaviour under varying conditions. The investigations underscore the potential of deep learning to improve motor performance, energy efficiency, and operational stability, showcasing NN model in minimizing errors and enhancing torque estimation accuracy. The research enlightened the reputation of advanced ML techniques in industrial automation, offering a promising direction for future research and development in PMSM torque.

V. AUTHOR'S CONTRIBUTION

Conceptualization: G.Sudeep and Dr.J N Chandra sekhar.
Methodology: G.Sudeep and Dr.J N Chandra sekhar.
Investigation: G.Sudeep and Dr.J N Chandra sekhar.
Discussion of results: G.Sudeep and Dr.J N Chandra sekhar.
Writing – Original Draft: G.Sudeep.
Writing – Review and Editing: G.Sudeep.
Resources: Dr.J N Chandra sekhar.

Supervision: Dr.J N Chandra sekhar.
Approval of the final text: G.Sudeep and Dr.J N Chandra sekhar.

VI. ACKNOWLEDGMENTS

The authors would like to express their sincere gratitude to Sri Venkateswara University College of Engineering for providing necessary guidance and support. We are also grateful to the anonymous reviewers for their constructive comments that helped us to improve the quality of this manuscript.

VII. REFERENCES

[1] Z.Q.Zhu, D Howe, "Electrical Machines and drives for Electric, Hybrid and Fuel Cell Vehicles", IEEE vol. 95, no. 95 pp. 746-765 April 2007.

[2] S. D. Pinto, C. Chatzikomis, A. Sorniotti and G. Mantriota, "Comparison of Traction Controllers for Electric Vehicles With On-Board Drivetrains", IEEE Trans., on Vehicular Technology vol. 66, no. 8, pp. 6715-6727, Aug-2017.

[3] M. Dalboni, D.Tavernini, U.Montanaro, A.Soldati, C. Concari, M. Dhaens, A. Sorniotti, "Nonlinear Model Predictive Control for Integrated Energy-Efficient Torque-Vectoring and Anti-Roll Moment Distribution", IEEE Trans., on Mechatronics, vol. 26, no. 3, pp. 1212-1224, June 2021.

[4] T. D. Batzel and K. Lee, "Electric Propulsion With the Sensorless Permanent Magnet Synchronous Motor: Model and Approach", IEEE Trans., on Energy Conversion, vol.20, no.4, pp.818-825, Dec 2005.

[5] S. Shinnaka and S. Takeuchi, "A New Sensorless Drive Control System for Transmissionless EVs Using a Permanent-Magnet Synchronous Motor", World Electr. Veh. J. , 1(1), 1-9, dec 2007.

[6] X. Liu, M. Li and M. Xu, "Kriging assisted on-line torque calculation for brushless DC motors used in electric vehicles", IEEE International Symposium on Industrial Electronics, July-2012, 10.1109/ISIE.2012.6237312.

[7] Y. Yan, J. Liang, T. Sun, J. Geng, Gang-Xie, and D. Pan. "Torque estimation and control of PMSM based on deep learning". Int. Conf. on Electrical Machines and Systems, Dec-2019.

[8] J.W. Jiang, Z. Chen, Y.H. Wang, T. Peng, S.L. Zhu, L.M. Shi "Parameter Estimation for PMSM based on a Back Propagation Neural Network Optimized by Chaotic Artificial Fish Swarm Algorithm" International Journal of Computers Communications & Control, vol.14(6), pp.615-632, December 2019.

[9] Luigi Colombo, Maria Letizia Corradini "An Embedded Strategy for Online Identification of PMSM Parameters and Sensorless Control" IEEE Transactions on control systems technology, vol.27, no.6, pp.2444-2452, Nov-2019.
[10]J Lee, J I Ha, "Temperature Estimation of PMSM Using a Difference-Estimation Feedforward Neural Network" IEEE Access, vol.8, PP.130855-130865, July 2020.

[11] Wilhelm Kirchgässner, Oliver Wallscheid and Joachim Böcker "Estimating Electric Motor Temperatures with Deep Residual Machine Learning" IEEE Trans., on power electronics, vol. 36, no.7, pp.7480-7488, July 2021.

[12] Luy Nguyen Tan, Thanh Pham Cong, Duy Pham Cong "Neural Network Observers and Sensorless Robust Optimal Control for Partially Unknown PMSM with Disturbances and Saturating Voltages" IEEE Trans., on power Electronics, vol. 36, no. 10, pp.12045-12056, Oct-2021.

[13] Hongyu Jie, Gang Zheng "Calibration of Torque Error of Permanent Magnet Synchronous Motor Base on Polynomial Linear Regression Model", IECON-2019, , October 2019.

[14] L. S. N. D. K. B. S. H. Oscar, "Deep Learning-Based Model Predictive Control for Resonant Power Converters", IEEE Trans., on Industrial Informatics, vol. 17, no.1, pp.409-420, Jan 2021.

[15] T. M. Breuel, "The Effects of Hyperparameters on SGD Training of Neural Networks", arXiv preprint arXiv:1508.02788, 2015, https://doi.org/10.48550/arXiv.1508.02788

[16] A. Brosch, O. Wallscheid, and J. Bocker. Data set: Torque characteristics ¨ of a permanent magnet motor - 74 million samples for data-driven learning. https://tinyurl.com/tt68bpz

[17]A.Brosch, O.Wallscheid and J.Bocker "Torque and Inductances Estimation for Finite Model Predictive Control of Highly Utilized Permanent Magnet Synchronous Motors", IEEE Trans., on Industrial Informatics, vol:17, no.12, pp. 8080-8091, December 2021.

Journal of Engineering and Technology for Industrial Applications

ISSN ONLINE: 2447-0228

ITEGAM-JETIA

Manaus, v10. n.50, p. 180-188. November/ December., 2024.
DOI: https://doi.org/10.5935/jetia.v10i50.1280

RESEARCH ARTICLE OPEN ACCESS

HYBRID UM-LT-AHE TECHNIQUE FOR CONTRAST ENHANCEMENT OF MEDICAL IMAGES

Kamoli A. Amusa[1], Olumayowa A. Idowu[2] and Abolaji O. Ilori[3]

[1,2] Department of Electrical and Electronic Engineering, Federal University of Agriculture, Abeokuta. Ogun State.
[3] Department of Electrical and Biomedical Engineering, First Technical University, Ibadan.

[1]http://orcid.org/0000-0002-9436-2349, [2]http://orcid.org/0000-0003-4892-3632, [3]http://orcid.org/0000-0002-2695-6479

Email: amusaka@funaab.edu.ng, olumayor2@gmail.com, abolaji.ilori@tech-u.edu.ng

ARTICLE INFO

Article History
Received: September 09, 2024
Revised: October 1, 2024
Accepted: November 10, 2024
Published: December 31, 2024

Keywords:
Hybrid,
Contrast,
Enhancements,
Medical,
Brightness.

ABSTRACT

This paper is concerned with combinations of un-sharp masking, logarithmic transformation and adaptive histogram equalization techniques to arrive at a hybrid method for enhancement different types of medical image' contrast. Motivation behind the hybridization is the need to have a contrast enhancement method that is not application specific and that can be deplored to several medical image enhancement. Four different types of medical images: X-ray, ultrasound, magnetic resonance and computer tomographic images are utilized in the evaluations of the proposed hybrid contrast enhancement method. As performance metrics, absolute mean brightness error, mean square error, peak signal to noise ratio and entropy are used. Comparative results both qualitative and quantitative, were conducted at the end of the research, and the proposed method out-perform other three (CLAHE, Fuzzy-based and Wavelet Transform-based) related selected methods in the field which used the same dataset in terms of testing accuracy. The enhancement quality of the proposed method was found to be satisfactory and can be used for any time of medical image, thus, the proposed hybrid technique produces better enhanced medical images from different medical image inputs.

I. INTRODUCTION

Image enhancement falls within the purview of computer vision with the aim of improving the visualization of asymmetric brightness level in images [1]. It is a technique widely utilized in medical image processing and analysis [2],[3] to modify a given picture such that desirable characteristics of the image are easier to recognize by automated image analysis systems [4] and aid accurate judgment from the image. Image enhancement represents one of the phases of digital image processing tasks, along with image detection, segmentation and classification [5]. The procedure of image enhancement encompasses a variety of approaches that geared towards improved image's aesthetic appeal, visual clarity and overall look of an image in order to facilitate easier extraction of its spatial characteristics [6]. In other word, through enhancement of an image, details of the image that are not readily visible in the original image right away become available. The need for the enhancement of an image may arise when the image data and the display system have different dynamic ranges, when the image is embedded with a lot of noise, or when the contrast is too low [4].

Image enhancement methods are divided into spatial domain-based and transformation domain-based approaches [5] - [6] Histogram Equalization (HE) is a frequently used spatial domain-based approach that produces a picture with a uniform distribution of intensity following equalization; however, if the histogram has high peaks, contrast is over-enhanced, resulting in a harsh and noisy image. Several other approaches have been used to address these shortcomings, including automatic image equalization using Gaussian mixture modeling [7], power-constraint contrast enhancements based on HE [8], and entropy maximization histogram modification for image enhancement [9], all of which were still deficient by causing a halo effect in high contrast areas [10]. In the transform-based approaches, one can find threshold transformation [11], log transformation [11], multi-scale retinex-based [12], image size dependent normalization [13], adaptive gamma correction-based algorithm [14], fractional order and directional derivatives [15], wavelet transform [16] and Non-

Subsampled Contourlet Transform (NSCT) [5]. Others are fuzzy logic-based and neuro-fuzzy method [11], [17].

A variety of apps provide a selection of photos with certain features, and the selection of augmentation techniques vary greatly based on particular requirements. The subject of this study is medical imaging. Globally, healthcare engineering is a significant and quickly growing field that includes illness prevention, diagnosis, treatment, and management as well as the maintenance and improvement of physical and mental health [18],[19]. In addition to diagnosing and treating diseases, medical imaging technologies are becoming more and more important for disease prevention, health screening, major disease screening, health management, early diagnosis, determining the severity of a disease, choosing a treatment plan, evaluating the effects of that plan, and rehabilitation [19]–[21]. As such, there has been a significant increase in the significance of medical imaging technology in healthcare delivery applications [19],[20].

Medical image enhancement has become standard practise due to its ability to improve different medical procedures, image-guided surgery, and illness detection and therapy [22]. Improving the clarity and quality of images is the goal of medical image enhancement, which also aims to improve the images' interpretability for human viewers. X-rays, Computed Tomography (CT), ultrasound, and Magnetic Resonance Imaging (MRI) are among the frequently used medical imaging [5]–[6], with the latter being especially helpful in the diagnosis of cerebrovascular diseases. The accuracy of doctors' diagnoses and treatments, where images of internal organs and human sub-systems are involved, is directly influenced by the quality of the images. This singular reason makes medical imaging an integral aspect of contemporary and modern medicine

II. THEORETICAL REFERENCE

Medical images are frequently bedeviled with effects of interference from sounds and electromagnetic sources, which often degrade the resultant image's quality. Furthermore, presence of noise and artifacts contribute uncertainty to the medical image in the form of ambiguous image segment homogeneity or ambiguous object-background contrast. These make segmentation and detection of contours and textures of the image very challenging [9].

A remapping technique called contrast enhancement modifies the image intensity distribution so that the entire image intensity range can be used [23]. This method has been used to improve the visual quality of photos, highlight important information, and highlight image aspects. For medical pictures, a variety of contrast enhancement techniques have been put forth. The Bihistogram Bezier curve contrast enhancement method was presented in [23], showing how well it works to emphasise important brain imaging features in low-resolution brain MR images [24]. A multimodal contrast enhancement strategy was proposed in [25] and successfully handled the problem of weak contrast in images of children's hand bones. In addition to the previously discussed techniques, the Hopfield Neural Network (HNN) is another way for image augmentation [26]. To ensure network stability throughout the training phase, this approach is said to have a few disadvantages [27], one of which is its propensity to converge to a fixed point [28]. Additionally, there could be a chance that the quality of the images decreases [29]. Notwithstanding these drawbacks, investigating various contrast enhancement techniques is still essential for developing the area of medical image enhancement and tackling particular problems related to various kinds of medical images.

NSCT technique introduced in [5] combined methods of adaptive thresholding and enhanced fuzzy set to meet the demands of medical image improvement. The fuzzy contrast function was improved through the adjustment of the normal inverse which was utilized in the creation of a new function for calculating the enhanced pixel gray membership. The new enhanced membership function together with the Laplace operator were used to improve the image details. The approach was able to boost the general contrast of an image, emphasize the features and contours of an image, and considerably improve the visual impression of an image; nevertheless, the algorithm's flexibility was ineffective. Other efforts to improve medical imaging include an approach to improving the visual look that makes use of the Bi-histogram Bezier Curve [23]. This technique focuses on improving MRI pictures that show a sudden leap in the knee. A different endeavour pertains to an altered iteration of the Hopfield Neural Network (HNN) methodology [30], which tackles the convergence issues linked to the conventional HNN approach. The goal of this update is to improve the HNN technique's overall efficacy in improving medical images. Additionally, a multimodal method has been investigated [6] that is intended for clinical imaging sensor applications. These varied methods demonstrate a dedication to honing procedures for a range of clinical settings and image types, and they highlight the continuous attempts to develop and improve in the field of medical image enhancement.

While those aforementioned methods and many others ensure improvement in the image contrast, there arises a problem of non-uniformity in enhancement and most importantly, over enhancement of certain portion of the image. There have been various modifications made to conventional histogram equalisation techniques in order to address the issue of over-enhancement. The contrast limited dynamic quadri-histogram equalisation [31], the minimum mean brightness error bi-histogram equalisation in contrast enhancement [32], the range limited weighted histogram equalisation (RLWHE) [33], the recursively separated weighted histogram equalisation (RSWHE) incorporating a normalised power law function [34], and the Recursive Mean-Separate Histogram Equalisation (RMSHE) intended for scalable brightness preservation [35] are noTab. among these techniques. The tendency towards over-enhancing in the final image remains a recurrent problem, even though these variations of the histogram equalisation (HE) technique have proven effective in producing high contrast enhancement and good brightness retention. Adaptive Gamma Correction with Weighted Distribution (AGCWD) is a revolutionary automated transformation approach that was developed [36] to solve the problems associated with RMSHE, RSWHE, and related techniques. To further address over-enhancement problems in medical image processing, the Triple Dynamic Clipped Histogram Equalisation based on Mean or Median (TDCHEM) approach [37] was put forth. The challenges presented by conventional histogram equalisation methods in medical image enhancement may be addressed by these creative approaches, which aim to achieve greater contrast while maintaining image quality. The two approaches AGCWD and TDCHEM are able to boost contrast and also prevent over-enhancement of images, however, none of them is able to retain brightness and preserve structures of images.

Several researches have been made in this area of contrast enhancements of medical images, various successes have been recorded and each technique with its identified shortcomings. Some of the shortcomings include the problem of over-enhancement, proper enhancement but brightness not preserved, some methods are not suiTab. for all types of medical images and so on. This study is primarily motivated by the shortcomings found in the previously described methods as well as the need for a low-complexity picture enhancing method. This work focuses on developing a hybrid algorithm for medical picture improvement that combines three different techniques: Un-sharp Masking (UM), Logarithm Transformation (LT), and Adaptive Histogram Equalisation (AHE). These three strategies were carefully chosen because they each have advantages over other alternatives in terms of robustness, low computational complexity, and short calculation times. By utilising the distinct benefits of each method, this hybrid strategy seeks to jointly address the issues raised by over-enhancing and computational complexity in medical picture enhancement.

III. MATERIALS AND METHODS

This study uses three different enhancing strategies in a cascaded manner. Un-sharp Masking (USM) is the first technique in this series, which is used to improve the image by sharpening edges and removing intrinsic blurring from the input medical image. Logarithm Transformation (LT) uses the output that is produced when USM is applied to the medical image. LT is specifically made to increase the brightness of the image's dark pixels, increasing its dynamic range. LT seeks to bring to light aspects that are buried inside the picture. The output is then passed into the Adaptive Histogram Equalisation (AHE) method after the LT step. AHE seeks to enhance the image's contrast even more. The planned tri-modal medical image enhancement strategy comes to a close with the final output of the AHE stage. The USM-LT-AHE medical image enhancement approach is the name given to this sequential process. These strategies were chosen because they have clear benefits over other approaches, such as being robust, efficient, and simple in terms of mathematical complexity.

A thorough block diagram is used in Fig. 1 to graphically represent the suggested hybrid UM-LT-AHE contrast enhancement technique. As shown in figure 1, the methodology is divided into five main stages: pre-processing (colour conversion), post-processing (colour conversion), Adaptive Histogram Equalisation (AHE), Logarithm Transformation (LT), and Un-sharp Masking (UM). The primary goals of this image processing approach are contrast enhancement and image de-blurring. The input image is specially de-blurred by the UM stage, and the contrast of the image is improved by the LT and AHE stages. We then emphasise each step of the proposed UM-LT-AHE medical image enhancement strategy, starting with the first image colour conversion. This methodical technique aims to solve issues with image quality and enhance both clarity and contrast in medical images.

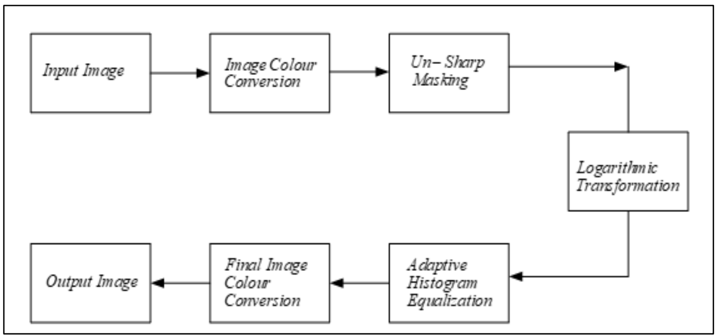

Figure 1: Block diagram of the proposed hybrid UM-LT-AHE method.
Source: Authors, (2024).

III.1 IMAGE COLOR CONVERSION

For the suggested hybrid UM-LT-AHE enhancement approach to be compatible and provide accurate colour rendering, two colour conversion stages must be included. Colour conversions are not required before the first processing steps or after the final output stages when the input is a grayscale image. However, colour conversion becomes an essential step when dealing with a colour image input. Prior to the Un-sharp Masking (UM) algorithm processing, the Red, Green, and Blue (RGB) components of the image are mapped into their equivalent Hue-Saturation-Value (HSV) on the input side. The output stage involves converting the processed image from the HSV mapping back to RGB equivalent using the Adaptive Histogram Equalisation (AHE) technique. The MATLAB environment facilitates the smooth execution of colour conversions for pre-processing and post-processing, with the rgb2hsv and hsv2rgb functions, respectively. Through these colour conversion steps, the suggested improvement method is made sufficiently flexible to handle both colour and grayscale images, offering a unified and uniform approach across many input conditions.

III.2 UN-SHARP MASKING

The Un-sharp Masking (UM) algorithm sharpens edges and areas with plenty of detail in a picture to highlight details that are otherwise hidden. This is accomplished by creating a corrective signal, which is basically an enlarged version of the input image's signal representation. A Laplacian filter, which has a negative centre coefficient, is used to generate the corrective signal. To recover the image's lost grey tones, this correction signal is then deducted from the original input image signal. Mathematically, the expression for the Un-sharp Masked input image at a pixel location (x, y) is represented as:

$$UM(x,y) = Original\ Image\ (x,y) Correction\ Signal(x,y) \quad (1)$$

In this equation, $UM(x,y)$ denotes the Un-sharp Masked pixel value at location (x, y), which is obtained by subtracting the Correction Signal at the same location from the corresponding pixel value in the original input image. This process results in an image that emphasizes fine details and enhances the overall sharpness of the edges within the original image.

The output image from UM stage that is fed into the input of LT stage is expressed as:

$$Y_{UM}(x,y) = I_o(x,y) + KI(x,y) \quad (2)$$

where $Y_{UM}(x,y)$ is the output image from the UM stage and K is a positive scaling factor that controls the level of achievable image de-blurring or sharpness level. The values for K is such that $0.2 \leq K \leq 0.9$ [38].

USM involves the following steps:

i. Get the input image that requires enhancement
ii. Generation of a blur copy of the input image using Laplacian of Gaussian (LoG) filter.
iii. Subtract blur copy from the input to give un-sharp masking image
iv. Multiplications of the un-sharp masking image by a fractional value “K”

Addition of the result in (iv) to the original image in (i).

III.3 LOGARITHMIC TRANSFORMATION

In the suggested enhancement scheme, the main goal of the Logarithm Transformation (LT) technique is to transfer the image's dark (or low) intensity values to brighter (or higher) values, increasing the visibility of features. Higher-intensity pixels are little impacted by the LT algorithm's application; instead, low-intensity pixels are mapped to high-intensity pixels. The expression for the logarithm transformation can be expressed mathematically as follows:

$$LT(x, y) = c.\log(1 + Original\ Image\ (x, y)) \quad (3)$$

Here, $LT(x, y)$ denotes the pixel value after the Logarithm Transformation at location (x, y) and c is a scaling factor. The logarithmic function $\log(1 + Original\ Image\ (x, y))$ is applied to the pixel values of the original image at the corresponding location. The addition of 1 in the logarithmic function helps avoid the issue of taking the logarithm of zero.

This transformation improves the contrast of the image overall by making details in the dark areas of the image more visible. The logarithmic function is a good choice since it preserves information in higher-intensity regions while extending the dynamic range of low-intensity values.

III.4 ADAPTIVE HISTOGRAM EQUALIZATION

The plot of the number of pixels n_k in an image against the intensity value k describes the image histogram, where $0 \leq k \leq 2^x - 1$ and x is the class unit of the image. In the context of this paper, 256 intensity levels are considered, resulting in a class unit of 8. This corresponds to an intensity value range between 0 (representing black) and 255 (representing white). For an image with a total number of pixels N the associated probability density function (PDF) is given:

$$P(k) = \frac{n_k}{N} \quad (4)$$

$P(k)$ is the probability density function at intensity value k
n_k is the number of pixels at intensity value k,
N is the total number of pixels in the image

The probability density function illustrates the possibility of coming across a pixel in the image with a certain intensity value. With 256 intensity levels in the provided context, the function characterises the distribution of pixel intensities throughout the image, offering important details about contrast, brightness, and general tonal qualities.

III.5 SUMMARY OF STEPS INVOLVED IN THE IMPLEMENTATION

The steps involved in the implementation of the proposed hybrid UM-LT-AHE contrast enhancement scheme for medical images:

1. Select the Type of Image:
   - Ascertain whether the input image is grayscale or colour.
2. Read Grayscale Pixel Values:
   - If the image is in grayscale, read each pixel's value.
3. Convert the RGB colour space to the HSV colour space if the image is coloured.
   - Examine the HSV's value component.
4. Sharp Masking Absence (UM):
   - As necessary, apply the Un-sharp Masking method to the results of steps (ii) or (iii).
5. Logarithm Transformation (LT):
   - Map the step (iv) output using a Logarithm Transformation mapping function.
6. Adaptive Histogram Equalisation (AHE):
   - Apply step (v)'s output to the Adaptive Histogram Equalisation with clipping.
7. Store Output (Grayscale):
   - Store the step (vi) output and move on to step (x) if the input image is grayscale.
8. Modify the Colour Image Value Component:
   - If the input image is coloured, use step (vi)'s result as the image's new V (value).
9. Combine H, S, and New V:
   - Combine the H and S components of the input image with the newly acquired V component from the previous step to create a new HSV colour space for the image.
10. RGB conversion:
    - Return the newly created HSV colour space from step (viii) to RGB colour space.
    - Keep the result stored.
11. Output Enhanced Image:

This is a version of the original input image that has been enhanced.

The developed hybrid UM-LT-AHE medical image enhancement approach was implemented using the MATLAB R2018a environment, which was set up on an HP EliteBook running Windows 10 with a core i5 processor, 64-bit architecture, and 4 GHz RAM. During implementation, a number of functions from the image processing toolbox were used, including rgb2hsv, hsv2rgb, imfilter, adapthisteq, and others.

A collection of sixteen test medical photos was used to assess how well the suggested UM-LT-AHE medical image enhancement method performed. These photographs cover a range of medical imaging modalities, such as ultrasound, X-ray, MRI, and CT scan images as shown in Table 1 and were taken from publicly accessible online databases. Both colour and grayscale photographs are included in the collection; each image format contributes four images.

Table 1: Descripption of images used for experiment.

Images	Ultrasound	X-ray	MRI scan	CT scan
(i)	multiple gestation	human elbow	cervical spine	gray scale abdominalcavity
(ii)	human kidney	human knee	human knee	healthy human heart
(iii)	human liver with gall bladder	human leg	human lung	brain tumor
(iv)	human liver	human toes	multiple fetal	color abdominal cavity

Source: Authors, (2024).

III.6 PERFORMANCE METRICS

By comparing its outcomes with existing methods from the literature, the suggested technique's performance in contrast enhancement is assessed using objective assessment criteria. For this, Absolute Mean Brightness Error (AMBE), Mean Square Error (MSE), Peak Signal-to-Noise Ratio (PSNR), and entropy are the four essential performance indicators used. When compared to the outputs of various contrast enhancement techniques in the literature, the suggested method is deemed superior if it produces an output image with the lowest AMBE, lowest MSE, highest PSNR, and highest entropy values.

Absolute Mean Brightness Error (MBE); the difference between the brightness level of the enhanced image and original image.

$$\boldsymbol{AMBE} = \mid E(y) - E(x) \mid \tag{7}$$

Where: $\boldsymbol{E(x)}$ = average intensity of input image; $\boldsymbol{E(y)}$ = average intensity of output image.

The output of this research was compared with those of other works using AMBE, the method yielding the least numerical value is adjudged best in performance in terms of brightness preservation.

Peak-Signal-to-Noise-Ratio (PSNR): is the evaluation standard of the reconstructed image quality, and is an important measurement feature. PSNR is measured in decibels. The higher the PSNR, the better the method.

$$PSNR = 10log_{10}\frac{R^2}{MSE} \tag{8}$$

Where $\boldsymbol{R} = \boldsymbol{2^{xbits}}$ which depends on image class

Entropy: This is a statistical measure of randomness that can be used to characterize the texture of an image. It is the measure of the content of an image. The higher the entropy, the better the method.

$$\boldsymbol{Entropy} = iP_i log_2 P_i \tag{9}$$

Where $\boldsymbol{P_i}$ is the probability that the difference between adjacent pixels is equal to $\boldsymbol{i}$.

IV. RESULTS AND DISCUSSIONS

Obtained simulation results from the proposed hybrid UM-LT-AHE method are compared with those from three other methods (CLAHE, Fuzzy and WT) in the literature, for image contrast enhancement.

What follows are the simulation results beginning with those of ultrasound images. The images in (a) are the original images before they were subjected to various enhancement techniques, (b)-(e) are the images after they have been enhanced with different enhancement methods; the Hybrid UM-LT-AHE, CLAHE, AHE and Fuzzy-based methods respectively. The level of enhancement on the images can be visualized in the output as shown in the Figure 2 to 5.

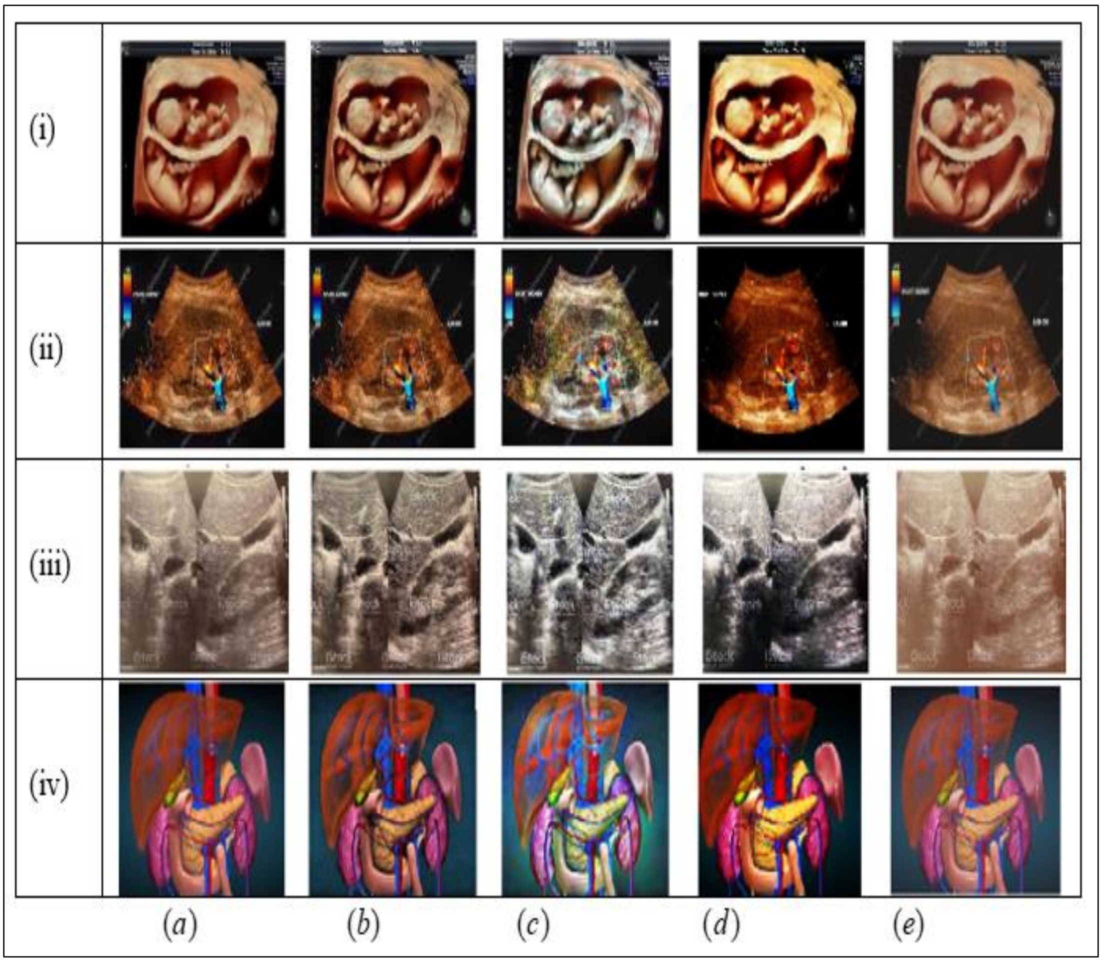

Figure 2: Simulation results using Ultrasound images (a)original image (b)UM-LT-AHE method (c)CLAHE method (d)Fuzzy-based method (e)WT method.
Source: Authors, (2024).

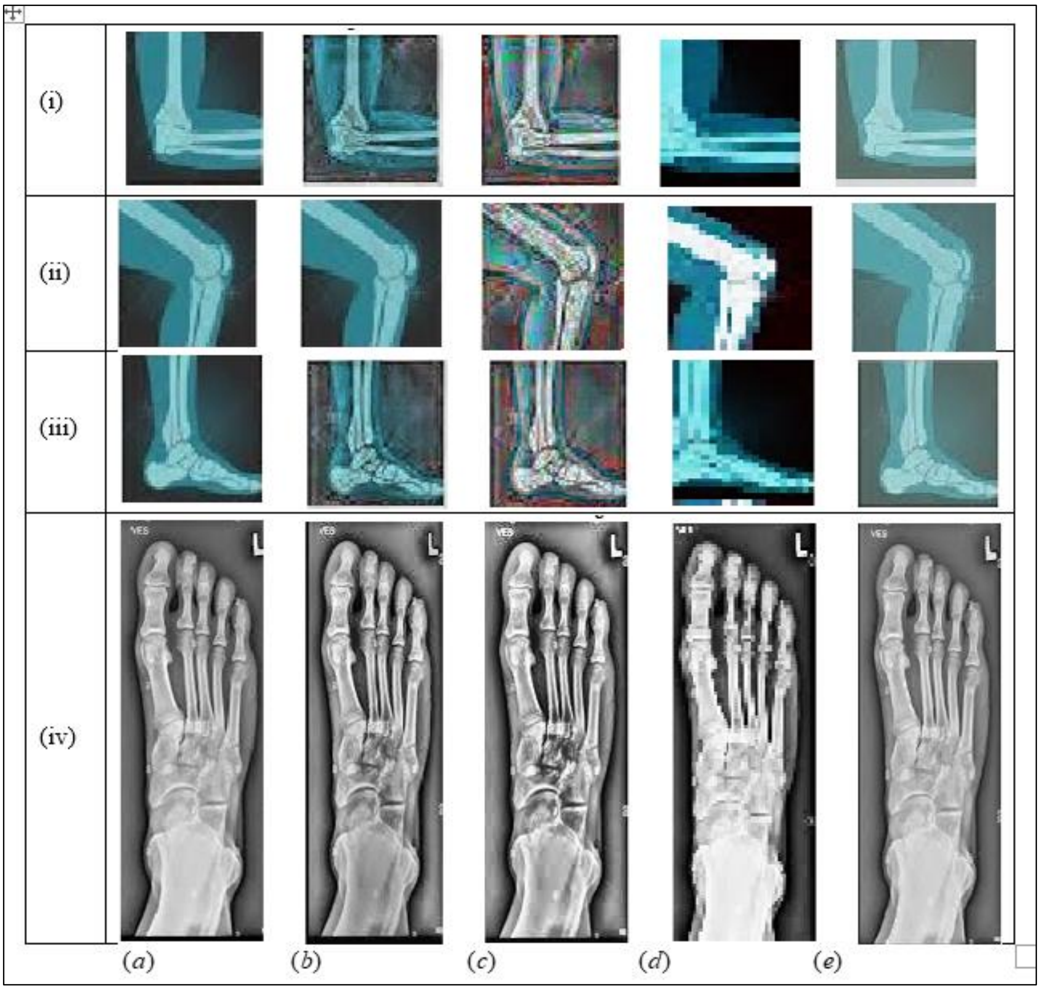

Figure 3: Simulation results using X-ray images (a)original image (b)UM-LT-AHE method (c)CLAHE method (d)Fuzzy-based method (e)WT method.
Source: Authors, (2024).

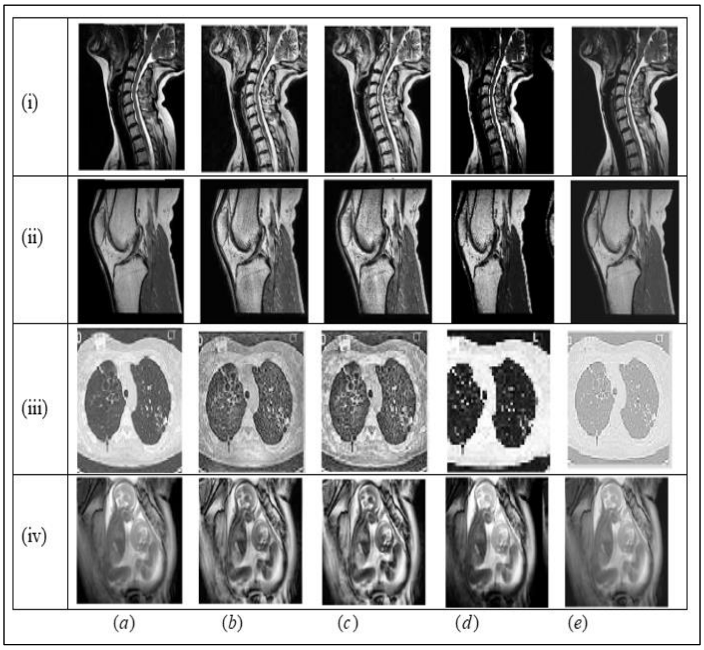

Figure 4: Simulation results using MRI scan images (a)original image (b)UM-LT-AHE method (c)CLAHE method (d)Fuzzy-based method (e)WT method.
Source: Authors, (2024).

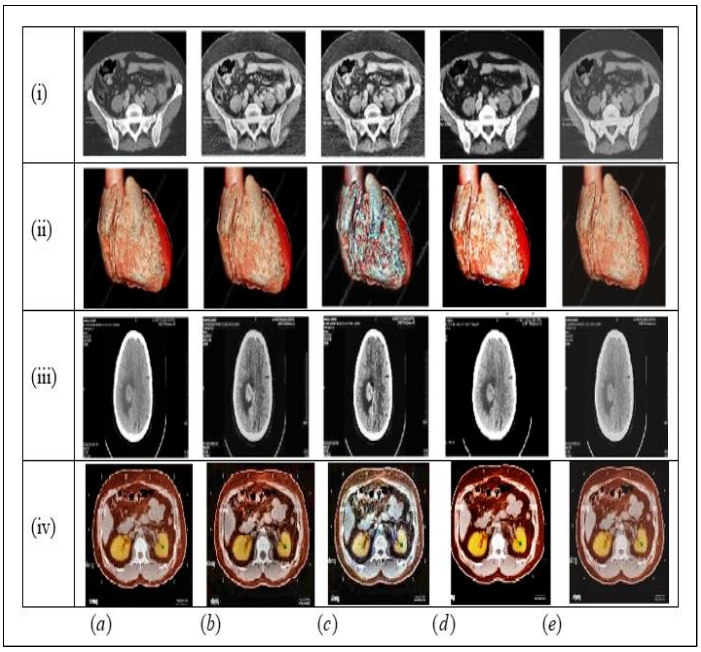

Figure 4: Simulation results using CT scan images (a)original image (b)UM-LT-AHE method (c)CLAHE method (d)Fuzzy-based method (e)WT method.
Source: Authors, (2024).

A cursory look at simulation results presented in Figure 2 to 5 for enhanced images of different types reveal that outputs of the proposed UM-LT-AHE medical image enhancement method fare better than other four methods employed in comparison. It is obvious that output images using the proposed UM-LT-AHE medical image enhancement method closely match the input test images than what obtains from other four methods used.

Next in the evaluation process is quantitative and objective evaluation of the performance of the UM-LT-AHE medical image enhancement method proposed in this work along with those of CLAHE, Fuzzy-based and Wavelet transform-based methods using those sixteen test images described in Table 1.

Table 2 to 4 present computed parametric results, starting with those of X-ray images.

Table 2: Evaluation results using X-ray images.

Parameters	CLAHE	Fuzzy-based	Wavelet-based	Proposed
ELBOW				
AMBE	186583	10.3738	39.6560	18.528
MSE	0.0910	0.0853	0.11225	0.0678
PSNR	23.9670	24.6105	21.8702	26.9127
Entropy	7.7059	6.5089	6.8866	7.5612
KNEE				
Parameters	**CLAHE**	**Fuzzy-based**	**Wavelet-based**	**Proposed**
AMBE	18.528	0.37373	36.446	1.0074
MSE	0.0866	0.0978	0.1040	0.0635
PSNR	24.4660	23.2496	22.6370	27.5704
Entropy	7.6671	6.6577	6.9027	7.4787
LEG				
Parameters	**CLAHE**	**Fuzzy-based**	**Wavelet-based**	**Proposed**
AMBE	19.5594	20.2151	34.3872	4.6719
MSE	0.0917	0.0723	0.1060	0.0703
PSNR	23.8899	26.2699	22.4391	26.5479
Entropy	7.6073	6.7336	6.9859	7.5064
FOOT				
Parameters	**CLAHE**	**Fuzzy-based**	**Wavelet-based**	**Proposed**
AMBE	5.0847	11.2024	15.1105	2.5408
MSE	0.0616	0.0775	0.0638	0.0553
PSNR	27.8784	25.5748	27.5273	28.9528
Entropy	6.2224	5.7115	5.5348	6.2548

Source: Authors, (2024).

Objective evaluation results involving X-ray images show that the proposed hybrid UM-LT-AHE contrast enhancement method performed better than each of CLAHE, fuzzy-based and wavelet transform-based methods. Specifically, the performance of the proposed method in this work surpasses those of others in terms of AMBE, MSE and PSNR Figures in all four images while it has entropy Figures that are slightly lower than those yielded by CLAHE in three of the test images

Table 3: Evaluation results using Ultrasound images.

Parameters	CLAHE	Fuzzy-based	Wavelet-based	Proposed
MULTIPLE GESTATION				
AMBE	18.4466	7.2810	12.4194	3.6492
MSE	0.0714	0.0723	0.0570	0.0523
PSNR	26.3917	26.2662	28.6539	29.5030
Entropy	7.1841	6.3418	7.0386	7.2399
HEALTHY KIDNEY				
Parameters	**CLAHE**	**Fuzzy-based**	**Wavelet-based**	**Proposed**
AMBE	27.5549	8.1986	17.7543	9.7369
MSE	0.0481	0.0228	0.0303	0.0287
PSNR	30.3426	37.8118	34.9762	35.5070
Entropy	6.9083	4.9430	6.2130	6.8636
HUMAN LIVER WITH GALL BLADDER				
Parameters	**CLAHE**	**Fuzzy-based**	**Wavelet-based**	**Proposed**
AMBE	8.7964	6.4803	18.9987	8.8073
MSE	0.0995	0.0901	0.1029	0.0715
PSNR	23.0714	24.0728	22.7391	26.382
Entropy	7.8810	7.8152	7.4250	7.6415
NORMAL LIVER				
Parameters	**CLAHE**	**Fuzzy-based**	**Wavelet-based**	**Proposed**
AMBE	25.845	10.7739	14.7473	0.58036
MSE	0.0690	0.0443	0.0513	0.0400
PSNR	26.7381	31.1763	29.7004	32.1825
Entropy	7.7775	6.9439	7.3239	7.3812

Source: Authors, (2024).

Results shown in Table 3 for ultrasound test images reveal a different scenario from that of X-ray images. While Fig.s obtained from the proposed hybrid UM-LT-AHE method are generally not the best, they are however, compare favorably with those adjudged to be best for ultrasound images. In fact, the marginal difference in those parameters is small as can be inferred from results involving 'healthy kidney' image where fuzzy-based method appear better than others as well as those of entropies returned by CLAHE for 'human liver with gall bladder' and 'normal liver'.

Table 4: Evaluation results using CT-scan images.

Parameters	CLAHE	Fuzzy-based	Wavelet-based	Proposed
GRAY SCALE ABDOMINAL CAVITY				
AMBE	17.3672	10.9913	11.4329	14.4132
MSE	0.0858	0.0666	0.0691	0.0783
PSNR	24.5553	27.0946	26.7278	25.4705
Entropy	7.6063	6.5047	6.8863	7.6202
HEALTHY HEART				
AMBE	2.7463	15.7666	13.4307	8.5005
MSE	0.0515	0.0789	0.0550	0.0348
PSNR	29.67	25.3993	29.0009	33.5753
Entropy	5.5869	4.9244	6.0456	5.7624
BRAIN TUMOR				
AMBE	4.5612	6.3451	16.7043	12.896
MSE	0.0407	0.0501	0.0403	0.0327
PSNR	32.0259	29.9346	32.1063	34.1945
Entropy	4.8102	30.751	44.571	4.8786
COLOR ABDOMINAL CAVITY				
AMBE	16.0203	24.185	14.8689	12.558
MSE	0.0695	0.0654	0.0593	0.0509
PSNR	26.6681	27.2683	28.2501	29.7763
Entropy	7.173	5.9548	6.7886	7.2027

Source: Authors, (2024).

Although parametric evaluation results CT scan of gray scale abdominal cavity image show that fuzzy-based method performed better than others in terms of AMBE, MSE and PSNR Figure, however, judging by the margin between corresponding values returned by the proposed hybrid UM-LT-AHE method, it can be safely said that the method compare well. Aside the results of gray scale CT scan of abdominal cavity, the proposed hybrid UM-LT-AHE method performed better than other methods, especially in terms of MSE and PSNR Figures. These observations are premised on results presented in Table 4.

Table 5: Evaluation results using MRI-scan images.

Parameters	CLAHE	Fuzzy-based	Wavelet-based	Proposed
CERVICAL SPINE				
AMBE	28.6652	**13.0575**	17.212	28.2196
MSE	0.0630	0.0937	**0.0406**	0.0604
PSNR	2.7654	23.6791	**32.0408**	28.0758
Entropy	6.8039	48.239	64.707	**68.113**
KNEE				
AMBE	13.0372	**96.004**	155.956	111.961
MSE	0.0638	0.1394	**0.0544**	0.0583
PSNR	27.5133	19.7026	**29.1072**	28.4297
Entropy	62.196	50.685	58.780	**62.251**
LUNG				
AMBE	20.2711	**18.5814**	37.828	24.3273
MSE	0.1279	0.1627	0.2150	**0.1150**
PSNR	20.563	18.1576	15.3711	**21.6259**
Entropy	**77.815**	65.790	64.779	76.419
MULTIPLE FETAL				
AMBE	13.4195	**7.2406**	12.6458	11.0239
MSE	0.0883	0.2131	0.0786	**0.0806**
PSNR	242.710	154.600	254.397	251.808
Entropy	78.333	71.747	74.522	77.251

Source: Authors, (2024).

Evaluation results using MRI scan images appear rather clumsy as mixed results are returned. One thing that is cleared from entries of Table 5, where MRI scan images results' are presented, is that the results of the proposed UM-LT-AHE method still compare well with those of other methods used for comparison.

IV.I. LIMITATION OF THE PROPOSED METHOD

The proposed method is limited to medical images drawn from CT scan, MRI images, Ultrasound scan and X-rays. Other medical images from other sources were not considered.

IV.II. FUTURE WORK

The method should be tested for its applicability in enhancement of many imaging applications such as underwater, astronomical, and consumer-based electronics.

V. CONCLUSIONS

We present a novel hybrid UM-LT-AHE technique in this work that is intended primarily to improve contrast in medical photos. This technique is noteworthy for its adaptability, as it can handle medical images in both grayscale and colour. Our assessment, carried out on a variety of test medical pictures including X-ray, ultrasound, CT, and MRI scan modalities, proved that the hybrid UM-LT-AHE contrast enhancement method that was suggested was effective. Its application to a variety of medical images was demonstrated by the results, which also showed that it produced accepTab. results for important assessment metrics like AMBE, MSE, PSNR, and entropy Figures. This highlights how well the technique works to improve contrast in a range of medical imaging situations, confirming its usefulness as a strong and adap table. instrument in the field of medical image processing. Furthermore, it was shown here that the proposed hybrid UM-LT-AHE method performed well than each of CLAHE, fuzzy-based and wavelet transform-based methods, on the average when deployed for contrast enhancement of the four aforementioned medical image types. Based on these findings, the proposed UM-LT-AHE method can be safely deployed for the enhancement of different types of medical images' contrast with satisfactory results for all types of images, something which was lacking in some other methods.

VI. AUTHOR'S CONTRIBUTION

Conceptualization: Kamoli A. Amusa and Olumayowa A. Idowu.
Methodology: Kamoli A. Amusa and Olumayowa A. Idowu.
Investigation: Olumayowa A. Idowu and Abolaji O. Ilori.
Discussion of results: Kamoli A. Amusa, Olumayowa A. Idowu and Abolaji O. Ilori.
Writing – Original Draft: Olumayowa A. Idowu and Abolaji O. Ilori.
Writing – Review and Editing: Kamoli A. Amusa and Abolaji O Ilori.
Supervision: Kamoli A. Amusa.
Approval of the final text: Kamoli A. Amusa, Olumayowa A. Idowu and Abolaji O. Ilori.

VIII. REFERENCES

[1] Z. Huang, Z. Wang, J. Zhang, Q. Li, and Y. Shi, "Image enhancement with the preservation of brightness and structures by employing contrast limited dynamic quadri-histogram equalization," *Optik (Stuttg).*, vol. 226, p. 165877, Jan. 2021, doi: 10.1016/j.ijleo.2020.165877.

[2] Z. Huang, X. Li, N. Wang, L. Ma, and H. Hong, "Simultaneous denoising and enhancement for X-ray angiograms by employing spatial-frequency filter," *Optik (Stuttg).*, vol. 208, p. 164287, Apr. 2020, doi: 10.1016/j.ijleo.2020.164287.

[3] Z. Huang, Q. Li, T. Zhang, N. Sang, and H. Hong, "Iterative weighted sparse representation for X-ray cardiovascular angiogram image denoising over learned dictionary," *IET Image Process.*, vol. 12, no. 2, pp. 254–261, Feb. 2018, doi: 10.1049/iet-ipr.2017.0518.

[4] Y. Abdallah and M. Siddig, Contrast Improvement of Chest Organs in Computed Tomography Images using Image Processing Technique Contrast Improvement of Chest Organs in Computed Tomography Images using Image, no. October. 2015.

[5] F. Zhou, Z. Jia, J. Yang, and N. Kasabov, "Method of Improved Fuzzy Contrast Combined Adaptive Threshold in NSCT for Medical Image Enhancement," *Biomed Res. Int.*, vol. 2017, pp. 1–10, 2017, doi: 10.1155/2017/3969152.

[6] Y. Yang, Y. Que, S. Huang, and P. Lin, "Multimodal Sensor Medical Image Fusion Based on Type-2 Fuzzy Logic in NSCT Domain," *IEEE Sens. J.*, vol. 16, no. 10, pp. 3735–3745, May 2016, doi: 10.1109/JSEN.2016.2533864.

[7] T. Celik and T. Tjahjadi, "Automatic Image Equalization and Contrast Enhancement Using Gaussian Mixture Modeling," *IEEE Trans. Image Process.*, vol. 21, no. 1, pp. 145–156, Jan. 2012, doi: 10.1109/TIP.2011.2162419.

[8] Chulwoo Lee, Chul Lee, Young-Yoon Lee, and Chang-Su Kim, "Power-Constrained Contrast Enhancement for Emissive Displays Based on Histogram Equalization," *IEEE Trans. Image Process.*, vol. 21, no. 1, pp. 80–93, Jan. 2012, doi: 10.1109/TIP.2011.2159387.

[9] Z. Wei, H. Lidong, W. Jun, and S. Zebin, "Entropy maximisation histogram modification scheme for image enhancement," *IET Image Process.*, vol. 9, no. 3, pp. 226–235, Mar. 2015, doi: 10.1049/iet-ipr.2014.0347.

[10] F. Zhou, Z. Jia, J. Yang, and N. Kasabov, "Method of Improved Fuzzy Contrast Combined Adaptive Threshold in NSCT for Medical Image Enhancement," *Biomed Res. Int.*, vol. 2017, pp. 1–10, 2017, doi: 10.1155/2017/3969152.

[11] N.S. Kuldeep, P. Anjali, and D. Prashant. A review on image enhancement techniques. *International Journal of Engineering and Applied Computer Science*, vol. 2, no. 7, pp. 978-995, 2017, doi: 10.24032/ijeacs/0207/05

[12] S. Chen and L. Zou. "Chest radiographic image enhancement based on multi-scale retinex technique". *Bioinformatics and biomedical engineering*, vol. 3, no. 1, pp. 1-3, 2009, doi: 10.1109/ICBBE.2009.5162500

[13] Z. Al-Ameen, G. Sulong and Md. Gapar, Md. Johar, "Enhancing the contrast of CT medical images by employing a novel image size dependent normalization technique", *International Journal of Bio-Science and Bio- Technology*, vol. 4, no. 3, pp. 63-68, Sep. 2002. https://www.earticle.net/Article/A207080

[14] F. Kallel, A. B. Hamida, "A new adaptive gamma correction based algorithm using DWT-SVD for non-contrast CT image enhancement", *IEEE Transactions on NanoBioscience*, vol. 16, Issue: 8, pp. 666 - 675, Dec. 2017. https://doi:10.1109/TNB.2017.2771350

[15] J. Guan, J. Ou, Z. Lai, Y. Lai, "Medical image enhancement method based on the fractional order derivative and the directional derivative", *International Journal of Pattern Recognition and Artificial Intelligence*, Vol. 32, no. 3, pp. 1857001 (22 pages), 2018. https://doi.org/10.1142/S021800141857001X

[16] L. Bibo, H. Wong, M. Chunli. "Biomedical image fusion with adaptive local geometrical structure and wavelet transforms", *ICESB: Maldives*. 2011, https://core.ac.uk/download/pdf/82517654.pdf

[17] T. Chiara. "An improved biomedical image enhancement scheme using type ll fuzzyset". *Applied soft computing*, vol. 25, pp. 293-308, 2014, doi: 10.1016/j.asoc.2014.09.004.

[18] P. Khong and D. Ghista, "Healthcare engineering for an efficient medical care system," *Int. J. Healthc. Technol. Manag.*, vol. 7, no. 5, p. 429, Dec. 2006, doi: 10.1504/IJHTM.2006.008430.

[19] S. Fu, M. Zhang, C. Mu, and X. Shen, "Advancements of Medical Image Enhancement in Healthcare Applications," *J. Healthc. Eng.*, vol. 2018, pp. 1–2, 2018, doi: 10.1155/2018/7035264.

[20] J. S. Duncan and N. Ayache, "Medical image analysis: progress over two decades and the challenges ahead," *IEEE Trans. Pattern Anal. Mach. Intell.*, vol. 22, no. 1, pp. 85–106, Jan. 2000, doi: 10.1109/34.824822.

[21] O. Idowu, K. Amusa, and A. Ilori, "Improved Enhancement Technique for Medical Image Processing," AJER, vol. 11, no. 01, pp. 126–137, 2022.

[22] R. Kaur and S. Kaur, "Comparison of contrast enhancement techniques for medical image," in *2016 Conference on Emerging Devices and Smart Systems (ICEDSS)*, Mar. 2016, pp. 155–159, doi: 10.1109/ICEDSS.2016.7587782.

[23] H. S. Gan *et al.*, "Medical image visual appearance improvement using bihistogram bezier curve contrast enhancement: Data from the osteoarthritis initiative," *Sci. World J.*, vol. 2014, pp. 1–13, 2014, doi: 10.1155/2014/294104.

[24] W. Z. W. Ismail and kok swee Sim, "Contrast enhancement dynamic histogram equalization for medical image processing application," *Int. J. Imaging Syst. Technol.*, vol. 21, no. 3, pp. 280–289, Sep. 2011, doi: 10.1002/ima.20295.

[25] H. Y. Chai, T. T. Swee, G. H. Seng, and L. K. Wee, "Multipurpose contrast enhancement on epiphyseal plates and ossification centers for bone age assessment," *Biomed. Eng. Online*, vol. 12, no. 1, p. 27, Apr. 2013, doi: 10.1186/1475-925X-12-27.

[26] S. Fu *et al.*, "Using Bihistogram Bezier Curve Contrast Enhancement : Data from the Osteoarthritis Initiative," *Optik (Stuttg).*, vol. 2021, no. June, p. 165877, Jan. 2021, doi: 10.1109/ICEDSS.2016.7587782.

[27] O. I. Abiodun, A. Jantan, A. E. Omolara, K. V. Dada, N. A. E. Mohamed, and H. Arshad, "State-of-the-art in artificial neural network applications: A survey," *Heliyon*, vol. 4, no. 11, p. e00938, Nov. 2018, doi: 10.1016/j.heliyon.2018.e00938.

[28] J. Gu *et al.*, "Recent advances in convolutional neural networks," *Pattern Recognit.*, vol. 77, pp. 354–377, May 2018, doi: 10.1016/j.patcog.2017.10.013.

[29] H. de Ridder, "Image processing and the problem of quantifying image quality," in *Proceedings 2001 International Conference on Image Processing (Cat. No.01CH37205)*, Nov. 2001, vol. 2, pp. 3–6, doi: 10.1109/ICIP.2001.958406.

[30] F. Alenezi and K. C. Santosh, "Geometric Regularized Hopfield Neural Network for Medical Image Enhancement," *Int. J. Biomed. Imaging*, vol. 2021, pp. 1–12, Jan. 2021, doi: 10.1155/2021/6664569.

[31] Soong-Der Chen and A. R. Ramli, "Minimum mean brightness error bi-histogram equalization in contrast enhancement," *IEEE Trans. Consum. Electron.*, vol. 49, no. 4, pp. 1310–1319, Nov. 2003, doi: 10.1109/TCE.2003.1261234.

[32] Soong-Der Chen and A. R. Ramli, "Contrast enhancement using recursive mean-separate histogram equalization for scalable brightness preservation," *IEEE Trans. Consum. Electron.*, vol. 49, no. 4, pp. 1301–1309, Nov. 2003, doi: 10.1109/TCE.2003.1261233.

[33] M. Kim and M. G. Chung, "Recursively separated and weighted histogram equalization for brightness preservation and contrast enhancement," *IEEE Trans. Consum. Electron.*, vol. 54, no. 3, pp. 1389–1397, Aug. 2008, doi: 10.1109/TCE.2008.4637632.

[34] S. C. Huang, F. C. Cheng, and Y. S. Chiu, "Efficient contrast enhancement using adaptive gamma correction with weighting distribution," *IEEE Trans. Image Process.*, vol. 22, no. 3, pp. 1032–1041, Mar. 2013, doi: 10.1109/TIP.2012.2226047.

[35] M. Agarwal and R. Mahajan, "Medical Image Contrast Enhancement using Range Limited Weighted Histogram Equalization," *Procedia Comput. Sci.*, vol. 125, no. 2017, pp. 149–156, 2018, doi: 10.1016/j.procs.2017.12.021.

[36] M. Zarie, H. Hajghassem, and A. Eslami Majd, "Contrast enhancement using triple dynamic clipped histogram equalization based on mean or median," *Optik (Stuttg).*, vol. 175, pp. 126–137, Dec. 2018, doi: 10.1016/j.ijleo.2018.08.082.

[37] N. Yehya Hassan and N. Aakamatsu, "Contrast Enhancement Technique of Dark Blurred Image," in *IJCSNS International Journal of Computer Science and Network Security*, 2006, vol. 6, no. 2, p. 223
A. Polesel, G. (Gianni) Ramponi, and V. J. Mathews, "Image Enhancement via Adaptive Unsharp Masking," *IEEE Trans. Image Process.*, vol. 9, pp. 505–510, Feb. 2000, doi: 10.1109/83.826787.

Journal of Engineering and Technology for Industrial Applications

ISSN ONLINE: 2447-0228

ITEGAM-JETIA

Manaus, v10. n.50, p. 189-195. November/ December., 2024.
DOI: https://doi.org/10.5935/jetia.v10i50.1311

RESEARCH ARTICLE OPEN ACCESS

ESTIMATION OF THE TIME OF OCCURRENCE OF THE MAXIMUM ELECTRICAL DEMAND BY SELECTING THE OPTIMAL CLASSIFICATION MODEL AND MAKING USE OF UNBALANCED DATA

César A. Yajure Ramírez[1] and Valesca M. Fuenzalida Sánchez[2]

[1] Universidad Central de Venezuela.
[2] Pontificia Universidad Católica de Chile.

[1]http://orcid.org/0000-0002-3813-7606, [2]http://orcid.org/0009-0001-6878-3852

Email: cyajure@gmail.com, vfuenzalidas@gmail.com.

ARTICLE INFO

Article History
Received: September 28, 2024
Revised: October 15, 2024
Accepted: November 10, 2024
Published: December 31, 2024

Keywords:
Evaluation metrics,
Machine learning,
Multi-criteria analysis,
Unbalanced classes,
Weighted sum.

ABSTRACT

Studies on electricity demand forecasting usually focus on the magnitude of the variable, however, the methodology used in this study also addresses the time at which the peak demand occurs, crucial for planning energy generation, smoothing the demand peaks and establishing differentiated rates. To predict the time of maximum demand, supervised machine learning algorithms were used: random forests, K nearest neighbors, support vector machine, and logistic regression. The dataset consists of hourly maximum and minimum demand data from 2021 to 2024 for a country in South America, including environmental factors such as temperature and seasonality. Since the data in the peak demand prediction variable is unbalanced, the study used oversampling techniques such as SMOTE-NC (synthetic instances of the minority classes to balance the data set). A multi-criteria decision-making approach is used to select the best classification model, considering model evaluation metrics as decision criteria. The most important conclusion drawn by the study is that the model obtained with the support vector machine algorithm turned out to be optimal, and successfully predicted the time of maximum demand on 15 of the 17 test days. The findings highlight the unbalanced nature of peak demand hours, which predominantly occur around 8 pm.

I. INTRODUCTION

Electrical demand forecasting methodologies usually focus on the magnitude of this variable, but in addition to this, determining the time in which this maximum demand occurs is very important for several reasons. For example, it is required for the purposes of determining the electrical generation that must be available to satisfy this maximum demand and thus smooth its peak [1]. Likewise, the company in charge of the electrical system could seek to reduce that maximum demand or temporarily transfer it to "flatten" the load curve, which brings us to the second reason, which is the establishment of differentiated rates for those high hours. demand [2]. Likewise, the temporal dependence between social practices and electrical energy consumption has become evident, with some of these specific practices having greater temporal dependence than others [3]. Then, knowing the time at which maximum demand occurs, the regulatory entity could implement policies for the rational and efficient use of electrical energy according to the types of users of the electrical system.

In addition, among the usual applications of forecasting the times of occurrence of maximum demand are smoothing of demand peaks, but also scheduling the charging of electric vehicles [4]. On the other hand, knowing the usual time at which the minimum power demand occurs is useful for the purposes of planning the mandatory shutdown of generation units for maintenance purposes, or even for planning the maintenance of elements of the transmission system and/or electrical distribution.

Therefore, the objective of this research is to forecast the time w3hen maximum demand will occur in a given geographic region, using data science methodology and selecting the best classification model. The supervised machine learning algorithms considered were random forests (RF), K-nearest neighbors (K-NN), support vector machine (SVC), and logistic regression (LR). To choose the best classification model, a multi-criteria technique is used in which the proposed models are the decision alternatives, and the performance evaluation metrics of the models are the decision criteria.

The topic of this research has been addressed previously, but without considering the multi-criteria approach. For example, [5] develop different models, one to predict whether the next day will be the day of maximum demand of the month, and another to predict the time of peak demand. They use machine learning algorithms to develop the models, and consider the maximum and minimum temperatures, among others, as explanatory variables of the models. The methodology was applied to the Duke energy system in North Carolina, United States. Of the 72 months of data considered, in 69 of them the models got the day of peak demand correct, and in 90% of the peak days, the actual time of peak demand was among the 2 hours with the highest probability. Likewise, [6] build classification models to predict the time of daily peak demand 24 hours in advance. They use several classification machine learning algorithms: Näive Bayes, Support Vector Machines (SVM), Random Forests, Adaptive Boosting (AdaBoost), Convolution Neural Network (CNN), LSTM neural network, and autoencoder type artificial neural network. The data used corresponds to the maximum hourly demand of the city of Ontario in Canada for the period from May 2003 to April 2008, differentiating the winter period from the summer period. They obtain that the artificial neural network is the one that has the best performance for both the winter period and the summer period. Furthermore, [7] presents an approach for developing a peak hour forecasting model, selecting the optimal model by applying a series of machine learning algorithms. To evaluate the model, they work with data from 57 regions of Russia corresponding to the period from January 2016 to January 2020. The algorithms considered were random forest classifier (RFC), decision tree classifier (DTC), nearest neighbors classifier (K-NN), and extra-tree classifier (ETC). The evaluation of the model performance is made based on the accuracy of the actual peak hour with respect to the predicted peak hour, considering one-, two-, and three-hour intervals of the most probable peak hours. The highest accuracy was obtained using the extra-tree classifier.

In their research, [8] presents a methodology to predict coincident peak demand events, including the day and time of event occurrence. The approach is based on performing Monte Carlo simulations to generate scenarios and estimators for this type of event. Additionally, [4] presents an open-source tool for electric energy forecasting through which a variety of methods for forecasting maximum demand, as well as its time of occurrence, are implemented. One of the case studies presented consisted of forecasting the hours of the day or days in a month or year, in which the maximum demand occurs. They worked with electricity consumption data, with a 5-minute resolution, from the New England region in the United States in 2020. It turned out that the model obtained with an artificial neural network of the LSTM type had better performance, with values for the metrics precision, recall, and accuracy, of 0.84, 0.84, and 0.83, respectively. Similarly, [9] proposes a model based on deep learning, to predict the k hours of the day with the highest and lowest demands. They evaluate their model using data from two years of electrical demand from an electrical microgrid that supplies 156 buildings. Its model based on an artificial neural network of the LSTM type was compared with other models: Linear Regression, Arima, and artificial neural network. They obtained that their four-layer LSTM network model had the best performance for both the k hours of high demand and for the k hours of low demand. Finally, [10] present a methodology to forecast the magnitude of maximum demand, as well as its time of occurrence, using two machine learning algorithms: Multiple Linear Regression and Gradient Boosting Machine. Among the explanatory variables, they consider the time, day of the week, month, holidays, and temperature. The results indicate that the regression performs better during seasons with low time variability, while the ensemble methods show greater accuracy in general.

The rest of the article is distributed as follows. Section 2 presents the theoretical background. Then, in section 3 the materials and method used in the research. Next, in section 4 the results obtained are analyzed and discussed. After that, there are the conclusions derived from the research carried out. Finally, bibliographic references are presented.

II. THEORETICAL REFERENCE

II.1 CLASS BALANCING TECHNIQUES

A data set is said to be imbalanced if the class we are interested in falls in the minority class and appears sparsely compared to the majority class, the minority class is also known as positive class, while the majority class is also known as negative class [11]. On the other hand, class imbalance is described as a large discrepancy between two classes of the same target variable, where one class is represented by many instances, while the other is only represented by a small number of instances [12].

Two strategies can be considered to counteract class imbalance: the data sampling approach, and the cost-sensitive learning approach. In this research we worked with the first approach, which could be approached using a sub-sampling method or an over-sampling method. The sampling methodology that selectively strips the majority class, while ensuring that the data set retains the meaningful information associated with this majority class, is known as a sub-sampling approach. While the sampling approach in which instances of the minority class are frequently replicated until a balanced class distribution is reached is known as an oversampling approach. In this work, over-sampling methods are used, among which the SMOTE method (Synthetic Minority Over-sampling Technique), the SMOTE-NC method (Synthetic Minority Over-sampling Technique for Nominal and Continuous), among others, stand out.

II.2 CLASSIFICATION MODELS PERFORMANCE METRICS

The following metrics are considered to evaluate the performance of the classification models: Accuracy, Precision, Recall, and F1. According to what was mentioned by [13], Accuracy "is defined as the sum of all correct predictions divided by the sum of all predictions", it is obtained using Equation (1). Precision "is related to the number of correct positive predictions," and is generated through Equation (2). The Recall metric "is related to the number of positive events correctly predicted" is achieved using Equation (3). The F1 metric "is known as the harmonic mean between precision and recall", is computed with Equation (4).

$$Accuracy = \frac{TP+TN}{TP+TN+FP+FN} \quad (1)$$

$$Precision = \frac{TP}{TP+FP} \quad (2)$$

$$Recall = \frac{TP}{TP+FN} \quad (3)$$

$$F1 = \frac{2\cdot(precisión\cdot recall)}{precisión+recall} \quad (4)$$

Where:

TP: True positives
TN: True negatives
FP: False positives
FN: False negatives

II.3 MULTI-CRITERIA DECISION MAKING

Multicriteria Decision Making (MCDM) is related to the treatment of decision problems in which more than one decision criterion is present to be considered for choosing the best option, within a group of alternatives [14]. MCDM is divided into two: multi-objective decision making (MODM), and multi-attribute decision making (MADM). Typically, MODM has an explicit goal and a continuous decision space, while MADM has an implicit goal and a discrete decision space [15].

The multi-attribute decision problem can be represented by its decision matrix of M rows and N columns. The element a_{ij} of this matrix shows the performance of the alternative A_i when evaluated by the decision criterion C_j, (i = 1, 2, 3, ..., M, and j = 1, 2, 3, ..., N). Each of the criteria has a relative importance weight wj, which is generally determined by the "decision maker". This is how, given a set of alternatives and decision criteria, we seek to establish the optimal alternative with the highest degree of "desirability" with respect to the decision criteria [16].

Ishizaka & Nemery [17] mention the taxonomy of decision problems proposed by Roy in 1981, that is: selection problems, classification problems, hierarchy problems, and description problems. In this research, the selection problem is addressed, in which the goal is to select the best alternative, according to a set of predetermined criteria. Similarly, we work with the Simple Additive Weighting (SAW) multi-criteria technique, also known as the weighted sum method, which is one of the simplest and most used decision-making methods [18]. It consists of four steps: preparing the decision matrix (M×N), preparing the normalized decision matrix, calculating the magnitude that represents the performance of each alternative, and ranking the alternatives according to their performance to select the best of them.

To generate the matrix of the second step, each of its components must be normalized using Equation (5) if it is a cost criterion, and Equation (6) if it is a benefit criterion. Likewise, to obtain the magnitude S_i of alternative i, mentioned in the third step, Equation (7) must be used.

$$\widetilde{a_{ij}} = \frac{\min a_{ij}}{a_{ij}} \quad (5)$$

$$\widetilde{a_{ij}} = \frac{a_{ij}}{\max a_{ij}} \quad (6)$$

$$S_i = \sum_{j=1}^{N} w_j \cdot \widetilde{a_{ij}} \quad (7)$$

III. MATERIALS AND METHODS

To analyze the data, the stages that make up a typical data science project were followed. These stages are establishment of the project objective(s), search for the data to be used, data processing, exploratory data analysis, data modeling, and decision making [19]. Figure 1 presents a diagram of the stages followed in the methodology.

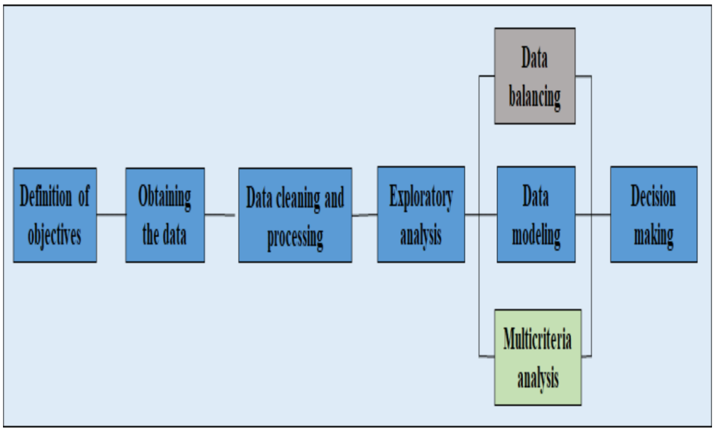

Figure 1: Research methodology.
Source: Authors, (2024).

The objective is to determine the time of occurrence of the maximum demand in a geographic area. The data is obtained from external and/or internal sources, in this case they correspond to the measurements of the maximum and minimum electrical demand, and their times of occurrence, for the area under study. Once the data is obtained, it usually must be cleaned and processed, applying the techniques described in [20]. For the exploratory data analysis, graphical and non-graphical descriptive statistics techniques are used, and from this analysis significant information could be obtained from the data. Modeling is then done using machine learning algorithms. Specifically, classification algorithms are used to forecast the time at which peak demand will occur in the coming days. With the results obtained in the two previous stages, we proceed to the decision-making stage. The stages mentioned so far, corresponding to the blue blocks in Figure 1, are typical of a data science project. In this research, a balancing stage is incorporated, since the data used is unbalanced and this characteristic affects the result returned by the models. Likewise, the multi-criteria analysis stage is incorporated to select the optimal classification model that is used to predict the time of occurrence of the maximum demand.

All the stages just presented are developed using the Python programming language and its respective libraries.

III.1 DATA CLEANING AND PROCESSING

The original data consists of the historical time series of the maximum hourly demand for the period 2021-2024 of a South American country. This series is processed to generate a time series with daily resolution, which contains the maximum demand of the day, the time at which this demand occurs, the minimum demand for the day, and the time at which this minimum demand occurs.

Additionally, the series includes the year, month, week, and day of the week. This daily time series includes information on holidays and working days, as well as a column for the maximum ambient temperature, and another for the average ambient temperature.

Considering the column of the months of the year, a column is created that indicates whether the corresponding day belongs to the historical rainy period or the historical drought period, since during the drought period the ambient temperature increases, and consequently the electricity demand grows, somehow affecting the time of occurrence of this demand.

Finally, from the peak demand hour column, a column is created that indicates whether for the respective day, the peak demand hour belongs to the afternoon hours (around 2 pm) or belongs to the hours of the night (around 8 pm).

IV. RESULTS AND DISCUSSIONS

This section analyzes the results obtained in the exploratory data analysis and data modeling stages.

IV.1 EXPLORATORY DATA ANALYSIS

First, it is important to determine the distribution of hours of maximum demand throughout the 2021-2024 study period, which is presented in Figure 2.

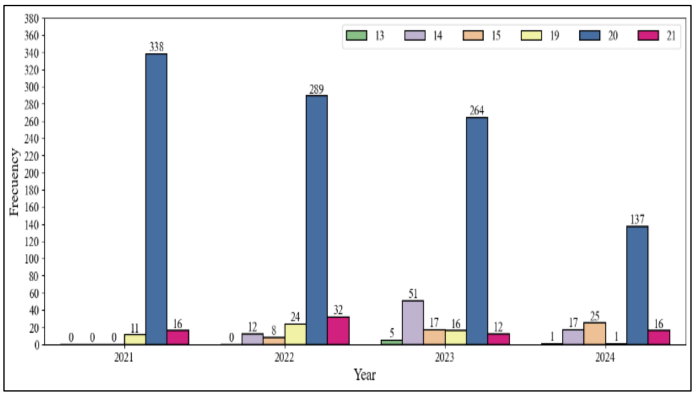

Figure 2: Distribution of hours of maximum demand per year.
Source: Authors, (2024).

From Figure 2, during 2021, the hours of maximum demand were all at night (hours 19, 20, and 21 of the day), which makes sense since in that year there was a greater presence of teleworking due to the pandemic. Likewise, for the entire period the time of maximum demand was mostly 8 pm, and that starting in 2022 the afternoon hours began to have a certain presence in the data on the time of maximum demand.

On the other hand, Figure 3 shows the distribution of the hours of maximum demand for each of the months of the year. It is observed that during the months of the last third of the year, 7 pm as the time for maximum demand has the greatest incidence, while until the month of August its presence is almost non-existent. Additionally, it is noted that the hours of maximum daytime demand intensify from the month of June until the month of October.

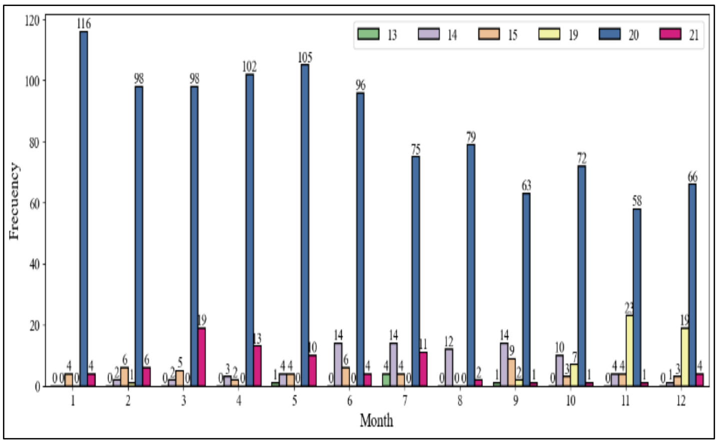

Figure 3: Distribution of hours of maximum demand per year.
Source: Authors, (2024).

Likewise, it is of interest to determine the distribution of the hours of maximum demand by weekday, which is presented in Figure 4. In this case, Monday is represented by the number “1”, and Sunday is represented with the number “7”.

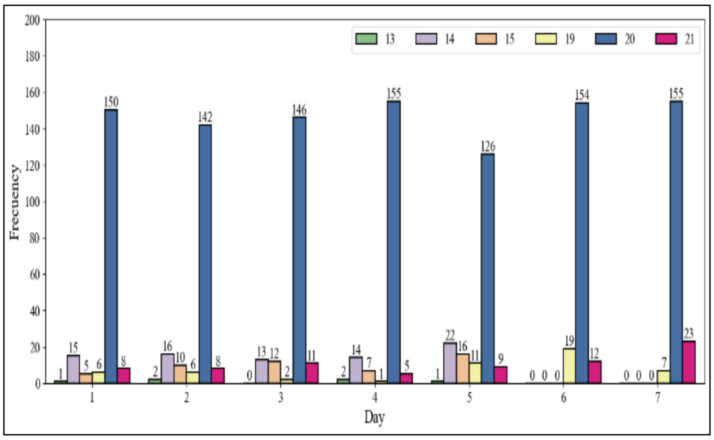

Figure 4: Distribution of hours of maximum demand by day.
Source: Authors, (2024).

It can be noted that, on Saturdays and Sundays, the hours of maximum demand correspond only to nighttime hours. On the other hand, it is observed that Fridays (day 5) are the days on which there are more hours of maximum demand during the afternoon, and they are also the days on which fewer hours of maximum demand coincide with 8 pm.

Additionally, Figure 5 presents the distribution of hours of maximum demand according to the type of day, to compare the behavior of weekdays with holidays and weekends. During weekdays 8 pm predominates, and 15.4% of the hours of maximum demand occur during the afternoons. The behavior of holidays is like that of Saturdays and Sundays, with 100% of the hours of maximum demand during the night and with a proportion of around 80% of the hours coinciding with 8 pm.

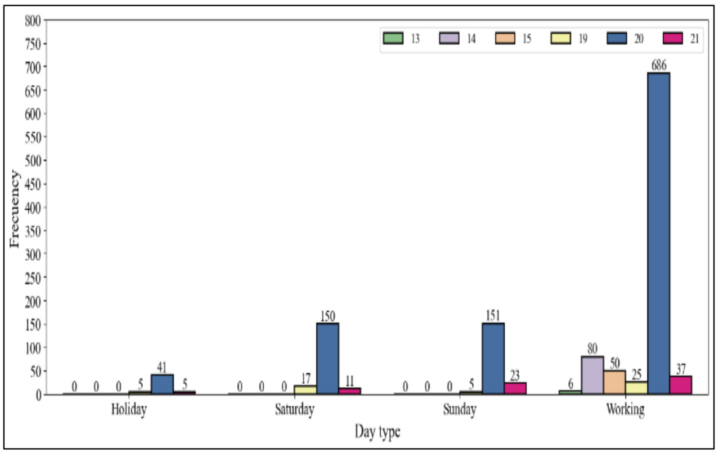

Figure 5: Distribution of hours of maximum demand by type of day.
Source: Authors, (2024).

IV.2 DATA MODELING

Next, the data modeling is presented to estimate the time of occurrence of the maximum electrical demand, for which supervised machine learning classification algorithms are used: K nearest neighbors, random forests, support vector machine, and logistic regression. In [21] the same classification algorithms are used to estimate the performance ratio of a solar PV plant, which also corresponds to a binary classification problem.

In this research, use is made of the daily maximum electricity demand data for the period 2023-2024, until 07/14/2024, to generate and train the models, and the remaining seventeen days until 07/31/2024 are used. to recalculate the performance evaluation metrics of said models. Likewise, data balancing techniques are used in combination with each of the models, since as observed in the exploratory analysis of the data, they are unbalanced around 8 pm, the time of maximum maximum demand. Specifically, the SMOTE-NC method was used, which is convenient when there is a data set with both numerical variables and categorical variables.

For each of the models, the data set was divided into two parts: training and testing, with a proportion of 80% for training and 20% for testing. Two possible times are considered: 2 pm and 8 pm, both with a variation of more or less one hour.

IV.2.1 RANDOM FOREST ALGORITHM

This is an algorithm that uses the bagging technique, which means aggregation by resampling, involving the manipulation of the training data set with resampling. From the training data set, multiple data sets are generated for training, and classification models are generated from each of them [22]. By having the classification models, predictions are made with each of them and the results are combined by taking the majority vote, that is, the result that is most repeated in the case of classification problems [23].

For the parameterization of the model, the number of estimators was set at 150, and to measure the quality of the forest the "gini" metric was used. To evaluate the model, the metrics were used: Accuracy, Precision, F1, and Recall. Table 1 shows the results obtained from the evaluation of the model in the testing phase.

Subsequently, the model is used to estimate the hour of maximum demand for the following seventeen days, from July 15 to 31, considering two options: 2 pm and 8 pm, both classes with a tolerance of 1 hour, that is, a range from 1 pm to 3 pm (13_14_15), and the other range from 7 pm to 9 pm (19_20_21). The results are compared with the actual values, and the new values of the evaluation metrics are presented in Table 2, while the estimated hours are presented in Table 3.

IV.2.2 K NEAREST NEIGHBORS ALGORITHM

This is an algorithm that is used both to generate regression and classification models, and falls within the category of supervised machine learning, and is also non-parametric [24]. However, the basic principle of this algorithm is to consider elements that are similar to each other (closest neighbors), so it is required to previously know the number of neighbors K to take into account. There are several methods to obtain the value of K, for example, [25] propose using cross-validation techniques. In our case, the optimal value of K was obtained by plotting the number of nearest neighbors versus accuracy, and the value of K that maximized this metric was selected. After evaluating the model in the testing phase, the values of the metrics presented in Table 1 were obtained.

Next, the model is used to estimate the hour of maximum demand for the period from July 15 to 31, considering two options: 2 pm and 8 pm, both classes with a tolerance of 1 hour, that is, a range from 1 pm to 3 pm, and the other range from 7 pm to 9 pm. The results are presented in Tables 2 and 3.

IV.2.3 SUPPORT VECTOR MACHINE ALGORITHM

Like the previous models, support vector machines can be used for both classification problems and regression problems, using the same operating principle. This algorithm uses the concept of kernel to convert the given data into a higher dimension, to achieve the so-called hyperplanes. The points located on each side of the hyperplane and that are closest to it are known as support vectors. There are four main types of kernels, namely linear, polynomial, sigmoid and radial basis function [26].

For our case study, the support vector classifier is used, and its default parameters are considered, which includes a radial basis function kernel. The trained model is used to make the forecast from the test data, and the results obtained are evaluated through the corresponding metrics. The metric values are presented in Table 1.

Next, the model is used to estimate the hour of maximum demand for the period from July 15 to 31, considering two options: 2 pm and 8 pm, both classes with a tolerance of 1 hour, that is, a range from 1 pm to 3 pm, and the other range from 7 pm to 9 pm. The results are presented in Tables 2 and 3.

IV.2.4 LOGISTIC REGRESSION ALGORITHM

Through the application of this algorithm, models for binary classification can be generated. According to [27], this technique "Is one of the most used linear statistical models for discriminant analysis." After performing a linear regression, the algorithm converts the output of this regression through a logistic function (hence its name), which is commonly the sigmoid function. This last function assigns a conditional probability for each of the classes. When applying this algorithm, all default parameters were taken, which included the Limited-memory Broyden, Fletcher, Goldfarb, and Shanno (lbgfs) optimization method. As was done with the other algorithms, the trained model is used to make predictions using the test set, and it was evaluated considering the corresponding metrics, whose values are presented in Table 1.

As with the previous models, Tables 2 and 3 present the results obtained after using the model to estimate the time of maximum demand for the period from July 15 to July 31.

Table 1: Metric results in the testing phase.

Metric	K-NN	RF	SVC	LR
Accuracy	0.765	0.844	0.777	0.737
Precision	0.793	0.848	0.807	0.735
F1	0.761	0.843	0.769	0.726
Recall	0.770	0.843	0.772	0.723

Source: Authors, (2024).

From Table 1 it can be noted that the random forest algorithm was the one that had the best performance according to the evaluation metrics considered. From Table 2 it can be noted that the K-NN and SVC algorithms were the best evaluated according to the metrics used.

Table 2: Metric results with new data.

Metric	K-NN	RF	SVC	RL
Accuracy	0.882	0.823	0.882	0.824
Precision	0.882	0.875	0.882	0.826
F1	0.882	0.813	0.882	0.824
Recall	0.882	0.813	0.882	0.826

Source: Authors, (2024).

In the same order of ideas, Table 3 presents the estimates of the time of maximum demand. It can be noted that using the K-NN model, the actual time of maximum demand was within the estimated range on 15 of the 17 days analyzed, as was the SVC model. In the case of the RF and RL models, the success was on 14 of the 17 days.

Table 3: Maximum demand hour estimation results.

Date	Actual time	K-NN	RF	SVC	RL
7/15/2024	14	13_14_15	19_20_21	13_14_15	13_14_15
7/16/2024	20	19_20_21	19_20_21	19_20_21	13_14_15
7/17/2024	15	13_14_15	19_20_21	13_14_15	13_14_15
7/18/2024	15	19_20_21	19_20_21	19_20_21	19_20_21
7/19/2024	20	13_14_15	19_20_21	13_14_15	13_14_15
7/20/2024	20	19_20_21	19_20_21	19_20_21	19_20_21
7/21/2024	20	19_20_21	19_20_21	19_20_21	19_20_21
7/22/2024	14	13_14_15	13_14_15	13_14_15	13_14_15
7/23/2024	15	13_14_15	13_14_15	13_14_15	13_14_15
7/24/2024	20	19_20_21	19_20_21	19_20_21	19_20_21
7/25/2024	14	13_14_15	13_14_15	13_14_15	13_14_15
7/26/2024	14	13_14_15	13_14_15	13_14_15	13_14_15
7/27/2024	20	19_20_21	19_20_21	19_20_21	19_20_21
7/28/2024	20	19_20_21	19_20_21	19_20_21	19_20_21
7/29/2024	13	13_14_15	13_14_15	13_14_15	13_14_15
7/30/2024	20	19_20_21	19_20_21	19_20_21	19_20_21
7/31/2024	20	19_20_21	19_20_21	19_20_21	19_20_21

Source: Authors, (2024).

IV2.5 MULTI-CRITERIA MODEL SELECTION

The SAW method is used to select the best model. The decision criteria to consider are Accuracy and F1, obtained in the testing phase, Accuracy and F1 obtained with new data, and the number of days that the respective model guessed correctly the time of maximum demand. The alternatives of the decision problem are the four models considered: K-NN, RF, SVC, and RL. The normalized decision matrix is shown in Table 4.

Table 4: Normalized decision matrix.

Decision alternatives	Decision criteria				
	Accuracy test	F1 test	Accuracy new	F1 new	Days of success
K-NN	0.906	0.903	1.000	1.000	1.000
RF	1.000	1.000	0.933	0.922	0.933
SVC	0.921	0.912	1.000	1.000	1.000
RL	0.873	0.861	0.934	0.934	0.933

Source: Authors, (2024).

After calculating the magnitudes of each of the alternatives, and ranking them from highest to lowest, the results presented in Table 5 are obtained, from which it is deduced that the optimal classification model is the one derived from the support vector machine algorithm (SVC), followed by the K-nearest neighbors (K-NN) model.

Table 5: Model hierarchy.

Model	S_i
SVC	0.982
K-NN	0.979
RF	0.945
RL	0.919

Source: Authors, (2024).

V. CONCLUSIONS

A methodology is presented that allows estimating the time of occurrence of the maximum electrical demand, using the optimal classification model, which was selected using multicriteria decision-making analysis. Within the methodology, a stage is included to balance the classes. After applying the weighted sum multicriteria decision-making method, it was obtained that the model derived from the support vector machine algorithm is optimal for estimating the time of occurrence of the maximum electrical demand. When evaluating the models with new data, this model correctly predicted the time of occurrence on 15 of the 17 days considered. According to historical data, the time of occurrence is in the afternoon around 2 pm, or at night around 8 pm. There is an imbalance in these hours of occurrence, with a clear tilt towards 8 pm, with a ratio of 75/25 with respect to all other hours for the period 2021-2024, and a ratio of 88/12 in the hours of occurrence. occurrence of the night with respect to the hours of the day, for the same study period.

VI. AUTHOR’S CONTRIBUTION

Conceptualization: César Yajure.
Methodology: César Yajure.
Investigation: César Yajure.
Discussion of results: César Yajure.
Writing – Original Draft: César Yajure and Valesca Fuenzalida.
Writing – Review and Editing: César Yajure and Valesca Fuenzalida.
Resources: César Yajure.
Supervision: César Yajure.
Approval of the final text: César Yajure.

VIII. REFERENCES

[1] Y. Xie, «Peak Load Hour Prediction,» 01 01 2022. [En línea]. Available: https://exergyenergy.com/wp-content/uploads/2022/01/Peak-load-Prediction-White-Paper.pdf.

[2] C. Candia, «ENERLINK,» 10 Julio 2024. [En línea]. Available: https://blog.enerlink.com/las-claves-del-cobro-de-demanda-en-horas-punta. [Último acceso: 10 Julio 2024].

[3] J. Torriti, «Understanding the timing of energy demand through time use data: Time of the day dependence of social practices,» Energy Research and Social Science, pp. 37-47. https://doi.org/10.1016/j.erss.2016.12.004, 2017.

[4] P. Bovornkeeratiroj, J. Wamburu, D. Irwin y P. Shenoy, «PeakTK: An Open Source Toolkit for Peak Forecasting in Energy Systems,» de Computing and Sustainable Societies, Seattle, WA, USA, 2022.

[5] T. Fu, H. Zhou, X. Ma, Z. J. Hou y D. Wu, «Predicting peak day and peak hour of electricity demand with ensemble machine learning,» Frontiers in Energy Research, pp. 1-11. https://doi.org/10.3389/fenrg.2022.944804, 2022.

[6] J. Liu y L. E. Brown, «Prediction of Hour of Coincident Daily Peak Load,» de IEEE Power & Energy Society Innovative Smart Grid Technologies Conference, Washington DC, USA , 2019.

[7] V. Voronin, F. Nepsha y M. Krasilnikov, «Short term forecasting peak load hours of regional power systems using machine learning methods,» CIGRE Science & Engineering (CSE), pp. 1-18, 2023.

[8] R. Carmona, X. Yang y C. Zeng, «Coincident Peak Prediction for Capacity and Transmission Charge Reduction,» arXiv:2407.04081, p. https://doi.org/10.48550/arXiv.2407.04081, 2024.

[9] A. Soman, A. Trivedi, D. Irwin, B. Kosanovic, B. McDaniel y P. Shenoy, «Peak Forecasting for Battery-based Energy Optimizations in Campus Microgrids,» de e-Energy '20: Proceedings of the Eleventh ACM International Conference on Future Energy Systems, Virtual, 2020.

[10] D. L. Donaldson, J. Browell y C. Gilbert, «Predicting the magnitude and timing of peak electricity demand: A competition case study,» IET Smart Grid, pp. 1-12. https://doi.org/10.1049/stg2.12152, 2023.

[11] A. Babajide Ebenezer1, O. Boyinbode y M. I. Oladunjoye, «A Comprehensive Analysis of Handling Imbalanced Dataset,» International Journal of Advanced Trends in Computer Science and Engineering, pp. 454-463. https://doi.org/10.30534/ijatcse/2021/031022021, 2021.

[12] T. Wongvorachan, S. He y O. Bulut, «A Comparison of Undersampling, Oversampling, and SMOTE Methods for Dealing with Imbalanced Classification in Educational Data Mining,» Information MDPI, pp. 4-15. https://doi.org/10.3390/info14010054, 2023.

[13] W. M. Lee, Python Machine Learning, Indianapolis: John Wiley & Sons, Inc., 2019.

[14] C. A. Yajure-Ramírez, «Enfoque multicriterio para la selección óptima de variables explicativas para modelos de pronóstico de la energía eléctrica de plantas solares fotovoltaicas,» Revista Tecnológica - Espol, pp. 83-98. https://doi.org/10.37815/rte.v35n3.1045, 2023.

[15] F. Eltarabishi, O. H. Omar, I. Alsyouf y M. Bettayeb, «Multi-Criteria Decision Making Methods And Their Applications– A Literature Review,» de Proceedings of the International Conference on Industrial Engineering and Operations Management, Dubai, UAE, 2020.

[16] E. Triantaphyllou, B. Shu, S. Nieto Sanchez y T. Ray, «Multi-Criteria Decision Making: An Operations Research Approach,» Encyclopedia of Electrical and Electronics Engineering, pp. 175-186., 1998.

[17] A. Ishizaka y P. Nemery, Multi-Criteria Decision Analysis - Methods and Software, West Sussex, United Kingdom: John Wiley & Sons, Ltd, 2013.

[18] H. Taherdoost, «Analysis of Simple Additive Weighting Method (SAW) as a Multi-Attribute Decision-Making Technique: A Step-by-Step Guide,» Journal of Management Science & Engineering Research, pp. 21-24. DOI: https://doi.org/10.30564/jmser.v6i1.5400, 2023.

[19] D. Cielen, A. D. B. Meysman y M. Ali, Introducing Data Science, Shelter Island, NY: Manning Publications Co., 2016.

[20] S. K. Mukhiya and U. Ahmed, Hands-On Exploratory Data Analysis with Python, Birmingham, UK: Packt Publishing Ltd., 2020.

[21] C. A. Yajure Ramírez, «Selección del modelo óptimo de predicción de la relación de desempeño de una planta solar fotovoltaica. Un enfoque multicriterio basado en algoritmos de aprendizaje automático,» Ciencia, Ingenierías y Aplicaciones INTEC, pp. 7-29. DOI: https://doi.org/10.22206/cyap.2023.v6i2.2935, 2023.

[22] J. Rogel-Salazar, Data Science and Analytics with Python, Boca Raton, FL: CRC Press Taylor & Francis Group, 2017.

[23] E. Russano y E. Ferreira Avelino, Fundamentals of Machine Learning Using Python, Oakville, Canadá: Arcler Press, 2020.

[24] M. E. Fenner, Machine Learning with Python for Everyone, Boston: Pearson Education, Inc., 2020.

[25] M. Maleki, N. Manshouri y T. Kayıkçıoğlu, «A Novel Simple Method to Select Optimal k in k-Nearest Neighbor Classifier,» International Journal of Computer Science and Information Security, pp. 464-469, 2017.

[26] R. Muthukrishnan y M. Jamila. S, «Predictive Modeling Using Support Vector Regression,» International Journal of Scientific & Technology Research, pp. 4863-4865., 2020.

[27] K. Kirasich, T. Smith y B. Sadler, «Random Forest vs Logistic Regression: Binary Classification for Heterogeneous Datasets,» SMU Data Science Review, p. https://scholar.smu.edu/datasciencereview/vol1/iss3/9, 2018.

Journal of Engineering and Technology for Industrial Applications

ITEGAM-JETIA

ISSN ONLINE: 2447-0228

Manaus, v10. n.50, p. 196-201. November/ December., 2024.
DOI: https://doi.org/10.5935/jetia.v10i50.1315

RESEARCH ARTICLE OPEN ACCESS

AN OVERVIEW OF IMPROVING LOGISTICS PROCESSES IN HEALTH FACILITIES: ISSUES, SOLUTIONS, AND CHALLENGES

Zdenek Smutny[1] and Katerina Svandova[2]

[1,2] Faculty of Informatics and Statistics, Prague University of Economics and Business, Prague, Czech Republic.

[1]http://orcid.org/0000-0002-6646-2991, [2]http://orcid.org/0009-0005-1664-3312

Email: zdenek.smutny@vse.cz, katerina.svandova@vse.cz

ARTICLE INFO

Article History
Received: September 29, 2024
Revised: October 15, 2024
Accepted: November 10, 2024
Published: December 31, 2024

Keywords:
Business process reengineering,
Healthcare,
Hospital,
Information technology,
RFID,
UWB.

ABSTRACT

Internal logistics processes in health facilities are complex and important to ensure health services and high-quality patient care. Therefore, the review is focused on issues, solutions and challenges related to logistic processes in health facilities. This review follows the PRISMA guidelines. Relevant studies were searched in the citation databases Web of Science and Scopus. The search was limited to articles published in English between 2000 and 2023. Based on the search and selection process, a total of 26 articles were included in the review. A qualitative content analysis was carried out. In this period analytical research dominates over design research. In terms of research strategies, a qualitative approach is preferred. The problem contexts addressed in the articles have been divided into five thematic areas. Most articles can be classified in the area dealing with sociotechnical interaction in internal logistics. The solutions presented in found articles can be divided according to the type of artefact into (1) formal approaches focused on models and algorithms, and (2) sociotechnical approaches focused on design of implementation frameworks. Challenges include the comparison of proposed solutions or their configurations in different problem contexts and regions. Further research should focus on organisational issues in internal logistics. Although the improvement of internal logistics in health facilities is a topic that has seen an increase in researcher interest over the last decade, there is a need to build a theoretical base on the findings of this research, which has been done only to a very limited extent. In terms of the use of new technologies, high persistence in the use of older IT-based solutions and rigidity can be observed in the implementation of new solutions.

I. INTRODUCTION

Internal logistics processes in health facilities are complex and important to ensure health services and high-quality patient care [1]. These processes can be improved through organisational changes, introducing new technological solutions or modifying procedures. To support processes in health facilities, information technology (IT) is very often implemented and must be used properly by healthcare staff. If ITs is not set up correctly in the organisation or if this set-up is circumvented, it can have negative consequences for the organisation. Not only in the healthcare industry, setting up the social and technical components of a sociotechnical system constitutes a challenge [2]. The diverse and extensive (sociotechnical) logistics systems and associated processes that are used in a particular health facility, increase the complexity of health and logistics management.

Properly configured internal logistics processes in health facilities can provide benefits, including but not limited to increased patient safety in medication administration, improved patient care, or reduced healthcare and healthcare facility operating costs [3]. Healthcare facilities are following the lead of manufacturing firms by applying approaches such as lean, business process reengineering, benchmarking [4] or deploying advanced systems based on IT and mathematical models to optimise these processes. The above underlines the relevance and importance of the topic of internal logistics processes.

Therefore, it is appropriate to prepare an overview that will address the issues, solutions and challenges related to logistics processes in health facilities over the last two decades. Before that, however, it is necessary to determine whether a similarly focused review article has not been published in the last decade.

Based on the keywords in the Methods and Materials section focusing on review articles, no thematically related or similarly focused overview was found in the Web of Science (WoS) and Scopus citation databases. Rather, review articles focus on benefits and critical success factors [5] or the importance of measuring internal logistics performance in hospitals [3]. It is therefore reasonable to prepare an overview that addresses the issues, solutions and challenges related to logistics processes in health facilities over the last more than two decades. An overview of such focus is beneficial for scholars who will be able to better navigate this topic area and further enable them to focus their analytical or design research on relevant areas and link it to other scholarly literature.

The article aims to review the issues, solutions, and challenges related to logistic processes in health facilities. Therefore, the authors focused on identifying problem contexts addressed in the thematically relevant articles, proposed technological solutions and challenges for future research. The following research questions (RQ) were proposed:

- RQ 1: What are the problem contexts addressed in the articles?
- RQ 2: What are the proposed technological solutions for solving problem contexts?
- RQ 3: What are the challenges for future research?

Answers to these research questions are beneficial for managers in health facilities as well as scholars who focus their research on improving logistics processes in health facilities. Managers get an overview of issues and types of proposed solutions. Scholars will find out what areas of research are covered and how much and what further research efforts are needed.

II. MATERIALS AND METHODS

This review was prepared according to PRISMA guidelines [6] and did not require ethics or institutional review board approval because data were collected by reviewing published peer-reviewed journal articles and papers from conference proceedings. The authors focused on international citation databases Web of Science and Scopus and the period from 2000 to 2023. Databases were searched on February 10, 2024, and only papers available in English were included. The keywords and queries used for searching databases are listed in Table 1.

Table 1: Search strategy in citation databases.

Citation databases	Used keywords / Query strings
Web of Science	"logistic process" OR "logistical process" (Topic) and "hospital" OR "clinic" OR "health facility" OR "healthcare center" OR "healthcare centre" (Topic)
Scopus	TITLE-ABS-KEY (("logistic process" OR "logistical process") AND ("hospital" OR "clinic" OR "health facility" OR "healthcare center" OR "healthcare centre"))

Source: Authors, (2024).

The searched articles were imported to the web-tool Rayyan (www.rayyan.ai) where the selection according to the abstract was carried out. Duplicate entries were removed. In the case of higher content matching, the source that most comprehensively summarized the given topic was selected based on the evaluation of the full text – an example could be the publication of a conference paper and an extended article in a journal. In that case, only the journal article was selected. Screening was conducted by examining the abstract in terms of inclusion criteria in Table 2 and defined research questions. The full text was used where it was impossible to decide on inclusion or exclusion based on the abstract.

Table 2: Inclusion and exclusion criteria.

Criterion	Inclusion	Exclusion
Type of article	Research journal article or conference paper	Any type of review, conference abstract or editorial material
Period	1 January 2000 to 10 February 2024	Before 1 January 2000 and after 10 February 2024
Language	English	All other languages
Research topic	Analytical and design research focused on improving logistics processes in health facilities	Any other
Multiple versions	Latest version	Previous versions

Source: Authors, (2024).

Inclusion in the review was verified based on full-text examination by both authors (Z.S. and K.S.) in mutual cooperation. Analytical and design-oriented articles relevant to the focus of this article were included. Figure 1 presents a flow diagram of the selection process. A complete list of all included papers can be found in the Appendix and supplementary material [7].

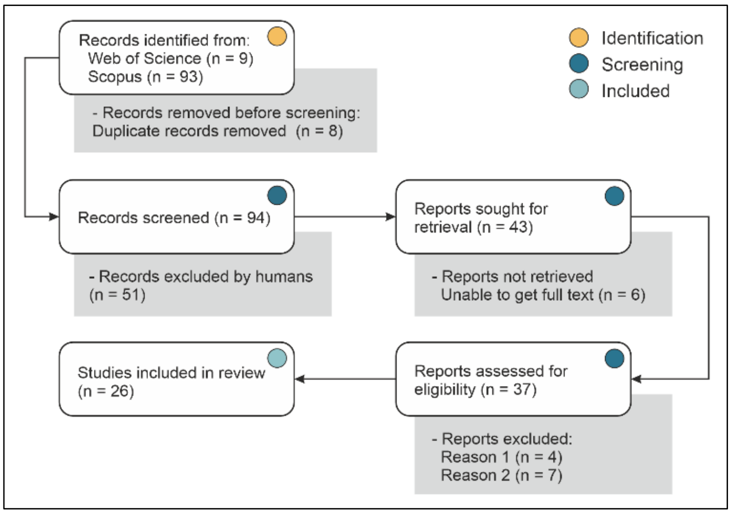

Notes: Reason 1: Several almost identical articles based on the same data were found. The paper that offered more detailed results was selected for the authors' overview. Reason 2: The article is not thematically relevant in its focus.

Figure 1: Flow diagram of the systematic review.
Source: Authors, (2024).

The information found was entered into a pre-prepared form, which included the following information: authors, year of publication, title of the work, country (first author's country of origin), research methodology, identified issues or article aim, technological solution of the problem context, results, and challenges for future work (see Appendix). A qualitative analysis of content was carried out to interpret text data through the systematic classification process.

III. RESULTS

Based on the search and selection process, a total of 26 papers were included in the review. Almost half of the articles were published in the last 5 years (2019–2023) and 21 articles in the last decade (2014-2023) as can be seen from Figure 2. From this, it can be concluded that the importance of this field has been increasing, especially in the last decade. As regards the first author's affiliations, authors from universities in Europe dominate (13 papers), followed by North America (6 papers), Asia (5 papers), and South America (2 papers). Thus, supporting the logistics processes of healthcare facilities is a topic that resonates especially in developed countries. Such countries have the financial resources to analyse and implement smart solutions in these facilities as well as the relevant research capacity.

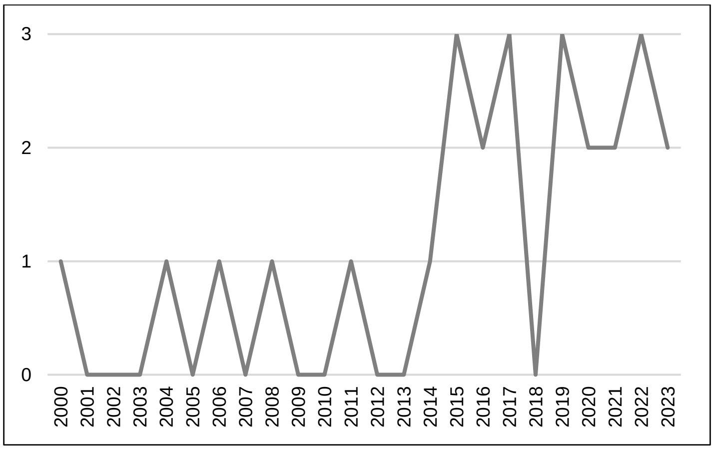

Figure 2: Distribution of the number of articles in individual years (N=26).
Source: Authors, (2024).

As regards the type of research, analytical research (17 papers) dominates over design research (9 papers) where artefacts/solutions are proposed. In terms of research approach, qualitative methods (16 papers) dominate over quantitative methods (10 papers). For this distribution, papers with design research were classified under solution evaluation; simulation and modelling were classified under quantitative approach; and mixed method studies were classified under qualitative approach. The quantitative approach was dominated by simulation and modelling, and the qualitative approach by case studies.

Furthermore, this section is divided into three thematic areas due to the focus of the paper. This involves identification of the problem contexts addressed in the articles, the proposed technological solutions and the challenges for future research.

III.1 PROBLEM CONTEXTS ADDRESSED IN THE ARTICLES

Most of the analytical and design-oriented articles address specific problem contexts associated with a particular health facility or institutional context in a given region. This is matched by the use of case studies as the main research strategy in 10 articles and the dominance of the use of qualitative research methods. Thematically, the authors divided the articles into five areas and an example was selected for each area, see Figure 3.

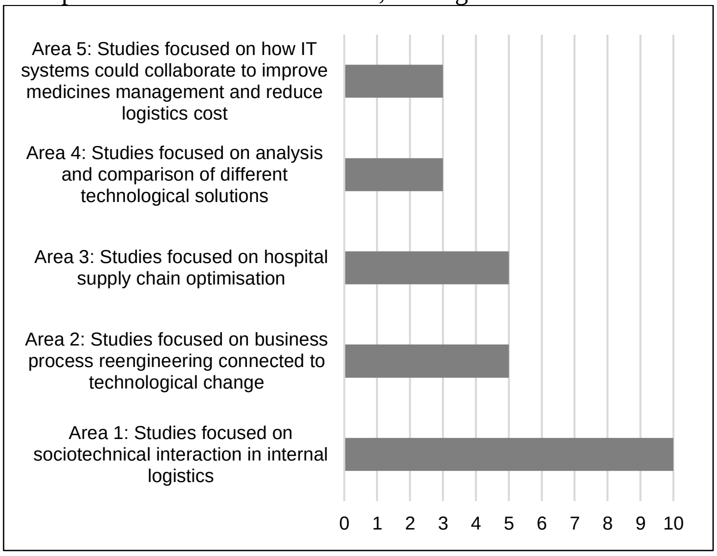

Figure 3: Distribution of the number of articles in identified five problem context areas (N=26).
Source: Authors, (2024).

Area 1: Studies focused on sociotechnical interaction in internal logistics, where 10 papers can be classified. An example is [8], where the authors use a large-scale qualitative analysis of a selected hospital in Brazil and use this to identify seven major problems mainly related to social aspects and information flows.

Area 2: Studies focused on business process reengineering connected to technological change, e.g. the transition from barcodes to Radio Frequency Identification (RFID) technology, where 5 papers can be classified. An interesting example is [9], which compares different configurations and technology combinations usable for track-and-trace systems and discusses the advantages and disadvantages of these configurations.

Area 3: Studies focused on hospital supply chain optimisation, most often using formal models to support managerial decision making, where 5 papers can be classified [3] present a formal logistics performance measurement framework that helps to manage the efficiency of particular logistics processes.

Area 4: Studies focused on analysis and comparison of different technological solutions (e.g. use of different readers) or proof of IT concept, where 3 papers can be classified. Careddaa et al. [10] compare the performance of inlays, fixed and handheld RFID readers in selected supply chain processes.

Area 5: Studies focused on how IT systems could collaborate to improve medicines management and reduce logistics cost, where 3 papers can be classified. [11] focused on identification of the main inefficiencies in internal logistics processes and offers RFID-based solutions to solve these problems.

III.2 PROPOSED SOLUTIONS

Engineering approaches bring solutions to problem contexts in the form of a designed artefact. For the articles found, the artefacts can be divided into two types that highlight two distinct approaches to the solution.

1) Formal approaches focusing on models and algorithms: These solutions are mainly used for decision-making support in logistics management [3], [12], [13], [14]. Most often, it involves modelling and simulation in order to support internal logistics. With the development and new possibilities to automate internal logistics processes, where big data is collected, new opportunities arise to optimise these sociotechnical systems using artificial intelligence approaches and formal models. An example is the creation of an ensemble model combining artificial neural network and particle swarm optimisation [15] in order to reduce the costs of health facilities and increase the serviceability in logistics. The optimisation of autonomous logistics systems is also addressed by the design of an algorithm [16] that aims to solve the fleet sizing and routing problem with synchronisation for automated guided vehicles with dynamic demands.

2) Sociotechnical approaches aiming at designing frameworks: This output represents realistic or conceptual guidelines that serve as support for implementation. The frameworks found describe business process reengineering in the context of RFID implementation [17], [18]. They aim to facilitate the transition of health facilities to RFID, whether this involves stand-alone or hybrid deployments.

However, some papers have looked at instantiating a solution that is already in use in practice [19], [20] in order to improve it – particularly the life cycle of pharmaceutical products. In addition to the aforementioned frameworks focused on business process reengineering, approaches can also be found with respect to a specific solution implementation and focusing on a holistic process view (including processes and activities, organisational structure, technology). An example is a study [21] that aims to reduce the number of errors in the particular logistics warehouse.

III.3 CHALLENGES FOR FUTURE RESEARCH

Improving and optimising logistics processes in health facilities ideally brings two main benefits: improved patient care and reduced costs of operating the health facility. Therefore, even suggestions for future research mention the need to continuously explore the potential of using new IT to improve patient care and to provide more evidence on the appropriateness of using certain metrics to manage logistics processes across process types, organisational boundaries, and regions [3], [19], [22]. This can be achieved by preparing review articles focused on the evaluation and comparison of proposed solutions, especially in the internal logistics of health facilities. These articles can focus on the identification of beneficial and negative factors that influence health care performance aspects [14].

The deployment of IT solutions in this kind of organisations brings certain issues and encounters organisational constraints. Any technological change alters the organisational dynamics and is inherently complex. Therefore, evaluating the economic benefits associated with a particular technological configuration and the cost of adoption in an organisation is also difficult. Therefore, a seemingly never-ending job of hospital managers is to compare different technological configurations and their economic benefits. In this context, for instance, Moatari-Kazerouni and Bendavid [18] suggest conducting a detailed cost analysis to assess the operational cost of implementing the RFID technology for further research. However, any "reduction in the time dedicated to logistics processes or associated errors at the health care departments is a contribution to enhance the health care provided" [21].

In addition to focusing on the technological component of sociotechnical systems in healthcare organisations, it is also necessary to examine the social aspects. Human factors in particular have been little researched in healthcare logistics [22]. Therefore, further research should focus less on technology and more on organisational issues [23]. In particular, papers from the last 5 years highlight the need for a sociotechnical perspective especially in the provision of internal logistics.

The possibilities of processing data collected by different systems in hospitals can also help with the optimisation of logistics processes. To this end, it is advisable to base the design of data processing on “real success cases, and analyse the causal links between the analytics capabilities and the organisational benefits” [23].

In the area of designing models to support managers' decision-making and optimising the hospital supply chain, further research should focus in particular on the comparison of the proposed models [13]. Furthermore, it is advisable to incorporate more into the models both subjective and objective weight assessments of the criteria. In other words, more use of subjective stakeholder ratings could be used as additional criteria or inputs to analytical models for effective decision-support systems [3].

IV. DISCUSSION AND CONCLUSION

The results presented in this overview show the approaches applied to improve logistics processes in health facilities. At least brief focus has been given to the technological aspects where high persistence of the use of previously implemented technologies can be observed.

In particular, the articles mention the use of technologies built on barcodes and RFID for monitoring medical inventories and equipment. At the same time, more advanced technologies can be found such as Ultra-Wide Band (UWB), which not only allows its use in the internal logistics of hospitals, but also in the monitoring of the patient's health condition or their movement inside the building [24], [25]. Although UWB was mentioned two decades ago as a technology to change many sectors including healthcare, this has not yet happened according to the authors' findings. Blockchain is also waiting for its greater deployment in practice, which increases the trustworthiness of the activities performed [26]. The healthcare sector is very rigid in this regard.

It can be stated that some authors [21], [27] focus on errors and issues in the field of logistics processes in health facilities to identify obstacles and barriers to logistic logistics management implementation in the medical supplies department and thereby improve the relevant processes. Nevertheless, no publication that would include in its proposal a solution regarding exception handlings related to the processes of internal logistics of health facilities was found. Exceptions are unexpected or unplanned events that can affect or completely interrupt processes. In a healthcare logistics environment, they can impact quality of care, patient safety, and healthcare costs. This could be, for example, the missing RFID of the medicine when sending it to the department, the failure of the automatic filer of the central pharmacy, or the failure of Wi-Fi during the scanning of the barcode when receiving medicines in the department. Exception handling should, therefore, be part of the analysis of the implementation of new technologies, the preparation of staff training and part of the monitoring after implementation. In the supply chain management environment, exceptions handling is an important part of the proposed track system [28]. For the logistics environment in general, a system proposal was presented to support end users in solving exceptions. The system can also help revise existing processes based on the most frequent exceptions. This is also a promising direction for further research.

In conclusion, there is a rapidly growing interest among researchers in improving internal logistics in health facilities, especially in developed countries. Qualitative approach dominates the research. Nevertheless, theorising and building a theoretical base in this area remains insufficient.

The presented overview also has several limitations. The authors focused only on international citation databases, so a limited number of databases were searched and many regional databases were omitted. At the same time, only papers published in English were included. All these facts could have led to distorted results and conclusions related to the research questions.

V. AUTHOR'S CONTRIBUTION

Conceptualization: Zdenek Smutny and Katerina Svandova.
Methodology: Zdenek Smutny and Katerina Svandova..
Investigation: Zdenek Smutny and Katerina Svandova..
Discussion of results: Zdenek Smutny and Katerina Svandova..
Writing – Original Draft: Zdenek Smutny and Katerina Svandova..
Writing – Review and Editing: Zdenek Smutny and Katerina Svandova
Resources: Zdenek Smutny and Katerina Svandova..
Supervision: Zdenek Smutny and Katerina Svandova..
Approval of the final text: Zdenek Smutny and Katerina Svandova.

VI. APPENDIX

In this Appendix, a list of articles included in this overview is presented in Table A1. The authors also prepared an online appendix, where more details on individual articles regarding the research methodology, identified issues or article aim, technological solution of the problem context, results, and challenges for future work can be found. The online appendix can be found at https://doi.org/10.5281/zenodo.xxx

Table 3: Articles included in the overview.

Authors	**Year**	**Title**	**Country***	**Research type**
Ritchie et al.	2000	The benefits of reverse logistics: the case of the Manchester Royal Infirmary Pharmacy	UK	Analytical research and recommendations
Eymann & Morito	2004	Privacy Issues of Combining Ubiquitous Computing and Software Agent Technology in a Life-Critical Environment	Germany	Analytical research
Fenies et al.	2006	A decisional model for the performance evaluation of the logistic process: application to the hospital supply chain	France	Design research
Jiao et al.	2008	Hospital Linens Inventory Control Re-engineering Based on RFID	China	Design research
Su et al.	2011	Logistics innovation process revisited: insights from a hospital case study	Taiwan	Analytical research
Romero	2014	Improving the Logistics Operations of the Hospital Pharmacy Using a Barcode-Rfid Identification System	Canada	Analytical research
Hargis et al.	2015	Barriers to Administering Intravenous Tissue Plasminogen Activator (tPA) for Acute Ischemic Stroke in the Emergency Department: A Cross-Sectional Survey of Stroke Centers	USA	Analytical research
Pinna et al.	2015	The drug logistics process: an innovative experience	Italy	Analytical research
Romero & Lefebvre	2015	Combining barcodes and RFID in a hybrid solution to improve hospital pharmacy logistics processes	Canada	Analytical research
Dursun	2016	Evaluation of Agile Suppliers Using Fuzzy MCDM Approach	Turkey	Analytical research
Caredda a et al.	2016	RFID technology for blood tracking: An experimental approach for benchmarking different devices	Italy	Analytical research
Moatari-Kazerouni & Bendavid	2017	Improving logistics processes of surgical instruments: case of RFID technology	USA	Analytical research
Longaraya et al.	2017	Using MCDA to evaluate the performance of the logistics process in public hospitals: the case of a Brazilian teaching hospital	Brazil	Analytical research
Feibert et al.	2017	Benchmarking healthcare logistics processes – a comparative case study of Danish and US hospitals	Denmark	Analytical research
Moons et al.	2019	Performance indicator selection for operating room supply chains: An application of ANP	Belgium	Analytical research
Dusseljee-Peute et al.	2019	The Value of Radio Frequency Identification in Quality Management of the Blood Transfusion Chain in an Academic Hospital Setting	Netherlands	Analytical research
Feibert & Jacobsen	2019	Factors impacting technology adoption in hospital bed logistics	Denmark	Analytical research
Ham et al.	2020	Identifying integration and differentiation in a Hospital's logistical system: a social network analysis of a case study	Netherlands	Analytical research
Bygstad et al.	2020	Developing and Organizing an Analytics Capability for Patient Flow in a General Hospital	Norway	Analytical research
Reis et al.	2021	Lessons from a Surgical Center SatelliteWarehouse in a	Brazil	Analytical research

Authors	Year	Title	Country*	Research type
		Large Brazilian Public Hospital		
Sirisawat & Hasachoo	2021	The Exploration and Investigation of Logistics Processes and Barriers for Medical Supplies Department: A case of Thai Public Hospital	Thailand	Analytical research
Lopez et al.	2022	Evaluating interaction between internal hospital supply chain performance indicators: a rough DEMATEL-based approach	Canada	Analytical research
Zhou	2022	The overall framework design of automatic logistics system using a hybrid ANN-PSO model	China, Malaysia hospitals	Design research
Aziez et al.	2022	Fleet Sizing of Healthcare Automated Guided Vehicles	Canada	Design research
Rochaa & Regob	2023	Reorganisation of the internal storage and distribution logistics in a hospital	Europe, Portugal	Exploratory and design research
Cappelle et al.	2023	Automated and Interference-Free Inventory Solution using Energy-Neutral BLE Tags	Belgium	Experimental study and design research

Source: Authors, (2024).

VII. REFERENCES

[1] Moons K, Waeyenbergh G, Pintelon L. Measuring the logistics performance of internal hospital supply chains – A literature study. Omega. 2019;82:205–17.

[2] Guest DE. The sociotechnical approach to work organization. Oxford Research Encyclopedia of Psychology. 2022 Sep 15; doi:10.1093/acrefore/9780190236557.013.905

[3] Moons K, Waeyenbergh G, Pintelon L, Timmermans P, De Ridder D. Performance indicator selection for operating room supply chains: An application of ANP. Operations Research for Health Care. 2019 Dec 1;23:100229.

[4] Feibert, D. C., Andersen, B., & Jacobsen, P. (2017). Benchmarking healthcare logistics processes – a comparative case study of Danish and US hospitals. Total Quality Management and Business Excellence, 30(1–2), 108–134.

[5] Von Eiff W. Quality management - Drug logistic and pharmacotherapy as critical success factors. Krankenhauspharmazie. 2009;30:411-15.

[6] Page MJ, McKenzie JE, Bossuyt PM, Boutron I, Hoffmann TC, Mulrow CD, et al. The PRISMA 2020 statement: an updated guideline for reporting systematic reviews. BMJ 2021;372:n71.

[7] Da Cunha Reis A, Oliveira RP, Ferreira LAF, De Souza CG. Lessons from a Surgical Center Satellite Warehouse in a Large Brazilian Public Hospital. Healthcare. 2021 Mar 8;9(3):297.

[8] Romero A, Lefebvre E. Combining barcodes and RFID in a hybrid solution to improve hospital pharmacy logistics processes. International Journal of Information Technology and Management. 2015 Jan 1;14(2/3):97.

[9] Caredda V, Orrú PF, Romagnoli G, Volpi A, Zedda F. RFID technology for blood tracking: An experimental approach for benchmarking different devices. International Journal of RF Technologies. 2016 Sep 13;7(4):209–28.

[10] Romero A. Improving the logistics operations of the hospital pharmacy using a Barcode-RFID identification system. In: Transactions on Engineering Technologies. 2014; Dordrecht: Springer. p. 733–47.

[11] Alexandre C., Féniès P., Rodier S. A decisional model for the performance evaluation of the logistic process: Application on consultation ambulatory unit of a hospital supply. In: 4th International Industrial Simulation Conference 2006. 2006; EUROSIS. p. 459-63.

[12] Longaray A, Ensslin L, Ensslin S, Alves G, Dutra A, Munhoz P. Using MCDA to evaluate the performance of the logistics process in public hospitals: the case of a Brazilian teaching hospital. International Transactions in Operational Research. 2017 Feb 15;25(1):133–56.

[13] Lopez DS, Garshasbi M, Kabir G, Bari ABMM, Ali SM. Evaluating interaction between internal hospital supply chain performance indicators: a rough-DEMATEL-based approach. International Journal of Productivity and Performance Management. 2021 Aug 13;71(6):2087–113.

[14] Zhou Y. The overall framework design of automatic logistics system using a hybrid ANN-PSO model. Engineering With Computers. 2021 Apr 16;38(S3):2515–31.

[15] Aziez I, Côté JF, Coelho LC. Fleet sizing and routing of healthcare automated guided vehicles. Transportation Research Part E Logistics and Transportation Review. 2022 May 1;161:102679.

[16] Jiao Y-Y., Zhen Y-W., Jiao R-J. Hospital Linens Inventory Control Re-engineering Based on RFID. In: 2008 IEEE Conference on Cybernetics and Intelligent Systems. 2008; IEEE. p. 612-7.

[17] Moatari-Kazerouni A, Bendavid Y. Improving logistics processes of surgical instruments: case of RFID technology. Business Process Management Journal. 2017 Apr 3;23(2):448–66.

[18] Pinna R, Carrus PP, Marras F. The drug logistics process: an innovative experience. The TQM Journal. 2015 Mar 9;27(2):214–30.

[19] Ritchie L, Burnes B, Whittle P, Hey R. The benefits of reverse logistics: the case of the Manchester Royal Infirmary Pharmacy. Supply Chain Management an International Journal. 2000 Dec 1;5(5):226–34.

[20] Rocha LA, Rego N. Reorganisation of the internal storage and distribution logistics in a hospital. Procedia Computer Science. 2023 Jan 1;219:1357–64.

[21] Feibert DC, Jacobsen P. Factors impacting technology adoption in hospital bed logistics. The International Journal of Logistics Management. 2019 Feb 11;30(1):195–230.

[22] Bygstad B, Øvrelid E, Lie T, Bergquist M. Developing and organizing an analytics capability for patient flow in a general hospital. Information Systems Frontiers. 2019 May 4;22(2):353–64.

[23] Jiang S, Skibniewski MJ, Yuan Y, Sun C, Lu Y. Ultra-Wide Band Applications in Industry: A Critical Review. Journal of Civil Engineering and Management. 2011 Sep 20;17(3):437–44.

[24] Pan, J. Medical Applications of Ultra-WideBand (UWB). 2008 Technical Report, Washington University; 2008 [cited 2024 Jul 23]. Available from: https://www.cse.wustl.edu/~jain/cse574-08/ftp/uwb.pdf

[25] Xia X, Lin X, Dong W, He Z. Design of traceability system for medical devices based on blockchain. Journal of Physics Conference Series. 2019 Oct 1;1314(1):012067.

[26] Sirisawat P., Hasachoo N. The Exploration and Investigation of Logistics Processes and Barriers for Medical Supplies Department: A case of Thai Public Hospital. In: Proceedings of the International Conference on Industrial Engineering and Operations Management. 2021; IEOM. p. 2287–93.

[27] Woo SH, Choi JY, Kwak C, Kim CO. An active product state tracking architecture in logistics sensor networks. Computers in Industry. 2009 Apr 1;60(3):149–60.

[28] Montani S. Prototype-based management of business process exception cases. Applied Intelligence. 2009 Feb 9;33(3):278–90..

Journal of Engineering and Technology for Industrial Applications

ITEGAM-JETIA

ISSN ONLINE: 2447-0228

Manaus, v10. n.50, p. 202-210. November/ December., 2024.
DOI: https://doi.org/10.5935/jetia.v10i50.1324

RESEARCH ARTICLE OPEN ACCESS

IMPLEMENTATION OF IOT IN IMPROVING THE EFFICIENCY OF HOSTAGE RELEASE OPERATIONS WITH THE QHBM METHOD

Dekki Widiatmoko[1], Kasiyanto[2], and Mokhammad Syafaat[3]

[1,2,3] Department of Electrical Engineering, Faculty of Enggineering, Army Polytechnic, Batu, East Java, Indonesia.

[1]http://orcid.org/0009-0009-8510-3925, [2]http://orcid.org/0009-0008-6483-5900, [3]http://orcid.org/0009-0001-6675-912X

Email: dekki101067@gmail.com, kasiyanto@poltekad.ac.id, syafaatarh96@poltekad.ac.id

ARTICLE INFO

Article History
Received: October 08, 2024
Revised: October 30, 2024
Accepted: November 10, 2024
Published: December 31, 2024

Keywords:
Internet of Things,
IoT,
Queen Honey Bee Migration,
QHBM,
Hostage Release Operations.

ABSTRACT

In an increasingly complex security context, hostage release operations require innovative strategies to improve efficiency and safety. This article discusses the application of Internet of Things (IoT) technology and the Queen Honey Bee Migration (QHBM) method in improving the effectiveness of these operations. Conventional methods often face drawbacks, such as a lack of direct monitoring and limited communication. This study proposes the use of QHBM algorithms for optimizing troop deployment and resource allocation based on real-time data from IoT. This study uses quantitative and simulation approaches to evaluate the effectiveness of QHBM in the management of rescue operations. The results of the analysis show that QHBM is more efficient in energy consumption and bandwidth usage, reducing energy consumption by up to 10% compared to conventional methods. QHBM also shows improved connectivity stability with stronger signals at more distant nodes. With these optimizations, QHBM successfully extends the life of battery-based devices and supports more nodes without network congestion. These findings show that the application of QHBM in IoT resource management can improve communication quality and operational efficiency, providing practical guidance for professionals in the military, law enforcement, and crisis management.

I. INTRODUCTION

In a world full of uncertainty and risk, hostage release operations represent a security challenge that requires innovative and effective solutions [1]. The key to success in this type of operation lies in the ability to respond quickly and precisely, while minimizing the risk to the hostages and rescue teams [2]. The conventional method of hostage release operations has several weaknesses, such as lack of direct monitoring, limited communication in remote areas, and difficulties in predicting hostage behavior [3], [4], [5]. All of these weaknesses can be overcome by the application of IoT technology and QHBM methods to improve accuracy, communication, and predictive analytics. The conventional approach to hostage release generally uses direct military tactics, manual negotiations, and situational assessments that are often based on limited intelligence [6], [7]. This method relies on slow information, suboptimal communication, and difficulty predicting the actions of the hostage, especially in unexpected or hard-to-reach terrain [8]. These limitations increase the risk for hostages and rescue teams, so it is necessary to update the strategy by utilizing technologies such as IoT and predictive methods such as QHBM to improve real-time monitoring, communication, and analysis of the situation [9].

The conventional method of hostage release operations has several weaknesses, such as lack of direct monitoring, limited communication in remote areas, and difficulties in predicting hostage behavior. All of these weaknesses can be overcome by the application of IoT technology and QHBM methods to improve accuracy, communication, and predictive analytics. The conventional approach to hostage release generally uses direct military tactics, manual negotiations, and situational assessments that are often based on limited intelligence. This method relies on slow information, suboptimal communication, and difficulty predicting the actions of the hostage, especially in unexpected or hard-to-reach terrain. These limitations increase the risk for hostages and rescue teams, so it is necessary to update the strategy by utilizing technologies such as IoT and predictive methods such as QHBM to improve real-time monitoring, communication, and analysis of the situation recent technological developments, particularly in the areas of the Internet of Things (IoT) and nature-inspired computing, offer new opportunities to improve the efficiency and effectiveness of hostage release operations [10]. Taking inspiration from natural phenomena, in particular the organized and efficient migration strategy of honey bees, this study proposes the use of the Queen Honey Bee Migration (QHBM) Algorithm as a tool to optimize troop placement and resource allocation [11]-[13].

QHBM algorithms allow for adaptation and flexibility in troop placement and resource management, taking advantage of the real-time data provided by IoT technologies by utilizing computational models inspired by the migration of honeybee queens, this approach aims to create a more responsive and dynamic operational strategy [14], [15]. The main objective of this study is to explore how the integration of advanced technologies and natural principles can bring about a paradigm shift in the execution of hostage rescue operations, potentially enhancing mission success [16].

Through detailed analysis and simulation, this study seeks to show how the application of QHBM can facilitate strategic decision-making in highly stressful and uncertain situations [13]. It underscores the importance of innovation and adaptation in the face of modern security challenges, and offers valuable insights for professionals in the military, law enforcement, and crisis management [15]-[17]. Thus, this research not only contributes to the academic literature but also offers practical guidance for the implementation of more effective and efficient hostage release strategies [18]-[20].

Research related to the Queen Honey Bee Migration (QHBM) algorithm and its application in tactical operations, such as hostage release, has been the focus of several studies. Several previous studies have discussed the use of optimization algorithms in military and security contexts, especially in terms of resource allocation and real-time data-driven decision-making.

Solving Multi-Objective Resource Allocation Problem Using Multi-Objective Binary Artificial Bee Colony Algorithm by Acar & Basçiftçi in 2021 [12]. The multi-objective binary artificial bee colony algorithm effectively solves multi-objective resource allocation problems with higher accuracy and fewer evaluations compared to other algorithms.

IoT Resource Allocation and Optimization Based on Heuristic Algorithm by Sangaiah et al in 2020 [21]. The whale optimization algorithm (WOA) effectively optimizes IoT resource allocation and scheduling, reducing total communication cost compared to other existing algorithms.

Adaptive Decision Method in C3I System by [22]. The adaptive decision method based on parallel computing and optimization theory effectively generates online trade-off strategies for command and control scenarios, ensuring dynamic response to environmental changes and task changes in the C3I system.

Mission success probability optimization for phased-mission systems with repairable component modules by [23]. The importance measure-based ACO (IMACO) algorithm effectively optimizes mission success probability in phased-mission systems with repairable component modules, maximizing performance while maintaining cost constraint.

Increasing the efficiency of hostage rescue strategies can be done by increasing the resources and adaptive capabilities of the methods used so that the number of hostages rescued is maximized with minimal losses [24], [25]. This study aims to increase the efficiency of hostage rescue operations by implementing the Queen Honey Bee Migration (QHBM) algorithm, which is expected to speed up response time, optimize resource allocation and increase mission success rates through more efficient and adaptive operational strategies.

II. RESEARCH METHODS

This study adopts quantitative and simulation approaches to evaluate the effectiveness of the Queen Honey Bee Migration (QHBM) Algorithm in optimizing troop deployment and IoT resource allocation in hostage rescue operations. This research is divided into several main stages, namely model development, operational simulation, and result analysis [26], [27].

The model adapts the operational scheme to an increasing number of military personnel, demonstrating how any personnel can be effectively deployed for hostage liberation, with the support of IoT technology and coordination from the command center [28].

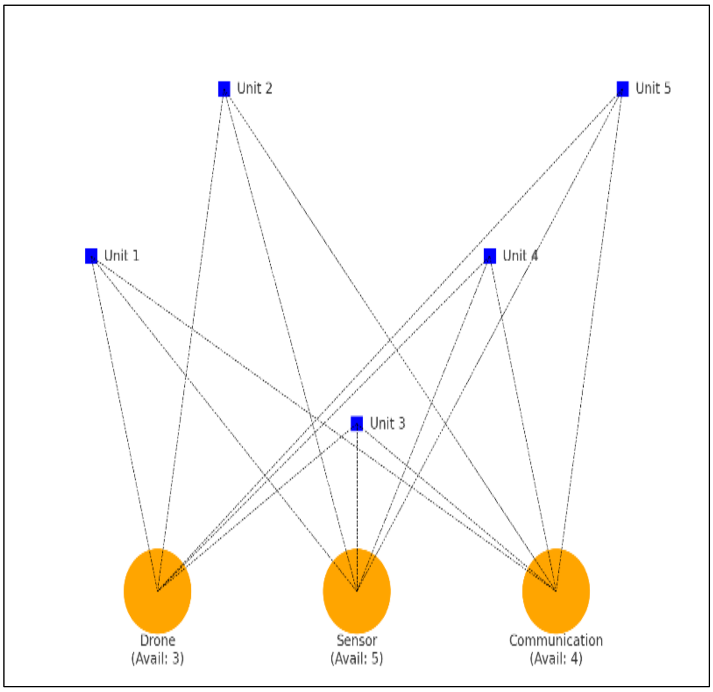

Figure 1: Hostage-Free Design Models of Each Location.
Source: Authors, (2024).

Figure 1 explains the City Operations Map which is still displayed with a gray line, the hostage locations are still marked with red dots, there are now 5 military personnel, each marked with a blue dot, the release route (dashed green line) now connects each military personnel to the nearest hostage location, the number of devices increases according to the number of military personnel, indicated by orange symbols, the location and function of the command center remains the same, marked in purple, and additional text explains the symbols and functions.

In the initial stage, researchers developed a computational model underlying the QHBM Algorithm, combining the principles of honeybee migration with the operational mechanics of special forces and IoT technology. This model is designed to optimize resource distribution and troop deployment based on variables such as hostage location, enemy presence, and environmental conditions [20], [24], [25].

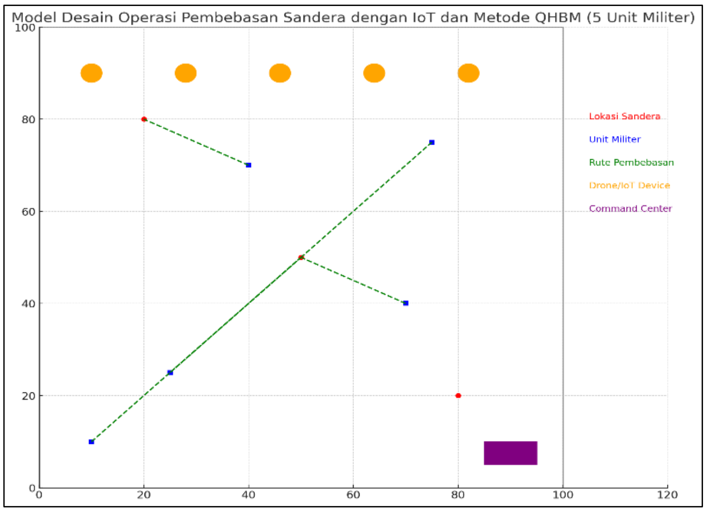

Figure 2: Resource Availability Design Model.
Source: Authors, (2024).

Figure 2 explains the military personnel Indicated by a blue box, and each unit is labeled from Unit 1 to Unit 5, IoT Resources shown with orange circles, each for 'Drone', 'Sensor', and 'Communication'. Dotted lines connect each military unit to each type of IoT resource, symbolizing the potential use of resources by each unit.

From Figure 2, the researchers integrated IoT resources, with 5 Devices attached to 5 military personnel and other communication systems, into the model to provide real - time data about the operating environment. This data is used by algorithms to make strategic decisions about troop placement and movement.

The simulation was conducted in a virtual environment created to simulate the scenarios of various hostage rescue operations. Each simulation focuses on a specific scenario, with variables set to test the effectiveness of the allocation and placement strategies generated by QHBM. Parameters such as response time, hostage safety, and mission success are measured to evaluate the performance of the algorithm.

The results of the simulation were then analyzed to assess the performance of QHBM in various scenarios. This analysis involves a comparison between the results of operations using conventional strategies and strategies optimized by QHBM. Assessment criteria include time efficiency, successful hostage release, and operational risk reduction. The Queen Honey Bee Migration (QHBM) Algorithm Design as a concept in IoT research is shown in the image below.

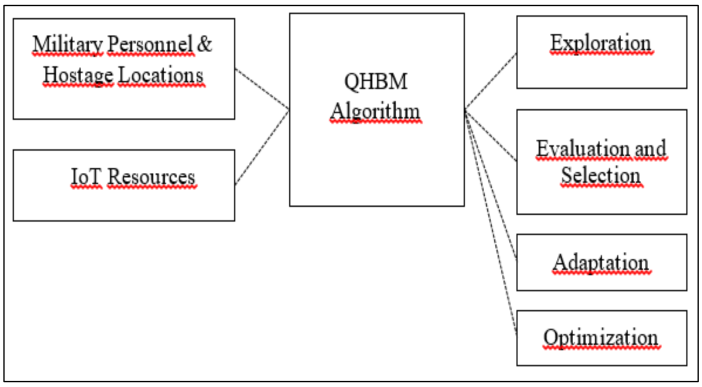

Figure 3: Design of the Queen Honey Bee Migration (QHBM) Algorithm as a concept in IoT research.
Source: Authors, (2024).

Figure 3 describes the military personnel & hostage location which explains the main aspects of the operation, namely the location of the hostages and the military personnel involved. Proper placement of personnel and mapping of hostage positions are very important because this information determines the strategy to be used in releasing the hostages.

The IoT resources section describes the various Internet of Things (IoT) resources used during the operation. IoT provides connected devices and sensors to monitor environmental conditions in real-time, as well as provide critical data on the position, signal, and condition of hostages and victims. The QHBM algorithm in this section explains the process of the QHBM algorithm which is responsible for optimizing resource usage. This algorithm helps in formulating operational strategies by adjusting IoT resources and optimizing the placement of military personnel to achieve better results. The implementation of this algorithm uses several stages such as exploration, evaluation & selection, adaptation and optimization.

Exploration at the initial stage of QHBM collects data on environmental and operational conditions. The information collected, such as enemy positions, hostages, and evacuation routes, is used to plan the next strategy. Evaluation & Selection where at this stage, the QHBM algorithm analyzes data from the exploration phase and selects the most effective strategy and resources based on environmental conditions and operational objectives. The adaptation stage of the QHBM algorithm adapts the operational approach according to environmental dynamics and feedback received during the operation. The strategy can change if the situation on the ground changes, such as hostage relocation or enemy movement. The stage ends with optimization where QHBM finds the best solution that suits the operational objectives, namely to safely release the hostages. This algorithm optimizes the efficiency of resource usage by considering existing constraints, such as energy, *bandwidth*, and time.

This research was conducted with parameters on the IoT network model with n movable nodes. As shown in table 1 below.

Table 1: Parameters for an IOT Network Model With N Movable Nodes, Based on The Given Description.

Not. Node (i)	**Posisi (Xi,1, Xi,2)**	**Energy Consumption (Ei)**	***Bandwidth* Usage for RSSI (Bi,RSSI)**	**Individual Purpose Function (fi)**	**Energy Consumption Limitation (Ei ≤ Emax)**	***Bandwidth* Limit for RSSI (Bi,RSSI ≤ BRSSI, max)**	**Position or Location Constraint (Xi, 1^2 + Xi, 2^2 ≤ $Rmax^2$)**
1	(Xi,1, 1, Xi, 2,1)	E1	Bi, RSSI 1	fi1	E1 ≤ Emax	Bi, RSSI1 ≤ BRSSI, max	Xi, $1,1^2$ + Xi, $2,1^2$ ≤ $Rmax^2$
2	(Xi,1, 2, Xi, 2,2)	E2	Bi, RSSI 2	FI2	E2 ≤ Emax	Bi, RSSI2 ≤ BRSSI, max	Xi, $1,2^2$ + Xi, $2,2^2$ ≤ $Rmax^2$
3	n	En	Bi, RSSI n	Fin	E3 ≤ Emax	Bi, RSSIn ≤ BRSSI, max	Xi, $1,n^2$ + Xi, $2,n^2$ ≤ $Rmax^2$

Source: [38].

Table 1 provides an overview of the attributes and constraints of each node in the movable IoT network model. For each ith node, position (Xi,1, Xi,2) is a coordinate or location in a two-dimensional plane.

$$d1 = \sqrt{(\text{Xi}, 1 - \text{Xo}, 1)^2 + (\text{Xi}, 2 - \text{Xo}, 2)^2} \quad (1)$$

X0,1 and X0,2 are the center or reference coordinates and energy consumption (Ei) is the energy consumption generated by the i-th node.

$$\text{Ei} = \text{Ptx} \cdot di^2 + \text{Prx} \cdot \text{Bi} \quad (2)$$

Ptx$\cdot di^2$ is a component that measures the energy spent on data transmission over a distance because transmission energy is usually proportional to the square of the distance, a factor is used di^2. Prx·Bi is a component that measures the energy spent on data transmission over a distance because transmission energy is usually proportional to the square of the distance, a factor is used.

$$\text{Bi,RSSI} = k \cdot (\text{RSSImax} - \text{RSSIi}) \quad (3)$$

Bi, RSSI is the bandwidth allocated to node i in Hz or Mbps. While k is a scale factor that is adjusted based on the network settings or communication technology used. RSSImax as the maximum or reference RSSI value (usually, −30dBm is considered a very strong signal). And RSSIi as the actual RSSI value received by node i. Furthermore, the individual objective function (fi) is the value of the individual objective function for node i obtained by the formula.

$$\text{fi} = \text{w1} \cdot \frac{1}{Ei} + \text{w2} \cdot \frac{1}{Bi} + \text{w3} \cdot \frac{1}{di} + \text{w4} \cdot \text{Kualitas Sinyal (RSSI)} \quad (4)$$

Ei is the energy consumption at node i, Bi as the bandwidth usage at node i, di as the distance of node i to the center or target. Signal quality (RSSI) is a measurement of the signal at node i, usually in dBm and w1,w2,w3,w4 as coefficients that determine how important each parameter is to the objective function. The value of w can be determined based on operational priorities, such as energy efficiency is more important than bandwidth usage.

$$(\text{Ei} \leq \text{Emax}) \quad (5)$$
$$(\text{Bi, RSSI} \leq \text{BRSSI, maks}) \quad (6)$$
$$Xi, 1^2 + Xi, 2^2 \leq Rmax^2 \quad (7)$$

The restrictions include energy consumption restrictions, bandwidth restrictions for RSSI and position or location restrictions used must meet the requirements in accordance with equation 5-7.

III. RESULT AND DISCUSSIONS

III.1 RESULT

Data generated from a BLE Beacon device detected on August 29, 2024. Each entry in the data shows the time, type, and various sensor parameters. Here are the key elements recorded:

1. Data is taken every few seconds, starting from 13:04:38 to 14:29:57.
2. The beacon used has a unique ID (example: 00050001-0000-1000-8000-00805F9B0131).
3. There is some sensor data that shows environmental conditions, including temperature conditions covering a temperature range that varies from 20.4°C to 23.8°C. Humidity conditions range from 57% to 71%.
4. There is raw data in hexadecimal format that may contain additional information about the condition or status of the beacon.
5. The RSSI (Received Signal Strength Indicator in dBm) value indicates the strength of the beacon signal, ranging from -79 dBm to -59 dBm, which gives an indication of how far the beacon is from the receiver.
6. The estimated distance to the beacon varies, ranging from 2.24 m to 10 m, which can be used for location analysis.

Table 2 is used for analysis and decision making in the context of beacon network management, where assessing the performance of each node is important in determining which nodes are the most efficient and effective in network operations.

Tabel 2: Best 5 Beacon Data.

Not. Node (i)	Posisi (Xi,1, Xi,2)	Energy Consumption (Ei)	*Bandwidth* Usage for RSSI (Bi,RSSI)	RSSI	Distance	Average
1	(10, 20)	50	10	-85	4.5	-40.25
2	(15, 25)	60	12	-80	4.0	-38.00
3	(30, 35)	70	14	-75	3.5	-35.75
4	(25, 40)	65	13	-70	3.0	-33.50
5	35, 45)	75	15	-65	2.5	-31.25

Source: Authors, (2024).

The table above shows data on the 5 best beacon nodes based on several parameters, namely position, energy consumption, bandwidth usage for RSSI (Received Signal Strength Indicator), RSSI value, distance, and average value.

Not. Node (i) in the table is a sequence number indicating the identification of each beacon node in the list, position (Xi,1, Xi,2) is the coordinate column of the position of each beacon node in the format (X, Y). For example, node 1 is at position (10, 20). Energy Consumption (Ei) shows the amount of energy consumed by each beacon node. Node 1 consumes 50 units of energy, while node 5 consumes 75 units of energy.

Bandwidth Usage for RSSI (Bi,RSSI) describes the bandwidth usage required to support RSSI measurements at each node. For example, node 1 uses 10 units of bandwidth, while node 5 uses 15 units. RSSI is the value of the signal strength received from the beacon node, measured in dBm (decibel-milliwatts). Higher values indicate better signal quality. Node 1 has an RSSI of -85 dBm, while node 5 has -65 dBm.

The distance column shows the distance between the beacon and the receiver in meters. For example, node 1 is 4.5 meters away from the receiver and the average column in the table shows an average value that may reflect the overall performance of the beacon nodes, but it needs further explanation on how this value is calculated. The average value for node 1 is -40.25, and for node 5 it is -31.25.

Table 3 below provides a comprehensive overview of the performance of each node in the IoT network. This information can be used for better decision making regarding energy management, bandwidth usage, and node placement in the network.

Table 3: Nominal Data of Research Results (5 Nodes).

Not. Node (i)	Posisi (Xi,1, Xi,2)	Energy Consumption (Ei)	*Bandwidth* Usage for RSSI (Bi,RSSI)	Individual Purpose Function (fi)	Energy Consumption Limitation (Ei ≤ Emax)	*Bandwidth* Limit for RSSI (Bi,RSSI ≤ BRSSI,max)	Position or Location Constraint (Xi, 1^2 + Xi, $2^2 \leq Rmax^2$)
1	(10, 20)	50	10	0.5	≤ 100	≤ 20	≤ 1000
2	(15, 25)	60	12	0.6	≤ 100	≤ 20	≤ 1000
3	(30, 35)	70	14	0.7	≤ 100	≤ 20	≤ 1000
4	(25, 40)	65	13	0.65	≤ 100	≤ 20	≤ 1000
5	35, 45)	75	15	0.75	≤ 100	≤ 20	≤ 1000

Source: Authors, (2024).

Table 3 presents data from five nodes in an IoT (Internet of Things) network. In table 3, the Node number (i) is a unique identifier for each node in the network, making it easy to reference a particular node. Position (Xi,1, Xi,2) indicates the position coordinates of each node in the format (X, Y). For example, node 1 is located at position (10, 20). Energy Consumption (Ei) describes the amount of energy used by each node. For example, node 1 consumes 50 units of energy, while node 5 uses 75 units of energy. Bandwidth Usage for RSSI (Bi,RSSI) indicates the amount of bandwidth used for RSSI measurements. Node 1, for example, uses 10 units of bandwidth. Individual Objective Function (fi) reflects the specific objectives of each node, with values indicating the effectiveness or efficiency of its function. For example, node 1 has a function value of 0.5. Energy Consumption Constraint (Ei ≤ Emax) indicates that the energy consumption of each node must be less than or equal to a predetermined maximum value (Emax), which in this table is 100 for all nodes. Bandwidth constraint for RSSI (Bi,RSSI ≤ BRSSI,max) states that the bandwidth usage for RSSI of each node must not exceed the maximum limit (BRSSI,max), which is set to 20 for all nodes.

Position or Location constraint ($Xi,1^2 + Xi,2^2 \leq Rmax^2$) states that the position of each node must be within a certain maximum range (Rmax). In this table, $Rmax^2$ is set to 1000 for all nodes, ensuring that the sum of the squares of the coordinates of the node positions does not exceed that value.

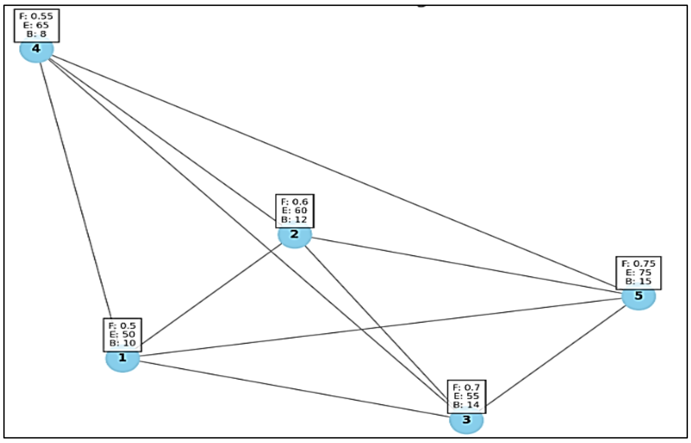

Figure 4: Parameters in IoT Network Model.
Source: Authors, (2024).

Figure 4 above is a visualization of an IoT network with moving nodes where. Each node is labeled with information about the Objective Function (F), Energy Consumption (E), and Bandwidth Usage (B). The connecting lines indicate the connections between nodes in the network.

The following are the steps for implementing the Queen Honeybee Migration Algorithm (QHBM) in optimizing hostage release operations, especially in terms of troop deployment and IoT resource allocation, as well as its comparison with conventional methods. The data provided will be used to create a table that includes a comparison between conventional methods and methods optimized with QHBM.

The Initial Population (Node) on each node in the IoT network shown in the table is a candidate solution. In this case, there are five nodes that are the objects of optimization. The fitness function for this optimization includes several important parameters, such as Energy consumption (Ei), bandwidth usage for RSSI (Bi, RSSI), RSSI value (signal strength), distance between node and receiver and location constraints (The node position must be within a predetermined range), the goal of optimization is to minimize energy consumption and bandwidth usage, while maximizing the RSSI value and minimizing the distance between node and receiver. In this algorithm, the queen bee (optimal node) mates with drones (other candidate solutions). The offspring solutions are evaluated based on a fitness function and the best performing one is selected. The node with the best fitness value is selected for migration to the next iteration. Nodes with low performance are ignored. The algorithm continues to update the solution until convergence is achieved, where the optimal solution (best node and resource arrangement) is found. Comparison with conventional methods is shown in Table 4.

Table 4: Comparison with Conventional Methods.

Parameters	Node 1	Node 2	Node 3	Node 4	Node 5
Energy Consumption (Ei)	50	60	70	65	75
***Bandwidth* (Bi,RSSI)**	10	12	14	13	15
RSSI (dBm)	-85	-80	-75	-70	-65
Distance (Meters)	4.5	4.0	3.5	3.0	2.5
Average	-40.25	-38.00	-35.75	-33.50	-31.25

Source: Authors, (2024).

Based on the information from Table 5 below, the QHBM Optimization model shows better performance than conventional methods in several aspects. In terms of energy efficiency, the QHBM model achieves a higher level, while the conventional method has only moderate energy efficiency. In addition, bandwidth usage in QHBM is more efficient because it is lower compared to conventional methods that use more bandwidth. In terms of signal strength (RSSI), the conventional method is not optimal, while the QHBM model is able to optimize the signal well. Regarding distance reduction, conventional methods do not undergo optimization, whereas QHBM succeeds in doing so. Finally, when it comes to resource allocation, conventional methods are static, while QHBM models offer dynamic resource allocation.

Table 5: Comparison of Model Performance.

Method	Energy Efficiency	*Bandwidth* Usage	Signal Strength (RSSI)	Minimize Distance	Resource Allocation
Metode Konvensional	Medium	High	Suboptimal	Not optimized	Static
Optimasi QHBM	High	Low	Optimal	Optimal	Dynamic

Source: Authors, (2024).

Based on the results shown in Table 6, each node shows variations in energy consumption, bandwidth usage, signal strength (RSSI), distance, and average performance. Node 1 has an energy consumption of 45 with a bandwidth of 9 and an RSSI of -80 dBm at a distance of 4.0 meters, resulting in an average performance of -38.0. Node 2 consumes more energy at 55, with a bandwidth of 10 and a better RSSI, i.e. -75 dBm at a distance of 3.5 meters, resulting in an average performance of -36.25. Meanwhile, Node 3 recorded an energy consumption of 65, a bandwidth of 11, and an RSSI of -70 dBm at a distance of 3.0 meters, resulting in an average performance of -33.75. At Node 4, energy consumption drops slightly to 60 with a bandwidth of 12 and an RSSI of -65 dBm at a distance of 2.5 meters, providing an average performance of -31.5. Node 5, which has the highest energy consumption of 70, bandwidth of 13, and the strongest RSSI of -60 dBm at a distance of 2.0 meters, recorded the best average performance of -29.75.

Table 6: QHBM Optimization Result Values.

Node	Energy Consumption (Ei)	*Bandwidth* (Bi,RSSI)	RSSI (dBm)	Distance (Meters)	Average Performance
1	45	9	-80	4.0	-38.0
2	55	10	-75	3.5	-36.25
3	65	11	-70	3.0	-33.75
4	60	12	-65	2.5	-31.5
5	70	13	-60	2.0	-29.75

Source: Authors, (2024).

Energy efficiency in the QHBM method table 6 shows that there has been a 10% energy saving on all nodes compared to the conventional method. Bandwidth usage is lower in the QHBM method, because the algorithm selects nodes that are more efficient in using resources. The optimized RSSI value provides better signal strength, which can increase the speed and stability of communication between nodes. The distance between the node and the receiver is optimized so that hostage release operations can be carried out faster and more efficiently.

Thus, the use of the QHBM algorithm in the context of IoT resource allocation and troop deployment can provide more efficient results compared to conventional methods, especially in terms of energy consumption, bandwidth usage, and communication signal quality. The QHBM method provides significant advantages over conventional methods, especially in terms of energy efficiency, bandwidth, signal strength, and node distance as shown in Figure 5.

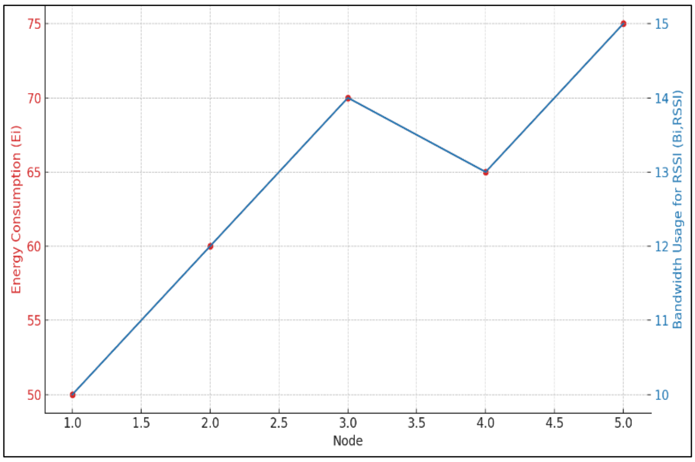

Figure 5: Energy Consumption and *Bandwidth* Usage Per Node.
Source: Authors, (2024).

The graph in Figure 5 shows the energy consumption and *bandwidth* usage for each node. The red line represents the energy consumption, while the blue line shows the *bandwidth* usage for RSSI. Each data point from a node is marked to make it easier to visualize the respective values.

The basis of the comparison between the Conventional method and the QHBM method for each node based on the four main parameters is shown in Figure 6.

Based on the graph in Figure 6 shown, there are four data visualizations related to node performance in the system. The energy consumption graph per Node (Top Left) shows the energy consumption for two methods, namely conventional (orange line) and QHBM (blue line). It can be seen that the conventional method always consumes higher energy compared to the QHBM method at each node. The highest energy consumption is at Node 3 for both methods, but the QHBM method provides significant energy savings at each node, especially Node 3 and Node 5.

The bandwidth usage graph per Node (Top Right) illustrates the bandwidth usage for both methods. Similar to the energy consumption pattern, the conventional method (orange) uses more bandwidth than the QHBM method (blue). The increase in bandwidth usage is seen along with the increase in nodes, but QHBM consistently uses less bandwidth.

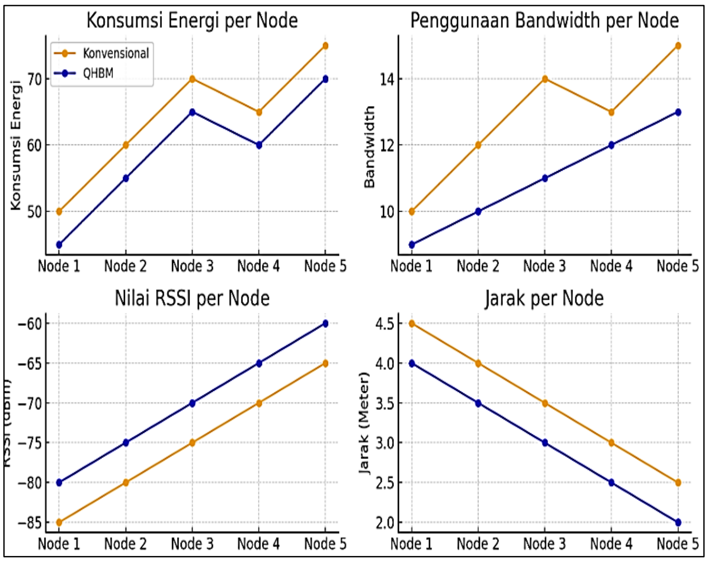

Figure 6: Comparison Chart Between Conventional Method and QHBM Method for Each Node Based on Four Main Parameters.
Source: Authors, (2024).

The RSSI Value graph per Node (Bottom Left) shows the RSSI (Received Signal Strength Indicator) signal strength for both methods. The RSSI value in the QHBM method is higher (closer to zero) than the conventional method, indicating a better signal received at the node using QHBM. The higher the RSSI value (more negative), the weaker the signal, so the QHBM method shows better performance in maintaining signal quality.

The Distance per Node graph (Bottom Right) shows the distance between nodes. Conventional methods tend to have a larger distance between nodes than the QHBM method. This means that in the QHBM method the nodes are closer to each other, which is likely to affect energy efficiency and bandwidth usage.

III.2 DISCUSSIONS

The QHBM method is overall more efficient than the conventional method in terms of energy consumption and bandwidth usage. In addition, the QHBM method also has better signal reception and keeps the distance between nodes shorter, which can contribute to the operational efficiency and communication quality of the network.

Based on the analysis of the QHBM optimization results shown in Table 6, there are several important interpretations related to aspects of energy performance, bandwidth usage, objective function, and position constraints. In terms of energy performance, all nodes show lower energy consumption than the maximum limit that has been set, which is 100. Node 5 recorded the highest energy consumption of 70, close to the limit, while the other nodes remained below it, showing the variation in efficiency between nodes.

In terms of bandwidth usage, all nodes operate within a maximum limit of 20, with node 5 recording the highest usage of 13, while the other nodes use lower bandwidth but remain within a secure limit.

From the perspective of the objective function, which signifies the relative efficiency of each node, node 5 has the highest function value of -29.75, which indicates optimal performance compared to other nodes. This shows that although node 5 uses more energy and bandwidth, it is more efficient than other nodes.

Regarding position constraints, all nodes comply with the existing constraints because all node coordinates are within the predetermined maximum limits. This indicates that each node operates in an optimal distance according to the set parameters.

Overall, these results show that QHBM optimization successfully manages resources efficiently, maintains a balance between energy consumption, bandwidth usage, and signal strength, and still adheres to position constraints. The interpretation of this data indicates that node 5 has the potential to perform better than other nodes, without violating existing limits.

In this section, the results of QHBM optimization compared to conventional methods show significant improvements in various parameters measured, such as energy consumption, bandwidth usage, signal strength (RSSI), distance, and average performance. This data is presented in the form of tables and graphs, which shows the difference in performance between the two methods.

Energy consumption is one of the main parameters measured, and QHBM optimization shows a decrease in energy consumption compared to conventional methods. This happens due to more efficient allocation of resources. The QHBM method is able to reduce energy use thanks to more optimal network management, especially on nodes farther away from the communication center, which use energy more efficiently.

In the use of bandwidth, QHBM optimization is also more efficient than conventional methods. With a more precise and dynamic bandwidth distribution, QHBM avoids excessive bandwidth usage and provides a more balanced distribution across all nodes. These results are seen in the graph visualization, where the QHBM method does not exceed the maximum bandwidth limit and still ensures optimal usage without degrading signal quality.

For signal strength (RSSI), QHBM shows significant improvement, especially in more distant nodes, where conventional methods often experience signal performance degradation. With QHBM optimization, the received signal strength is more consistent across the network, resulting in more stable connectivity. The graph also shows improvements in signal strength, especially on nodes in medium to long positions.

In terms of distance, QHBM optimization is more effective than conventional methods, which often do not provide optimal performance on nodes that are far from the signal center. With QHBM, the distance between nodes and communication centers is better managed, so that nodes at the edge of the network still receive a strong and stable signal.

Finally, the average performance shows a significant improvement in the nodes that use QHBM. The value of each node's destination function indicates that although QHBM uses more energy and bandwidth on multiple nodes, the overall efficiency is still higher than conventional methods. This is due to QHBM's ability to dynamically adjust resource allocation based on network conditions in real-time.

The increase in performance variables in the QHBM method, compared to the conventional method, is due to the ability of QHBM to be more effective in managing resources. With a quantum-based approach, QHBM enables more adaptive, dynamic, and coordinated resource allocation, which reduces resource waste, improves signal stability, and maximizes energy efficiency, resulting in more optimal network performance.

IV. CONCLUSIONS

The QHBM method is superior to the conventional method in several important aspects such as energy consumption, bandwidth usage, signal quality, and spacing between nodes. This makes QHBM a more efficient choice for network systems that require optimal performance under limited conditions such as power and bandwidth. The energy consumption efficiency of the QHBM method is proven to be more efficient in energy usage than the conventional method at each node. The energy consumption of the QHBM method is consistently lower, indicating that this method can extend the life of battery-dependent devices or nodes.

The bandwidth usage of the QHBM method is also more efficient in bandwidth usage for RSSI compared to the conventional method. The decrease in bandwidth usage in QHBM allows for more efficient usage and may support more nodes without experiencing network congestion. The RSSI value of the QHBM method indicates better signal quality (stronger) compared to the conventional method. A stronger signal indicates more stable and reliable communication between nodes. The QHBM method maintains a shorter distance between nodes than the conventional method, which has the potential to improve communication efficiency and reduce signal loss. Shorter distances between nodes usually allow for more efficient data transmission and with less energy required.

V. AUTHOR'S CONTRIBUTION

Conceptualization: Dekki Widiatmoko, Kasiyanto, and Dodo Irmanto.
Methodology: Dekki Widiatmoko, Kasiyanto, and Dodo Irmanto.
Investigation: Dekki Widiatmoko, Kasiyanto, and Dodo Irmanto.
Discussion of results: Dekki Widiatmoko, Kasiyanto, and Dodo Irmanto.
Writing – Original Draft: Dekki Widiatmoko, Kasiyanto, and Dodo Irmanto.
Writing – Review and Editing: Dekki Widiatmoko, Kasiyanto, and Dodo Irmanto.
Supervision: Dekki Widiatmoko, Kasiyanto, and Dodo Irmanto.
Approval of the final text: Dekki Widiatmoko.

VII. ACKNOWLEDGMENTS

This research collaborates to support consultation on writing and data analysis by postgraduate lecturers in the Department of Electronics Engineering, Elkasista Study Program, Army Polytechnic to support the data used In the preparation of this report, the author received a lot of help from various parties. Therefore, the author expresses his gratitude to A family that is always morally motivated and tirelessly supports with prayer that never stops so that the author can complete this research. Thanks to Mr. Briggen TNI DR. Rachmat SW, CIP, MM, MTR(ARE), As a Former Commander of Poltekad, thanks to all superiors and colleagues at the Kodiklatad Poltekad, and all friends of Electrical Engineering Lecturers at Army Polytechnic. May Allah SWT always give a reward for the deeds and goodness that have been given. Although it has been reviewed and worked on seriously, the writing of this thesis is still far from perfect, due to the limitations of knowledge and skills possessed, so that all criticisms and suggestions are accepted to be used as guidelines in compiling a more perfect next report. The author hopes that this report can be useful for the author in particular and readers in general.

VIII. REFERENCES

[1] A. Spall, M. Van Der Auwera, J. Gerstner, Y. M. Taalab, and R. Wunderlich, "Safety and Security in International Humanitarian Missions – Assessing the Stress Level of Responders in Critical Situations during a Realistic Full-Scale Training," *Prehosp. Disaster Med.*, vol. 34, no. 6, pp. 575–579, Dec. 2019, doi: 10.1017/S1049023X19005016.

[2] S. Zhang, L. Li, S. Wang, L. Liu, F. Yang, and Z. Wang, "3D Aircraft Path Planning for Hostage Rescue by Artificial Immunity Algorithm," *IOP Conf. Ser. Mater. Sci. Eng.*, vol. 490, no. 4, p. 042005, Apr. 2019, doi: 10.1088/1757-899X/490/4/042005.

[3] T. Prathima, V. S. V. S. Varma, K. Prathyush, and A. Govardhan, "Detection of Armed Assailants in Hostage Situations- A Machine Learning Based Approach," in *Proceedings of the 3rd International Conference on Intelligent Communication Technologies and Virtual Mobile Networks, ICICV 2021*, Institute of Electrical and Electronics Engineers Inc., Feb. 2021, pp. 774–781. doi: 10.1109/ICICV50876.2021.9388476.

[4] D. J. Neller, T. C. Healy, T. K. Dao, S. Meyer, and D. B. Barefoot, "Situational Predictors of Negotiation and Violence in Hostage and Barricade Incidents," *https://doi.org/10.1177/00938548211017926*, vol. 48, no. 12, pp. 1770–1787, May 2021, doi: 10.1177/00938548211017926.

[5] B. Jones, A. Tang, and C. Neustaedter, "Remote Communication in Wilderness Search and Rescue," in *Proceedings of the ACM on Human-Computer Interaction*, ACMPUB27New York, NY, USA, Jan. 2020, pp. 1–26. doi: 10.1145/3375190.

[6] G. M. Vecchi, G. K. H. Wong, P. W. C. Wong, and M. A. Markey, "Negotiating in the Skies of Hong Kong: The Efficacy of the Behavioral Influence Stairway Model (BISM) in Suicidal Crisis Situations," *Aggress. Violent Behav.*, vol. 48, pp. 230–239, Sep. 2019, doi: 10.1016/J.AVB.2019.08.002.

[7] A. R. Grubb, S. J. Brown, P. Hall, and E. Bowen, "From Deployment to Debriefing: Introducing the D.I.A.M.O.N.D. Model of Hostage and Crisis Negotiation," *Police Pract. Res.*, vol. 22, no. 1, pp. 953–976, Jan. 2021, doi: 10.1080/15614263.2019.1677229.

[8] J. Son and S. Lee, "Hidden Enemy Visualization Using Fast Panoptic Segmentation on Battlefields," in *Proceedings - 2021 IEEE International Conference on Big Data and Smart Computing, BigComp 2021*, Institute of Electrical and Electronics Engineers Inc., Jan. 2021, pp. 291–294. doi: 10.1109/BIGCOMP51126.2021.00061.

[9] C. Fathy and S. N. Saleh, "Integrating Deep Learning-Based IoT and Fog Computing with Software-Defined Networking for Detecting Weapons in Video Surveillance Systems," *Sensors 2022, Vol. 22, Page 5075*, vol. 22, no. 14, p. 5075, Jul. 2022, doi: 10.3390/S22145075.

[10] A. Douklias, M. Krommyda, and A. Amditis, "Resilient Communications for the First Responders at the Field," in *Proceedings - 2021 Asia-Pacific Conference on Communications Technology and Computer Science, ACCTCS 2021*, Institute of Electrical and Electronics Engineers Inc., Jan. 2021, pp. 37–42. doi: 10.1109/ACCTCS52002.2021.00016.

[11] X. Xu, J. Hao, and Y. Zheng, "Multi Objective Artificial Bee Colony Algorithm for Multi-Stage Resource Leveling Problem in Sharing Logistics Network," *Comput. Ind. Eng.*, vol. 142, p. 106338, Apr. 2020, doi: 10.1016/J.CIE.2020.106338.

[12] Z. Yilmaz Acar and F. Başçiftçi, "Solving Multi-Objective Resource Allocation Problem Using Multi-Objective Binary Artificial Bee Colony Algorithm," *Arab. J. Sci. Eng.*, vol. 46, no. 9, pp. 8535–8547, Sep. 2021, doi: 10.1007/S13369-021-05521-X/METRICS.

[13] G. J. Jong, Aripriharta, Hendrick, and G. J. Horng, "A Novel Queen Honey Bee Migration (QHBM) Algorithm for Sink Repositioning in Wireless Sensor Network," *Wirel. Pers. Commun.*, vol. 95, no. 3, pp.

3209–3232, Aug. 2017, doi: 10.1007/S11277-017-3991-Z/METRICS.

[14] P. Tam, S. Math, C. Nam, and S. Kim, "Adaptive Resource Optimized Edge Federated Learning in Real-Time Image Sensing Classifications," *IEEE J. Sel. Top. Appl. Earth Obs. Remote Sens.*, vol. 14, pp. 10929–10940, 2021, doi: 10.1109/JSTARS.2021.3120724.

[15] Aripriharta and G. J. Horng, "A New Defect Diameter Prediction using Heart Sound and Possibility to Implement as IoT Healthcare," *Mob. Networks Appl.*, vol. 28, no. 6, p. 2076, Dec. 2023, doi: 10.1007/S11036-023-02201-Y.

[16] M. Oqail Ahmad and R. Z. Khan, "An Efficient Load Balancing Scheduling Strategy for Cloud Computing Based on Hybrid Approach," *Int. J. Cloud Comput.*, vol. 9, no. 4, pp. 453–469, 2020, doi: 10.1504/IJCC.2020.112317.

[17] K. H. Wibowo, Aripriharta, I. Fadlika, G. J. Horng, S. Wibawanto, and F. W. Y. Saputra, "A New MPPT based on Queen Honey Bee Migration (QHBM) in Stand-alone Photovoltaic," in *IEEE International Conference on Automatic Control and Intelligent Systems, I2CACIS 2019*, Institute of Electrical and Electronics Engineers Inc., Jun. 2019, pp. 123–128. doi: 10.1109/I2CACIS.2019.8825025.

[18] A. Yuliia, "Directions of Adaptation of Domestic Enterprises to Changing Financial Conditions," *J. Bus. Intellect. Cap.*, vol. 21, no. 1, pp. 78–81, 2023, doi: 10.32782/2415-8801/2023-1.14.

[19] S. Tulchynska, O. Popelo, R. Tulchinskiy, O. Popelo, and T. Tkachenko, "Innovative Development as Determinant of Corporate Economic Security," *Oppor. Challenges Sustain.*, vol. 1, no. 1, pp. 52–60, 2022, doi: 10.56578/ocs010106.

[20] A. Gruszczak and M. Kolaszyński, "Understanding Contemporary Security: A Prolegomenon to the Interplay Between Technology, Innovation and Policy Responses," *J. Politeja - Pismo Wydz. Stud. Międzynarodowych i Polit. Uniw. Jagiellońskiego*, vol. 19, no. 79, pp. 5–16, 2022.

[21] A. K. Sangaiah, A. A. R. Hosseinabadi, M. B. Shareh, S. Y. B. Rad, A. Zolfagharian, and N. Chilamkurti, "IoT Resource Allocation and Optimization Based on Heuristic Algorithm," *Sensors 2020, Vol. 20, Page 539*, vol. 20, no. 2, p. 539, Jan. 2020, doi: 10.3390/S20020539.

[22] K. Gao, H. Wang, J. Nazarko, and M. Jarocka, "Adaptive Decision Method in C3I System," *Comput. Intell. Neurosci.*, vol. 2022, no. 1, p. 6967223, Jan. 2022, doi: 10.1155/2022/6967223.

[23] J. Zhao, S. Si, Z. Cai, P. Guo, and W. Zhu, "Mission Success Probability Optimization for Phased Mission Systems With Repairable Component Modules," *Reliab. Eng. Syst. Saf.*, vol. 195, p. 106750, Mar. 2020, doi: 10.1016/J.RESS.2019.106750.

[24] Y. Y. Chiu, H. Omura, H. E. Chen, and S. C. Chen, "Indicators For Post-Disaster Search and Rescue Efficiency Developed Using Progressive Death Tolls," *Sustainability*, vol. 12, no. 19, p. 8262, Oct. 2020, doi: 10.3390/SU12198262.

[25] B. Liu, J. B. Sheu, X. Zhao, Y. Chen, and W. Zhang, "Decision Making on Post-Disaster Rescue Routing Problems From the Rescue Efficiency Perspective," *Eur. J. Oper. Res.*, vol. 286, no. 1, pp. 321–335, Oct. 2020, doi: 10.1016/J.EJOR.2020.03.017.

[26] R. O. Sikveland, H. Kevoe-Feldman, and E. Stokoe, "Overcoming Suicidal Persons' Resistance Using Productive Communicative Challenges during Police Crisis Negotiations," *Appl. Linguist.*, vol. 41, no. 4, pp. 533–551, Aug. 2020, doi: 10.1093/APPLIN/AMY065.

[27] S. Aebischer Perone, F. Althaus, F. Chappuis, N. Aguirre Zimerman, E. Martinez, and S. Regel, "Psychological Support Post-Release of Humanitarian Workers Taken Hostage: The Experience of the International Committee of the Red Cross (ICRC)," *Br. J. Guid. Counc.*, vol. 48, no. 3, pp. 360–373, May 2020, doi: 10.1080/03069885.2018.1461193.

[28] P. Pramono, M. A. Habibi, F. I. Kusuma, S. Sujito, S. Suprayitno, and S. Azzahra, "Automatic Coffee Bean Roaster Machine to Improve Production Quality and Efficiency for Coffee Business," *Pengabdi. Masy.*, vol. 4, no. 3, pp. 6450–6454, Aug. 2023, doi: 10.31004/CDJ.V4I3.17530.

Journal of Engineering and Technology for Industrial Applications

ISSN ONLINE: 2447-0228

ITEGAM-JETIA

Manaus, v10. n.50, p. 211-218. November/ December., 2024.
DOI: https://doi.org/10.5935/jetia.v10i50.1329

RESEARCH ARTICLE OPEN ACCESS

ENHANCING OPTICAL DISTRIBUTION POINT PLACEMENT: A DECISION SUPPORT SYSTEM INTEGRATING WEIGHTED PRODUCT METHOD, CONTENT-BASED FILTERING, AND LOCATION-BASED SERVICES

Viktor Handrianus Pranatawijaya[1], Widiatry Widiatry [2] and Dea Jeany Lestari[3]

[1,2,3] Informatics Engineering Department, Faculty of Engineering, University of Palangka Raya, Indonesia

[1]https://orcid.org/0000-0002-3301-0702, [2]https://orcid.org/0009-0005-1956-5815, [3]http://orcid.org/0009-0002-8047-0039

Email: viktorhp@it.upr.ac.id, widiatry@it.upr.ac.id, chdjeany1601@gmail.com

ARTICLE INFO

Article History
Received: October 09, 2024
Revised: October 30, 2024
Accepted: November 10, 2024
Published: December 31, 2024

Keywords:
Optical Distribution Point,
Decision Support System,
Weighted Product Method,
Content-Based Filtering,
Location-Based Services.

ABSTRACT

The Optical Distribution Point (ODP) is a crucial element in fiber-optic internet networks, playing a key role in ensuring efficient service delivery. This study presents an integrated Decision Support System (DSS) that combines the Weighted Product Method (WPM), Content-Based Filtering (CBF), and Location-Based Services (LBS) to optimize ODP placement in urban areas. By considering multiple criteria such as ODP categories, customer preferences, and business types, the DSS provides a data-driven approach to strategic decision-making. The system's ability to recommend ODPs based on customer needs, while visualizing key data through LBS, enhances the effectiveness of network expansion strategies. This comprehensive framework improves decision-making in urban internet services and offers a scalable solution for optimizing network infrastructure. The study demonstrates the potential of combining analytical models with user-focused technology to streamline service deployment and improve customer satisfaction.

I. INTRODUCTION

In the world of fiber-optic communication, the Optical Distribution Point (ODP) is like the heart of the network, playing a crucial role in delivering fast and reliable internet services. Think of it as the essential hub where connections are made, ensuring that data travels efficiently from one place to another. However, to truly maximize its effectiveness, we need to strategically place these ODPs in urban areas, taking into account factors such as their proximity to users, capacity, and operational conditions [1], [2]. Monitoring the capacity of ODPs is vital not just for installation, but also for ensuring that customers receive the high-quality service they expect [3–6].

This research introduces a novel Decision Support System (DSS) that aims to optimize the placement of ODPs using the Weighted Product method. By analyzing various factors—like customer preferences, ODP recommendations, and data from local business surveys—this system helps identify the best locations for ODPs[7], [8]. The ultimate goal is to enhance decision-making and support effective business strategies in our increasingly connected urban environments [9].

To make these recommendations even more precise, we've incorporated a Content-Based Filtering approach. This means that the system takes into account what customers want, focusing on their specific needs such as proximity and service types [10]. By aligning the recommendations with user preferences, we can identify the most promising areas for promoting ODP services [11].

Moreover, integrating Location-Based Service (LBS) technology adds another layer of depth to our DSS. It allows us to visualize ODP data in real-time, providing interactive maps that display essential information such as capacity and distances from potential customers [12], [13]. Despite advancements in DSS, the integration of multiple decision-making techniques remains limited, and existing literature often addresses these methodologies in isolation, missing out on their combined strengths. This study aims to fill this gap by proposing a comprehensive DSS that seamlessly integrates the Weighted Product method, Content-Based Filtering, and LBS technology. This robust framework not only enhances ODP placement but also strengthens the overall decision-making process in urban internet service provision [14], [15].

In this study, we seek to answer a fundamental question: **How can we effectively optimize ODP placement to improve**

service delivery for urban customers? Our objectives include developing a comprehensive DSS framework that merges the Weighted Product method, Content-Based Filtering, and LBS while also acknowledging the challenges of data accuracy and scalability. By tackling these issues, we aim to contribute valuable insights to the field of telecommunications and network optimization, ultimately enhancing customer experiences in urban settings.

II. RELATED WORKS

The development of Decision Support Systems (DSS) for recommending the placement of Optical Distribution Points (ODPs) in internet networks has gained attention in recent years, focusing on the application of advanced technologies and analytical methods to enhance service efficiency and effectiveness. Several studies have explored various approaches related to DSS, the Weighted Product method, Content-Based Filtering, and data visualization using Location-Based Services (LBS).

A DSS is defined as an interactive information system designed to provide data analysis, modeling, and manipulation to support decision-making processes [16]. Weighted Product (WP) is a well-established method utilized within Multi-Attribute Decision Making (MADM), where the attributes of each alternative are multiplied by their respective weights, allowing for efficient decision-making [16]. For instance, a study that applied the WP method to determine optimal village funding solutions, demonstrating its efficacy in integrating multiple criteria for effective decision support [17]. The WP method is versatile and effective in educational settings, particularly in selecting exemplary students and teachers. It ensures objective and systematic decision-making by evaluating multiple criteria, similar to other methods like Technique for Order Preference by Similarity to Ideal Solution (TOPSIS) and Analytical Hierarchy Process (AHP), which are also used for student selection [16], [18], [19]. This versatility underscores the method's broad applicability across different domains within education.

Content-Based Filtering (CBF) in recommendation systems focuses on providing personalized item suggestions based solely on user preferences, independent of other users' inputs. CBF systems rely on data attributes and user profiles to generate recommendations, addressing cold start issues by analyzing item content and user feedback to measure item similarity [20]. This approach builds a user profile based on explicit or implicit data provided by the user, such as past interactions with items, and uses this profile to recommend new items that match the user's preferences [20–22].

This approach has proven effective in various applications, from media recommendations to restaurant selections. For example, implementing a CBF system for restaurant recommendations can significantly enhance the selection process and improve user satisfaction by providing tailored suggestions based on individual preferences and behaviors [23–26]. Additionally, Content-based filtering is commonly used to suggest items based on user likes and past actions, leveraging attributes like movie genre, director, and user ratings and cosine similarity is a key evaluation metric used to measure the similarity between items, regardless of their dimensions, and is commonly employed in content-based recommendation systems [27], [28].

Location-Based Services (LBS) enhance decision-making by providing real-time, location-specific information through the integration of GIS, positioning technologies, and communication networks. Their applications span various fields, including tourism, emergency services, and navigation, making them indispensable tools in modern geographic data visualization and interaction [28–30].

The key features of Location-Based Services (LBS) that contribute to enhancing user experience in mapping services include personalized information retrieval, real-time traffic information, and the ability to provide location-specific and customized services [31–33]. The integration of LBS technology in decision support systems facilitates informed choices based on accurate spatial data by enabling the collection of GPS data logs, location chronicles, and the deployment of multi-criteria decision analysis (MCDA) tools for personalized decision outcomes [33], [34]. The enumerations of citations in the body of the article must be sequenced in the order in which they appear, according to the example shown below.

III. PROPOSED METHOD

The framework for the proposed method in this study integrates Decision Support Systems (DSS) with Content-Based Filtering (CBF) and Location-Based Services (LBS) to optimize Optical Distribution Point (ODP) selection for fiber-optic network expansion. The method is structured into several stages, each of which contributes to a comprehensive and data-driven decision-making process. Figure 1 below explains the method proposed in this study.

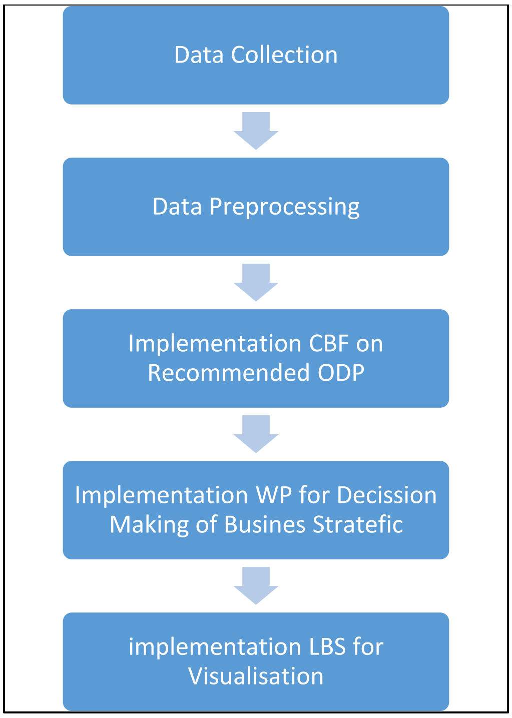

Figure 1: The Architecture of Proposed Method.
Source: Authors, (2024).

III.1 DATA COLLECTION

Relevant data are gathered, ODP data included information such as the ODP name, geographic coordinates, total capacity, the number of empty, filled, and reserved charging ports, and the ODP category. In addition, customer data, consisted of the customer's business name, location coordinates, the chosen service package, and the current status of their order, are collected. Finally, business survey data captured the business name, address, coordinates, and the type of business participating in the survey. This information forms the dataset used for the subsequent analysis.

III.2 DATA PREPROCESSING

Data preprocessing involves cleaning and transforming the raw data to ensure consistency, completeness, and accuracy [35], [36]. This step includes removing duplicates, handling missing values, and standardizing the data format. The preprocessed dataset is then divided into relevant criteria for further analysis. For instance, ODP capacity, distance from the customer, and business categories are considered critical factors in the decision-making process.

III.3 CONTENT BASED FILTERING

The next step involves applying Content-Based Filtering (CBF) to recommend ODPs based on customer preferences and service needs [37]. The CBF algorithm leverages data related to ODP attributes (e.g., proximity to customers, type of business, and customer demand in a specific area) to filter and recommend the most suitable ODPs for promotional targeting. By tailoring recommendations according to customer-specific preferences, the system increases the likelihood of successful service installations, enhancing customer satisfaction [38].

The process begins with data collection, where the data used comes from data collected within 250 m of the user point. The data used is ODP data such as distance, ODP category, and check highway. Next, the criteria values are weighted according to the data used. Next, the cosine similarity calculation is performed for points within a 250 m radius of the user point. After the cosine similarity results are obtained, a list of recommendation results based on these two calculations is displayed. The criteria weighting process uses the criteria rules as in Data Table 1.

Table 1: Recommendation ODP Criteria.

No.	Recommendation Criteria
1)	Distance from ODP to Potential Customer Location < 250m
2)	Does Not Cross Protocol Road
3)	ODP Category

Source: Authors, (2024).

To facilitate calculations between data, the data needs to be converted into a numerical scale. In Tables 2, 3, and 4 are the assessments of each criterion.

Table 2: ODP Category Criteria.

Criteria	Value	Description
Black	0	Not Good
Red	1	Less Good
Yellow	2	Fairly Good
Green	3	Good

Source: Authors, (2024).

Table 3: Check Highway Criteria.

Criteria	Value	Description
Passed	0	Not Good
Not Passed	1	Good

Source: Authors, (2024).

Table 4: Distance Criteria.

Criteria	Value	Description
> 250 m	0	Very Poor
<= 250 m	1	Not Good
<= 200 m	2	Less Good
<= 150 m	3	Fairly Good
<= 100 m	4	Good
<= 50 m	5	Very Good

Source: Authors, (2024).

After data collection and weighting based on criteria have been carried out, the development of a recommendation system with Content Based Filtering is continued by calculating Cosine Similarity between the value of the user and the detected ODP in order to get recommendation results. The calculation process will be carried out in Experiments and Results.

III.4 WEIGHTED PRODUCT

The filtered ODP recommendations are further analyzed using the Weighted Product (WP) method, a widely used Multi-Criteria Decision Making (MCDM) technique. The WP method is applied to rank the potential ODP locations based on multiple factors, including proximity, capacity, and demand. Each factor is assigned a weight that reflects its importance to the decision-making process. By multiplying the ratings of each alternative by its corresponding attribute values and raising them to their assigned weights, the WP method provides a clear ranking of ODPs, identifying areas with the highest potential for business growth.

III.4.1 alternatives

To apply the Decision Support System with the Weighted Product Method, it is necessary to determine the alternative as the output under consideration. Alternatives are a set of different objects, each of which has the same opportunity to be selected by the decision maker [7], [16], [39]. Alternatives are the different options being evaluated. For instance, in selecting teachers for a school, each teacher represents an alternative with unique qualifications and performance metrics [16]. The alternatives used in this study are listed in Table 5

Table 5: Alternatives.

No.	Alternatives
A1	250 m to the north
A2	250 m to the south

Source: Authors, (2024).

III.4.2 criteria

Criteria are standards used to evaluate and compare alternatives in decision making42. Criteria help assess the advantages and suitability of each option, making it easier to choose the most appropriate one to achieve the goal. The following in Table 6 are the criteria that will be used for the decision-making process.

Table 6: Criteria.

No.	Criteria
C1	ODP Categories
C2	Non-Subscriber Business Count
C3	Business Type
C4	ODP Count

Source: Authors, (2024).

III.4.3 weight of each criteria

The following is the weighting of each ODP category criterion, namely the most recommended ODP category, the number of unsubscribed businesses, the most business types, the number of recommended ODP.

Table 7: Weight of ODP Category Criteria.

Criteria	Value	Description
Black	1	Not Good
Red	2	Less Good
Yellow	3	Good
Green	4	Very Good

Source: Authors, (2024).

Table 7 above is the weighting of the ODP Category Criteria. This ODP consists of two types of ODP, namely 8 port ODP and 16 port ODP. The Green category is an ODP with 8 - 6 available ports for 8 ports and 16 - 11 for 16 ports, which is the category with the most available ports. The Yellow category is an ODP with 5 - 3 available ports for 8 ports and 10 - 5 for 16 ports, which is a category with quite a lot of available ports. The Red category is an ODP with 2 -1 available ports for 8 ports and 4 - 1 for 16 ports, which is the category with the least available ports. The Black category is an ODP with 0 available ports, which is a category with no available ports and cannot be used.

Table 8: Weight of Non-Subscriber Business Count Criteria.

Criteria	Value	Description
Few Non-Subscribers	1	Less Good
Many Non-Subscribers	2	Good
Most Non-Subscribers	3	Very Good

Source: Authors, (2024).

In Table 8 above is the weighting of the Number of Unsubscribed Business Criteria, which is done by comparing the number of customers from order data and the amount of survey data from businesses that have not subscribed. The highest number of unsubscribed is obtained from the number of business surveys that are more than the number of customers. The number of subscriptions is a condition where the number of business surveys is equal to the number of customers. The number of unsubscribed is not much obtained from the comparison of the number of business surveys that are smaller than the number of customers.

Table 9: Weight of Business Type Criteria.

Criteria	Value	Description
Small Business	1	Less Good
Medium Business	2	Good
Large Business	3	Very Good

Source: Authors, (2024).

Table 9 above shows the weighting of the business type criteria, which is divided into 3 types of businesses classified according to the scope and amount of Internet network usage, namely small businesses, medium businesses, and large businesses. Small Businesses consist of Other, Public Facilities, Real Estate (Housing Complex), Business Service. Medium businesses consist of Gov Office, Enterprise, Retail & Distribution, and Manufacturing. Large Businesses consist of Media & Communication, Education, Health, Finance, and Hospitality & Tourism.

Table 10: Weight of ODP Count Criteria.

Criteria	Value	Description
Few ODPs	1	Less Good
Moderate ODPs	2	Good
Many ODPs	3	Very Good

Source: Authors, (2024).

The weighting of the criteria for the number of ODPs available is shown in Table 10 above. For classification, less than 8 is worth 1, less than 16 is worth 2, and greater than or equal to 24 is worth 3.

III.4.4 weighted normalized values

The following is a weight normalization where the weight value used has been determined on the basis of the evaluation priorities of the agency in question. Please refer to Table 11 for more details.

Table 11: Weighted Normalized Value.

No.	Criteria	Value	Normalized Value
C1	ODP Categories	4	0.26
C2	Non-Subscriber Business Count	5	0.33
C3	Business Type	3	0.2
C4	ODP Count	3	0.2

Source: Authors, (2024).

After weighting based on criteria and normalizing the weight of the criteria has been obtained, the development of a decision support system with the Weighted Product algorithm is continued with the calculation of alternatives per criterion from the user point used, calculation of the decision matrix, calculation of the vector (S) and ends with the calculation of preferences (Vi) in order to get results. The calculation process will be carried out in Experiments and Results.

IV. EXPERIMENTS AND RESULTS

IV.1 CONTENT BASED FILTERING FOR RECOMMENDATION ODP

At this stage will continue the process of developing the Content Based Filtering Recommendation System, namely the calculation of Cosine Similarity. Where previously the data collection process had been carried out to weight the criteria. For this calculation process, one user point will be used which is located at **latitude -2.188012** and **longitude 113.895569**. To calculate cosine similarity on ODP data is to use the following formula in Eq. (1).

Cosine Similarity

$$\mathrm{sim}(a,b) = \frac{\mathrm{n}(\mathrm{A} \cap \mathrm{B})}{\sqrt{(\mathrm{n}(\mathrm{A} \cap \mathrm{B}))}} \quad (1)$$

Where:

- sim(a,b) = Similarity score between user item and ODP item
- n(A) = Number of features of the user item
- n(B) = Number of features of the ODP item
- n(A ∩ B) = Number of features common to both the user item and the ODP item

To determine n(A), values are assigned based on the criteria of distance, category, and road status from the user, yielding the following.

User = [distance <= 50, category = green, check highway = not passed]

n(A) = [5,3,1]

Next, the values of n(B) are gathered from ODP data within a 250 m radius of the user point, as shown below on Table 12.

Table 12: Detected ODP Data.

ODP Name	Distance (m)	Category	Check Highway
ODP-PLK-FQ/006	59.95	Yellow	Not Passed
ODP-PLK-FQ/048	161.60	Green	Not Passed
ODP-PLK-FBD/007	225.88	Red	Passed
ODP-PLK-FQ/051	163.77	Red	Not Passed
ODP-PLK-FBD/035	135.16	Yellow	Passed

Source: Authors, (2024).

The detected data is converted using a scale for each of the criteria, resulting in the following in Table 13.

Table 13: ODP Data Conversion Based on Criteria.

ODP Name	Distance (m)	Category	Check Highway
ODP-PLK-FQ/006	4	2	1
ODP-PLK-FQ/048	2	3	1
ODP-PLK-FBD/007	1	1	0
ODP-PLK-FQ/051	2	1	1
ODP-PLK-FBD/035	3	2	0

Source: Authors, (2024).

The following calculations determine the cosine similarity for the nearest ODP recommendation system. The following table summarizes the similarity calculations between the user and the detected ODPs, ordered from highest to lowest similarity score. See Table 14 for details.

Table 14: ODP Data Conversion Based on Criteria.

2	Cosine Similarity	Order
ODP-PLK-FQ/006	0.98778	1
ODP-PLK-FQ/048	0.98450	2
ODP-PLK-FBD/007	0.90453	3
ODP-PLK-FQ/051	0.90619	4
ODP-PLK-FBD/035	0.67612	5

Source: Authors, (2024).

Thus, the recommended ODP for the user is as per the results in Table 14, with the top recommendation being ODP-PLK-FQ/006, followed by ODP-PLK-FBD/035 for last.

IV.2 WEIGHTED PRODUCT FOR DECISION MAKING OF BUSINESS STRATEGIC

This phase involves the development of the Decision Support System using the Weighted Product Algorithm, which includes alternative weighting per criterion based on the user point, decision matrix calculations, vector (S) calculations, and preference (Vi) value calculations. The user point coordinates are **latitude -2.188012** and **longitude 113.895569**.

After weighting each criterion, the ratings for each alternative based on the user's location were determined. Below is an example rating for each alternative according to the criteria. See Table 15.

Table 15: Alternatives per Criterion.

Alternatives	Criteria			
	C1 (ODP Category)	C2 (Non-Subscriber Business Count)	C3 (Business Type)	C4 (ODP Count)
A1	Yellow	The most	Intermediate	3
A2	Red	The most	Large	2

Source: Authors, (2024).

In Table 16, this matrix is then used in the next step to calculate the weighted score for each alternative, which allows comparison between A1 and A2 based on the importance weight of each criterion.

Table 16: Decision Matrix Value.

Alternatives	Criteria			
	C1	C2	C3	C4
A1	3	3	2	1
A2	2	3	3	1

Source: Authors, (2024).

The vector value determination utilizes the converted data from the alternative criteria as shown in the table. The vector (S) is calculated using the following Eq. (2).

Vector Values (S)

$$S_i = \prod_{j-1}^{n} X_{ij} W_j \quad (2)$$

Once all vector values are identified, preference values are calculated using the Eq. (3).

Preference Values (Vi)

$$V_i = \frac{\prod_{j-1}^{n} X_{ij} W_j}{\prod_{j-1}^{n} (X_j^{w}) W_j} \quad (3)$$

Based on the calculations through vector (S) and Preference (Vi), the highest value is found in alternative A1. Thus, the Decision-Making System for the Priority Promotion Area is set for A1, or 250 m north of the User Point. See Table 17 for more details.

Table 17: Weighted Product Values.

Alternatives	Si	Vi	Order
A1	2.1964	0.506	1
A2	2.1435	0.494	2

Source: Authors, (2024).

IV.3 LOCATION BASED SERVICE FOR VISUALITATION RESULT OF DECISION MAKING

The outcomes of the calculations using cosine similarity and the weighted product provide a strategic business decision that can be viewed in the application interface as illustrated in Figure. 2.

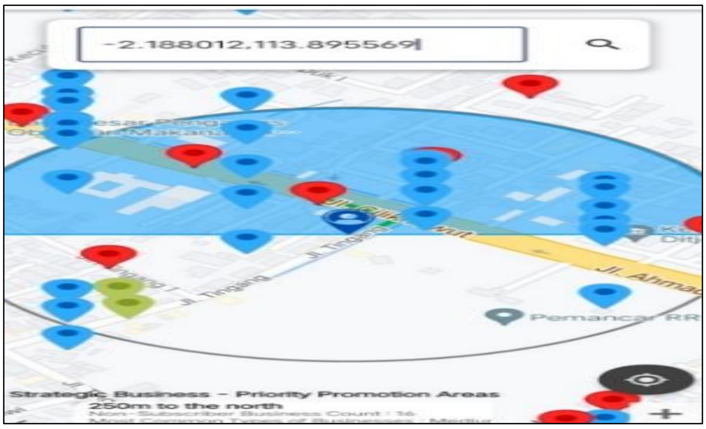

Figure 2: Location Based Service of Strategic Business.
Source: Authors, (2024).

In the application, four markers are visible: the user marker, red marker (ODP), blue marker (non-subscribing businesses), and green marker (customers). From the user point, a 250 m radius is delineated by a straight line dividing the northern and southern sections. The display at the bottom shows a list of DSS results for the business strategy, indicating priority promotion areas. Based on the top result in the list, the corresponding area on the map is colored, clearly indicating the priority region.

V. DISCUSSION

The integration of the Weighted Product Method (WPM), Content-Based Filtering (CBF), and Location-Based Services (LBS) into a Decision Support System (DSS) has yielded significant insights into optimizing Optical Distribution Point (ODP) placement in urban fiber-optic networks. Our results demonstrate not only the efficacy of this integrated approach but also its practical applications in enhancing service delivery.

The recommendation of ODP-PLK-FQ/006, which achieved a high **Cosine Similarity score of 0.98778**, reflects a strong alignment between the ODP's characteristics and user needs. This finding underscores the importance of incorporating user-specific preferences into the decision-making process, as emphasized in the Introduction. By tailoring ODP selections based on proximity and service categories, we enhance customer satisfaction and ensure that services are readily accessible.

The application of the WPM facilitated a structured ranking of alternatives based on multiple criteria, confirming that a multi-criteria approach is essential for making informed decisions. The preference scores for **Alternative A1 (250 m north)** and **Alternative A2 (250 m south)** highlight how nuanced factors like ODP category and business type can influence optimal placements. These insights contribute to a deeper understanding of the criteria that matter most in the context of urban internet services.

While our study achieves significant milestones, such as demonstrating the practicality of integrating WPM, CBF, and LBS, several limitations must be acknowledged. The accuracy of the recommendations is contingent on the quality and completeness of the input data. Missing or outdated information from customer surveys could lead to suboptimal ODP placements, which could impact overall service quality. Furthermore, while our DSS performed effectively within the scope of this study, its scalability in larger urban environments with complex network demands has yet to be tested.

One of the most innovative aspects of this study is the seamless integration of diverse methodologies into a single DSS framework. By leveraging LBS technology for real-time visualizations, we can provide stakeholders with interactive maps that enhance understanding of spatial relationships. This capability not only aids in decision-making but also serves as a valuable tool for communicating strategies to network engineers and business managers. The practical application of this system has the potential to revolutionize how ODP placements are approached in urban settings.

In conclusion, this study demonstrates that a comprehensive DSS integrating WPM, CBF, and LBS can significantly improve the optimization of ODP placements in urban environments. However, unresolved issues remain, particularly regarding data accuracy and system scalability. Future research should focus on testing the DSS in larger, more dynamic urban contexts to evaluate its robustness and adaptability.

To further enhance the effectiveness of the Decision Support System (DSS), we recommend incorporating machine learning algorithms to enable the system to adaptively learn from incoming data, improving its responsiveness to changes in customer demand and market conditions. Additionally, collaborating with telecommunication companies and urban planners to access more comprehensive datasets will enhance the accuracy and reliability of the recommendations. Lastly, continuously engaging with end-users to gather feedback can help refine the system, ensuring it remains aligned with customer needs and expectations. By addressing these recommendations, future iterations of the DSS can become even more effective in optimizing Optical Distribution Point (ODP) placements, ultimately leading to enhanced service delivery in urban networks.

VI. CONCLUSIONS

In conclusion, this research underscores the critical role of Optical Distribution Points (ODPs) in enhancing fiber-optic internet services. By integrating a Decision Support System (DSS) that employs the Weighted Product Method, Content-Based Filtering, and Location-Based Services, we have developed an innovative framework that effectively addresses the challenge of optimizing ODP placement in urban areas.

Our findings reveal that this multi-faceted approach not only improves decision-making by aligning ODP placement with customer needs and preferences but also enhances overall service delivery. Specifically, we have shown that considering various criteria—such as the number of ODPs, non-subscribing businesses, and business types—leads to more informed decisions and better strategic planning.

This study answers the research objective by demonstrating how the proposed DSS can streamline the decision-making process, ultimately facilitating the efficient deployment of ODPs where they are needed most. Looking ahead, we believe that further refining this system will empower stakeholders to adapt to the dynamic landscape of urban internet infrastructure, ensuring that service delivery remains responsive to customer demands.

By embracing this comprehensive approach, we contribute valuable insights to the telecommunications field and set the stage for future innovations that will enhance urban connectivity.

VII. AUTHOR'S CONTRIBUTION

Conceptualization: Viktor Handrianus Pranatawijaya, Widiatry Widiatry and Dea Jeany Lestari.
Methodology: Viktor Handrianus Pranatawijaya, Widiatry Widiatry and Dea Jeany Lestari.
Investigation: Viktor Handrianus Pranatawijaya, Widiatry Widiatry and Dea Jeany Lestari.Two.
Discussion of results: Viktor Handrianus Pranatawijaya, Widiatry Widiatry and Dea Jeany Lestari.
Writing – Original Draft: Viktor Handrianus Pranatawijaya, Widiatry Widiatry and Dea Jeany Lestari.
Writing – Review and Editing: Viktor Handrianus Pranatawijaya, Widiatry Widiatry and Dea Jeany Lestari. **Resources:** Viktor Handrianus Pranatawijaya, Widiatry Widiatry and Dea Jeany Lestari.
Supervision: Viktor Handrianus Pranatawijaya, Widiatry Widiatry and Dea Jeany Lestari.
Approval of the final text: Viktor Handrianus Pranatawijaya, Widiatry Widiatry and Dea Jeany Lestari.

VIII. REFERENCES

[1] Y. A. Auliya et al., "Optimizing the routing of optical distribution points on a fiber network using modified genetic algorithm (GA's) with a travelling salesman problem approach," in The 7th International Conference Of Combinatorics, Graph Theory, And Network Topology 2023, AIP Publishing, 2024, p. 030049. doi: 10.1063/5.0222824.

[2] R. Sidik and Y. Ray, "Interactive Map-Based Optical Distribution Point (ODP) Mapping," Journal of Engineering Science and Technology, vol. 16, no. 3, pp. 2128–2138, 2021.

[3] S. Ashraf and A. K. Bardhan, "A location and capacity-allocation game model for two competing online delivery platforms seeking new customers," Electronic Commerce Research, Aug. 2024, doi: 10.1007/s10660-024-09891-w.

[4] X. Zhou, Y. Ding, C. Wu, J. Huang, and C. Hu, "Measuring the Spatial Allocation Rationality of Service Facilities of Residential Areas Based on Internet Map and Location-Based Service Data," Sustainability, vol. 11, no. 5, p. 1337, Mar. 2019, doi: 10.3390/su11051337.

[5] G. Smaragdakis, N. Laoutaris, K. Oikonomou, I. Stavrakakis, and A. Bestavros, "Distributed Server Migration for Scalable Internet Service Deployment," IEEE/ACM Transactions on Networking, vol. 22, no. 3, pp. 917–930, Jun. 2014, doi: 10.1109/TNET.2013.2270440.

[6] G. Kontsevik, V. Tikhevich, and S. Mityagin, "Enhancing Urban Planning Through Improved Connectivity: A Genetic Algorithm Approach for Optimal Service Placement," in Computational Science and Its Applications – ICCSA 2024, 2024, pp. 395–407. doi: 10.1007/978-3-031-64605-8_27.

[7] D. Wira Trise Putra and A. Agustian Punggara, "Comparison Analysis of Simple Additive Weighting (SAW) and Weigthed Product (WP) In Decision Support Systems," MATEC Web of Conferences, vol. 215, p. 01003, Oct. 2018, doi: 10.1051/matecconf/201821501003.

[8] D. G. H. Divayana, "Simulation of the weighted product method integrated with the CSE-UCLA evaluation model," in THE 8TH INTERNATIONAL CONFERENCE ON TECHNOLOGY AND VOCATIONAL TEACHERS 2022, 2024, p. 030004. doi: 10.1063/5.0214095.

[9] R. Hou, X. Ye, H. B. O. Zaki, and N. A. B. Omar, "Marketing Decision Support System Based on Data Mining Technology," Applied Sciences, vol. 13, no. 7, p. 4315, Mar. 2023, doi: 10.3390/app13074315.

[10] A. Nair and R. Mathews, "Challenges and Solutions in Recommender Systems," in Proceeding of the International Conference on Computer Networks, Big Data and IoT (ICCBI - 2019), 2020, pp. 188–194. doi: 10.1007/978-3-030-43192-1_21.

[11] K. Pasrija and K. Mittal, "A Survey of Recent Advances in Recommendation Systems," in IOT with Smart Systems, 2022, pp. 589–597. doi: 10.1007/978-981-16-3945-6_58.

[12] G. Kaur and R. Gupta, "A Study on Location Based Services and TTP based Privacy Preserving Techniques," in 2021 International Conference on Advances in Computing and Communications (ICACC), IEEE, Oct. 2021, pp. 1–5. doi: 10.1109/ICACC-202152719.2021.9708364.

[13] A. Rathod and V. Jariwala, "Scalable Collaborative Approach For Privacy Preservation In Location Based Services," Indian Journal of Computer Science and Engineering, vol. 13, no. 1, pp. 1–10, Feb. 2022, doi: 10.21817/indjcse/2022/v13i1/221301301.

[14] J. Samuel et al., "UD-SV: Urban data services and visualization framework for sharing multidisciplinary research," Transactions in GIS, vol. 27, no. 3, pp. 841–858, May 2023, doi: 10.1111/tgis.13049.

[15] M. T. Cepero Garcia and L. G. Montane-Jimenez, "Visualization to support decision-making in cities: advances, technology, challenges, and opportunities," in 2020 8th International Conference in Software Engineering Research and Innovation (CONISOFT), IEEE, Nov. 2020, pp. 198–207. doi: 10.1109/CONISOFT50191.2020.00037.

[16] A. Tohir et al., "Decision Support System using WP Algorithm for Teacher Selection," J Phys Conf Ser, vol. 1845, no. 1, p. 012028, Mar. 2021, doi: 10.1088/1742-6596/1845/1/012028.

[17] T. Hastono and F. Syah, "Alternative Solutions for Determining Village Funds Using Weight Product Method," IOP Conf Ser Mater Sci Eng, vol. 835, no. 1, p. 012029, Apr. 2020, doi: 10.1088/1757-899X/835/1/012029.

[18] Setiawansyah, A. A. Aldino, P. Palupiningsih, G. F. Laxmi, E. Delisa Mega, and I. Septiana, "Determining Best Graduates Using TOPSIS with Surrogate Weighting Procedures Approach," in 2023 International Conference on Networking, Electrical Engineering, Computer Science, and Technology (IConNECT), IEEE, Aug. 2023, pp. 60–64. doi: 10.1109/IConNECT56593.2023.10327119.

[19] Y. S. Bagi, S. Suyono, and M. F. Tomatala, "Decision Support System for High Achieving Students Selection Using AHP and TOPSIS," in 2020 2nd International Conference on Cybernetics and Intelligent System (ICORIS), IEEE, Oct. 2020, pp. 1–5. doi: 10.1109/ICORIS50180.2020.9320823.

[20] Y. Ariyanto and T. Widiyaningtyas, "A Systematic Review Of Movie Recommender Systems," Journal of Engineering and Technology for Industrial Applications, vol. 10, no. 47, pp. 34–41, Jul. 2024, doi: 10.5935/jetia.v10i47.1052.

[21] S. Sridhar, D. Dhanasekaran, and G. Charlyn Pushpa Latha, "Content-Based Movie Recommendation System Using MBO with DBN," Intelligent Automation & Soft Computing, vol. 35, no. 3, pp. 3241–3257, 2023, doi: 10.32604/iasc.2023.030361.

[22] N. R. Kota, V. Padmanabhan, and W. N. Bhukya, "Content Based Network Representational Learning for Movie Recommendation (CNMovieRec)," in Multi-disciplinary Trends in Artificial Intelligence (MIWAI 2023), 2023, pp. 112–123. doi: 10.1007/978-3-031-36402-0_10.

[23] Q. Nguyen, V. Nguyen, D. Tran, T. Mai, and T. Quan, "Star2vec: From Subspace Embedding to Whole-Space Embedding for Intelligent Recommendation System (Extended Abstract)," in Computational Data and Social Networks (CSoNet 2019), 2019, pp. 70–71. doi: 10.1007/978-3-030-34980-6_7.

[24] Y. Afoudi, M. Lazaar, and M. Al Achhab, "Impact of Feature selection on content-based recommendation system," in 2019 International Conference on Wireless Technologies, Embedded and Intelligent Systems (WITS), IEEE, Apr. 2019, pp. 1–6. doi: 10.1109/WITS.2019.8723706.

[25] M. Arulprakash, M. Joshikha, and C. Khemka, "Food recommender system using content based filtering," 4TH INTERNATIONAL CONFERENCE ON INTERNET OF THINGS 2023: ICIoT2023, vol. 3075, no. 1, 2024, doi: 10.1063/5.0217594.

[26] M. T. Mishan, A. L. Amir, M. H. Bin Mohd Supir, A. L. Kushan, N. Zulkifli, and M. H. Rahmat, "Integrating Business Intelligence and Recommendation Marketplace System for Hawker Using Content Based Filtering," in 2023 4th International Conference on Artificial Intelligence and Data Sciences (AiDAS), IEEE, Sep. 2023, pp. 200–205. doi: 10.1109/AiDAS60501.2023.10284691.

[27] S. S, Madhumitha. S, Sushma. R, S. M, Subitsha. M, and Swetha. S, "Certain Investigations on Cognitive based Movie Recommendation system using Pairwise Cosine Similarity," in 2023 9th International Conference on Advanced Computing and Communication Systems (ICACCS), IEEE, Mar. 2023, pp. 2139–2143. doi: 10.1109/ICACCS57279.2023.10112790.

[28] M. K. Delimayanti et al., "Web-Based Movie Recommendation System using Content-Based Filtering and KNN Algorithm," in 2022 9th International Conference on Information Technology, Computer, and Electrical Engineering (ICITACEE), IEEE, Aug. 2022, pp. 314–318. doi: 10.1109/ICITACEE55701.2022.9923974.

[29] M. E. Elalami, I. A. Elshafei, and H. E. Abdelkader, "Location-Based Services Using Web-Gis By An Android Platform To Improve Students' Navigation During Covid-19," J Theor Appl Inf Technol, vol. 100, no. 10, 2022, [Online]. Available: www.jatit.org

[30] M. Deidda, A. Pala, and G. Vacca, "An example of a tourist location-based service (LBS) with open-source software," Applied Geomatics, vol. 5, no. 1, pp. 73–86, Mar. 2013, doi: 10.1007/s12518-012-0097-x.

[31] V. Paliulionis, "Issues of integrating GIS and mobile technologies in location-based services," Geodesy and cartography, vol. 30, no. 4, pp. 117–122, Aug. 2012, doi: 10.3846/13921541.2004.9636654.

[32] V. Poornima and R. Ganesan, "Implementation of health information system using Location Based Services," in 2014 IEEE International Conference on

Advanced Communications, Control and Computing Technologies, IEEE, May 2014, pp. 1692–1696. doi: 10.1109/ICACCCT.2014.7019397.

[33] D. Parmar and U. P. Rao, "Dummy Generation-Based Privacy Preservation for Location-Based Services," in Proceedings of the 21st International Conference on Distributed Computing and Networking, New York, NY, USA: ACM, Jan. 2020, pp. 1–1. doi: 10.1145/3369740.3373805.

[34] S. Ganapati, "Mobile Location-Based Service (LBS) Apps for the Public Sector," in Routledge Handbook on Information Technology in Government, Routledge, 2017, pp. 108–123. doi: 10.4324/9781315683645-7.

[35] F. Xiao et al., "A Data Processing Method for Load Data of Electric Boiler with Heat Reservoir," in Intelligent Computing Theories and Application (ICIC 2021), 2021, pp. 395–405. doi: 10.1007/978-3-030-84529-2_33.

[36] S. M. Mostafa, "Towards improving machine learning algorithms accuracy by benefiting from similarities between cases," Journal of Intelligent & Fuzzy Systems, vol. 40, no. 1, pp. 947–972, Jan. 2021, doi: 10.3233/JIFS-201077.

[37] H. Zitouni, S. Meshoul, and K. Taouche, "Enhancing Content Based Filtering Using Web of Data," in Computational Intelligence and Its Applications (CIIA 2018), 2018, pp. 609–621. doi: 10.1007/978-3-319-89743-1_52.

[38] N. Belacel, G. Wei, and Y. Bouslimani, "The K closest resemblance classifier for amazon products recommender system," in ICAART 2020 - Proceedings of the 12th International Conference on Agents and Artificial Intelligence, SciTePress, 2020, pp. 873–880. doi: 10.5220/0009155108730880.

[39] Nurmahaludin, G. R. Cahyono, J. Riadi, and I. Wardiah, "Decision support system for the selection of rice varieties using weighted product method," J Phys Conf Ser, vol. 1450, no. 1, p. 012059, Feb. 2020, doi: 10.1088/1742-6596/1450/1/012059.

Journal of Engineering and Technology for Industrial Applications

ISSN ONLINE: 2447-0228

ITEGAM-JETIA

Manaus, v10. n.50, p. 219-227. November/ December., 2024.
DOI: https://doi.org/10.5935/jetia.v10i50.1344

RESEARCH ARTICLE OPEN ACCESS

OPTIMIZING PORTER ASSIGNMENTS IN HOSPITAL: A MATHEMATICAL MODELING APPROACH FOR WORKLOAD BALANCING

Chawis Boonmee[1] and Phavika Mongkolkittaveepol[2*]

[1,2] Department of Industrial Engineering, Faculty of Engineering, Chiang Mai University, Chiang Mai, Thailand 50200

[1]https://orcid.org/0000-0002-3656-513X, [2] https://orcid.org/0009-0006-4342-6513

Email: chawis.boonmee@cmu.ac.th, phavika.m@cmu.ac.th

ARTICLE INFO

Article History
Received: October 22, 2024
Revised: October 30, 2024
Accepted: November 10, 2024
Published: December 31, 2024

Keywords:
Assignment problem,
Mathematical model,
Porter assignment,
Hospital,
Workload balancing.

ABSTRACT

This case study addresses the staffing challenges faced by a hospital's porter service, which is currently insufficient to meet patient needs effectively. Due to the lack of a systematic task assignment mechanism, the head of the porters' center has had to manage patient transport manually, leading to unequal workload distribution among porters. This research aims to rectify this operational issue by developing a mathematical model and a user-friendly program for optimizing porter assignments. The methodology includes extensive data collection on existing protocols and factors affecting operations. A mathematical model is formulated with the objective of minimizing monthly workload deviations among porters. The model is executed using Excel Solver, producing an optimal assignment solution. Additionally, Visual Basic for Applications (VBA) in Excel is utilized to create a practical program for real-world application. A quantitative comparison of the standard deviation in cumulative workload from September 2022 reveals a significant improvement: the proposed program reduced the standard deviation by 5,907 seconds, or 76.17%. This outcome highlights the effectiveness of the new solution in achieving a more balanced distribution of porter assignments, thereby enhancing operational efficiency.

I. INTRODUCTION

Due to the recent elevation of the case study hospital to the status of a central healthcare facility catering to patient referrals from hospitals within the Chiang Mai, Lamphun, and Mae Hong Son provinces in Thailand, accompanied by its advancement as a high-level center of expertise in accident care, the hospital has garnered approval for a substantial expansion of its bed capacity to 700 beds in the fiscal year 2022. Concomitantly, there has been a marked escalation in the utilization rates.

The extant responsibilities of porters at the case study hospital encompass the intricate coordination of patient movements within the wheelchair and stretcher services, inclusive of a spectrum of associated tasks. A pivotal facet of the porter's duties resides in their imperative to function within stringent temporal constraints while managing a sizable and demanding workload. This is precipitated by the exigency for porters to promptly furnish services to incoming patients, facilitating their expeditious transfer to diagnostic examination rooms or designated patient wards.

An examination of hospital data reveals a discernible and escalating influx of patients seeking treatment at the case study hospital annually. Within this cohort, a subset necessitates assistance in their mobility to access different departments within the hospital for requisite medical interventions. The responsibility for patient transport falls under the purview of the "Porter Center," currently operational at six strategic locations, encompassing the Accident Building, Emergency Room (ER), Outpatient Department (OPD), as well as specific points such as X-RAY, MRI, CT, and U/S. Additionally, the porter services extend to the Inpatient Department (IPD).

Each porter contends with a substantial daily workload, heightened by the increased demand for services and the multifaceted nature of assigned tasks. Nevertheless, the prevailing task assignment framework lacks a transparent mechanism for the equitable distribution of responsibilities among porters, resulting in an imbalanced workload distribution. Consequently, some porters bear a disproportionate burden, leading to fatigue due to the physical demands involved in patient transport, preparatory activities, and sanitation tasks. This is particularly pronounced for porters handling patients with substantial body weight, predisposing them to fatigue or potential musculoskeletal injury. These challenges have tangible implications, resulting in service delays that impact both patient experience and hospital operational efficiency.

The task assignment predicament aims at optimizing the allocation of available resources to maximize benefits. Task assignment is a methodological process in problem-solving to find the most appropriate solution. Ordinarily, task assignment is performed by supervisors, and decisions are influenced by their personal perspectives. However, reliance on personal perspectives may lead to an inequitable distribution of tasks among porters. This necessitates the application of task assignment algorithms to enhance work efficiency and minimize work duration for each porter.

Additionally, this research conducted a root cause analysis of the task assignment problem for porters at the case study hospital by studying the distribution data using the Why-Why Analysis tool. The results are elucidated in Figure 1.

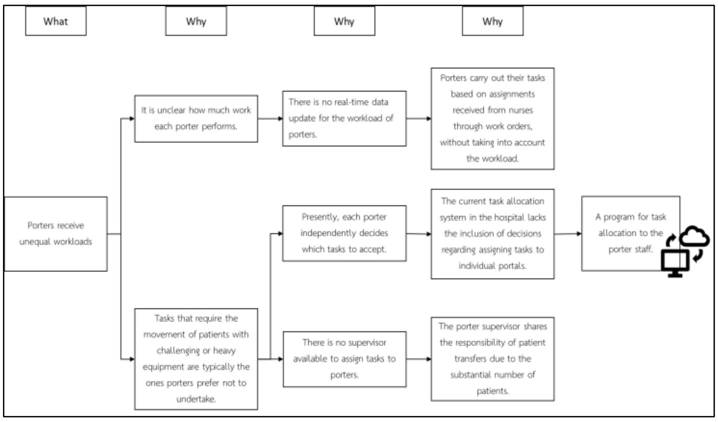

Figure 1: Why-Why analysis chart for the issue of porters' work assignment.
Source: Authors, (2024).

Therefore, this research proposes the utilization of Linear Programming as a tool to address task assignment problems. Linear Programming is a problem-solving tool in Operations Research, employing mathematical models to assist in problem-solving. It is effective in covering problems with limited resources and providing optimal results. This research applies Excel Solver as a software tool to solve the task assignment problem, utilizing mathematical models to prescribe conditions for porter task assignments. The mathematical model aims to propose the absolute cumulative workload deviation of porters on a daily basis as the objective function. Moreover, this research employs Visual Basic for Applications (VBA) to create a program for decision-making in task assignments to porters, aimed at achieving optimal workload balance.

II. THEORETICAL REFERENCE

In recent years, there has been a significant focus on applying mathematical modeling and optimization techniques in the healthcare sector [1], particularly in the domains of workforce scheduling and task assignment. This literature review provides a comprehensive overview, shedding light on the role of mathematical models in optimizing healthcare operations, with a specific focus on nurse scheduling and task assignment problems. [2] contribute to this field by applying mathematical modeling techniques to nurse scheduling at Surasat General Hospital, aligning with global efforts to ensure efficient nurse scheduling for high-quality patient care and the well-being of healthcare professionals. The literature review indicates a growing interest in utilizing mathematical models to optimize healthcare operations, considering factors such as staff availability, skill mix, and patient demand.[3], [4] provide valuable insights into daily patient-nurse assignments and load-balancing nurse-to-patient assignments, respectively. The former introduces Constraint Programming (CP) models, enhancing scalability and accuracy, while the latter emphasizes the superiority of Constraint Programming over Mixed-Integer Quadratic Programming (MIQP) in addressing workload variance. Additionally, other researchers, including [5-7] contribute to the discourse on nurse assignment.

The application of optimization extends to ambulance transports, as shown by [8], addressing the challenge of hospital overloading during unusual demand shifts in emergency medical services (EMS) systems. They propose a load-balancing optimization algorithm developed in collaboration with Columbia University and the Fire Department of the City of New York, emphasizing a proactive approach to prevent hospital overload during unexpected incidents. [9] address real-time optimization challenges in Emergency Medical Services (EMS) with a survival-based framework, focusing on maximizing patient survival while balancing EMS workload. Their approach, validated in a New York City case study, demonstrates significant improvements in response times for life-threatening emergencies, efficient workload balancing, and potential cost savings through integrating ride-hailing services.

To apply optimization techniques to porter assignment in hospitals, [10] extend mathematical modeling to task assignment and distribution for hospital porters, emphasizing the shift from traditional scheduling problems to broader resource allocation challenges within healthcare settings. This underscores the importance of workload balance for both nursing staff and ancillary services, highlighting the holistic nature of healthcare operations. [11] emphasize the crucial role of porters in hospital operations and address transparency in their movements through an Indoor Location-Based Porter Management System (LOPS). This system provides real-time location information to the dispatcher, enabling hospitals to enhance porter team efficiency and streamline daily operations for improved patient care. [12] highlight critical considerations in patient transportation within hospitals, integrating the needs of hospital managers, patients, and porters into a mathematical model. The tailored Tabu search algorithm used in solving the model demonstrates efficiency, producing high-quality solutions in a short time frame that outperform those generated by typical real-world planning approaches. The research emphasizes the trade-off between the interests of hospital managers, patients, and porters, underscoring the significance of holistic and optimized patient transport systems in healthcare settings.

In conclusion, these studies collectively reflect a growing trend in healthcare operations research, emphasizing the need for systematic, quantitative approaches to address scheduling, task assignment, and resource optimization challenges. The literature suggests that mathematical modeling, particularly linear programming and other optimization techniques, is increasingly becoming integral to decision-making processes in healthcare operations. This trend aligns with the broader paradigm shift towards data-driven decision-making and evidence-based management in healthcare, contributing to a broader understanding of the role of quantitative methods in enhancing efficiency and quality of service delivery in healthcare and other industries.

III. MATERIALS AND METHODS

In this research, the methodology comprises a multi-step investigation and analysis approach to address the task assignment and workload distribution challenges faced by hospital attendants at the case study hospital in Chiang Mai. The methodology is structured into distinct sections:

1. Examination of Current Attendant Workflow at hospital.

The initial phase of this research focused on analyzing the current workflow and assignment protocols for attendants at the case study hospital, located in Chiang Mai. The investigation encompassed various aspects such as task delegation mechanisms, procedures from task assignment to patient transfer completion, the daily workforce count, equipment utilization during patient transfers, established routes for attendants, location mapping of the attendant center, and overall hospital infrastructure. Additionally, this study explored various contributory factors leading to delays in patient transfers. Data was primarily sourced through consultations with the head of the attendant center at the case study hospital and supplemented with relevant prior research.

2. Exploration of Mathematical Modeling Principles and Excel Solver Application.

The research subsequently delved into studying pertinent mathematical modeling theories to facilitate the development of an appropriate model for task assignment optimization. Utilizing Microsoft's Excel Solver tool, the study aimed to generate objective functions and constraint equations essential for solving the attendant task distribution problem. Furthermore, the research incorporated Visual Basic for Applications (VBA) within the Microsoft Excel environment to formulate and implement the requisite codebase.

3. Data Collection.

A meticulous data collection process ensued, focusing on gathering detailed information regarding attendant workflows, equipment usage, established patient transfer routes, and attendant work schedules. The objective was to identify prevalent operational challenges and analyze underlying causal factors. This comprehensive data served as the foundation for subsequent mathematical modeling efforts.

4. Mathematical Model Development for Problem Resolution.

The subsequent phase of the research utilized equipment usability as a metric to evaluate the complexity of attendant tasks. A mathematical model was developed to quantify the cumulative workload for each attendant based on the time-intensive nature of assigned tasks. This model employed the Mean Deviation (M.D.) formula to quantify the absolute average deviation from the mean workload.

5. Validation of the Mathematical Model.

To ascertain the efficacy and accuracy of the developed mathematical model, a validation process was undertaken. Small-scale data simulations were conducted to test the model's capabilities in optimizing task assignments and reducing workload discrepancies effectively.

6. Program Development for Attendant Task Allocation.

This phase involved the creation of a user-friendly program, incorporating the previously developed mathematical model within a Microsoft Excel VBA framework. The program aimed to automate task assignments for attendants at the case study hospital, ensuring equitable workload distribution among staff members.

7. Results Analysis and Conclusion.

The penultimate phase entailed a comprehensive analysis of outcomes derived from comparing standardized workload data with model-generated results. The research aimed to determine the model's efficacy in minimizing workload standard deviations and enhancing operational efficiency. Finally, this research culminated in summarizing the achieved milestones, compiling findings

IV. RESULTS AND DISCUSSIONS

IV.1 DATA COLLECTION

1. Attendant Work Log Data Collection

Data was gathered from attendants at the case study hospital, encompassing their work logs, which included information such as attendant names, patient transfer equipment used, additional transfer equipment utilized, the respective origin and destination departments involved in patient transfers, and the corresponding time expended on each patient transfer. A total of 2,428 data sets were amassed to facilitate the computation of workload weighting.

2. Building-to-Building Distance Data Collection

Building-to-building distances within the case study hospital were measured utilizing Google Maps. In addition, real-time measurements of distances were obtained, extending from the building's front to the elevator, employing specialized tools to offer a pragmatic representation of travel distances. Average distances were calculated, and a conversion to vertical distances was conducted by adopting a standard height of 3 meters per floor.

IV.2 MATHEMATICAL MODEL

The mathematical model, concerning the objective function, aims to minimize the absolute average deviation of the workload of attendants each month. The workload is evaluated based on the distance and the speed of the equipment used in patient transfers, including additional transfer accessories. The transformation of distances and the equipment used in patient transfers into a unified unit of measurement is necessary for a comprehensive assessment of the cumulative workload of attendants. This transformation ensures a clearer representation of workload weights in terms of time.

1. Calculating the Average Speed of Patient Transfer Equipment and Additional Transfer Accessories for Cumulative Workload Assessment:

To compute the average speed, the distance between departments, obtained through data collection, is utilized along with the time spent on tasks. The time data retrieved from the system is initially in Epoch Time format.

$$\frac{\text{Epoch Time}}{86{,}400} + 25{,}569 \quad (1)$$

Subsequently, it is converted into standard time format. After the conversion, the time is represented in regular seconds, enabling the calculation of the average speed of patient transfer equipment and additional transfer accessories used in patient transfers as shown in Table 1.

Table 1: Average speed ratios for the 7 criteria.

Criteria	Overall Speed Ratio	True Instances	Average Speed (m/s)
Wheelchair	211.57	160	1.32
Wheelchair + Saltwater/Rubber Tube/Foley Catheter	14.51	19	0.76
Crutch	68.66	97	0.71
Crutch + Saltwater/Rubber Tube/Foley Catheter	56.37	92	0.61
Crutch + Ventilator	2.90	5	0.58
Crutch + O2	9.92	31	0.32
Crutch + Over	1.57	8	0.20

Source: Authors, (2024).

2. Mathematical Model Using the Absolute Average Deviation Component:

Indices

i : Set of attendants (i = 1, 2, …, n)

j : Set of assigned tasks (j = 1, 2, .., m)

k : Set of workdays (k = 1, 2, …, k)

Parameters

w_{ij}^{k}: Cumulative workload of attendant i assigned to task j accumulated from day 1 to day k.

mean^k: The average cumulative working time of attendants at present

e_i: Deviation value of attendant i.

Decision Variable

x_{ij} : Equals 1 when attendant i is assigned task j; otherwise, it is 0.

e_i^+ : Deviation value of attendant i when e_i is greater than 0

e_i^- : Deviation value of attendant i when e_i is less than 0

Objective function

$$Min\ Z = \frac{\sum_{i=1}^{n} |e_i|}{n} \quad (2)$$

Constraints

$$e_i = mean^k - \sum_{j=1}^{m} w_{ij}^k x_{ij} \quad \forall_{i,k} \quad (3)$$

$$\sum_{i=1}^{n} x_{ij} = 1 \quad \forall_j \quad (4)$$

$$\sum_{j=1}^{m} x_{ij} = 1 \quad \forall_i \quad (5)$$

$$x_{ij} = \{0,1\} \quad \forall_{i,j} \quad (6)$$

Equation (2) presents the objective function with the aim of finding the absolute deviation average of cumulative working time for the attendant with the lowest value. This equation is derived from the absolute deviation average equation, where the variable e_i can be obtained from the difference between the average cumulative workload of all attendants on day k and the cumulative workload of attendant i performing task j from day 1 to k as shown in Equation (3). Regarding the constraint equations, they enforce that each task is assigned to only one attendant, expressed in Equation (4) , and that each attendant must be assigned one task. Since the system involves assigning tasks sequentially, additional tasks are created equal to the number of attendants. These artificially generated tasks facilitate the optimization process of the Hungarian method, as outlined in Equations (5) . The decision variable (x_{ij}) is binary, reflecting the decision to perform or not perform a task, expressed in Equation (6).

Based on the proposed mathematical model, it is observed that the absolute deviation of attendant i (e_i) is subject to absolute value, indicating that e_i can be either positive or negative. To conform to the standard format of linear programming problems, the variable e_i is transformed into $e_i = e_i^+ - e_i^-$. To achieve this transformation, it is required that both e_i^+ and e_i^- are greater than or equal to 0, as stated in Equations (12) and (13). In summary, the objective function aims to minimize the sum of absolute workload deviations for each attendant in each month divided by the total number of attendants (n). Therefore, the reformulation of mathematical model is presented as follows.

Objective function

$$Min\ Z = \frac{\sum_{i=1}^{n} (e_i^+ + e_i^-)}{n} \quad (7)$$

Constraints

$$e_i^+ - e_i^- + \sum_{j=1}^{m} w_{ij}^k x_{ij} = mean^k \quad \forall_{i,k} \quad (8)$$

$$\sum_{i=1}^{n} x_{ij} = 1 \quad \forall_j \quad (9)$$

$$\sum_{j=1}^{m} x_{ij} = 1 \quad \forall_i \quad (10)$$

$$x_{ij} = \{0,1\} \quad \forall_{i,j} \quad (11)$$

$$e_i^+ \geq 0 \quad \forall_i \quad (12)$$

$$e_i^- \geq 0 \quad \forall_i \quad (13)$$

IV.3 MODEL VALIDATION

In the validation phase of the mathematical model, the accuracy of the mathematical model and the constraint equations used to solve the problem is examined to determine if tasks can be assigned to attendants to achieve balance. This involves simulating small-scale data to test the mathematical model, allowing it to produce results more efficiently. In this section, Microsoft Excel Solver is employed as a tool for testing. The objective function, decision variables, and various constraints of the Solver are specified. The objective function aims to minimize the absolute deviation average of cumulative workload for attendants in each month. The Microsoft Excel Solver is used to test whether the mathematical model can efficiently allocate tasks to attendants while achieving the minimum absolute deviation average of cumulative workload. This validation process ensures that the model accurately represents the problem and can provide optimal solutions.

IV.4 PROBLEM DEVELOPMENT

In the program development section, the researchers opted to use Microsoft Excel as their programming tool for allocating tasks to hospital attendants at the case study hospital, aiming to achieve a balanced workload. Microsoft Excel allows the integration of Visual Basic for Applications (VBA) code into its spreadsheet application, facilitating the creation of a user-friendly program. This program, once developed, will automate the task allocation process based on the mathematical model created.

The researchers designed the program using VBA with the objective of creating a systematic and user-friendly tool for practical use. The program's workflow is illustrated in Figure 2.

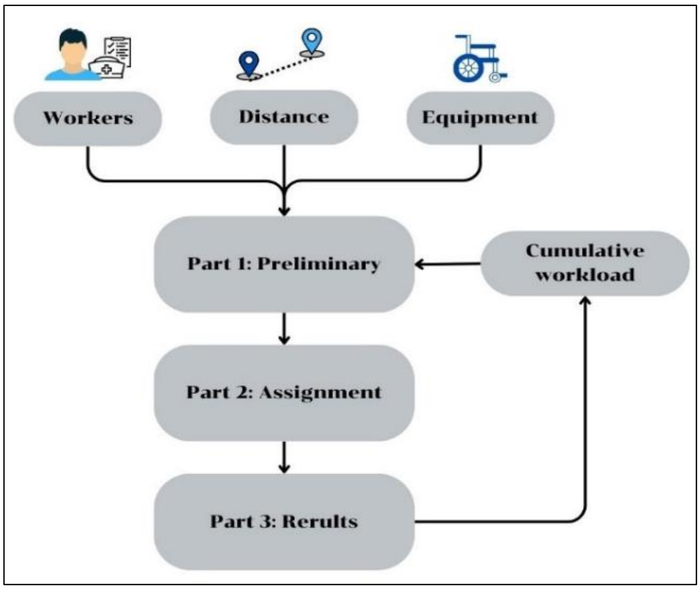

Figure 2: Workflow of the program.
Source: Authors, (2024).

The program is divided into three main parts:

Part 1: Preliminary

This part is responsible for data input, including the list of attending staff, the origin and destination departments for patient transfers, and the equipment used. It calculates the workload based on the distance traveled, equipment speed, and assigns this workload to be used in the task assignment process in Part 2.

Part 2: Assignment

This section utilizes the mathematical model to allocate tasks. It displays the assignment results from the Solver tool, showing which attendant is assigned which task and the corresponding workload. The results are then sent to Part 3.

Part 3: Results

This part displays the task assignment results obtained from Part 2. The results are added to the cumulative workload from previous rounds, and the new cumulative workload is sent back to Part 1 to inform task assignment decisions in the next round.

The three-part structure ensures a clear and organized workflow for the program, making it efficient and user-friendly for real-world applications.

IV.5 RESULTS ANALYSIS

The obtained data is subjected to further analysis, focusing on the results obtained from the actual work records of attendants who received task assignments. This data has been previously collected for the month of September (2022), consisting of a total of 456 records. The information includes the names of assigned attendants, the origin and destination departments for patient transfers, as well as the equipment used for the transfers, including auxiliary equipment. This data is input into a program to calculate the workload for each task. Subsequently, the calculated workload values are used to update the cumulative workload of each attendant. The cumulative workload obtained from task assignments using the old method is then compared with the cumulative workload obtained from task assignments using the mathematical model created by the Excel Solver tool. The results are recorded and presented in Table 2 for further analysis.

In scrutinizing Table 2 and Figure 3, a conspicuous observation emerges regarding the standard deviation values of cumulative workload among transport staff members. Specifically, the standard deviation associated with the conventional task assignment method stands at 7,754 seconds, eclipsing the analogous metric derived from the simplistic program, which registers at 1,847 seconds. This dichotomy underscores the superior equilibrium achieved by the program in workload distribution during the month of September compared to the traditional approach. Furthermore, discernible workload variations among staff members can be attributed to discrepancies in the number of workdays for certain individuals during that month.

In the subsequent analysis, a robust statistical examination was undertaken to assess the statistical significance of the difference in standard deviations in cumulative workloads between the traditional assignment method and the utilization of the straightforward program. The null hypothesis (H_0) posits the equality of standard deviations ($\sigma_1 = \sigma_2$), while the alternative hypothesis (H_1) asserts that the standard deviation associated with the traditional method surpasses that of the uncomplicated program ($\sigma_1 > \sigma_2$).

The examination of cumulative workload data for hospital transport staff at the case study hospital during September has revealed noteworthy insights. The conventional assignment method yielded a variance of 60, 120 and 711 in cumulative workloads, while the utilization of a program for task assignments resulted in a significantly lower variance of 3, 412, and 865. A meticulous comparative analysis of these cumulative workload variances indicates a profound statistical impact on the workload distribution among hospital transport staff.

Table 2: Comparison of task assignment results between the traditional method and after implementing the morning and afternoon shifts model in august, 2022.

Staff First Name	The actual number of working days	Before	After
		Time of cumulative workloads (Second)	Time of cumulative workloads (Second)
A	8	6,996	6,523
B	18	11,068	9,198
C	18	31,001	9,895
D	11	15,786	11,251
E	3	1,671	3,212
D	21	19,122	10,016
G	16	14,228	10,064
H	12	8,957	10,017
I	12	9,350	9,938

J	13	8,386	9,360
K	6	4,147	10,376
L	11	10,750	9,913
M	5	1,166	9,383
N	7	3,771	8,767
O	5	3,520	7,659
P	4	1,642	9,382
Q	4	2,665	9,264
Mean		9,072	9,072
SD		7,754	1,847

Source: Authors, (2024).

Note: In the section about some attendants having different cumulative workload values than other attendants, this is due to the fact that in that month, those specific attendants had fewer actual working days compared to other attendants.

The empirical findings suggest that the implementation of the straightforward program for task assignments has a substantial influence on reducing the variance in cumulative workloads. The statistical significance of this impact is robust, attaining a 95% confidence level. Additionally, the p-value derived from the F-test, being less than 0.05, leads to the rejection of the null hypothesis (H0: $\sigma_1 = \sigma_2$) and the acceptance of the alternative hypothesis (H*1*: $\sigma_1 > \sigma_2$). This implies that the program significantly contributes to minimizing the variability in cumulative workloads, fostering a more consistent distribution among the hospital transport staff.

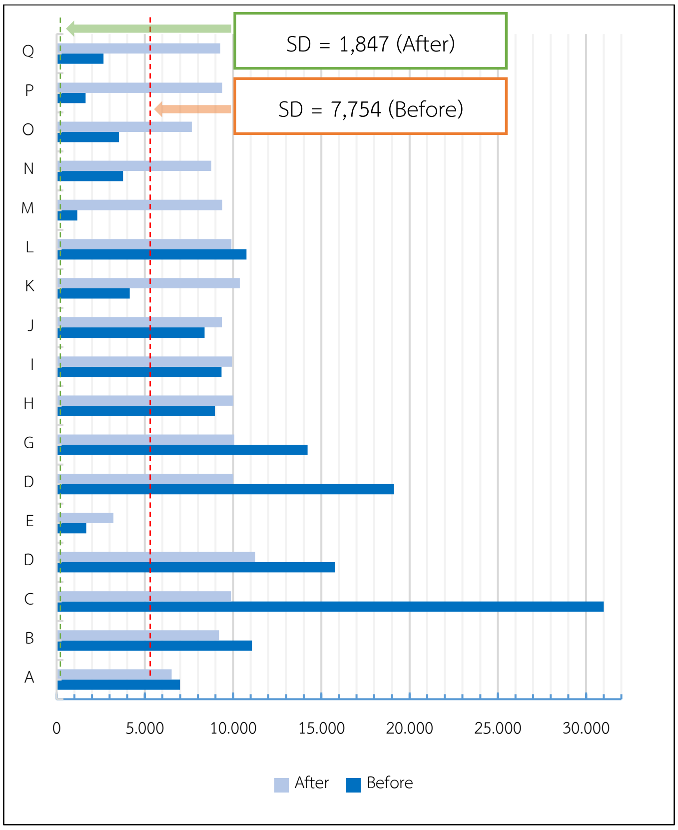

Figure 3: Comparison graph of workload results before and after optimization.
Source: Authors, (2024).

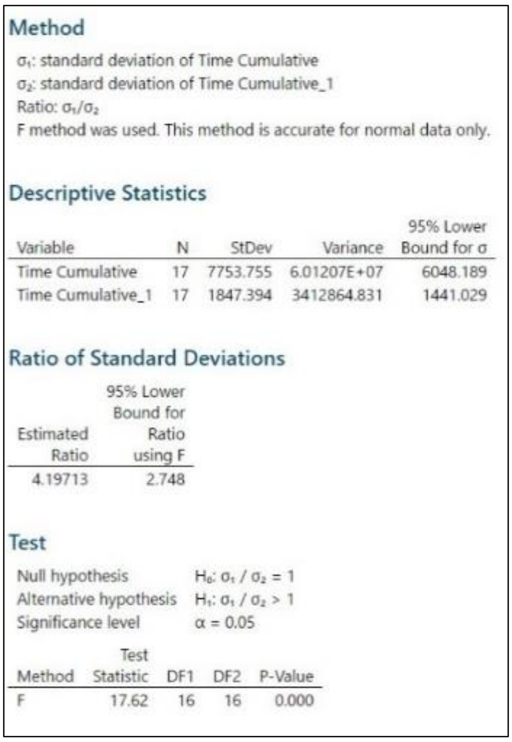

Figure 4: Statistical Analysis using F-Test.
Source: Authors, (2024).

Table 3: Summary of user satisfaction evaluation for the program.

Satisfaction Aspect	Satisfaction	
	Mean Score	Percentage
1. Operational Processes / Program Workflow	4.5	90
1.1 Program Workflow Pattern	4	80
1.2 Program Task Execution Capability	5	100
2. Program Efficiency	3.6	72
2.1 Accuracy and Precision	4	80
2.2 Alignment with Objectives	3	60
2.3 Data Accuracy and Currency	4	80
2.4 User-Friendliness	4	80
2.5 Program Stability	3	60
3. User-Friendliness	3	60
3.1 Overall Program Design Suitability	3	60
3.2 Ease of Use and Simplicity	3	60
4. Program Quality	4	80

4.1 Future Usability of the Program	4	80
4.2 Satisfaction with Program Usage	4	80
Overall Score	3.78	75.6

Source: Authors, (2024).

Note:
Mean satisfaction scores interpretation:
4.51 - 5.00: Highly Satisfied
3.51 - 4.50: Satisfied
2.51 - 3.50: Moderate Satisfaction
1.51 - 2.50: Dissatisfied
1.00 - 1.50: Highly Dissatisfied
Satisfaction percentage interpretation:
91 - 100%: Highly Satisfied
71 - 90%: Satisfied
51 - 70%: Moderate Satisfaction
31 - 50%: Dissatisfied
21 - 30%: Highly Dissatisfied

The empirical findings in Figure 4 suggest that the implementation of the straightforward program for task assignments has a substantial influence on reducing the variance in cumulative workloads. The statistical significance of this impact is robust, attaining a 95% confidence level. Additionally, the p-value derived from the F-test, being less than 0.05, leads to the rejection of the null hypothesis (H0: $\sigma_1 = \sigma_2$) and the acceptance of the alternative hypothesis (H_1: $\sigma_1 > \sigma_2$). This implies that the program significantly contributes to minimizing the variability in cumulative workloads, fostering a more consistent distribution among the hospital transport staff.

In conclusion, the application of the program for task assignments has demonstrated not only practical efficacy but also statistical significance, affirming its positive influence on mitigating the variability in cumulative workloads for hospital transport staff at the case study hospital.

Following the statistical analysis using the F-Test with Minitab software, the examination of the standard deviations of cumulative workloads for hospital transport staff, both assigned tasks using the traditional method and the newly introduced program, revealed a statistically significant reduction in workload variance. The ensuing standard deviation values were then utilized to calculate the proportional reduction in workload variance before and after the implementation of the program, with the comprehensive findings meticulously compiled into a thorough report.

Additionally, the program, meticulously crafted by the researcher, was presented to the head of the transport center for practical application. The opportunity for hands-on usage allowed the center's head to gain profound insights into the intricacies of the program's operational processes. A detailed evaluation form was subsequently administered, focusing on four key dimensions: 1) Process or operational workflow, 2) Program efficiency, 3) User-friendliness, and 4) Program quality.

The culmination of the evaluation process yielded an overall satisfaction level with a mean score of 3.78, indicating a commendable degree of contentment. Notably, the assessment of operational processes (Dimension 1) stood out with the highest satisfaction level, attaining a mean score of 4.5. Simultaneously, program efficiency (Dimension 2) garnered a satisfactory mean score of 3.6. User-friendliness (Dimension 3) achieved a moderate satisfaction level, obtaining a mean score of 3, while program quality (Dimension 4) secured a high satisfaction level with a mean score of 4. The nuanced satisfaction ratings are meticulously detailed in Table 3**.**

IV.6 MANAGERIAL INSIGHTS

The managerial insights derived from this research provide valuable information and recommendations for decision-makers and managers. Here are some key managerial insights:

1. Efficiency Improvement through Program Implementation: The implementation of the program has resulted in increased operational efficiency. The program's task execution capability and workflow pattern received high satisfaction scores (100% and 80%, respectively). Managers can infer that adopting this program enhances overall efficiency in task management.

2. Accuracy and Data Quality: Users expressed satisfaction with the program's accuracy and precision, data accuracy, and currency (80% satisfaction for each). This suggests that the program contributes to maintaining high data quality. Managers should recognize the importance of accurate information for decision-making processes.

3. User-Friendly Design: The program's overall design suitability and ease of use received moderate satisfaction scores (60%). Managers should consider investing in further user interface enhancements to make the program more user-friendly, potentially leading to increased satisfaction and productivity.

4. Stability and Future Usability: Program stability received a satisfaction score of 60%, indicating room for improvement. Managers should focus on enhancing the stability of the program to ensure a seamless user experience. Additionally, the positive response regarding the future usability of the program (80%) suggests that continued investment in the program is worthwhile.

5. Holistic Program Quality: The overall program quality, including its ability to meet objectives and user satisfaction, scored 80%. Managers can interpret this as a positive indication that the program is perceived as valuable and meets the needs of the users. Continuous quality monitoring and updates should be implemented to sustain high satisfaction levels.

6. Employee Training and Support: To address areas of lower satisfaction, particularly in user-friendliness, managers should consider implementing training programs or providing additional support to users. This can help users adapt to the program more easily and increase overall satisfaction.

7. Strategic Decision-Making: The insights gained from the research can inform strategic decision-making regarding the use and enhancement of the program. Whether it involves refining the user interface, improving stability, or planning for the program's future use, managers can strategically allocate resources for maximum impact.

8. Continuous Feedback Loop: Establishing a continuous feedback loop with end-users can further enhance the program's effectiveness. Regularly soliciting feedback, addressing concerns, and implementing user-driven improvements contribute to long-term user satisfaction and sustained program success.

By considering these insights, managers can make informed decisions to optimize the use of the program, improve user satisfaction, and align organizational processes with strategic objectives.

V. CONCLUSIONS

The researcher has embarked on the systematic aggregation of data, encompassing information derived from the work logging software employed by the transport staff. This dataset is instrumental in the derivation of speed parameters for the equipment integral to patient transport, both in terms of primary conveyance apparatus and ancillary devices. Furthermore, pertinent data concerning inter-departmental distances is compiled to facilitate the computation of workload metrics. Subsequently, a mathematical model is conceived, characterized by the optimization of the objective function—specifically, the minimization of the absolute deviation in cumulative workload values across each month, as articulated in Equation (4). The ensuing imperative is the meticulous validation of the mathematical model's precision, a task undertaken through the simulation of petite-scale data using the Excel Solver functionality within the Microsoft Excel milieu. The outcomes of this simulation attest to the model's efficacy in task assignment, demonstrating a predilection for staff members with reduced cumulative workloads, thus aligning seamlessly with the stipulated research objectives.

Post-validation, the research trajectory pivots towards the development of a rudimentary program. This choice leans towards Microsoft Excel due to its adeptness in accommodating Visual Basic for Applications (VBA) code amalgamated into the fabric of Visual Basic applications within the Microsoft Excel ecosystem. The program's elementary nature engenders an automatic generation of results predicated on assigned tasks, leveraging the underlying mathematical model. A trial deployment of the program ensues, utilizing authentic work data from the transport staff in September, juxtaposing the outcomes against the actual task assignments. This comparative analysis reveals a noteworthy reduction in the standard deviation of the cumulative workload for transport staff—from 7,754 seconds to 1,847 seconds—constituting a consequential diminution of 76.17%.

In the vein of suggestions for augmentative refinement, it is posited that the program could be elevated through the infusion of code in alternative languages, thereby concomitantly enhancing processing velocity and broadening the gamut of tasks within its purview [13]. Anticipating scenarios involving the engagement of temporary staff, prospective iterations may contemplate the integration of additional conditions to accord precedence to the task allocation for daily wage laborers. Instances where transport staff undergoes transient work cessation and subsequent resumption would necessitate programmatic adjustments to forestall the imposition of unduly burdensome tasks upon returning staff members. Moreover, a prudent course of action entails the delineation of an upper limit for the workload value, preempting the assignment of tasks that surpass manageable thresholds.

Further considerations advocate for program refinements catering to scenarios typified by consecutive or overlapping task assignments. A nuanced modification would entail the incorporation of supplementary conditions stipulating that actively engaged transport staff should be exempted from the reception of new tasks. This adaptive measure ensures that the program mitigates the challenge of consecutively or concurrently assigned tasks. Additionally, programmatic adaptations beckon the integration of functionalities permitting nursing personnel to input data into the system. This symbiotic interfacing allows the mathematical model ingrained in the system to systematically process information and proactively apprise the transport center regarding new tasks, subsequently allotting these tasks to available transport staff.

Moreover, this research can provide actionable insights that can be applied to SME, enabling enhanced operational efficiency, resource optimization, and overall competitiveness through the adaptation of workload balancing and mathematical modeling principles.

VI. AUTHOR'S CONTRIBUTION

Conceptualization: Chawis Boonmee.
Methodology: Chawis Boonmee.
Investigation: Chawis Boonmee and Phavika Mongkolkittaveepol.
Discussion of results Chawis Boonmee and Phavika Mongkolkittaveepol.
Writing – Original Draft: Chawis Boonmee.
Writing – Review and Editing: Chawis Boonmee and Phavika Mongkolkittaveepol.
Resources: Chawis Boonmee.
Supervision: Chawis Boonmee and Phavika Mongkolkittaveepol.
Approval of the final text: Chawis Boonmee and Phavika Mongkolkittaveepol.
Corresponding author: Phavika Mongkolkittaveepol.

VII. ACKNOWLEDGMENTS

This research is part of the project "A Strategic Roadmap Toward the Next Level of Intelligent, Sustainable, and Human-Centered SME: SME 5.0" from the European Union's Horizon 2021 research and innovation program under the Marie Skłodowska-Curie Grant agreement No. 101086487.

VIII. REFERENCES

[1] C. Boonmee and C. Kasemset, "The improvement of healthcare management in Thailand via IE tools: A survey," in Proceedings of International Conference on Industrial Engineering and Operations Management, Bangkok, Thailand, Mar. 2019, pp. 264–274.

[2] R. Bojaras and Y. Yothee, "Nurse scheduling model by integer linear programming (A case study: The Fort Sunpasitthiprasong hospital)," Thai Journal of Operations Research, vol. 7, no. 2, pp. 20–29, 2019.

[3] P. Schaus, P. Van Hentenryck, and J.-C. Régin, "Scalable load balancing in nurse to patient assignment problems," in Proceedings of the 2009 International Conference on Operations Research, 2009, pp. 248–262. doi: 10.1007/978-3-642-01929-6_19.

[4] W.-Y. Ku, T. Pinheiro, and J. C. Beck,"CIP and MIQP models for theload balancing nurse-to-patient assignment problem," in Proceedings of the 2014 International Conference on OperationsResearch, 2014, pp. 424–439. doi: 10.1007/978-3-319-10428-7_32.

[5] O. Riklikiene, O. Didenko, R. Ciutiene, A. Daunoriene, and R. Ciarniene, "Balancing nurses' workload: A case study with nurse anaesthetists and intensive carenurses," Economics & Sociology, vol. 13, no. 2, pp. 11–25, Jun. 2020. doi: 10.14254/2071-789X.2020/13-2/1.

[6] P. Schaus and J.-C. Régin, "Bound-consistent spread constraint: Application to load balancing in nurse-to-patientassignments," EURO Journal on Computational Optimization, vol. 2, no. 3, pp. 123–146, Aug. 2014. doi: 10.1007/s13675-013-0018-8.

[7] J. Sangai and A. Bellabdaoui, "Workload balancing in nurse scheduling problem modelsand discussion," in 2017 International Colloquium on Logistics and Supply Chain Management (LOGISTIQUA), IEEE, Apr. 2017, pp. 82–87. doi: 10.1109/LOGISTIQUA.2017.7962878.

[8] E. Dolan et al., "Hospital load balancing: A data-driven approach to optimize ambulance transports during the COVID-19 pandemic in New York City," SSRN ElectronicJournal, 2022. doi: 10.2139/ssrn.4094485.

[9] Y. Essus, R. De La Fuente, and A. Venkitasubramanian, "Real-timeoptimization for relocation and dispatching of Emergency Medical Services with balanced workload and outsourced ride-hailing services," Comput. Ind. Eng., vol. 187, p. 109823, Jan. 2024. doi: 10.1016/j.cie.2023.109823.

[10] T. Jaikaew andP. Nomraksaksri, "Software prototype design for patient transport system for porters and administration at NakornpingHospital," Project, Chiang Mai University, Chiang Mai, 2020.

[11] C.-R. Lee, E. T.-H. Chu, H.-C. Shen, J. Hsu, and H.-M. Wu, "An indoor location-based hospital porter management system and trace analysis," Health Informatics J., vol. 29, no. 2, Apr. 2023. doi: 10.1177/14604582231183399.

[12] A. Fröhlich von Elmbach, A. Scholl, and R. Walter, "Minimizing the maximal ergonomic burden in intra-hospital patient transportation," Eur. J. Oper. Res., vol. 276, no. 3, pp. 840–854, Aug. 2019. doi: 10.1016/j.ejor.2019.01.062.

[13] C. Boonmee, K. Akarawongsapat, W. Wisittipanich, W. Chattinnawat, and K. Khwanngern, "Differential evolution for cleft lip and/or cleft palate patient treatment scheduling problems: a northern Thailand hospital case study," Ann. Oper. Res., vol. 335, no. 1, pp. 563–595, 2024. https://doi.org/10.1007/s10479-023-05769-6

Journal of Engineering and Technology for Industrial Applications

ITEGAM-JETIA

ISSN ONLINE: 2447-0228

Manaus, v10. n.50, p. 228-234. November/ December., 2024.
DOI: https://doi.org/10.5935/jetia.v10i50.1356

RESEARCH ARTICLE OPEN ACCESS

NEURAL NETWORK EDDY CURRENT NON-DESTRUCTIVE EVALUATION OF CONDUCTIVE COATINGS THICKNESS

Islam Nacer Eddine El Ghoul*[1], A.E. Lakhdari[2], S. Bensaid[3], A. Aissaoui[4], A.T. Ouamane[5]

[1] Scientific and technical research center of arid regions (CRSTRA), Algeria.
[2,3,4,5] University of Bouira, Algeria.

[1]http://orcid.org/0000-0002-9044-7214, [2]http://orcid.org/0000-0002-4803-4512, [3]http://orcid.org/0000-0002-2512-5040
[4]http://orcid.org/0009-0009-1943-4080, [5]http://orcid.org/0000-0002-7723-6834

Email: islammlili@yahoo.com, lakhdari_ala@yahoo.fr, bensaid2011@gmail.com, azeddine.aissaoui@gmail.com, altarek07@yahoo.fr

ARTICLE INFO

Article History
Received: October 27, 2024
Revised: October 30, 2024
Accepted: November 10, 2024
Published: December 31, 2024

Keywords:
EC-NDE,
ANN-ML,
Thickness measurement,
Multilayer material,
Conductive coating.

ABSTRACT

The proposed study is a machine learning application using a Neural Network for the prediction and identification of the thickness of aluminum placed over a steel plate. Two thousand and five hundred datasets with the eddy current method of different aluminum plate thicknesses above a steel plate and working frequencies of EC-sensor were generated using experimentally validated analytical models in our previous research. The data has three input parameters (normalized resistance, normalized reactance, and frequency) and one output (thickness). The ANN architecture involves careful consideration of the number of hidden layers and neurons within the model. The acquired data was split into two sections: the first section was used to train and test the selected model, and the second section was used to test the model on untrained data to demonstrate its high accuracy. The results obtained, as mentioned in the article, prove the validity and sensibility of the chosen model.

I. INTRODUCTION

Industrial components commonly surface treated through the application of engineering coatings, conferring new functional properties to the material surface like hardness, electrical conductivity, and thermal insulation...etc. The material composition of coatings, and desired properties such as thickness and adhesion to substrates, is controlled by specific deposition techniques and processes, i.e., PVD, CVD, electroplating, thermal spray, and others. Regardless of the selected process, rigorous control over coating quality is essential to ensure that the treated surfaces meet specified standards. When the coating parameters such as thickness is out of required specifications; the performance will be then negatively altered. Hence, the ability of the assessment of coating properties by the mean of non-destructive method offers a crucial importance for many industrial sectors such as aerospace, energy. In fact, Non-destructive evaluation techniques are based on determining the inherent physical and mechanical characteristics of a material without damaging or affecting its intended functionality, and subsequently using the resulted data to decide and predict its performance in the suitable applications [1].

Eddy current testing (NDE-EC) among other is a highly sensitive and less costly non-destructive evaluation technique compared to other methods. It is widely used particularly to detect geometric defects of material. Several experimental works have established that NDE-EC is a robust and reproductible technique to measure and reveal cracks, corrosion failure and thickness of protective coatings [2–8] .

NDE-EC modeling is also an additional study that can aid to better understanding the corresponding electrical and magnetic phenomena. Many research efforts have focused on the modeling and simulation of NDE-EC. Commonly the modeling study is associated with an inversion problem analysis in order to characterize or identify either the physical or geometric properties of the materials, or to optimize the inspection process [9], [10]. Design, development, and optimization of eddy current as non-destructive evaluation (NDE-EC) have been successfully developed through analytical [2], [3], [6–8], [11], [12] and numerical modeling [4], [5], [10], [13–16] based on electromagnetic systems.

The principle of thickness measurement by NDE-EC, is based on induced voltage or impedance change in a coil which is positioned above the plate to be measured. When alternating current is added at different frequencies in the coil an eddy-current is generated at different depths of the conductive plate providing a beneficial electromagnetic parameter information to measure and evaluate the thickness [2],[4], [5–8],[11],[12],[14],[16],[17].

According to Huang et al, NDE-EC is a relevant experimental technique to determine thin coatings thickness by the placement of the impedance of a coil probe above a coated multilayered plate using the swept-frequency eddy current testing method [14]. The studied phenomenon was described theoretically by Dodd and Deeds in [18], [3], [19] being a solution of the analytical expression of the coil impedance. Whereas, the optimization can be conducted by some methods such as artificial intelligence optimization to iteratively determine the thickness of coating layer based on the coil impedance.

Several artificial intelligence algorithms such as artificial neural networks (ANN) have proven successfully a good capability of managing, modeling, forecasting [20], [21], and predicting various aspects in electromagnetic, mechanical, and geometrical characterization, [22], [23].

As a data-driven computational model, artificial neural networks (ANN) can learn from given examples and ascertain the relationship between inputs and outputs without passing by a physical model, which can decrease the strong need for further extensive research.

The present work is a complementary study to the previous one of [24]. Where, they had experimentally validated analytical models developed by Dodd and Deeds and Theodoulidis et al [19], [25]. In fact, the main objective is firstly modeling of eddy current sensor-based system that allows thickness measurement of an aluminum layer in multilayer material in accurate and fast way the thickness of the aluminum plate (coating) placed on steel substrate over a wide range of frequencies. Secondly, the investigation of future values prediction for an aluminum plate thickness by ANN model. Where, training and testing datasets were initially produced using the previously validated models [24].

An artificial neural network (ANN) model has been created using the acquired datasets. Our artificial neural network (ANN) design considers the optimum arrangement of hidden layers and neurons in the model. The obtained data was divided into two parts: the initial part was used for training and evaluating the selected model, while the next one was used to evaluate the model's performance on untrained data, demonstrating its accuracy in the forecast of thickness. The collected results demonstrate the selected model's accuracy and sensitivity.

II. DATASET PREPARATION

Our study assumes that the provided problem is an axisymmetric eddy current. We adapt the system utilized in previous works (Figure 1) [3], [24]. A cylindrical coil of rectangular cross-section serves as the excitation source, positioned above a two-layer material where the first layer is a conductive material (aluminum) and the bottom layer is a ferromagnetic material (steel). Once more, the computation of the coil impedance changes induced by eddy current in the multilayer conductor is of primary concern [3], [24].

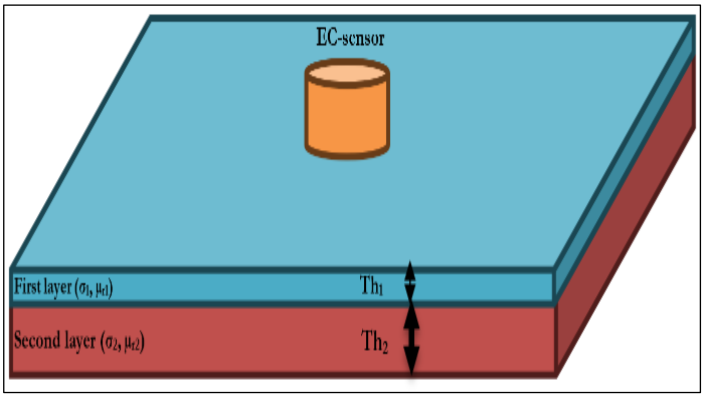

Figure1: Issue description.
Source: Authors, (2024).

The material to be evaluated has fixed physical parameters: two homogeneous layers of constant electric conductivity (σ) and relative magnetic permeability (μ_r). The distance between the coil and the material (lift-off) is fixed at 0.01 mm. It indicates how much the induced eddy currents alter the coil impedance and how much the coil is electromagnetically coupled to the material. The coil, top, and bottom layers extend to infinity in the third coordinate (z). The thickness of the first layer is changed from 0.01 to 0.25 mm, and the thickness of the steel layer is fixed to 5mm.

Tables 1 and 2 summarise the physical and geometrical properties of the material and coil used, respectively.

Table 1: The physical and geometrical properties of the material.

Multilayer material	Electrical conductivity (MS/m)	Relative magnetic permeability	Thickness of plate (mm)
First layer (Aluminum)	35.5	1	From 0.01 to 0.25
Second layer (Steel)	4.2	50	10

Source : Authors, (2024).

Table 2: Geometrical properties of the coil.

Coil parameter	
Outer diameter	19.4 mm
Inner diameter	10 mm
Height	4 mm
Lift-off	0.01 mm
Number of spires	406

Source: Authors, (2024).

Dodd and Deeds formulation [18] and the developed model by [3], [19] give an electromagnetic analytical solution to this problem. The magnetic vector potential *A* formulation in all regions satisfies the equation (1):

$$\left(\begin{array}{c} \frac{\partial^2 A}{\partial r^2} + \frac{1}{r}\frac{\partial A}{\partial r} - \frac{A}{r^2} + \frac{\partial^2 A}{\partial z^2} = \\ (j\omega\mu_r\mu_0\sigma)^2 A - \mu_0 I \delta(r_1 r_0)\delta(z_1 z_0) \end{array} \right) \quad (1)$$

δ is the penetration depth and I is the coil current, The total impedance of the coil is the sum of the individual coil impedance Z0 and the change in impedance Z produced by the conductive layer system. This change in impedance is a result of the presence of eddy currents within the system, which can be explained using the superposition principle. Having obtained the equation for Z0, equation (2) our task now is to calculate the value of ΔZ.

$$\begin{pmatrix} \Delta Z = \Delta R - j\Delta X = (R_c - R_0) + j(X_c - X_0) \\ = \dfrac{j2\pi\omega_{i0}}{r^2} \displaystyle\int_{r_1}^{r_2} \int_{z_1}^{z_2} A^{(ec)}\,(r_1 Z) drdz \end{pmatrix} \quad (2)$$

Equations (3) and (4) are used to compute the normalized resistance and reactance of the sensor for a range of frequencies and thicknesses of the aluminum layer as shown in Figure 2 and 3. Figure 4 illustrate the impedance normalised plane.

$$R_n = \frac{R_c - R_0}{X_0} \quad (3)$$

$$X_n = \frac{X_c}{X_0} \quad (4)$$

R_n and X_n are respectively the normalized resistance and normalized reactance. R_c and X_c are respectively the resistance and reactance of the eddy current sensor. R_0 and X_0 are respectively the sensor resistance and reactance sensor resistance without existence of material.

By varying the thickness of the first layer and the signal frequency by powering the sensor in an interval of 100 Hz up to 10 kHz with a step of 100 Hz, we obtained one hundred data points for each thickness. Furthermore, the thickness variation was from 0.01 mm to 0.25 mm with a step of 0.01 mm. In the end, we obtained data from 25 samples of the thickness of the first layer, and each one has 100 frequency calculations. At the end, three variables are in the input layer and a single output layer, each containing 2500 samples. The analytic model defined the normalized resistance and reactance, which proved the experimental solution to this problem in [24].

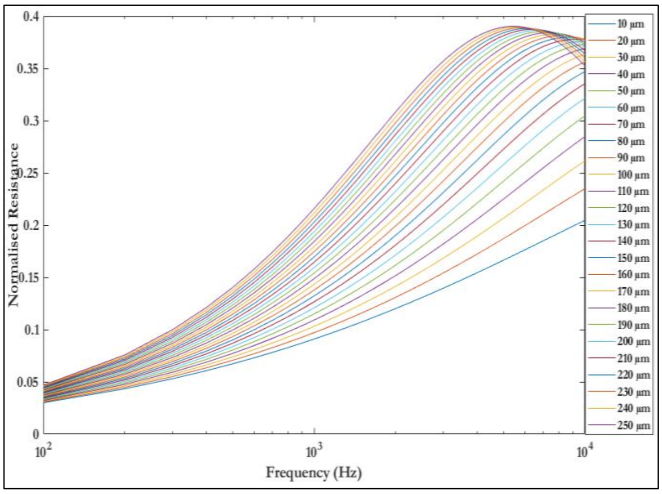

Figure 2: Normalized resistance.
Source: Authors, (2024).

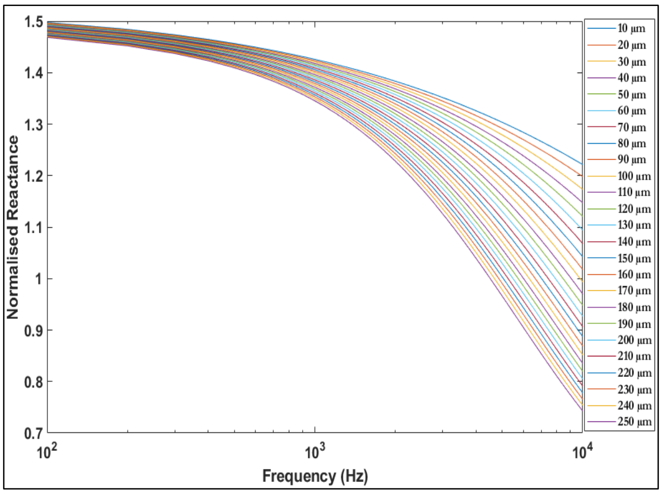

Figure 3: Normalized reactance.
Source: Authors, (2024).

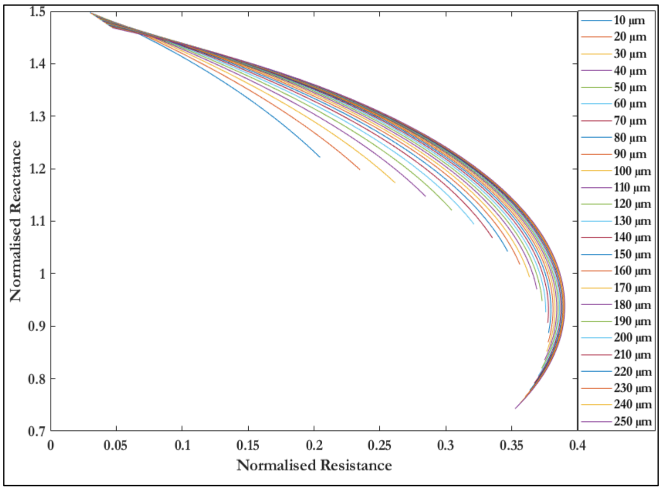

Figure 4: Impedance plane diagram.
Source: Authors, (2024).

III. ARTIFICIAL NEURAL NETWORK

This section delves into the development and training of an Artificial Neural Network (ANN) model for precise coating thickness prediction in eddy current testing scenarios. The ANN model is structured with an input layer, one or more hidden layers, and an output layer. The dataset is crucial for training the model to find relationships between input variables (normalized resistance, reactance, frequency) and output variables (thickness of the aluminum layer).

The ANN architecture involves careful consideration of the number of hidden layers and neurons within the model. Iterative testing determines that the optimal performance is achieved with 12 neurons in a hidden layer. The activation functions, specifically the sigmoid function in hidden layers and a linear function in the output layer, contribute to the model's capacity to learn complex relationships within the data. Figure (5) show the implemented ANN model's structure. The input layer of the Artificial Neural Network (ANN) is composed of essential parameters, including the responses of the coil at various frequencies. These variables play a pivotal role in providing the necessary input for the network to evaluate and predict the output layer, which presents the thickness of the coating layer. The ANN comprises 12 hidden layers, each contributing to the network's ability to capture intricate patterns inherent in structural responses. The activation functions are employed in these layers to introduce non-linearities crucial for accurate prediction. The training process involves using a neural fitting application, where 85% of the dataset is randomly selected for training the model. The iterative nature of this process allows the model to adjust its internal parameters to minimize the mean square error (MSE), optimizing its ability to predict coating thickness accurately.

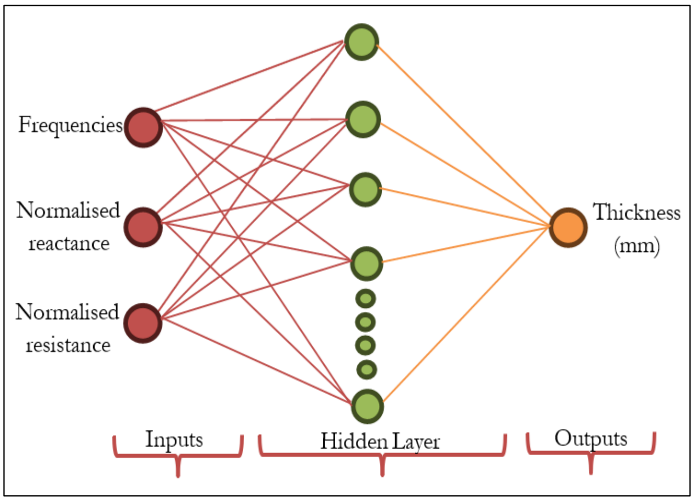

Figure 5: The implemented ANN model's structure.
Source: Authors, (2024).

Fine-tuning hyperparameters is a crucial step in enhancing the model's performance, including optimizing the learning rate and batch size to achieve the best convergence during training. After training, the model's performance is rigorously tested on the remaining 15% of the dataset. Evaluation metrics such as R-squared (R^2) and Mean Squared Error (MSE) provide insights into how well the model generalizes to new, unseen data.
The loss function of the regression ANN models was the mean square error (MSE), as expressed as follow:

$$Mse = \frac{1}{n}\sum_{1}^{n}(Th_s - Th_p)^2 \quad (5)$$

Were:

Th_s is simulated thickness values and Th_p is Predicted thickness values.

IV. RESULTS AND DISCUSSIONS

The regression ANN model was used to predict the thickness of the first layer of a multilayer material, which is an aluminum thin plate over a thick steel plate.
The network is a two-layer feedforward network with a sigmoid transfer function in the hidden layer and a linear transfer function in the output layer. The layer size value defines the number of hidden neurons, which have 12 neurons. You can see the network architecture in Figure 6. The network plot updates to reflect the input data. In this study, the data has three inputs (features) and one output. To show that it is feasible to apply a well-trained ANN model to untrained datasets, we only used the data from the thickness plate ranging from 0.01 mm to 0.2 mm for training and testing the selected ANN in our study. The remaining data was obtained for test the untrained data.

The training performance of our neural network model is displayed in Figure 7, which also shows the mean squared errors (MSE) for the training and test data throughout the epochs.

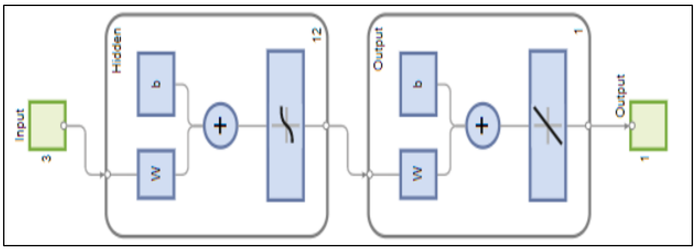

Figure 6: ANN Structure.
Source: Authors, (2024).

The vertical axis shows the mean square error, and the horizontal axis shows the number of epochs. The blue line, which rapidly decreases until stabilizing, represents the error on the training set. The red line represents the error on the test set. The black horizontal dotted line denotes the highest performance during training, and the blue circle denotes the optimal performance, which arrived at epoch 815 with an MSE of 5.2282e-10. This shows that the model performed exceedingly well on the test data, and the model has successfully learned the training dataset.

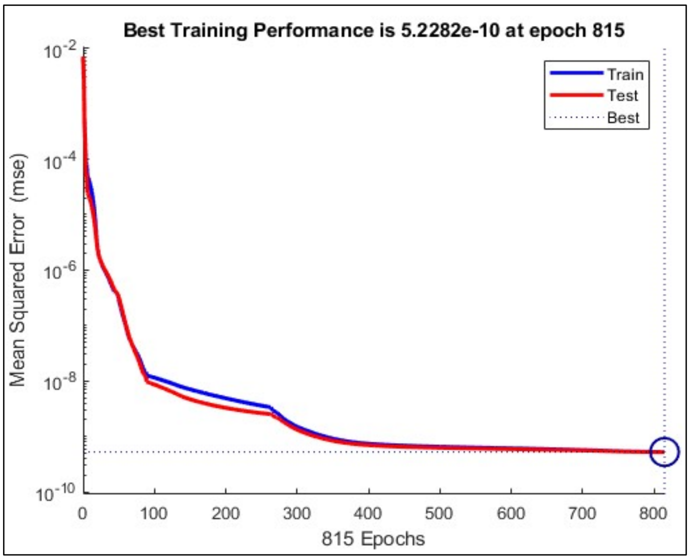

Figure 7: ANN performance.
Source: Authors, (2024).

To further substantiate the training performance, Figure 8 displays the error histogram plot for the training dataset. It displays data points known as outliers or those whose fits are noticeably poorer than those of the majority of the data. In our training model, there are no outliers in the data because the majority of the data lies on the zero-error line, and all errors fall between -5.1e-5 and 6.73e-5, which supports the performance results in Figure 7. The artificial neural network's performance is evaluated by calculating the variance between the test dataset's true values and the network's predicted values. The correlation between the first layer's anticipated and simulated thicknesses is displayed in Figure 9. The training and testing datasets had 1700 and 300 instances, respectively. For the training and testing datasets, the corresponding R^2 values were 1, and the regression lines had slopes of (1×Target+1.5e-7) and (1×Target+2.7e-6), respectively. Regression line slopes and R^2 values were both near 1.0, suggesting that the results that were predicted by the regression ANN model matched well with the analytical simulation results.

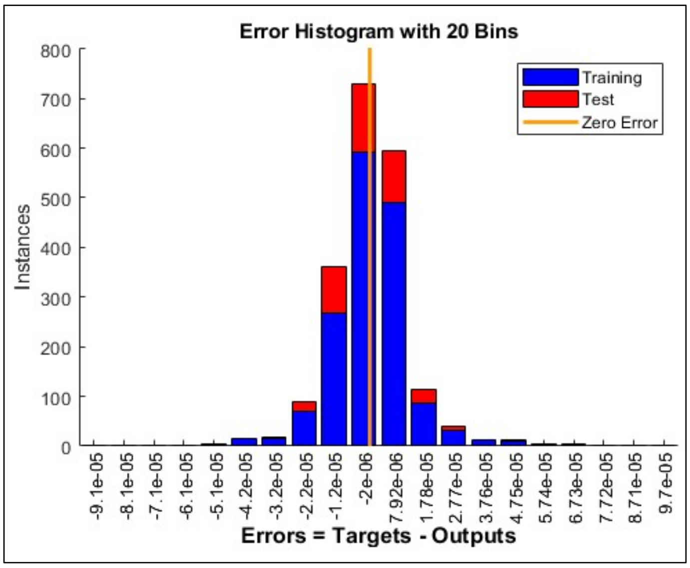

Figure 8: ANN histogram regression.
Source: Authors, (2024).

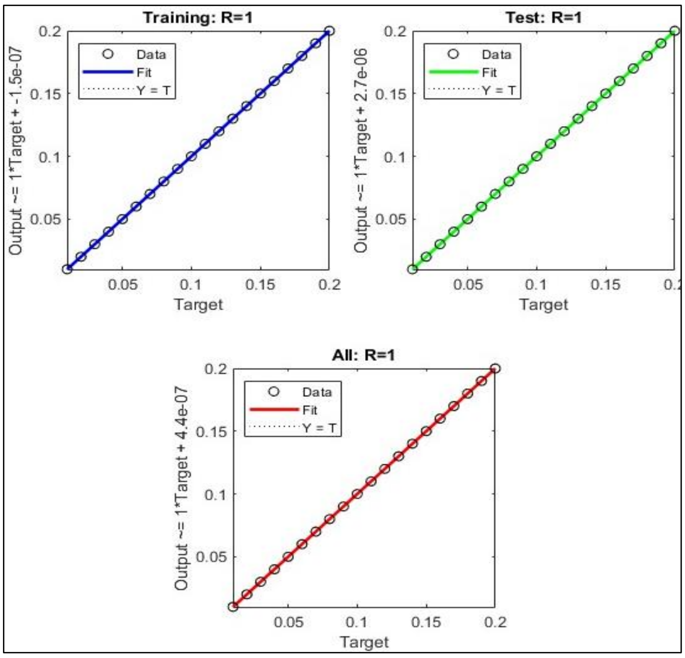

Figure 9: ANN regression.
Source: Authors, (2024).

After determining the most effective data processing approach, it became imperative to validate the applicability of the well-trained Artificial Neural Network (ANN) model to datasets that were not part of the initial training. All other input datasets that did not participate in the training and testing of the ANN model, which is the data obtained from the thicknesses of the first plate from 0.21 mm to 0.25 mm, were chosen. The simulated and predicted thicknesses of five cases of untrained inputs are illustrated in Figure 10 and Figure 11.

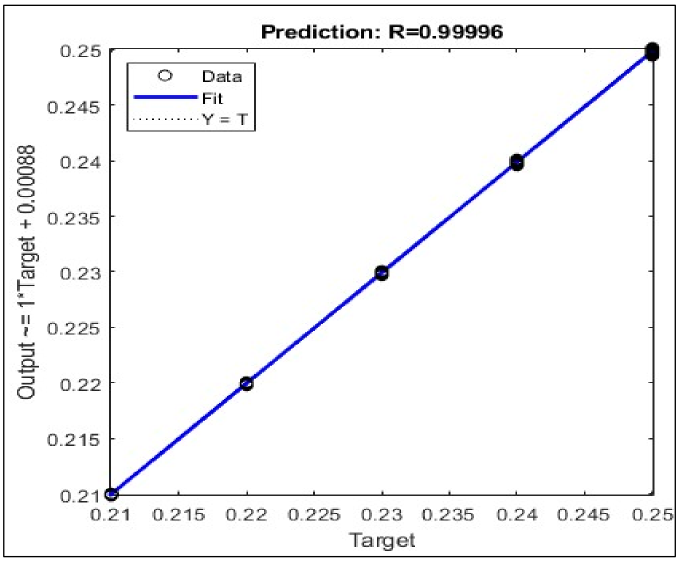

Figure 10: Regression of untrained predicted thicknesses.
Source: Authors, (2024).

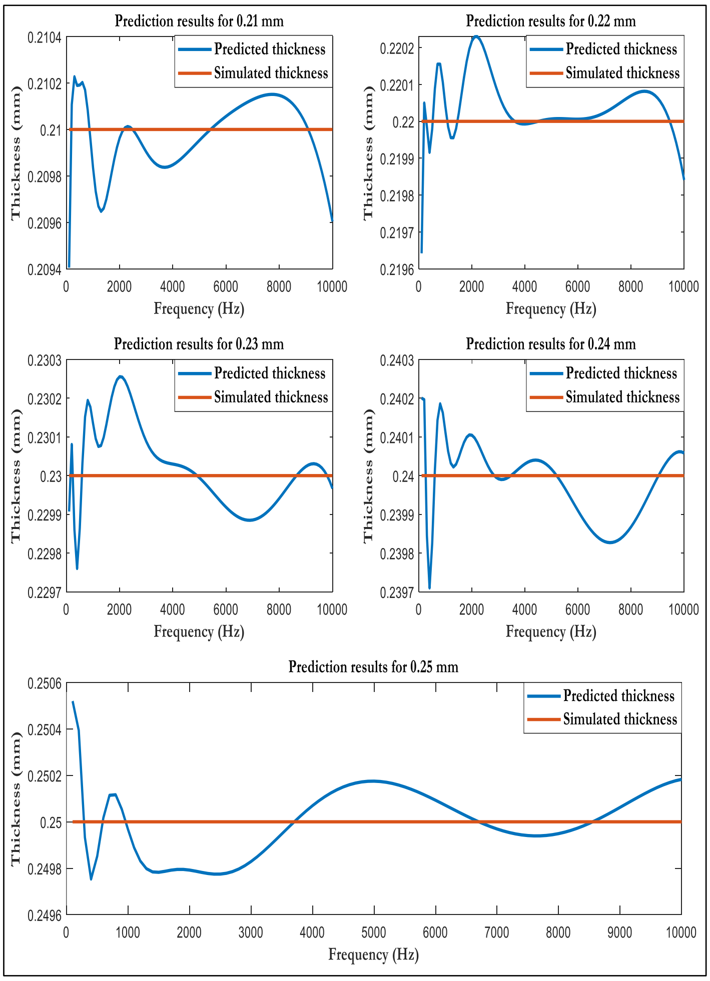

Figure 11: Results obtained for untrained data.
Source: Authors, (2024).

V. CONCLUSIONS

Two thousand and five hundred datasets with the eddy current method of different aluminum plate thicknesses above a steel plate and working frequencies of EC-sensor were generated using experimentally validated analytical models in our previous research. The values of the thickness measurement of the first layer predicted by the ANN model were almost identical with the simulated results.

Under the different thicknesses of the plate and working frequency of the sensor, the R^2 and MSE of the testing dataset were 1 and ,5.22e-10 respectively. The practicality of implementing the proficiently trained ANN model on untrained datasets was successfully demonstrated with R^2 equal to 0.99996. The model parameters, such as the number of neurons in the hidden layer and the choice of the activation function, have been systematically studied, and the developed ANN model gave quite good prediction results. In this study, we avoided those errors by searching for the optimal number of neurons and trying training with Bayesian regularization.

VI. AUTHOR'S CONTRIBUTION

Conceptualization: Islam Nacer Eddine El Ghoul, A. E. Lakhdari, S. Bensaid, A. Aissaoui, A.T. Ouamane.
Methodology: Islam Nacer Eddine El Ghoul, A. E. Lakhdari, S. Bensaid, A. Aissaoui, A.T. Ouamane.
Investigation : Islam Nacer Eddine El Ghoul, A. E. Lakhdari, S. Bensaid, A. Aissaoui, A.T. Ouamane.
Discussion of results: Islam Nacer Eddine El Ghoul, A. E. Lakhdari, S. Bensaid, A. Aissaoui, A.T. Ouamane.
Writing – Original Draft: Islam Nacer Eddine El Ghoul, A. E. Lakhdari, S. Bensaid, A. Aissaoui, A.T. Ouamane.
Writing – Review and Editing: Islam Nacer Eddine El Ghoul, A. E. Lakhdari, S. Bensaid, A. Aissaoui, A.T. Ouamane.
Supervision: Author Two and Author Three.
Approval of the final text: Islam Nacer Eddine El Ghoul, A. E. Lakhdari, S. Bensaid, A. Aissaoui, A.T. Ouamane.

VII. REFERENCES

[1] W. Giurlani, E. Berretti, M. Innocenti, and A. Lavacchi, "Measuring the thickness of metal coatings: A review of the methods," Coatings, vol. 10, no. 12, pp. 1–36, 2020, doi: 10.3390/coatings10121211.

[2] C. C. Tai, J. H. Rose, and J. C. Moulder, "Thickness and conductivity of metallic layers from pulsed eddy-current measurements," Review of Scientific Instruments, vol. 67, no. 11, pp. 3965–3972, 1996, doi: 10.1063/1.1147300.

[3] L. Yong, T. Theodoulidis, and G. Y. Tian, "Magnetic field-based eddy-current modeling for multilayered specimens," IEEE Transactions on Magnetics, vol. 43, no. 11, pp. 4010–4015, 2007, doi: 10.1109/TMAG.2007.904930.

[4] H. Nebair, A. Cheriet, I. N. El Ghoul, B. Helifa, S. Bensaid, and I. K. Lefkaier, "Bi-eddy current sensor based automated scanning system for thickness measurement of thick metallic plates," International Journal of Advanced Manufacturing Technology, vol. 96, no. 5–8, pp. 2867–2873, 2018, doi: 10.1007/s00170-018-1753-z.

[5] A. E. Lakhdari, A. Cheriet, and I. N. El-Ghoul, "Skin effect based technique in eddy current non-destructive testing for thickness measurement of conductive material," IET Science, Measurement and Technology, vol. 13, no. 2, pp. 255–259, 2019, doi: 10.1049/iet-smt.2018.5322.

[6] J. Xu, J. Wu, B. Wan, W. Xin, and Z. Ge, "A novel approach for metallic coating detection through analogizing between coil impedance and plane wave impedance," NDT and E International, vol. 116, no. 37, p. 102308, 2020, doi: 10.1016/j.ndteint.2020.102308.

[7] J. Wang et al., "Thickness Measurement of Magnetic Absorbing Coating on Metallic Surface by Localized Spoof Surface Plasmon-Based Sensor," IEEE Sensors Journal, vol. 21, no. 24, pp. 27433–27440, 2021, doi: 10.1109/JSEN.2021.3102065.

[8] W. Guo et al., "High precision thickness evaluation of thermal barrier coating with high frequency eddy current testing method," NDT and E International, vol. 140, no. October, p. 102963, 2023, doi: 10.1016/j.ndteint.2023.102963.

[9] P. Huang, Z. Bao, H. Pu, X. Huang, L. Xu, and Y. Xie, "Extraction of LIF features using sweep-frequency eddy current for conductivity and thickness evaluation of non-magnetic metallic plates," Measurement: Journal of the International Measurement Confederation, vol. 208, no. January, p. 112444, 2023, doi: 10.1016/j.measurement.2023.112444.

[10] S. Harzallah, R. Rebhi, M. Chabaat, and A. Rabehi, "Eddy current modelling using multi-layer perceptron neural networks for detecting surface cracks," Frattura ed Integrita Strutturale, vol. 12, no. 45, pp. 147–155, 2018, doi: 10.3221/IGF-ESIS.45.12.

[11] D. M. Depth-varying, "Analytical Solution in Eddy-Current Testing of Magnetic Properties," vol. 27, no. 5, pp. 4360–4365, 1991.

[12] G. Hu, R. Huang, M. Lu, L. Zhou, and W. Yin, "Measurement of radius of a metallic ball using eddy current testing based on peak frequency difference feature," Measurement: Journal of the International Measurement Confederation, vol. 184, no. May, p. 109876, 2021, doi: 10.1016/j.measurement.2021.109876.

[13] S. Harzallah, M. Chabaat, and K. Chabane, "Numerical study of eddy current by finite element method for cracks detection in structures," Frattura ed Integrita Strutturale, vol. 11, no. 39, pp. 282–290, 2017, doi: 10.3221/IGF-ESIS.39.26.

[14] R. Huang, M. Lu, A. Peyton, and W. Yin, "Thickness Measurement of Metallic Plates with Finite Planar Dimension Using Eddy Current Method," IEEE Transactions on Instrumentation and Measurement, vol. 69, no. 10, pp. 8424–8431, 2020, doi: 10.1109/TIM.2020.2987413.

[15] A. E. Lakhdari, A. Cheriet, B. Lamamra, B. Bellouti, S. Bensaid, and I. N. El Ghou, "Gap Estimation of Disbanding Failure Appears in Hybrid Laminate Material by Means of an Eddy Current Evaluation," Proceedings of 2018 3rd International Conference on Electrical Sciences and Technologies in Maghreb, CISTEM 2018, pp. 14–18, 2018, doi: 10.1109/CISTEM.2018.8613357.

[16] J. Xu, D. Wang, and W. Xin, "Coupling Relationship and Decoupling Method for Thickness and Conductivity Measurement of Ultra-Thin Metallic Coating Using Swept-Frequency Eddy-Current Technique," IEEE Transactions on Instrumentation and Measurement, vol. 71, pp. 1–9, 2022, doi: 10.1109/TIM.2022.3190533.

[17] P. Huang, Z. Bao, H. Pu, X. Huang, L. Xu, and Y. Xie, "Extraction of LIF features using sweep-frequency eddy current for conductivity and thickness evaluation of non-magnetic metallic plates," Measurement: Journal of the International Measurement Confederation, vol. 208, no. 24, pp. 1–9, 2023, doi: 10.1016/j.measurement.2023.112444.

[18] C. V. Dodd and W. E. Deeds, "Analytical solutions to eddy-current probe-coil problems," Journal of Applied Physics, vol. 39, no. 6, pp. 2829–2838, 1968, doi: 10.1063/1.1656680.

[19] T. Theodoulidis and E. Kriezis, "Series expansions in eddy current nondestructive evaluation models," Journal of Materials Processing Technology, vol. 161, no. 1-2 SPEC. ISS., pp. 343–347, 2005, doi: 10.1016/j.jmatprotec.2004.07.048.

[20] R. Wazirali, E. Yaghoubi, M. S. S. Abujazar, R. Ahmad, and A. H. Vakili, "State-of-the-art review on energy and load forecasting in microgrids using artificial neural networks, machine learning, and deep learning techniques," Electric Power Systems Research, vol. 225, no. June, p. 109792, 2023, doi: 10.1016/j.epsr.2023.109792.

[21] M. Sharifzadeh, A. Sikinioti-Lock, and N. Shah, "Machine-learning methods for integrated renewable power generation: A comparative study of artificial neural networks, support vector regression, and Gaussian Process Regression," Renewable and Sustainable Energy Reviews, vol. 108, no. March, pp. 513–538, 2019, doi: 10.1016/j.rser.2019.03.040.

[22] L. Huang and X. Huang, "Research on registration error prediction of large size measurement field based on finite element and artificial neural network," International Journal of Advanced Manufacturing Technology, pp. 4589–4603, 2023, doi: 10.1007/s00170-023-12608-2.

[23] Q. Zhou et al., "Prediction of the mechanical behavior of steel-aluminum flow drill screw joints using artificial neural network," International Journal of Advanced Manufacturing Technology, pp. 4553–4567, 2023, doi: 10.1007/s00170-023-12563-y.

[24] I. N. El Ghoul, A. Cheriet, S. Bensaid, and A. E. Lakhdari, "Accurate measurement of Aluminum layer thickness in a multilayer material using eddy

current sensor," in Proceedings of 2016 International Conference on Electrical Sciences and Technologies in Maghreb, CISTEM 2016, Institute of Electrical and Electronics Engineers Inc., Oct. 2017. doi: 10.1109/CISTEM.2016.8066777.

[25] Dodd C. V. and Deeds W. E., "Analytical solutions to eddy current probe coil problems," Journal of Applied Physics, vol. 39, no. 6, p. 2829{2838, 1968.

Journal of Engineering and Technology for Industrial Applications

ISSN ONLINE: 2447-0228

ITEGAM-JETIA

Manaus, v10. n.50, p. 235-242. November/ December., 2024.
DOI: https://doi.org/10.5935/jetia.v10i50.1433

RESEARCH ARTICLEOPEN ACCESS

VAULTGUARD: THE ADVANCED KEYLESS SECURITY SYSTEM

Dr. Yogita Mane [1], Dr. Neeta Patil[2], Akshay Agrawal[3], Sanketi Raut[4], Vishal Shinde[5]

[1,3,4] Department of Information Technology, Universal College of Engineering, University of Mumbai, Vasai
[2,5] University of Mumbai, Mumbai.

[1]https://orcid.org/0000-0002-7097-2193, [2]http://orcid.org/0009-0003-1532-3996, [3]http://orcid.org/0000-0002-8722-7181, [4]https://orcid.org/0000-0002-7097-2193, [5]https://orcid.org/0009-0009-3256-3012,

Email: yogita.ydmane@gmail.com, npat78691@gmail.com, akshay1661@gmail.com, sanketiraut28@gmail.com, mailme.vishalshine@gmail.com

ARTICLE INFO

Article History
Received: November 28, 2024
Revised: November 30, 2024
Accepted: December 10, 2024
Published: December 31, 2024

Keywords:
2 Factor Authentication,
WebAuthn,
Biometric Recognition,
Keyless Vault,
FIDO2.

ABSTRACT

The VaultGuard is a cutting-edge password management solution designed to enhance security, convenience, and user experience. A full-featured research work named VaultGuard is developed to assist users in safely creating, organizing, and storing strong passwords for a variety of online accounts and programs. This paper offers a wide range of features, including secure storage for multiple encrypted passwords using AES256 on cloud, Random key generation algorithm for creating an advanced password, updating user password timely, and a user-friendly dashboard for managing and organizing login information. The system provides a seamless registration process using Fast Identity Online 2 algorithm (FIDO2) with Web Authentication (WebAuthn) component, allowing users to securely login without needing any password. To further enhance security, the research paper employs AES256 Algorithm to safeguard stored passwords, protecting them from unauthorized access and data breaches. The system also proactively monitors the age of passwords and sends SMS and email notifications to users when their passwords are older than a predetermined time period, such as a month, prompting them to update their passwords for added security. By combining the convenience of password management with authentication, strong encryption, and proactive password monitoring, the VaultGuard sets a new standard for secure and user-friendly password management systems, effectively addressing the shortcomings of traditional methods with 97.66 % accuracy and 98.63% precision.

I. INTRODUCTION

In today's digital era, effective password management is crucial for ensuring online security and privacy. The VaultGuard Research paper is a comprehensive software solution designed to help users securely store, organize, and generate strong passwords for their various online accounts and applications. The VaultGuard enables users to store and manage their login credentials for different websites and services in a centralized, encrypted database. It requires a Passkey to access the stored passwords, making it more convenient and secure than memorizing multiple passwords [1], [2].

A Password-Based Authentication System Based on the CAPTCHA [3], represents Artificial Intelligence (AI) inspired security methods needed to secure communications in the era of quantum computing. The VaultGuard is a secure storage component that protects the user's sensitive information using strong encryption techniques [4]. This ensures that, even if the vault is compromised, the stored passwords remain secure and unreadable. The research paper offers a functionality to automatically create random passwords with a minimum length of 8-20 characters using a combination of uppercase letters, lowercase letters, 0-9 digits, and special symbols. It also displays the time required to crack the password by a supercomputer, few methods like Brute Force Attack, Dictionary Attack, Rainbow

Tables etc. can be used providing an estimate of its strength and use cases as mentioned in below Table 1 [5].

Table 1: Comparative Analysis of Different Password Cracking Algorithms.

Algorithm	Method	Strengths	Use Cases
Brute Force	Exhaustive Search	Guaranteed to find the password; simple implementation	Recovering short or weak passwords.
Dictionary Attack	Wordlist Matching	Fast; effective against weak passwords.	Cracking user-chosen weak passwords.
Rainbow Tables	Hash Lookup	Reduces time for cracking hashes; requires less computation than brute force.	Cracking stored hashed passwords.

Source: Authors, (2024).

To promote better password practices, the research paper includes functionality to monitor password age. If a user's password is older than 1 month, the server sends an email and an SMS notification to remind the user to update their password [6]. The VaultGuard Research paper is a robust and feature-rich solution for safeguarding sensitive login information, reducing the risk of data breaches, and promoting better password practices. It combines convenience, security, and advanced features to provide a comprehensive password management experience for users.

I.1 OBJECTIVES

The objectives of proposed research work are as follows.

- **To Implement Passwordless Authentication System:** Utilize FIDO2 with WebAuthn component standards to provide a secure, passwordless login system that mitigates the risks associated with traditional password-based authentication methods.
- **To provide Secure Password Storage:** Employ AES 256-bit encryption to ensure the secure storage of user-generated passwords within a MongoDB database, protecting sensitive user information from unauthorized access and data breaches.
- **To Automate Password Manager:** Integrate an automatic password generator that not only creates strong, randomized passwords combining uppercase letters, lowercase letters, 0-9 digits, and special symbols but also informs users about the estimated time required for this password to be cracked by a supercomputer.
- **To provide Proactive Security Notifications:** Develop a system that actively monitors the age of stored passwords and automatically notifies users via email and SMS when passwords need updating, thus maintaining high security standards over time.
- **To enhance User Experience:** By employing NodeJS and EJS, deliver a responsive, user-friendly interface that simplifies user interactions while maintaining high performance and security.

The overarching objectives of this research paper are to provide a comprehensive solution that not only secures user data but also enhances usability and promotes better password hygiene among users. This initiative is aligned with current trends in cyber security, aiming to reduce cyber risk through innovative technological advancements.

I.2 LITERATURE REVIEW

The study [1] presents "Building and Examining a Watchword Store that Impeccably Stows away Passwords from itself called SPHINX", which remains secure indeed when the secret word director itself has been compromised. In SPHINX, the data put away on the gadget is hypothetically autonomous of the user's ace watchword. Besides, an assailant with full control of the gadget, indeed at the time the client interacts with it, learns nothing about the ace secret word – the secret word is not entered into the gadget in plaintext frame or in any other way that may spill data on it.

In this inquiry about work [2], the creators dive profoundly into the offline word reference assaults on the database of passwords (PW) or indeed hashed PW are harmed as a single server break-in leads to numerous compromised PWs. In this respect, utilizing Physical Unclonable Capacities (PUFs) to increment the security of PW chief frameworks has been as of late proposed. Utilizing PUFs permits supplanting the hashed PW with PUF reactions, which give an extra equipment layer of security. In this way, indeed with getting to the database, an enemy ought to have physical control of the PUF to discover the PWs.

A Password-Based Confirmation Framework Based on the CAPTCHA, as portrayed [3], speaks to Manufactured Insights (AI) motivated security strategies required to secure communications in the period of quantum computing. This article presents a challenge-response password-based verification framework based on the Totally Mechanized Open Turing test to tell Computers, People Separated (CAPTCHA) AI difficult issues. In this framework, a server sends a challenge content to a client, and at that point the client produces an arbitrary picture and mixes the challenge content inside this irregular picture utilizing his watchword. At that point the client sends the produced picture to the server. The server extricates the challenge content from the sent picture utilizing his duplicate of the client's secret word. If the extricated challenge content is the same as the sent challenge content, at that point both the client's and the server's duplicates of the secret word coordinate and the client is authenticated.

The work [4] investigates the interesting world of propositions to handle the issue of watchword spillage of prevalent websites like Linked-In, Adobe, Gmail, Yahoo, eHarmony, etc. by utilizing energetic watchword arrangement and improved hash Calculation. Here, a calculation is created that will produce watchword arrangements powerfully depending on the recurrence of characters. Time complexity is computed, and it is found that the calculation works quickly. Since the calculation makes watchword arrangements powerfully, it will be intense for the aggressor to figure the characteristics of the secret word database.

The investigate study [5,6] basically centers on reinforcing the passkey section convention and securing the gadgets against detached listening in and dynamic Man-in-the center (MITM) assaults in both Bluetooth Essential Rate/Enhanced Information Rate (BR/EDR) and Bluetooth Moo Vitality (Bluetooth LE). This strategy can be utilized for any gadget which employs the passkey passageprotocol.

The work [7],[8] leads to key experiences almost the trouble of supplanting passwords. Not as it were does no known plot come near to giving all craved benefits: none indeed holds the full set of benefits that bequest passwords as of now give. In specific, there is a wide range from plans advertising minor security benefits past bequest passwords, to those advertising critical security benefits in return for being more exorbitant to send or more troublesome to utilize. This research paper concludes that numerous scholarly recommendations have fizzled to pick up footing since analysts once in a while consider a adequately wide run of real-world limitations.

I.3 EXISTING SYSTEMS

The current landscape of password management and authentication systems is characterized by a reliance on traditional password-based mechanisms [1-10], which pose numerous security challenges. Despite advancements in cryptographic practices, many systems continue to depend on passwords that users often find difficult to manage and remember, leading to compromises in security practices such as the reuse of passwords across multiple sites.

The introduction of two-factor authentication (2FA) [11] has provided an additional layer of security; however, it often adds complexity to the user experience and does not eliminate the fundamental vulnerabilities associated with password theft or loss. Moreover, many 2FA implementations remain susceptible to phishing and man-in- the-middle attacks, which can intercept or replicate the second fator[12].

Password managers have become popular for storing and generating secure passwords, yet they also concentrate risk by storing multiple passwords in a single location, often protected by a single master password [13]. Every credential that is stored is vulnerable if the master password is hacked. Furthermore, these systems do not inherently encourage or enforce strong password creation, nor do they typically address the issue of password aging, leaving users with potentially vulnerable accounts over time.

Recent developments in the field have seen the adoption of password-less authentication methods, such as biometrics and hardware tokens, which offer improved security by eliminating the need for stored secrets that can be stolen or lost. However, these technologies often require additional hardware or specific environmental conditions, which can limit their accessibility and general usability.

In summary, while existing systems have made strides towards enhancing security and user convenience, significant challenges remain, particularly in terms of security robustness, user experience, and accessibility. These challenges underscore the necessity for innovative solutions like “VaultGuard,” which seeks to address these gaps through the integration of advanced encryption, password-less authentication, and proactive security measures.

I.4 LIMITATION ON EXISTING SYSTEM

The limitations of the existing systems are as follows;

- Password managers that store user data in a centralized server can pose a risk if the server is compromised or becomes unavailable [13].
- Some password managers may not support all operating systems, browsers, or devices, which can limit accessibility for users working across multiple platforms.
- Synchronization issues may arise when using password managers across multiple devices, leading to inconsistencies or delays in accessing passwords.
- Despite the convenience of password managers, some users may find them complex or intimidating to set up and use, which could hinder adoption and usage.
- While some password managers are free, others may require a subscription, which can be a barrier for users who prefer a free solution or are unwilling to pay for additional features [12].
- If a user's master password is compromised, all the stored passwords within the password manager become vulnerable. Implementing additional security measures, such as two-factor authentication, can help mitigate this risk, but it remains a limitation of password-based systems [13].

I.5 PROBLEM STATEMENT

In today's digital age, managing multiple online accounts with unique and robust passwords has become a challenging task for individuals and organizations. Users often struggle to remember complex passwords or resort to using the same passwords across multiple websites, which can lead to security vulnerabilities. Traditional password-based authentication systems are susceptible to various threats, such as weak passwords, phishing attacks, and data breaches. Existing password management systems may not offer adequate protection against unauthorized access, leaving sensitive data vulnerable.

Users often lack the knowledge and resources to create strong, unique passwords for their accounts, further compromising their security. Creating and managing complex passwords can be time-consuming and cumbersome, leading to frustration and decreased user adoption. Ensuring the security of stored passwords is a significant challenge, and data breaches can have severe consequences for both individuals and organizations.

To address these challenges, the VaultGuard aims to develop a comprehensive and secure password management solution that incorporates a robust password generator, a secure password vault, and encryption algorithms to safeguard sensitive information. By offering a user-friendly and highly secure password management system, the study aims to improve password security, reduce the burden of managing multiple passwords, and enhance overall digital security for users.

II. PROPOSED SYSTEM

To address the limitations identified in existing password management and authentication systems, “VaultGuard” introduces a comprehensive solution that emphasizes security, usability, and proactive management. The proposed system integrates several key innovations and improvements over traditional methods:

Passwordless Authentication using FIDO2 with WebAuthn component: “VaultGuard” utilizes the FIDO2 standard to enable passwordless authentication. This method significantly reduces the risk of password-related breaches by eliminating the need for users to remember and manage traditional passwords, thus also decreasing vulnerability to phishing and brute-force attacks.

AES 256-Bit Encryption: All passwords generated or stored within the system are encrypted using the Advanced Encryption Standard (AES) with a 256-bit key, currently the gold standard in encryption. This ensures that even if data is intercepted, it remains protected against unauthorized access.

Automated Random Password Generator: The system includes a feature to automatically generate complex passwords using a mix of uppercase letters, lowercase letters, numbers, and symbols. It also provides an estimate of how long different algorithms or techniques would take to crack each password, helping users understand their password strength better..

Proactive Password Aging and Notification System: "VaultGuard" actively monitors the age of stored passwords and notifies users via email and SMS when it is time to update their passwords. This feature helps maintain high security standards by ensuring that passwords are regularly updated and not left vulnerable over time.

User-Friendly Interface: The application is developed using NodeJS for the backend and Embedded JavaScript Templates (EJS) for the frontend, providing a smooth and responsive user experience. This approach allows for quick interactions and a more intuitive user interface, which is accessible even to users with minimal technical expertise.

By combining these features, "VaultGuard" not only provides a more secure method of managing passwords but also enhances the overall user experience, making it a versatile and robust solution in the domain of digital security.

The following Fig. 1 shows a multi-layered architecture which follows the Advanced Password Manager to ensure security, scalability, and performance. The system comprises a client-side interface built using modern web technologies, a password generator module, a password vault backed by AES 256 encryption, WebAuthn integration for password less login, and automatic password aging notification functionality. The system architecture also includes a robust database layer using MongoDB for storing encrypted user passwords. The application server handles requests, processes user data, and communicates with the database to ensure seamless user experience. The system architecture is designed to be modular, secure, and scalable, making it an ideal solution for managing passwords and enhancing digital security in the modern era.

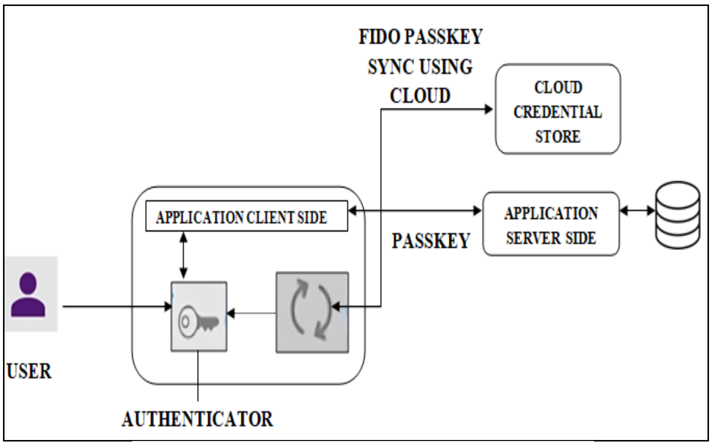

Figure 1: VaultGuard System Architecture.
Source: Authors, (2024).

Client Side: represents the user interface that users utilize to engage with the system; this is usually a web browser or an application.

Web Server (Backend): Acts as the intermediary between the client-side interface and the database. It hosts the application logic, including API endpoints for handling user requests.

Application Logic (API): Handles user authentication, password management, and notification services. It includes modules for WebAuth authentication, password generation, and expiry notification.

MongoDB Database: Stores user data, including user information (name, email, mobile number) and passwords. It consists of collections for users and passwords, enabling CRUD operations.

The arrows indicate the flow of data and interactions within the system: Users interact with the client-side interface, making HTTP(S) requests. The web server receives these requests and forwards them to the application logic. The application logic processes the requests, interacts with the MongoDB database as needed, and sends responses back to the client. Database queries are executed to read or modify user data stored in the MongoDB database. The notification service may also interact with external services (e.g., email and SMS gateways) to send notifications to users.

The advantages of the proposed system are that it provides password-less login having secure password storage. It also generates random passwords and provides password expiry reminders to the users. It also provides Better Security Compliance consisting of Multi-factor Authentication.

III. METHODOLOGY

As shown in Fig. 2, when the user tries to sign in it first checks whether the user is signed in previously or not, if not then it would prompt the user to sign in first. When registering, it would ask for which device it wants to use for authentication, the user can use the same current device in which he/she is browsing or they can select any other device to use to authenticate them. Then it would use FIDO2/WebAuthn to register users and save the users data in the MongoDB Database. If the user is already authenticated it would let the user to authenticate themselves and then access the dashboard. The dashboard shows the total number of passwords saved and the number of passwords needed to be updated.

Further it also allows users to "Create a Vault" where users can save passwords by adding website name, username and password and saving it. Additionally, it has the ability to determine how strong a password is and how long a supercomputer would need to break it. It also has the feature to generate a random password consisting of uppercase letters, lowercase letters, numbers, symbols which would be too hard to be cracked as shown in the section below.

It also has another section called "Vault" where users can see all the previously saved passwords.

Role of Authenticator (WebAuthn):-

1. The user tries to login to a website
2. The website prompts the user to authenticate
3. The user authenticates against their authenticator
4. Via the browser, the authenticator signs and returns a response to the website.
5. The website verifies the authenticator response.
6. The user is logged in.
7.

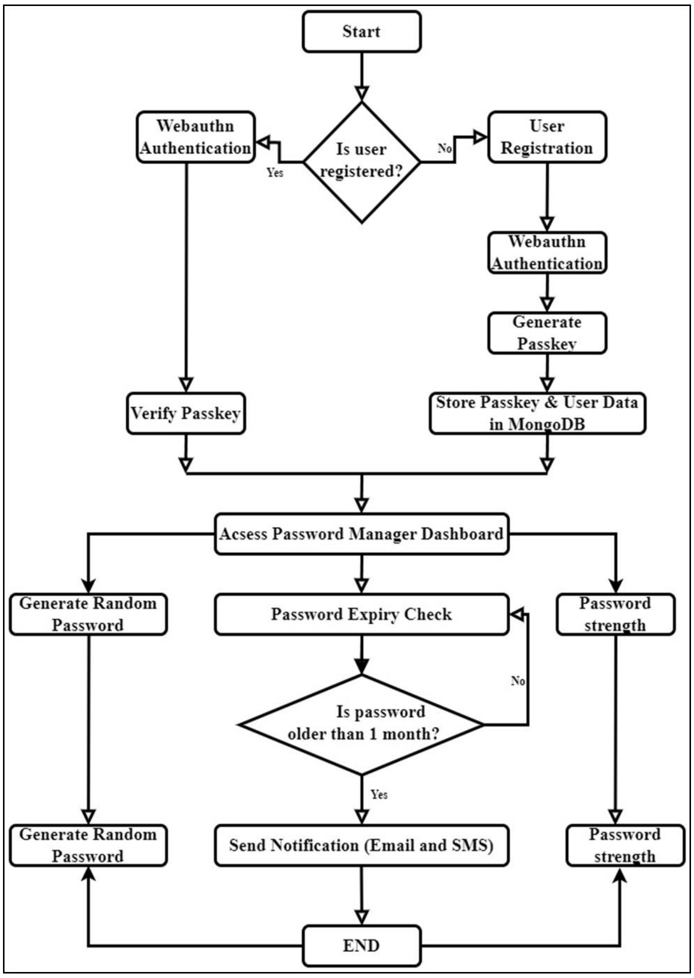

Figure 2: Flowchart of VaultGuard.
Source: Authors, (2024).

IV. RESULTS AND DISCUSSIONS.

The result set for the VaultGuard system includes various test cases that cover the primary functionalities and features of the platform. The registration and login process are a critical aspect of the platform, and it should be thoroughly tested to ensure that users can register and log in to the platform without any issues. This includes testing the password-less login using WebAuthn and verifying that the device is connected using valid credentials.

The normal functions of the VaultGuard, such as viewing, adding, editing, and deleting passwords, should also be tested to ensure that users can manage their passwords effectively. The system should allow users to generate a new random password and display the estimated time to crack this password, ensuring that users can create strong and secure passwords. The search functionality should be tested to ensure that users can search for a specific password quickly and efficiently.

The password aging notification feature should be tested to ensure that users receive notifications via email and SMS when their password is older than one month. This feature is essential for maintaining the security of user accounts and ensuring that users regularly update their passwords.

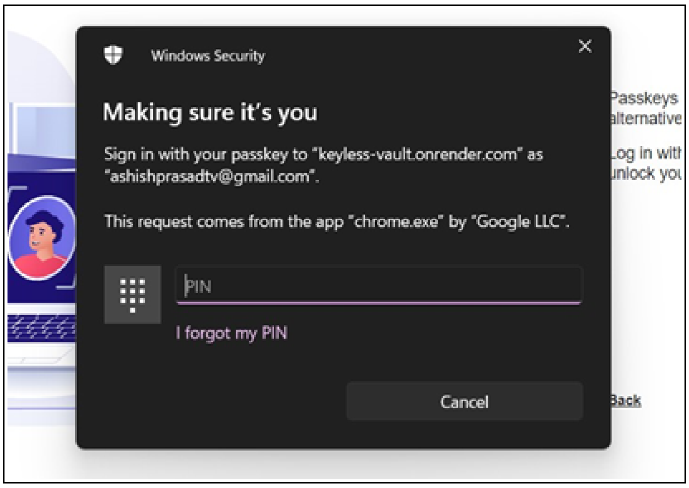

Figure 3: Same Device SignIn.
Source: Authors, (2024).

While logging into the device using the same device as shown in Fig. 3, it shows this prompt to let the user sign in or register itself using the system prompt popup to sign in using the system pin generated by the user during login.

Figure 4: Create Vault.
Source: Authors, (2024).

As a result, the system allows the user to save the password in the vault and to generate a new random password with letters including uppercase, lowercase, numbers and symbols as shown in Fig. 4. It also shows the strength of the password and Estimated Cracking Time by Brute Force Algorithm.

Figure 5: Email Notification.
Source: Authors, (2024).

When the password is older than 1 month the server will send a mail to the user that the password needs to be updated as shown in Fig. 5.

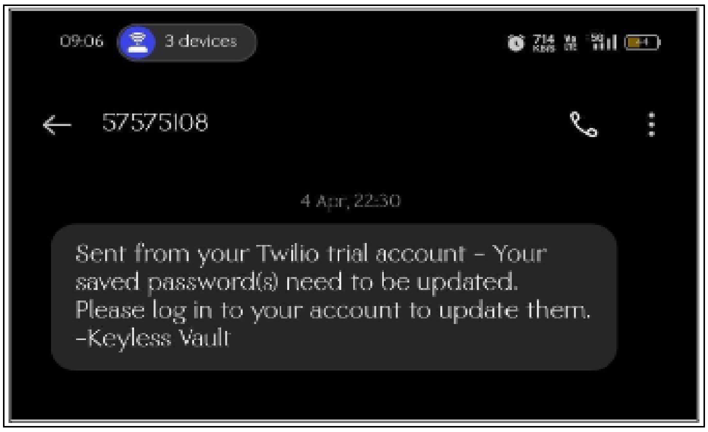

Figure 6: SMS Notification.
Source: Authors, (2024).

Fig. 6 displays that the server also sends an SMS Notification to the registered users' mobile number reminding him/her to update its password as it is older than 1 month.

Figure 7: Using different device to Sign In.
Source: Authors, (2024).

While logging into the device using any other device, it shows a QR code, which the user has to scan using its smartphone which when scanned will prompt the user to sign in using his/her device and save the pass keys in that device and allow them to use the same device in future to sign in to the dashboard as shown in Fig. 7.

Figure 8: VaultGuard Dashboard.
Source: Authors, (2024).

Figure. 8 shows the dashboard consisting of the total number of passwords saved and the number of passwords needed to be updated.

Table 2: Comparative Analysis.

Sr No.	Research paper Title	Proposed Methodology	Drawbacks
1	VaultGuard: The Advanced Keyless Security System	FIDO2/WebAuthn	may not integrate well with specific third-party applications
2	Building and Studying a Password Store that Perfectly Hides Passwords from Itself [1]	SPHINX	work on non-confidential channel, limited adoption
3	Resilient Password Manager Using Physical Unclonable Functions [2]	PUF	Such a scheme cannot operate without a backup in case of catastrophic failure of the PUFs. Extra Hardware level security
4	A Password- Based Authentication Based on the CAPTCHA AI Problem.[3]	CAPTCHA AI	Limited Accessibility, Adversarial Attacks, False Positives
5	Securing password using dynamic password policy generator algorithm [4]	Dynamic Password Generator	Memory Load, Training and Education, Increased Support Requests

Source: Authors, (2024).

Overall, the test cases for the VaultGuard system should ensure that the platform is secure, user-friendly, and functional. The testing covers all the primary functionalities and features of the platform, including registration, login, password management, random password generation, and password aging notification. The testing should also ensure that the platform is compliant with relevant security standards and regulations.

V. PERFORMANCE METRICS

Understanding the critical elements that affect an accuracy of a Keyless Vault (a password manager based on FIDO2/WebAuthn) is necessary to determine its accuracy. Accuracy here refers to the system's capacity to appropriately approve authorized users and deny illegal ones.

Definitions:

True Positive Ratio (TPr): Legitimate users who are correctly authenticated.

False Positive Ratio (FPr): Unauthorized users who are incorrectly authenticated.
True Negative Ratio (TNr): Unauthorized users who are correctly rejected.
False Negative Ratio (FNr): Legitimate users who are incorrectly rejected.
The research work has been tested for 150 legitimate authentication attempts and 150 unauthorized authentication attempts. Out of the 150 legitimate users, 145 are correctly authenticated (TPr), and 05 are incorrectly rejected (FNr). Out of the 150 unauthorized users, 148 are correctly rejected (TNr), and 02 are incorrectly authenticated (FPr).

Accuracy Metrics:

1. Accuracy: Accuracy gives the overall correctness of the system, combining both authentication successes and failures.

Accuracy = (TPr + TNr) / (TPr + TNr + FNr + FPr) (1)

Accuracy = (145+148) / (145+148+02+05) = 293 / 300

Accuracy = 0.9766 = 97.66 %

2. Precision (for accepted users): Precision represents how well the system avoids false positives, i.e., how many of the users it accepts are actually legitimate.

Precision = TPr / (TPr + FPr) (2)

Precision = 145/(145+02) = 0.9863 = 98.63%

3. Recall (also known as True Positive Rate or Sensitivity): Recall indicates how many legitimate users are correctly authenticated.

Recall = TPr / (TPr + FNr) (3)

Recall = 145/(145+05) = 0.9666 = 96.66%

4. False Positive Rate (FPR): FPR shows the likelihood that an unauthorized user gets authenticated.

False Positive Rate = FPr / (FPr + TNr) (4)

False Positive Rate (FPR) = 02/(02+148) = 0.0133

%False Positive Rate (%FPR)= 1.33%

5. False Negative Rate (FNR): FNR is the likelihood that an authenticated user will have their authentication refused.

False Negative Rate = FNr / (TPr + FNr) (5)

False Negative Rate (FNR) = 05/(145+05) = 0.0333

%False Negative Rate (%FNR)= 3.33%

Table 3: Feature Analysis.

Paper	Algorithm used	Encryption Technique	SMS Notification	Mail Notification
[1]	secure multiparty computation (MPC)	homomorphic encryption	NO	NO
[2]	PUF-based key generation	AES	NO	NO
[3]	dynamic password policy generator	SHA or PBKDF2	NO	NO
[4]	CAPTCHA AI	SHA-256	NO	NO
Proposed System	FIDO2/WebAuthn	AES 256	YES	YES

Source: Authors, (2024).

The proposed system VaultGuard sets a new standard for secure and user-friendly password management systems, effectively addressing the shortcomings of traditional methods with 97.66 % accuracy, 98.63% precision recall value as 96.66%, FPR & FNR as 1.33 % and 3.33% respectively.

VI. CONCLUSION

The “VaultGuard” represents a significant advancement in password management and authentication technology. Through its integration of FIDO2/WebAuthn for password-less authentication and AES 256-bit encryption for secure password storage, this system addresses the major vulnerabilities inherent in traditional password-based systems. The implementation of these technologies not only enhances security but also improves the user experience by simplifying the authentication process and reducing the cognitive load on users.

Moreover, the addition of an automated password generator and a proactive password aging and notification system further strengthens the system's security posture by ensuring that passwords are both strong and regularly updated. The user-friendly interface, developed with NodeJS and EJS, ensures that the system is accessible to a broad range of users, thus promoting better security practices across diverse user groups.

“VaultGuard” also benefits from the scalability and performance capabilities of MongoDB, making it suitable for deployment in environments ranging from small businesses to large enterprises. The system's focus on compliance and regular security audits guarantees that it remains effective against evolving cybersecurity threats[14][16].

In conclusion, “VaultGuard” is not just a tool for securing passwords but a comprehensive platform for promoting a more secure digital environment. Its innovative approach to password management could potentially set a new standard for how personal and organizational security is managed in an increasingly interconnected world.

.

VII. AUTHOR’S CONTRIBUTION

Conceptualization: Dr. Yogita Mane, Dr. Neeta Patil and Akshay Agrawal
Methodology: Dr. Yogita Mane, Sanketi Raut and Vishal Shinde.
Investigation: Dr. Yogita Mane, Akshay Agrawal.
Discussion of results: Dr. Yogita Mane, Dr. Neeta Patil, Akshay Agrawal, Sanketi Raut and Vishal Shinde.
Writing – Original Draft: Dr. Yogita Mane. Akshay Agrawal.
Writing – Review and Editing: Sanketi Raut and Dr. Neeta Patil.
Resources: Vishal Shinde and Akshay Agrawal.
Supervision: Dr. Yogita Mane, Dr. Neeta Patil and Vishal Shinde.
Approval of the final text: Dr. Yogita Mane, Dr. Neeta Patil, Akshay Agrawal, Sanketi Raut and Vishal Shinde.

VIII. REFERENCES

[1] M. Shrivanian, N. Saxena, and S. Jarecki, “Building and Studying a Password Store that Perfectly Hides Passwords from Itself,” in Proc. IEEE 37th International Conference on Distributed Computing Systems (ICDCS), 2017.

[2] M. Mohammadi Nodoushan, B. Cambou, and C. R. Philabaun, “Resilient Password Manager Using Physical Unclonable Functions,” in Proc. IEEE 41st International Conference on Distributed Computing Systems (ICDCS), 2021.

[3] M. Alajmi, I. Elasshry, and H. S. El-sayed, “A Password-Based Authentication System Based on the CAPTCHA AI Problem,” in Proc. IEEE 37th International Conference on Distributed Computing Systems (ICDCS), 2017.

[4] A. Singh and S. Raj, “Securing password using dynamic password policy generator algorithm,” August 8, 2021.

[5] J. Bonneau, “The science of guessing: Analyzing an anonymized corpus of 70 million passwords,” in Proc. IEEE Symp. Secur. Privacy, 2012, pp. 538–552.

[6] I. Dacosta, M. Ahamad, and P. Traynor, "Trust no one else: Detecting MITM attacks against SSL/TLS without third-parties," in Proc. Eur. Symp. Res. Comput. Secur., 2012, pp. 199–216.

[7] J. Bonneau, C. Herley, P. C. Van Oorschot, and F. Stajano, "The quest to replace passwords: A framework for comparative evaluation of web authentication schemes," in Proc. IEEE Symp. Secur. Privacy, 2012, pp. 553–567.

[8] M. Gusev, S. Ristov, G. Velkoski, and P. Gushev, "Alert Notification as a Service," in Proc. 2014 37th International Convention on Information and Communication Technology, Electronics and Microelectronics (MIPRO).

[9] D. J. Bernstein, M. Hamburg, A. Krasnova, and T. Lange, "Elligator: Elliptic-curve points indistinguishable from uniform random strings," in Proc. ACM SIGSAC Conf. Comput. Commun. Secur., 2013, pp. 967–980.

[10] S. S. Madugula, "Improvement of Passkey Entry Protocol for Secure Simple Pairing," in Proc. 2023 International Conference on Cyber-Enabled Distributed Computing and Knowledge Discovery (CyberC).

[11] S. Chiasson, P. C. van Oorschot, and R. Biddle, "A usability study and critique of two password managers," in Proc. 15th Conf. USENIX Secur. Symp. - Vol. 15, 2006, Art. no. 1.

[12] S. Kumar, S. Huzaimah, Y. Binti, and A. Hamid, "Real time mailbox alert System via SMS or Email," in Proc. 2007 Asia-Pacific Conference on Applied Electromagnetics.

[13] R. Chatterjee, J. Bonneau, A. Juels, and T. Ristenpart, "Cracking resistant password vaults using natural language encoders," in Proc. IEEE Symp. Secur. Privacy, 2015, pp. 481–498.

[14] W. Ford and B. S. Kaliski Jr , "Server-assisted generation of a strong secret from a password," in Proc. 9th IEEE Int. Workshops Enabling Technol.: Infrastructure Collaborative Enterprises, 2000, pp. 176–180.

[15] M. J. Freedman, Y. Ishai, B. Pinkas, and O. Reingold, "Keyword search and oblivious pseudorandom functions," in Proc. 2nd Int. Conf. Theory Cryptography. 2005, pp. 303–324.

[16] M. Georgiev, S. Iyengar, S. Jana, R. Anubhai, D. Boneh, and V. Shmatikov, "The most dangerous code in the world: Validating SSL certificates in non-browser software," in Proc. ACM Conf. Comput. Commun. Secur., 2012, pp. 303–324.

Journal of Engineering and Technology for Industrial Applications

ITEGAM-JETIA

Manaus, v10. n.50, p. 243-250. November/ December., 2024.
DOI: https://doi.org/10.5935/jetia.v10i50.1452

ISSN ONLINE: 2447-0228

RESEARCH ARTICLE OPEN ACCESS

EVALUATION OF WI-FI MESH NETWORKS FOR READING ELECTRICITY CONSUMPTION

Carlos Bazán Prieto[1] and Alberto Bazán Guillén[2]

1 Universidad Central "Marta Abreu" de Las Villas – UCLV. Santa Clara - Villa Clara, Cuba.
2 Universitat Politècnica de Catalunya – UPC. Barcelona, España.

[1] http://orcid.org/0000-0002-2810-9599, [2] http://orcid.org/0000-0001-8634-6907

Email: cabazan@uclv.edu.cu, alberto.bazan@upc.edu

ARTICLE INFO

Article History
Received: November 28, 2024
Revised: November 30, 2024
Accepted: December 10, 2024
Published: December 31, 2024

Keywords:
Energy meters,
Wi-Fi mesh networks,
ESP-12.

ABSTRACT

In Smart electrical networks, the Advanced Metering Infrastructure allows bidirectional communication between the service company and the customers. It includes smart meters and a communication infrastructure, which among other functions, is responsible for reading electricity consumption and billing. Cable or wireless technologies are used for the exchange of information between the networks that comprise it. In Cuba there is no such Advanced Metering Infrastructure, the reading of electricity consumption is carried out manually by an operator, reader-collector. That is why we are working on a project where traditional meters are modified by adding a Wi-Fi communications module that allows wireless access. This work evaluates the possibility of interconnecting several modified meters with wireless modules to form a mesh network. Protocols, programming tools, metrics to evaluate performance, scenarios, and experiments are described. As a result, the possibility of forming a mesh network is verified, with the exchange of information, with the requirements of self-configuration and self-repair of the network. This allows the reader-collector to read consumption from any point on the network through a smart device.

I. INTRODUCTION

Smart grids (SG) are a solution to supply electricity from generation points to consumers, which adapts to the current and future energy expectations of humanity. Different definitions of SG are presented in [1–3], from which it is described as an advanced electrical network with a bidirectional energy flow that spans from the point of generation to consumption. It uses Information and Communications Technologies (ICT) to improve the reliability, security and efficiency of the electrical system. It has the ability to self-repair, adapt, be resistant and sustainable, as well as open to future modifications, as it is equipped with present and future standards for components, devices and systems in general. A series of technologies, operations and various smart devices are involved here, such as Smart Meters (SM), smart appliances, renewable energy resources, electric vehicles, flexible charging, smart dialers, various energy efficiency programs and smart end users [1]. The SG architecture consists of three main systems: energy, communication and information. These require the use of ICT for the exchange of data at high speeds while maintaining reliability and security. The Advanced Metering Infrastructure (AMI) is what makes these operations possible, allowing the management and regulation of energy generation and consumption. AMI also allows bidirectional communication between the service provider company and customers, which includes consumption billing data. In Cuba there is no AMI, its implementation would require changes to equipment, electrical and communications networks at a very high cost. The Cuban residential sector represents more than 60% of total consumption, has approximately 4,056,865 users with an average monthly consumption of 185kWh [4], with traditional meters. An operator, called a reader-collector, performs the tasks of reading electricity consumption and collecting the bill; both processes are carried out manually and monthly. The operator must move on foot through the area assigned to him. For reading, a small terminal (PDA) or more recently a mobile device with the appropriate application and in some cases infrared reading equipment is used. The limitation in both cases is that the operator has to have access to the meter or at least a very close line of sight to it. This makes reading impossible in some scenarios, for example, a closed house. In addition, there may be errors in manual reading, anomalies in consumption due to lack of appropriate measurements, readings outside established dates, cases of fraud, and others. On the other hand, savings are not encouraged or consumption habits are influenced. The amount to be charged each month is derived only from the notation of the previous and current month's reading.

Based on the above, a low-cost alternative solution was proposed, with free software and hardware. This alternative reuses traditional residential meters and adds reading facilities to users and the reader-collector [5]. The alternative proposes adding an electronic device to existing residential energy meters, capable of reading consumption remotely, turning them into advanced energy meters. The electronic device contains, among other elements, an ESP-12 module (ESP8266 Ai-Thinker) [6] that allows the exchange of consumption data via Wi-Fi. The communication capabilities as a base radio, as well as a Wi-Fi access point, give this advanced meter the facilities for local communication with the user [5]. This technology could also be used for the interconnection between modified meters, through Wi-Fi mesh networks, more specifically the ESP-WIFI-MESH networks, derived from them. This operation represents a saving of resources, expanding the network coverage area, which would allow the reader-collector to read the electricity consumption in an easier and faster way.

ESP-WIFI-MESH is a network protocol built on the Wi-Fi protocol that allows numerous devices (nodes) spread over a large physical area to be interconnected under a single network. The network is capable of self-organizing and self-repair. In [7] a wireless mesh network based on ESP8266 devices is evaluated using the PainlessMesh library, to collect data such as the temperature and humidity of fruit boxes or containers when they are stored or transported in refrigerated chambers. The performance of the network is evaluated in terms of delivery ratio and delivery delay, which consequently affects the energy consumption and therefore the lifetime of the network.

The performance results were affected by the increase in the number of sensor nodes, message sending rate, and message payload size, as expected. In [8], a mesh network is built using NodeMCU ESP 8266 and NodeMCU ESP 32 with two types of sensors, DHT 11 and DHT 22. The communication delay with line of sight and without line of sight is evaluated. The results give a shorter delay time in the line-of-sight condition for all connected nodes. In [9] the performance of ESP8266 mesh network has been tested and evaluated. A network consisting of two nodes has a single-hop delay of 2.49 ms.

As expected, a larger number of nodes tends to increase the network delay even for the same hop distance. An evaluation of data rate performance is also performed. It is found that a node can receive up to 461 messages/sec and 28 messages/sec for a payload of 10 bytes and 4400 bytes, respectively. It is also observed that sending messages with a payload greater than 4400 bytes results in broken and incomplete messages. With ESP 32, in [10] a MESH network of sensors is established using an ESP-MESH network protocol for real-time indoor and outdoor air quality monitoring. The performance of the MESH network is estimated in terms of packet loss rate (PLR), packet failure rate (PFR), and packet delivery rate (RPD). The RPD value is greater than 97% and the PMR and PER value for each active node is less than 1.8%, which is below the limit. The results show that the ESP-MESH network protocol offers considerably good quality of service, mainly for medium area networks.

This work aims to evaluate the possibility of interconnecting several modified energy meters with the ESP-12 modules, to form a mesh network, to increase the coverage area and facilitate the reading process.

II. COMMUNICATIONS NETWORK

By adding the ESP-12 module to traditional residential energy meters, one or more users can interact with the device via Wi-Fi. However, since there is no form of communication between the modified energy meters, the collection of information from the reader-collector is difficult. Since to read it, it must access each energy meter, extract its data and move on to the next one. The protocol and network functions related to the interconnection facilities of a mesh network are described below. As well as, the programming tools available for the mesh network, which allow better interaction between its nodes.

II.1 ESP-WIFI-MESH NETWORK PROTOCOL

ESP-WIFI-MESH [11] is a network protocol built on the Wi-Fi protocol that allows numerous devices (ESP-12 nodes) spread over a large physical area to be interconnected under a single network. The network is capable of self-organizing after the selection of a root node from which downward connections are formed layer by layer until all nodes have joined the network. It is also capable of self-repair by detecting and correcting failures that occur when the connection between any of the nodes is interrupted, or it becomes unstable.

With ESP-WIFI-MESH the nodes are not required to connect to a single central node (unlike Wi-Fi networks that have an AP and each node establishes a connection with it). Instead, connections are established between neighboring nodes, and each of them is mutually responsible for relaying each other's transmissions. Therefore, this type of networks has a much larger coverage and is less susceptible to overload, since the number of nodes allowed in the network is not limited by a single central node [11]. ESP-WIFI-MESH allows nodes to simultaneously act as a station and an AP. Therefore, a node can have multiple downstream connections using its softAP (software-defined access point) interface and a single upstream connection using its station interface. Therefore, a tree-shaped network topology is obtained with a parent-child hierarchy formed by multiple layers as shown in Figure 1. On the other hand, ESP-WIFI-MESH is a multi-hop network. Therefore, nodes transmit their own packets and simultaneously serve as repeaters for other nodes. This allows any pair of nodes within the network to communicate as long as any path exists at the physical layer (through one or more wireless hops). The total number of nodes that the ESP-WIFI-MESH network can support depends on the maximum number of layers allowed in the network and the maximum number of downstream connections that each node can have, both variables can be configured to limit the size of the network [11].

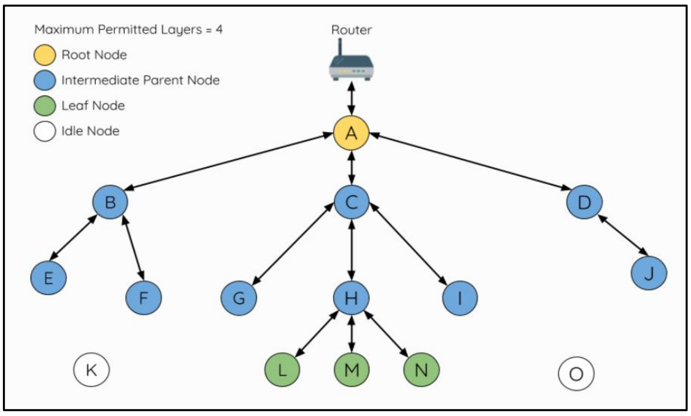

Figure 1: Types of nodes in ESP-WIFI-MESH.
Source: [11], (2024).

ESP-WIFI-MESH recognizes four types of nodes shown in Figure 1. The top node of the network is called the root node (node A). It serves as the only interface between the ESP-WIFI-MESH network and an external IP network, only one can exist on the network and its upstream connection is a conventional router. The nodes located in the maximum allowed layer of the network are assigned as leaf nodes (L, M and N nodes). They are not allowed to have downstream connections (child nodes), therefore they can only transmit or receive their own packets, but not forward packets from other nodes. These nodes ensure that no more layers are added to the network. Some nodes without a softAP interface are also designated in this category since they do not meet the requirements to establish downward connections. The intermediate nodes to the previous classifications are the so-called intermediate parent nodes (nodes B, C, D, E, F, G, H, I and J). These nodes must have a single upstream connection (a single parent node), and can have zero to multiple downstream connections (child nodes). They are capable of transmitting and receiving packets, but also forwarding packets sent from their upstream and downstream connections. Nodes of this type that do not have child nodes (nodes E, F and J) are not classified as leaf nodes, as they can form descending connections in the future. Finally, inactive nodes (K and O nodes) are those that have not yet joined the network, but may form an upstream connection with an intermediate parent node or will try to become the root node under the right circumstances [11].

Nodes that can form downstream connections transmit signaling frames periodically, allowing other nodes to detect their presence and know their status. Inactive nodes receive the frames to generate a list of possible parent nodes, with one of which they will form an upstream connection. To prevent this connection from being weak ESP-WIFI-MESH implements a received signal strength indication (RSSI) threshold mechanism for signaling frames. If a node detects a signaling frame with an RSSI lower than a pre-configured threshold, the transmitting node will not be considered to form an uplink. To choose the parent node among the possible candidates, the inactive node takes into account the layer where the candidate is located and the one located in the shallowest layer of the network (including the root node) has priority, in order to minimize the number total network layers. If there are several parent node candidates within the same layer, it will be preferred to have fewer child nodes, in order to balance the number of downward connections between nodes in the same layer. On the other hand, ESP-WIFI-MESH allows the user to define their own algorithm to select a predefined parent node, or force a node to only connect to a specific parent node [11].

II.2 NETWORK CONSTRUCTION

Building an ESP-WIFI-MESH network involves selecting a root node from which downward connections are formed layer by layer until all nodes have joined the network. Before starting the network formation, each node must be configured with the same: mesh network identifier, router configuration and softAP configuration. The root node can be designated during configuration or chosen dynamically based on the signal strength between each node and the router. Once selected, it will create an upstream connection with the router and from there the second layer will be formed with the inactive nodes in the range of the root node, becoming intermediate parent nodes. The remaining inactive nodes will connect to the intermediate parent nodes within their range, becoming intermediate parent nodes or leaf nodes, depending on the number of layers allowed in the network. The process is repeated until there are no idle nodes left in the network or until the maximum layer allowed in the network has been reached, therefore the remaining nodes will remain idle indefinitely.

In automatic root node selection, each idle node will transmit its MAC address (to identify each node in the network) and its RSSI value with the router through Wi-Fi signaling frames. Each node will then simultaneously search for signaling frames from other idle nodes, and if a node detects a frame with a stronger RSSI it transmits the contents of the frame. The process is repeated for a pre-configured minimum number of iterations and will result in the signaling frame with the strongest RSSI being propagated throughout the network. Finally, each node individually checks its vote percentage (number of votes/number of nodes participating in the election) and the one that contains a value greater than a pre-configured threshold will become the root node of the network. If more than one node meets the threshold requirements, there will be several root nodes within the same ESP-WIFI-MESH network, resulting in the creation of multiple networks. This conflict can be resolved automatically by internal ESP-WIFI-MESH mechanisms. However, conflicts where two or more root nodes have the same SSID (public name of a WLAN that serves to differentiate it from other wireless networks in the area) are not handled. Once a root node is chosen, ESP-WIFI-MESH does not automatically change it unless it is disconnected from the network.

If some nodes in the network are powered on asynchronously (separated by several minutes) the final structure of the ESP-WIFI-MESH network may differ from the ideal case where all nodes are powered on at the same time. The lagging node should join the network like any other idle node, even though it may have a stronger RSSI with the router. If this were the designated root node, all other nodes in the network will remain idle until the lagging node is powered on. Likewise, if it is a designated parent node, its child will remain inactive until it powers on. Finally, child nodes can change their upstream connections to another parent node in a lower layer, this process occurs autonomously and following the same threshold mechanism explained [11].

II.3 NETWORK SELF-REPAIR

ESP-WIFI-MESH can detect and correct failures that occur when the connection between any of the nodes is interrupted, or becomes unstable. Child nodes will autonomously select a new parent node and form an upstream connection to it to maintain network interconnectivity. If the root node fails, it will be detected by the nodes connected to it (second layer), which will initially try to reconnect to the root node. After several failed attempts, the second layer nodes will start a new round of electing a new root node following the process described above, and the remaining nodes will form upstream connections with it or a neighboring parent node if they are not in range. If the root node and several nearby layers fail, the top layer that is still functioning will begin the root node election process. When an intermediate parent node fails, a similar procedure is followed since the disconnected child nodes will search for possible parent nodes. Then each child node will individually select a new parent node and form an upstream connection with it. If there are no potential parent nodes for any child node, it remains inactive indefinitely [11].

II.4 PROGRAMMING TOOLS

The painlessMesh library [12] allows the implementation of the ESP-WIFI-MESH protocol and creating mesh networks using ESP-12 modules. Below are the functions that are of interest for this job:

- *void receivedCallback(uint32_t from, String &msg):* every time this node receives a message, this routine will be called, where *from* is a variable of type integer and size 32 bits corresponding to the identification of the sender of the message and *msg* is the message sent (in this case a string, but it can be any type of data).
- *void newConnectionCallback(uint32_t nodeId):* is triggered every time a node establishes a new connection, where *nodeId* is the ID of the new node connected to the mesh.
- *void changedConnectionCallback():* runs every time a connection on the network changes (a node leaves or joins the network).
- *void nodeTimeAdjustedCallback (int32_t offset):* it is executed when the network adjusts the time, so that all nodes are synchronized, offset is the offset.

III. MATERIALS AND METHODS

To evaluate the possibility of interconnecting several modified energy meters with the ESP-12 modules, the parameters to be evaluated are defined and three scenarios are formed with characteristics of mesh networks. With these conditions, the verification experiments are carried out [13].

III.1 PARAMETERS FOR NETWORK EVALUATION

It is necessary to define certain parameters to measure the quality of the ESP-WIFI-MESH network, as well as evaluate its behavior in different scenarios. In this work, the following are used: the power of the received signal as a measure of quality, as well as the network discovery time and the network recovery time as distinctive measures of this type of networks.

The signal power level (in dBm) perceived by a device in wireless networks (RSSI) [14] is the parameter used by Wi-Fi transceivers to adapt their modulation and coding scheme so that the optimal data rate. The modulation scheme that supports high-speed transmission requires a high signal-to-noise ratio, which is correlated with a strong RSSI.

The network discovery time or convergence time is defined in [15] as the time interval that elapses from the start-up of the devices until the complete formation of the network. The latter refers to the state in which each node is able to communicate with any other node through a route defined in its routing table. To carry out the measurement, each node was configured to periodically send a “measurement update” packet. To quantify the time it takes a node to discover the network, each node records a timestamp when it starts up (*t_start*). Every time a node discovers a network and decides to join it, it records another timestamp (*t_join*), then the difference between both timestamps (*t_join-t_start*) is the time it took the node to discover the network [16]. The value of this difference corresponding to the last node to join the network is the network discovery or convergence time.

The recovery or self-repair time of ESP-WIFI-MESH networks is defined in [16] as the recovery latency parameter. Which is the amount of time it takes the network to detect a node breakdown and take the appropriate actions to repair the network. To measure the same, whenever a node detects that it may have lost connectivity, it records a timestamp (*t_(connection lost)*) and initiates a connectivity test. If the result confirms the loss of connectivity, the node is released from said link and begins a channel exploration procedure (other possible connections). When it discovers a hub in the vicinity and decides to join it, it records another timestamp (*t_join*). The difference between both brands (*t_join-t_(connection lost)*) is the time it took for the node to recover connectivity and therefore, the time it took for the network to recover.

III.2 DESCRIPTION OF THE SCENARIOS AND EXPERIMENTS

The experiments are carried out from three ESP-12 modules (nodes) whose Id are shown in Figure 2, which illustrates a possible network topology with two levels. There is one ESP-12E nodeMCU and two ESP-12E SoM. The dashed lines represent the Wi-Fi connections between them.

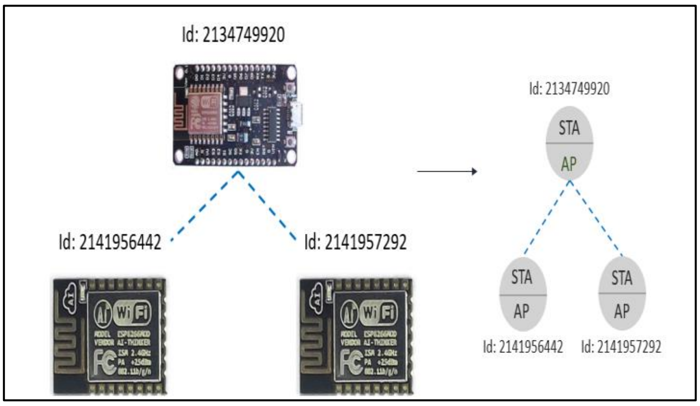

Figure 2: ESP-WIFI-MESH Network.
Source: Authors, (2024).

In addition, a possible network diagram is shown, where the stations (STA) of the modules with Id 2141956442 and 2141957292 respectively, connect to the access point (AP) of the remaining module (Id 2134749920). Therefore, the node with Id 2134749920 acts as a bridge (root), so that the two remaining nodes (intermediate parents) can establish communication.

Three scenarios were implemented in adjoining rooms and exterior hallways, separated by reinforced concrete walls, the details of which are shown in Figure 3. The legend specifies the meaning of each shape belonging to Figure 3 and the black arrows are the dimensions of distance between the nodes. Finally, the blank spaces on the walls in Scenario 3 represent the doors to the rooms.

These scenarios are equivalent to the situations of several energy meters in the same room, in the case of an apartment building. As well as several energy meters that are in separate houses a short distance away, located inside and outside the houses. In scenarios 1 and 2, the nodes have a direct line of sight, only the distances vary, while in scenario 3, two of the modules are inside the rooms and a third in the hallway, therefore, there is no line of sight between any of them.

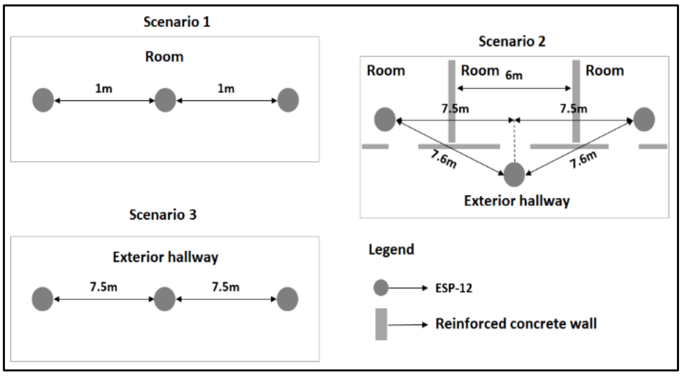

Figure 3: Sampling scenarios.
Source: Authors, (2024).

The first experiment is to verify that the three nodes can connect to each other forming the ESP-WIFI-MESH network. To verify that the connection is established, all nodes send a broadcast message, and the recipient prints the messages received through its serial port. A web server is used with the objective of simulating a possible interface between the reader-collector and the network of modified energy meters, where information on the connection states is also displayed. Actions were carried out on the network to evaluate its response to situations that correspond to real problems. For example, modules were intentionally turned off (simulating the possible failure of a modified energy meter) and a module that was turned off during network establishment was turned on (simulating a new modified energy meter in the area), among others. The network should not be affected in any case due to its self-healing and self-configuring properties.

The second experiment is aimed at evaluating the parameters in different scenarios, with the greatest amount of data possible, and presenting the result of the average values in each case. By having three modules, disconnecting an extreme node from the network (a node that only has a connection with another node) does not provide information. In this case, the network loses a node. However, since there is no bridge connection between the two remaining nodes, an interruption does not occur, only the topology changes.

IV. RESULTS AND DISCUSSIONS

The first connectivity experiment is performed in a local scenario like scenario 1 in Figure 3, using broadcast messages. By exchanging information between the three nodes, the self-configuration of the ESP-WIFI-MESH networks was verified, since the network was created automatically and all the nodes were able to send messages between them.

The reader-collector must be able to collect data from the modified energy meters by connecting with their smart device (phone, tablet, laptop, among others) to the network formed by them. To test this function, we create a web server and a function that returns the connection status in the form of a table. The columns **Id Node**, **Value** (in this case a random value from 1000 to 5000 will be displayed that simulates the current electricity consumption), the **Connection status** and the **Id** of the nodes that are connected to the network. In addition, a "*****" is used next to the Id of the node that serves as the AP for the intelligent device that simulates the reader-collector interface. The result of this operation is shown in Figure 4, where a diagram of the possible topology of said network is also shown.

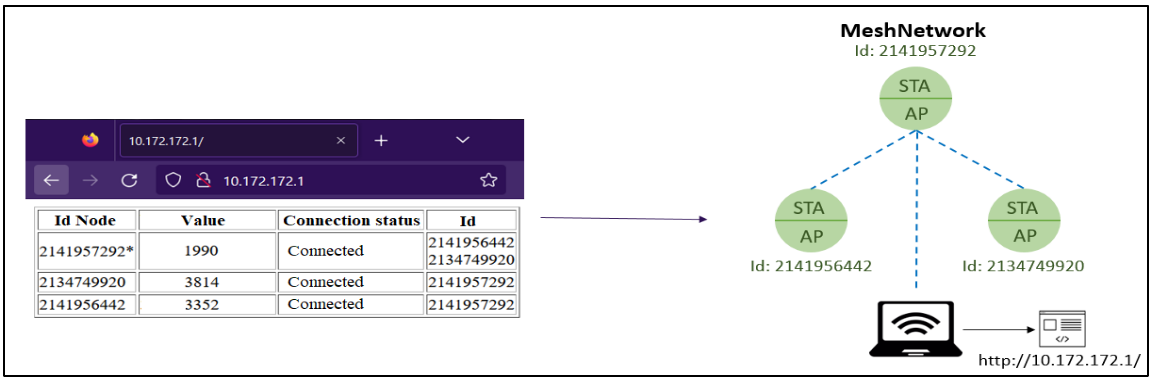

Figure 4: Network with all nodes connected.
Source: Authors, (2024).

The green circles in Figure 4 represent the turned on nodes, the blue dashed lines represent the Wi-Fi connections between all devices, and the web page that the laptop accesses is illustrated by specifying its domain. In this case, the network is accessed through the node with Id 2141957292, this means that the laptop is connected to the AP of that node. If a node leaves the network, it reorganizes itself due to its self-healing and self-configuring features. To verify this, the module that acted as a bridge node between the rest (Id: 2141957292) was intentionally turned off. In Figure 5, the turned off module is represented in gray, and it is shown how the remaining nodes connect to each other and the laptop accesses the network through another node. The Id of the nodes with which the connection is established is displayed, "-" indicates that the node has no connections because it is not active on the network. This process was done automatically and takes a few seconds. Then the module was turned on again, and in seconds, it was integrated back into the network forming a different topology.

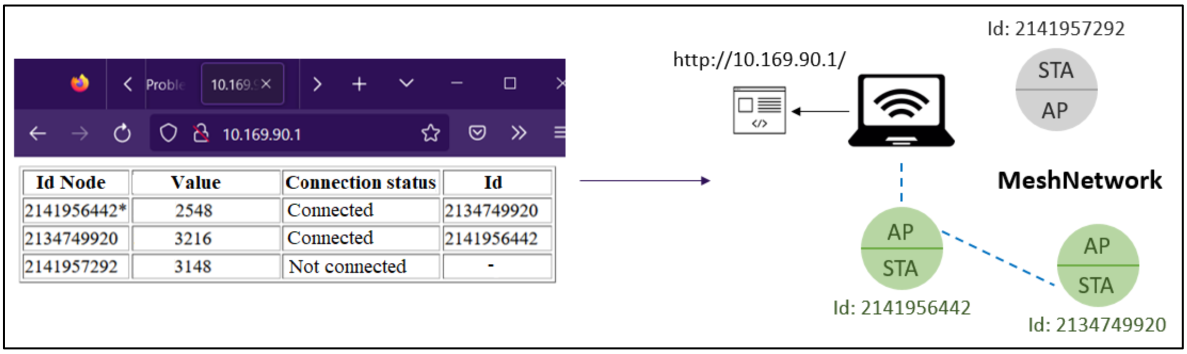

Figure 5: Network with two connected nodes.
Source: Authors, (2024)

After establishing the network and checking its correct operation, the code was modified with the objective of evaluating the previously defined parameters, with the second experiment. Network discovery and recovery times were calculated from a list of network events, which are broadcast messages that are modified each time a change occurs in the network topology. The values are sent through the serial port and are managed through another web page. The parameters are evaluated in the three scenarios. The results of the evaluation of scenario 1 are presented below, as an example.

The results of each of the five tests in scenario 1 are shown in Table 1. For each test, several measurements are made and the average values are presented. The RSSI values are in the range of -30dBm to -60dBm, which are associated with an ideal signal, which was expected, since there are no obstacles and the distance between the ESP-12 is small. From the average times in each test, it is obtained that in scenario 1 the network discovery time is approximately 2.6122 seconds.

Table 1: Network and RSSI discovery times for scenario 1.

Test	Parameter	Id: 2134749920	Id: 2141956442	Id: 2141957292	Average
1	Time (ms)	2951	2224	2874	2683
	RSSI (dBm)	-	-55	-48	-
2	Time (ms)	2708	2287	2364	2453
	RSSI (dBm)	-51	-50	-	-
3	Time (ms)	2610	2209	2745	2521.33
	RSSI (dBm)	-57	-47	-	-
4	Time (ms)	2910	2206	3053	2723
	RSSI (dBm)	-51	-48	-	-
5	Time (ms)	2813	2280	2949	2680.67
	RSSI (dBm)	-45	-54	-	-

Source: Authors, (2024).

In some of the tests, the node that functioned as a bridge for the remaining nodes was intentionally disconnected, to measure the network's recovery time in the event of its loss. Figure 6 shows the network topologies before and after said action, where the green color indicates that the node is on and the gray color is off, the black arrows correspond to distance levels and the blue dashed lines represent the connections through Wi-Fi of the nodes. Where Id 2141957292 identifies the bridge node. By disconnecting the bridge node, the remaining nodes lose connection between them and are unable to exchange information. Figure 7 shows the events corresponding to the node with Id 2141956442. After approximately 14,854 seconds (in Figure 7, t = 361053 - 346199) the network is reestablished, with a new topology. This time is calculated taking into account the times of the node with Id 2141956442, the same procedure is followed for the network discovery time, calculating the recovery times seen from each node and averaging them. In Figure 6, the RSSI value in the node with Id 2141956442 also increases as the distance with its new AP decreases.

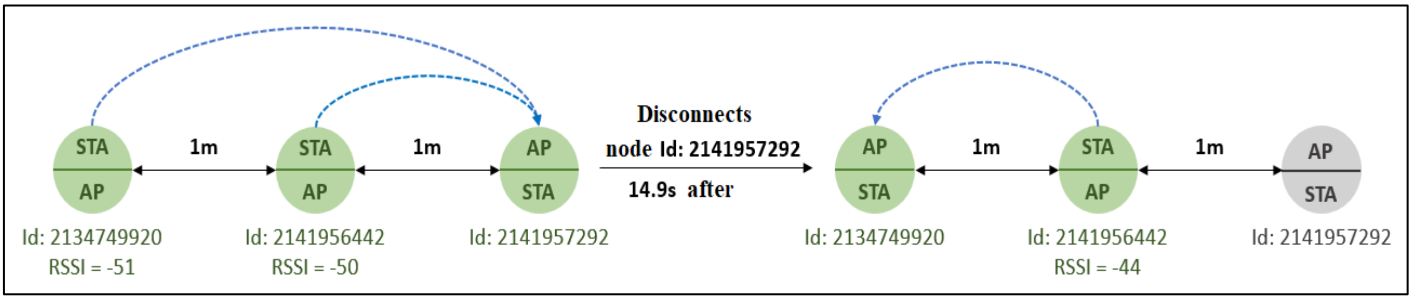

Figure 6: Topology changes in test 2.
Source: Authors, (2024).

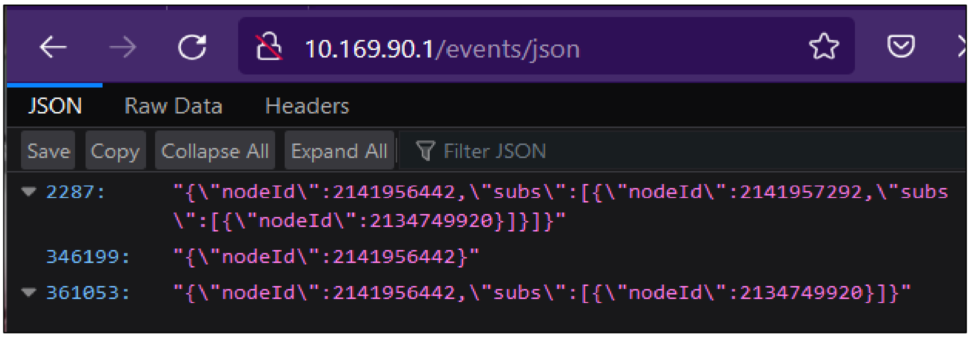

Figure 7: Events of the node with Id 2141956442 in Test 2.
Source: Authors, (2024).

Similar treatment was carried out with each of the scenarios. Table 2 shows a comparison between the results for each scenario, with the average values of several trials. Network discovery times remain almost constant when only the distance between modules increases (scenarios 1 and 2, in Figure 3), even though the signal strength decreases considerably. Furthermore, when the bridge node was intentionally disconnected from the network, and the distance increased further in some cases, the RSSI decreased as expected. However, when the modules have no line of sight between them by walls (scenario 3 in Figure 3), the network formation time increases by approximately 0.368 seconds (compared to scenario 2 in Figure 3). Obstacles also affected the RSSI, which decreases reaching unacceptable values (less than -90dBm).

Table 2: Comparison of the results of each scenario.

Scenerios	Network discovery time (s)	Network recovery time (s)	RSSI Range
1	2.6122	20.78675	(-45) – (-
2	2.797732	28.126	(-60) – (-
3	3.166268	72.043	(-70) – (-

Source: Authors, (2024).

Network recovery times vary in each of the scenarios. Figure 3 shows that the maximum distance between two nodes is 2m in scenario 1 and 15m for scenarios 2 and 3 respectively. Therefore, when the intentionally disconnected node was the bridge (scenarios 2 and 3 in Figure 3), the distance between the remaining nodes increased. The recovery times for scenarios 1 and 2 differ by 7.34s, only due to the increase in said distance, which brings with it a decrease in the RSSI value. In this case not very considerable, since it continued in the same range as for its initial configuration. However, in scenario 3 the value of this parameter increases considerably (43.917s compared to scenario 2 where the distance remains constant), in addition the RSSI decreases, reaching values below the minimum acceptable signal state. Therefore, the existence of obstacles that reduce the intensity of the received signal (in this case reinforced concrete walls) affects network recovery times more.

V. CONCLUSIONS

It is possible to form an ESP-WIFI-MESH network with the ESP-12 modules using the painlessMesh library, which meets the self-configuration and self-healing requirements. By accessing one of its nodes, the data stored in the remaining nodes can be obtained. Therefore, it is possible to form a mesh network between the modified energy meters, allowing the exchange of information between them and its collection, so that the coverage area is increased. This allows the reader-collector to read consumption from any point on the network through a smart device. The evaluation of the network parameters in the different scenarios also demonstrated its viability for this purpose. However, when deploying the new energy meters it is important to take into account the obstacles and distances between them in each of the areas. The distance between the modules has a direct impact, decreasing the RSSI. This decrease can cause loss of connection stability or the most critical result, a complete loss of connection. On the other hand, some materials (such as reinforced concrete walls) can cause signal attenuations, this results in delays in the discovery time and fundamentally in the network recovery time. Tests must be carried out with the modified energy meters in real environments and the type of antenna to be used must be evaluated, so that the greatest possible coverage is guaranteed.

VI. AUTHOR'S CONTRIBUTION

Conceptualization: Carlos Bazán Prieto and Alberto Bazán Guillén.
Methodology: Carlos Bazán Prieto and Alberto Bazán Guillén.
Investigation: Carlos Bazán Prieto and Alberto Bazán Guillén.
Discussion of results: Carlos Bazán Prieto and Alberto Bazán Guillén.
Writing – Original Draft: Carlos Bazán Prieto and Alberto Bazán Guillén.
Writing – Review and Editing: Carlos Bazán Prieto and Alberto Bazán Guillén**.**
Resources: Carlos Bazán Prieto and Alberto Bazán Guillén.
Supervision: Carlos Bazán Prieto and Alberto Bazán Guillén.
Approval of the final text: Carlos Bazán Prieto and Alberto Bazán Guillén.

VII. REFERENCES

[1] S. S. Refaat, O. Ellabban, S. Bayhan, H. Abu-Rub, F. Blaabjerg, and M. Begovic, Smart Grid and Enabling Technologies. 2021. doi: 10.1002/9781119422464.

[2] M. R. Hossain, A. M. T. Oo, and A. B. M. S. Ali, "Smart Grid", in Smart Grids: Opportunities, Developments, and Trends, A. B. M. S. Ali, Ed. London: Springer, 2013, pp. 23–44. doi: 10.1007/978-1-4471-5210-1_2.

[3] G. Dileep, "A survey on smart grid technologies and applications", Renew. Energy, vol. 146, pp. 2589–2625, Feb. 2020, doi: 10.1016/j.renene.2019.08.092.

[4] "Electricidad en Cuba: entre el costo y la tarifa", https://www.juventudrebelde.cu/cuba/2020-12-13/electricidad-en-cuba-entre-el-costo-y-la-tarifa (accessed Oct. 12, 2022).

[5] A. Bazán Guillén, "Infraestructura escalable para lectura remota de contadores de energia de energía eléctrica", Tesis de Maestría en Telemática, Universidad Central "Marta Abreu" de Las Villas, 2022.

[6] "ESP-12E Datasheet", https://datasheet4u.com/datasheet-pdf/AI-Thinker/ESP-12E/pdf.php?id=1258546 (accessed Nov. 03, 2022).

[7] L. Santos, T. Costa, JMLP. Caldeira, VNGJ. Soares. "Performance Assessment of ESP8266 Wireless Mesh Networks", Information. 2022; 13(5):210. https://doi.org/10.3390/info13050210

[8] N.A. Afifie, A.W.Y. Khang, A.S. Bin Ja'afar, A.F.B.M. Amin, W.A. Indra, S.G. Herawan and A.B. Ramli, 2021. "Evaluation Method of Alsayaydeh, J.A.J Mesh Protocol over ESP32 and ESP8266", Baghdad Science Journal. 18, 4(Suppl.) (Dec. 2021), 1397. https://doi.org/10.21123/bsj.2021.18.4(Suppl.).1397

[9] Yoppy, R. H. Arjadi, E. Setyaningsih, P. Wibowo, M. I. Sudrajat, IOP Conf. Series: Journal of Physics: Conf. Series 1230 (2019) 012023, doi:10.1088/1742-6596/1230/1/012023

[10] A.U. Khan, M.E. Khan, M. Hasan, W. Zakri, W. Alhazmi, T. Islam, "An Efficient Wireless Sensor Network Based on the ESP-MESH Protocol for Indoor and Outdoor Air Quality Monitoring", Sustainability. 2022; 14(24):16630. https://doi.org/10.3390/su142416630

[11] "ESP-WIFI-MESH - ESP32 - ESP-IDF Programming Guide v4.4.2 documentation", https://docs.espressif.com/projects/esp-idf/en/stable/esp32/api-guides/esp-wifi-mesh.html (accessed Nov. 03, 2022).

[12] G. Martín, "Intro to painlessMesh", Oct. 18, 2022. Accessed: Nov. 05, 2022. [Online]. Available: https://github.com/gmag11/painlessMesh

[13] A. Arkhipenko, "Task Scheduler", Nov. 05, 2022. Accessed: Nov. 05, 2022. [Online]. Available: https://github.com/arkhipenko/TaskScheduler

[14] Yoppy, R. H. Arjadi, H. Candra, H. D. Prananto, and T. A. W. Wijanarko, "RSSI Comparison of ESP8266 Modules", in 2018 Electrical Power, Electronics,

Communications, Controls and Informatics Seminar (EECCIS), Oct. 2018, pp. 150–153. doi: 10.1109/EECCIS.2018.8692892.

[15] E. Giacomini, F. D'Alterio, A. Lacava, and F. Cuomo, "BLUES: A Self-organizing BLE Mesh-network Paradigm for IoT Environments," in 2020 IEEE 21st International Symposium on "A World of Wireless, Mobile and Multimedia Networks" (WoWMoM), Aug. 2020, pp. 409–414. doi: 10.1109/WoWMoM49955.2020.00075.

[16] P. Kulkarni, S. Gormus, Z. Fan, and F. Ramos, "AMI Mesh Networks—A Practical Solution and Its Performance Evaluation", IEEE Trans. Smart Grid, vol. 3, no. 3, pp. 1469–1481, Sep. 2012, doi: 10.1109/TSG.2012.2205023.